Investigating and Exploiting Best Practices in Hit Identification and Hit to Lead Chemistry

Jennifer Borthwick

PhD 2016

Department of Pure and Applied Chemistry

Declaration of Authenticity and Author's Rights

This thesis is the result of the author's original research. It has been composed by the author and has not been previously submitted for examination which has led to the award of a degree.

The copyright of this thesis belongs to GSK in accordance with the author's contract of employment with GSK under the terms of the United Kingdom Copyright Acts. Due acknowledgement must always be made of the use of any material contained in, or derived from, this thesis.

Signed: Date:

Abstract

A fragment-based drug discovery (FBDD) effort was carried out against the enzyme target BCATm. This resulted in elucidation of novel binding interactions against the enzyme. Several series of inhibitors were identified, these are the first known small molecule inhibitors of this enzyme. The compounds identified contained several examples which exhibited potent enzyme binding, excellent activity in a cellular assay and excellent DMPK profiles, making them high quality tools for target validation experiments.

A comparative data analysis was carried out to compare the physicochemical properties of molecules discovered by FBDD, high throughput screening (HTS) and encoded library technology (ELT) against BCATm. This showed that the properties of the ELT derived molecules were consistently outside of the established areas of physicochemical properties for drugs and leads, whilst the HTS and FBDD derived compounds largely sat within the desired space. This analysis was extended to clinical candidates against a range of targets described in the literature as being discovered by a range of different techniques. Only slight trends for improved properties for FBDD derived molecules were observed.

A phenotypic HTS hit against tuberculosis was identified to be acting through inhibition of the enzyme DprE1. This molecule had physicochemical properties which were far from the established limits for drug molecules. Through careful optimisation, using methodologies first established for FBDD, a lead series with much improved properties was derived. The lead molecules had potent inhibition of DprE1, were efficacious in halting the growth of *Mycobacteria tuberculosis in vitro*, had excellent DMPK properties and also showed good efficacy in *in vivo* models of tuberculosis.

2

Acknowledgements

The completion of this work would not have been possible without the help and support of many people. I would like to begin by thanking my industrial supervisor, Rob Young for the many hours he has put into reading and refining this work, and for insightful discussions and suggestions throughout the course of the projects. Equally important are the contributions of my academic supervisor, Colin Suckling who has always been an interesting and astute adviser and collaborator with whom to discuss this work. Also thanks to both Colin and Rob for their support and encouragement to persevere when things got tough.

Words cannot express how important the love, support and encouragement of my family have been in motivating me to complete my PhD. I am especially grateful to my husband, Scott who has been unwavering in his support and belief in me. Also to Scott and my two sons, James and Douglas who have put up with me spending far too many weekends and holidays writing and studying without complaints, and always with smiles on their faces for me at the end of a long day. My wonderful parents, Anne and Jim and parents-in-law Susan and Finlay have frequently travelled from Scotland and spent countless days babysitting to allow me to work on my thesis and have always been ready with a glass of wine and words of encouragement. Thank you.

There are many colleagues from GSK I need to thank. All those who have contributed to this work with excellent science, including Rob Young, Ben Whitehurst, Sophie Bertrand, Nicolas Ancellin, Paul Carter, Ryan Bingham, Chun-wa Chung, Claus Spitzfaden, Peter Francis, Don Somers, Nerina Dodic, Sarah Smith, Yoshiaki Washio, Benjamin Beaufils, Andy Hobbs, Archie Argyrou, Monica Cacho-Izquierdo, Julia Castro-Pichel, Laura Vela-Glez del Peral and Joaquin Rullas-Trincado. Also, thank you to the many colleagues who have spent their time on proof-reading, data integrity checking and legal approvals: Lisa Sloan, Mark Hillier, Fatema Sardharwalla, Chun-wa Chung, Metul Patel, Chris Edwards, Shenaz Benully, Laura Vela-

Glossary and Abbreviations

ADME: Absorption, distribution, metabolism, excretion

Animal Studies: All animal studies were ethically reviewed and carried out in accordance with European Directive 2010/63/EU and the GSK Policy on the Care, Welfare and Treatment of Animals

ATP: Adenosine triphosphate

ATR: Attenuated total reflectance

BACE-1: Beta-secretase 1

BCAA: Branched chain amino acid

BCATc: Cytosolic branched chain aminotransferase

BCATm: Mitochondrial branched chain aminotransferase

Bcl-2: B-cell lymphoma 2

BEH: Ethylene bridged hybrid

BEI: Binding efficiency index

Biological Data: All biological data quoted in this thesis is an average of at least 2 test occasions, unless stated otherwise

BOC: *Tert*-butyl carbamate

Candidate: A molecule which has been selected after lead optimisation as suitable for progression to pre-clinical and then clinical development

CDI: Carbonyl diimidazole

CDK: Cyclin-dependant kinase

CFU: Colony forming unit

ChromlogD$_{7.4}$:Chromatographic logD measured at pH 7.4

Cl$_b$: Whole blood clearance

Clint h/m: Intrinsic clearance measured in human and mouse microsomes[1]

CLND solubility: Measures precipitation from DMSO solution by chemi-luminescent nitrogen detection[2]

CNS: Central nervous system

COMU: (1-Cyano-2-ethoxy-2-oxoethylidenaminooxy)dimethylamino-morpholino-carbenium hexafluorophosphate

CSD: Cambridge structural database

CYP: Cytochrome P450

DBU: 1,8-Diazabicyclo[5.4.0]undec-7-ene

DCM: Dichloromethane

DFG loop: Asp-Phe-Gly (DFG) motif at the N terminus of the activation loop of a kinase

DIPEA: *N,N*-diisopropylethylamine

DMF: *N,N*-dimethylformamide

DMPK: Drug metabolism and pharmacokinetics

DMSO: Dimethyl sulfoxide

DNA: Deoxyribonucleic acid

DPA: Decaprenylphosphoryl arabinose

DPR: Decaprenylphosphoryl ribose

DprE1: Decaprenylphosphoryl-β-D-ribose 2'-epimerase

DprE2: Decaprenylphosphoryl-D-2-ketoerythro pentose reductase

DPX: Decaprenylphosphoryl-D-2-keto-erythro-pentofuranose

ED_{99}: Effective dose 99 %

E-GGPR: 2E,6E,10E-Geranylgeranylphosphoryl-β-D-ribose

ELT: Encoded library technology

F%: Oral bioavailability

FAD: Flavin adenine dinucleotide

FaSSIF: solubility in simulated intestinal fluid in the fasted state[3]

FBDD: Fragment based drug discovery

FDA: US food and drug administration

FeSSIF: solubility in simulated intestinal fluid in the fed state[3]

Focussed Screening: The screening of a smaller set of compounds than for an HTS which are considered more likely than a random set to be active at the target being screened.

FPR: Farnesylphosphoryl-β-D-ribose

FTIR: Fourier transform infrared spectroscopy

GABA: γ-aminobutyric acid

GI: Gastro-intestinal

GPCR: G-protein coupled receptor

GSK: GlaxoSmithKline

HATU: N,N,N',N'-tetramethyl-O-(7-azabenzotriazol-1-yl)uronium hexafluorophosphate

HBA: Number of hydrogen bond acceptors

HBD: Number of hydrogen-bond donors

HepG2 cytotoxicity: Ability of compound to kill HepG2 (a human hepatoblastoma cell line) cells[4]

hERG: Human ether-a-go-go related gene

Hit: A molecule which has robust measured activity at a given target

HIV: Human immunodeficiency virus

HMBC: Heteronuclear multiple bond correlation

HOBt: Hydroxybenzotriazole

HPLC: High performance liquid chromatography

HRMS: High resolution mass spectroscopy

HSQC: Heteronuclear single quantum correlation

HTS: High-throughput screening

Human biological samples: The human biological samples were sourced ethically and their research use was in accord with the terms of the informed consents

IC_{50}: Half-maximal inhibitory concentration

InhA: Isoniazid target

IPA: Propan-2-ol

IQR: Inter-quartile range

IR: Infrared

ITC: Isothermal titration calorimetry

K_d: Dissociation constant for binding

Knowledge based discovery: Starting hits are designed by analogy to known active compounds at the target of interest

LCMS: Liquid chromatography mass spectrometry

LE: Ligand efficiency

Lead: A series of molecules which are considered suitable to investigate further in lead optimisation. Typically would have activity at the target of interest, SAR, good physicochemical properties and indications of good pharmacokinetics and limited off-target activities.

LELP: Ligand efficiency logP

LLE: Lipophilic ligand efficiency

LLE_{AT}: Lipophilic ligand efficiency as defined at Astex

$logD_{xx}$: Distribution coefficient at pH xx.

$logS_w$: The log of the intrinsic aqueous solubility

logP: The partition coefficient of the neutral compound between octanol and water

LTA4H: Leukotriene-A4 hydrolase

MDAP: Preparative mass directed HPLC

MDI: Metabolism-dependent inhibition

MDR: Multi-drug resistant

MEC: Minimum effective concentration

2-MeTHF: 2-Methyltetrahydrofuran

MIC: Minimum inhibitory concentration

MMP: Matrix metalloproteinase

MP: Melting point

MW: Molecular weight (Da)

NAD: Nicotinamide adenine dinucleotide

Natural product based discovery: Screening of libraries of natural products and their close analogues

NET: Norepinephrine transporter

NIH: US National Institutes of Health

NMR: Nuclear magnetic resonance

NOESY: Nuclear Overhauser effect spectrospcopy

PAIN: Pan-assay interference compound

PD: Pharmacodynamics

$Pd_2(dba)_3$: Tris(dibenzylideneacetone)dipalladium(0)

PDB: Protein data bank

PFI: Property forecast index = chromlog$D_{7.4}$ + number of aromatic rings

Phenotypic screening: Diversity screening carried out in a whole cell or organism where the measured output is the desired phenotypic effect, rather than activity at a given biological target

PK: Pharmacokinetics

PLP: pyridoxal phosphate

PMP: pyridoxamine phosphate

PPAR: Peroxisome proliferator-activated receptor

PPB: Plasma protein binding

PPM: Parts per million

QC: Quality control

QT interval: The time between the start of the Q wave and the end of the T wave in the heart's electrical cycle

RFID: Radio frequency identification

ROESY: Rotating frame nuclear Overhauser effect spectroscopy

RTB: Number of rotatable bonds in a molecule

SAR: Structure-activity relationship

SDM: Site directed mutagenesis

SMARTS: Smiles arbitrarty target specifications, a language for specifying molecular substructures

$S_N Ar$: Nucleophilic aromatic substitution

SPE: Solid phase extraction

STD: Saturation transfer difference

$T_{1/2}$: Half-life

TB: Tuberculosis

TBME: *Tert*-butyl methyl ether

TDR: Totally drug resistant

TFA: Trifluoroacetic acid

THF: Tetrahydrofuran

T_m: Thermal shift

UPLC: Ultra performance liquid chromatography

UV: Ultraviolet radiation

Vd_{ss}: Volume of distribution at the steady state

Virtual screening: Computational screening of a library of molecules at a target of interest to identify a subset that are likely to bind, which can then be tested

XDR: Extensively drug resistant

Table Of Contents

1. Introduction

1.1 The Drug Discovery Process and the role of Medicinal Chemistry

The aim of drug discovery science is to design, test and bring small molecules to market as novel treatments for human diseases. This is a long, complex process, which takes most pharmaceutical companies around a decade,[5] costs on average $1.8 billion[6] and is frequently subject to failure.[7] The ability of the pharmaceutical industry to succesfully identify and progress to market new drugs is becoming exponentially poorer over time. Eroom's Law[8] states that the cost to discover and develop each FDA approved new drug roughly doubled every nine years between 1950 and 2010.

Target Identification

Identifying the biological target is the first step in the drug discovery process. In the past, drug molecules were identified on the basis of their behaviour in diseased cells or even whole animals. However, modern drug discovery has increasingly focussed on identifying single biological targets for intervention.

This target is a biomolecule, most commonly a protein, that can have its activity modulated by the drug molecule to ameliorate the disease of interest. The basic research linking the target protein to the disease can take many forms: genetic analysis of tissues from patients;[9] the use of knock-out genes or antisense technology in animal models or cell lines;[10] or simply understanding the cellular pathways that are involved in a given disease.[5] It has been suggested that this reductionism of identifying a single molecular target to treat a complex disease may be an overly simplistic approach, and a potential cause of the crisis of productivity affecting pharmaceutical R&D.[8,11]

Until recently, the proteins identified as drug targets by pharmaceutical researchers tended to be 'functional' enzymes or receptors, with known endogenous agonists, antagonists or substrates. By their nature, these proteins had well-characterised binding sites amenable to modulation by

small molecules, and their pharmacology could be readily investigated using their known ligands. Increasingly, in the post-genomics era, potential drug targets being investigated include 'non-enzymes', which may be involved in regulation of gene transcription, chaperoning, subcellular transport or formation of multi-protein complexes.[12] The functions of these targets are dependent on protein-protein interactions and so pharmacological intervention may be more difficult. It is likely that the binding sites would be less optimised for small molecule binding and that the necessary biological assays needed to investigate potential modulators would be more complex to set up, run and interpret.

As a result, it has become even more important to carry out further experiments to understand if the protein identified is 'druggable'. Researchers need to deduce if a drug-like molecule could interact with the target to provide a treatment for the disease without causing unwanted side effects.[13] It is at this stage in the process that medicinal chemists typically become involved. Their role would be to assess the chemical tractability of the protein. This could be by examining the binding site, if an X-ray crystal structure is available, or by comparing known ligands of the protein of interest or its close relatives with concepts of drug-like molecules. In some cases, it is necessary to identify novel chemical 'tools' that display the desired pharmacological effect at the target to test the hypothesis in animal models of disease.

Hit Identification

Once a drug target has been identified, the next step is to identify a potential drug molecule with the desired pharmacological effect on the target. The drug needs to be able to reach the site of action at an appropriate concentration and to stay there for a suitable duration of time. It also must not cause excessive side effects. Identifying this candidate drug molecule is the main role of the medicinal chemist, as part of a multi-functional team of scientists.

The first step in this process is the identification of a 'hit' starting point. A hit molecule is defined as a compound that displays some measurable activity at the target and that the medicinal chemistry team deem to be suitable for further exploration. Hit identification is commonly achieved by screening a large set of diverse compounds against the protein of interest, a process known as high throughput screening (HTS).[14]

Another approach is to design starting points from the chemical structure of the endogenous or other known ligands (knowledge based design). The use of *in silico* screening against the known or modelled structure of the protein active site is also common.[15] There has recently been increasing interest in growing drug-like molecules from small, weakly binding 'fragments' (Fragment Based Drug Discovery, FBDD).[16] This report focuses on the use of FBDD as a tool in hit identification and compares the outcomes with other hit finding techniques. The relevant hit finding techniques will be discussed in more detail later in this introduction.

Lead Optimisation

Once the starting hit is identified, the medicinal chemist must use an iterative process of designing, synthesising and testing potential molecules to improve their properties, known as lead optimisation. A lead molecule would be a molecule derived from the starting hit, which shows improved properties over the hit, and warrants more detailed investigation. During the lead optimisation process, the binding affinity of the hit for the target protein typically needs to be increased. However, other important properties of the molecule must also be optimised simultaneously to provide a candidate drug molecule. A candidate molecule is the single final compound that results from the lead optimisation process, which is considered to be the most promising molecule to be the marketed drug. The factors that are considered during optimisation can be broadly divided into three major issues that must be addressed. The first of these is the effect that the drug molecule has on the body, known as pharmacodynamics (PD). The second issue is how the body treats the drug, which as known as pharmacokinetics (PK). The combination of

pharmacokinetics and pharmacodynamics (PK/PD) defines the relationship between the dose of drug administered and the therapeutic effects. The final area that needs to be considered during lead optimisation is ensuring that the drug does not display unwanted side effects.

Within the area of pharmacokinetics, a number of parameters relating to the absorption, distribution, metabolism and excretion (ADME) of the drug must be optimised.[17] The drug molecule must be capable of reaching its site of action following administration, which could be orally, by injection, inhalation or transdermally. This describes the absorption component of the profile. In order to achieve this, the drug molecule must be soluble in biological fluids (mostly comprised of water) but also be capable of being absorbed across lipophilic biological membranes to allow it to enter the blood and, if required, penetrate cells where the target resides. The distribution of the drug will effect whether it is present at its site of action at a suitable concentration to exert its pharmacological effect. If, for example, the drug is strongly bound to proteins in the body it may be difficult to achieve a sufficient concentration at its target. The drug must be metabolised at such a rate that it is present in the body long enough to exert its desired effect without accumulating to toxic levels. Finally, the drug (or its metabolites) must be excreted from the body; this is usually through the kidneys (urine) or in the faeces.

The ADME profile of the drug is evaluated in both *in vivo* and *in vitro* models. *In vitro* testing can allow for rapid and high throughput evaluation of compounds. This includes measuring solubility and protein binding levels in plasma, stability in hepatocytes or microsomes and binding to metabolic enzymes especially the cytochrome P450 enzymes.[18] Molecules are also studied in whole animal *in vivo* studies of DMPK where the combined effects of the absorption, distribution, metabolism and elimination of the drug can be studied in a more realistic and complex biological environment.

Early assessment of the potential of a drug to cause unwanted side effects mainly involves *in vitro* testing. Some toxicity may be due to modulating the activity of the target protein, in which case all drug molecules that act through

this target would be expected to display similar adverse effects. This is known as mechanism based toxicity. However, many side effects are caused by the drug molecule interacting with alternative proteins. This could be specific to the target class of interest. For example, drugs that interact with a kinase target frequently bind to other kinases, which can cause undesirable effects. For this reason, kinase drug discovery programmes typically have to screen all molecules of interest against a sub-set of the kinome to assess and optimise selectivity.[19] Any functional protein could be modulated by the drug molecule. One example is the ion channel hERG (Human ether-a-go-go related gene). Drug molecules that bind and inhibit this channel prolong the QT interval of the heart-beat and can cause serious cardiac events, which are sometimes fatal.[20] In the decade to 2005, QT elongation, mainly due to hERG inhibition, was the most common reason for drugs to be withdrawn from the market.[21] For these reasons, most drug discovery projects now monitor *in vitro* hERG inhibition routinely as a marker for cardiotoxicity.

Late in lead optimisation, candidate molecules are often assessed in *in vivo* animal models of the disease being studied to test for efficacy.[17] These PK/PD studies can begin to predict the dose that would be required to treat the disease. *In vivo* toxicity tests in animals are also carried out to understand the potential for toxic effects in a whole organism system.

Drug Development

Once a candidate drug molecule has been identified, the drug development process begins. The first stage of this process is pre-clinical development. During this phase, longer and more complex animal toxicity experiments are carried out in several species.[22] At this stage, research to find a suitable manufacturing route to the drug molecule, which should be high-yielding, reproducible, economical and environmentally benign, is conducted.[23] An ideal form and formulation of the drug must be found that allows the drug to be suitably stored and administered.[24]

The final step in the process before a drug can be launched is clinical testing.[25] This is initially carried out in a small number of healthy human volunteers to test for tolerability and exposure (Phase I). In Phase II trials, the drug is tested in patients with the disease in question to determine if it provides an efficacious treatment. If successful, the drug is progressed to Phase III trials that involve large numbers of patients to provide the required evidence of efficacy and safety to achieve regulatory approval.

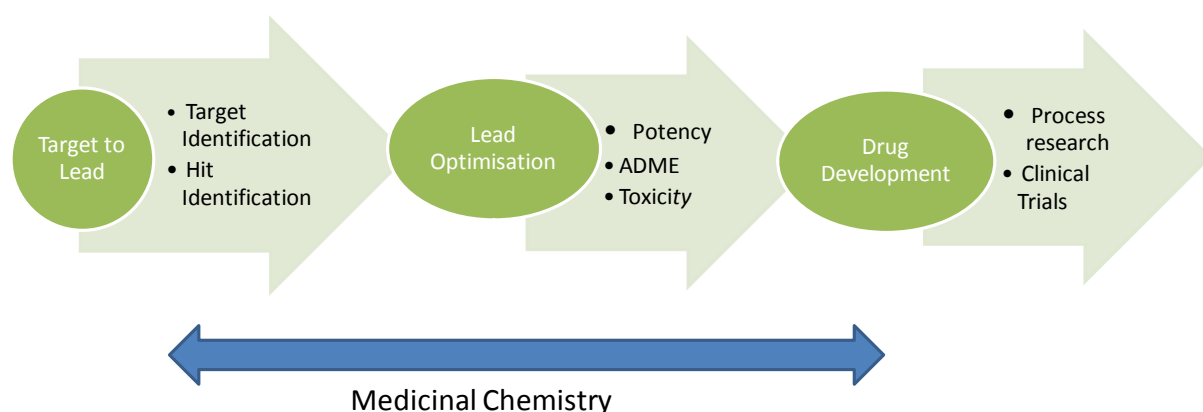A summary of the drug discovery and development process is given in *figure 1.1.*

Figure 1.1: The drug discovery process, highlighting the role of the medicinal chemist.

1.2 **Attrition in Drug Discovery and Physicochemical Properties of Drugs**

A major challenge facing the pharmaceutical industry is the very high rate of attrition in drug candidates during the development process. The current success rate of candidates to market is approximately 11%.[7] Even a small change to these attrition rates could have a profound effect on the fortunes of the pharmaceutical industry. The three highest causes of drug attrition in the year 2000 were lack of efficacy, commercial considerations and toxicity. Lack of efficacy in humans would most likely be caused by poor target selection, or by the drug failing to reach its target as a result of a poor ADME profile. Commercial decisions are often influenced by issues such as competitor

activity or changing regulatory requirements, which are difficult to predict by discovery scientists. Toxicity could either be due to mechanism based toxicity, or be due to the chemical properties of the molecule. Therefore, of these three causes, toxicity and lack of efficacy could both be influenced by the properties of the drug molecule. Addressing the properties of drug candidate molecules in discovery is one approach which could reduce failure in development and result in more new drugs successfully being launched to market.

One of the main physicochemical properties of a molecule that is important in determining its likely success as a drug is the lipophilicity or hydrophobicity. Experimentally, this is often measured as the partition coefficient of the neutral compound between octanol and water (logP).[26] There are several software programmes available to estimate the logP of a molecule, giving a calculated logP (clogP).[27] As the partition coefficient will change drastically depending on the charge of a molecule, the distribution coefficient (logD) is often measured.[28] This is the partition coefficient of an ionisable molecule at a given pH. In the study of drug molecules, physiological pH of 7.4 is considered the most relevant pH[29] and this result is generally quoted as $logD_{7.4}$. As for logP, it is possible to predict logD, the clogD, at any given pH. As these calculations rely on a pK_a estimate as well as an estimate of lipophilicity they are often less reliable than clogP calculations.[30] A chromatographic method of measuring logD, $chromlogD_{7.4}$, has been reported.[31] The authors suggest that this method is more reliable, especially for poorly soluble and highly lipophilic compounds. ChromlogD is on a different scale to traditional logD and the values for chromlogD are typically two log units higher. The $chromlogD_{7.4}$ measurement is used in this report for all measured logD experiments.

The influential work of Lipinski[32] established the so-called 'rule of 5' from an analysis of a set of oral small molecule drugs, which were expected to have good absorption. The conclusion from this analysis was that absorption was strongly correlated with no more than one failure of the following rules:

molecular weight <500 Da; logP < 5, number of hydrogen bond acceptors <10 and number of hydrogen bond donors <5. In the last decade, this work has been expanded upon and further refined.

A recent review of the effect of lipophilicity on a range of ADMET (absorption, distribution, metabolism, excretion and toxicology) parameters[33] suggested that to achieve a molecule with a favourable multifactorial profile there is a narrow logD window of between -1 and 3. Gleeson carried out an analysis of the effect of physicochemical properties on a range of parameters used in drug discovery to evaluate drug candidates[34] and established that increasing molecular weight or logP generally had a detrimental effect on measured solubility, permeability, oral bioavailability, volume of distribution, plasma protein binding, hERG channel binding and cytochrome P450 inhibition. Researchers at Pfizer analysed a large set of compounds that had *in vivo* toxicity data associated with them and established that molecules with clogP > 3 and polar surface area (PSA) < 75 $Å^2$ had a much increased chance of exhibiting toxicological effects.[35]

More recently, focus has turned to the relative aromatic or aliphatic character of candidate molecules. It has been shown that molecules with higher relative proportions of saturation are more soluble and have less promiscuous binding to proteins.[36] It was also observed that the proportion of saturation increases throughout the development process, suggesting that highly unsaturated molecules have a higher risk of attrition. An analysis of GSK molecules confirmed that the average number of aromatic rings decreases as compounds pass through development[37] and that high aromatic ring count is associated with poor solubility, high plasma protein binding, cytochrome P450 inhibition, and hERG channel binding. This work has recently been extended to show that carboaromatic rings have a more detrimental effect than heteroaromatics and that fused ring systems are preferable to the same number of rings arranged separately in a molecule.[38]

The combination of aromaticity and lipophilicity has been considered with the introduction of the 'solubility forecasting index' (SFI, *equation 1.1*).[39]

$$\text{SFI} \ = \ \text{clogP} \ + \ \text{number of aromatic rings} \qquad \textit{[Equation 1.1]}$$

The SFI should be below 5 to have a high probability of achieving aqueous solubility. This concept has been applied to a number of other important parameters in drug discovery, with the 'property forecasting index' (PFI) where a PFI <5 has also been shown to correlate with low plasma protein binding, low microsomal clearance, low hERG activity and lower promiscuity against a range of protein targets (see figure 1.2 for an example).[31] This calculation was shown to be even more effective when chromlogD$_{7.4}$ measurements are used in place of clogP (*equation 1.2*).

$$\text{PFI} = \text{chromlogD}_{7.4} + \text{number of aromatic rings} \quad \textit{[Equation 1.2]}$$

The PFI using chromlogD$_{7.4}$ should be less than 7 for the optimisation of most parameters.[*] However, permeability was shown to require a higher PFI, with the best compounds having a PFI around 7. This reflects the higher lipophilicity required to cross biological membranes and highlights the general requirement for medicinal chemists to produce molecules with balanced physicochemical profiles. In general, drug molecules were found to have low PFI values.

---

[*] chromlogD$_{7.4}$ is on a different scale to clogP hence the 2-unit difference in the maximum value
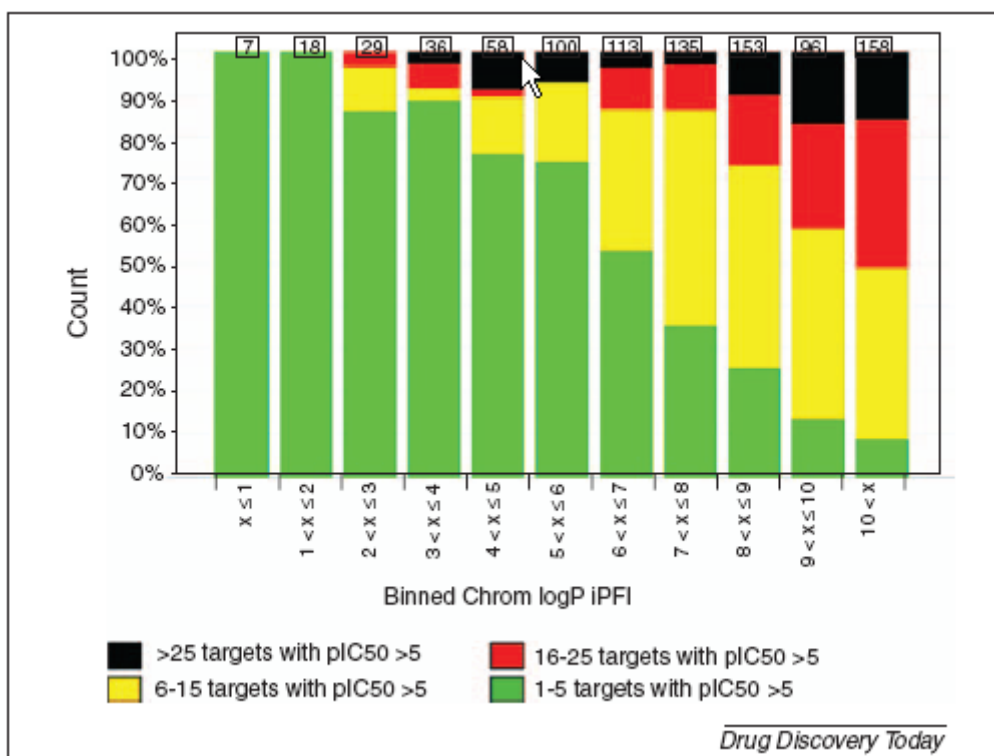
Figure 1.2: Relationship between PFI and target promiscuity. Reproduced from reference [31]

Taken together, these analyses all show compelling evidence that, in order to improve a molecule's chance of reaching market, care should be taken to design compounds with suitable physicochemical properties. There has been some criticism in the literature of the statistical techniques used to infer these correlations.[40,41] However, even these authors concede that there is a strong link between physicochemical properties and probability of success for any given candidate drug molecule. In particular, molecular size, lipophilicity and relative aromatic character are simply calculated properties that dictate much of a molecule's chance of success. In this context, it is perhaps surprising to note that during the same period of rising awareness of the importance of physicochemical properties the average logP and molecular weights of the candidate molecules advanced by major pharmaceutical companies actually increased.[42]

One potential explanation for this observation is that potency at the biological target can usually be most easily improved by increasing logP and molecular

complexity and that early lead optimisation programmes have increasingly focussed on potency optimisation.[43] However, it has been shown that marketed drugs actually display on average relatively modest potencies at their biological targets combined with optimal ADME profiles.[44] The focus on potency at the expense of other important ADME properties has possibly been driven by the fact that potency is cheap and fast to measure in a high throughput fashion compared with more complex *in vivo* experiments.

It has been shown that there is a link between the protein family of the drug target being explored and the molecular weight and lipophilicity of the molecules synthesised by medicinal chemists.[45] This implies that some proteins have intrinsically more 'drug-like' chemical requirements from ligands than others.

Another suggested cause of the increasingly poor physicochemical profiles of molecules in drug discovery programmes is the limited range of synthetic chemistry methods being utilised by medicinal chemists. It has been suggested that the use of increasing chemical automation and a focus on numbers of compounds synthesised has encouraged medicinal chemists to restrict their synthetic arsenal to a relatively small number of reactions. These tend to be reactions which are reproducible and straightforward to set up and purify, especially in organic solvents, which favour lipophilic molecules.[46] In fact, it has been shown that even when chemists target compounds with a range of lipophilicities from a chemical array, the lower logP products are the most likely to fail, leading to so-called 'logP drift' in the profile of the synthesised set of compounds.[47] These synthetic issues have consequences for both the nature of chemical libraries from which hits are derived and in lead optimisation.

It has even been shown that the organisation within which a drug discovery programme takes place can have an influence on the physicochemical properties of derived drug candidates (*figure 1 .3*).[48] This demonstrates that to a certain extent, the control of properties is within the medicinal chemists' domain, if they are sufficiently disciplined and have support from colleagues

and managers to pursue more attractive drug molecules, perhaps at the expense of time and/or cost.
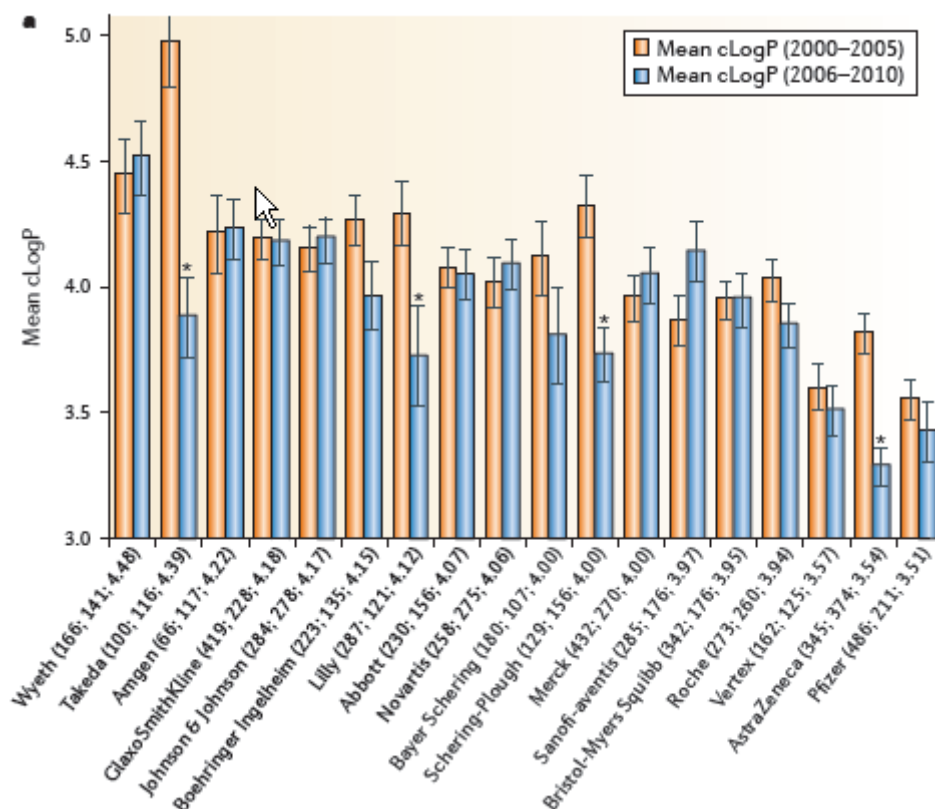

Figure 1.3: Average clogP profile for patented compounds from a range of pharmaceutical companies. Numbers in parentheses are: the number of targets for the period 2000 – 2005, the number of targets for the period 2006 – 2010, and the mean logP for the period 2000 – 2010. Reproduced with permission from reference [48]

It is clear that, although medicinal chemists may in theory understand the importance of controlling physicochemical properties, they find this difficult to do in practice whilst attempting to optimise potency at the target protein. There is, therefore, a genuine need for new methods and tools to assist medicinal chemists in this task.

1.3   Hit Discovery Techniques

One question that this thesis seeks to address is what effect, if any, does the method of identifying a hit compound have on the nature of lead and candidate molecules derived from the hit. In particular, this project will

examine three potential hit finding methodologies: high throughput screening (HTS); encoded library technology (ELT); and fragment based drug discovery (FBDD).

High Throughput Screening

High throughput screening is currently the most widely-used technique to generate chemical starting points for lead optimisation within the pharmaceutical industry.[49] The process involves testing a large library of structurally diverse compounds (of the order 10^6) in a biochemical assay to identify compounds with the desired pharmacological profile.[50] The biochemical assay is typically performed with a solution of the isolated protein of interest, although whole cell systems are becoming increasingly popular as screening technology has improved.[49] The overall success rate in generating a suitable chemical starting point for further optimisation is currently around 50 %.[49]

In order to carry out a high throughput screen it is necessary to assemble a suitable library of compounds. The compounds within the library should be as diverse from one another as possible, in order to allow the maximum probability that a ligand for the protein being screened can be found.[51] The molecules in the library should also have a suitable physicochemical property profile to allow space for optimisation.[52] Suggested suitable properties from one group were:

- number of heavy atoms 10-27,
- clogP 0-4,
- number of rotatable bonds ≤ 8,
- number of hydrogen bond donors ≤ 4,
- number of hydrogen bond acceptors ≤ 7.[53]

It is important that the compounds in the library do not contain functional groups which may lead to toxicity, such as nitro groups or alkylating agents.[54]

It is also important to remove functional groups which interfere with typical screening technologies and can generate assay false-positives, the so-called 'pan assay interference compounds' (PAINS).[55] Commercially available compounds largely fall outside the range of chemical space required by these tight restrictions. Estimates put the number of available compounds suitable for inclusion in a high throughput screening library at between 1 and 3 % of a typical vendor's catalogue.[47,52] Although it is difficult to obtain data on most pharmaceutical companies' screening libraries, it is thought that they are largely made up of proprietary compounds due to the lack of suitable commercially available compounds. When comparisons have been made between the screening libraries of different pharmaceutical companies, it has been estimated that the overlap of compounds is at most 10 %.[56] The requirements to acquire and store large numbers of compounds which are not commercially available effectively limits the ability to carry out high throughput screening to those who are able to make this investment. Recently, publically funded bodies, such as the NIH, have made screening libraries available to researchers who have no access to pharmaceutical company screening libraries in an effort to widen access to high throughput screening.[57]

As well as obtaining a compound collection for screening, it is important to develop a suitable biochemical assay to carry out the screen. The screening technology to be used is, in part, selected by the nature of the biological system being studied. It is typical to use radiolabels or fluorescence to measure activity, either by tagging the protein, its endogenous or other known ligands, or a downstream product of the biochemical process.[58] Another important consideration when choosing a biochemical system to use is the robustness of the data generated, in terms of being able to discriminate between genuinely active compounds and false positives or negatives.[59] The cost of running the screen must also be optimised; the quantity and cost of reagents used as well as the time taken to complete the screen are important considerations.[58]

There is also a significant effort required in the HTS process to interpret and validate the screening output to ensure that the hits identified are genuine. This process requires robust statistical analysis of the data generated.[59] The compound hits must be examined to ensure they are not interfering with the assay detection technology[55] or as a result of compound aggregation.[60] It should be noted that the need to separate real hits from 'noise' in the assay means that there is a lower level of activity below which genuine actives will not be detected. Smaller molecules are generally found in this low-activity space and so the hits with the most attractive physico-chemical properties are often not detected. The sample of compound tested must be analysed and often repurified or resynthesised to verify that the observed activity is due to the assigned molecular structure and not an impurity. Finally, the medicinal chemist must prioritise which hits to pursue further, based on the properties of the molecule and the level of biochemical activity.

Encoded Library Technology

Encoded library technology is a technique used to screen libraries of many millions or even billions of compounds, which are each tagged with a unique DNA sequence, which acts as a code for the structure of the screened compound.[61] The compounds are synthesised in a split and pool fashion, onto a DNA duplex. An example library synthesis is shown in *figure 1.4*. The library shown had over 802 million unique structures contained within it. As each synthetic step is carried out in the presence of DNA, the chemistry must all be amenable to aqueous conditions at ambient temperatures. The supposed strength of this methodology is in the vast number of compounds which can be screened simultaneously. However, it must be remembered that since all compounds in a given library are synthesised *via* the same route, they will share elements of their chemical structure to a certain extent.
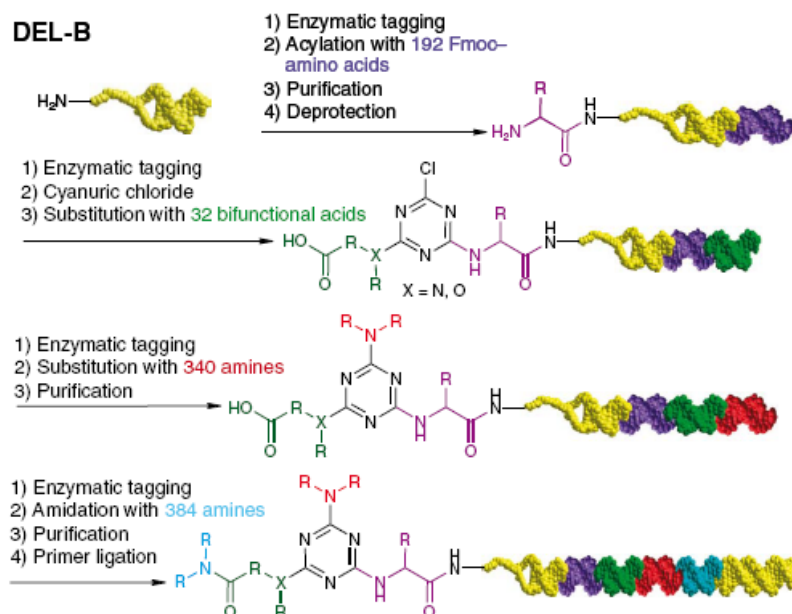
Figure 1.4: A typical ELT synthetic library synthesis. Coloured double-helix represents the DNA tags, which act as codes for the monomers added to the small molecule in each synthetic step. Reproduced with permission from reference [61]

The screening of an ELT library takes place by immobilising the protein of interest onto a solid matrix and then incubating with a solution of all members of the encoded library. The immobilised protein is then washed to remove non-binding members of the library and finally denatured, so that bound compounds are released back into solution. The DNA 'code' is then read using high throughput sequencing and the data is viewed on a 3-dimensional cube, where each 'spot' represents a compound, which was detected as binding.[62] An example data set is shown in *figure 1.5*. A line on a plot like this denotes where a particular library building block, or 'feature' as they are referred to, is present in a number of compounds that are binding. A plane represents two features are maintained across a set of binding compounds.
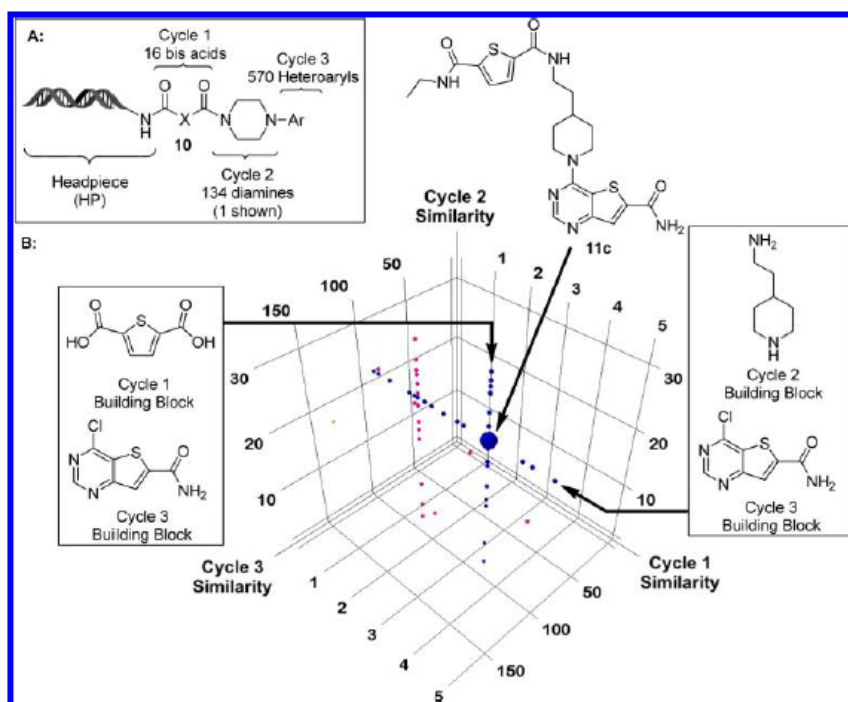
Figure 1.5: Data generated from an ELT screen against SIRT3. Reproduced with permission from reference [62]

The final step in the ELT process is to validate the hits generated by synthesising them off of DNA and screening in a biochemical assay where the protein is not immobilised. Compounds are selected for synthesis by combining the preferred features generated from the lines and planes in the cubes into exemplar molecules, as is illustrated in *figure 1.5*.[62] The binding for the compounds chosen for synthesis may not translate into activity in a biochemical assay for a number of reasons. It is possible that the DNA tag may be binding rather than the small molecule, or the DNA tag may have altered the conformation of the small molecule, so it does not adopt the same binding mode when free in solution. Equally, the compounds could be binding with the solid support used to immobilise the protein or the protein conformation could be affected by being immobilised. The compounds could be genuinely binding to the protein but at a binding site which has no functional consequence. For these reasons, it is vitally important to complete the validation step of off-DNA synthesis before considering any molecules as genuine hits.

There are a number of researchers in this emerging field who follow a broadly similar approach, using DNA coding to synthesise and screen large combinatorial libraries.[63-65]

Fragment Based Drug Discovery

One new paradigm that has recently emerged as a solution to improving physicochemical properties is fragment based drug discovery (FBDD). The theoretical basis for this approach is that by beginning the drug optimisation process with small, weakly binding, but highly efficient ligands ('fragments'), potency can be gradually built up. This allows control of the molecular properties by aiming to maintain the highly efficient interactions of the hit.

Background to FBDD and screening libraries

The theoretical premise for FBDD results from considering the relationship between molecular complexity and probability of forming a positive binding interaction. Models of protein-ligand binding predict that as the ligand molecules become smaller in size the probability of an energetically favourable binding interaction increases.[66,67] The simplest explanation for this effect is that, as ligands become more complex, the chances of an unfavourable 'clash' with the protein surface increases. This phenomenon is illustrated schematically in *figure 1.6*. This effect has been confirmed experimentally in several studies, which have shown that fragment screening hit rates are generally higher than for traditional high throughput screening.[68]

Figure 1.6: The molecular complexity argument. Fragment molecules (blue) are more likely to be accommodated by a protein binding site (green) due to their size than larger ligands (red), where the probability of an unfavourable clash is higher.

Since the number of hypothetical organic molecules that can exist increases exponentially with the number of atoms in the molecule,[69] fragment libraries

can sample chemical diversity more effectively than libraries of drug-like compounds.[70] For example, calculation of the potential number of feasible organic molecules containing 11 heavy atoms enumerated 26 million molecules.[69] A library of just 26,000 compounds, which would be practically possible to synthesise, store and screen, could sample 1 % of this chemical space. When a similar enumeration was carried out for molecules containing up to 17 heavy atoms, 166 billion potential molecules were found.[71] A similar 1 % sampling of this chemical space would require over 1.6 billion molecules, which would be prohibitive using currently available technologies. To contextualise these numbers, it is worth noting that the estimated total output of all organic synthesis to date is around 100 milliion compounds.[71] As an aside, these calculations show that the relative size of a fragment library can have a reasonable effect on the diversity of compounds held within it. However, even doubling the size of a high throughput screening collection from 1 to 2 million compounds will have virtually no effect on the proportion of available chemical space being sampled.

For these reasons, as well as practical considerations of how many compounds can reasonably be screened, a typical fragment library for screening is generally of the order of 500-10,000 compounds compared with approximately 10^6 compounds in a typical high throughput screening library. Other important criteria to consider when building a screening library for fragments are the average and maximum molecular weight and logP of the compounds, the solubility of the compounds and the purity of the compound samples. As the compounds will likely be screened from a very high concentration sample it is important that they are extremely soluble, and so have a low logP. The 'rule of three' has been proposed as a guide to the limit of molecular properties in a fragment library.[72] This suggests maximum values for a range of properties as follows:

- Molecular weight < 300 Da;
- Number of hydrogen bond donors ≤ 3;
- Number of hydrogen bond acceptors ≤ 3;
- clogP ≤ 3.

In contrast, typical HTS hits reported in the literature have an average molecular weight of 359 Da and clogP of 3.8.[72,73]

Fragment Screening

The screening techniques that are used to detect fragment hits also differ from those used in high throughput screening. Although biochemical assays such as those used for high throughput screening can be adapted to screen fragment libraries, their use is limited by the maximum concentration of organic compound and DMSO solvent that can be tolerated by the assay system.[74] This often means that the weakest binding fragments cannot be detected by biochemical methods. A more common approach for fragment screening is to use a biophysical method that directly measures the binding of the ligand to the protein. These techniques include various NMR methods, Surface Plasmon Resonance (SPR), Isothermal Titration Calorimetry (ITC), fluorescence based thermal shift (T_m) and X-ray crystallography. The techniques used in this study will be described in more detail below.

Saturation Transfer Difference by NMR (STD by NMR) is an NMR method that detects changes in the ligand ^{1}H NMR spectrum. A selection of proton signals of the methyl groups in the protein are irradiated and if a ligand is bound then the saturation is transferred to the ligand and an increase in the size of the ligand peaks is observed.[75] The STD by NMR experiment is illustrated schematically in *figure 1.7.* The advantage of using a ligand detected method rather than a protein detected method is that isotopically labelled protein is not needed and an NMR spectrum of the ligand is generated during the experiment, providing a purity and structural integrity check of the fragment sample. The size of the STD effect increases in proportion with the size of the protein, due to a slower tumbling rate in solution, so this method is not suitable for very small proteins. The experiment is typically carried out with high ligand concentrations (up to 1 mM) and low protein concentrations (usually 10-50 µM) so the amount of protein needed is relatively small. The experiment can be run in 5-10 minutes

and can be performed using pools of compounds making it suitable for use as a medium throughput screening tool. An example of the data obtained from an STD experiment run on a pool of compounds is shown in *figure 1.8*.
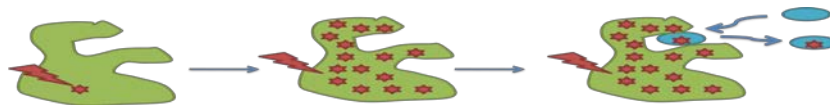

Figure 1.7: The STD by NMR experiment. Selective irradiation of a small number of protons in the protein (green) is saturated throughout the whole protein with continued irradiation (red stars). If a ligand (blue) is bound this saturation is also transferred to the ligand and is observed as an increase in the intensity of the ligand ^1H NMR peaks.

Figure 1.8: STD by NMR results for a pool of compounds screened against BCATm. Two spectra, with (blue) and without (red) protein irradiation are recorded for a mixture of fragment compounds. The difference (green) is the STD spectrum. Compounds which bind show a large green peak, while no STD green peak is observed for non-binders. Provided by Claus Spitzfaden.

Fluorescence based thermal shift screening relies on measuring the stabilising effect of a ligand binding to a protein by measuring changes to the protein's denaturation point. A fluorescent dye, which interacts preferentially with the unfolded protein, is used to observe the melting point and the midpoint of the protein unfolding transition (T_m) is measured.[76] In the presence of a ligand that binds to the protein, the complex is stabilised and

the temperature at which it unfolds is increased. The result is reported as the difference in T_m (ΔT_m) between the bound and unbound state. An example of the melting curves observed in a typical T_m experiment is shown in *figure 1.9*. Although it is conceptually appealing to consider the size of the ΔT_m measured as being proportional to the affinity of binding, in practice this is often not the case. The ligand may bind to both the folded and unfolded state of the protein or may bind to more than one site on the surface. A T_m assay requires only small amounts of protein and can be run very quickly using automated high throughput screening equipment on large numbers of samples (up to hundreds of thousands),[76] making it the highest throughput method amongst the readily available biophysical techniques.
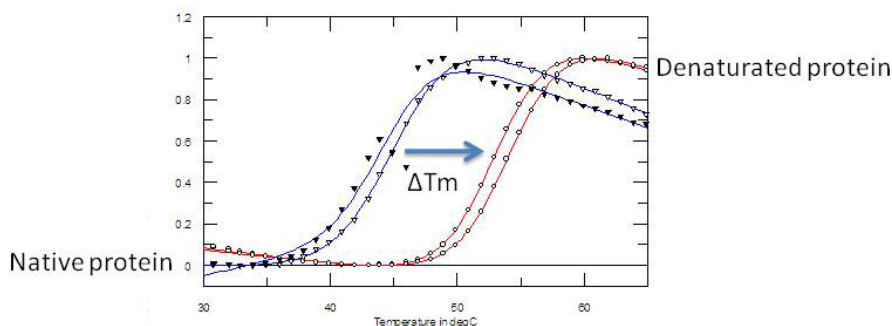
Figure 1.9: Typical data observed in a T_m experiment. Provided by Chun-Wa Chung, GSK.

Isothermal titration calorimetry (ITC) is a technique that directly measures the heat that is absorbed or produced upon titrating a ligand into a protein solution, i.e. the enthalpy of binding.[77] By repeating this experiment at varying concentrations of the ligand, a dissociation constant for binding, K_d can be determined from which the Gibbs free energy of binding can be derived. This technique can be used to determine the binding constant, stoichiometry, enthalpy and entropy of binding. As the ITC experiment makes a direct measurement of the binding process and has no added probes, it provides a uniquely detailed and precise insight into the ligand-protein interaction. However, each complete calorimetric titration typically requires a few hundred μg of protein and so this technique is impractical for use as a

primary screening method and is more often used as a hit confirmation method.[76] An example of ITC data is shown in *figure 1.10.*
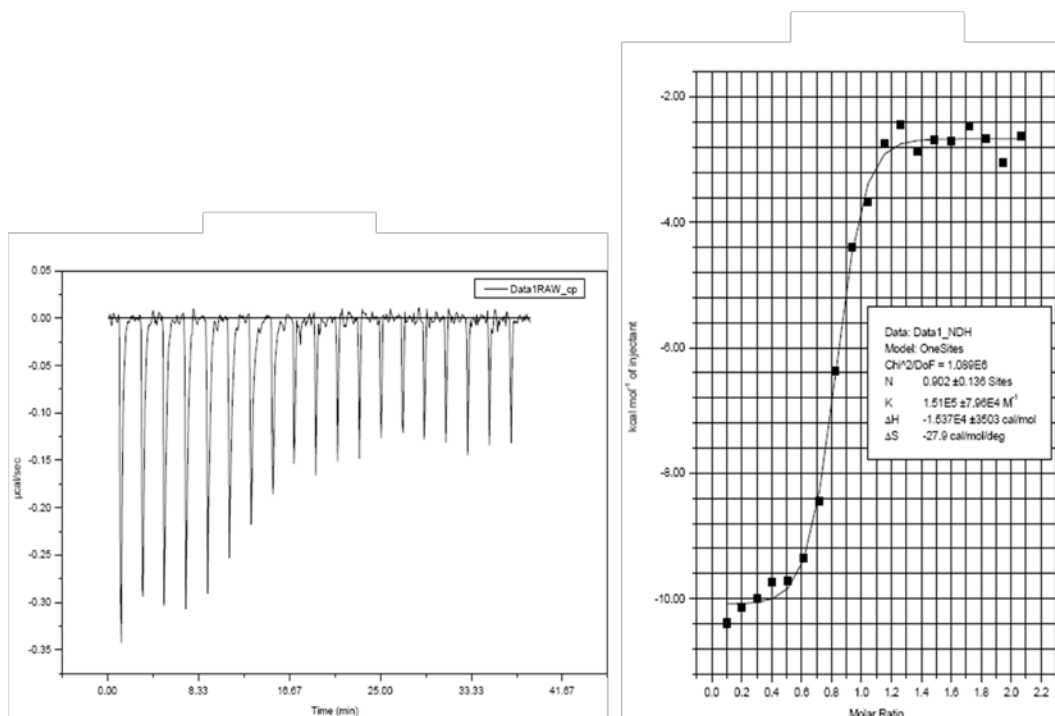

Figure 1.10: Experimentally determined ITC curves: Left – titration curve of heat change of solution upon titrating ligand into protein; Right – derived dose-response curve. Provided by Peter Francis, GSK.

Following identification of fragment hits by a biophysical method, their activity is often confirmed in a high-concentration biochemical assay and their binding modes are determined using X-ray crystallography. Once all of this information has been collected, the chemical optimisation phase of the FBDD process can begin.

Fragment Optimisation and Ligand Efficiency Measures

The chemical optimisation of fragment hits into lead-like molecules was initially assumed by medicinal chemists to be extremely challenging as the binding potency needed to be increased from the mM to the nM range. Previous experience in optimising high throughput screening derived hits had shown that increasing potency from the μM range to the nM range often required for a candidate could frequently require intense investigation by

large teams of chemists over many months. It was predicted that this situation would be even more difficult for weakly active fragment hits. In fact, this has not proven to be the case. Fragment specialist companies such as Astex Therapeutics claim to have been able to derive nM potency leads from fragment hits in only 20-100 molecules in some cases.[78] There are three main reasons for this apparent success in optimisation. The first is the fact that fragment hits are inherently easier to optimise as they do not generally contain structural features that are not contributing to the binding, as is often observed with high throughput screening hits. A schematic representation of this concept is shown in *figure 1.11*. The second contributor to success is the use of structure based drug design to optimise hits and the third is the focus on efficiency of binding during the optimisation process.

Figure 1.11: Fragments screening versus HTS screening. The fragment hits (blue) although weak have very specific and efficient interactions with the protein. HTS hits (red) contain structural elements that are not contributing to binding or display non-ideal binding, but which may be difficult to remove.

The intensive use of X-ray crystallography and structure based design in fragment optimisation has become a standard component of the FBDD methodology for most practitioners. A recent analysis shows that the chances of deriving a potent (<100 nM) lead from a fragment hit increases from 33% to 93% when structure-based design is used.[79] There are three main approaches to using structure based design to optimise fragment hits, which are illustrated schematically in *figure 1.12*. The first and most common is to use fragment growing or evolution, which aims to design larger molecules that have additional interactions with the protein.[80] This relies on the fragment maintaining a constant binding site during evolution. The second approach is fragment linking, in which two fragment hits identified in different pockets are linked together to provide a more potent lead. Intuitively this

would seem to be a sensible approach and there are some successful examples of this in the literature.[81,82] However, in practice it can be extremely difficult to design a linking group between the two fragments that does not disrupt the binding of at least one of them. The third approach is fragment merging, which is a hybrid of the first two approaches.[83] The fragment hit is optimised by aiming to add the interactions with the protein observed in other fragment hit structures. Importantly, this is achieved by designing new molecules that are calculated to have optimised binding rather than trying to simply link the two fragment structures.
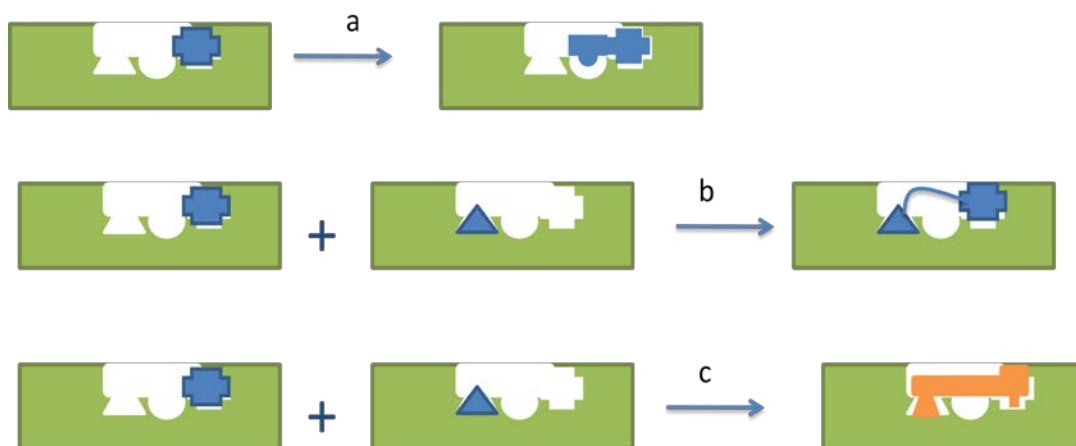
Figure 1.12: Approaches to fragment optimisation: (a) fragment growing; (b) fragment linking; (c) fragment merging.

Ligand efficiency measures are another important feature of the fragment optimisation process, which allow researchers to ensure that the changes they make to their fragment hits are constructive in terms of building towards leads with high potency and favourable physicochemical profiles. The ligand efficiency is defined as a measure of the binding energy per non-hydrogen (heavy) atom and the formula used to calculate it is shown in *equation 1.3.*[84]

$$LE = \frac{\Delta G}{HAC} = -\frac{RTln\text{K}_d}{HAC} \approx \frac{(1.36 \times pKi \text{ or } pIC_{50})}{HAC}$$

[Equation 1.3: LE = ligand efficiency; ΔG = Gibbs free energy of binding; R = the gas constant; T = temperature in Kelvin; K_d = dissociation constant; pK_i = -log(inhibitor constant); pIC_{50} = -log(conc. of inhibitor that gives 50% inhibition); HAC = heavy atom count.]

For a typical candidate molecule with a molecular weight of 500 (approximately 38 heavy atoms) and a potency of 10 nM the ligand efficiency would equal 0.3. Therefore, fragment hits with a ligand efficiency equal to or greater than 0.3 are more favoured for optimisation and a major aim in the optimisation process is to maintain the ligand efficiency above this value. An alternative to the ligand efficiency measure is the binding efficiency index (BEI) defined as shown in *equation 1.4.*[85]

$$BEI = \frac{pKi \text{ or } pIC_{50}}{MW \text{ in kDa}} \qquad \textit{[Equation 1.4: MW = molecular weight]}$$

The BEI can be easily distorted by the presence of very heavy atoms such as halogens. For this reason, the ligand efficiency measures as calculated in equation 1.3 will be used throughout this report.

As well as monitoring the size of drug molecules it is important to monitor and optimise their lipophilicity. The lipophilic ligand efficiency (LLE) has therefore been introduced as an important measure to guide optimisation.[86] LLE is calculated by the formula given in *equation 1.5*.

$$LLE = pIC_{50} \text{ or } pKi - clogP \qquad \textit{[Equation 1.5]}$$

For a molecule with 10 nM potency and a clogP of 3 the LLE is 5 therefore a useful guide is that a drug molecule should ideally have an LLE value above 5. Although this is a useful metric for evaluating leads and candidates, it is less useful for evaluating fragments. Fragments generally have very low potency, which requires them to have negative clogP values to maintain an LLE above 5. As a consequence of this, researchers at Astex therapeutics have introduced the Astex LLE (LLE_{AT}),[87] which is corrected for the number

of heavy atoms, as for the ligand efficiency measure. The Astex LLE also contains a scaling factor so that ideal compounds also have an LLE_{AT} above 0.3, which eases comparison with LE. The definition of LLE_{AT} is given in *equation 1.6.*

$$LLE_{AT} = 0.111 + \frac{[1.36(pIC_{50} \text{ or } pKi - cLogP)]}{HAC}$$ *[Equation 1.6]*

The Astex LLE measurement will be the preferred LLE figure used throughout this report.

Another suggested measurement for lipophilic ligand efficiency is the ligand efficiency logP (LELP, equation 1.7).[73] The claimed advantages for this method are similar to those for the Astex LLE, in that it combines ligand efficiency and logP in a single measure. The authors suggest that an LELP value of between 0 and 7.5 is ideal and that during optimisation, the LELP should move towards 0 as the potency increases.

$$LELP = \frac{logP}{LE}$$ *[Equation 1.7]*

Applications of FBDD

Although FBDD has only existed as a cohesive methodology for the last decade, it has been enthusiastically adopted by several biotechnology and pharmaceutical companies with impressive results. A number of reviews have been published,[88-90] which describe a large number of successful lead optimisation campaigns against a range of biological targets including kinases, proteases, nuclear receptors and phosphatases. At least 13 clinical candidates derived from FBDD starting points have been described.[89]

As the results of FBDD begin to reach fruition in the clinic, the molecules found by this technique can be compared to other molecules acting against the same targets to determine if fragment-derived compounds offer any advantage in terms of physicochemical properties. An example analysis is shown in *figure 1.13* for the dual PPAR agonist class of drugs. The fragment-derived clinical candidate Indeglitazar **1.2**, along with the fragment hit **1.1**

from which it was optimised are shown.[91] The molecular weight, clogP and calculated PFI of **1.2** are significantly lower than other clinical candidates in this class, Aleglitazar[92] **1.3** and Muraglitazar[93] **1.4**. The same is true when comparing **1.2** to the only marketed drug in this class Saroglitazar **1.5**.[94] Compounds **1.3, 1.4** and **1.5** were all identified using a knowledge based approach incorporating features of known PPAR ligands.
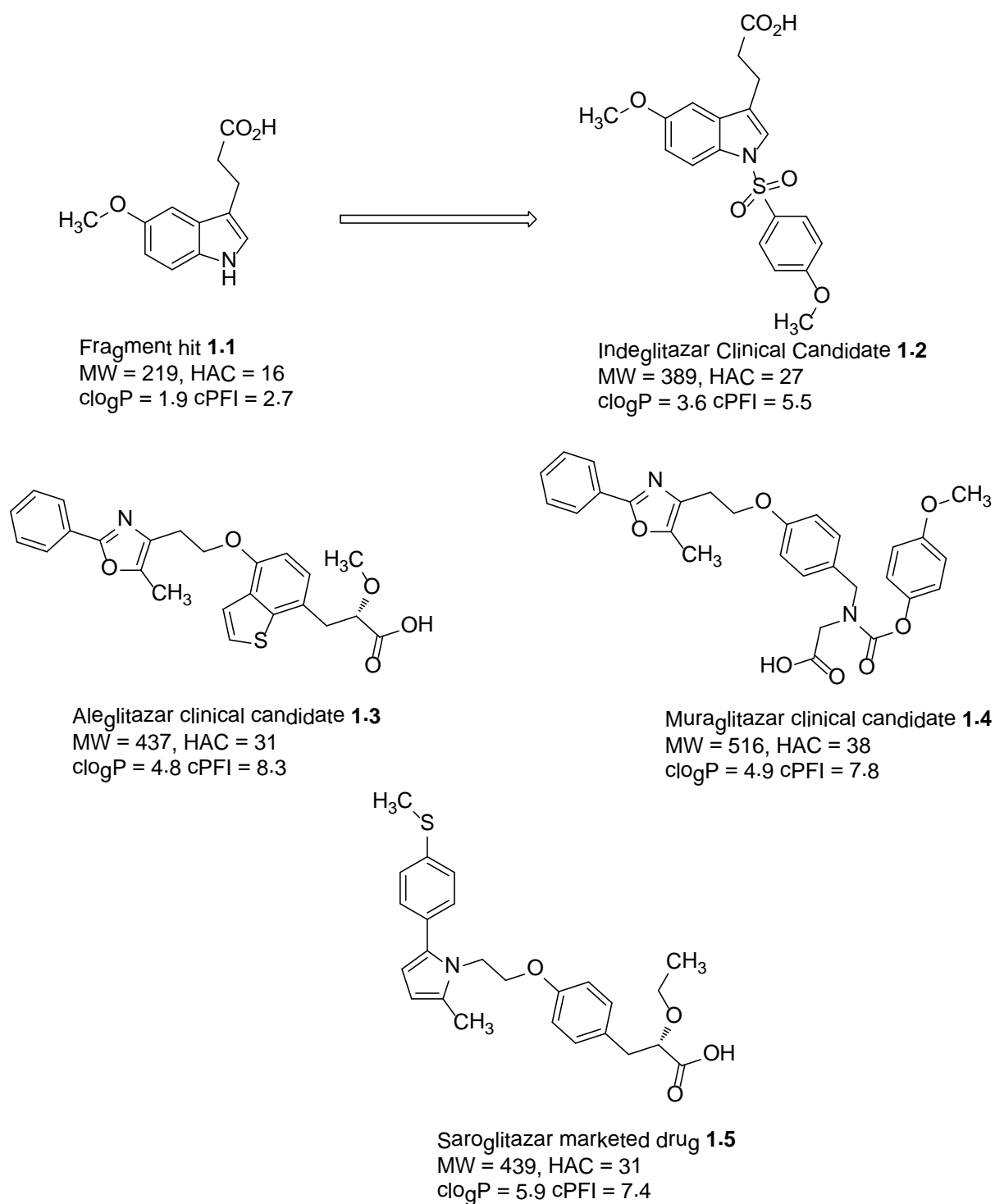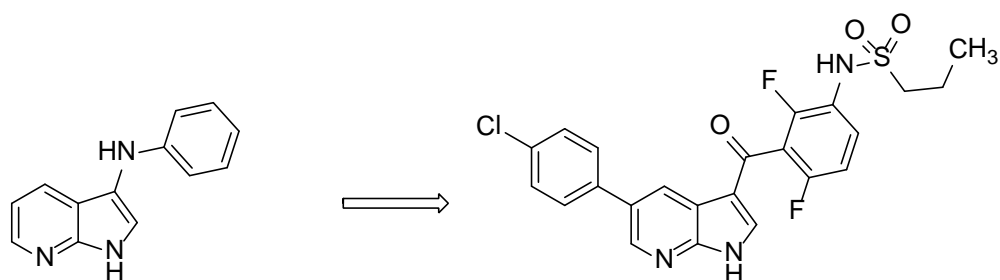
Fragment hit **1.1**
MW = 219, HAC = 16
clogP = 1.9 cPFI = 2.7

Indeglitazar Clinical Candidate **1.2**
MW = 389, HAC = 27
clogP = 3.6 cPFI = 5.5

Aleglitazar clinical candidate **1.3**
MW = 437, HAC = 31
clogP = 4.8 cPFI = 8.3

Muraglitazar clinical candidate **1.4**
MW = 516, HAC = 38
clogP = 4.9 cPFI = 7.8

Saroglitazar marketed drug **1.5**
MW = 439, HAC = 31
clogP = 5.9 cPFI = 7.4

Figure 1.13: Comparison of dual PPAR agonists

In 2011, the FDA approved Vemurafenib **1.7** (*figure 1.14*), a B-Raf inhibitor for treatment of melanoma, which is the first marketed drug discovered by an FBDD approach.[95] The physicochemical properties of this molecule are

largely similar to those of the one other marketed B-Raf inhibitor, Dabrapenif **1.8**, which was derived from a hit discovered by screening of a targeted kinase library of compounds.[96] These data illustrate that following an FBDD approach will not in itself be a panacea for all of the difficulties in medicinal chemistry. It is still important for medicinal chemists to use a disciplined approach in lead optimisation to derive final compounds with good properties. The question of whether the method of identifying hits has a significant effect on the properties of derived molecules will be examined in more detail as one of the main areas of study in this project.

Fragment hit **1.6**
MW = 209, HAC = 16
clogP = 3.2 cPFI = 6.8

Vemurafanib marketed drug **1.7**
MW = 490, HAC = 33
clogP = 4.1 cPFI = 9.4
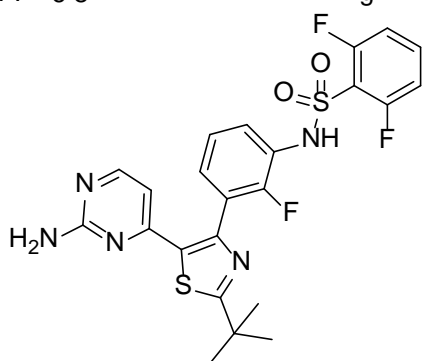
Dabrafenib marketed drug **1.8**
MW = 519, HAC = 35
clogP = 4.6 cPFI = 9.2

Figure 1.14: Comparison of B-Raf Inhibitors

1.4   Molecular Recognition

As discussed above, an essential component of the chemical optimisation of fragment hits is the use of structure-based design to improve affinity of the ligands at the target of interest. In order to do this successfully, it is important to have a good understanding of the factors that influence the energetics of ligand-protein interactions. This is a theoretical problem that has been addressed in the scientific literature for over a hundred years.[97] However, although the individual components of binding can be rationalised and, in some cases, measured experimentally, it is still impossible to predict even within several orders of magnitude the likely free energy of binding for a hypothetical drug-target interaction.[98] This implies that there is still much that remains to be understood. The following section provides a review of what is known about the different contributions to free energy of binding and highlights some of the caveats that need to be considered when attempting to apply this knowledge in a predictive sense.

Models of Molecular Recognition

One of the earliest attempts to rationalise non-covalent molecular recognition was by Fischer who proposed the 'lock and key' model.[99] This model considers the ligand and protein as rigid bodies, which, if they have complementary shape and polarity, fit together as a key fits into a lock. Although this model has some intuitive value it is a drastic over-simplification of the dynamic effects present in a solution equilibrium process.

This model was further refined to the more realistic 'induced-fit' model.[100] In this model, the ligand and the protein undergo conformational adjustments on binding, to allow the most energetically favourable complex to be formed. This model is sometimes described as the 'hand in glove' model, which is a useful analogy of both partners adjusting their shape to accommodate binding. In some cases, the ligand can cause large structural changes in the protein, opening up previously unobserved induced binding pockets. A good

example of this is the 'DFG loop', which is observed in two conformations – 'in' or 'out' for several kinases.[101]

An alternative to the induced fit model is the 'selected fit' model[102] where the ligand selects and stabilises a conformation of the protein from several that exist in equilibrium in solution. The induced fit and selected fit models can both be useful and each may be considered more or less relevant dependent on the individual circumstances of the binding event being considered. A summary of the different models of binding is shown in *figure 1.15*.
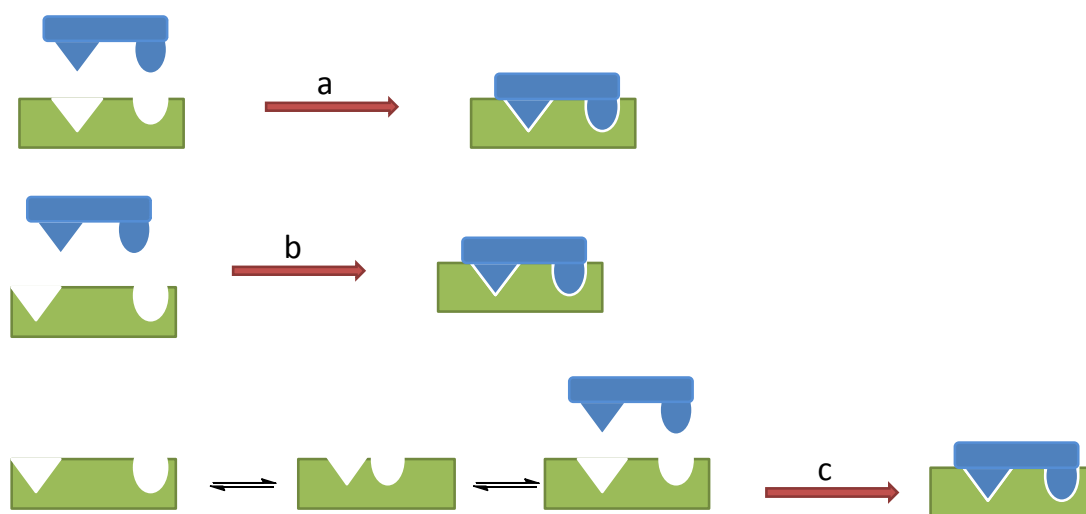
Figure 1.15: Models of molecular recognition: (a) Lock and Key – the protein and ligand are considered as rigid bodies that bind when they have good shape and polar complementarity; (b) Induced Fit – the protein and/or ligand must adjust its conformation to allow binding; (c) Selected Fit – the ligand selects one of a number of conformations present in equilibrium.

Energetics of Binding

The Gibbs free energy of binding (ΔG) between a protein and drug molecule is related to the experimentally determined binding constant, K_d as given in *equation 1.8*, where R is the molar gas constant and T is the temperature in Kelvin.

$$\Delta G = -RT ln K_d \qquad [Equation\ 1.8]$$

The Gibbs free energy is composed of the enthalpic (ΔH) and entropic (ΔS) terms as related in *equation 1.9*.

$$\Delta G \; = \; \Delta H - T \Delta S \qquad [Equation\ 1.9]$$

Since the enthalpy of binding can be measured experimentally (e.g. by ITC) it is possible to partition the measured binding energy into its constituent enthalpic and entropic terms. However, these experimentally derived values cannot themselves describe which particular favourable or unfavourable interactions between the protein, ligand and solvent are responsible for the measured binding. Partitioning of the different contributions to binding is given in *equation 1.10*.[103]

$$\Delta G = \Delta G_{trans+rot} + \Delta G_{conform} + \Delta G_{polar} + \Delta G_{hydrophobic} + \Delta G_{vdW}$$

[*Equation 1.10*]

In this equation:

- $\Delta G_{trans+rot}$ denotes the energetic difference between the translational and rotational degrees of freedom for the ligand and protein compared with the complex;

- $\Delta G_{conform}$ accounts for the difference in conformational energy upon binding;

- ΔG_{polar} is the contribution made to binding by polar interactions;

- $\Delta G_{hydrophobic}$ is the contribution from the hydrophobic effect;

- ΔG_{vdW} is the difference in energy due to van der Waals' effects. Each of these contributions to binding is discussed in further detail below.

Translational and Rotational Energy

The change in translational and rotational free energy upon ligand binding is an entirely entropic change and is always an unfavourable contribution to ΔG. The ligand and protein in solution each have three degrees of rotational freedom and three degrees of translational freedom (x,y and z axes) giving a total of twelve degrees of freedom. Upon complexation this is reduced to just six.[103] The size of this energetic cost has been calculated to be in the region of 50-70 kJmol^{-1}.[104]

Conformational Energy

Similarly to the translational and rotational free energetic cost of binding, there is an unfavourable entropically driven cost due to the reduction in the number of conformations of ligand and protein available after binding.[105] When the ligand and protein are in solution they are able to move freely between energetically similar conformations. However, a binding event typically involves 'freezing out' of a single particular conformation of each partner, which can accommodate binding.

This phenomenon could be exploited in structure based design.[106] If the preferred conformation of a ligand when bound is known, then pre-organisation of the ligand in a rigid arrangement should reduce the entropic cost of freezing out the bioactive conformation and so decrease the free energy of binding. In practice, it is often difficult to achieve the desired increase in affinity by rigidifying ligands. This could be due to the requirements for the geometry of the compound to be exactly complementary to the protein if no ligand motion is possible.

An example of attempted pre-organisation is the formation of a cyclopropyl group to phosphotyrosine groups in peptide ligands.[107] Importantly, no heavy atoms are added or removed when making this change so the two molecules have the minimum additional alterations in addition to the conformational restraint. The Src SH2 ligand **1.9** was modified to produce the more rigid ligand **1.10** (*figure 1.16*), which was expected to have improved binding as a result of lower entropic cost of conformational restriction. ITC confirmed this entropy hypothesis. However, the binding constants of **1.9** and **1.10** were approximately equal as the enthalpy of binding of **1.10** decreased. A similar experiment was carried out for the Grb SH2 binding ligands **1.11** and **1.12**. In this case **1.12** was found to have a higher binding affinity than **1.11**. However, the ITC experiment showed that the entropic barrier to binding had actually increased for **1.12** and that its improved binding was enthalpically driven. Examination of the various ligand protein crystal structures in these experiments failed to provide an explanation for the observed effects. This

example highlights the limitations of using structure based design for optimisation. It is actually extremely difficult to modify a ligand so that its binding will only differ by one enthalpic or entropic interaction. It is very possible that the binding will improve as a result of the modification, but it is important to remember that the source of the improved binding may not be that which was hypothesised in the compound design.
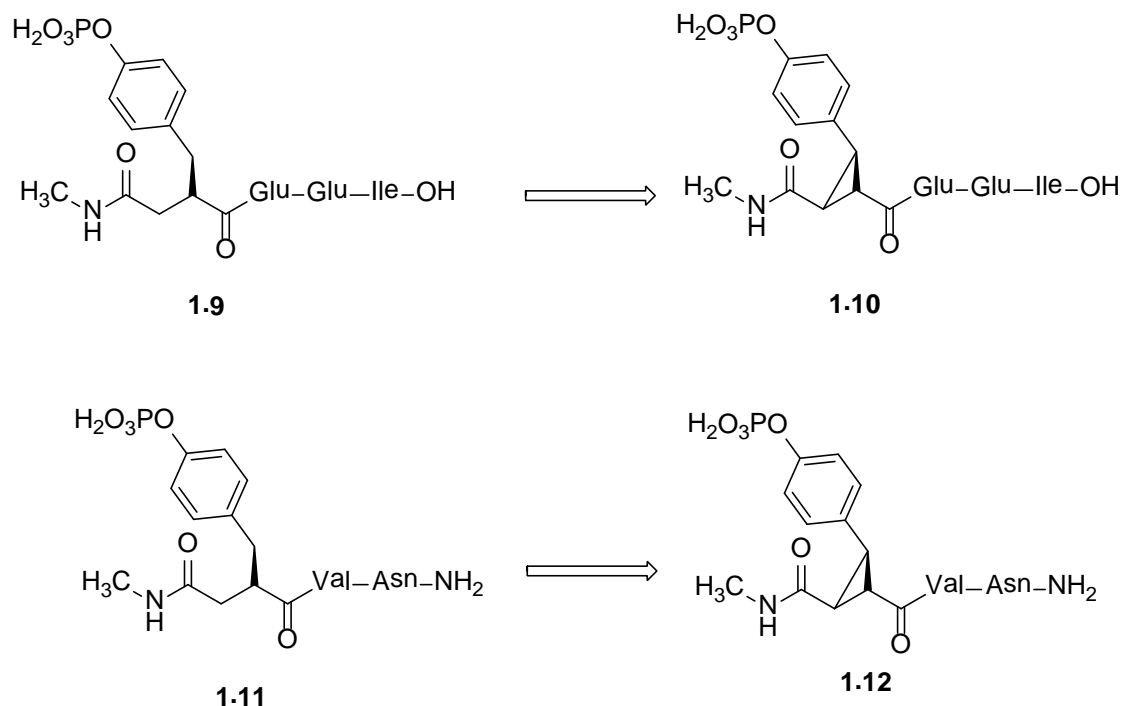

Figure 1.16: Peptide ligands tested as models of conformational restriction

Taken together the terms of $\Delta G_{trans + rot}$ and $\Delta G_{conform}$ account for the majority of the entropic cost of binding a ligand and a protein. This overall cost is relatively similar across most systems. Overcoming this barrier to binding with fragment molecules could account for the fact that it is then relatively easy to increase the potency by many orders of magnitude.[108] An example of this is of a fragment with a measured binding affinity of 100 µM (-22.8 kJ/mol), which has to overcome a total entropic barrier to binding of 20 kJ/mol. This fragment is actually contributing -42.8 kJ/mol of favourable interactions to the overall binding energy. When the fragment is optimised to a larger, more potent molecule of 3 nM potency (-48.6 kJ/mol) to a good approximation the barrier to binding will be the same as for the fragment (see

figure 1.17). This means the optimised compound forms -68.6 kJ/mol of productive interactions. The original fragment hit contained the majority of the positive interactions despite the 33,000 times lower binding affinity. This analysis also helps to explain the frequently observed result that the structure of a fragment hit varies very little during optimisation.
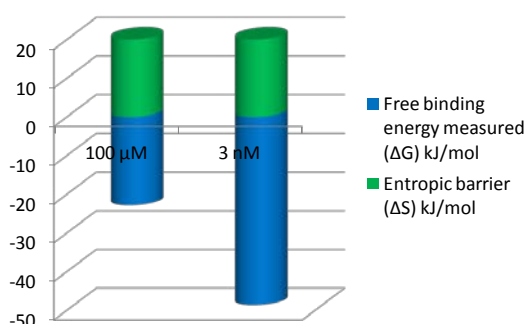
Figure 1.17: Free energy differences between fragment hit (100 µM) and optimised lead (3 nM) showing fragment hit already contains majority of positive interactions required.

Polar Interactions

The polar interactions between a ligand and protein are the easiest to rationalise by X-ray crystallography and so are frequently afforded the most attention in structure based design. The polar interactions are largely enthalpic in character and generally provide a positive contribution to the binding energy.

Of the polar interactions, hydrogen bonds are the most important specific interactions in biological recognition. A hydrogen bond is defined as the non-covalent interaction between a donor, which is a polarised X-H bond (e.g. OH, NH, SH) and an acceptor, which is an electronegative atom (e.g. F, O, N).[97] Studies of large numbers of crystal structures in the Cambridge Structural Database (CSD) and the Protein Data Bank (PDB) have defined that hydrogen bonds display very particular lengths and geometries.[109] For instance the median distance between an amide C=O and an OH is 2.75 Å, whilst an NH donor has a median distance of 2.9 Å, suggesting that OH is a

stronger donor than NH. Charged interactions are typically stronger than neutral ones. The median distance between a carboxylate and ammonium is 2.79 Å, increasing to 2.83 Å for a neutral amine and 2.9 Å for the distance between a neutral carboxyl group and an amine. The preferred angle for a hydrogen bond interaction C=O····H is 120°. Due to the precise distance and geometric requirements of hydrogen bonds, their presence can help to make the binding of a ligand specific for a single protein. The pK_{BHX} database[110] contains a measured scale of the relative hydrogen-bonding acceptor strengths of various functional groups that can be useful in drug design.

An analysis of the relationship between the number of hydrogen bonding interactions and the binding affinity has been carried out for a set of 80 protein-ligand complexes.[111] The binding affinities were found to increase by roughly one order of magnitude per hydrogen bond, but this was only a general trend and there was a large variance in the data. This analysis suggests that, although forming hydrogen bonds can be favourable for drug-target interactions, it cannot always be expected to give a positive increase in binding affinity. This can be explained by considering the total number of hydrogen bonds present in the equilibrium process. If the drug and protein molecule are both forming strong hydrogen bonds to water then there will be no enthalpic benefit to replacing these with newly formed hydrogen bonds in the ligand-protein complex.[112]

An example of this effect is the binding of ligands containing phosphonamides, phosphonates and phosphinates to thermolysin (*figure 1.18*).[113] The NH linker has a hydrogen bond to water in solution and to a backbone carbonyl in complex with the protein. Therefore there is no change in the overall number of hydrogen bonds upon ligand binding so the energetic contribution of the hydrogen bond is close to zero. This is evidenced by the fact that replacement of NH by CH_2 generally has little influence on the binding affinity. However, when the NH is replaced by an O linker there is a very large increase in K_i. The oxygen atom will have its hydrogen bonding potential fully satisfied in aqueous solution but cannot form a hydrogen bond

upon ligand binding. In fact, not only is a hydrogen bond removed but there is also an unfavourable clash between the lone pairs on the ligand O and the backbone carbonyl.
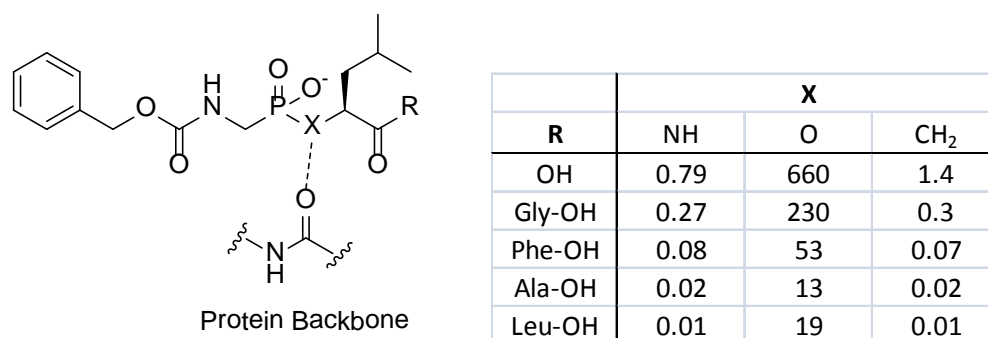

R	X		
	NH	O	CH$_2$
OH	0.79	660	1.4
Gly-OH	0.27	230	0.3
Phe-OH	0.08	53	0.07
Ala-OH	0.02	13	0.02
Leu-OH	0.01	19	0.01

Figure 1.18: Thermolysin Inhibitors tested with Ki values (µM)

Further studies on the energetics of hydrogen bonding have been carried out by site directed mutagenesis (SDM) to tyrosine tRNA synthase.[114] The residues that contained hydrogen bond acceptors known from crystallography to be important to substrate binding (Asp-78, Tyr-169, Gln-173) were deleted. An estimated value of the contribution of a neutral hydrogen bond was calculated to be equivalent to a relatively modest increase of 2 to 15-fold in binding affinity.

Halogen bonding is an observed polar interaction that has many similarities to hydrogen bonding. The heavier halogens, chlorine, bromine and iodine exhibit polarisation along their C-X bond resulting in an 'electropositive crown' opposite the bond at the tip of the halogen atom.[115] This allows the halogen to act as a Lewis acid and interact with Lewis bases such as oxygen, nitrogen, sulphur and aromatic rings. A review of published crystal structures of protein kinase inhibitors suggests that halogen bonds are an important and frequently observed interaction in drug-protein interactions.[116] The strengths of the halogen bonds increases with the size of the halogen and can also be affected by the electronegativity of the other substituents on the C-X carbon.[109]

The π-electron cloud of aromatic rings can interact with cations, such as ammonium[117] or with other aromatic rings or hydrogen bond donors[109,118] and produce productive binding. When two aromatic rings interact, the geometric requirements are very precise. *Ab initio* calculations of the benzene dimer suggest two almost isoenergetic conformations, the T-shaped (edge-to face) or parallel (off-stacked) interactions (*figure 1.19*).[119] Both of these geometries have been frequently observed in protein-ligand structures. The strengths of π-π interactions can be increased by making the 'acceptor' more electron rich or by making the 'donor' ring in T-shaped interactions more electron poor.[109]
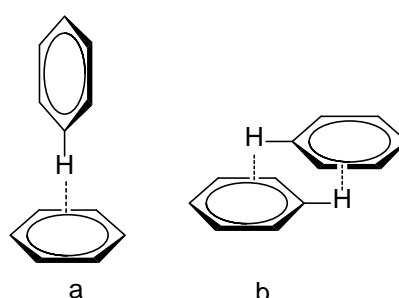
Figure 1.19: π-π interactions in benzene: (a) T-shaped; (b) off-stacked

The relative strengths of the different polar interactions are indicated by their average bond lengths, as given in *table 1.1.*[109]

Type of Interaction	Average bond length (Å)	
Hydrogen bond	2.5 - 3.0	
Halogen bond	3.0 - 3.5	Increasing bond strength ↑
π-π	3.4 -3.8	
Cation-π	3.4 - 4.0	

Table 1.1: Relative bond lengths of different polar interactions

The Hydrophobic Effect and Displacing Water Molecules

The hydrophobic effect describes the often large positive contribution to binding that can be achieved by burying non-polar surface area.[120] The effect arises from the fact that when a non-polar ligand and protein are solvated in water the water molecules immediately surrounding the solutes are more

ordered than bulk water. When the ligand and protein associate, the solvating water is liberated to bulk, which gives an increase in entropy resulting in a favourable free energy change (*figure 1.20*). There is also an enthalpic benefit as the solvent water molecules are unable to form hydrogen bonds to the non-polar regions of the ligand and protein but can fully satisfy their hydrogen-bonding potential in bulk water. Oil-water partitioning experiments have been used to quantify the hydrophobic effect, which estimate that burying a methyl group should give a 3.5-fold increase in binding affinity.[109]
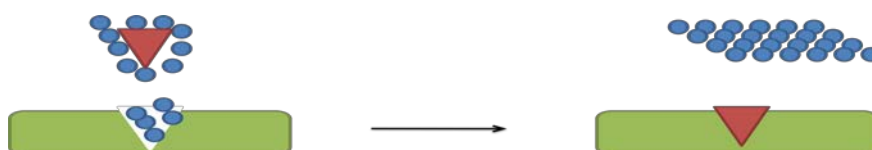
Figure 1.20: The Hydrophobic Effect – returning solvent molecules to bulk solvent upon ligand binding is enthalpically and entropically favourable

A related question to address is the energetic cost or benefit of replacing a water molecule, which is consistently observed at the same position in the protein active site by x-ray crystallography, with a ligand. The issue of whether displacing a water molecule with a ligand is energetically favourable is complex and has received much attention in the literature.[121] In each case, the energetic outcome for binding of a ligand at the expense of water will depend on the nature of the water molecule's binding site. This could be, for instance, due to the number of hydrogen bonding interactions with the protein and whether the water is in a protein groove or close to bulk solvent. The outcome will also depend on the usual energetic considerations for ligand binding, such as desolvation of the ligand, enthalpic contribution based on the new hydrogen bonds formed and entropic cost of adopting a single conformation of ligand and protein. As such, there are currently no reliable methods for estimating how favourable displacing the water molecule in each case is, although there is a wealth of anecdotal evidence in the literature describing cases where displacing a conserved water molecule results in increased binding,[122,123] or conversely in decreased binding.[124] This is an emerging area of research, and some researchers have begun to publish

methods based on molecular mechanics simulations to predict the energies of bound water molecules.[125] To date, these methods have demonstrated potential in explaining existing SAR.[126-128] The future challenge for these methods is demonstrating predictive use in a design setting.

Van der Waals' Interactions

The final term to be considered from equation 1.10 is the contribution of van der Waals' interactions to the binding energy. This term accounts for the favourable interactions that are formed by having optimal van der Waals' distances between the ligand and protein molecules and can be considered as the term that accounts for 'shape complementarity'.[103] In a systematic study of the effect of van der Waals' binding on a set of related protease inhibitors, it was found that there was a linear correlation between the Gibbs binding energy and the van der Waals' radii of different atoms which were added.[129] It was determined that each atom could contribute up to 2 kcal mol^{-1} (a smaller contribution to binding than for adding a new hydrogen bonding interaction), which resulted in an approximately 2-fold improvement in affinity.[129]

The relationship between the K_d and the lipophilic contact area between ligand and protein for 80 complexes has been analysed.[111] These data showed a general trend for an increased binding affinity with increasing lipophilic contact area but with a large spread in the data. The contribution to binding from the lipophilic contact area can be considered as a combination of the hydrophobic effect and the van der Waals' interactions.

The terms ΔG_{polar}, $\Delta G_{hydrophobic}$ and ΔG_{vdW} together represent the terms in the binding relationship that can be modified to modulate the overall binding affinity in drug discovery.

Enthalpy and Entropy in Binding

It has been frequently observed in ligand-protein complexes that when changes are made to the ligand structure the overall binding energy may not

change by much. By using ITC experiments it has been shown that the enthalpy of binding does change by a large amount but that this is offset by an approximately equal and opposite change in the entropy.[130] This phenomenon has been termed enthalpy-entropy compensation. It can be understood intuitively by considering the induced-fit model of binding. As the enthalpy of binding becomes more favourable, the complex is held together more tightly so the entropy loss is greater. Although this effect is often observed, it is not ubiquitous, as it is possible in many cases to optimise binding affinities. Currently, prediction of whether or not enthalpy-entropy compensation will dominate a particular system is not possible and this phenomenon is generally poorly understood.

An emerging area of research is the analysis of the evolution of marketed drugs over time against a particular target class.[131] Drugs launched later must by definition be superior to their predecessors in some way to achieve approval. ITC analyses suggest that the drugs that are launched later tend to have more enthalpically driven binding than earlier drugs in the same class. An example analysis is shown in *figure 1.21* for the HIV-1 protease inhibitors. There is a trend over time to enthalpically stronger binding as the drugs become more potent, selective and less prone to develop resistance problems.
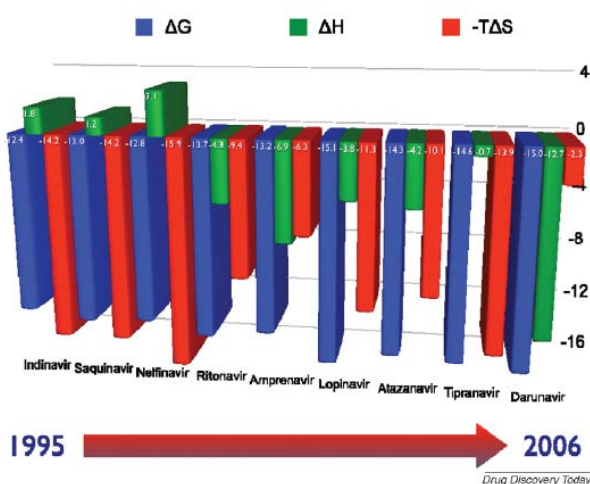
Figure 1.21: Thermodynamic binding profiles of HIV-1 protease inhibitors. Reproduced with permission from reference [131]

The current hypothesis is that more enthalpic binding will be driven by polar interactions rather than the hydrophobic effect or van der Waals' interactions so the drug molecules will be more polar and have lower logP values.[132] It has been suggested that drug researchers should aim to optimise enthalpic binding but this could often be very difficult to achieve in practice, due to enthalpy entropy compensation. This is an area of research that is likely to become more prominent over the coming years.

Molecular Modelling

The overall aim of molecular modelling is to be able to predict the binding mode and affinity between a given ligand and protein. Most packages currently in use treat the protein as a rigid body using an X-ray crystal derived structure and allow the ligand to be flexible to find a low energy docking pose.[133] This is a pragmatic approach based on the impractically large computational power that would be required to allow flexibility in both ligand and protein. In practice, this approach has some utility in predicting binding poses of compounds that are structurally related to ligands with known binding modes, or in screening out proposed compounds that are very unlikely to be accommodated in the site.[98] However, techniques currently in use are generally not able to predict binding energies or even to provide meaningful rank ordering of compounds that are predicted to display positive binding.[98]

In this project, docking has been used with these limitations in mind. The general approach used was to modify the structure of a known ligand for which an experimentally derived structure was known, minimise the proposed structure in the site, and then examine the proposed binding mode by eye, to determine if there were additional positive interactions with the protein or obvious steric or electronic clashes. This approach was carried out as a collaboration between a molecular modeller and medicinal chemist and was used to prioritise proposed structures for synthesis. Although a relatively conservative methodology was used, there are still risks that the binding mode may not be appropriately predicted. It has often been observed that

making relatively small changes to a ligand can sometimes completely alter its binding mode and this is especially true of small, weakly binding fragment molecules.[134]

Another molecular modelling methodology that has been used in this project is the GRID software available from Molecular Discovery Ltd. This experiment involves minimising a number of small molecular 'probes' such as methyl, amine nitrogen, carbonyl oxygen or hydroxyl within the binding pockets to identify areas where these may make productive interactions.[135] This experiment is useful in generating spaces to computationally grow existing ligands with particular groups.

1.5   Project Aims

Against a backdrop of increasing attrition in drug discovery,[8] the output of medicinal chemistry programmes has become less effective.[42] As the discipline of medicinal chemistry becomes increasingly unfit for purpose, it risks becoming obsolete. Therefore, it is important and urgent that practitioners of medicinal chemistry examine and critically evaluate standard practices and seek improvements. This project aims to examine the relative importance of the quality of a starting hit versus medicinal chemistry practice in influencing the quality of the derived lead. This work will aim to make recommendations to improve outcomes, in particular in hits to leads optimisations. This study takes three parts.

Firstly, a fragment screen was carried out and hits were optimised against an enzyme target. Care was taken to ensure that the screening was exhaustive and that the hits chosen for optimisation had good physicochemical properties. The outcome of this experiment examined the lead which was ultimately generated and discussed whether the high quality starting point resulted in a high quality lead.

This study was then extended by comparing the FBDD derived lead to other leads generated at GSK against the same target using different hit discovery

methods. This work aimed to investigate whether hit generation by FBDD could offer the advantages many of its proponents claimed. These comparisons were further extended by comparing published clinical candidates against a range of biological targets discovered by FBDD or other methods to elucidate if any differences in candidate quality could be observed.

Finally, an attempt was made to assess the impact that medicinal chemistry practice can play in affecting outcomes in hit to lead optimisation. An enzyme HTS hit with poor physicochemical properties was optimised using some of the medicinal chemistry philosophies and methods common in FBDD optimisations. This work aimed to understand if the quality of the hit from FBDD is the important factor in improved outcomes, or whether it is the rigour and discipline in optimisation that is often a feature of FBDD optimisations that is more important.

2. Mitochondrial Branched-Chain Aminotransferase (BCATm) Inhibitors

2.1 Introduction

BCATm Inhibition and Obesity

This project describes the application of FBDD in the identification and optimisation of inhibitors of the enzyme mitochondrial branched chain aminotransferase (BCATm). BCATm converts branched chain amino acids (BCAAs, leucine, isoleucine and valine) into their corresponding α-keto acids. Over the past few years, evidence has linked this enzyme to obesity in animals and humans and so inhibition of this enzyme has the potential to be a treatment for obesity and related diseases.

High protein diets (such as Atkins[TM] diet), BCAA supplements or leucine supplements have been demonstrated to increase energy expenditure and reduce food consumption in humans leading to lower body weights.[136] These data suggest that increasing branched chain amino acid levels *in vivo* by a pharmacological mechanism such as BCATm inhibition may have similar effects. However, studies in genetically mutated obese rodents (ob/ob mice and Zucker rats), as well as diet induced obese mice and humans, show that these individuals have higher BCAA levels than lean animals and they exhibit lower levels of expression of BCATm.[137] Interestingly, these effects are reversed in humans who lose weight following gastric bariatric surgery. Knock-out mice that have no gene coding for BCATm have been bred and studied.[136] These animals appear healthy, viable and exhibit an interesting metabolic phenotype. When fed a high-fat diet, they consume more food, but weigh less, and have lower levels of body fat than wild-type mice. They also display improved insulin sensitivity and glucose tolerance. The knock-out mice were shown to have higher energy expenditure, which was not linked to mechanisms such as increased movement, but instead was demonstrated to be due to a futile cycle of protein synthesis and degradation being

established (both of which are energy consuming processes). This is consistent with the fact that leucine is known to stimulate protein synthesis while α-keto acids inhibit protein degradation.[136] *Figure 2.1* illustrates the effect of BCATm inhibition on these processes. At the outset of this work, potent pharmacological inhibition of BCATm by a small molecule had not been reported. Based on the literature evidence of the effects of this enzyme on metabolism, identifying a suitable small molecule to investigate transient pharmacological inhibition was a useful experiment to elucidate if this mechanism could provide a treatment for obesity and related conditions, such as type II diabetes.
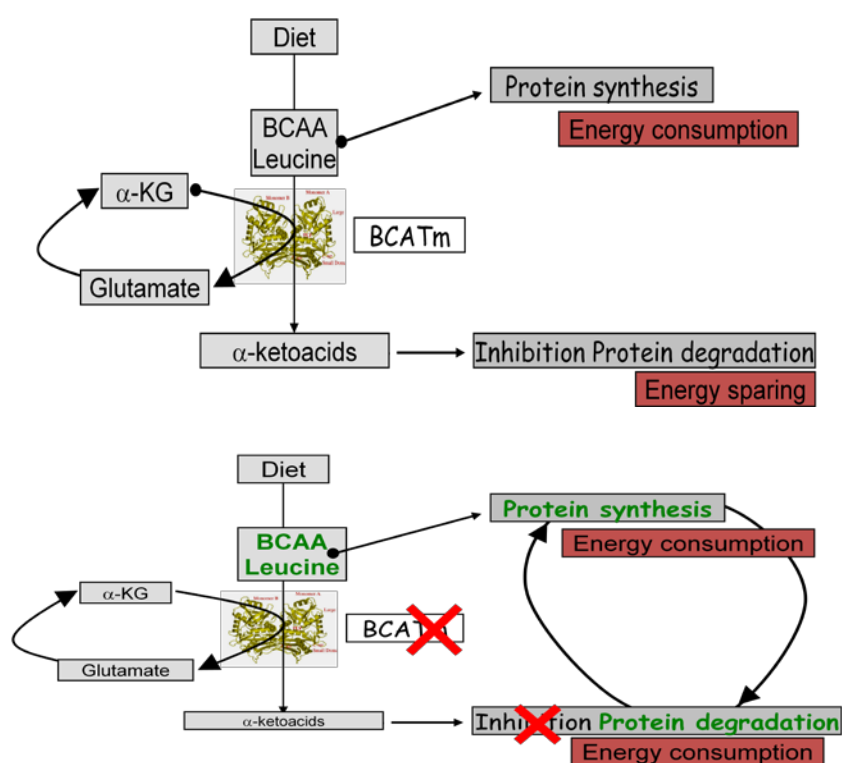
Figure 2.1: Schematic illustrating the metabolic consequences of BCATm inhibition. Figure provided by Nicolas Ancellin, Lipid Metabolism DPU, GSK

Structure and function of BCATm

Human BCATm (hBCATm) exists as a dimer, each subunit of which is made up of two domains, the small domain and the large domain.[138] A ribbon diagram of the tertiary structure of the protein is shown in *figure 2.2*.
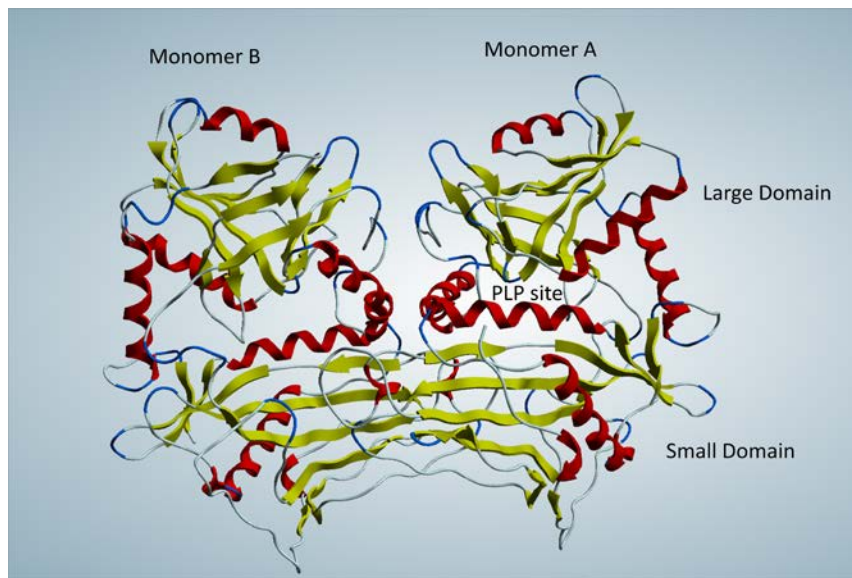
Figure 2.2: Ribbon Diagram of structure of hBCATm, showing both monomers, the small and large domains and the catalytic site, where the cofactor PLP is bound (PDB code 1ekf).

The biochemical reaction catalysed by BCATm is illustrated in *figure 2.3*.[139] At the start of the cycle, the co-factor pyridoxal phosphate (PLP) is covalently bound to the enzyme *via* a lysine residue. This lysine is then displaced by the α-amino group of an incoming BCAA substrate. The imine formed is converted to the corresponding α-keto acid. In the course of the reaction, the co-factor is released from its covalent bond to the enzyme as pyridoxamine phosphate (PMP). A complementary half-reaction occurs to complete the cycle, where α-ketoglutarate is transaminated to glutamate and the PLP form of the enzyme is regenerated.
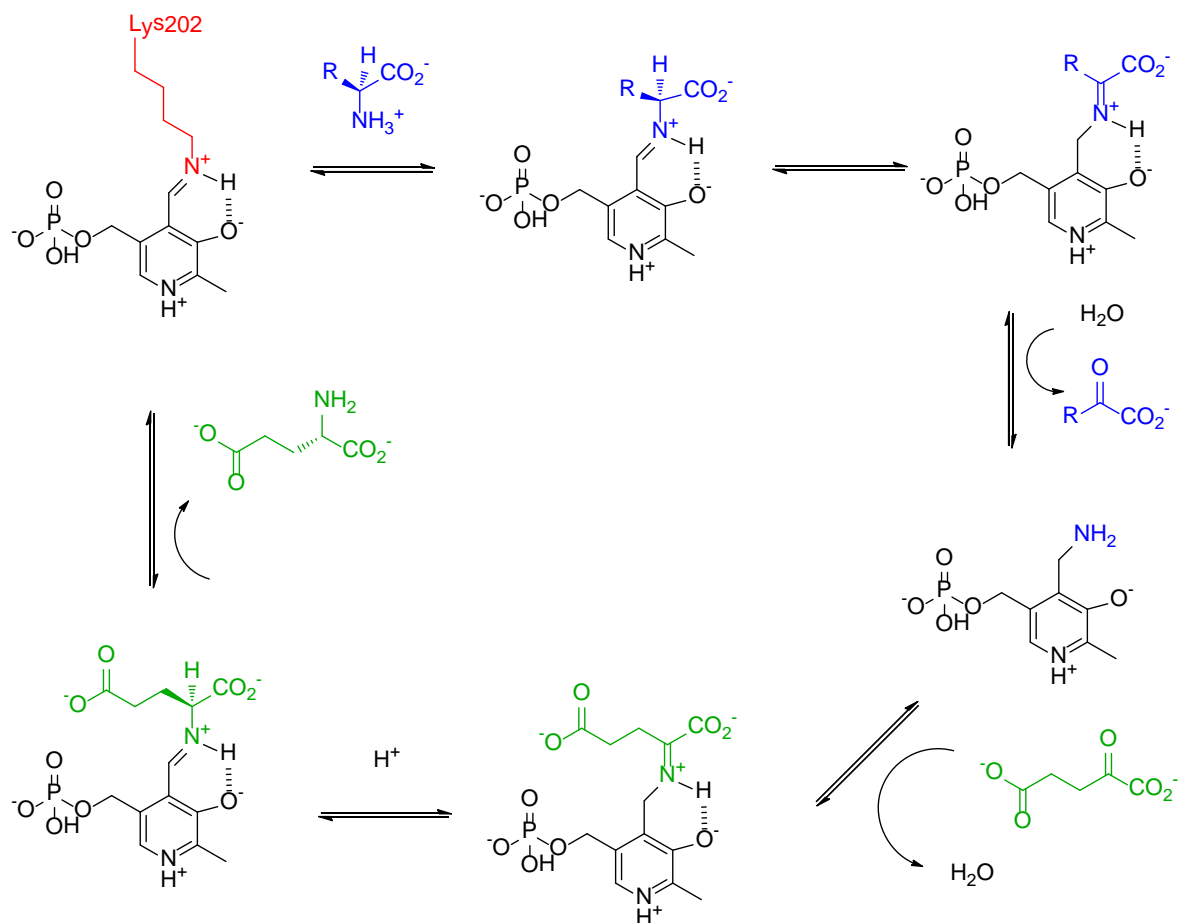
Figure 2.3: Biochemical reaction catalysed by BCATm. Black = cofactor, PLP or PMP; Red = BCATm protein; Blue = BCAA substrate/α-ketoacid product; Green = α-ketoglutarate/glutamate

Figure 2.4 shows an overlay of the active site of the enzyme with the PLP covalently bound,[138] and with the PMP form present with one of the reaction products, α-ketovaline bound.[140] The PMP is slightly twisted relative to the PLP position and the key lysine residue, which forms the covalent interaction (Lys-202) also moves slightly. Otherwise, the structures of the two forms of the enzyme are very similar.
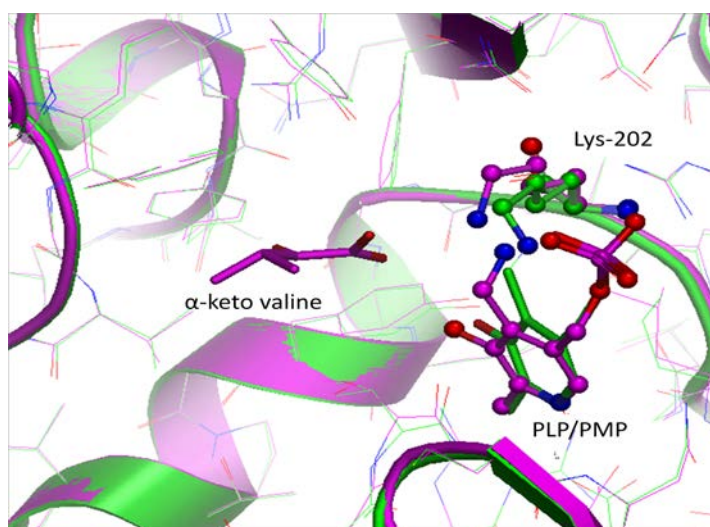
*Figure 2.4: hBCATm active site showing **PLP form** (PDB code 1ekf) and **PMP form** (PDB code 1kta)*

BCAT Isoforms and Expression

There are two known isoforms of BCAT enzyme, BCATm and the cytosolic form, BCATc. The human forms of these enzymes share 58% amino acid sequence homology.[141] The BCATm isoform is expressed ubiquitously, with very high levels in the stomach, pancreas and salivary glands; consistent with its role in protein metabolism.[142] The BCATc enzyme has much more limited expression and appears to be confined to the brain, ovary and placenta.[143]

In the brain, BCATc is vital in the synthesis of the essential neurotransmitter glutamtate, from which the additional neurotransmitters glutamine and γ-aminobutyric acid (GABA) are also derived.[144] In order to avoid CNS-related side-effects, which could be caused by interfering with normal brain levels of these neurotransmitters, it was important that any BCATm inhibiting drug molecule did not inhibit centrally-expressed BCATc. This could potentially be achieved either by finding a molecule that selectively inhibits BCATm over BCATc or by identifying a dual inhibitor that was unable to cross the blood-brain barrier.

Known BCAT Inhibitors

At the outset of this work, no selective inhibitors of BCATm had been described in the literature. The antiepileptic drug Gabapentin, **2.1** (*figure 2.5*), which has similar structure features to the BCAA substrates of BCAT is an inhibitor of BCATc (amongst other targets) but has no effect on BCATm.[145]

2·1
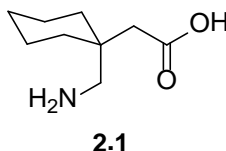
Figure 2.5: Chemical structure of Gabapentin

Researchers at Pfizer investigated BCATc inhibitors as potential treatments for neurodegenerative diseases and disclosed a series of sulfonyl hydrazide inhibitors such as **2.2** (*figure 2.6*).[146] These compounds generally exhibited micromolar IC_{50} values for BCATc inhibition and had approximately 10-fold lower activity at BCATm. *Figure 2.7* shows a crystal structure of compound **2.2** in the BCATc active site[146] overlaid with the same compound in the BCATm active site (GSK data generated by Don Somers). The binding mode in both enzymes is very similar, which accounts for the poor selectivity observed. The phenyl ring occupies a lipophilic pocket adjacent to the PLP substrate. There is a hydrogen bond formed between the hydrazide NH and the backbone carbonyl of Thr-240. There is also an off-stacked π-π interaction between the inhibitor benzofuran and Tyr-173. The position of Tyr-173 is approximately 5 Å different between the two isoforms, due to some residue differences in the loop it is part of. The position of Tyr-173 in BCATc is more amenable to forming the π-stacking interaction, which may explain the slightly improved binding at BCATc versus BCATm.
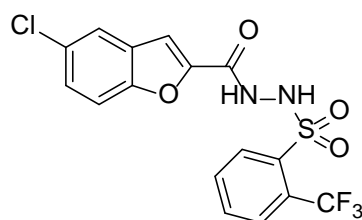
2.2

*Figure 2.6: Chemical structure of published BCATc inhibitor **2.2***
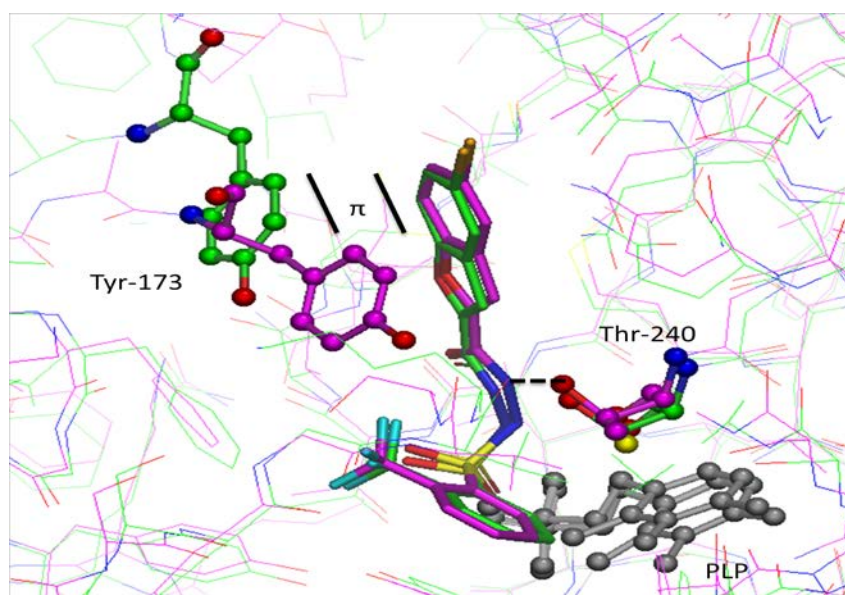
*Figure 2.7: Crystal structure of compound **2.2** in **BCATc** (PDB code 2abj) and in **BCATm** (residue numbers are for BCATm).Hydrogen bonding and π-stacking interactions are highlighted.*

Researchers at Abbott described an NMR based assay to carry out fragment screening at BCATc.[147] Several fragment hits were identified with IC_{50} values in the 10-500 μM range. These included some aryl sulfonyl hydrazides. The authors do not describe any BCATm activity or any optimisation of these hits.

2.2 Project Aims

The overall aim of this project was to apply FBDD methodology to contribute to the identification of potent inhibitors of BCATm that would be suitable to be used as tool molecules to effectively test the relevance of this target to diseases of metabolism and potentially be suitable candidates for further lead optimisation. In theory, targetting good physicochemical properties should

give rise to compounds with good DMPK profiles and low risk in developability assays. During the progress of the project, the potential of FBDD to be used in drug discovery to identify lead molecules with good overall physicochemical properties was monitored. The effects of these properties on the factors contributing to attrition such as poor pharmacokinetics and off-target effects was also explored within the context of the leads identified. A final aim was to critically assess and suggest improvements and refinements in the application and practice of FBDD methodology in drug discovery.

2.3 Fragment Screening

Design of Fragment Screening Cascade

In this project I fulfilled the role of Fragment Programme Coordinator which meant that I had overall matrix responsibility for the successful prosecution of the fragments screening and optimisation effort. In collaboration with colleagues from the screening departments, we designed a cascade of assays to identify hits and determined appropriate criteria to progress compounds into crystallography. My colleague Sophie Bertrand and I were jointly responsible for defining the strategy for chemical optimisation of all of the hits and for making prioritisation decisions. The particular contribution of colleagues to this work will be identified in each section.

In designing an appropriate cascade of screening assays, a number of questions were considered.

- What assays would be practically accessible within a reasonable time-scale and would be capable of screening an appropriate number of compounds (in this case, the GSK fragment library of 1056 compounds);
- What kinds of hits could be identified from each assay, i.e. would the hits identified by different assays bind to different forms of the protein, would different assays be biased towards different chemical subsets of compounds, what information does each assay provide about the hit;

- How many hits might be identified by each assay. It was important to design a cascade that would identify as many genuine hits as possible, to fully explore the diversity of binding modes and chemical matter generated;

- How to have confidence that the hits identified were genuine inhibitors and not assay false positives;

- The screening cascade should provide a final set of hits with sufficient data associated with them to allow meaningful prioritisation decisions to be made about which compounds to begin medicinal chemistry optimisation on.

With all of these considerations in mind, it was decided to screen the GSK fragment collection of 1056 compounds through three assays concurrently: a biochemical assay, an STD by NMR assay and a T_m assay. It was decided to triage hits through X-ray crystallography and only to progress to chemistry hits for which a liganded structure could be obtained. Each of these assays will now be described in more detail, with a discussion for the rationale of screening in each assay and the caveats which were considered when interpreting data.

Saturation Transfer Difference by NMR assay (STD NMR)

This assay was developed and run by Claus Spitzfaden, GSK. When carrying out screening of BCATm, it was important to consider that the enzyme cycled between two forms; the PLP-bound and free-PMP forms (see *figure 2.3).* By consideration of the enzyme's catalytic cycle, it was not thought that inhibition of one particular form of the enzyme would give rise to superior inhibitors and so it was important to seek inhibitors of both forms. It was found that the different forms of the protein could be isolated and characterised, and also that interconversion between these was possible by adding an excess of either leucine or α-keto glutarate as appropriate. Therefore, the decision was made to carry out the STD NMR screening on a sample where both forms of the protein were mixed in a single NMR tube. An advantage of this approach

was the potential to allow inhibitors of either form to be detected, however the assay would not provide information as to whether the detected hits bound to either PLP, PMP or both forms of the enzyme. The screening was carried out with pools of five compounds in each tube, to allow the experiment to be carried out within a reasonable time-frame. The pools had been selected with reference to the individual compounds' ^{1}H NMR spectra, to ensure that the peaks did not overlap and to allow identification of a particular hit molecule within any given pool. In this assay, a hit was defined as any compound which gave an STD-signal:noise ratio of greater than or equal to 4:1. This value was selected retrospectively to provide a reasonable number of hits (34) to be progressed into X-ray crystallography. If a higher or lower hit rate had been observed, this cut-off would have been adjusted. Since the size of the STD signal is not proportional to the binding strength, but rather to the off-rate,[148] this choice of cut-off would likely have resulted in some genuine hits being missed. Another caveat with the hit-set identified by STD NMR was, that to avoid interference from protein NMR signals, only the aromatic region of the spectrum was interrogated. This meant that compounds in the fragment library which did not contain any aromatic protons could not be detected by this method. Molecules identified by the STD NMR assay with the pragmatically chosen cut-off were simply classified as hits and no attempts to use this data to quantify their binding were made.

Thermal Shift Assay (T$_m$)

Due to the inherent limitations of high concentration binding assay determinations, an orthogonal biophysical screen is commonly employed in a fragment triage and a T$_m$ assay was selected. This assay was developed and screened by Peter Francis, GSK. Since the denaturation temperatures of the PLP (73 °C) and PMP (54 °C) forms of BCATm were found to be so different, the decision was taken to carry out the T$_m$ assay with each of the forms screened separately. All of the compounds were tested against each form. The high-throughput nature of the T$_m$ experiment allowed for this additional information to be gathered quickly and easily. All compounds

which gave a ΔT_m of greater than 1 °C against either form were classified as hits. As with the STD NMR experiment, this value was selected to provide a practical number of hits to progress into X-ray crystallography. It was again likely that the hit set identified by this technique using a pragmatic cut-off to define hits would be incomplete, so it was considered important to use both biophysical screening techniques concurrently.

High Concentration Functional Biochemical Assay

As a complementary approach to the biophysical techniques, a high concentration functional biochemical assay was also used (developed by Ryan Bingham, GSK and screened by Sarah Smith, GSK). The assay used was a coupled assay (*figure 2.8*). The glutamate product of the BCATm reaction was monitored by its oxidation back to α-ketoglutarate by the enzyme L-Glutamate Oxidase. This reaction also produces hydrogen peroxide which can be reduced to water by the enzyme horseradish peroxidase. The final coupled reduction reaction was carried out using Amplex^{TM} red which acts as the electron donor to horseradish peroxidase and is thus oxidised to resorufin, a highly coloured, fluorescent compound, which was then quantified using automated fluorescence detection. One risk of using a coupled assay such as this to detect inhibitors is that compounds which inhibit either of the coupled enzymes in the cascade would also be identified as inhibitors. In order to mitigate this risk, a decoupled assay, which does not contain the initial BCATm mediated step, was run at the same time. Any compounds which display similar inhibition in both assays were considered to be acting via a non-specific mechanism and were discarded. In using this approach, it is possible that genuine BCATm inhibitors were discarded simply because they also happened to inhibit one of the other enzymes. This could be especially likely for small, fragment molecules, which simply have more chances of binding to a given protein by some means.[66,67] The biochemical assay provided an advantage over the biophysical techniques in that it detected molecules that inhibited the enzyme turnover, rather than compounds that simply bound to the protein. However, the limit of

detection was likely higher for the biochemical assay and so the weakest binders would not be detected. The biochemical assay was the only one to give a quantifiable measure to allow the compounds to be ranked in order of their inhibitory activity and to calculate ligand efficiency values.
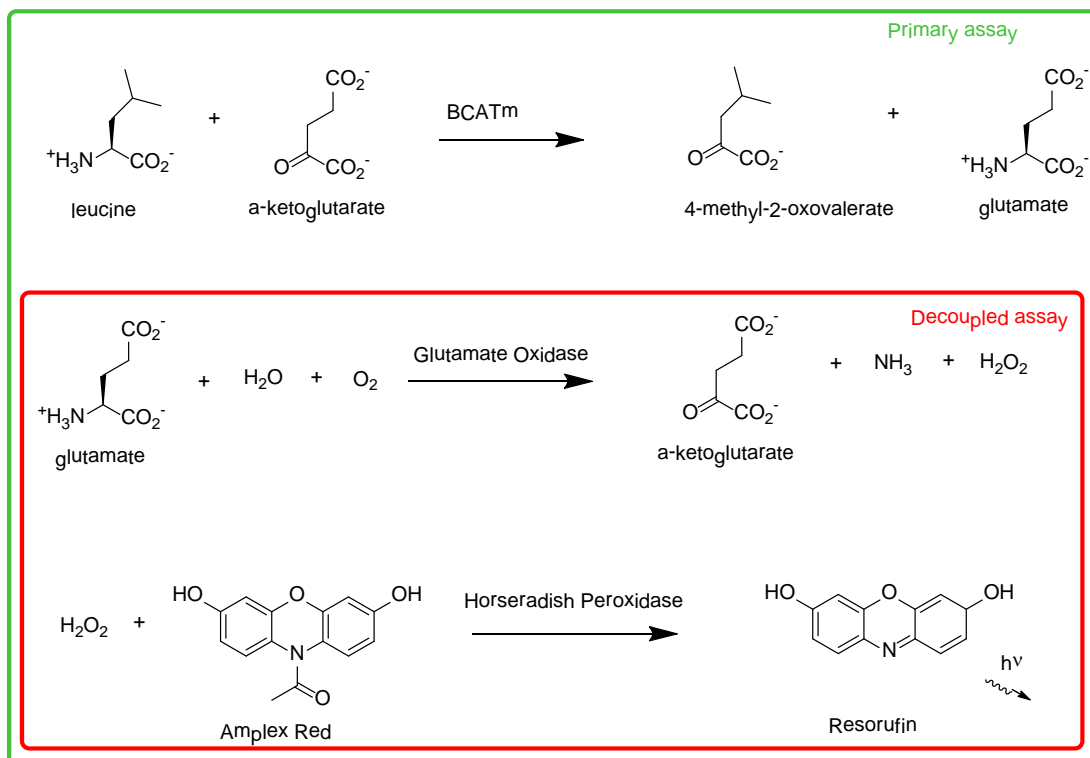
Figure 2.8: Coupled reactions exploited in biochemical assay. Assay sequence is in green box, with decoupled specificity assay shown in red box.

X-Ray Crystallography

Consistent with established best practice in FBDD,[79] the identified hits were not considered suitable for optimisation until a liganded X-ray protein structure was obtained. The crystallography was carried out by Don Somers, GSK. High concentration solutions (40 mM - 60 mM) of the ligand of interest were soaked into preformed crystals for one to fourteen days. The X-ray data were generally collected at a synchrotron source although some structures were obtained using GSK's internal X-ray source. The structures obtained had resolutions between 1.8 and 2.4 Å. Although crystals of both the PLP and PMP forms of the BCATm were used in the soaking experiments, the initial hits only yielded complexes with the more stable PLP form. Therefore it

was not feasible to progress any of the hits identified as putative PMP-form binders due to a lack of structural guidance.

Results of Fragment Screen
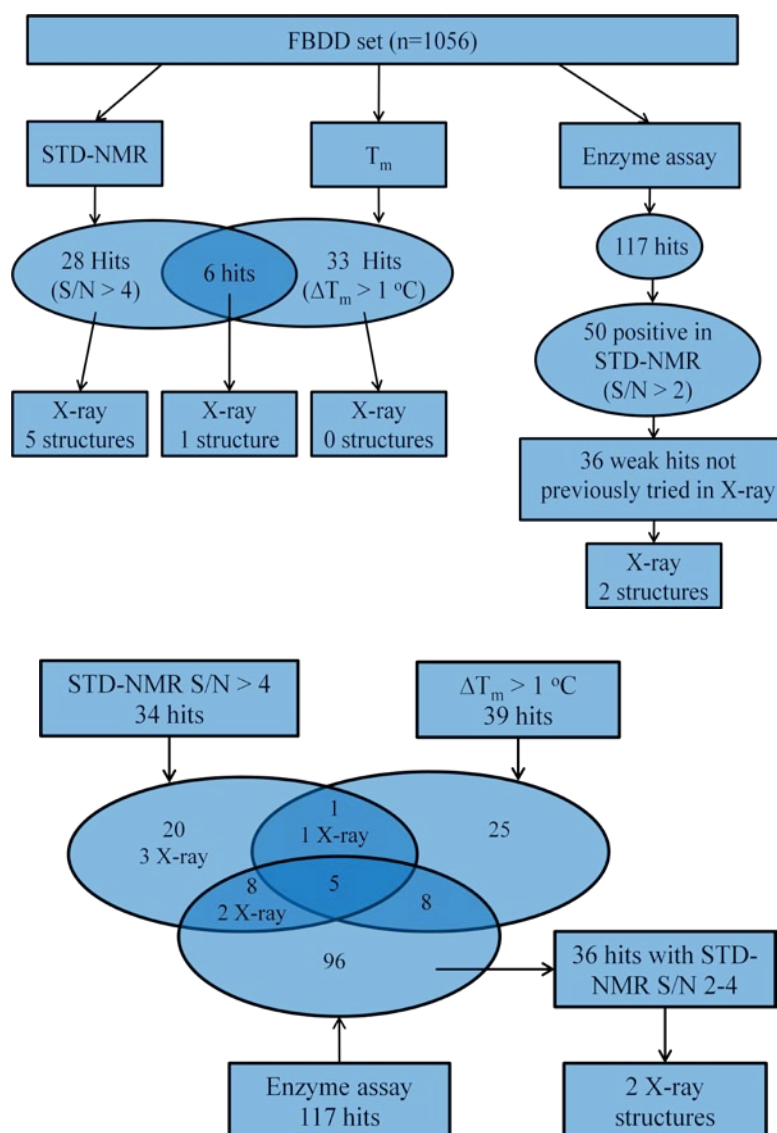
Figure 2.9: Flow and Venn diagrams illustrating the output of the fragment screening campaign, showing number of hits identified by each screening technique and the logic employed for X-ray prioritisation, plus the distribution of those which yielded X-ray crystal structures.

A summary of the results of the fragment screen is given in *figure 2.9.* The hit rates for the biophysical assays were relatively low at around 3 %. Also, the overlap of hits between these two assays was low, with only 6 out of the 61 identified hits being detected by both biophysical techniques. This result was

consistent with the finding of others, that multiple fragment screens do not give hit sets with good overlap.[149] The biophysical assays used in these experiments were detecting fragment hits which had binding affinities around the limit of detection for these techniques. Therefore, it is not surprising that they detected different hit sets.

The overall success rate of crystallography was low. There are a number of potential reasons for this.

- As discussed earlier, BCATm cycles between two forms of the enzyme during the biochemical reaction, with the PLP co-factor either covalently bound or free. At the time of screening, only the bound form had yielded crystal structures so it is possible that the hit ligands which failed in crystallography interacted preferentially with the unbound form.

- The compounds tested could have destroyed the crystal packing when they were soaked into the crystals.

- The compounds may have bound to a conformation of the protein which was present in the solution assays but was not the form which crystallised.

- The compounds could have been too poorly soluble to reach the high concentrations needed to soak very weakly binding ligands into a crystal system.

- The weakly binding fragments could have occupied several binding modes which were similar in energy, resulting in weak electron density being observed throughout the binding site.

Ideally, the biochemical screening would have been carried out in parallel with the NMR and T_m assays. This would have allowed additional prioritisation of compounds for crystallography, and the arbitrary cut-offs used in the biophysical assays may not have been required. However, the biochemical assay was not available in time to complement the biophysical

screening so a pragmatic decision was taken to carry out the screening in two stages.

The biochemical assay identified 117 compounds which generated meaningful dose-response curves and had no activity in the decoupled specificity assay. This number of compounds was too high to progress directly into crystallography. Therefore, a triage using STD NMR data was used, since this had been previously shown to have some ability to predict crystallography success.

- Of the 117 hits identified in the biochemical assay, 16 had a high signal to noise ratio in the STD-NMR so had already been attempted in crystallography.

- There were a further 36 compounds which had biochemical activity and also had an STD signal to noise ratio of between 2 and 4.

- Crystallography of these was attempted with only two succeeding to produce a bound crystal structure.

Since the number of crystal structures of confirmed hits was low (8 compounds in total) some additional work was carried out to identify additional structures. Around the same time as the fragment screening was carried out, a high throughput screen (HTS) was also run. This provided additional information to complement the fragment screening output. A computational approach (by Stephen Pickett, GSK) was used to find similar structures to the fragment hits which had shown weak activity in the HTS. The 42 compounds identified were tested in the STD NMR assay, with those which had detectable binding being progressed to crystallography. This approach resulted in a further two liganded crystal structures of fragment-like molecules being obtained.

Another approach which was used to generate more structures was to further investigate the six compounds which had been identified by both the T_m and STD NMR assays. Only one of these compounds had resulted in a bound

crystal structure of a complex, but the fact that they were detected by the two orthogonal assays suggested that they were likely to be genuinely binding to the protein. The GSK compound collection was searched for available compounds which were close analogues of these six hits. This work was a carried out by myself, Sophie Bertrand and Stephen Pickett. The analogue searching was a mixture of substructural searching of the cores of the identified hits to find larger compounds and similarity searching using Tanimoto scoring[150] to identify similar compounds to the fragment hits. To ensure the compounds screened were fragment-like and soluble, a molecular weight and clogP cut-off was applied to the compounds identified. This varied by series depending on the molecular weight and clogP of the hits and also by the number of analogues identified. Finally, the compound sets were examined by eye to remove any which contained undesirable functionality, such as reactive intermediates, or protecting groups. The compounds identified were screened in the biochemical assay and also in the STD NMR assay. Any compounds identified which had high potency in the biochemical assay or exhibited strong binding in the STD NMR experiment were progressed to crystallography. In total a further 32 compounds were studied in X-ray crystallography, which resulted in another three liganded crystal structures from two distinct chemical series.

2.4 Fragment Screening Hits

The fragment screening hits were evaluated based on a number of criteria to determine which compounds should be progressed into medicinal chemistry optimisation. The binding modes of the hits were examined in detail to identify opportunities to improve activity. The ligand efficiency and likely synthetic ease of optimisation for each compound was also considered. The details for each hit will now be discussed.

2.3
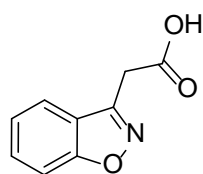
pIC$_{50}$ <2.9, clogP = 0.78, 13 heavy atoms

STD NMR hit

*Figure 2.10: Compound **2.3***

The crystal structure of fragment **2.3** (*figure 2.11*) shows that the benzisoxazole made van der Waals' type interactions in a lipophilic pocket in front of the PLP co-factor and that the carboxylic acid carbonyl acted as a hydrogen bond acceptor in a hydrogen bond with a backbone NH.
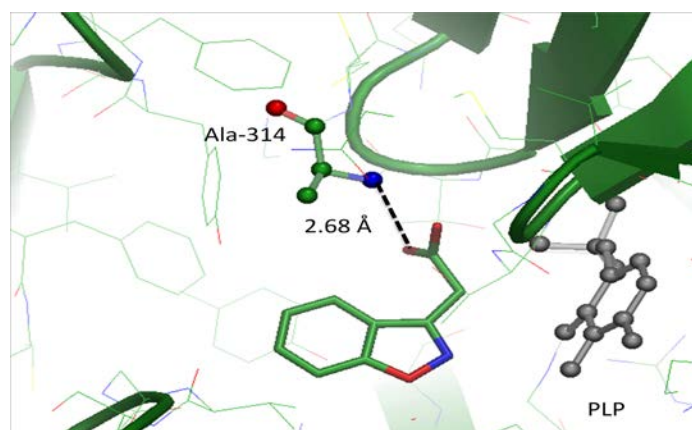
*Figure 2.11: Crystal structure of compound **2.3**, showing interactions observed*
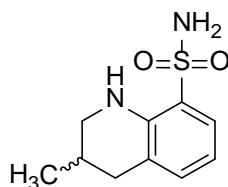
2.4

pIC$_{50}$ <2.9, clogP = 1.25, 15 heavy atoms

T$_m$ and STD NMR hit

*Figure 2.12: Compound **2.4***
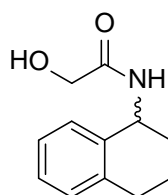
2.5

pIC$_{50}$ <2.9, clogP = 1.57, 15 heavy atoms

STD NMR hit

*Figure 2.13: Compound **2.5***

An overlay of compounds **2.3**, **2.4** and **2.5** (*figure 2.14*) shows the similarities in the binding modes of these three fragment hits. The hydrogen bond acceptors were superimposed, suggesting that it was this interaction that was key for the binding of these fragments. The lipophilic and aromatic cores of these molecules occupied similar positions, but the pocket appeared to accommodate slight differences in the core position, to allow the hydrogen bond acceptors to occupy a more favourable location. Since these molecules possessed similar binding modes, and could access similar vectors by substitution, it is possible to employ a strategy often used in fragment optimisation know as vectorial clustering. This involves identifying relationships between fragment hits such as these and clustering them by their binding interactions rather than by chemical similarity or structure, as may be done, for instance, in clustering of HTS hits. A decision can then be taken to optimise only one of the clustered hits based on an advantage such

as superior chemical tractability, physicochemical properties, functional groups, potency, or ligand efficiency.
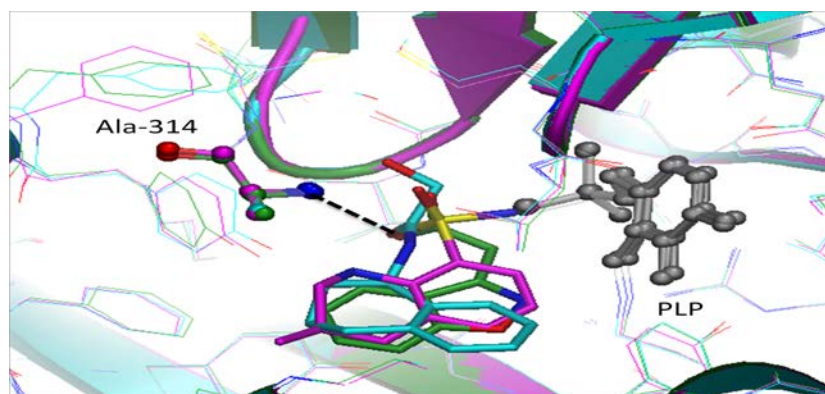
Figure 2.14: Overlaid structures of compounds 2.3, 2.4 and 2.5, showing similar binding modes
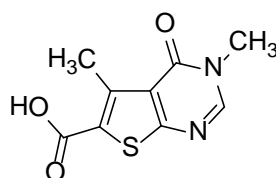

2.6

$pIC_{50} = 4.2^{a}$, clogP = 0.62, 15 heavy atoms
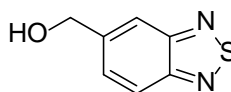
STD NMR hit

LE = 0.38 LLE$_{AT}$ = 0.43

Figure 2.15: Compound 2.6. [a]Compound tested inactive ($pIC_{50} < 4.2$) on 3 out of 34 test occasions.

The crystal structure of compound **2.6** (*figure 2.16*) showed that it occupied a distinct binding site from compounds **2.3**, **2.4** and **2.5**. The site adjacent to the cofactor is instead occupied by ethylene glycol which was present in the crystallisation medium. The aromatic core of compound **2.6** formed a π-stacking interaction with a phenylalanine residue at the bottom of the pocket (Phe-30). The amide carbonyl acted as a hydrogen bond acceptor to a lysine NH at the back of the pocket. An overlay of compound **2.6** with compound **2.3** (*figure 2.17*) showed that the binding pocket for this fragment was induced by the presence of the ligand. The π-stacking phenylalanine (Phe-

30) moves by around 2 Å, while a tyrosine residue (Tyr-173) makes a dramatic move of around 6 Å.
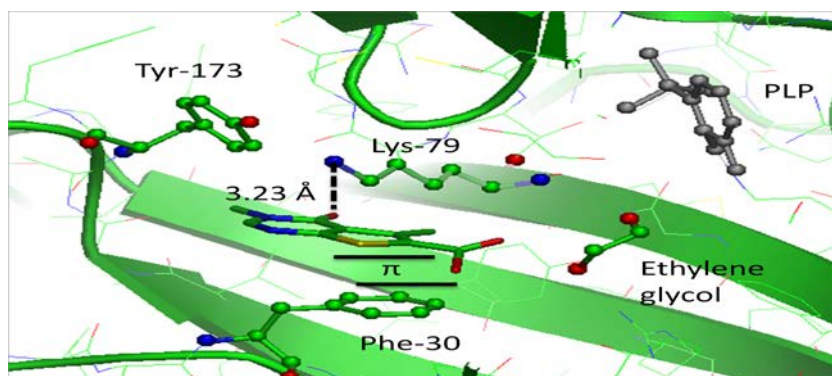
*Figure 2.16: Crystal structure of compound **2.6**, showing interactions observed.*
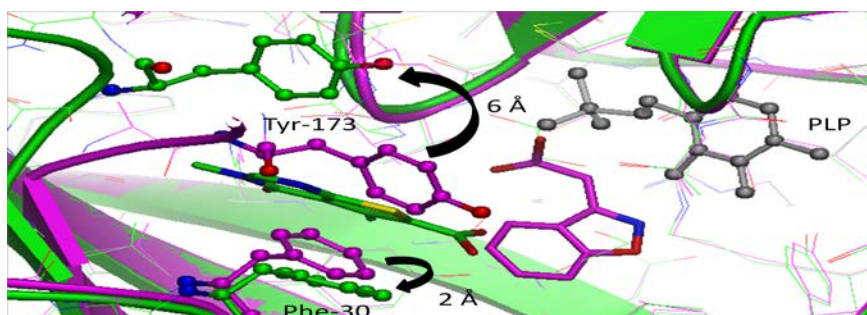
*Figure 2.17: Overlaid structures of compounds **2.6** and **2.3**, showing movement of residues to allow opening of induced π-stacking pocket*
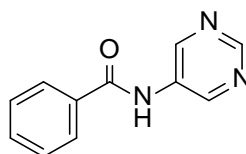
2.7

$pIC_{50} = 3.0^a$, clogP = 1.31, 15 heavy atoms

STD NMR hit

LE = 0.27 LLE_{AT} = 0.23

*Figure 2.18: Compound **2.7**. [a]Compound tested inactive ($pIC_{50} < 2.9$) on 1 out of 2 test occasions.*

The crystal structure of compound **2.7** (*figure 2.19*) showed that the pyrimidine ring formed a similar π-stacking interaction with Phe-30 as compound **2.6**, whilst the phenyl ring occupied a similar lipophilic aromatic pocket to compounds **2.3**, **2.4** and **2.5**. The tyrosine residue, which moved to open the induced pocket in the structure of **2.6** (Tyr-173) was completely disordered in this structure. There were no hydrogen bonding interactions between the fragment's heteroatoms and the protein, which may explain the poor ligand efficiency observed. An overlay of compound **2.7** with hits **2.3** and **2.6** (*figure 2.19*) shows that compound **2.7** was an effective bridge between the two binding sites identified, and demonstrated that it was possible to have both sites occupied simultaneously. Although this compound had low potency and ligand efficiency this result illustrated the value of crystallising hits with this profile, as it provided structural insights which were useful for the optimisation of other fragments.
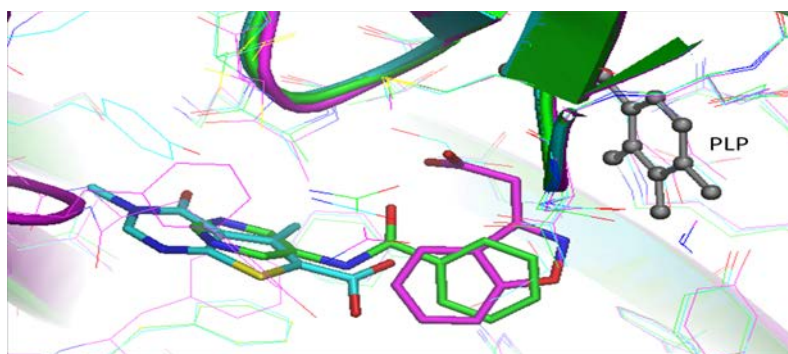
*Figure 2.19: Overlaid structures of compounds **2.7, 2.3** and **2.6**, showing **2.7** bridging two binding sites*

2.8

pIC_{50} <2.9, clogP = 1.96, 11 heavy atoms.

STD NMR hit

*Figure 2.20: Compound **2.8**.*

The X-ray crystal structure of compound **2.8** in the protein revealed that it did not bind in the enzyme's catalytic site but instead was observed at the interface between the protein dimers. This binding mode would not be expected to result in enzyme inhibition and indeed no biochemical activity was observed. This result illustrates one of the potential drawbacks of using biophysical methods which can detect binding for screening. There are many potential pockets on most protein structures which could accommodate small fragment-like molecules. The hits identified may genuinely bind to the protein with well-defined binding modes, but the biophysical assays used do not discriminate between functional binding, which can inhibit the biological activity, and binding in pockets which have no biological effects.
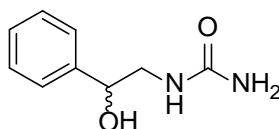
2.9

pIC_{50} = 3.1,[a] clogP = -0.2, 13 heavy atoms

Weak (2 < signal:noise < 4) STD NMR hit

LE = 0.33 LLE_{AT} = 0.45

*Figure 2.21: Compound **2.9**. [a]Compound tested inactive (pIC_{50} < 2.9) on 1 out of 2 test occasions.*

Hit **2.9** occupied a similar binding pocket (*figure 2.22*) to that found for compounds **2.3**, **2.4** and **2.5** with the urea carbonyl making the key hydrogen bonding interaction with the backbone alanine NH. The induced pocket was in the 'closed' conformation. The *(S)*-enantiomer was selectively observed in the crystal structure from the racemic mixture soaked. This molecule also had an additional interaction. The pendant alcohol displaces a water molecule, which was conserved in most of the other structures. This water or alcohol formed a hydrogen bonding interaction with a tyrosine residue in the bottom of the pocket. This interaction can be observed in the overlay between compounds **2.9** and **2.3** (*figure 2.22*).
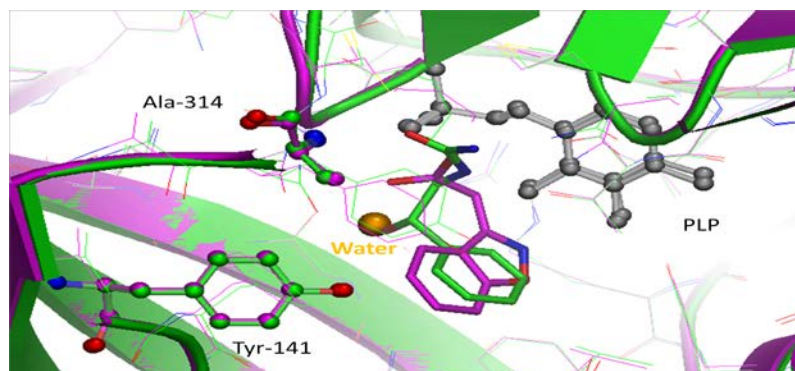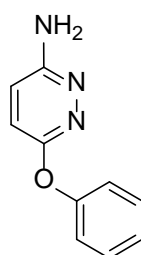
*Figure 2.22 Overlaid structures of compounds **2.9** and **2.3**, showing displaceable **water molecule***

2.10

pIC_{50} = 3.9, clogP = 1.6, 14 heavy atoms

Weak (2 < signal:noise < 4) STD NMR hit

LE = 0.38, LLE_{AT} = 0.33

*Figure 2.23: Compound **2.10***

The phenyl ring of compound **2.10** occupied the lipophilic binding site occupied by compounds **2.3**, **2.4**, **2.5** and **2.9**. The pyridazine ring formed a π-stacking interaction with the Phe-30 residue whilst the ring nitrogen atoms are likely to be interacting with the solvent water (*figure 2.24*). Interestingly, the nature of the π-stacking interaction is different to what was previously observed (e.g. with fragment **2.6**), with the phenylalanine ring rotating by 90° relative to the previously observed position. This can be visualised with an overlay of compound **2.10** with **2.6** (*figure 2.24*).
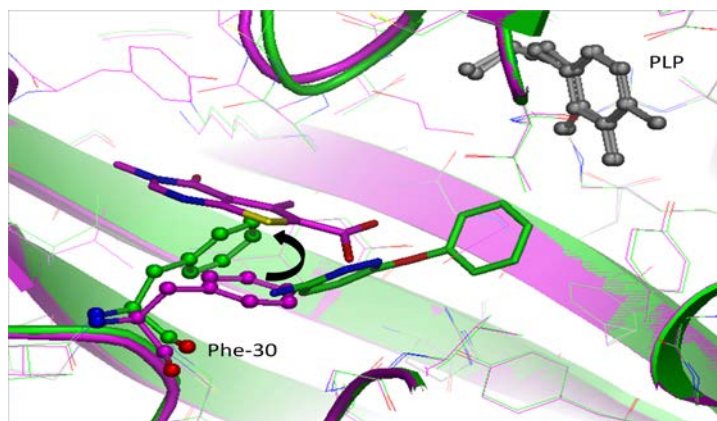
Figure 2.24: Overlaid structures of compounds 2.10 and 2.6, showing movement of Phe-30
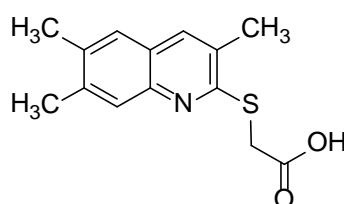
2.11

pIC_{50} = 6.1, clogP = 3.8, 18 heavy atoms

HTS hit identified through similarity searching of **2.3**

LE = 0.48 LLE_{AT} = 0.30

Figure 2.25: Compound 2.11

The crystal structure of hit **2.11** (figure 2.26), showed the acid carbonyl formed a hydrogen bonding interaction with Ala-314, which formed the hydrogen bond with compounds **2.3**, **2.4** and **2.5**. There was also a π-stacking interaction with a tyrosine residue (Tyr-141). This induced π-stacking pocket is formed under the π-stacking pocket formed with compound **2.6**. The phenylalanine residue (Phe-30) moved by approximately 3.5 Å from its position with **2.6** bound to accommodate **2.11**.
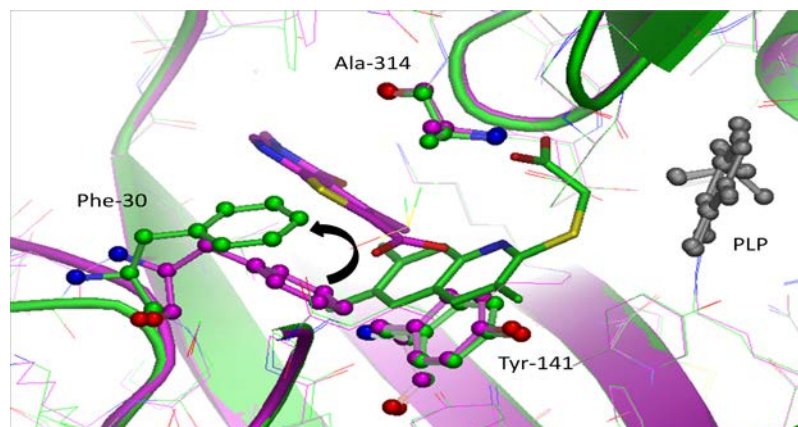
Figure 2.26: Overlaid structures of compounds 2.11 and 2.6, showing movement of Phe-30 to open π-stacking pocket.
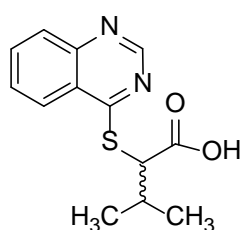
2.12

pIC_{50} = 5.1, clogP = 2.69, 18 heavy atoms

HTS hit identified through similarity searching of **2.3**

LE = 0.39 LLE_{AT} = 0.29

Figure 2.27: Compound 2.12

Compound **2.12** was another hit identified from the HTS results which appeared from its structure to be related to compound **2.11** (*figure 2.27*). It had lower activity than compound **2.11** and so was initially considered to provide structure activity relationship (SAR) information on this series. However, when the crystal structure was obtained (*figure 2.28*) this fragment was found to have a quite different binding mode from compound **2.11**. Compound **2.12** occupied the π-stacking pocket observed for compound **2.6** with additional hydrogen bonding interactions between the carboxylic acid carbonyl with Arg-143 and Tyr-70 of the 2nd dimer of the protein in the complex. The *(R)*-enantiomer of **2.12** was the only one observed by crystallography from the racemic mixture. These stark differences observed

for two structures which look very similar in two-dimensional space highlights the importance of obtaining structural data for as many compounds as possible. This is especially true for weakly binding fragment hits, where the possibility for movement in the binding site is high, and can lead to false assumptions being made.
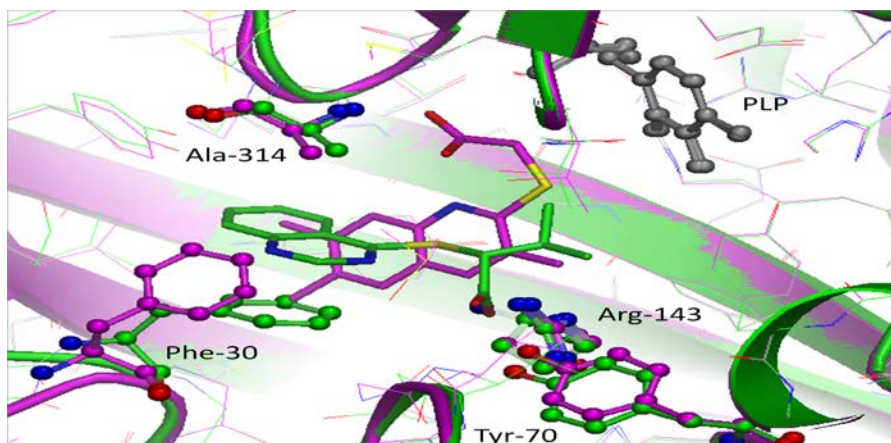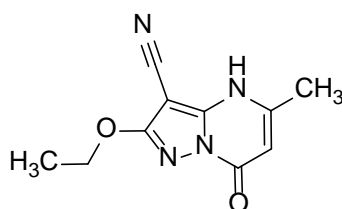

Figure 2.28: Overlaid structures of compounds 2.11 and 2.12, showing different binding modes
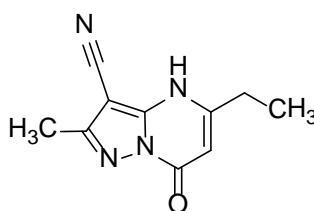
2.13

pIC$_{50}$ = 3.3,[a] clogP = -0.21, 16 heavy atoms

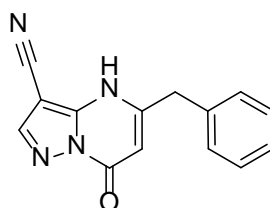Tm and STD NMR hit, no crystal structure obtained

LE = 0.28 LLE$_{AT}$ = 0.41

2.14

pIC$_{50}$ = 4.4,[b] clogP = 0.14, 15 heavy atoms

LE = 0.40 LLE$_{AT}$ = 0.50

2.15

pIC$_{50}$ = 4.6, clogP = 0.77, 19 heavy atoms

LE = 0.33 LLE$_{AT}$ = 0.39

*Figure 2.29: Compounds **2.13**, **2.14** and **2.15**. [a]Compound tested inactive (pIC$_{50}$ < 2.9) on 1 out of 2 test occasions. [b]Compound tested inactive (pIC$_{50}$ < 3.2) on 2 out of 3 test occasions*

The related fragment structures **2.14** and **2.15** were identified as analogues of the T$_m$ and STD NMR dual hit compound **2.13**, which itself failed to yield a liganded crystal structure (*figure 2.29*). An overlay of compounds **2.14** and **2.15** (*figure 2.30*) showed a slight movement of the core between the two

structures. The nitrile group was displacing the conserved water molecule that was also displaced by **2.**9. The pendant benzyl group in compound **2.15** occupied the lipophilic pocket in front of the co-factor which was also occupied with aromatic groups for compounds **2.3**, **2.4** and **2.5**.
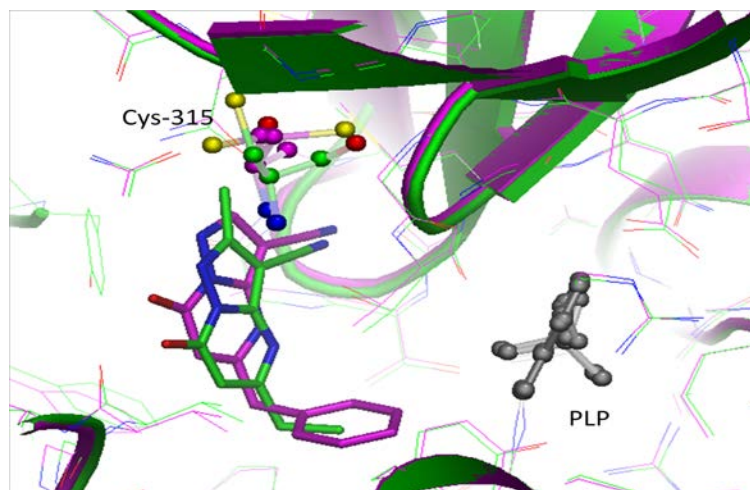
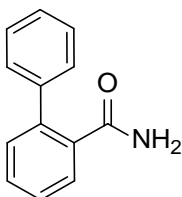*Figure 2.30: Overlaid structures of compounds 2.14 and 2.15, showing interactions observed*
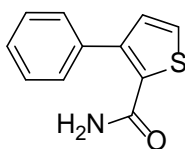
2.16

$pIC_{50} = 3.8$, clogP = 1.9, 14 heavy atoms

Tm and STD NMR hit, no crystal structure obtained

LE = 0.37 LLE$_{AT}$ = 0.29

2.17

$pIC_{50} = 3.8$, clogP = 2.08, 15 heavy atoms

LE = 0.35 LLE$_{AT}$ = 0.26

*Figure 2.31: Compounds **2.16** and **2.17***

Compound **2.17** was identified as an analogue of the T_m and STD NMR dual hit **2.16** (*figure 2.31*). The binding mode was similar to that of compounds **2.3**, **2.4** and **2.5** (*figure 2.32*). The amide carbonyl acted as a hydrogen-bond acceptor to Ala-314. There was an additional hydrogen-bond between the amide NH$_2$ and the backbone carbonyl of Thr-240).
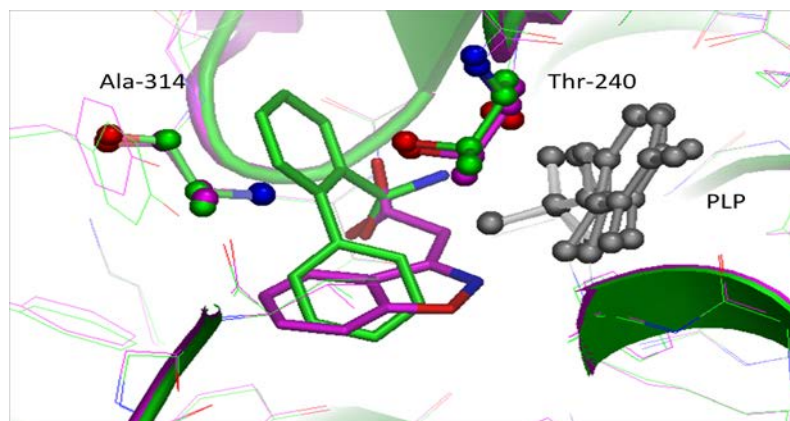
*Figure 2.32: Overlaid structures of compounds **2.17** and **2.3**, showing similar binding modes*

The fragment screening results revealed important new information about binding of ligands to the BCATm enzyme, with a number of new binding modes discovered. It was found that the ligand binding site for BCATm was highly mobile, with ligands seemingly inducing several binding pockets. This mobility of the binding site would have made predicting binding interactions for the fragment hits on the basis of their two-dimensional structures extremely challenging, and highlighted the importance of obtaining as much crystallographic structural data as possible. Another observation from the fragment hits was that, although there was diversity in the binding modes, a number of binding 'hot-spots' were identified (*figure 2.33)*; all of the hits made at least one of these interactions with the protein. The most notable of these was the lipophilic pocket adjacent to the PLP, hydrogen bonding with Ala-314, π-stacking with Phe-30 and displacement of the water molecule adjacent to Cys-315. The design and output of the fragment screening has now been published.[151] The binding of all of the hits is summarised in *table 2.1.*
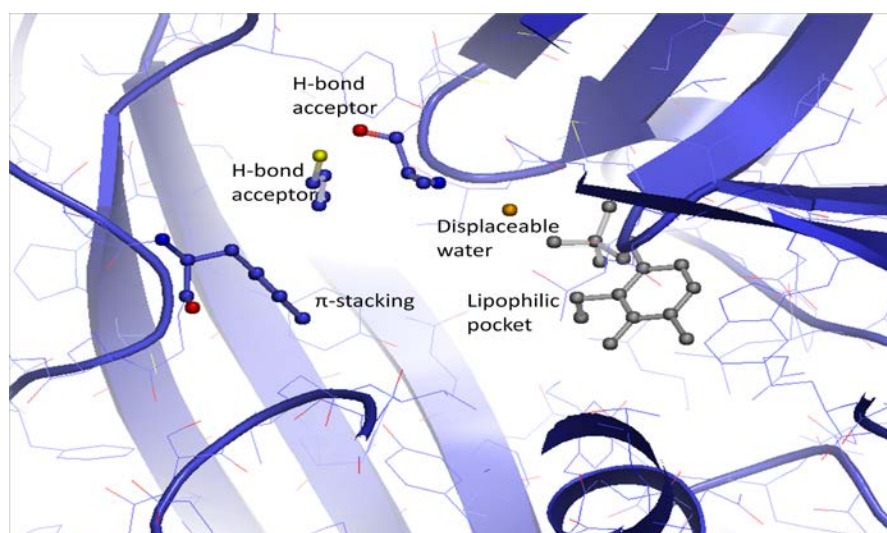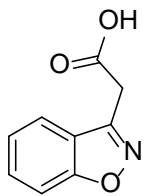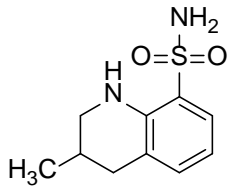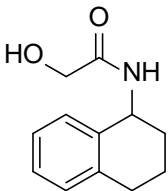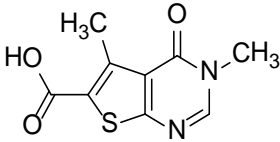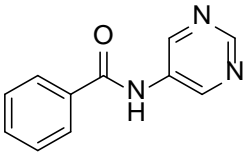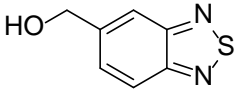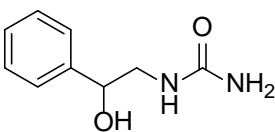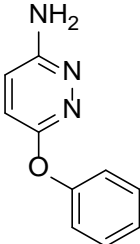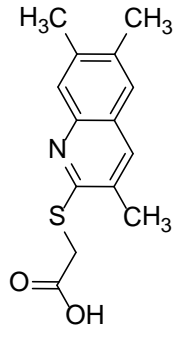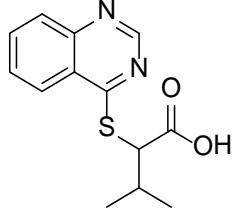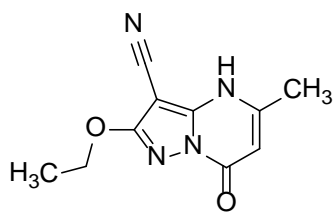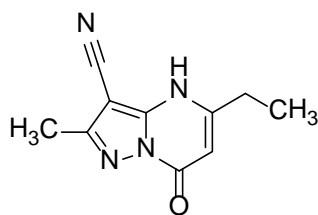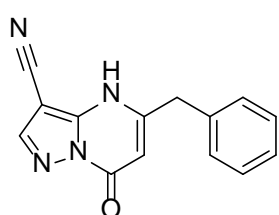
Figure 2.33: Binding hot-spots identified by fragment screening for BCATm

Compound Number	Structure	Source	Binding Mode
2.3		STD-NMR	PLP lipophilic pocket, Hydrogen bond acceptor to Ala-314
2.4		T_m and STD-NMR	PLP lipophilic pocket, Hydrogen bond acceptor to Ala-314
2.5		STD-NMR	PLP lipophilic pocket, Hydrogen bond acceptor to Ala-314

2.6		STD-NMR and biochemical	π- stacking to Phe-30, Hydrogen bond acceptor to Lys-79
2.7		STD-NMR and biochemical	π- stacking to Phe-30, PLP lipophilic pocket
2.8		STD-NMR	Interface between protein dimers (no functional effect)
2.9		STD-NMR and biochemical	PLP lipophilic pocket, Hydrogen bond acceptor to Ala-314, Displacement of water adjacent to Cys-315
2.10		STD-NMR and biochemical	π- stacking to Phe-30, PLP lipophilic pocket

2.11		HTS hit with similarity to fragment hits	Hydrogen bond acceptor to Ala-314
2.12		HTS hit with similarity to fragment hits	π- stacking to Phe-30
2.13		T_m, STD-NMR and biochemical	No crystal structure obtained
2.14		Analogue of **2.13**	PLP lipophilic pocket, Displacement of water adjacent to Cys-315
2.15		Analogue of **2.13**	PLP lipophilic pocket, Displacement of water adjacent to Cys-315
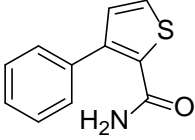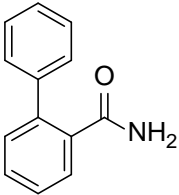
2.16		T$_m$, STD-NMR and biochemical	No crystal structure obtained
2.17		Analogue of **2.16**	PLP lipophilic pocket, Hydrogen bond acceptor to Ala-314

Table 2.1: Summary of fragment hits identified with their binding hot-spots

2.5 Fragment Prioritisation

These data were reviewed and considered with fragment clustering and merging strategies as part of a discussion between myself, Sophie Bertrand and Stephen Pickett. We recommended priority of series for initial investigation by the team of medicinal chemists as follows.
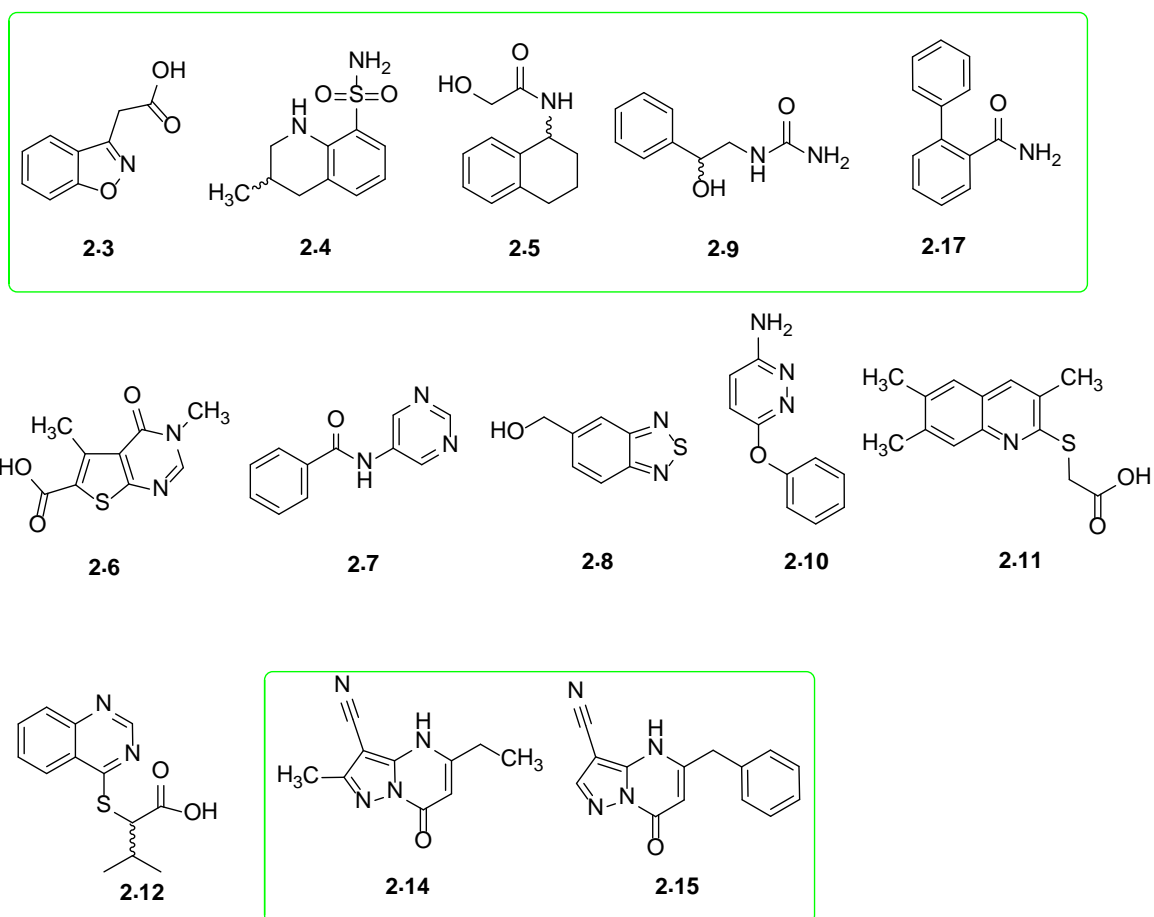
Figure 2.34: Summary of all structures considered for optimisation. Green boxes indicate fragment hits which are contained in the same vectorial cluster.

The cluster containing compounds **2.3**, **2.4**, **2.5**, **2.9** and **2.17** was explored through compounds **2.3** and **2.4** simultaneously. Compound **2.5** was given lower priority for chemistry as it was considered to be less synthetically tractable than introducing the desired interactions in compounds **2.3** and **2.4**. Compound **2.9** was not chosen for chemical optimisation as it contained a urea group, which is often found to confer poor aqueous solubility and to be associated with unsuitable properties in experimental molecules.[152] Compound **2.17** was not selected for optimisation as it had a much higher clogP relative to compounds **2.3** and **2.4**. Compounds **2.3** and **2.4** were both advanced in parallel initially as they had similar physicochemical properties and lacked biochemical activity so it was difficult to differentiate between them.

Compound **2.6** was selected for optimisation as it occupied a distinct binding site and had high potency, LE and LLE$_{AT}$.

Compound **2.7** was attractive for optimisation as it bridged the two major binding sites but made no hydrogen-bonding interactions so could potentially be optimised by targeting the interactions observed for compounds **2.3**, **2.4**, **2.5**, **2.6**, **2.9** and **2.17**. However, since compound **2.7** was a simple biaryl amide, many analogues were available, either commercially or in the GSK compound collection, so searches and selections were made to do this.

Compound **2.10** appeared to offer an attractive starting point for optimisation as it had high LE and LLE$_{AT}$ values and contributed a unique interaction with Phe-30. It was explored through testing available analogues from the GSK collection; however, none of these analogues showed a significant increase in potency over the initial hit. It was then decided not to pursue compound **2.10** further.

Compounds **2.11** and **2.12** contained a structural motif which had been shown in previous studies in our group to be chemically reactive, due to the presence of an electrophilic centre adjacent to the thioether, a relatively good leaving group. This functionality was believed likely to engender activity in biochemical assays due to chemical reactivity rather than specific binding effects. The substructure of concern is shown in *figure 2.35*.
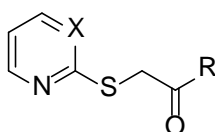
Figure 2.35: Potentially Reactive Substructures: X = N or C, R = N or O.

The concerns over the reactivity of compounds **2.11** and **2.12** were confounded by the fact that the two compounds appeared similar, but were shown to occupy such different binding sites in the crystal structure.

Generally, when closely related molecules exhibit different binding modes, they are binding relatively weakly to the protein and can access several binding sites which have similar energies. Since these compounds were apparently highly potent in the biochemical assay it was feared that their binding affinity was actually much lower and the biochemical effects observed were resulting from the compounds reacting with the proteins and not due to the binding observed crystallographically. To address these concerns, the binding K_d and stoichiometry were measured using an ITC experiment, to compare the biophysically measured binding affinity with the biochemical IC_{50}. The ITC experiments were carried out by Peter Francis and Chun-Wa Chung, GSK. Compound **2.11** exhibited a binding curve which was consistent with 1:1 stoichiometry of binding. The derived $K_d = 6.6$ μM, was of a similar magnitude to the biochemical IC_{50} of 0.5 μM. Compound **2.12** showed a very weak response in the ITC experiment, which resulted in a poorly fitted dose-response curve. The only conclusion that could be reliably determined from this result was that the binding of compound **16** was close to the limit of detection for the ITC experiment. On the basis of these experiments we recommended an optimisation effort on compound **2.11** but not **2.12**.

Compounds **2.14** and **2.15** occupied a different binding mode from any of the other fragments, had high potency, promising LE and LLE_{AT} values and subsequently presented the opportunity to access a pocket occupied by an HTS hit (not shown) therefore these were selected for optimisation. The term fragment guided optimisation has been coined for such a hybdridisation approach and the successful growth and optimisation of the series was published[153] and was favourably reviewed in a Journal of Medicinal Chemistry *viewpoint* article.[154]

2.6 Fragment Optimisation

The remainder of this chapter will focus on the optimisation of compounds **2.3**, **2.14** and **2.15**. Additional optimisation of other fragment hits were investigated by colleagues in the team.

Optimisation of Compound 2.3

2.3
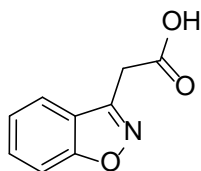
pIC_{50} <2.9, clogP = 0.78, 13 heavy atoms
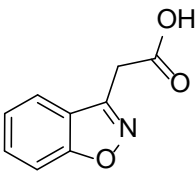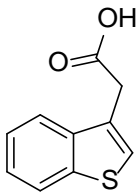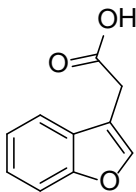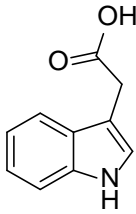
*Figure 2.36: Compound **2.3***

The initial goal for optimising compound **2.3** was to improve potency with maintenance of efficiency so that the SAR could be tracked using the biochemical assay and as a first step towards a lead compound. Three strategies were adopted to grow the fragment with the aim of increasing potency and maintaining efficiency, whilst maintaining good physicochemical properties.

SAR analysis of available analogues

I carried out a search of the GSK compound collection using similarity and substructure methods to find available analogues of compound **2.3.** Point changes were particularly chosen to facilitate initial SAR exploration. Some of the close analogues tested showed activity in the biochemical assay (*table 2.2*). Replacing the benzisoxazole with either benzothiophene (**2.18**) or benzofuran (**2.19**) gave an improvement in the potency. The indole, benzimidazole, indazole and benzotriazole analogues (**2.20-2.23**) were all inactive in the biochemical assay. The compounds tested were not an exhaustive set of heterocycles but based on these results, I recommended not to synthesise any further heterocyclic cores. The differences in activity

between the heterocyclic cores could be explained on the basis that less polar groups are preferred in the lipophilic pocket. Similarly, small lipophilic substituents on the benzisoxazole core also showed improved potency over the original hit (methyl, methoxy, **2.24** – **2.26**), presumably by improving van der Waals' interactions in the lipophilic pocket. Importantly, this approach of acquiring potency through lipophilic interactions still maintained the LLE_{AT} figure in an appropriate range for further optimisation.

Compound	Structure	pIC_{50}	LE/LLE_{AT}
2.3		<2.9	
2.18		3.5[a]	0.37/0.22
2.19		3.5[a]	0.37/0.27
2.20[c]		<3.2	
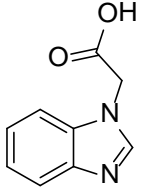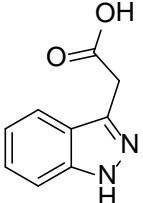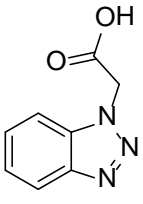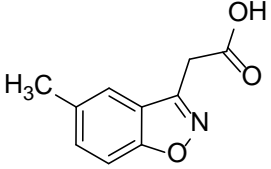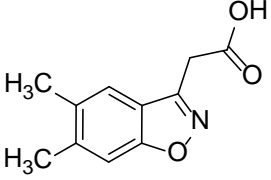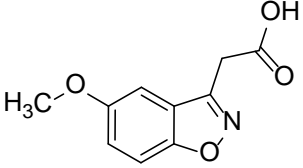
2.21		<3.2	
2.22		<2.9[d]	
2.23		<3.2	
2.24		3.4[a]	0.33/0.31
2.25		3.8[b]	0.35/0.30
2.26		3.6[d]	0.33/0.34

*Table 2.2: Available analogues of **2.3** tested. [a]Compound tested inactive (pIC_{50} < 3.2) on 1 out of 2 test occasions. [b]Compound tested inactive (pIC_{50} < 3.2) on 1 out of 3 test occasions. [c] Compound tested as both free acid and sodium salt. [d] Compound tested n = 1*

Targeting induced π-stacking pockets

The first design strategy employed to improve the potency of compound **2.3** was a fragment merging approach to access the induced pockets accessed by compounds **2.6** or **2.11** that exploited π-stacking interactions. An overlay of compounds **2.3**, **2.6** and **2.11 (**with the protein removed for simplicity,

figure 2.37) suggested that substitution of the benzisoxazole in positions 4, 5 or 6 could potentially access one of the targeted regions. The screening of analogues confirmed that small substituents on the phenyl ring were tolerated which further validated this approach.
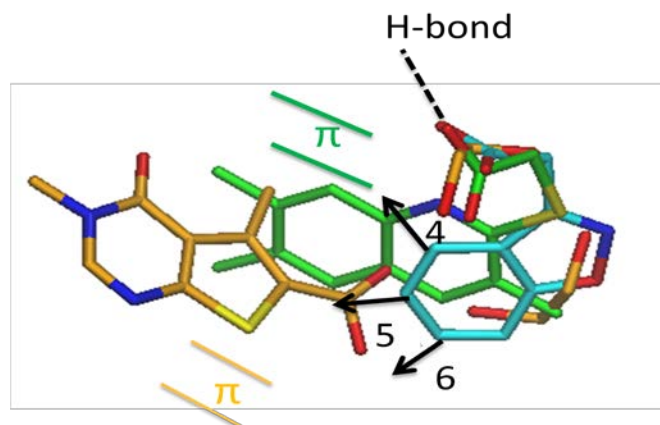
*Figure 2.37: Overlay of compounds **2.3**, **2.6** and **2.11***

A number of benzisoxazole analogues were synthesised by reacting commercially available 4-hydroxycoumarins with hydroxylamine (*scheme 2.1*).[155] Acidification of the aqueous reaction mixture resulted in precipitation of the desired products with no further purification required.
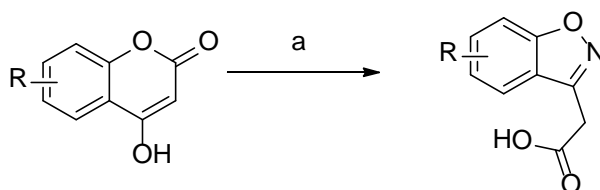
Scheme 2.1: Synthesis of benzisoxazole acetic acids from hydroxycoumarins. Reagents and conditions: (a) Hydroxylamine (50 % in water), 70 °C, 24 h, 50 -85 %.

Docking experiments (carried out by Stephen Pickett, GSK) predicted that 5-aryloxy substituents on compound **2.3** were most likely to add potency. The 5-phenoxy compound (**2.27**) was docked into the protein crystal structure liganded with either **2.6** or **2.11**, and was thus predicted to form π-stacking interactions with Phe-30 in both cases (*figure 2.38*). The appropriately

substituted coumarins were unknown in the literature, so synthesis of 6-phenoxycoumarin **2.30** was required.

a)

2.27

b)

c)
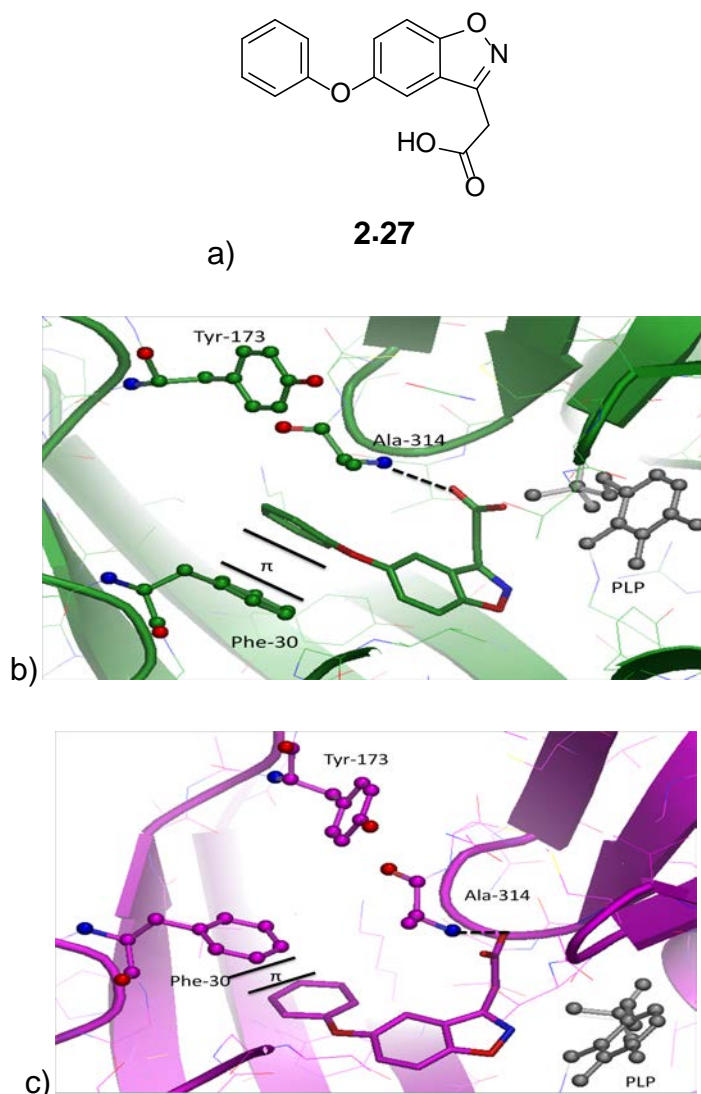
*Figure 2.38: Dockings generated of proposed compound **2.27** (a) in (b)* ***crystal structure generated for compound 2.6*** *and (c)* ***crystal structure generated for compound 2.11***. *π-Stacking interactions being targeted with Phe-30 are shown.*

The most common route to 4-hydroxycoumarins in the literature is by cyclisation of *ortho*-acetyl phenols with diethylcarbonate using sodium hydride as base.[156-158] This reaction was precedented for synthesis of 6-methoxy[158] and 6-ethoxy[159] 4-hydroxycoumarins but not for the desired 6-phenoxy system. The appropriate ketone **2.29** was synthesised from 4-phenoxyphenol **2.28** (*scheme 2.2*) by Fries rearrangement under Lewis acid

catalysis of the acetate ester. A one-pot process was attempted using boron trifluoride as the Lewis acid[160] but the reaction stopped at the ester intermediate stage, which was isolated. The rearrangement of the ester was achieved using aluminium chloride. The cyclisation of **2.29** to the 4-hydroxycoumarin **2.30** was then attempted using diethylcarbonate and sodium hydride.
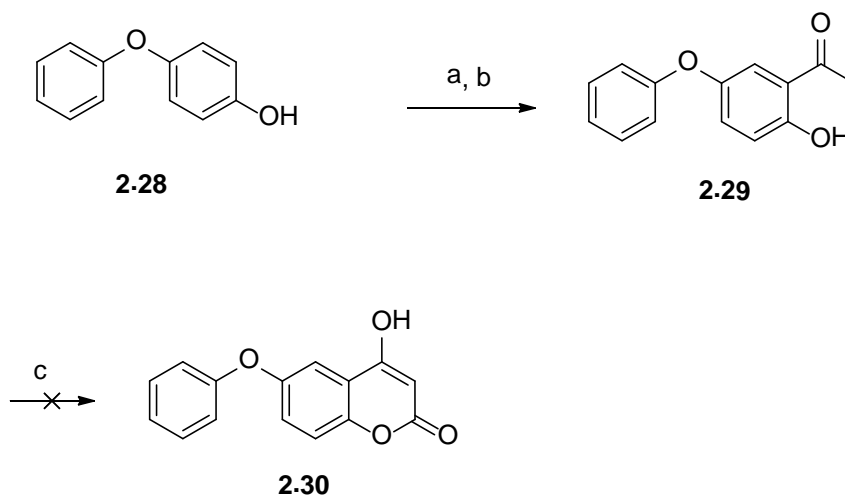
Scheme 2.2: Attempted synthesis of **2.30**. Reagents and conditions: (a) Acetic acid, boron trifluoride diethyl etherate (1.1 eq.), 80 – 100 °C, 3 days; (b) Chlorobenzene, aluminium chloride (1 eq.) 130 °C, 4 h, 36 % over 2 steps; (c) Sodium hydride, diethyl carbonate, various conditions, no reaction.

The conversion of **2.29** to **2.30** was attempted several times using variations of the conditions shown in *scheme 2.2*. The reaction was attempted using toluene as solvent or in diethylcarbonate. The ethanol formed during the reaction was removed azeotropically from the toluene solution. In all cases, LCMS analysis of the crude reaction mixture showed remaining starting material and a peak with mass corresponding to the carbonate intermediate **2.31** (M^+ = 301, M^- = 299, **2.31**, *scheme 2.3*).
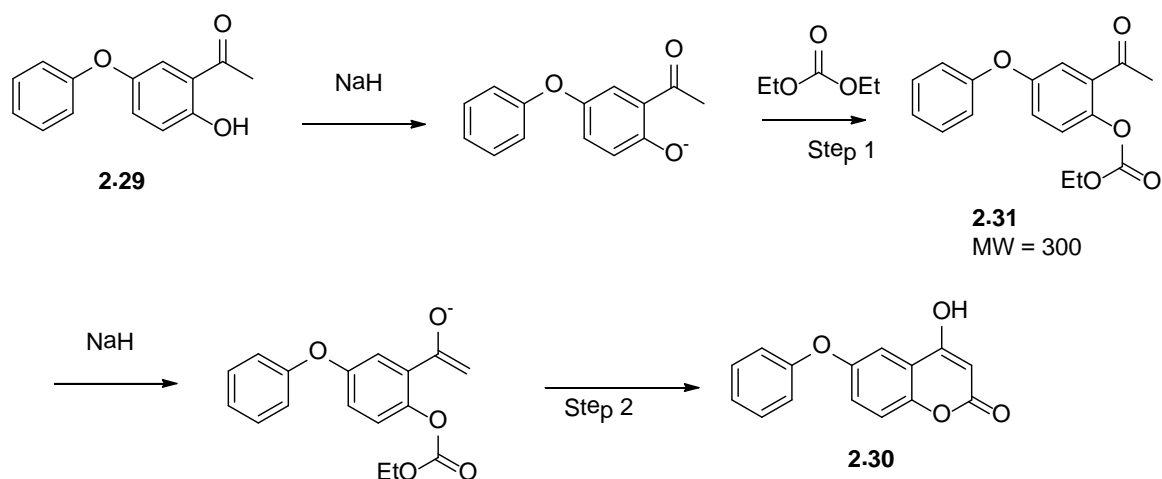
*Scheme 2.3: Proposed mechanism for desired conversion of **2.29** to **2.30***

The first step in the reaction, the conversion of **2.29** to **2.31** was activated by the presence of the *para*-phenoxy substituent. For the second step, conversion of **2.31** to **2.30**, the phenoxy group was *meta* to the nucleophile and so de-activated the reaction to the extent where it did not proceed. These effects would be expected to be less pronounced for the precedented[158,159] methoxy- and ethoxy- analogues.

A review of the literature found several alternative routes for the synthesis of 4-hydroxycoumarins. These included selenium-assisted carbon-monoxide addition to *ortho*-acetyl phenols,[161] Baker-Venkataraman rearrangement to give a phenol precursor for cyclisation[162] and tellurium-mediated cyclisations.[163] A one-pot reaction of the starting phenol **2.28** with Meldrum's acid, followed by cyclisation using Eaton's reagent (a solution of phosphorus pentoxide in methanesulfonic acid) was chosen (*scheme 2.4*).[164] The 6-methoxy analogue was one of the products described in the paper but the phenoxy group was not exemplified. The first step of the reaction was performed under solvent-free conditions. LCMS analysis indicated formation of the desired intermediate **2.32**. However, addition of Eaton's reagent appeared to result in decomposition of the components. LCMS indicated tentative evidence for desired product but it was not possible to isolate this.

Scheme 2.4: Attempted one-pot formation of **2.30**. Reagents and conditions: (a) 1:1 mixture, 70 °C 4 h, product not isolated; (b) Eaton's reagent (excess as solvent) 20 °C 2 h, 0 %.

An alternative approach to the synthesis of the 5-phenoxy benzisoxazole not involving synthesis of the coumarin ring was researched. A range of copper-catalysed coupling conditions to substitute with phenol onto several relevant intermediates was investigated, using caesium carbonate as base.[165] The coupling was attempted on the 5-bromobenzisoxazole acid (**2.33**), the 4-hydroxy-6-bromo coumarin (**2.34**), and the 5-bromobenzisoxazole t-butyl ester (**2.35**). Several ligands were tried and addition of potassium iodide was tested to convert the bromide substrates to iodides *in situ* (*figure 2.39, table 2.3*). The phenanthroline-derived ligand **2.36** is a bidendate ligand of the type commonly used in copper-mediated *O*-arylations.[166] Trispolyoxaalkyl amines such as **2.37** are good phase transfer catalysts which help to solubilise the copper salts used.[167] The imino pyridine ligand **2.38** has been recently reported as a highly efficient ligand for copper-mediated *O*-arylations.[168] It is postulated that the electron rich pyridine nitrogen can facilitate oxidative addition, whilst the imine group withdraws electrons from the copper complex, encouraging the reductive elimination of the product.

None of the conditions attempted with catalytic copper present provided any desired product (*table 2.3,* entries 1 – 9). Stoichiometric copper and ligand **2.36** were successful in performing the required transformation using the coumarin substrate **2.34** (entries 14 and 15) but not on the benzisoxazole

substrate **2.33** (entries 10-13). Crude LCMS results of the reaction suggested that addition of potassium iodide appeared to increase the yield of product formed (entry 14 vs. entry 15) so the reaction was scaled up using these conditions (*scheme 2.5*).

2.33   **2.34**   **2.35**

2.36   **2.37**   **2.38**
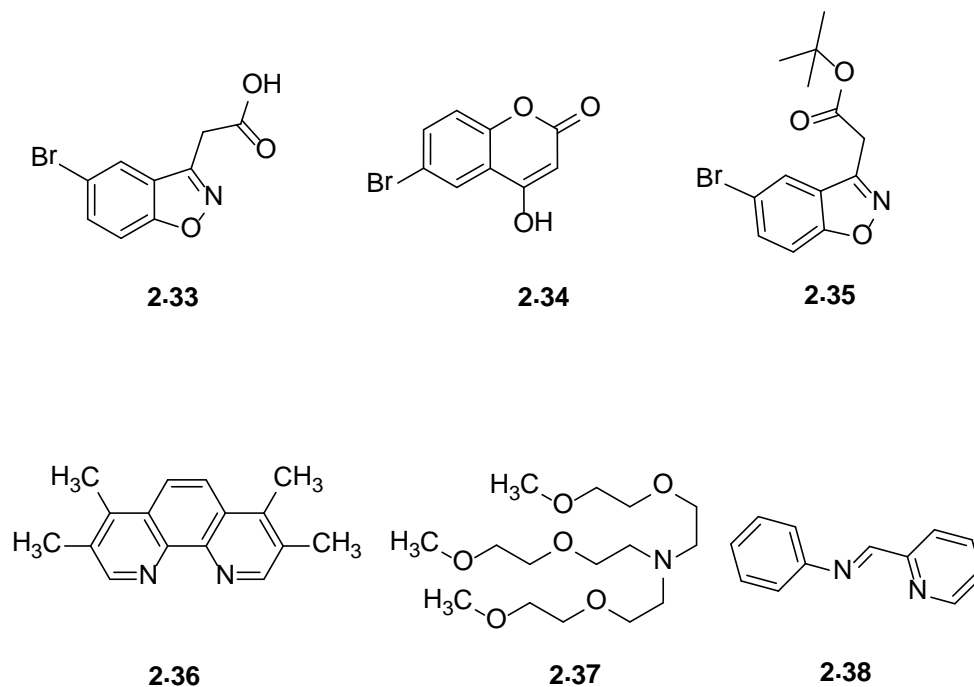
Figure 2.39: Substrates and ligands studied in optimisation experiments

Entry	Substrate	Ligand	KI Present	Equivalents of Copper	Result
1	**2.33**	**2.37**	No	0.5	No reaction
2	**2.33**	**2.38**	No	0.2	No reaction
3	**2.33**	**2.37**	Yes	0.2	No reaction
4	**2.33**	**2.36**	No	0.2	No reaction
5	**2.33**	**2.36**	Yes	0.2	No reaction
6	**2.35**	**2.36**	No	0.2	No reaction
7	**2.35**	**2.36**	Yes	0.2	No reaction
8	**2.35**	**2.38**	No	0.2	No reaction
9	**2.35**	**2.38**	Yes	0.2	No reaction
10	**2.33**	**2.36**	No	1.5	No reaction
11	**2.33**	**2.36**	Yes	1.5	No reaction
12	**2.33**	**2.38**	No	1.5	No reaction
13	**2.33**	**2.38**	Yes	1.5	No reaction
14	**2.34**	**2.36**	No	1.5	Crude LCMS showed 3 % product
15	**2.34**	**2.36**	Yes	1.5	Crude LCMS showed 10 % product

Table 2.3: Results of optimisation experiments
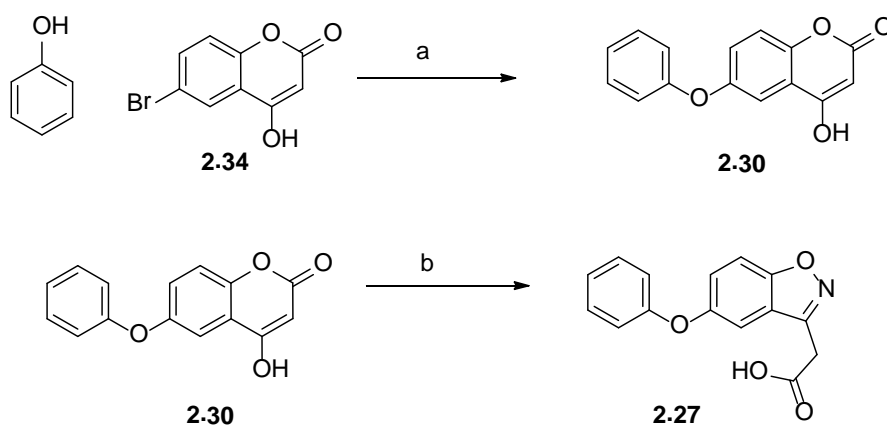
*Scheme 2.5: Conditions used to synthesise **2.27**. Reagents and conditions: (a) cesium carbonate (1 eq.), potassium iodide (1 eq.), phenanthroline **2.36** (0.5 eq.), copper (I) iodide (1.5 eq.), DMF, microwave 150 °C, 2.5 h, 4 %; (b) Hydroxylamine (50 % in water), 70 °C, 24 h, 45 %.*

When compound **2.27** was initially submitted to the BCATm assay it was found to have a pIC_{50} = 5.1. However, the stock sample of **2.27** used to generate this datum was analysed by LCMS as part of the QC process. This experiment indicated that the purity of the compound had decreased from 100 % at the time of synthesis to 69 %. This was likely to have been either due to degradation, or the introduction of another compound during handling. Accordingly, **2.27** was resynthesised and its stability in DMSO was monitored by LCMS and ^{1}H NMR for 15 days at room temperature during which time no degradation was observed. The LCMS QC of the new stock sample indicated a purity of 100 %. On retest, the pure sample was found to have a BCATm pIC50 < 3.2, which implied that the measured activity on the first test occasion was due to contamination with an unknown compound.

Interestingly, the X-ray crystal structure of compound **2.27** bound to BCATm (*figure 2.40*) showed that the desired induced π-stacking pocket (as observed for fragment hit **2.3**) was opened and the interaction with Phe-30 was achieved. The observed electron density for the phenoxy group was weaker than for the rest of the molecule and the protein, suggesting that this part of the structure was mobile. This result suggested that the positive enthalpic contribution to binding generated with the added π-stacking, as well as increased binding due to the hydrophobic effect and van der Waals' interactions, may not have been sufficient to compensate for another negative contribution to binding. This result demonstrated that designing compounds using docking techniques cannot always be relied upon to yield increased affinity. Given the synthetic difficulty and poor activity no further work with this connectivity was pursued
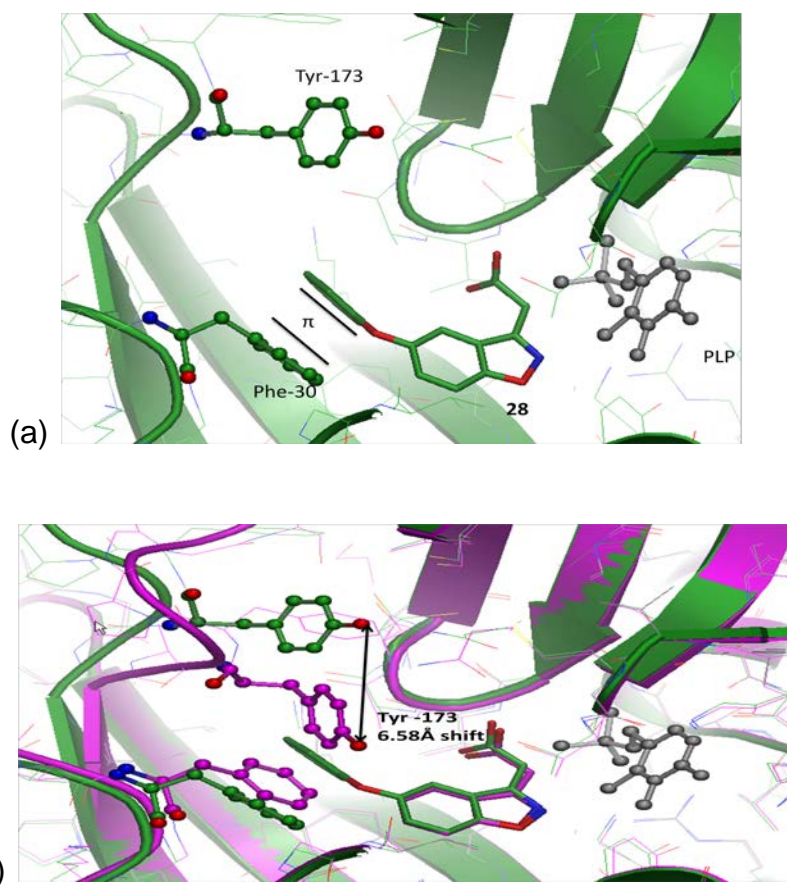
Figure 2.40: (a) X-ray crystal structure of 2.27 with BCATm showing π-stacking interaction with Phe-30; (b) Overlay of 2.27 with fragment hit 2.3 (no phenoxy substituent) showing opening of induced pocket between Phe-30 and Tyr-173.

Summary of core substitutions

A summary of the SAR observed around the benzisoxazole core of hit **2.3** from synthesised and available analogues are shown in *figure 2.41* and the data are shown in *table 2.4*. Compounds **2.39 - 2.47** were synthesised by Charlene Fournier, Industrial Placement Student, GSK under my supervision, using condensation of 4-hydroxy-coumarins with hydroxylamine as described previously in scheme 2.1.
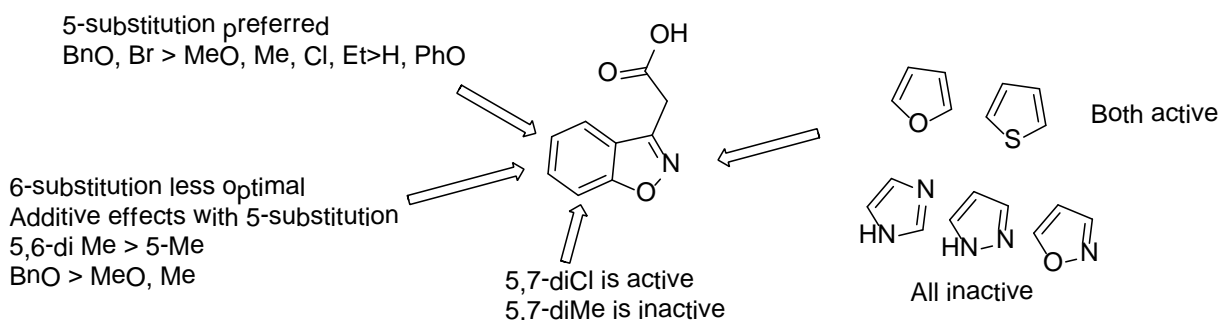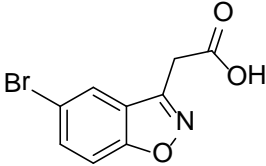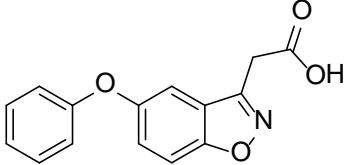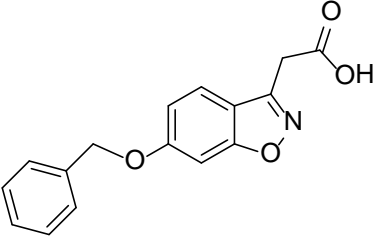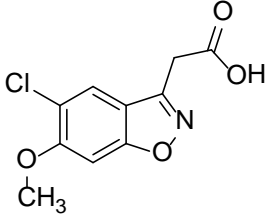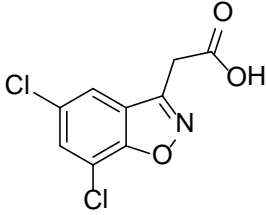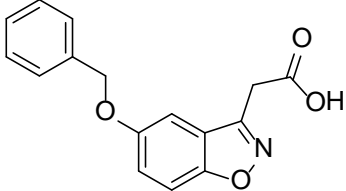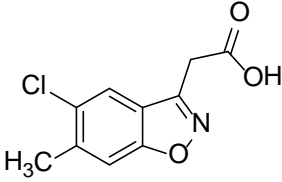
Figure 2.41: SAR summary of analogues of **2.3**

The most potent compound identified was the 5-benzyloxy derivative **2.39** (pIC_{50} = 4.1, LE = 0.27, LLE_{AT} = 0.19). In general, small subsitutents such as chloro and methoxy reflected the modest potencies observed from the analogue searching with other small groups such as methyl. The 6-substitution was generally less preferred for substitution although it could cause subtle effects such as the 5,6-dimethyl compound **2.25** (table 2.2, pIC_{50} = 4.1, LE = 0.38, LLE_{AT} = 0.32) having higher affinity than the 5-methyl analogue **2.24** (table 2.2, pIC_{50} = 3.4, LE = 0.33, LLE_{AT} = 0.31). The 5,6-dimethyl compound **2.25** had the same activity in the assay as the benzyloxy compound **2.42** but achieved this activity with many fewer atoms, hence the significantly higher ligand efficiency values.

There were few examples synthesised with 7-substitution. The 5,7-dimethyl compound **2.46** had a pIC_{50} value of less than 3.2 whilst the 5,7-dichloro compound **2.41** showed modest activity (pIC_{50} = 3.7, LE = 0.33, LLE_{AT} = 0.23).

It was possible to replace the benzisoxazole core with benzofuran or benzothiophene rings to give slightly more potent compounds (table 2.2).

Compound	Structure	pIC_{50}	LE/LLE$_{AT}$
2.33		3.7^a	0.36/0.30
2.27		<3.2	
2.39		3.5	0.23/0.15
2.40		3.5	0.30/0.28
2.41		3.7	0.34/0.23
2.42		4.0	0.26/0.18
2.43		3.3^b	0.30/0.22
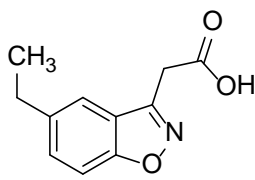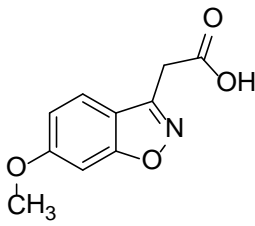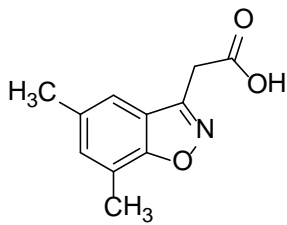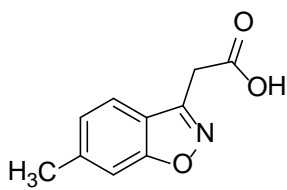
2.44		<3.2
2.45		<3.2
2.46		<3.2
2.47		<3.2

Table 2.4: Results from substituting benzisoxazole core. [a]Compound tested inactive (pIC_{50} < 3.2) on 1 out of 5 test occasions. [b]Compound tested inactive (pIC_{50} < 3.2) on 1 out of 2 test occasions.

The overall conclusions from this area of work were that it was possible to achieve modest activity increases through modulation of the core, but that productive growth in another direction would be required to achieve the high pIC_{50} values required to progress this series further.

Growing from carboxylic acid
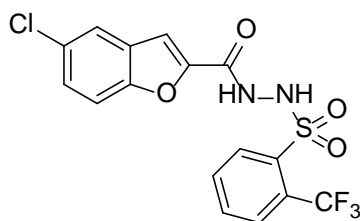
2.2

*Figure 2.42: Chemical structure of published BCATc inhibitor **2.2***

An overlay of fragment hit **2.3** with the published BCATc inhibitor **2.2** [146] bound to the BCATm protein (*figure 2.43*) indicated a potential vector for growth accessible by derivatisation of the carboxylic acid. A set of readilly available amines was used to enumerate virtual amide products from the acid **2.3** and these were docked into the protein pocket observed in the X-ray structure of **2.3** (by Stephen Pickett, GSK). The amides which were found to best overlay with the literature compound **2.2** were selected for synthesis. In general, this docking experiment favoured amides derived from primary amines, with a methylene or ethylene linker to an aliphatic or aromatic ring. Some of the suggested amide products were available in the GSK compound collection and a selection were synthesised from the potent dimethyl benzisoxazole acid **2.25** using standard HATU coupling conditions (*scheme 2.6*).
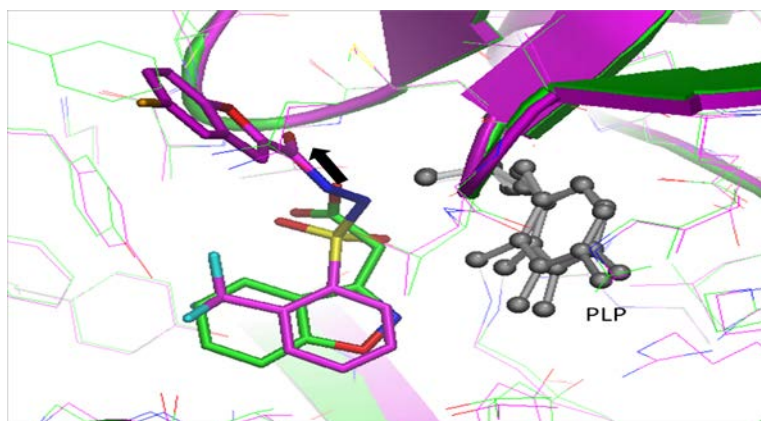
*Figure 2.43: Overlaid structure of **2.3** with **2.2**, showing potential vector for growing **2.3***
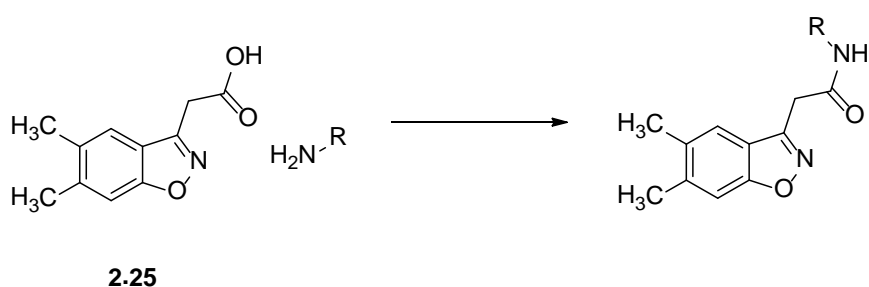
Scheme 2.6: Amide formations. Reagents and conditions: DCM, HATU (2 eq.), DIPEA (3 eq.), room temperature, 24 h, 10 – 79 %.

In total 36 amide derivatives were tested, but only five of these (**2.48** to **2.53**, *table 2.5*) showed any measurable activity in the biochemical assay. (The inactive compounds are shown in Appendix A2.1, table A2.1, compounds **2.54** – **2.83**.) These five compounds had low LE and LLE$_{AT}$ values suggesting that they made sub-optimal interactions with the protein. No clear SAR was established, not helped by the fact that the compounds were close to the limit of detection in the assay. Those which were active did not appear to show any preference for ring size or linker length, over the inactive analogues. The docking in this series was not predictive of improved potency, which may have been due to the protein changing its conformation depending on the actual ligand binding. In this scenario it is likely that a diversity-driven array to explore potential substituents may be the most pragmatic solution when the chemistry is so tractable. This experiment had explored the binding in the top pocket, with a variety of different linker lengths

to aryl or aliphatic rings or alkyl chains. The conclusion from this exploration is that growing in this direction was not fruitful for increasing potency with efficient interactions.
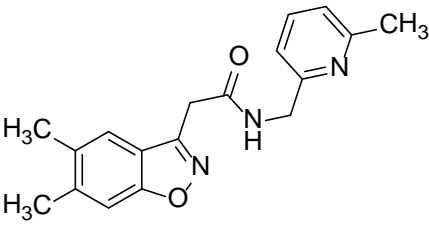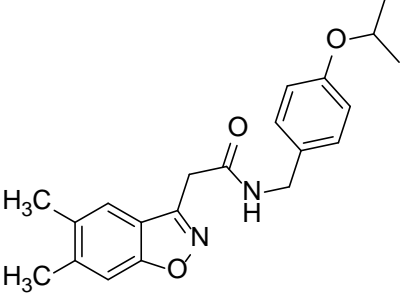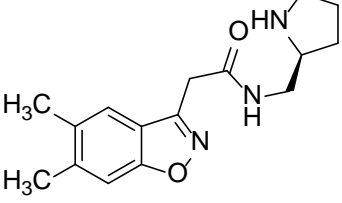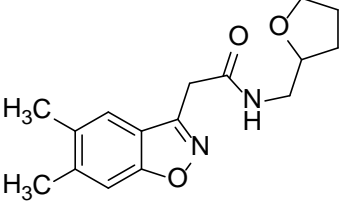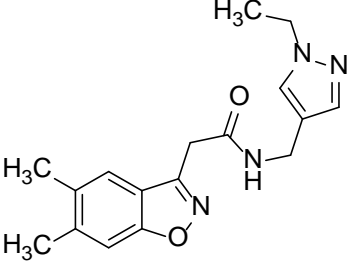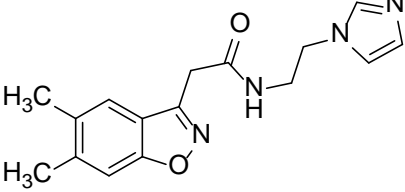
Compound	Structure	pIC_{50}	LE/LLE_{AT}
2.48		3.7	0.22/0.21
2.49		4.0	0.32/0.23
2.50		3.4	0.22/0.22
2.51		3.4	0.22/0.21
2.52		3.4	0.20/0.21
2.53		3.3	0.21/0.25

Table 2.5: Active compound results from amide formations

113

Based on the poor potencies and ligand efficiencies resulting from explorations around hit **2.3**, my recommendation to the team, which was endorsed, was not to pursue further optimisation of this series.

Optimisation of Fragments 2.14 and 2.15

Introduction to initial optimisations

2.13
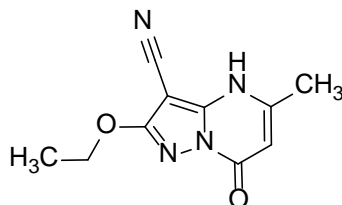
$pIC_{50} = 3.3$,[a] $clogP = -0.21$, 16 heavy atoms

$LE = 0.28$ $LLE_{AT} = 0.41$
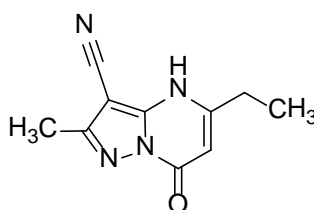
2.14

$pIC_{50} < 3.2$,[b] $clogP = 0.14$, 15 heavy atoms

2.15
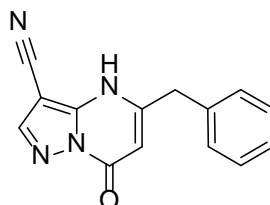
$pIC_{50} = 4.6$, $clogP = 0.77$, 19 heavy atoms

$LE = 0.33$ $LLE_{AT} = 0.39$

*Figure 2.44: Compounds **2.13**, **2.14** and **2.15**. [a]Compound tested inactive ($pIC_{50} < 2.9$) on 1 out of 2 test occasions. [b]Compound tested active ($pIC_{50} = 4.4$) on 1 out of 3 test occasions*

As described in section 2.4 (Fragment Screening Hits), fragment **2.13** was identified as a hit by both T_m and NMR screening, but a co-crystal could not be obtained. Thirteen analogues of compound **2.13**, which were available in

the GSK compound collection, were tested in the biochemical and NMR assays. Seven actives were progressed to crystallography, whence **2.14** and **2.15** afforded liganded crystal structures. These highly ligand efficient compounds were considered excellent starting points for optimisation and this result demonstrated the value that can be derived by carrying out fragment expansion to give more options towards successful crystallography.

Progress with optimisation of compounds **2.14** and **2.15** was expedited when a very closely related compound (**2.84,** *figure 2.45*) was identified by high throughput screening (HTS) of BCATm and gave a liganded structure.
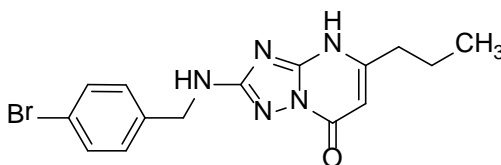
2.84

$pIC_{50} = 6.2$, clogP = 2.42, 22 heavy atoms

LE = 0.39 LLE$_{AT}$ = 0.34

*Figure 2.45: Compound **2.84***

Compound **2.84** had a triazole ring in place of the cyano-pyrazole identified in the fragment hits and had a 3-benzylamino triazole substitutent. HTS hit **2.84** was approximately 10-fold more potent at BCATm than the fragment-derived compounds **2.14** and **2.15**.

The overlaid crystal structures of **2.14** and **2.84** (*figure 2.46*) showed that the binding pocket of the pendant bromophenyl ring in **2.84** was blocked by a methionine side-chain (Met-241) in the fragment structure of **2.14**. This side-chain rotated through 180° to accommodate the larger ligand. This movement had not previously been observed in any other BCATm protein structures and so exploitation of this interaction would probably have been inconceivable by traditional fragment growth techniques.
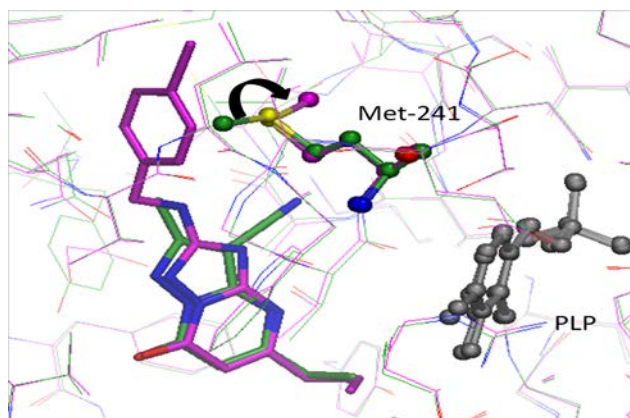
*Figure 2.46: Overlay of cyanopyrazole fragment hit **2.14** with HTS derived triazole **2.84**, showing movement of Met-241.*

One way to test if the core identified in the fragment hit was a more efficient core than the compound identified by HTS was to make a hybrid structures with the cyanopyrazole core from compounds **2.14** and **2.15** with the same substituents found on HTS compound **2.84**. Such compounds were synthesised by Laura Gummer, Industrial Placement student, GSK under the supervision of Rob Young (*figure 2.47)*. Compound **2.85** was approximately 10-fold more potent than the HTS hit **2.84** and had higher ligand efficiency values.
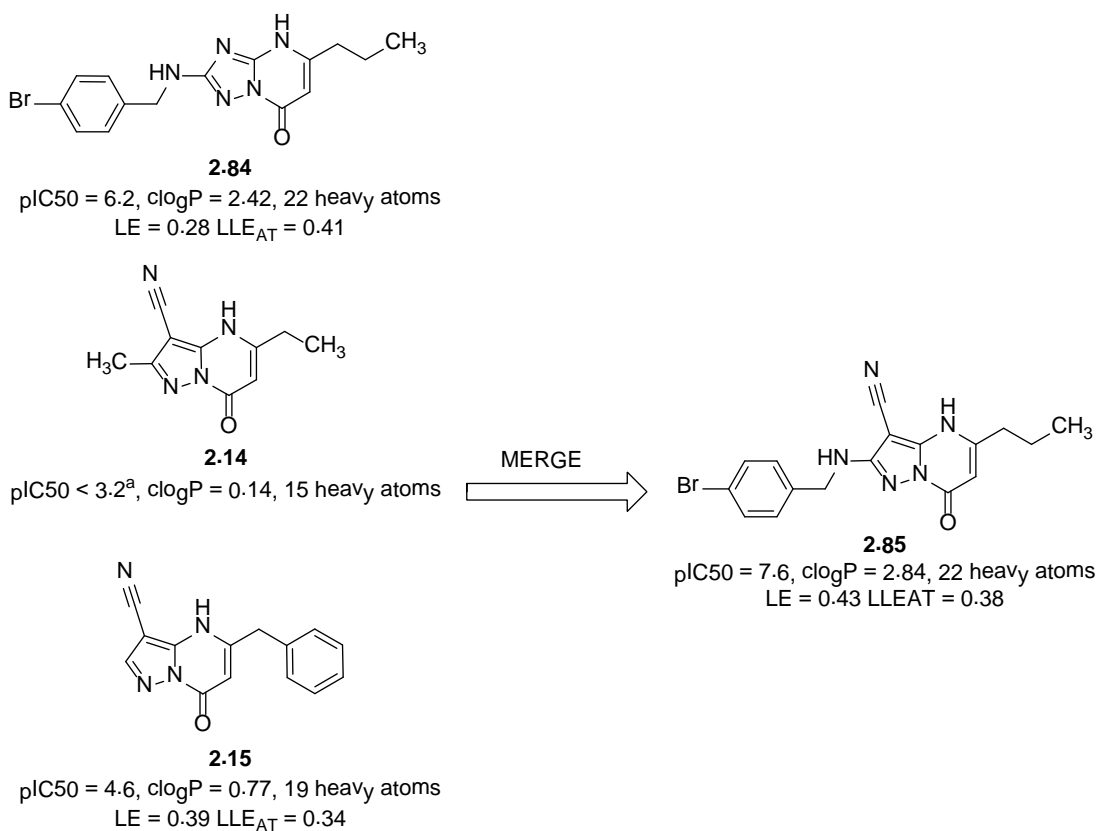
*Figure 2.47: Compound **2.85** derived from merging fragment and HTS-derived hits. [a]Compound tested active (pIC$_{50}$ = 4.4) on 1 out of 3 test occasions.*

This large increase in pIC$_{50}$ derived from replacing the triazole with a cyanopyrazole ring could not simply be rationalised by the addition of hydrogen bonding interactions. The X-ray structure showed the nitrile to be interacting with a backbone NH (Cys-315) but with an angle which was outside of the normal range for an optimal hydrogen bonding contact. X-ray crystal structures of the two compounds were overlaid (*figure 2.48*), showing the nitrile group on compound **2.85** displacing a water molecule which was present when the triazole **2.84** is crystallised**.** An X-ray structure of compound **2.85** was not obtained, but its improved lipophilicity analogue (**2.86**) with the Br replaced by Cl was used to give structural insight.
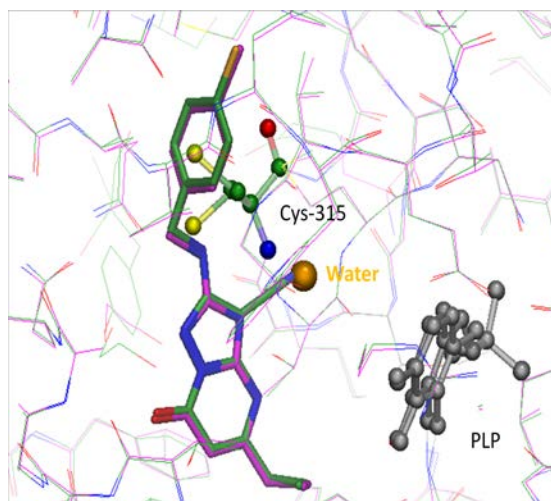
*Figure 2.48: Overlay of HTS triazole **2.84** with fragment-derived cyanopyrazole **2.86** showing displacement of a water molecule*

The increase in activity would indicate that displacing this particular water molecule was energetically favourable. This result was also corroborated computationally using software to generate GRID maps,[135] which aim to identify the areas of a binding pocket which are energetically favoured for the binding of small molecule fragments or 'probes'. When the GRID analysis was carried out on this binding pocket (*figure 2.49*, by Stephen Pickett, GSK) the position where the water was observed experimentally was not indicated to be a favoured position for water molecules. Additionally, hydrophobic probes, such as methyl groups were identified as having a good chance of making productive contacts in this region, which further supported the idea that this water molecule was not in an optimal environment (see introduction section 'The Hydrophobic Effect and Displacing Water Molecules for further discussion).
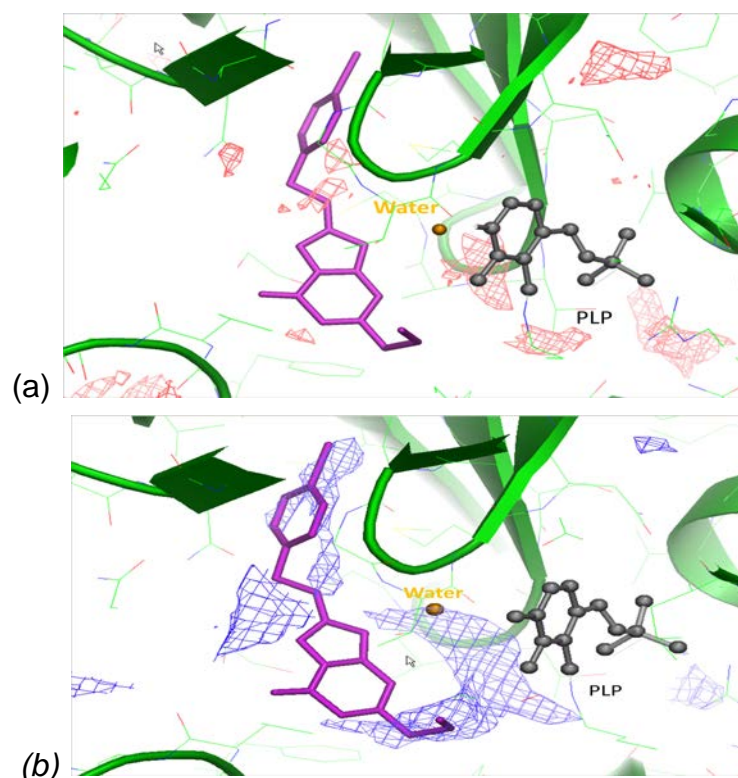
*Figure 2.49: GRID maps around HTS triazole hit **2.84**: (a) Water maps in red do not overlay with experimentally derived water position; (b) Methyl maps in blue do overlay with experimentally derived water position, suggesting that a hydrophobic group in this position may be energetically more favourable than water.*

Based on these initial experiments, optimisation of the cyanopyrazole compounds was carried out by my colleagues Rob Young, Laura Gummer and Yoshiaki Washio. SAR exploration mainly focused on identifying the preferred substituents on the benzylamino group and alternatives to the propyl chain. This optimisation was very successful, identifying several compounds with enzyme pIC_{50} values greater than 7, and activity in a cellular BCATm assay of pIC_{50} greater than 6. The compounds identified also had excellent DMPK profiles in mice: high oral bioavailabilities (> 80 %); low whole blood clearance values (< 1 ml/min/kg); long half-lives (6 - 12 hours); and moderate-high plasma protein binding (96 – 99 %). These properties appear to validate the premise that fragment-derived compounds, if optimised with careful attention paid to physiochemical properties, will result in compounds which have fewer DMPK issues than those derived from other hit finding methods. Chapter 3 will explore how general this result is. At this

stage consequently, the goal of identifying suitable tool molecules to evaluate the *in vivo* effects of BCATm inhibition had been achieved.

Whilst the evaluation of these molecules was ongoing, further optimisation and exploration of the series continued. The aim of this work was to comprehensively explore the SAR of the molecules as well as investigating the effects of altering the physicochemical profiles of the compounds. My work focussed on replacement of the benzylamino group.

Replacement of benzylamino group

A typical part of lead optimisation is to discharge risks associated with particular functional groups. For example, a particular group may need to be replaced in order to circumvent intellectual property concerns or because it was found to have a toxicity risk. As part of the lead optimisation of this cyanopyrazole series, alternatives to the benzylamino group were investigated, which would reduce the overall number of aromatic rings in the compounds. The initial SAR exploration carried out had shown that replacing the propyl chain with phenyl or heteroaromatic rings could increase BCATm potency but that these derivatives containing four aromatic rings generally had poorer aqueous solubility and DMPK profiles than the compounds with alkyl substituents. This observation is consistent with predictions that increasing the number of aromatic rings in a molecule generally has detrimental effects on these properties.[37]

The X-ray crystal structure of compound **2.86** complexed with BCATm (*figure 2.50*) showed that the benzylamino linker passed through a narrow channel into a lipophilic pocket where the substituted aromatic ring fitted snugly. There was very good shape complementarity between the ligand and the protein, both around the linker, and in the pocket occupied by the *para*-substitued phenyl ring. It was challenging to design non-aromatic replacements for the benzylamino group which could be accommodated in this narrow channel and also effectively fill the planar binding pocket of the aryl ring.
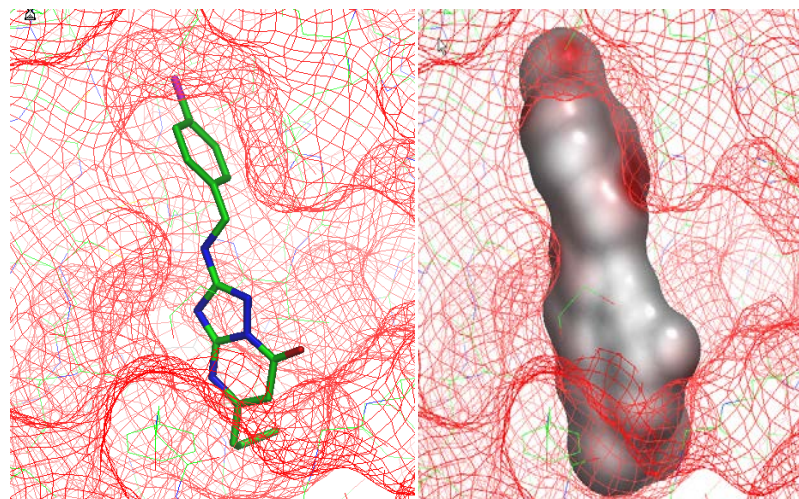
*Figure 2.50: X-ray crystal structure of **2.86** in BCATm, showing stick model of ligand and space-filling representation.*

My design of potential replacements for the benzylamino group yielded structures that were docked into the BCATm active site by Stephen Pickett GSK. The GRID maps were also used to identify potential additional interactions which could be accessed in the linker region.
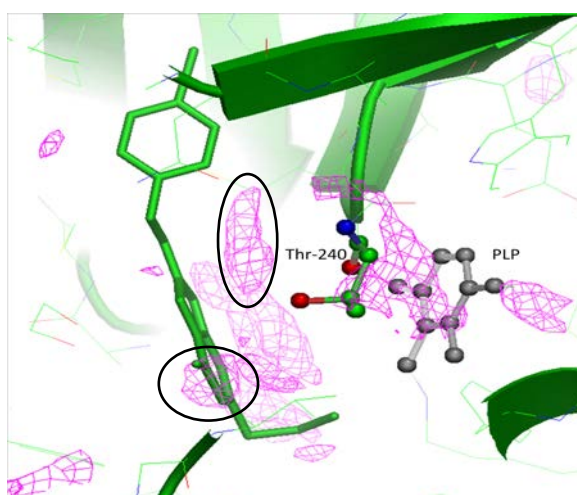
*Figure 2.51: GRID maps around HTS hit **2.84**. The map illustrated areas of density where productive interactions with a carbonyl group would be expected, for example, adjacent to the benzyl amino linker (circled),and an area of density coinciding with the pyrimidinone carbonyl (circled).*

The GRID map with a carbonyl probe superimposed on the bound structure of compound **2.84** (*figure 2.51)* indicated an area of positive density adjacent to the linker region, suggesting introduction of a carbonyl group could potentially yield productive binding. This was due to the proximity to a backbone NH (Thr-240) from which an additional hydrogen-bonding interaction appeared feasible. Additional confidence in the predictions of this GRID map was gained as an area of carbonyl density was predicted overlying with the experimentally observed position of the pyrimidinone carbonyl group.[153] The docking of my virtual compounds with linkers containing a carbonyl group indicated that compounds with cyclic amides of the general structure shown in *figure 2.52* were attractive replacements for the benzyl amino group, based on the favourable orientation of the carbonyl within the GRID map density.
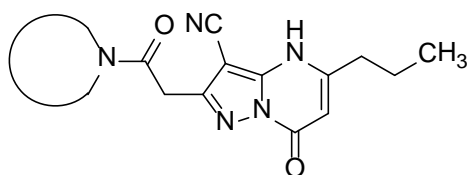
Figure 2.52: General structure of designed replacements for benzyl amino group.

The docking pose of the pyrrolidine amide **2.87** (*figure 2.53*) shows that the amide carbonyl occupied a favourable position to interact with the NH of Thr-240 and that the amide linker held the ring in a relatively flat conformation, allowing the compound to fill the narrow channel and enter the lipophilic pocket. The pyrrolidine ring was not expected to fill the pocket as well as the substituted phenyl ring does. Compounds with five- and six-membered rings were targeted for synthesis to investigate the shape and size requirements of the pocket.
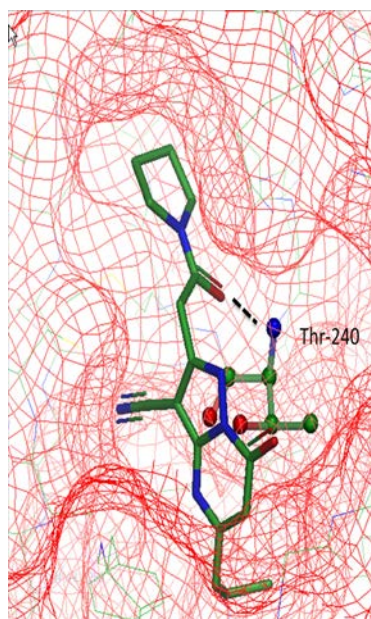
*Figure 2.53: Designed pyrrolidine amide compound **2.87** docked into the BCATm pocket showing potential hydrogen bond with Thr-240 and planar access to llipophilic pocket.*

The synthesis of the targeted amides (*scheme 2.7)* began with the condensation reaction between a β-keto ester **2.88** and commercial aminopyrazole **2.89** to form the pyrazolepyrimidinone core **2.90**. Selective hydrolysis of the alkyl nitrile to an ethyl ester in the presence of an aryl nitrile was achieved using a saturated solution of HCl gas in ethanol.[169] The identity of the product formed (**2.91**) was confirmed by an HMBC signal from the ester carbonyl C (168.8 ppm) to both of the ethyl ester methylene protons (4.14 ppm) and the protons of the methylene adjacent to the ring (3.9 ppm) (by Steve Richards, GSK, see *figure 2.54*). No hydrolysis of the aryl nitrile was observed. The syntheses of test compounds **2.87** and **2.93** were completed using standard ester hydrolysis and HATU amide formation conditions.
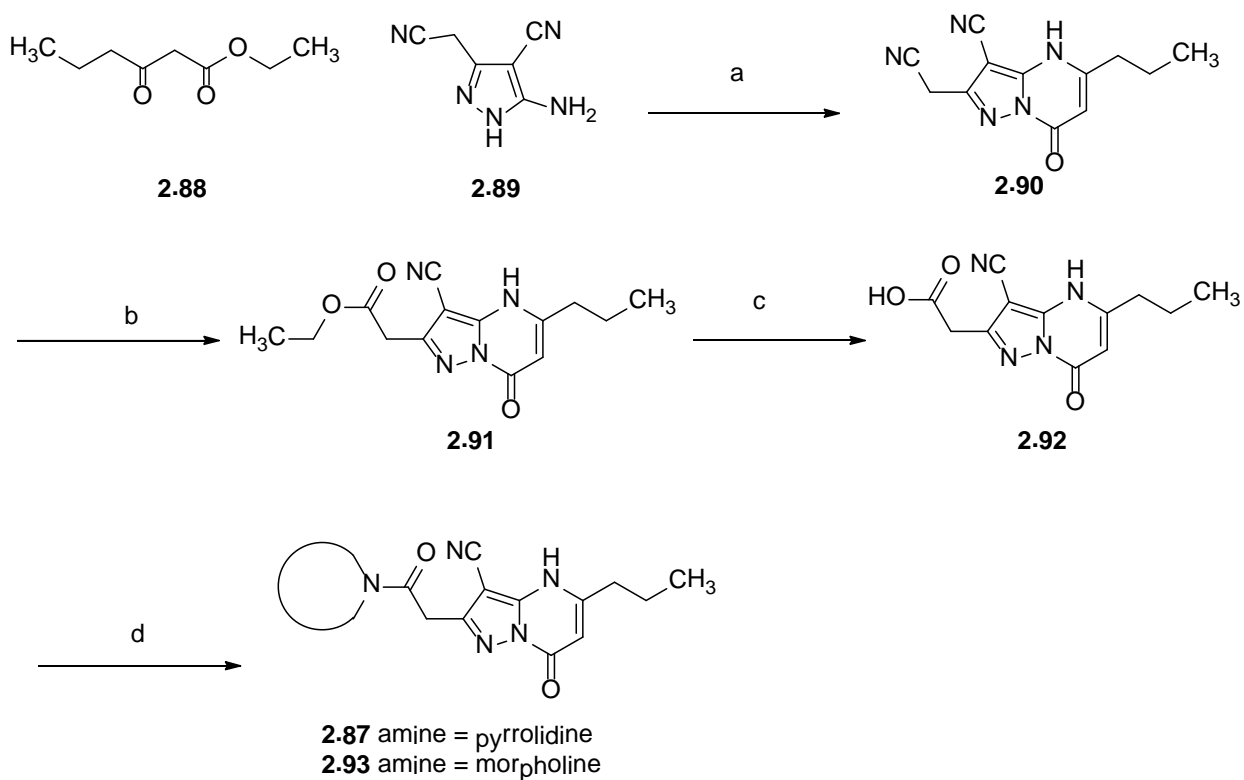
Scheme 2.7: Synthesis of cyclic amide analogues **2.87** and **2.93**. Reagents and conditions: (a) Acetic acid, water, 120 °C, 2 days, 33 %; (b) 1,4-dioxane, ethanol, HCl (g), -30 °C, 2.5 h, 46%; (c) 2-methyltetrahydrofuran, methanol, water, lithium hydroxide(10 eq.), room temperature, 24 h, 55 %; (d) DMF, HATU (1.2 eq.), DIPEA (2 eq.), amine (2 eq.), room temperature 24 h, 57 – 64 %.
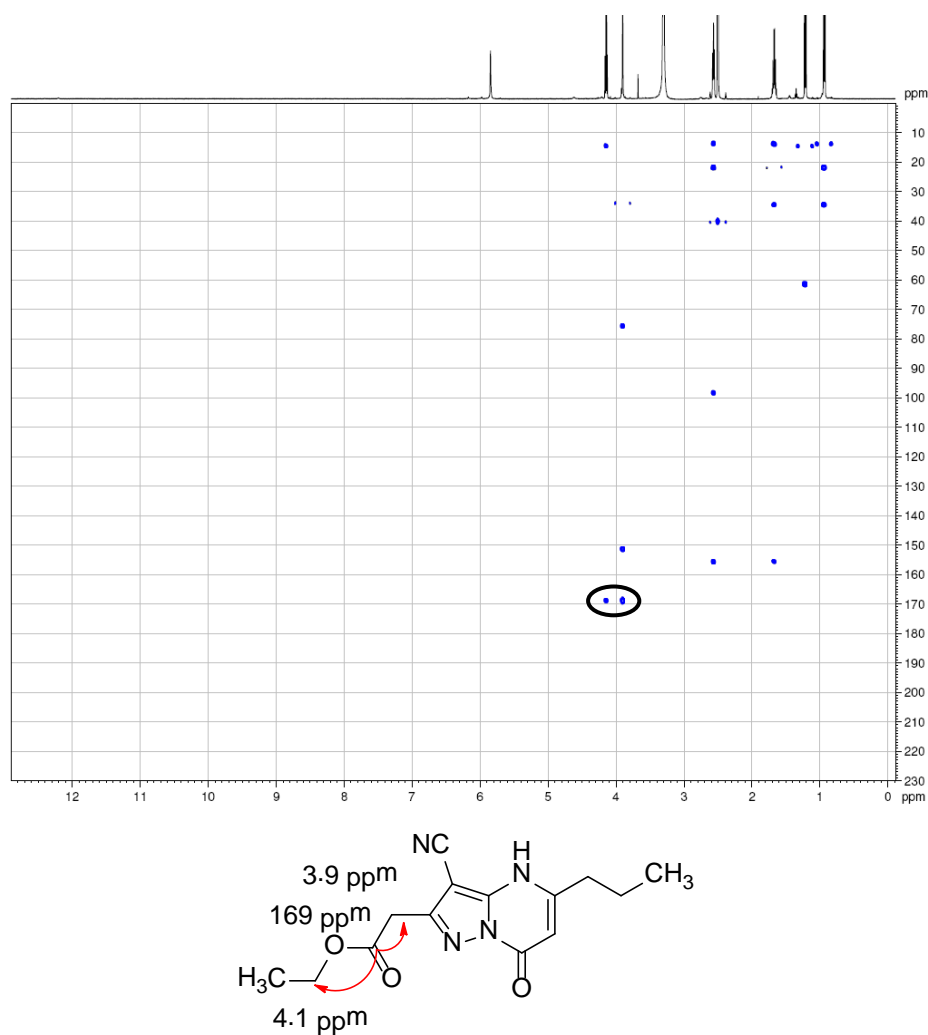
Figure 2.54: Observed correlations in ^{13}C *HMBC Spectrum of* ***2.91*** confirming structure

Each of the two amides synthesised exhibited high pIC_{50} values at BCATm (*figure 2.55*), with pyrrolidine **2.87** approaching the activity levels of the better benzyl amino linked compounds such as **2.85**. The LE and LLE_{AT} values were also high. The LLE_{AT} value for **2.87** was considerably higher than for **2.85,** which reflected the significantly lower clogP value which was obtained by replacing the halogen-substituted benzyl amino group with the pyrrolidine amide.
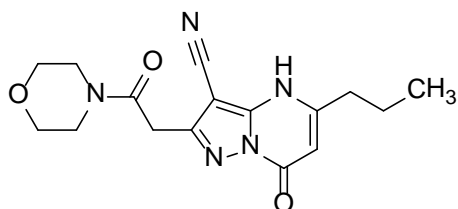
2·93

pIC$_{50}$ 5.1[a], clogP -0.50, 24 heavy atoms
LE 0.29; LLE$_{AT}$ 0.43
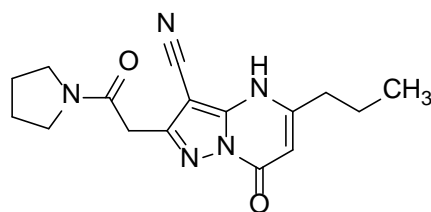
2·87

pIC$_{50}$ 6.3, clogP -0.05, 23 heavy atoms
LE 0.38; LLE$_{AT}$ 0.49

*Figure 2.55: Screening results for amide compounds **2.93** and **2.87**.*
[a] Compound tested n = 1.

An X-ray crystal structure of **2.87** bound to BCATm was obtained (*figure 2.56*), which indicated a binding mode almost identical to the one predicted by the docking experiment, making the hydrogen bonding interaction as desired of the carbonyl with the N-H of Thr-240. In this case, the use of docking was highly predictive of binding mode and was also capable of prioritising compounds for synthesis which would have high enzyme inhibition.
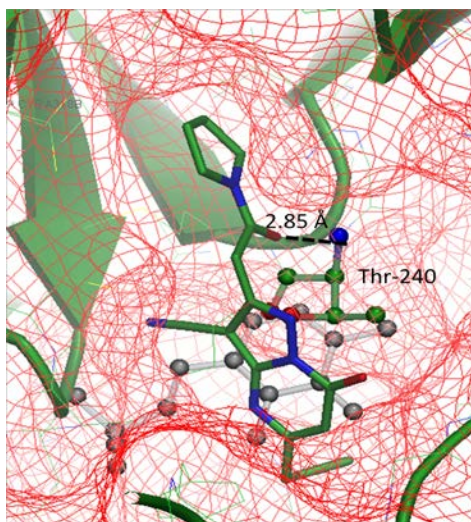
*Figure 2.56: X-ray crystal structure of **2.87** bound to BCATm.*

The crystal structure of the morpholino- compound **2.93** was also obtained (*figure 2.57)* in an attempt to rationalise the 100-fold lower potency at the

enzyme compared to **2.87**. It appears that the morpholine ring's larger size and shape positioned the ring atoms in closer proximity to the protein surface, requiring more flexing of the protein to accommodate it. The carbonyl to N-H hydrogen bonding distance was also slightly longer for this analogue, suggesting that the ligand was unable to adopt a conformation with a favourable hydrogen-bonding vector. This was rationalised by a likely clash of the morpholine ring on moving the carbonyl closer to the backbone NH of Thr-240. The morpholine ring also contained an oxygen atom, which was placed in a relatively lipophilic pocket and not making contact with any hydrogen bond donors. There would be an energy penalty associated with removing this atom from an aqueous solution, where it would be hydrogen bonded to the water molecules, then burying it in a lipophilic region of the protein without making productive interactions, which would also contribute to **2.93**'s lower activity. The presence of the oxygen would also be expected to withdraw electrons away from the amide carbonyl, making it a poorer hydrogen bond acceptor.
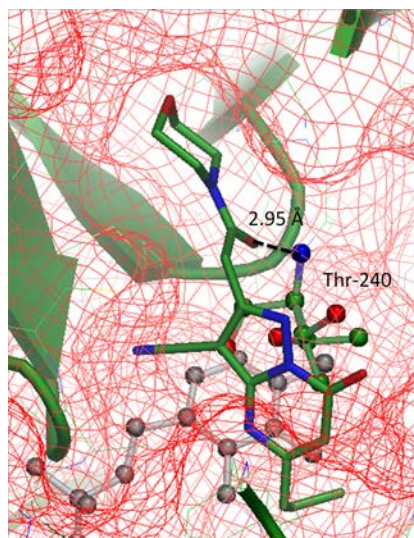
*Figure 2.57: X-ray crystal structure of **2.93** bound to BCATm.*

Compound **2.87** was further profiled to assess its suitability for further progression or SAR expansion (*figure 2.58*), including a cellular BCATm inhibition assay and an *in vivo* DMPK evaluation in mice (carried out by Benjamin Beaufils, GSK). No cellular activity for **2.87** was observed. This

result could be explained by the very low lipophilicity of the molecule, which would be expected to make it more difficult for the compound to cross biological membranes; the measured chromlogD$_{7.4}$ was 0.98: a very low value on this scale, which is typically 2 log units higher than traditional shake flask octanol-water logD measurements.[31]. The low lipophilicity and high fraction of sp^3 atoms of **2.87** contributed to the high measured solubility[39] in aqueous buffer (pH = 7.4) and very low plasma protein binding (PPB). However, the compound also exhibited high whole blood clearance (Clb), a short half-life (T$_{1/2}$) and low oral bioavailability (F%), which combined with the poor cell activity make this particular compound unsuitable for further progression.
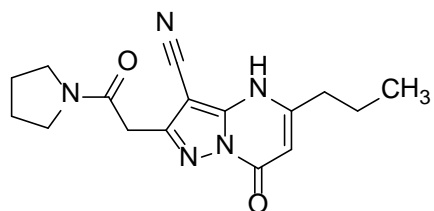
2.87
pIC50 = 6.3
cell pIC50 < 5.0[a]
chromlogD7.4 = 0.98, PFI = 3.0
Solubility from solid = 392 mg/ml
PPB = 40%
Clb = 70 ml/min/kg
T1/2 = 0.2 h
Vdss = 1.2 l/kg
F% = 7%

*Figure 2.58: Data on further profiling of compound **2.87**.* [a] Compound tested n = 1.

The poor DMPK profile of this compound could have been due to its very low logD, as it is likely that a molecule with this profile could have been excreted rapidly by the kidneys, even without enzymatic metabolism (expected to be low given the low lipophilicity). The low logD and high solubility would also limit absorption of the drug across the wall of the GI tract, which could contribute to the low oral bioavailability observed.

One way to address the poor DMPK profile of compound **2.87** could be to increase the lipophilicity of the compound slightly. This could be achieved either by adding lipophilic substituents to the pyrrolidine ring, or by replacing the propyl chain with a more lipophilic group. These ideas will be discussed further in the future work section.

Based on the promising activity observed for compounds **2.87** and **2.93**, further SAR exploration of this series was initiated. For synthetic ease, a set of available secondary amines were selected and coupled to an acid intermediate bearing the triazole core, as a large quantity of the appropriate acid was available. The design of the amine set I selected was primarily driven by the premise of trying to fill the pocket better by adding substituents which would occupy a similar position to the *para*-halogen in the benzylamino series. The synthesis was prosecuted by Charlene Fournier, Industrial Placement student, GSK under supervision by myself and Sophie Bertrand.

The results from this array are given in *table 2.6*. The pyrrolidine (**2.94**) and morpholine (**2.95**) triazolo amides were synthesised to ensure that an SAR benchmark could be set between the cyanopyrazole and triazole series. These two triazolo compounds were approximately 10-fold less active than the corresponding cyanopyrazoles, consistent with previous observations. Therefore, SAR conclusions from this array could be applied to the cyanopyrazole series, in order to further boost any activity/property enhancements. In general, all amines with 6-membered rings were less active in the assay, confirming the observed result for **2.95**. Adding small halogen or methyl substituents to the smaller rings did not give the increase in activity which was expected if a productive halogen interaction was made as with the halo aryls of the benzylamino series. This may be because these substituents were approaching the protein from a chiral sp^3 atom, rather than from the planar phenyl vector available in the benzylamino series. The incorporation of fluorine atoms would also be expected to weaken the amide carbonyl's hydrogen bond to the backbone, which might have reduced the binding affinity of the compounds, especially if the fluorine did not itself add a

specific positive contribution to binding. Aside from morpholine amide, few polar atoms were studied in the lipophilic pocket. The *N*-methyl piperazine compound **2.101** was inactive, which indicated that charged motifs were not well tolerated in this region.
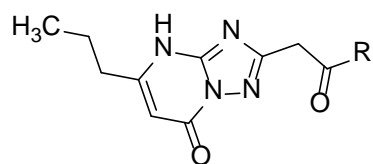
Compound	R	pIC$_{50}$	LE/LLE$_{AT}$
2.94		5.9[a]	0.39/0.56
2.95		4.4 [a]	0.27/0.47
2.96		5.6 [a]	0.38/0.60
2.97		5.2 [a]	0.68/0.61
2.98		5.1	0.30/0.45
2.99		5.2 [a]	0.32/0.46
2.100		5.5 [a]	0.3/0.55
2.101		<4.2 [a]	
2.102		<4.2 [a]	
2.103		<4.2 [a]	
2.104		<4.2 [a]	

Table 2.6: Exploration of amides in triazole series. [a] Compound tested n = 1.

132

2.7 Conclusions and Suggestions For Further Work

In summary, this fragment project delivered potent, cell active inhibitors of BCATm, with good DMPK profiles which allowed target validation experiments to be carried out. This was a significant achievement, given that no inhibitors of this target with sub-micromolar IC_{50} values were previously reported. These results have demonstrated the potential of fragment based drug discovery to quickly deliver candidate-quality molecules.

There were several important factors in achieving this outcome.

- The screening strategy adopted made use of several orthogonal assays, along with iterative screening of available analogues and identified a diverse set of starting points for chemistry.

- The use of structure based design to rationally optimise the fragment hits allowed the binding pocket to be thoroughly explored.

- The synthetic chemistry strategy made use of small arrays where appropriate, along with custom synthesis of designed analogues to test important hypotheses. This allowed definitive decisions to be reached on each series investigated.

- A focus on ligand efficiency values and physicochemical properties during the fragment optimisation resulted in lead compounds which had profiles consistent with good developability properties. These could potentially have size and lipophilicity increased later in lead optimisation, if desired, to improve potency or other properties.
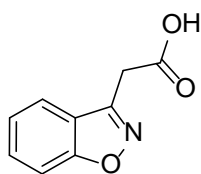
*Fgure 2.61: Fragment hit **2.3***

Several potential vectors for the growth of fragment **2.3** (figure 2.61), or merging with other known ligands, were investigated. This exploration was systematic and thorough but failed to identify any areas where the activity of the compound could be increased in a ligand efficient manner. Therefore, a decision was taken based on all of the data generated to discontinue work in this area. No future work is proposed based on compound **2.3**.
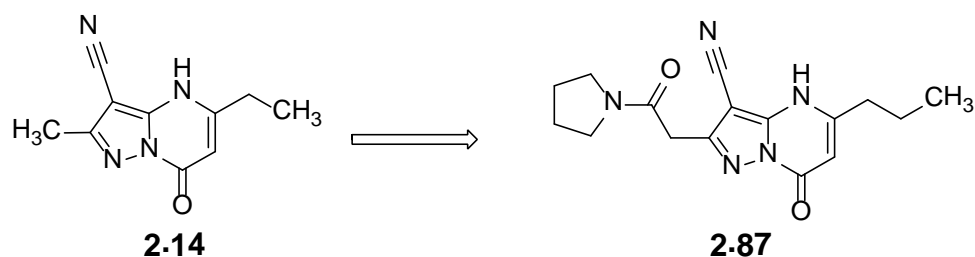
*Figure 2.62: Fragment hit **2.14** and optimised compound **2.87***

Optimisation of the cluster representing compound **2.14** did achieve molecules with profiles which were able to give confidence in experiments that helped to explore target validation and had the potential to become drug candidates. The discovery of the alternative linker in compounds such as **2.87** represented a useful progression in this series. Further work would be required to optimise the DMPK properties in this latter series. Two areas are proposed to address this:

1. Increase logD by replacing the propyl chain with more lipophilic aliphatic and aromatic groups.

R = branched and longer chain alkyls, aryl
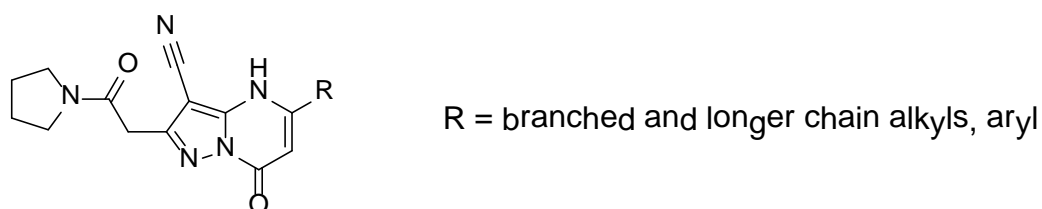
*Figure 2.63: Suggested Optimisation of **2.87** by replacing propyl chain with more lipophilic groups*

2. Substitute the pyrrolidine 3- and 4- positions with groups which could increase lipophilicity. If the pyrrolidine ring is partially unsaturated, or the substituent is a spirocycle then these could also potentially mimic the 4-halogen substituent which has been shown to increase activity in the benzyl amino linked series.

R = Me, Cl, Br   Spirocyclic systems
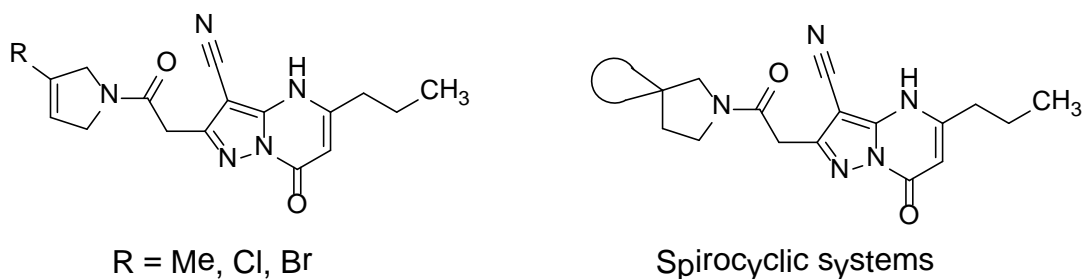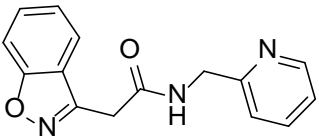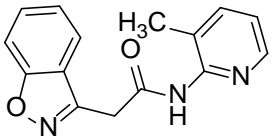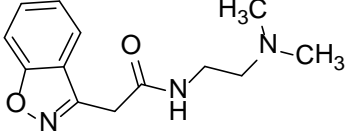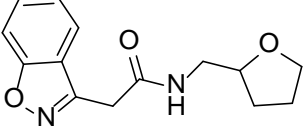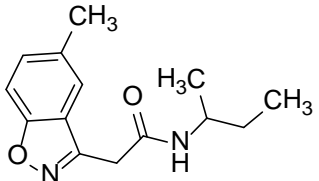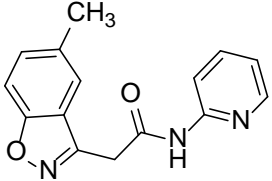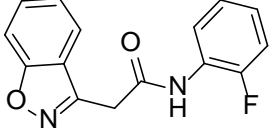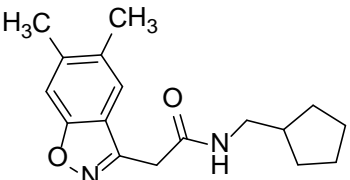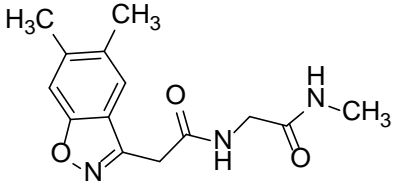
*Figure 2.64: Suggested optimisation of **2.87** by substituting pyrrolidine ring*
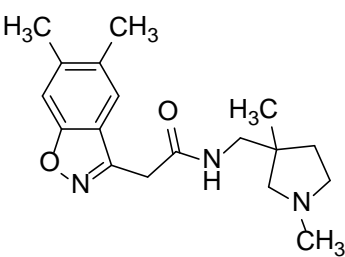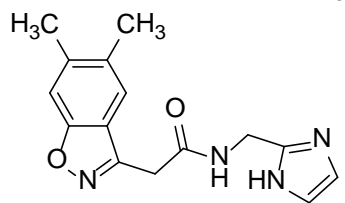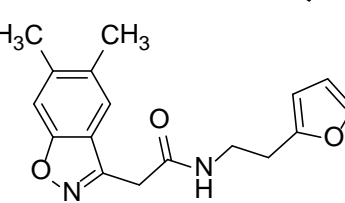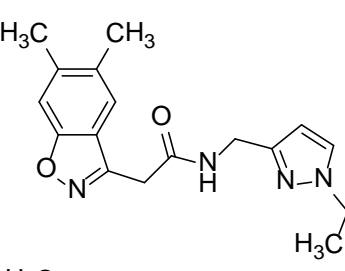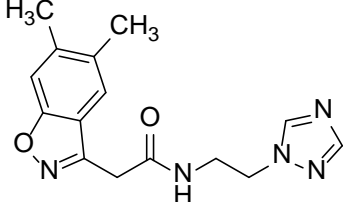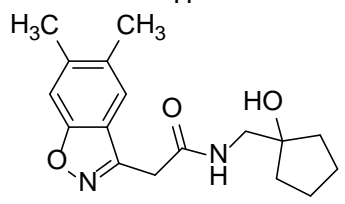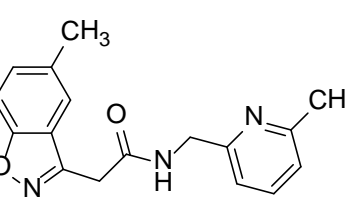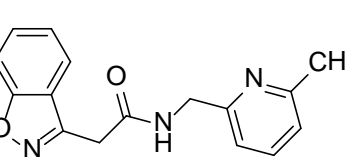
Due to the strategic decision by groups within GSK to discontinue work on this project, it was not possible to put these ideas into practice.

A final area for exploring the conclusions from this work was to compare and contrast the relative success of the fragment based screening effort with other hit finding methods which were used to seek BCATm inhibitors. This analysis examined the relative hit rates between the different hit finding methods used and also investigated whether there are any significant differences in the physicochemical properties of lead molecules generated by the different methods. This analysis is reported in chapter 3.

Appendix 2.1: SAR Tables

Compound	Structure	pIC50
2.54		<3.2[a]
2.55		<3.2
2.56		<3.2 [a]
2.57		<3.2 [a]
2.58		<3.2 [a]
2.59		<3.2 [a]
2.60		<3.2 [a]
2.61		<3.2 [a]

2.62	<3.2
2.63	<3.2 [a]
2.64	<3.2 [a]
2.65	<3.2
2.66	<3.2 [a]
2.67	<3.2 [a]
2.68	<3.2
2.69	<3.2
2.70	<3.2

137

2.71		<3.2
2.72		<3.2
2.73		<3.2[b]
2.74		<3.2 [a]
2.75		<3.2 [a]
2.76		<3.2 [a]
2.77		<3.2
2.78		<3.2

138
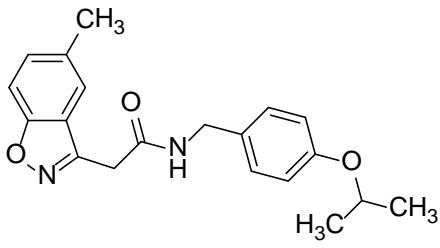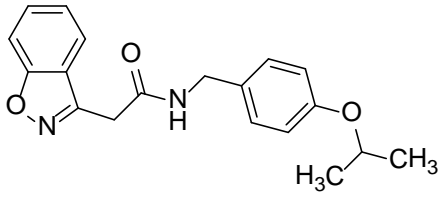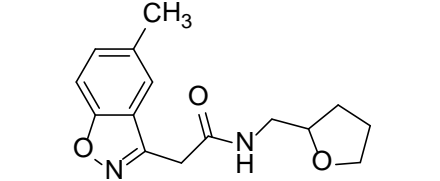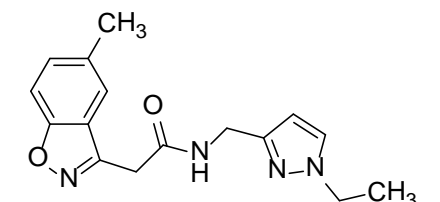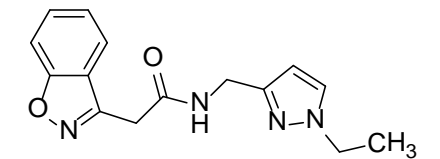
2.79		<3.2 [a]
2.80		<3.2 [a]
2.81		<3.2 [a]
2.82		<3.2 [a]
2.83		<3.2 [a]

Table A2.1: Structures of inactive amide derivatives. [a] Compound tested
n = 1. [b]*Compound tested active (pIC$_{50}$ = 3.4) on 1 out of 2 test occasions.*
*Compounds **2.54** – **2.64** were obtained from the GSK compound collection.*
The remainder were synthesised by me.

3 Comparison of Hit Finding Techniques and their Impact on Progression

3.1 Introduction

This chapter aims to investigate some of the literature claims[78,79] that the use of FBDD techniques in hit discovery and further optimisation provides an advantage in terms of the quality of derived leads, and in the lesser effort required in lead optimisation over other common hit finding techniques. Initially, these questions were challenged by investigating data generated at GSK against a single target, BCATm (chapter 2), comparing FBDD with HTS and ELT screening outputs. Although useful comparisons could be made by examining one target in detail, more general trends were investigated across many organisations and biological targets using a range of hit generation techniques, where direct comparisons were available. A review of known fragment-derived clinical candidates and their predecessor hits was carried out and compared with clinical candidates for the same biological targets discovered by other means, including FBDD, HTS, phenotypic screening and various target based screening of focussed sets, natural products and knowledge based sets.

Previous Studies Quantifying Sources of Medicinal Chemistry Success

The understanding of what underlying trends and practices made drug discovery campaigns was perceived to be key to addressing the very high attrition rates which have been observed in the pharmaceutical industry in recent decades.[7] The discipline of medicinal chemistry can affect the chances of success either in the selection of initial hits for optimisation, or in the optimisation from hits to candidates. Therefore, considerable efforts have been reported in the literature trying to rationalise how medicinal chemistry might become more successful in lead identification and optimisation in attempts to address high attrition rates. It is now well established that the physicochemical properties of potential drug molecules are associated with their chances of progressing through clinical development (see Chapter 1

Introduction for further details). Thus physicochemical profiles of molecules are often used to quantify the likely quality of medicinal chemistry output in the literature. Efficiency metrics (ligand efficiency and lipophilic ligand efficiency) have also been commonly employed to compare the quality of different molecules binding to the same target.[170]

Comparisons of drug molecules with the leads from which they are derived have established that, on average, leads tended to have superior physicochemical properties to the corresponding drugs derived from them.[171] Lead optimisation programmes have generally resulted in an increase in molecular size and lipophilicity as potency, selectivity and DMPK properties are optimised.[171] However, it has also been demonstrated that the fundamental chemical structure is remarkably well-maintained on moving from lead to drug, implying that the defined structure of the lead is important in determining the chemical make-up of the eventual drug.[172] Interestingly, ligand efficiency was shown, on average, to be maintained from lead to drug.[173] These observations have profound consequences for medicinal chemistry as they imply that from the initial identification of a starting chemical structure, the boundaries within which the medicinal chemist is able to work are relatively narrow and so there is limited opportunity to improve the quality of the molecule. An important question arising from these literature analyses is whether the apparent limited structural diversification on progressing from lead to candidate is due to the maintainence of binding interactions, which have not allowed significant scaffold changes without dramatic losses of binding. This assumption could be challenged with an alternative proposition; that the observed historical patterns emerged simply from a conservatism of practice in medicinal chemistry (ie, medicinal chemists only made analogues which were structurally very close to the hit or lead), which could be overcome if researchers were willing to accept higher levels of risk in the initial optimisation phase. This question was explored in more detail in the following chapter (chapter 4), where attempts were made to dramatically improve the physical properties of a hit molecule during optimisation.

The observation that the physicochemical properties of molecules usually show an increase in lipophilicity and concomitant reduction in solubility during lead optimisation has led to a focus on the quality of starting points, with the introduction of the concept of leadlikeness to describe molecules which are smaller and less lipophilic than druglike molecules, leaving room for increases during optimisation.[43,174] Some examples of suggested parameters for defining fragment-like, lead-like and drug-like are given in *table 3.1*. The bounds of these terms have been subject to some debate and refinements, but the general principle that molecules become larger, more lipophilic, and have increased numbers of donors and acceptors on moving from fragment to lead to drug has been documented in several puclications.[42,43,46,72]

Fragment-Like Congreve 'Rule of 3'	Lead-Like Hann and Oprea	Drug-Like Lipinski 'Rule of 5'
MW ≤ 300	MW ≤ 460	MW ≤ 500
clogP ≤ 3	-4 ≤ clogP ≤ 4.2	clogP ≤ 5
HBD ≤ 3	$logS_w \geq -5$	HBD ≤ 5
	RTB ≤ 10	HBA ≤ 10
	HBD ≤ 5	
	HBA ≤ 9	
	Ring ≤ 4	

Table 3.1: Literature suggested properties for fragment-like[175], lead-like[174] and drug-like[32] chemical space.

Morphy noted that the nature of the biological target is very important in determining the physicochemical profile of hits and leads.[45] For example, comparison of around 1600 optimisation programmes revealed that peptidic GPCRs, transferases and nuclear receptors on average had much higher molecular weight and clogP ligands than ion channels, monoamine GPCRs and transporters.[45] This is an important caveat to consider when comparing different hits and leads; to have meaningful conclusions it is necessary to make comparisons between molecules acting at the same targets.

An analysis was published by Keserü and Makara which attempted to explore the impact of hit-finding methods on the properties of the derived hits and leads.[73] There are some caveats which must be considered when

examining the conclusions of this paper. Firstly, the paper aimed to compare hits and leads, which were identified as such within medicinal chemistry publications. However, these terms (especially lead) are subject to qualitative interpretation and may be used to mean quite different levels of optimisation by different organisations. Therefore, leads in different publications may not represent a useful comparison to one another as they will all represent a different point on the optimisation pathway between hits and clinical candidates. A second issue with this analysis is that the authors did not make their comparisons between molecules acting at the same biological targets. This was partially addressed by a detailed comparison of ligands against a single target (BACE-1). Nonetheless, this paper reached some very interesting general conclusions, which acted as a basis for further investigation.

The major comparison between HTS hits with other hits (including fragment-derived, natural product and virtual screening approaches) showed that the HTS hits had physicochemical properties that were on average worse than starting points from other sources. However, there were few observed differences after lead optimisation. Lead molecules had similar average molecular weights regardless of screening source and non-HTS derived leads were found to have only slightly lower logP values than HTS-derived leads. Ligand efficiency data indicated some potentially important observations. The average LE of HTS leads was higher than non-HTS leads. However, the LELP[73] (a measure of lipophilic ligand efficiency, = logP/LE) was lower for fragment and natural product leads than for HTS leads, suggesting that HTS leads make less effective use of polar atoms. The authors therefore suggested that fragment and natural product screening could be considered to produce more attractive starting points than HTS. These conclusions were supported again with an additional data set[176], where fragment leads were shown to have lower LELP values than HTS leads, and that leads which resulted in marketed drugs had lower average LELP values than either of these sets.

Another important publication by Leeson and St.-Gallay compared the effects of organisational factors on the outputs of medicinal chemistry.[48] This paper compared the properties of structures included in patents filed by a range of drug-discovery companies and importantly, made direct comparisons between particular targets. The average clogP value differed by 0.95 log units between the best and worst practitioners and the average molecular weight differed by 69 Da when the comparisons were corrected for biological targets (*figure 3.1*). The authors attempted to quantify the impact of fragment-based research by comparing patented structures from Astex, a company specialising in fragment screening to large pharmaceutical companies, which were assumed to have carried out most hit identification by HTS. They noted marked differences between the two sets of compounds, with the Astex compounds having significantly better physicochemical properties. Their conclusions were that (i) there appeared to be a significant quality emphasis for medicinal chemistry teams in different organisations and (ii) that there was an indication that higher quality molecules emerged from fragment screening and optimisation, based on the Astex data.
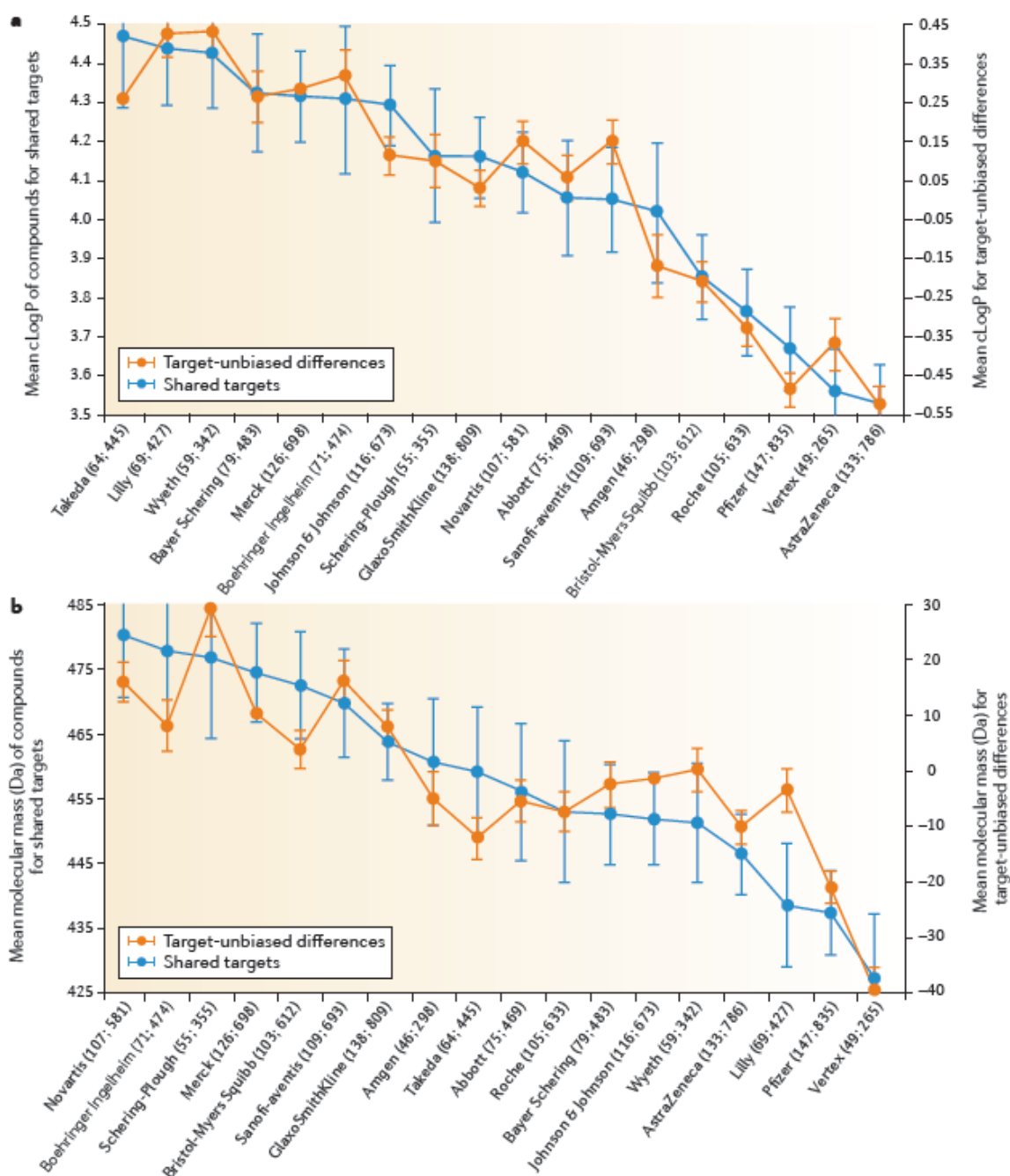
Figure 3.1: Differences in (a) mean clogP and (b) mean molecular mass for patented compounds at a range of companies. The orange lines represent target-unbiased values and the blue lines represent values corrected for shared targets. Reproduced with permission from reference [48]

The work described in this chapter aimed to further explore trends, akin to these published analyses to try to further substantiate the implications of hit-finding techniques on medicinal chemistry optimisations, with a particular focus on the impact of FBDD.

3.2 Results and Discussion

BCATm Hits to Leads Optimisations from Different Screening Techniques

As described in chapter 2, an FBDD approach was used to identify hit and establish lead molecules for BCATm. Concurrently, GSK also carried out BCATm screening by HTS and encoded library technology (ELT, see chapter 1 introduction for more details of this technique). Therefore, the data generated from these efforts represented a useful and unique case to examine the relative advantages and disadvantages of each of these three methodologies.

In order to compare these techniques, all of the data for compounds tested in the BCATm project were extracted from the GSK data repository and SMARTS[177,178] were used to define different sub-structural classes, which were annotated according to screening origin (FBDD, HTS or ELT). Stephen Pickett, GSK assisted with defining the SMARTS strings. The substructures selected for the analysis were those for which significant hits to leads chemistry was carried out, and are shown generically in table 3.2. To allow a reasonable comparison between the techniques, only those series derived from FBDD which achieved an optimised $pIC_{50} \geq 5$ were considered. The data were then visualised using the TIBCO Spotfire™[179] software and differences between the screening methodologies were interrogated for patterns and trends in numbers of compounds synthesised, physicochemical properties and efficiencies.
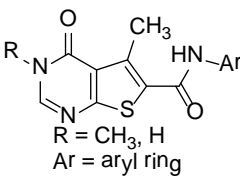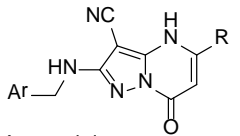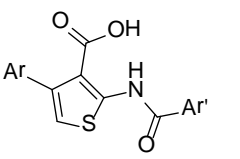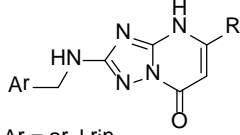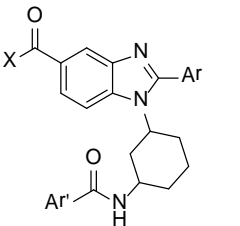
Series	Structure	Lead?	Issues	BCATm pIC_{50} for lead	DMPK for lead
FBDD Series 1	$R = CH_3$, H; Ar = aryl ring	No	Potency, DMPK (short $t_{1/2}$, high Cl_b, low F %)	n/a	n/a
FBDD Series 2	Ar = aryl ring; R = alkyl chain or $(CH_2)nAr$	Yes		7.8	F % = 47 %, $t_{1/2}$ = 6.8 h, Cl_b = 0.63 ml/min/kg, V_{dss} = 0.35 l/kg
HTS Series 1	Ar, Ar' = aryl ring	Yes		7.6	F % = 56 %, $t_{1/2}$ = 5.7 h, Cl_b = 5.9 ml/min/kg, V_{dss} = 1.9 l/kg
HTS Series 2	Ar = aryl ring; R = alkyl chain or $(CH_2)nAr$	No (but closely related FBDD lead)	Potency	n/a	n/a
ELT Series	$X = CH_3NH$ or OH; Ar, Ar' = aryl ring	Yes		6.6	F % = 10 %, $t_{1/2}$ = 1.4 h, Cl_b = 23 ml/min/kg, V_{dss} = 1.3l/kg

Table 3.2: Summary of series from different techniques for which significant hits to leads chemistry was carried out

There were two series explored for FBDD and HTS and only one series investigated for ELT (*table 3.2).* Note that the FBDD and HTS screens detected structurally similar molecules, which were ultimately merged as described in chapter 2. One lead was identified for each technique. In this context, a lead was defined by the programme team, for which some lead

optimisation chemistry was pursued. The HTS and FBDD-derived leads had similar pIC_{50} values and good DMPK profiles, suitable for progression to *in vivo* experiments. However, the lower clearance and longer half-life of the FBDD-derived lead molecule was considered by the project team to confer an advantage for chronic dosing experiments, and so only this lead was progressed to these studies. The ELT-derived lead was approximately 10-fold less potent and had a less optimal DMPK profile, with lower oral bioavailabilty, higher clearance and shorter half-life than the leads found from the other screening techniques. These data illustrated that even within a single project at a single research organisation, the definition of what might constitute a lead molecule could vary greatly and so comparisons between these must be treated with some caution.

	FBDD 2 series 1 lead generated	HTS 2 series 1 lead generated	ELT 1 series 1 lead generated
Total number of compounds	356	378	162
Number of pIC_{50} > 5 compounds (%)	190 (53 %)	146 (39 %)	114 (70 %)
Number of pIC_{50} > 5 compounds with LE > 0.3 (%)	163 (46 %)	123 (33 %)	8 (5 %)

Table 3.3: Number of compounds synthesised by screening technique

Table 3.3 shows a summary and comparisons between the synthetic effort required to evaluate each of the series, as measured by the number of compounds synthesised. One lead was identified from each screening technique, so from this initial measure it could be considered that the techniques were equally successful in terms of optimisation required. In the case of HTS and FBDD, 2 series were pursued in hits to leads chemistry to identify 1 lead series, whereas 1 series was investigated from ELT. The average number of compounds synthesised per series to move from a hit to lead was roughly similar.

Next, the frequency of synthesised compounds exhibiting enzyme potency above a threshold was examined. ELT-derived molecules were found to have pIC_{50} values above 5 in 70 % of cases. This could be due to the fact that the ELT screening methodology contains a large number of similar analogues, and so hit confirmation chemistry is carried out using already partially optimised substitution patterns. Interestingly, this high level of SAR understanding did not shorten the synthetic effort required to identify a lead molecule. In the case of this project, initial hit molecules from ELT were highly potent but had poor DMPK properties (high clearance and low oral bioavailability), so the bulk of the synthetic effort in hit to lead optimisation was focussed on addressing these DMPK issues. For HTS, only 39 % of the synthesised compounds exhibited high enzyme potency. However, the initial hits had again exhibited high enzyme potency and much of the hit to lead synthetic effort was focussed on improving their DMPK properties. Perhaps because the SAR was less well understood at the outset of chemistry, this resulted in a higher proportion of weakly active and inactive compounds. The FBDD generated compounds represented an intermediate position, with 53 % of synthesised compounds displaying an enzyme pIC_{50} greater than 5. In the case of the FBDD hit to lead effort, the majority of the synthesis was focussed towards improving enzyme potency. The initial hits were, as expected, extremely weak inhibitors and the optimisation was strongly driven by hypotheses from structure-based design. The focus on structural rationale for design of molecules in FBDD should account for the higher success rate in synthesising potent compounds.

The ligand efficiency of each series was also compared (see Chapter 1 Introduction for a discussion of ligand efficiency metrics). In this comparison, ELT performed very poorly, with only a handful of the synthesised compounds displaying desirable levels of ligand efficiency, i.e. above 0.3. In contrast, the majority of the potent compounds synthesised in both HTS and FBDD screening were also ligand efficient. The poor performance of ELT against this measure could be attributed to the inherent size of the molecules, which mutli-cycle construction of the very large combinatorial

libraries from which they are derived would dictate. It has been shown that as the complexity of a given ligand increases, the chances that an unfavourable clash with the protein host increases,[66] and so this would be expected to give rise to poor ligand efficiency for more complex molecules. It could be argued that an inherent advantage of FBDD is that by building up lead molecules iteratively from small, weak, but ligand efficient starting points, the derived leads should maintain ligand efficiency; by targeting and exploiting polar interactions good physicochemical properties should be achievable for molecules of comparable enzyme potencies. It was important to explore this question by examining the optimisation processes for this target in more detail and then also to investigate how general this result might be, by looking at other targets.

Comparison of Physicochemical Properties of Hits and Leads from Different Screening Techniques

In the following analyses, comparing the physicochemical profiles of the compounds from the different techniques, only those compounds with an enzyme pIC_{50} greater than 5 were considered. This restriction ensured that the FBDD hit compounds, and close analogues, which would be expected to have very desirable properties but very poor activity, were not preventing a meaningful like-for-like comparison with the compounds from the other methods.
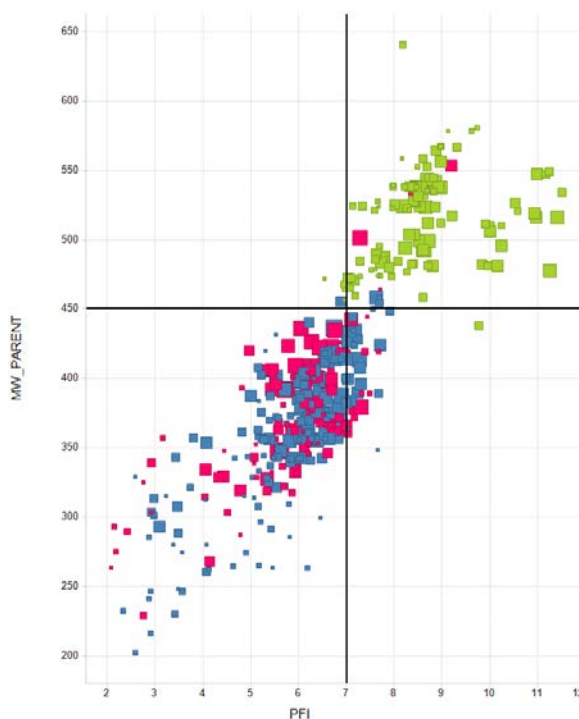
Figure 3.2: Plot of molecular weight against measured PFI comparing different hit finding techniques. The spots are coloured by technique: HTS (pink), FBDD (blue) and ELT (green). The spots are sized by BCATm enzyme potency: larger spots represent more potent molecules. Reference lines are shown for desirable values of molecular weight 450 and PFI 7.

When molecular weight and PFI[31] (ChromlogD$_{7.4}$ + number aromatic rings, see Chapter 1 Introduction) were examined (*figure 3.2*), a clear pattern was apparent between molecules synthesised as ELT hit analogues and those for the other two techniques. It is striking that all of the ELT molecules were found outside of the desired area of physicochemical space defined by molecular weight and PFI, whilst the HTS and FBDD compounds fell largely within it. Interestingly, no statistical difference was observed when comparing HTS and FBDD derived structures.

These data trends were also visualised using box plots (*figure 3.3* and *3.4*) (see *Appendix 3.1* for a detailed description of these plots). The box plots confirmed that for FBDD and HTS both the median and mean values for molecular weight and PFI were very similar to one another, and that the ELT compounds were occupying a distinct area of physicochemical space.

	HTS	Fragment	ELT	Alpha level = 0.05
Count	146	190	114	Root MSE = 48.995
Median	363.39	362.345	521.41	sqrt(2)q* = 3.326
Outliers	3	3	1	
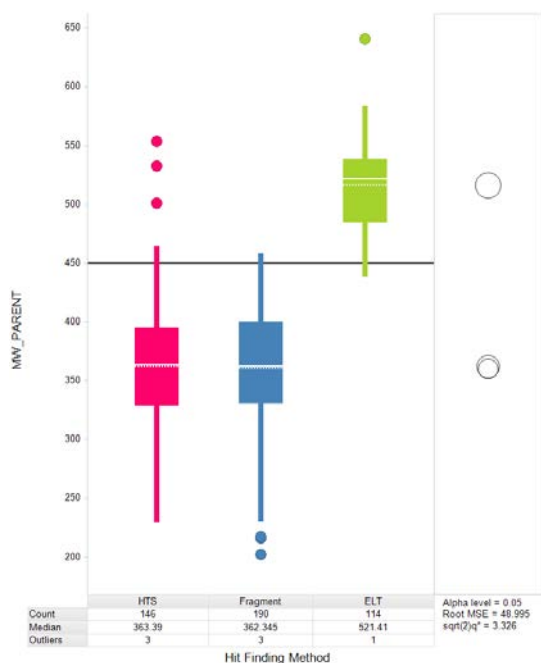
Figure 3.3: Box plot showing molecular weight values comparing different hit finding techniques. The boxes are coloured by technique: HTS (pink), FBDD (blue) and ELT (green). A reference line is shown for a desirable value of molecular weight 450.

	HTS	Fragment	ELT	Alpha level = 0.05
Count	113	174	110	Root MSE = 1.225
Median	6.09	6.035	8.515	sqrt(2)q* = 3.327
Outliers	10	11	10	

Figure 3.4: Box plot showing measured PFI values comparing different hit finding techniques. The boxes are coloured by technique: HTS (pink), FBDD (blue) and ELT (green). A reference line is shown for a desirable value of PFI 7.
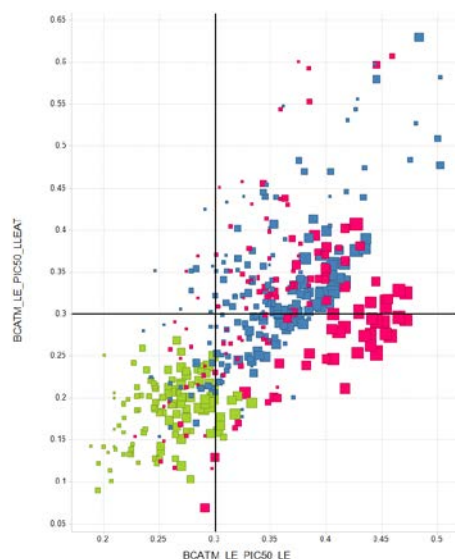
Figure 3.5: Plot of LLE$_{AT}$ against LE comparing different hit finding techniques. The spots are coloured by technique: HTS (pink), FBDD (blue) and ELT (green). The spots are sized by BCATm enzyme potency: larger spots represent more potent molecules. Reference lines are shown for desirable values LE and LLE$_{AT}$ 0.3.

When LE and LLE$_{AT}$ were compared (*figure 3.5*), the clearest pattern observed was that ELT-derived compounds mostly fell outside of desired efficiency space, whereas HTS and FBDD derived compounds mostly occupied the >0.3 area for LE. When examining lipophilic efficiency, the FBDD and HTS compounds appeared to separate, with the FBDD compounds showing superior lipophilic efficiencies. This observation concurs with the conclusions of Keserü and Makara, who also found that on average across many targets, FBDD derived leads had better lipophilic efficiencies than HTS ones.[73]
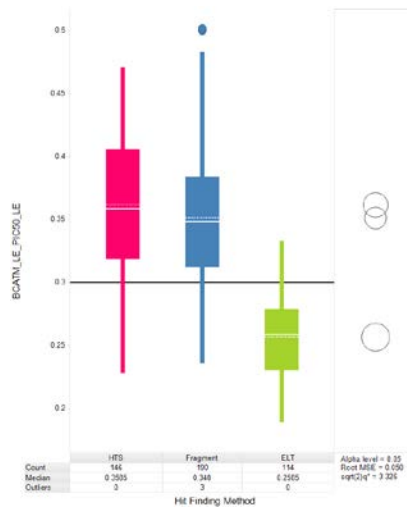
Figure 3.6: Box plot showing LE values comparing different hit finding techniques. The boxes are coloured by technique: HTS (pink), FBDD (blue) and ELT (green). A reference line is shown for a desirable value of LE 0.3.
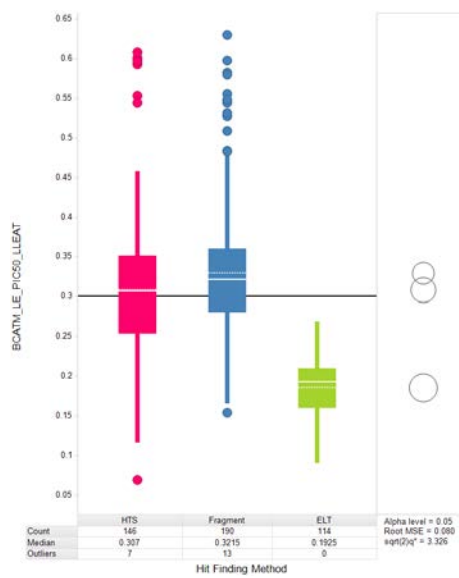
Figure 3.7: Box plot showing LLE$_{AT}$ values comparing different hit finding techniques. The boxes are coloured by technique: HTS (pink), FBDD (blue) and ELT (green). A reference line is shown for a desirable value of LLE$_{AT}$ 0.3.

The box plots of the efficiency data (*figures 3.6* and *3.7*) confirmed that the average efficiency values for ELT were significantly different to FBDD and HTS for both of the measures used. However, the overlapping circles between HTS and FBDD for both efficiency measures confirmed that the differences were not statistically significant.

An analysis of the measured aqueous solubility of the molecules was also carried out to determine whether there were any patterns which could be observed for this important determinant of a molecule's chances of successful development.
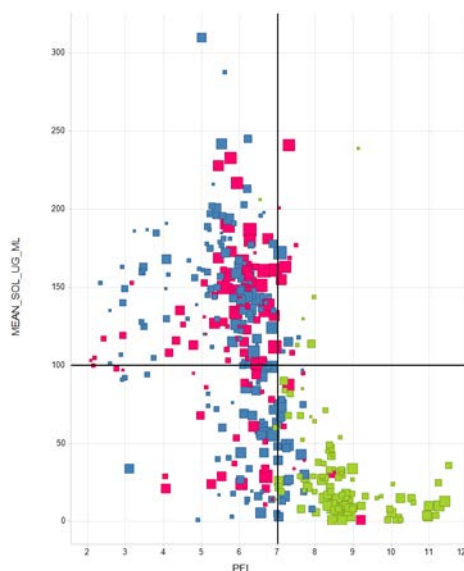
Figure 3.8: Plot of measured solubility (µg/mL) against measured PFI comparing different hit finding techniques. The spots are coloured by technique: HTS (pink), FBDD (blue) and ELT (green). The spots are sized by BCATm enzyme potency: larger spots represent more potent molecules. Reference lines are shown for desirable values solubility 100 µg/mL and PFI 7.
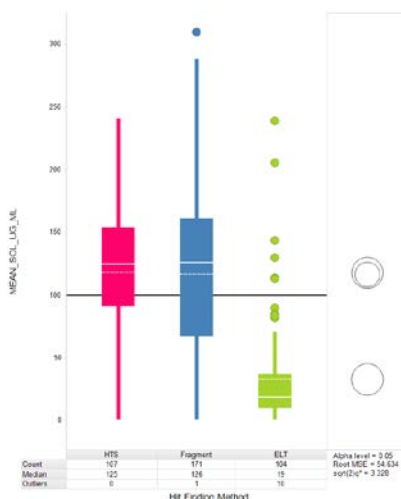
Figure 3.9: Box plot showing measured solubility values comparing different hit finding techniques. The boxes are coloured by technique: HTS (pink), FBDD (blue) and ELT (green). A reference line is shown for a desirable value of solubility 100 µg/mL.

Figure 3.8 shows a plot of the measured solubilities of the molecules as plotted against the measured PFI. This data confirmed that for all of the molecules studied the reported trend[31] of lower solubility being associated with high PFI was confirmed. The ELT compounds all had high measured PFI and low solubility. The HTS and FBDD compounds had more desirable properties, with the FBDD compounds occupying the extremes of low PFI and high solubility. The box plot (*figure 3.9*) once again confirmed that the ELT molecules were significantly distinct from the HTS and FBDD molecules. The average solubility values for HTS and FBDD compounds showed a strong overlap, although the data extended into a higher solubility range for the FBDD compounds than for HTS.

Comparison of Evolution of Properties During Optimisations for Different Screening Techniques

The analyses described so far sought to interrogate the average properties of all of the molecules synthesised during the course of the project. However, drug discovery seeks to identify one single candidate molecule. The properties of molecules used to delineate SAR are not necessarily important if they help the medicinal chemistry team to move along a trajectory towards

a candidate molecule. Therefore it would be instructive to examine the trajectory of the optimisation process over time to understand if and how the hit-finding method plays a role in facilitating progress towards a candidate-like molecule.
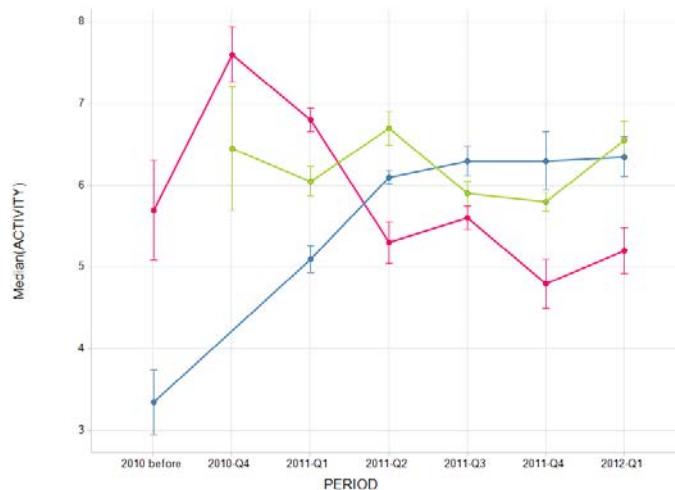
Figure 3.10: Median pIC$_{50}$ of synthesised compounds over time (with error bars showing the standard error for more details of statistical techniques see Appendix 3.1). The lines are coloured by technique: HTS (pink), FBDD (blue) and ELT (green).

When the median pIC$_{50}$ of synthesised compounds was examined over the time period of the optimisation (*figure 3.10*), some interesting observations were made. The median pIC$_{50}$ of ELT compounds was high when chemistry began and continued to be maintained at a similar level. As discussed above, this screening methodology by definition tests many molecules with the same sub-structure, so the SAR could be explicit from the initial screen. In the case of this project, the chemists optimising these compounds had a good understanding of how to achieve enzyme inhibition within this series and focussed most of their synthetic effort in trying to optimise DMPK, specifically high clearance, while maintaining activity. In the case of HTS-derived molecules, extremely potent molecules were quickly identified. The chemistry team was again focussed on improving clearance, which often resulted in a reduction in enzyme potency. The FBDD compounds displayed a quite different profile, as would be expected. The initial hits were weakly active and the chemical optimisation gradually produced more and more active

compounds, arriving at a potency level similar to the ELT compounds. In this case, the chemistry team did not need to invest significant effort in DMPK optimisation, as the compounds which resulted from potency optimisation were found to have very good DMPK profiles. This outcome was postulated to be due to the chemistry team rigidly controlling the physicochemical properties of the molecules during optimisation, which resulted in optimised compounds with a higher probability of successful progression.

Some interesting potential trends arose from these observations. Might achieving good DMPK be more likely if potency is optimised using an FBDD based approach where close attention is paid to ligand efficiency and optimised compounds contain the minimum chemical framework required for a given level of activity? If so, is it easier to optimise potency or DMPK? Is the best starting point a hit that requires significant effort to build potency or a potent hit which requires DMPK optimisation? These strategic questions could be fundamental to improving the discipline of medicinal chemistry and were considered again in chapter 4 using the example of a single optimisation.

Figure 3.11: Median LE (top) and LLE$_{AT}$ (bottom) of synthesised compounds over time (with error bars showing the standard error). The lines are coloured by technique: HTS (pink), FBDD (blue) and ELT (green). A reference line is shown for a desirable value of LE and LLE$_{AT}$ 0.3

On examining evolution of efficiency metrics over the course of optimisation (*figure 3.11*), some interesting trends were observed. An opinion often expressed by practitioners of FBDD is that the efficiency of a given chemical series is relatively fixed and can be very difficult to improve.[180] This concept is used to triage by ligand efficiency when selecting hit series to begin

working on. In the plots shown above, this seems to be the case for the ELT series, where both LE and LLE$_{AT}$ began low and remained at a similar level throughout the optimisation process. In the case of the FBDD series, the LE of the initial starting points was maintained at a similar level throughout the optimisation. However, the lipophilic efficiency was initially very high, but dropped (to a still quite acceptable level) as a cost of enhancing potency. This was consistent with key polar interactions that the molecules made with the protein being already present in the hit molecule and that most of the potency gains in optimisation were due to additional lipophilic interactions. If this result was general, it would have implications for how best to select fragment hits for optimisation. If potency increases are more easily added through lipophilic interactions then the importance of LLE$_{AT}$, or another lipophilic efficiency measure in selecting hits for optimisation would be the key criteria. The HTS series displayed a different profile again. The initial LE of the hit was high, but this dropped as less potent molecules were synthesised during SAR exploration and DMPK optimisation. The LLE$_{AT}$ value was maintained at a similar level throughout the optimisation.
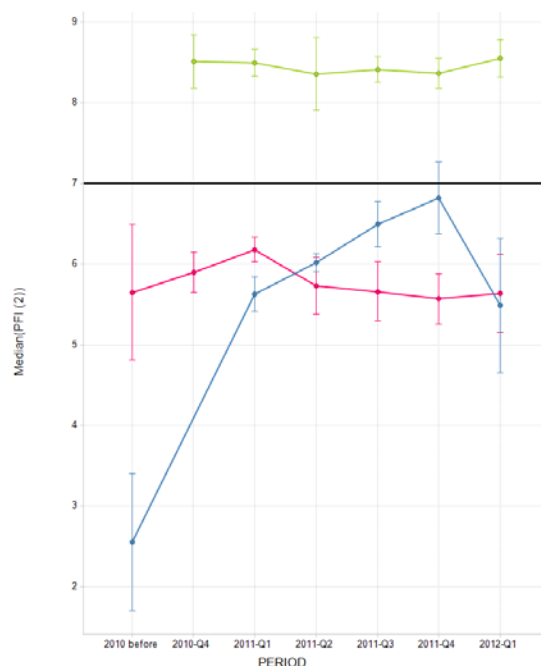
Figure 3.12: Median measured PFI of synthesised compounds over time (with error bars showing the standard error). The lines are coloured by technique: HTS (pink), FBDD (blue) and ELT (green). A reference line is shown for a desirable value PFI 7.

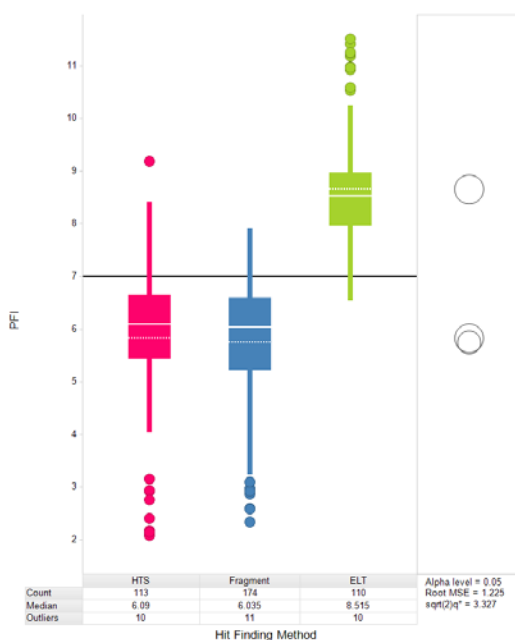When the measured PFI values were studied (*figure 3.12*), they were shown to display a similar pattern to the LLE_{AT} plot. This is not surprising, as both metrics contain a measure of compound lipophilicity. The ELT molecules had very little change in properties during optimisation. FBDD compounds became more lipophilic and increased in PFI as potency was optimised, whilst HTS compounds maintained similar PFI values throughout optimisation.

An alternative strategy for understanding the hit to lead journey would be to study the properties of all of the synthesised compounds and how these compare to the starting hits and final leads (*figure 3.13*)
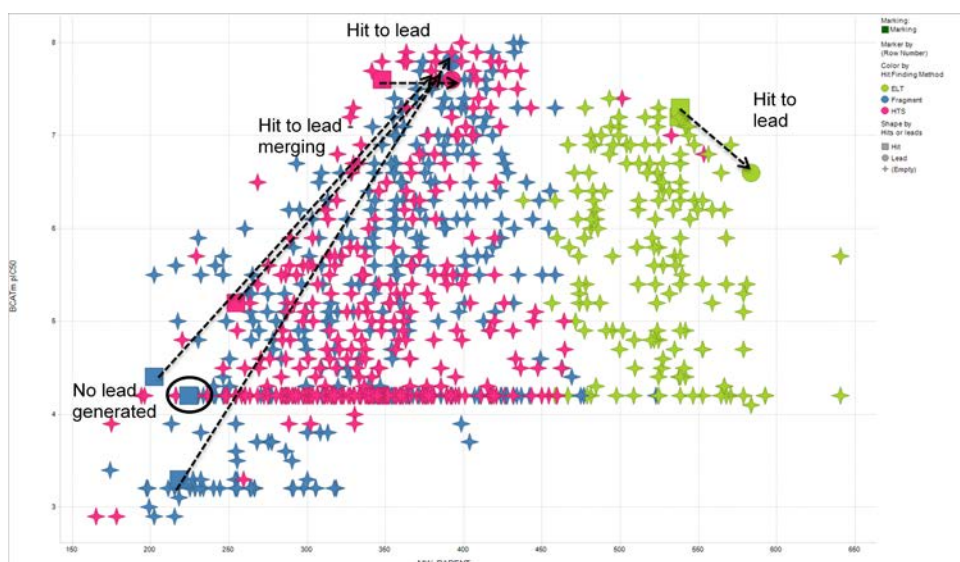
Figure 3.13: Plot of pIC$_{50}$ against measured molecular weight comparing different hit finding techniques. The spots are coloured by technique: HTS (pink), FBDD (blue) and ELT (green). The spots are shaped by status of compound: hit (square), lead (circle), other compounds synthesised during optimisation (cross).

The original hits and leads are marked on *figure 3.13*, along with all of the compounds which were synthesised during optimisation. For the ELT series, the initial hits identified were two of the most potent molecules in the series. This is a commonly observed outcome for ELT, as has been discussed earlier. All of the other green points shown represent compounds which were subsequently synthesised in an attempt to optimise clearance. The obtained lead molecule, which had an improved DMPK profile, had lower enzyme inhibition and was a larger molecule than the starting point. For the HTS series, it can be seen that the hit and lead molecule were very similar. However, a significant synthetic effort was required to identify the one molecule which demonstrated similar activity with an improved DMPK profile from the hit. The FBDD optimisation showed the expected potency increase. There were 2 related fragment hits and a similar HTS hit which were merged to provide the lead molecule shown. The optimisation of this series mainly focused on improving potency, in an atom efficient manner. The optimised molecules were found to have the most suitable profile of all three leads to be used in a chronic dosing animal model, despite the similar potency profile to

the other leads. All three optimisation campaigns required similar synthetic effort in terms of number of compounds synthesised to reach a lead. Therefore it seems difficult to answer the question of whether potency or DMPK are more easily optimised. However, the fact that the FBDD lead had the most preferred DMPK profile, and was the compound progressed furthest along the project's critical path, suggested that despite a significant synthetic effort, the DMPK profile could not be as fully optimised for the other two leads. In effect, the FBDD lead was of a higher quality for further advancement than the other leads. Therefore from these data, it may be concluded that a superior overall profile resulted from investing a similar chemical effort in optimising potency than in optimising DMPK.

Comparison of Hits to Candidates Optimisations from Literature Sources

Although the detailed analysis described above provided some potentially interesting observations about the outcomes of different screening approaches on one project, there are a number of issues associated with making generalised conclusions on this basis. The analysis was only associated with a single screening target, BCATm, but prosecuted at 3 different sites within a single research organisation, and so the observed trends should be regarded with some caution if broader learnings are required. The advantage of using this approach was that access to all data gathered in the same assays for each compounds synthesised was feasible, which is not usually the case when examining literature data. However, it was believed that it would be instructive to perform some similar analyses on publically accessible data, which would have different strengths and weaknesses for analysis. Although literature data are often snapshots and incomplete data sets are often presented, they provide opportunities to make comparisons across multiple targets and multiple organisations.

Since the definition of a lead molecule is open to interpretation, and being defined differently in different organisations, at different times and on different targets, it was decided to conduct a literature review that would compare only

declared clinical candidates. As a clinical candidate must pass some regulatory approval before being tested in human subjects, it was assumed that all clinical candidates had undergone significant levels of optimisation.

To generate a list of candidates identified by fragment screening, a 2012 review by Erlanson, which published a list of 17 fragment-derived clinical candidates was used as a basis for this excercise.[181] The targets of these 17 candidates were then mined in the Pharmaprojects™[182] database to identify additional candidates, discovered using other modalities. For clinical candidates which had multiple targets (mostly kinases) in Pharmaprojects™ the summary information in the database was used to identify a major target. This effort generated a list of 120 clinical candidates in total against 13 distinct biological targets.

To research how each candidate was discovered, structure searches in SciFinder™[183] identified relevant publications, describing hit finding methods and optimisation processes.[184-231,232-241] The hit finding methods encompassed screening protocols based on FBDD, HTS, knowledge based, focussed screening, phenotypic screening and natural products. Many of the clinical candidates investigated had few details published and so these compounds had 'unknown' recorded as hit finding method in the data file and were thus considered for the purposes of this analysis as an average candidate for any given target, against which the hit finding methods could be compared.

There were some adjustments needed to the initial list of FBDD candidates published by Erlanson.[181] The candidates Linifanib,[194] SNS-314,[209] LP-261[238] and AUY-922[190] were all classified by Erlanson as stemming from an FBDD approach but the medicinal chemistry papers did not corroborate this. Therefore, the classification was changed to reflect the approaches described in the papers. Candidate LY-517717 had no literature found in the SciFinder™ search describing its identification. It was unclear how this compound was identified as FBDD by Erlanson but this classification was retained. For candidate LEE-011 (an additional candidate identified in the

Pharmaprojects search for CDK candidates) no medicinal chemistry publication was identified but it was presumed that FBDD was the hit-finding method as it was developed at Astex (an FBDD specialist research company). Finally, for PLX-5568 no structure was found and so this compound was removed from the input list of FBDD-derived candidates.

Where no pXC_{50} was available from a medicinal chemistry paper, the Aureus™[242] database was searched to determine if the pXC_{50} was recorded anywhere in the published literature. Ceara Rea, GSK carried out the Aureus™ database search. The SciFinder™ searches by structure were also used to identify the earliest published patent exemplifying the candidate structure. The number of compounds exemplified in this patent was recorded to investigate whether this value could be used as a measure for the synthetic effort required to develop a clinical candidate in each case. All of the literature mining described was carried out between January and March 2014 and represented literature published between 1980 and 2014.

A data file was generated including the name, structure and pXC_{50} of the clinical candidate in each case, along with the biological target, company name and name, structure and pXC_{50} of the hit and annotation of the hit finding method, if disclosed. To this were added calculated physicochemical properties of each structure identified, including molecular weight, clogP, PFI and fraction of sp^3 atoms. The LE, LLE and LLE_{AT} values were also computed. The data in Pharmaprojects™ were also used to record the stage of clinical development the candidate had reached and whether its development was still ongoing or had been halted. All of the data generated were visualised and analysed using TIBCO Spotfire™ software.

Comparisons of Physicochemical Profiles of Hits and Candidates from Different Hit Finding Techniques

The data were interrogated to try to identify any trends or patterns associated with the different hit finding methods, e.g. did different sources lead to clinical candidates with different physicochemical profiles? As some of the hit finding

methods had very few, or sometimes only one clinical candidate for each biological target, statistical analyses of the data set were not meaningful. Therefore, no statistical quantification of the data was possible, so conclusions drawn below are based on observed patterns.

The initial analysis compared different physicochemical properties of the candidates to understand if the hit finding method resulted in candidates with different properties. A typical outcome is shown in *figure 3. 14* for calculated PFI.
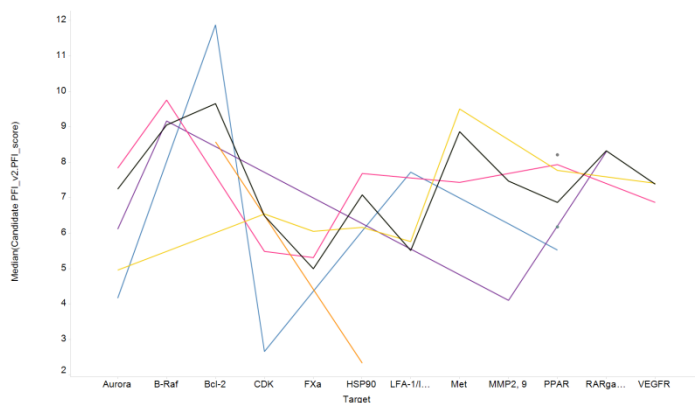
Figure 3.14: Median calculated PFI of clinical candidates against different targets. The lines are coloured by technique: unknown (black), FBDD (blue), focussed screening (purple), HTS (pink), knowledge based (yellow) and natural product (orange).

Figure 3.14 shows a comparison of the resulting PFI values of clinical candidates by hit finding technique for a range of targets. The FBDD candidate for Bcl-2 had the highest PFI of all compounds shown in the plot, but in other targets FBDD generally led to candidates with lower than average PFI. Out of the 11 targets examined, the FBDD candidates had lower PFI than the black line representing the typical candidate in 8 cases. This effect was much more marked against some targets (eg aurora, CDK and LTA4H), where there were several PFI units difference than for others (e.g. Factor Xa and MMP2 and 9). The HTS candidates tracked closely with the black line, which could be explained by the fact that many of the unknown hit finding methods represented by this line would have been HTS. None of

166

the other hit finding techniques appeared to show any particular patterns with PFI.

A similar analysis was carried out for other physicochemical properties. The results are summarised in *table 3.4* and the corresponding data plots are shown in *Appendix 3.2*.

Property studied	Figure Number	Conclusions
PFI	3.14	FBDD resulted in lower values than average in 8 out of 11 targets
clogP	A3.3	FBDD and HTS both lower than average
Molecular weight	A3.4	No differentiation for most techniques, knowledge-based higher than average
Fraction sp^3	A3.5	FBDD higher than average for 6 out of 11 targets

Table 3.4: Summary of comparisons of clinical candidates from different hit finding techniques

In general, only the FBDD-derived candidates were shown to have a pattern towards improved physicochemical properties when studied across a range of different measures of molecule quality. However, given the currently available data, these trends were not quantifiable. The clinical candidates with the poorest overall properties (Bcl-2 candidates Navitoclax[210] and ABT-199[219]) were discovered by FBDD at Abbott, which is an indication that medicinal chemistry practice is also a very important factor in contributing to the properties of candidates. This is also demonstrated by the fact that there are high quality candidates (e.g. PF-4217903 for Met[241]) discovered by HTS, which generally appeared to identify few candidates with attractive physicochemical properties.

Comparisons of Optimisation Journeys from Hits to Candidates for Different Screening Techniques

As well as investigating the properties of clinical candidates discovered by different techniques, it would also be useful to investigate how the optimisation journeys compare by screening method. An important caveat to consider when examining these data is that the work described in the literature was likely to be a selective snapshot of the medicinal chemistry optimisation and will not contain all of the details of work carried out. Therefore, it would not be possible to complete an analysis as detailed as that which was presented for BCATm at GSK. Nonetheless, it is possible to draw comparisons between identified hits and leads and to infer from these some indications of the likely optimisation trajectories. The only hit finding techniques for which there were sufficient numbers of hit and candidate pairs published to allow meaningful comparisons to be made were FBDD and HTS, so all analyses which follow focus on comparing these two techniques.

A typical analysis is shown for ligand efficiency, in *figures 3.15* and *3.16*.

FBDD:
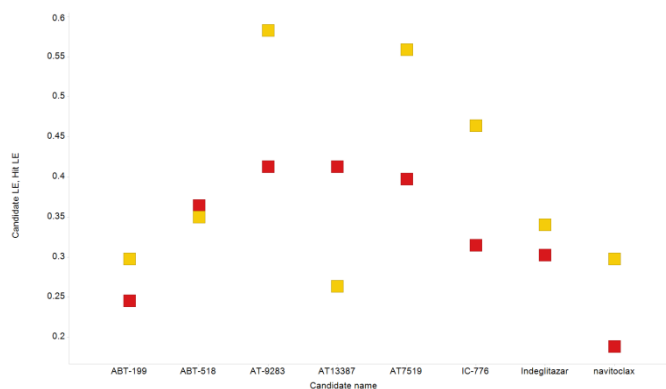
HTS:
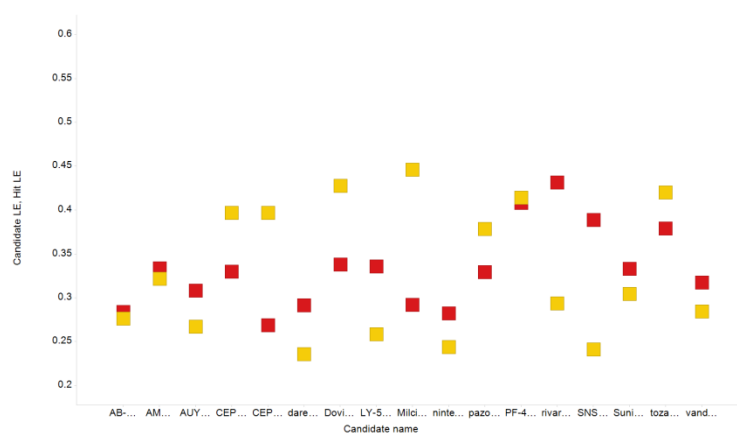
Figure 3.15: Comparison of hit (yellow) and candidate (red) ligand efficiences for a range of candidates from FBDD (top) and HTS (bottom).

In *figure 3.15*, the change of ligand efficiency during optimisation is compared for FBDD and HTS. For FBDD, most compounds showed either a decrease in LE or little change. There was only one pairing for which a substantial increase was observed, suggesting that it is generally difficult to improve the LE of a fragment hit. The outcome for BCATm, where optimisation increased the average LE of synthesised compounds by approximately 0.1 units may therefore be considered unusual, but clearly not isolated. The HTS compounds generally showed little change in LE during optimisation, although there were 3 examples of a large decrease (>0.1) in LE for an HTS compound and 2 examples where LE increased by a similar amount.

	Count	Median	Outliers
Hit LE (FBDD)	16	0.344857	0
Candidate LE (FBDD)	16	0.33925	0
Hit LE (HTS)	34	0.304381	0
Candidate LE (HTS)	34	0.329697	4

Alpha level = 0.05
Root MSE = 0.076
sqrt(2)q* = 3.698
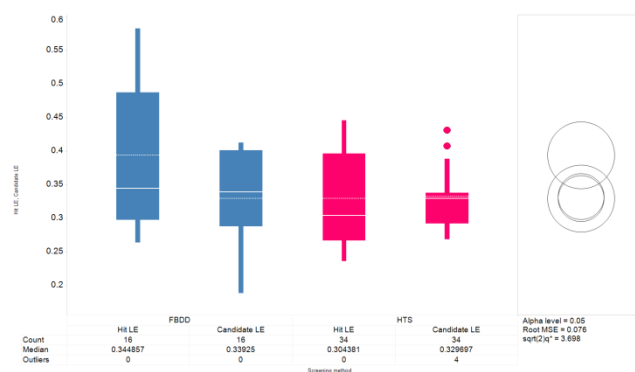
Figure 3.16: Box plot analysis of hit and candidate ligand efficiency values for FBDD (blue) and HTS (pink).

When examining how the median and mean ligand efficiency values changed during optimisation in the box plot in *figure 3.16*, it was shown that there was no statistically significant difference between hit and candidate ligand efficiency values for each technique. These data were consistent with the published work of Perola[173] who observed that there was on average little change in ligand efficiency between leads and drugs. The spread of the data indicated that it was more possible to find very highly efficient hits (LE > 0.45) from fragment screening than for HTS, but *figures 3.15* and *3.16* illustrate that these extremely high ligand efficiencies were not usually maintained during optimisation. The isolated examples from both screening techniques where LE could be substantially improved or decreased may point to a contribution from medicinal chemistry practice , for example designed shape complementarity or serendipidous findings being able to profoundly improve ligand efficiency.

Similar studies were carried out for other properties which evolved during optimisation. The results are summarised in *table 3.5* and the corresponding data plots are shown in *Appendix 3.2*.

Property studied	Figure Number	Conclusions
Ligand efficiency	3.15 and 3.16	On average remained constant from hit to candidate for both techniques. No statistically significant difference between FBDD and HTS derived candidate LE
Potency	A3.6 and A.37	FBDD increased by 2-8 log units from hit to candidate, HTS by 1-2 log units. No statistically significant difference between FBDD and HTS derived candidate pIC_{50}.
LLE	A3.8	Increased from hit to candidate for FBDD, no pattern observed for HTS.
LLE_{AT}	A3.9 and A3.10	No pattern observed from hit to candidate. No statistically significant difference between FBDD and HTS derived candidate LLE_{AT}
LELP	A3.11	No statistically significant differences between the techniques, or between hits and candidates

Table 3.5: Summary of comparisons of optimisations from hit to candidates for FBDD and HTS

In addition to examining the evolution of compound properties during optimisation, another potentially important measure of the quality of a hit compound is the effort required to optimise the hit into a candidate. It is difficult to get a measure of this effort from the medicinal chemistry literature, as researchers tend to publish only the key compounds in their optimisation, viewed from the perspective of succesful completion of optimisation. The patent literature was interrogated to establish if this could provide a more accurate snapshot of the synthetic effort required to reach a clinical candidate. For each of the 120 clinical candidates studied above, the earliest patent containing the candidate structure was retrieved and the number of exemplified compounds recorded.[243-292,293-331] These values were compared to establish if the number of exemplified compounds in patents could provide any discernible patterns. The number of compounds recorded varied between 1 and 8662, with no obvious patterns observed in the data. It is

likely that the variations in numbers of exemplified compounds was mainly due to different patenting strategies at different companies, rather than these values providing a true indication of the synthetic effort involved in the different lead optimisations. Therefore, from the publically available data, there was no reliable information to quantify the effort involved in optimising the hits from different screens.

Comparison of Outcomes for Candidates Derived from Different Hit Finding Techniques

The final, and arguably most important measure of compound quality that could be extracted from the publically available data was how far the clinical candidates studied progressed through clinical development. This information was available from annotation of the candidates in the PharmaProjects™ database.

Figure 3.17: Advancement of the 120 clinical candidates through clinical development, showing spread of calculated PFI values. The spots are coloured by hit finding technique: unknown (black), FBDD (blue), focussed screening (purple), HTS (pink), knowledge based (yellow) and natural product (orange). Spots are shaped by candidates' current status: discontinued (square), still active (circle).

	Ph I	Ph II	Ph III	Marketed	Total
Numbers in each phase for all compounds	22	53	28	17	120
Numbers discontinued by phase for all compounds	14 (64 %)	21 (40 %)	14 (50 %)	1 (6 %)	50 (42 %)
Numbers in each phase for FBDD compounds	3	9	0	1	13
Numbers discontinued by phase for FBDD compounds	3 (100 %)	5 (56 %)	0	0	8 (62 %)

Table 3.7: Numbers of compounds advanced to each phase of development

Figure 3.17 and *table 3.7* summarise the different stages of development reached by compounds from different screening techniques. To date, only one FBDD derived compound (the BRaf inhibitor Vemurafenib[224]) has reached the market. There are also no FBDD derived compounds in phase 3, with higher than average failure rates in phases 1 and 2 apparent from the limited data. It is unclear as yet whether this poorer than average performance in clinical development is due to FBDD technology being comparatively more recently implemented than the other forms of hit discovery, or there being inherent features of the derived molecules which made them more difficult to advance. Another possibility is that some of the early practitioners of FBDD advanced compounds, which were less ideal than an average clinical candidate, simply to achieve proof of concept for the technology, and potentially gain support for further discovery efforts. This is a question for future research: it would be instructive to carry out a similar analysis of FBDD compounds in clinical development in another decade when the field has matured, and the fruits of current discovery efforts have had the chance of being further advanced in the clinic. With the data currently available there is simply insufficient evidence to determine if these attrition rates are a genuine feature of FBDD molecules or are due to insufficient numbers of compounds to allow statistically meaningful analysis.

3.3 Conclusions and Suggestions for Further Work

From the analyses carried out here, there was certainly tentative evidence that compounds derived from FBDD screening may have an advantage over those found by other methods. In the BCATm work carried out at GSK, this was most evident in the comparison of FBDD and HTS with ELT, where FBDD and HTS molecules were generally found to have improved physicochemical properties over ELT compounds. The comparisons between FBDD and HTS molecules did not establish any statistically significant differences. However, the ultimate lead derived from FBDD was progressed further by the project than the HTS lead, reflecting the improved pharmacokinetic exposure and free fraction, even if this was not evident in comparing average properties of all of the molecules synthesised during optimisation. In the more comprehensive study made of multiple clinical targets across the pharmaceutical industry some weak patterns emerged suggesting FBDD derived clinical candidates had improved physicochemical properties over those from HTS and other methods. In both studies, these conlcusions were rather weak and there were indications that medicinal chemistry practice was as important in determining the quality of candidate drug molecules. FBDD technology is perhaps not sufficiently established and embedded to have shown its long-term worth; it will be interesting to observe in coming years how the method matures and impacts drug pipelines as compounds progress.

The conclusions which a practicing medicinal chemist can draw from these analyses are that ideally, one should begin optimisation from as high quality a hit as possible, and that these are slightly more likely to be discovered by FBDD than other commonly used techniques. However, if only poorer quality hits are available for optimisation rigorous control of molecular properties and ligand efficiency have enabled successful optimisation of high quality candidates. These principles were illustrated in chapter 4, where optimisation of an HTS hit with non-ideal physicochemical properties was prosectued.

These analyses should prove useful to the discipline of medicinal chemistry as they provide chemists with a framework of information on how they might have the best chances of being successful, allowing them to load the dice in a game with inherently poor odds of a positive outcome. Therefore, it is important to continue to interrogate data in this way as more information becomes available either in the public domain, or within single research organisations. There were some questions left unanswered by this analysis which could be explored in future studies. Specifically, how much effort is required to optimise molecules from different hit finding techniques, and also how successful will FBDD ultimately prove in identifying marketed drugs.

Appendix 3.1: Statistical Methods Employed in Chapter 3

Box plots are used in chapter 3 to visualise and compare sets of data. The significance of the various lines and points on a box plot are discussed using an example shown in Figure A3.1 below.
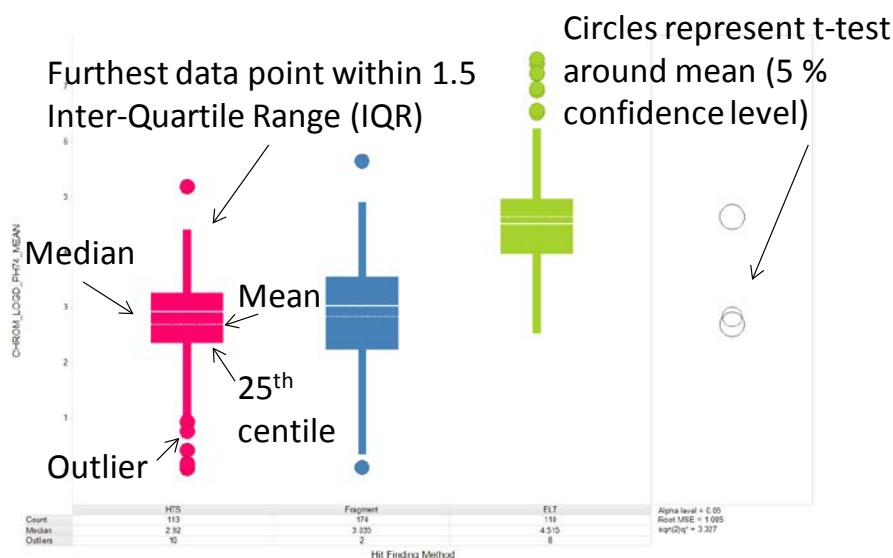
Figure A3.1: Example Box Plot with annotations.
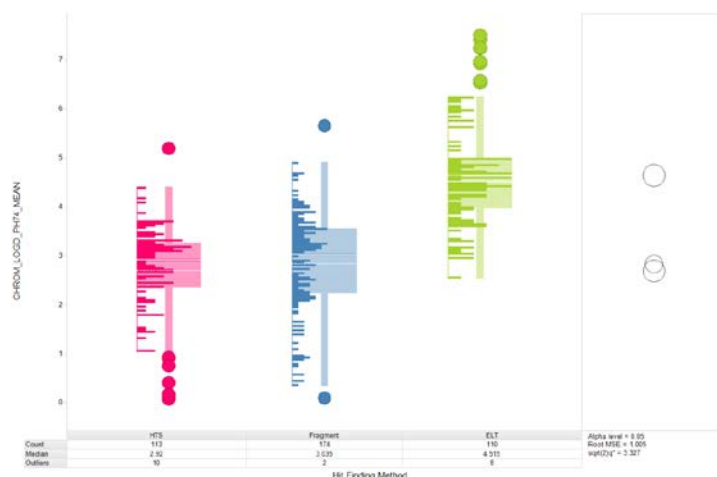
Figure A3.2 Box plot from FigureA 3.1 showing data distribution.

The box in the box plot represents the range of the data from the 25th to the 75th centile (ie, half of the data points fall within the box). The median is

represented by the solid white line and the mean is shown by the dotted white line. The distance from one end of the box to the other (25th-75th centile) is defined as the inter-quartile range (IQR). The solid lines extending from the box reach as far as the furthest data point that falls within 1.5 times the IQR. Any data points falling outside this limit are defined as outliers and are represented as individual data points. The circles on the right of the plot are centred on the mean of each data set and the circumferences represent the limits of Student's t-test[332] around the mean with a 5 % confidence level. Any circles which partially or completely overlap can be considered to not have a statistically significant difference in their means, whilst clear separation of the circles indicates confidence that the means have a statistically significant difference. The distribution of the full data set is shown superimposed on the box plots in figure A3.2, showing that the data sets are unevenly distributed, accounting for the unsymmetrical sizes of the resulting boxes and bars.

The standard error is shown on a number of plots as a measure of variability present in the data presented. The standard error is calculated by dividing the standard deviation of the data set by the square root of the number of samples in the data set (n).[333] It is by definition always smaller than the standard deviation, and becomes smaller as n increases and the true average of the data becomes more accurately known. It is a useful error calculation to apply when comparing data sets of different sizes, as in chapter 3.

Appendix 3.2: Figures from Data Analysis from Clinical Candidates
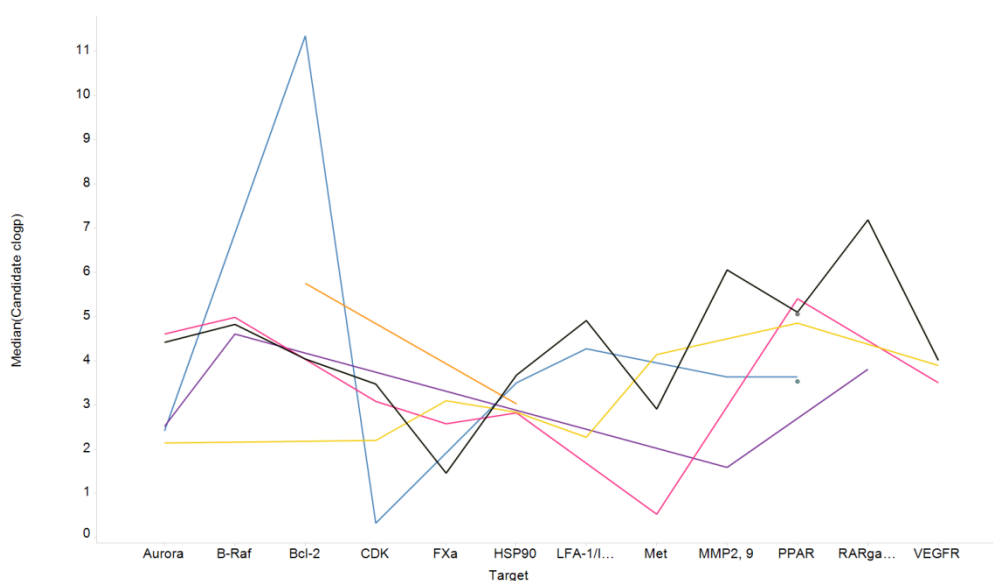
Figure A3.3: Median clogP of clinical candidates against different targets. The The lines are coloured by technique: unknown (black), FBDD (blue), focussed screening (purple), HTS (pink), knowledge based (yellow) and natural product (orange).
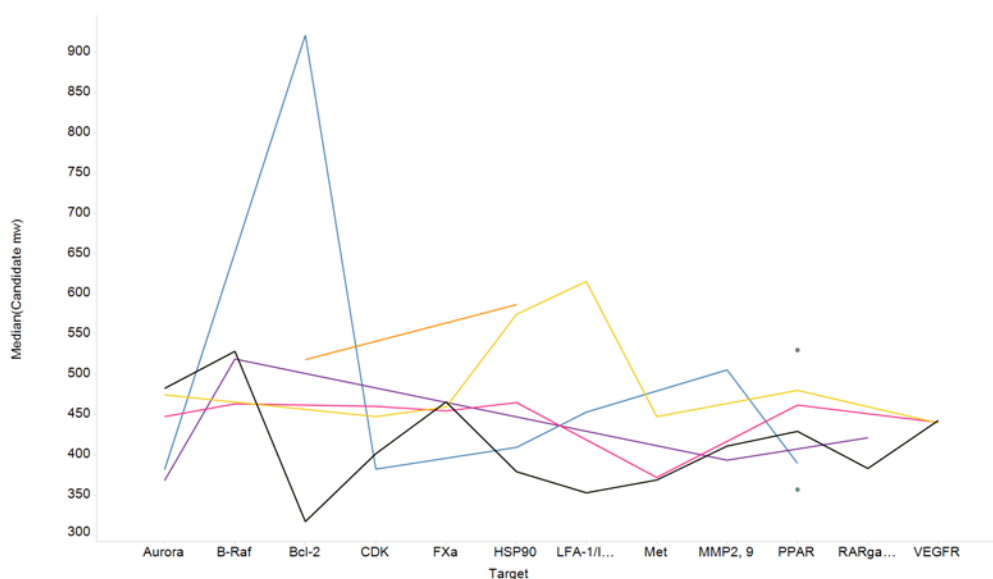
Figure A3.4: Median molecular weight of clinical candidates against different targets. The lines are coloured by technique: unknown (black), FBDD (blue), focussed screening (purple), HTS (pink), knowledge based (yellow) and natural product (orange).
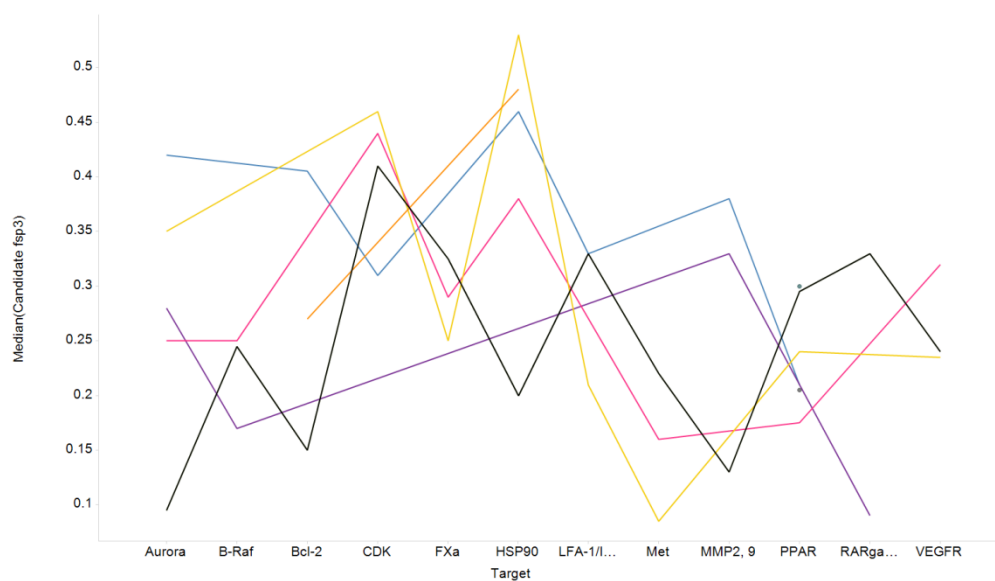
Figure A3.5: Median fraction of sp³ atoms (fsp³) of clinical candidates against different targets. The lines are coloured by technique: unknown (black), FBDD (blue), focussed screening (purple), HTS (pink), knowledge based (yellow) and natural product (orange).

FBDD:
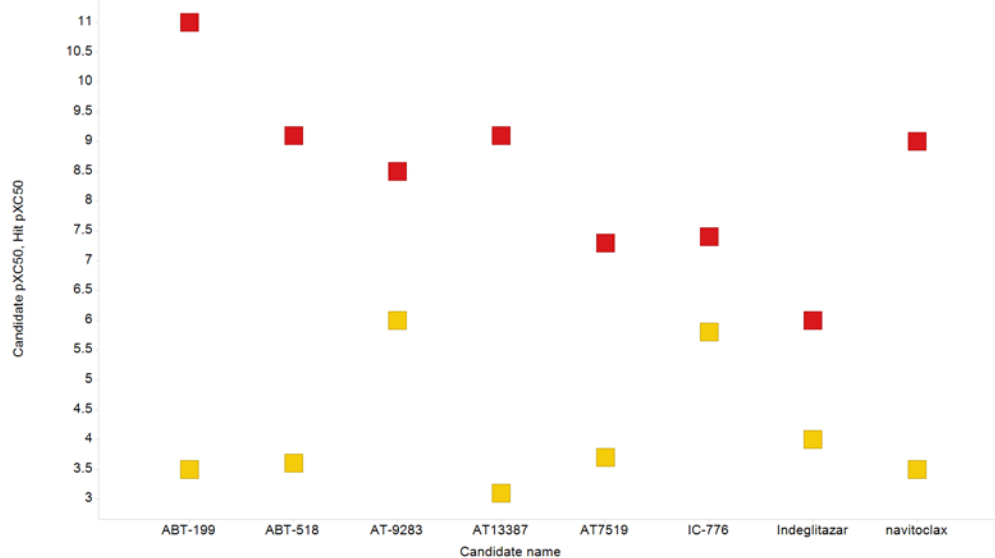
HTS:
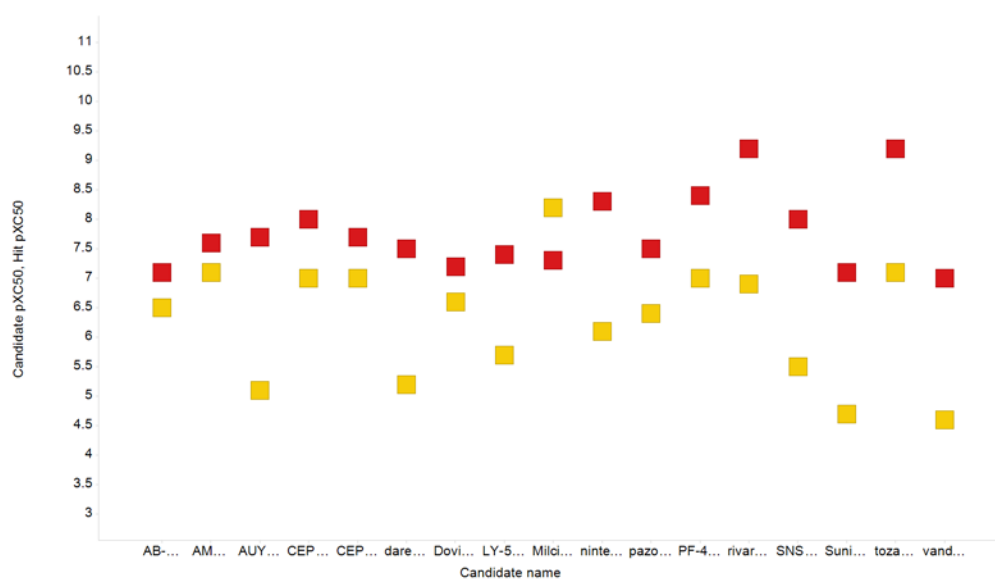
Figure A3.6: Comparison of hit (yellow squares) and candidate (red squares) pXC$_{50}$s for a range of candidates from FBDD (top) and HTS (bottom).

	FBDD		HTS		
	Hit pXC50	Candidate pXC50	Hit pXC50	Candidate pXC50	
Count	16	16	34	34	
Median	3.65	8.75	6.5	7.6	
Outliers	2	0	0	4	

Screening method

Alpha level = 0.05
Root MSE = 0.999
sqrt(2)q* = 3.698
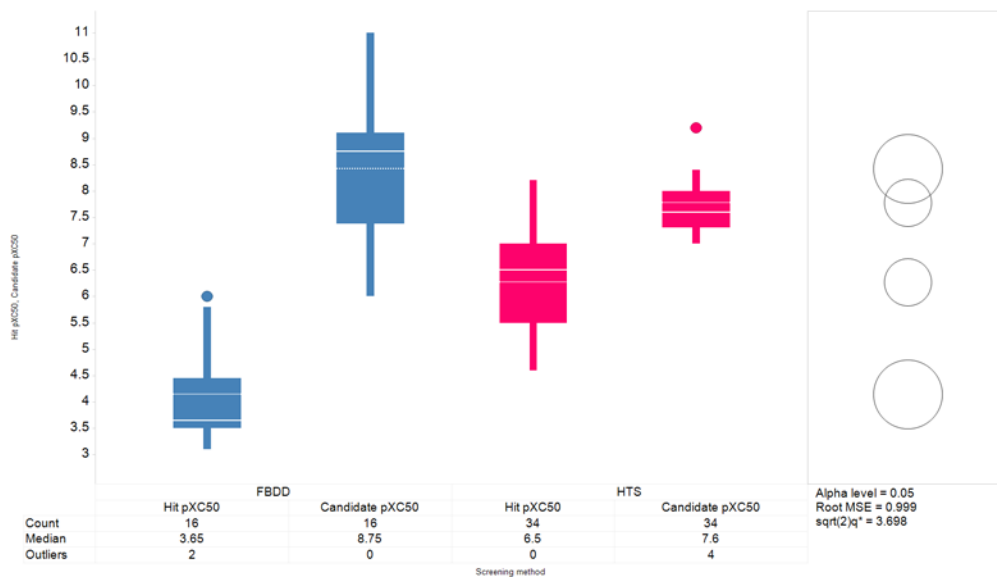
Figure A3.7: Box plot analysis of hit and candidate pXC$_{50}$ values for FBDD (blue) and HTS (pink).

FBDD LLE:
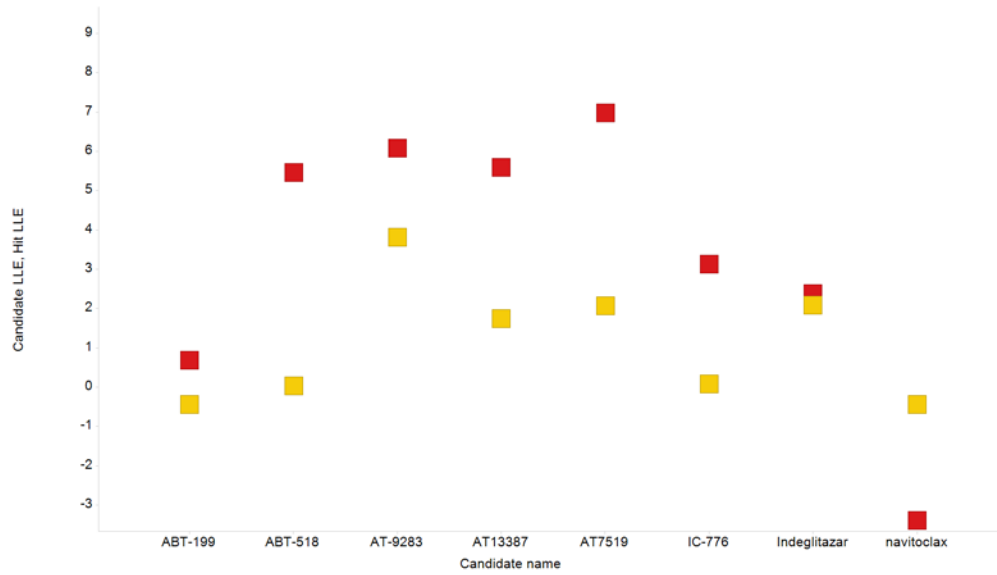
HTS LLE:
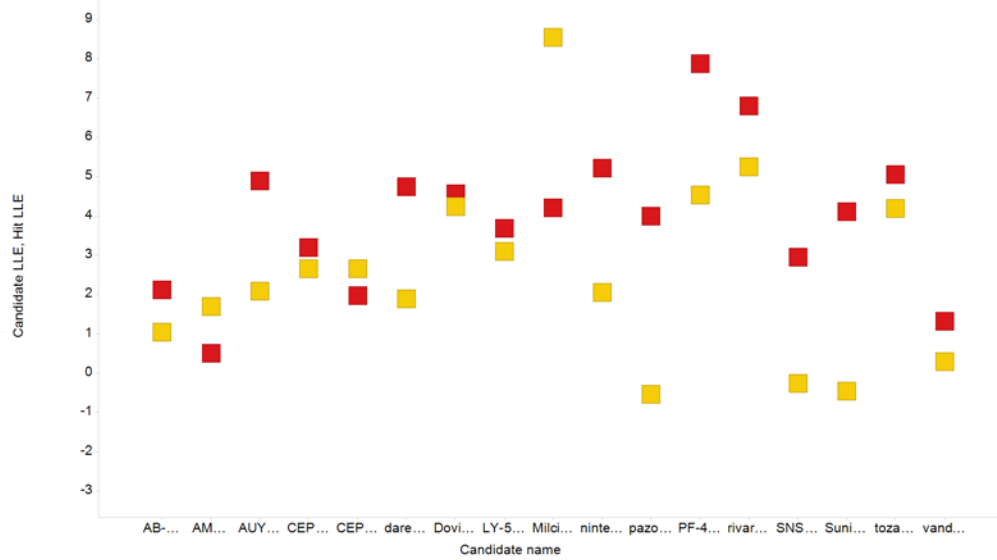
Figure A3.8: Comparison of hit (yellow) and candidate (red) LLEs for a range of candidates from FBDD (top) and HTS (bottom).

FBDD LLE$_{AT}$
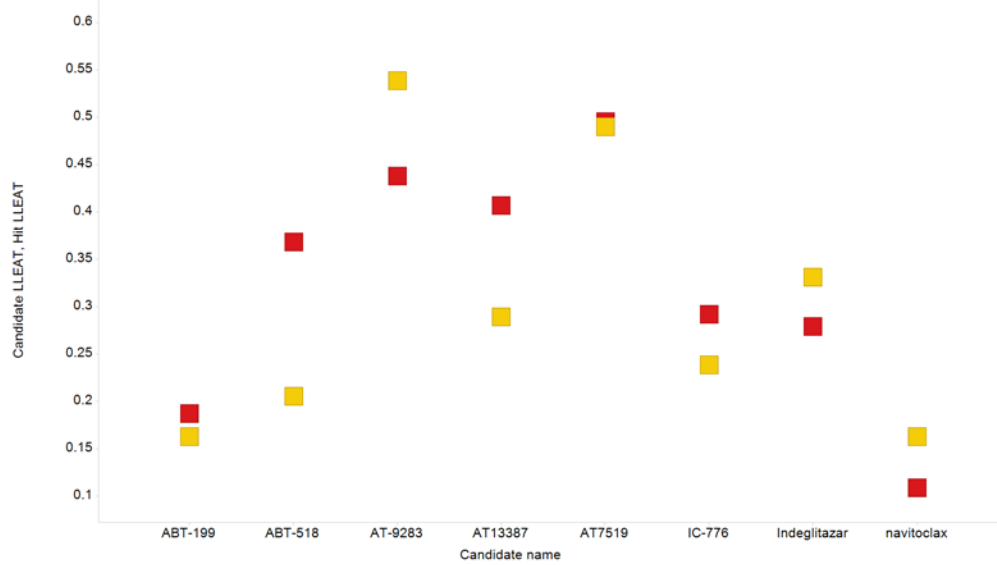
HTS LLE$_{AT}$

Figure A3.9: Comparison of hit (yellow) and candidate (red) LLE$_{AT}$s for a range of candidates from FBDD (top) and HTS (bottom).

	FBDD		HTS		Alpha level = 0.05
	Hit LLEAT	Candidate LLEAT	Hit LLEAT	Candidate LLEAT	Root MSE = 0.107
Count	16	16	34	34	sqrt(2)q* = 3.698
Median	0.264131	0.330043	0.262038	0.322867	
Outliers	0	0	2	6	
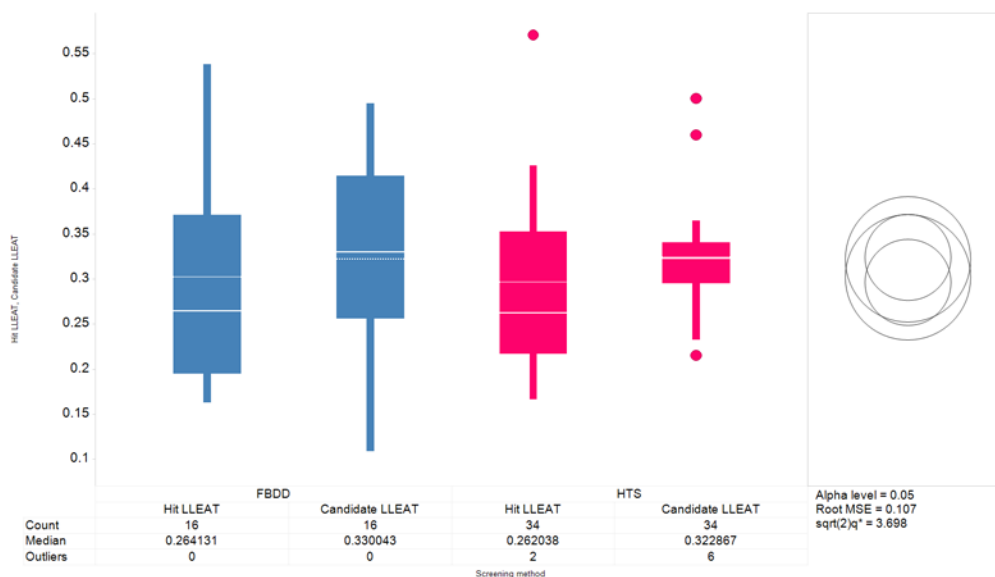
Figure A3.10: Box plot analysis of hit and candidate LLE$_{AT}$ values for FBDD (blue) and HTS (pink).

	FBDD		HTS		Alpha level = 0.05
	Hit LELP	Candidate LELP	Hit LELP	Candidate LELP	Root MSE = 10.125
Count	8	8	17	17	sqrt(2)q* = 3.770
Median	7.92316	10.9907	11.2794	10.9249	
Outliers	0	2	0	0	
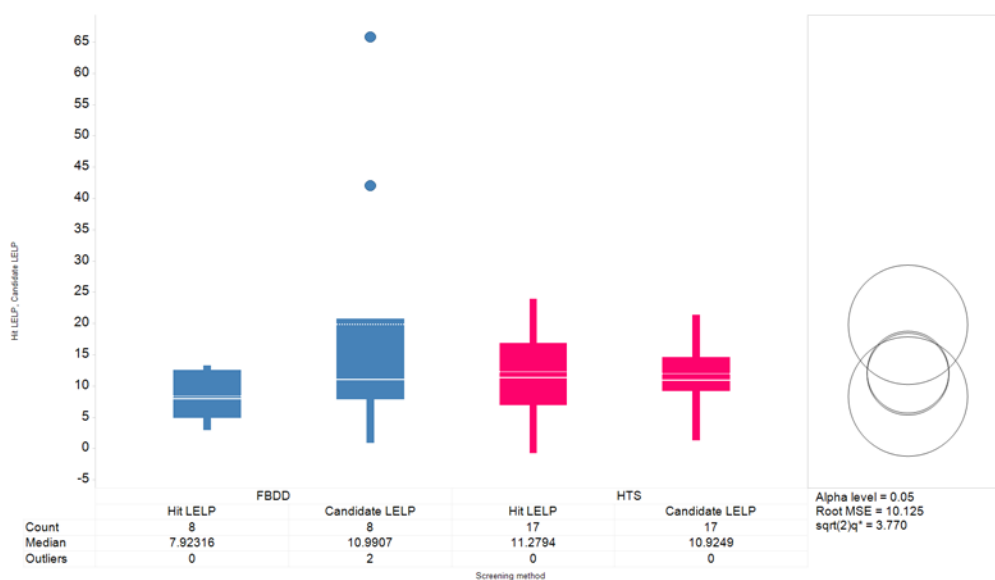
Figure A3.11: Box plot analysis of hit and candidate LELP values for FBDD (blue) and HTS (pink).

4. DprE1 Inhibitors

4.1 Introduction

This chapter describes the optimisation of a phenotypic HTS hit shown to act against decaprenylphosphoryl-β-D-ribose 2'-epimerase (DprE1), an enzyme involved in cell wall synthesis of *Mycobacterium tuberculosis*. The aim of this work was to explore the most effective way to optimise potency at the target, whilst also aiming to maintain the most attractive physicochemical profile possible. An important aspect of this work was that the starting hit had poor physicochemical properties, and no liganded structures were available to enable design. Therefore identifying optimised lead compounds with an attractive profile was a challenging goal, which would require a high degree of discipline and rigour in the medicinal chemistry to be achieved. This challenge represented a test of the relative importance of good practice in medicinal chemistry during optimisation compared with the quality of the starting point.

Tuberculosis

Tuberculosis is believed to be the most deadly infectious disease in human history, killing over 1 billion people in the last 200 years, and continuing to kill at a rate of more than 1 million people per year.[334] Tuberculosis is a highly contagious infectious disease which causes chronic cough, sputum production, weight loss, fever and often death in untreated patients.[335] Tuberculosis is caused by infection with the bacterium *Mycobacterium tuberculosis.* It is estimated that 2 billion people worldwide are infected with *M. tuberculosis*, and around 10 % of these will develop active tuberculosis, with the remainder remaining asymptomatic with latent disease.[336] It is a disease which disproportionately affects the world's poor, particularly in developing nations. The risk factors for developing active disease include overcrowding, poor nutrition, co-infection with HIV, increased age, and alcohol, drug and tobacco consumption.[337]

Infection with *M. tuberculosis* is caused by inhalation of infected droplets, which are exhaled in the cough of active tuberculosis sufferers. The droplets can remain viable in the atmosphere for several hours, and the infectious dose is thought to be as low as a single bacterium, resulting in highly effective transmission of the bacteria from host to host.[338] The bacteria are quickly taken up by phagocytic cells in the lungs, including macrophages, neutrophils, monocytes and dendritic cells.[339] These cells associate together to form a mass known as a granuloma or tuberculoma, inside of which *M. tuberculosis* can replicate. In latent disease, bacteria are enclosed in this granuloma and the infected host does not experience any symptoms.[338] When the host's immune response cannot maintain containment of the bacteria within the granuloma, which may be due to additional factors including HIV infection, vitamin deficiency or old age, active disease will result.[337] The granuloma decays, ruptures and releases bacteria into the patient's airways, causing the symptoms of active tuberculosis and further spread of the disease.[338]

Current Treatments for Tuberculosis

There are a number of drugs available which are effective treatments for tuberculosis, although current recommended treatment regimes involve a combination of these for a period of at least six months, extending up to three years for some patients.[335] The long treatment time required is a result of the ability of *M. tuberculosis* to reside in a latent state, and also the unusually slow rate of replication; *M. tuberculosis* divides every 15-20 hours, whilst most bacteria divide in timescales in the order of minutes.[337]

Mycobacteria possess a complex cell wall, which is present in addition to the normal plasma membrane made up of phospholipids found in animal cells. The outer cell wall of mycobacteria consists of several covalently attached layers.[340] The first layer beyond the membrane is the periplasmic space,a compartment between the membrane and the cell wall, containing dissolved components.[341] The inner cell wall is the peptidoglycan, made up of the sugars *N*-acetylglucosamine and muramic acid attached to polypeptide side

chains, which are more extensively cross-linked than in other bacteria.[340] The peptidoglycan layer is linked to the arabinogalactan layer, another polysaccharide.[340] This is in turn esterified at the outer layer by a mycolic acid layer.[340] Finally there is a region of free lipids.[340] This complex wall (*figure 4.1*) protects the bacterium and makes it very difficult for drug molecules to penetrate into the cell. However, the particular biochemistry of its construction also provides a number of potential targets for drug molecules, which can disrupt the synthesis or maintenance of the cell wall.[342]
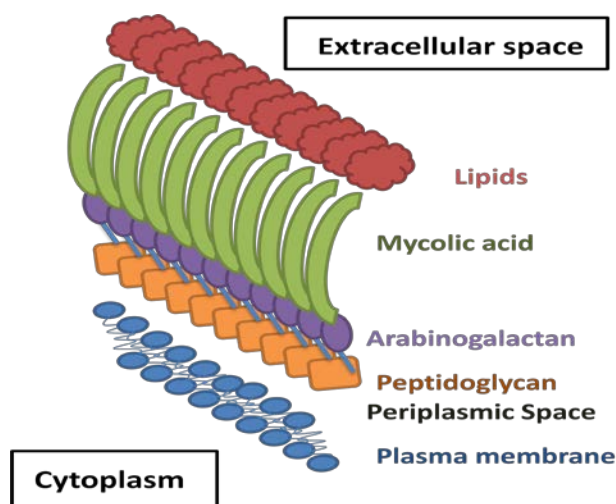
Figure 4.1: Schematic diagram of mycobacterium cell wall
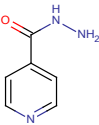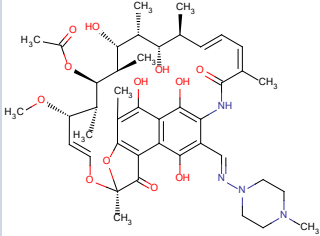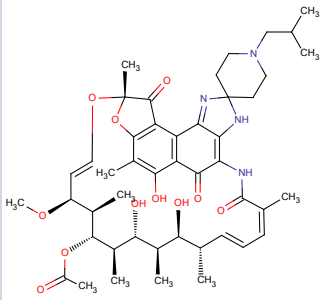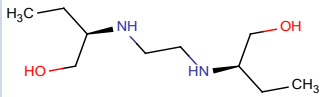
A summary of the most commonly used drugs to treat tuberculosis is given in *Table 4.1*. [342-351] These can be classified as either broad-spectrum antibiotics or tuberculosis-specific drugs.[352] The broad spectrum antibiotics include rifampicin and rifambutin, the aminoglycosides, such as streptomycin, and the fluoroquinolones, such as levofloxacin.[352] The specific anti-tuberculosis drugs include isoniazid, ethambutol and pyrazinamide.[352] Some drugs used to treat tuberculosis (e.g. isoniazid and the broad-spectrum antibiotics) are bactericidal, meaning they kill the bacteria, whilst others (e.g. ethambutol and pyrizamide), are bacteriostatic, simply preventing reproduction.[352] These differing mechanisms are one reason why the drugs are most effective when given in combination.
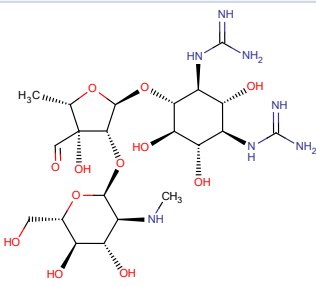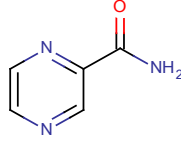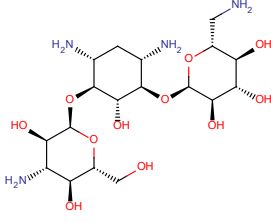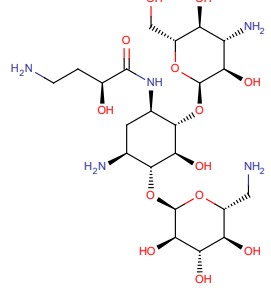
The available treatments for tuberculosis are problematic for several reasons. Importantly, many of them have potentially serious side effects with low
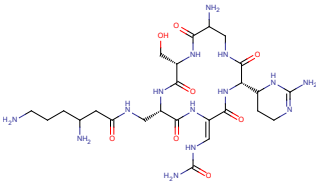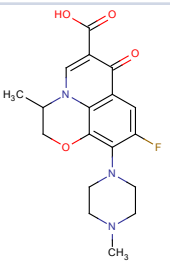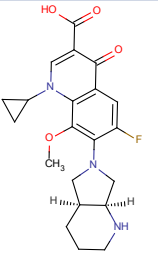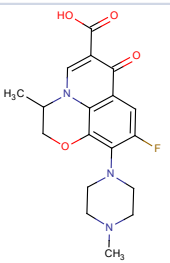
therapeutic windows. Some are incompatible with HIV medication, or unsuitable for certain groups of patients such as young children. The expense of some broad spectrum antibiotics can limit access in some countries and the injectable medications are difficult to administer to patients over the time periods required for effective treatment, applying a further burden on stretched resources. The most pressing problem in treating tuberculosis however, is the growing emergence of drug resistant strains of *M. tuberculosis.*

Drug resistance is thought to have emerged partly through poor patient compliance during the necessary long drug treatment regimes, which have potential for serious side effects. The drug resistant strains of *M. tuberculosis* are classified as multi-drug resistant (MDR), extensively drug resistant (XDR) and even totally drug resistant (TDR).[337] MDR tuberculosis is defined as being resistant to isoniazid (**4.1**) and rifampicin (**4.2**), the main front-line treatments.[337] XDR tuberculosis is also resistant to any fluoroquinolone (e.g. levofloxacin **4.10**, moxifloxacin **4.11** and ofloxacin **4.12**) and one of the injectable amino-glycosides (kanamycin **4.7**, amikacin **4.8** and capreomycin **4.9**).[337] TDR tuberculosis, as the name suggests, is resistant to all of the available first and second-line treatments (compounds **4.1** – **4.14** in *table 4.1*).[347] Treatment of drug resistant tuberculosis takes a minimum of 20 months, using combinations of drugs with potentially serious side-effects.[347] For XDR, the cure rate is only around 60 % for patients who are not infected with HIV and is close to 0 % for those who have HIV co-infection.[347] The desperate need for new treatments for tuberculosis is highlighted by the recent approval of the ATP-synthase inhibitor bedaquiline, **4.15**, which shows effective activity against drug-resistant TB[353] and so achieved approval despite clinical trials in which some deaths could have been attributed to the cardiovascular side-effects of this drug.[354] Similarly, the nitroimidazole delamanid **4.16** has recently received conditional approval in Europe for treatment of MDR tuberculosis, after the completion of phase II studies, which showed efficacy in patients, along with QT-elongation as a side-effect.[351] It is clear that tuberculosis treatment remains an area of very high

unmet medical need. New treatments targeting drug-resistant disease, shortening treatment times and reducing the combination of drugs administered are urgently required. Drugs which act at novel targets could be expected to address these needs and so this is a particular area of focus in the anti-tuberculosis field.

Drug Name	Structure	Mechanism of action	Site of action	Year approved	Method administration	Molecular weight	clogP	Comment
Isoniazid **4.1**		InhA and multiple other targets	Mycolic acid	1952	Oral	137.14	-0.67	Black box warning - hepatotoxic
Rifampicin **4.2**		Transcription inhibitor	Cytoplasm	1971	Oral	822.94	3.71	Incompatible with many anti-retrovirals
Rifabutin **4.3**		Transcription inhibitor	Cytoplasm	1992	Oral	847.01	4.73	Alternative to Rifampicin for HIV patients. Higher cost
Ethambutol **4.4**		Unknown	Arabinogalactan	1967	Oral	277.23	0.12	Not suitable for young children. Can cause loss of sight

Name	Structure	Mechanism	Site	Year	Administration	MW	LogP	Notes
Streptomycin **4.5**		Protein synthesis inhibitor	Cytoplasm	1946	Injection	581.59	-3.46	Not widely used as it must be injected Black box warning - neurotoxic (risk of deafness)
Pyrazinamide **4.6**		Unknown	Plasma membrane	1971	Oral	123.11	-0.68	Only effective in combination with other Anti-TB drugs
Kanamycin **4.7**		Protein synthesis inhibitor	Cytoplasm	1973	Injection	484.50	-7.06	Black box warning - neurotoxic (risk of deafness)
Amikacin **4.8**		Protein synthesis inhibitor	Cytoplasm	1981	Injection	585.60	-8.58	Black box warning - neurotoxic (risk of deafness)

Capreomycin **4.9**		Protein synthesis inhibitor	Cytoplasm	1971	Injection	668.71	-6.70	Black box warning - neurotoxic (risk of deafness)
Levofloxacin **4.10**		DNA gyrase inhibitor	Cytoplasm	1996	Oral and injection	361.37	0.65	Broad spectrum antibiotic. Not suitable for pregnant women or children.
Moxifloxacin **4.11**		DNA gyrase inhibitor	Cytoplasm	1999	Oral and injection	401.44	-0.50	Broad spectrum antibiotic. Not suitable for pregnant women or children.
Ofloxacin **4.12**		DNA gyrase inhibitor	Cytoplasm	1990	Oral and injection	361.37	0.65	Broad spectrum antibiotic. Not suitable for pregnant women or children.
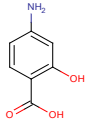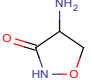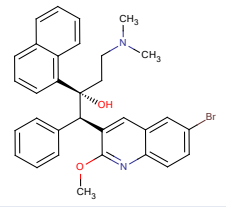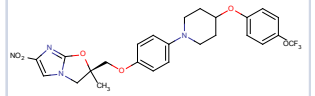
Para–aminosalicylic acid **4.13**		Folate synthesis inhibitor	Cytoplasm	1948	Oral	153.14	1.06	Causes gastrointestinal side effects
Cycloserine **4.14**		Inhibits synthesis and use of D-Ala, inhibits peptidoglycan	Ribosome	1964	Oral	102.09	-2.42	Causes neurological side effects
Bedaquiline **4.15**		ATP synthase inhibitor	Plasma membrane	2012	Oral	525.49	6.70	Black box warning - increased risk of death compared to placebo, causes QT prolongation
Delamanid **4.16**		Mycolic acid biosynthesis inhibitor	Mycolic acid	2014	Oral	534.48	5.25	Conditional approval in Europe only for MDR TB. Ph III data awaited. Causes QT prolongation

Table 4.1: Drugs currently used in the treatment of Tuberculosis

Decaprenylphosphoryl-β-D-Ribose 2'-Epimerase (DprE1)

In 2009, a promising new drug target for tuberculosis was identified when potent bactericidal molecules identified by phenotypic screening against *M. tuberculosis* were profiled.[355] Genetic analysis of mutant resistant strains determined that the anti-tuberculosis effect was a result of inhibiting the enzyme decaprenylphosphoryl-β-D-ribose 2'-epimerase (DprE1).[355] DprE1, along with its partner, decaprenylphosphoryl-D-2-ketoerythro pentose reductase (DprE2) enable the epimerisation of decaprenylphosphoryl ribose (DPR) to decaprenylphosphoryl arabinose (DPA) (*scheme 4.1*).[356] This pathway is believed to be the bacteria's only source of arabinans, which are essential for construction of the arabinogalactan component of the cell wall.[357]

Scheme 4.1: Conversion of DPR to DPA by the action of the enzymes DprE1 and DprE2

DprE1 causes oxidation of the ribose in DPR to the corresponding ketone, DPX. The electron acceptor in this step is the cofactor flavin adenine dinucleotide (FAD), which is converted to its reduced form $FADH_2$.[358,359] The second step in the sequence is reduction of the DPX to give the epimerised product DPA by the nicotinamide adenine dinucleotide (NAD) dependent enzyme DprE2.

Studies have shown that DprE1 is an excellent potential target for new anti-tuberculosis drugs, as mycobacteria with reduced expression of functional protein are not viable.[360,361] Additionally, analysis of 240 *M. tuberculosis* strains isolated from patient populations, including MDR and XDR variants contained no mutations in the DprE1 gene, confirming that this gene is highly evolutionarily conserved.[362] There is no equivalent gene in humans, reducing the risk of mechanism-related toxicity.[362] DPR is situated in the periplasmic space on mycobacteria, enabling access for potential drug molecules without having to penetrate to the intracellular space.[363]

BTZ-403 **4.20**
DprE1 pIC$_{50}$ not reported
MIC = 2.3 nM
MW =431, clogP = 2.45
calc PFI = 8.7

4.21
DprE1 pIC$_{50}$ not reported
MIC = 0.1 nM
MW =449, clogP = 3.13
calc PFI = 8.3

PTBBTZ-169 **4.22**
DprE1 pIC$_{50}$ not reported
MIC < 19 ng/mL (< 4 nM)
MW =455, clogP = 6.6
calc PFI = 11.2

4.23
DprE1 pIC$_{50}$ not reported
MIC =80 nM
MW =361, clogP = 3.0
calc PFI = 6.5

4.24
DprE1 pIC$_{50}$ not reported
MIC =3.1 μM
MW =344, clogP = 4.3
calc PFI = 9.6

4.25
DprE1 pIC$_{50}$ not reported
MIC not reported
MW =260 clogP = 2.9
calc PFI =7.6

Figure 4.2: Nitro-containing DprE1 inhibitors

Figure 4.2 shows the original hit used to identify DprE1, BTZ-403 (**4.20**),[355] along with analogues which were the result of subsequent optimisation (**4.21,**

4.22).[364,365] As these molecules were identified by screening compounds against whole cell *M. tuberculosis* and the target subsequently identified as being DprE1, the level of DprE1 inhibition was not measured. Instead, the minimum inhibitory concentration (MIC), an important measure of activity for antimicrobials was quoted. An MIC value is defined as the lowest concentration of compound that inhibits the visible growth of a microorganism following overnight incubation.[366] BTZ-403 was subsequently shown to be active against MDR and XDR strains of *M. tuberculosis*, and both BTZ-403 and PTBBTZ-169 were active in an *in vivo* model of tuberculosis in mice.[355,365]

Figure 4.2 also shows a selection of other nitro-containing compounds, **4.23**,[356] **4.24**[367] and **4.25**,[368] which were all identified using similar phenotypic screening protocols. SAR studies have shown that all of the molecules in *figure 4.2* experienced significant increases in their MIC values if the nitro moiety was absent. The role of the nitro group has been elucidated using studies of resistant mutants,[369] mass spectrometry[370,371] and X-ray crystallography.[359] These showed that the nitro group of BTZ-403 was reduced to a nitroso, likely by the $FADH_2$ form of DprE1 and then formed a covalent semimercaptal linkage with Cys-394 of DprE1 (*scheme 4.2*). It is likely that this mechanism of action is common to all of the nitro-containing DprE1 inhibitors which have been identified.[372]
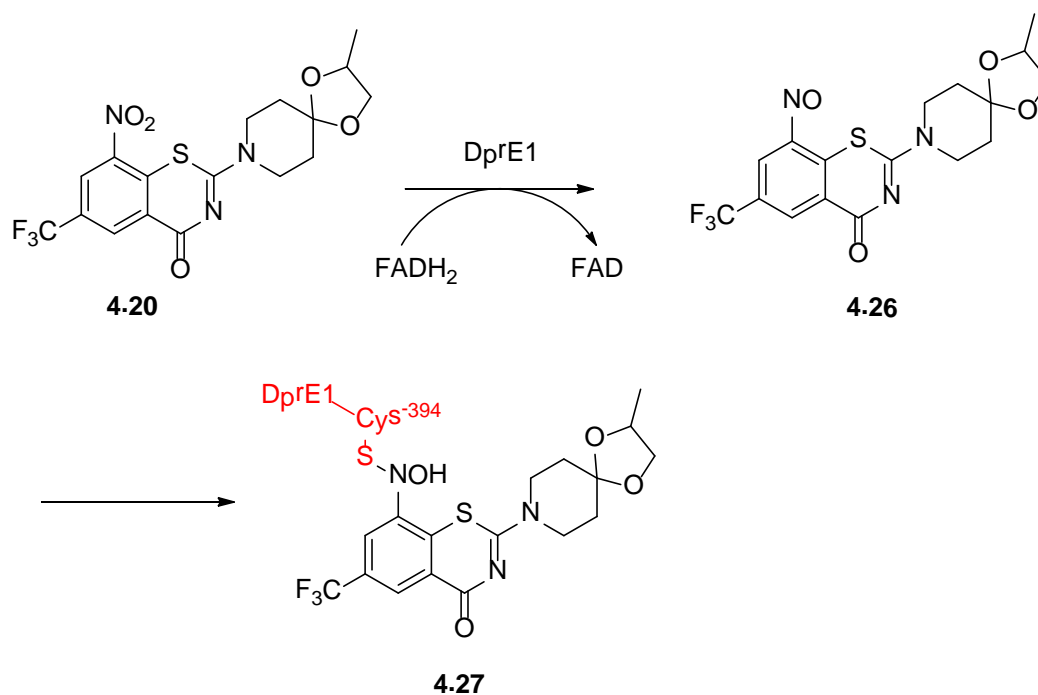
Scheme 4.2: Mechanism of BTZ-403 interaction with DprE1

Covalent binding of drugs to their targets, has historically been considered a risky tactic to employ, due to the potential for off-target reactivity, potentially leading to side-effects or toxicity.[373] These risks are increasingly being considered as manageable if a covalent inhibitor can be identified, which selectively forms its reactive functionality locally to the target of interest, such as is the case for these nitro-containing DprE1 inhibitors.[373] However, in spite of being present in some drugs, nitro-containing compounds are generally considered to have a high risk of causing cytotoxicity, as they are known to be reduced by other metabolic enzymes to reactive intermediates (e.g. nitroso) and such products can damage DNA by covalent modifications or bind to proteins.[374] Therefore the nitro-containing DprE1 inhibitors represent a class of compounds which have potential liabilities, thus making them higher risk for development.
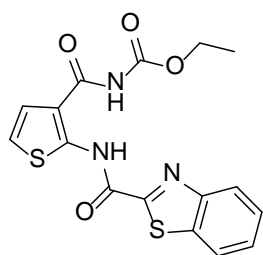
4.28
DprE1 pIC50 not reported
MIC = 27 nM
MW = 375, clogP = 3.6
calc PFI = 9.1
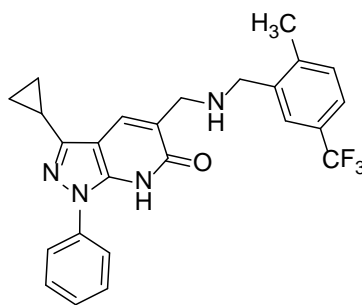
4.29
DprE1 pIC$_{50}$= 8 (*M. Smeg.*)
MIC = 100 nM
MW = 452, clogP = 3.8
calc PFI = 9.5
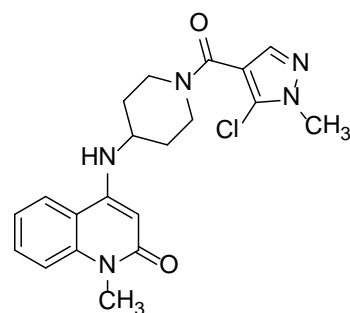
4.30
DprE1 pIC$_{50}$= 6.9 (*M. Smeg.*)
MIC = 25 μM
MW = 400, clogP = 0.94
calc PFI = 6.0
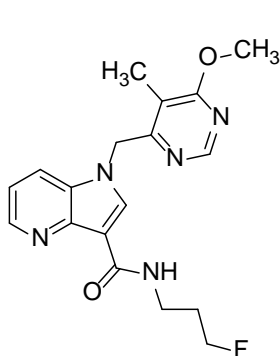
4.31
DprE1 pIC$_{50}$= 7.9 (*M. Smeg.*)
MIC = 2.3 μM
MW = 357, clogP = 1.8
calc PFI = 5.9
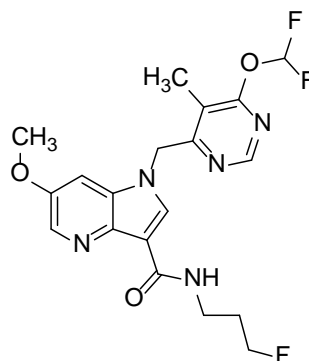
4.32
DprE1 pIC$_{50}$= 8.3 (*M. Smeg.*)
MIC = < 0.39 μM
MW = 423, clogP = 2.6
calc PFI = 6.8

Figure 4.3: Non-nitro containing DprE1 inhibitors. Enzyme potencies for DprE1 are reported, for the Mycobacterium smegmatis (M. smeg.) isoform. The MIC values reported are against M. tuberculosis.

Figure 4.3 shows the structures of other known DprE1 inhibitors, which do not contain nitro groups and are thus expected to be non-covalent binders.[375-379] However, compounds **4.28** and **4.29** have very high calculated PFI values and so may carry developability risks. Compound **4.28** also contains a 2-amino-3-carboxy thiophene, a functional group known to act as a PAIN (pan-assay interference compound) due to its inherent reactivity.[55] Compound **4.30** has a considerably higher MIC value than the other compounds, so it seems that activity may have been compromised for

198

superior physicochemical properties. The azaindole series represented by **4.31** and **4.32** appears to be the most promising of the published DprE1 inhibitors, as these molecules are potent enzyme inhibitors with low MIC values, better physicochemical properties and contain no functional groups which are known to carry high developability risks.

There is no suggestion in the literature that any of the known DprE1 inhibitors have advanced into clinical trials, and it is likely that several high quality clinical candidates would be required to achieve a successful drug approval. Therefore, there is still considerable scope for new DprE1 inhibitors to be discovered, especially from new chemical classes. This chapter will describe the identification of a new lead series of DprE1 inhibitors starting from an HTS hit.

4.2 Results and Discussion

Identification of Pyrimidine Series

GSK recently published 177 confirmed hits from a phenotypic high throughput screen, measuring inhibition of *Mycobacterium bovis* BCG growth.[380] *M. bovis* was used as a surrogate for *M. tuberculosis* as it requires lower levels of biosafety containment, and is therefore more convenient to handle in a high throughput screening environment.[380] The hits were published with the intention of inspiring further work by the scientific community to determine the mechanism or further optimise these hits. One molecule identified by this screen, **4.33** (*figure 4.4*) was later shown to be an inhibitor of DprE1 as its MIC value increased when tested in a strain of *M. tuberculosis* which over-expresses DprE1.[381]
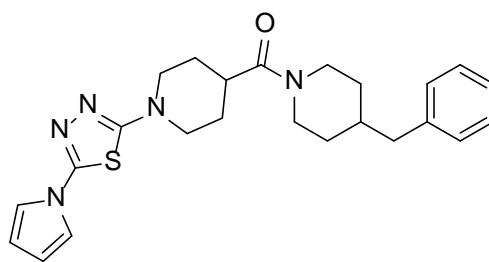
4.33

*Figure 4.4: Structure of over-expressor DprE1 hit **4.33***

Parameter	4.33	Target Value Tractable Hit	Target Value Lead
DprE1 pIC$_{50}$	7.3*[a]	>5	>6
MIC (µM)	3.7	< 50	< 10
LE, LLE$_{AT}$	0.32*, 0.30*	>0.27	>0.27
PFI	9.4	<7	<7
clogP	3.0	<5	<5
CLND solubility (µM)	<1		>200
FaSSIF solubility (µg/mL)	Not measured		>100
Cytotoxicity HepG2 pIC$_{50}$	<4.0	<5	<4
DMPK	Clint h/m (ml/min/g) = 9.9, 7.5		Suitable profile for *in vivo* dosing
Off-target effects	Not measured		No major off-target liabilities

*Table 4.2: Measured profile of **4.33** compared to desired profile of tractable hits and leads, as agreed by DprE1 programme team *DprE1 pIC$_{50}$ values above 7.3 are approaching tight binding limit of assay and should be treated with caution.[a] Compound tested inactive (pIC$_{50}$ < 4) on 2 out of 62 test occasions*

Table 4.2 compares the data gathered on compound **4.33** with the desired profile that the GSK DprE1 team had defined for a tractable hit and a lead. Compound **4.33** in many respects represented a very good starting point for optimisation. It was a highly potent inhibitor of DprE1, which translated into an excellent MIC value for a starting hit. The compound had good efficiency metrics. Importantly, **4.33** was not a general cytotoxic agent, demonstrated

by its having no measurable potency in the HepG2 cytotoxicity assay. However, **4.33** was very lipophilic, which combined with a structure containing three aromatic rings, resulted in a PFI value 2 units higher than the preferred maximum. This less than ideal physicochemical profile translated into very low solubility and poor intrinsic clearance values, predictive of a poor *in vivo* DMPK profile. Since lipophilicity and molecular size generally increase during chemical optimisation,[43] the profile of this molecule could have been considered unacceptable as a starting point. However, since **4.33** had promising activity against DprE1, and importantly, a very good MIC, analogue searching was initiated.

The GSK compound collection was mined for molecules which possessed a related structure to **4.33** but had lower predicted PFI values. This work was carried out by Ian Wall and Rob Young, GSK. The molecules identified in the substructure search were tested in the DprE1 assay (*appendix 4.1*), which identified the truncated compound **4.34** (*figure 4.5, table 4.3*). Although compound **4.34** had lower DprE1 potency and MIC activity than **4.33**, it had a lower PFI value, which translated into much improved measured solubility.
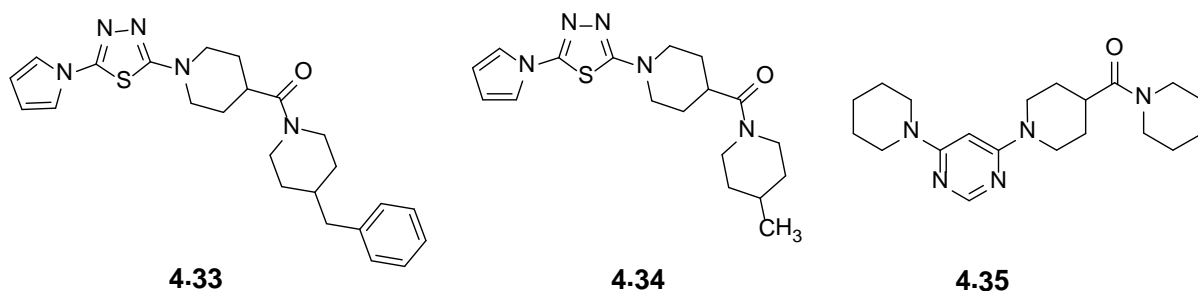
*Figure 4.5: Results of analogue searching – progression from compound **4.33** to **4.34** and **4.35***

Parameter	4.33	4.34	4.35
DprE1 pIC_{50}	7.3*[a]	6.3	5.8
MIC (µM)	3.7	20.8	34.2
LE, LLE_{AT}	0.32*, 0.30*	0.35, 0.37	0.31, 0.34
PFI	9.4	7.1	5.8
clogP	3	1.6	1.5
CLND solubility (µM)	<1	328	>405
Cytotoxicity HepG2 pIC_{50}	<4.0	<4.0	<4.0

*Table 4.3: Comparison of profiles of **4.33**, **4.34** and **4.35**. *DprE1 pIC_{50} values above 7.3 are approaching tight binding limit of assay and should be treated with caution. [a] Compound tested inactive ($pIC_{50} < 4$) on 2 out of 62 test occasions*

Additional similarity searching of the GSK collection was carried out by Ian Wall and Rob Young, using compound **4.34** as the entry structure. This resulted in the identification of **4.35**, where the pyrrole thiadiazole core had been exchanged for piperidine pyrimidine. This molecule had a further 1 unit reduction in PFI, resulting in very high solubility. The DprE1 pIC_{50} and MIC values were comparable to those for **4.34**.
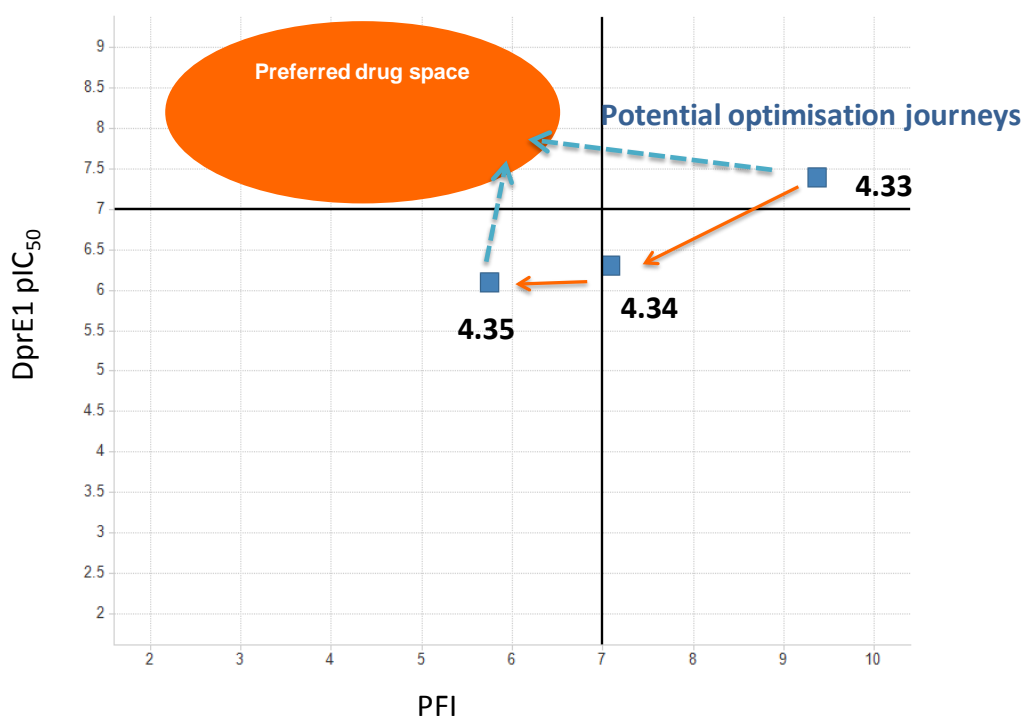
*Figure 4.6: Plot of DprE1 pIC$_{50}$ vs PFI for compounds **4.33, 4.34** and **4.35**, showing ideal drug space and potential optimisation journeys from hit to drug.*

The scaffold hopping exercise resulting in the discovery of **4.35** from **4.33** represents a move towards a more favourable area of physicochemical space, which warranted further investigation. As shown from the hypothetical optimisation journeys in *figure 4.6*, it would be more typical to grow **4.35** slightly whilst improving potency than it would be to maintain activity for **4.35** whilst simultaneously reducing PFI. Although **4.35** was less active than **4.33**, it retained good ligand efficiency and represented a more attractive hit when its whole profile and potential for optimisation was considered and so it was decided to begin hit to lead chemistry around this structure. Compound **4.35** was resynthesised to confirm its activity from a new sample before analogue synthesis began.

Two molecules were initially tested (**4.36** and **4.37**, *table 4.4*), which combined the new piperidine pyrimidine core with the substituents found on **4.33** and **4.34**. The purpose of this experiment was to determine if the SAR was transferable between the thiadiazole series and the pyrimidine series.
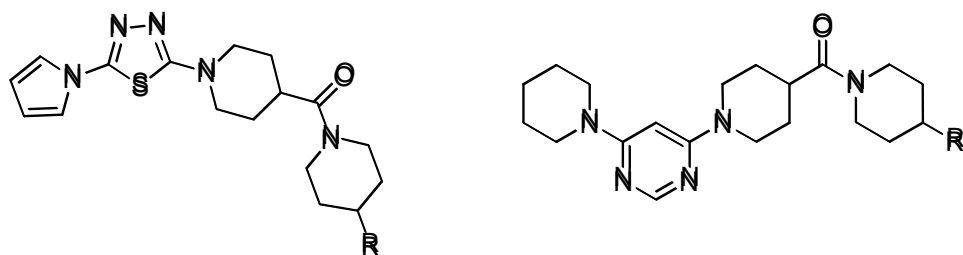
Parameter	4.33 R = CH$_2$Ph	4.34 R = CH$_3$	4.36 R = CH$_2$Ph	4.37 R = CH$_3$
DprE1 pIC$_{50}$	7.3*[a]	6.3	7.1	6.5
MIC (µM)	3.7	20.8	3.5	15.6
LE, LLE$_{AT}$	0.32*, 0.30*	0.35, 0.37	0.29, 0.26	0.33, 0.34
PFI	9.4	7.1	8.9	6.5
clogP	3.0	1.6	3.4	2.0
CLND solubility (µM)	<1	328	28	>488

Table 4.4: Comparison of thiadiazole series and pyrimidine series. *DprE1 pIC$_{5o}$ values above 7.3 are approaching tight binding limit of assay and should be treated with caution. [a] Compound tested inactive (pIC$_{50}$ < 4) on 2 out of 62 test occasions

Comparing compounds **4.36** and **4.37** with their thiadiazole analogues **4.33** and **4.34** showed that the pyrimidine series consistently achieved approximately 0.5 units lower PFI values, translating to improved solubility. The pyrimidine series maintained similar levels of activity to the thiadiazole series in both the DprE1 and MIC assays. Therefore, it was concluded that the bis-piperidinyl pyrimidine ring represented a lower PFI replacement for the pyrrolyl thiadiazole with consistent SAR.

Optimisation of pyrimidine series – replacement of left hand piperidine

Although compounds containing the pyrimidine ring had lower PFI values than the thiadiazole hit, the series was still on the edge of desired property space. Therefore, further lowering of the PFI of the series was required to find a series of compounds which could provide acceptable activity and PFI within the same molecule. The replacement of pyrrolyl thiadiazole with bis-

piperidinyl pyrimidine without loss of activity suggested that the left hand side of the molecule could be a promising area to explore.

A set of small amines was selected which were predicted to be less lipophilic than piperidine. The PFI values of the targets were predicted with both methyl and benzyl substituents on the right hand side piperidine ring, and only those compounds which had predicted PFI values below 7 were selected for synthesis. The compounds were synthesised according to the routes shown in *scheme 4.3.*
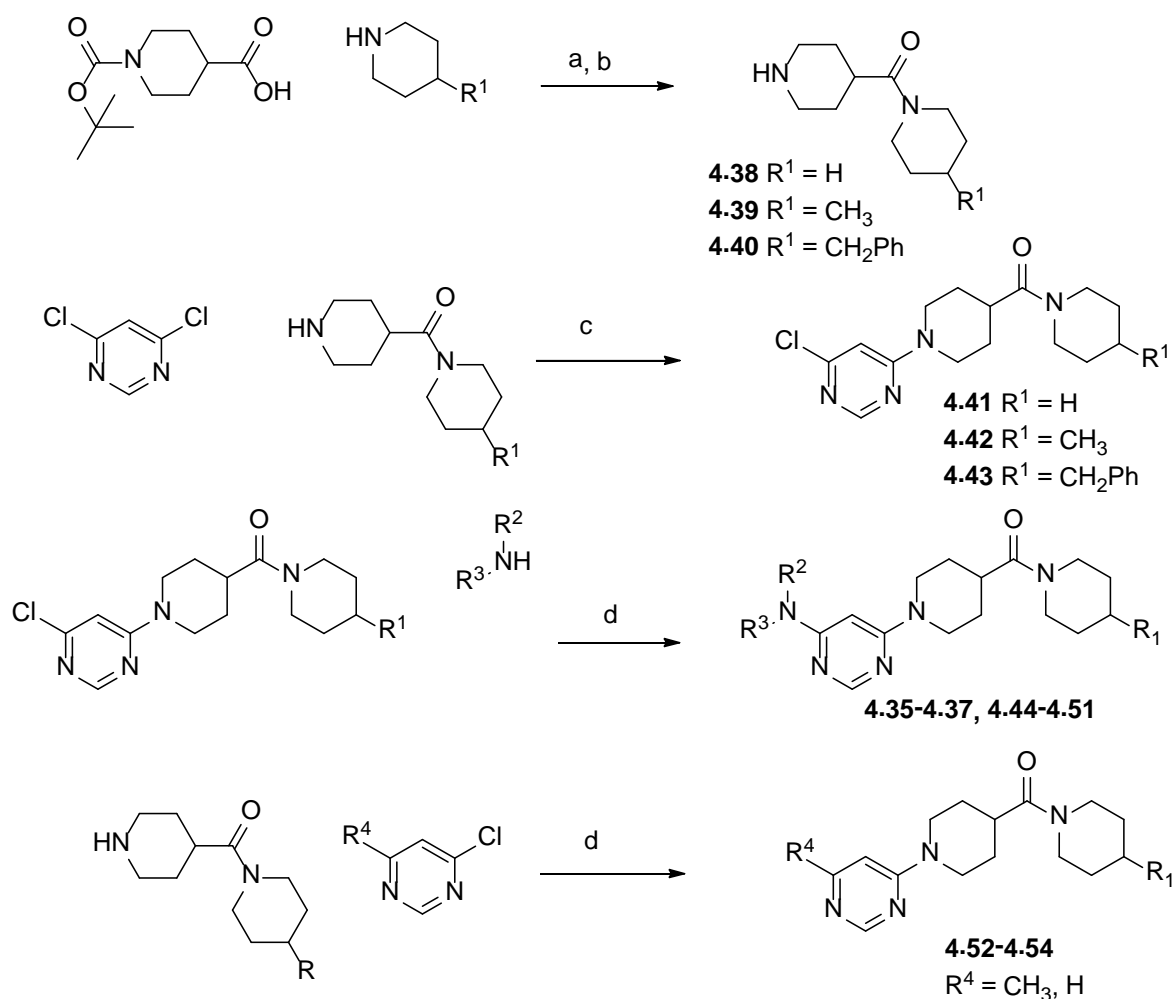
Scheme 4.3: Synthesis of compounds containing replacements for left hand side piperidine. Reagents and conditions: (a) Substituted piperidine (1.2 eq.), COMU (2 eq.), N,N-diisopropylethylamine (3 eq.), N,N-dimethylformamide, room temperature, 2 – 20 h; (b) Hydrochloric acid (4 M in dioxane) (5 eq.), room temperature, 0.5 – 17 h, 91-100% over 2 steps; (c) N,N-diisopropylethylamine (2 eq.), ethanol, microwave, 150 °C, 5 min.; (d) Amine (5 eq.), N,N-diisopropylethylamine (2 eq.), ethanol, microwave, 150 °C, 1 h, 19-43 % over 2 steps.

The bis-piperidine amides **4.38, 4.39** and **4.40** were formed by COMU-mediated amide bond formation,[382] followed by BOC-deprotection. Sequential nucleophilic aromatic substitutions onto 4,6-dichloropyrimidine afforded the final products. The versatility of this route enabled the three steps to be performed in any order, depending on where any structural diversity was to be introduced. The two nucleophilic aromatic substitutions

were carried out in one microwave vial, with the second amine simply pipetted into the vial on completion of the first reaction. These reactions were carried out in an appropriate volume of solvent (0.5-0.9 mL) to allow direct injection of the crude reaction mixture onto mass-directed prep-HPLC at the end of the reactions without the need to carry out any work-up or evaporation. The designed route allowed rapid exploration of piperidine replacements.
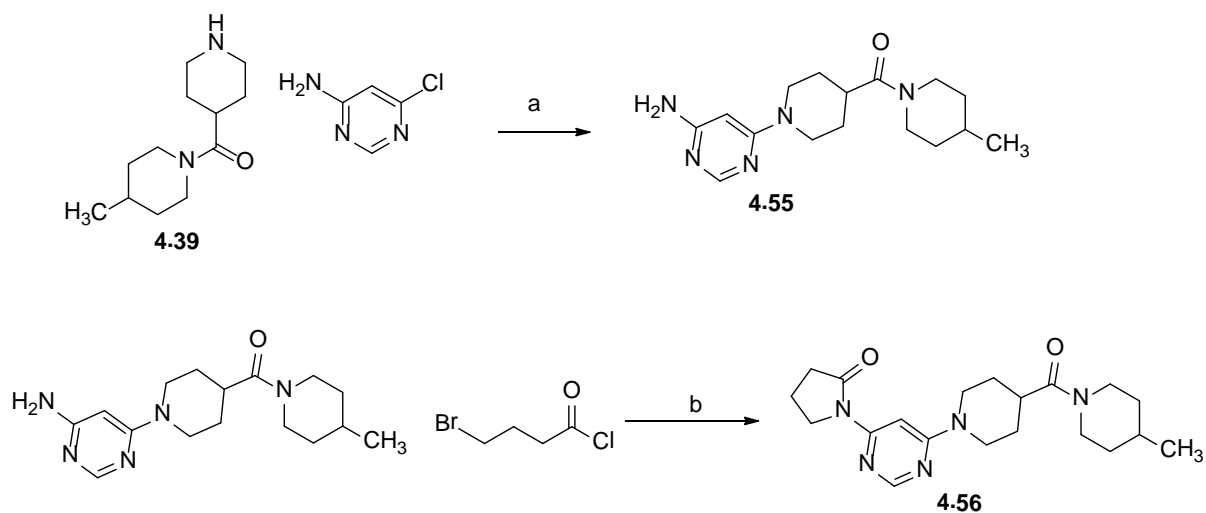
*Scheme 4.4: Synthesis of compound **4.55**. Reagents and conditions: (a) N,N-diisopropylethylamine (2 eq.), ethanol, microwave, 150 °C, 5 min.; (b) Potassium carbonate (3 eq.), ethanol, room temperature, 6 d 2 % over 2 steps.*

The lactam analogue **4.56** was synthesised as shown in *scheme 4.4.* Nucleophilic substitution of the previously formed amine **4.39** onto commercially available 4-amino-6-chloropyrimidine yielded the desired intermediate **4.55**. Subsequent reaction with 4-bromobutanoyl chloride under basic conditions yielded the desired product **4.56**. The reaction was very low-yielding, but sufficient material was obtained for biological testing and so the conditions were not optimised.
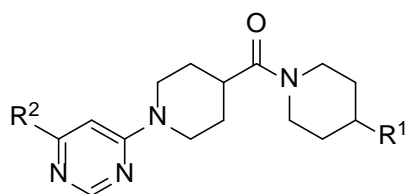
Compound	R^1	R^2	DprE1 pIC50	MIC / μM	Calculated PFI	Measured PFI
4.44	CH_3		6.0	15.6	3.3	4.9
4.45	CH_3	$N(CH_3)_2$	5.0	125.0	4.8	5.0
4.46	CH_3		5.9	23.4	5.0	5.5
4.47	CH_3		< 4.0	> 125.0	3.3	4.1
4.48	CH_3		4.7	> 125.0	5.8	6.1
4.49	CH_3		< 4.0	> 125.0	6.5	6.6
4.50	CH_2Ph		7.6*	0.6	6.6	7.4
4.51	CH_2Ph		4.7	125.0	5.7	6.7
4.52	CH_3	CH_3	< 4.0	> 125.0	4.8	4.4
4.53	CH_3	H	< 4.0	> 125.0	4.0	4.1
4.54	CH_2Ph	H	4.8	> 125.0	6.2	6.8
4.56	CH_3		4.7	> 125.0	4.6	5.0

*Table 4.5: Results of left hand piperidine replacement. *DprE1 pIC$_{50}$ values above 7.3 are approaching tight binding limit of assay and should be treated with caution.*

Table 4.5 shows the results from the synthesised compounds. The measured PFI values were mostly a little higher than the predicted values, which resulted in some synthesised compounds with higher than targeted PFI. The SAR around the left hand piperidine was quite restricted and most of the groups synthesised were less active than the parent piperidine. Only the morpholine group showed a similar level of activity, within assay limits, to piperidine, but with around a 1.5 unit reduction in measured PFI compared with the piperidine compounds. In particular, benzyl compound **4.50** represented an important milestone in this series, being the first compound to achieve a sub-micromolar MIC value. This compound was thus more fully profiled as shown in *table 4.6*.
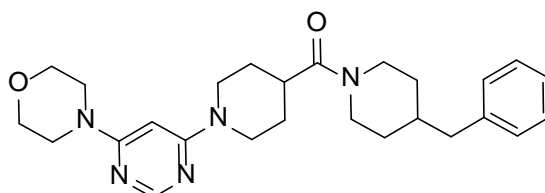
Parameter	4.50
DprE1 pIC$_{50}$	7.6*
LE, LLE$_{AT}$	0.32*, 0.34*
PFI	7.4
clogP	2.1
Basic pKa	5.2
MIC (µM)	0.6
Intracellular MIC (µM)	0.07
DprE1 Over-expressor MIC (µM)	>16
Antibacterial panel MIC (µg/mL)	>128
Cytotoxicity HepG2 pIC$_{50}$	4.2[a]
CLND solubility (µM)	280
FaSSIF solubility (µg/mL)	10 (free base), 26 (HCl salt)
FeSSIF solubility (µg/mL)	80 (free base), 559 (HCl salt)
DMPK	Clint h/m (ml/min/g) = 4.4, 13.5 CYP 3A4 pIC50 <4.0, low MDI risk
Off-target effects	Phospholipidosis induction pMEC < 4.0 hERG pIC$_{50}$ = 4.9

*Table 4.6: Full profile of **4.50**. *DprE1 pIC$_{5o}$ values above 7.3 are approaching tight binding limit of assay and should be treated with caution. [a] Compound tested inactive (pIC50 < 4.0) on 2 out of 4 test occasions.*

Highly potent **4.50** translated its enzyme activity into a low MIC value, which was gratifyingly a further 10-fold lower when measured in the likely more disease-relevant intracellular assay in macrophages.[383] The compound was tested in a strain of *M. tuberculosis* which over-expressed DprE1 and its MIC was shown to increase substantially, indicating that the anti-tuberculosis effect observed in the MIC assays could be attributed to the DprE1 activity of **4.50**. Importantly, **4.50** was shown not be a general cytotoxic agent, being weakly active in the HepG2 cytotoxicity assay, and inactive against an antibacterial panel of 19 common bacterial strains, including *E. coli* and

Staph. aureus, as expected from the mechanism of action, a process unique to mycobacteria. Although the PFI value of **4.50** was substantially reduced in comparison to the piperidine-containing analogue **4.36**, it was still slightly higher than the aspirational value of below 7. Although **4.50** was highly soluble in the high-throughput precipitation from DMSO solution measurement using chemi-luminescent nitrogen detection (CLND), the profile was more complex in simulated intestinal fluid. Compound **4.50** was very poorly soluble in the simulated intestinal fluid in fasted state (FaSSIF), although the solubility was higher in the fed model (FeSSIF) and particularly for the HCl salt. The compound was found not to inhibit the CYP 3A4 P450 metabolic enzyme and was also found to be a low risk for metabolism-dependent inhibition (MDI) of CYP 3A4. However, the measured intrinsic clearance values were rather high for good oral exposure *in vivo*. Screening for undesired off-target effects identified that **4.50** did not appear to have a risk of drug-induced phospholipidosis, but that it did exhibit moderate inhibition of the hERG channel.
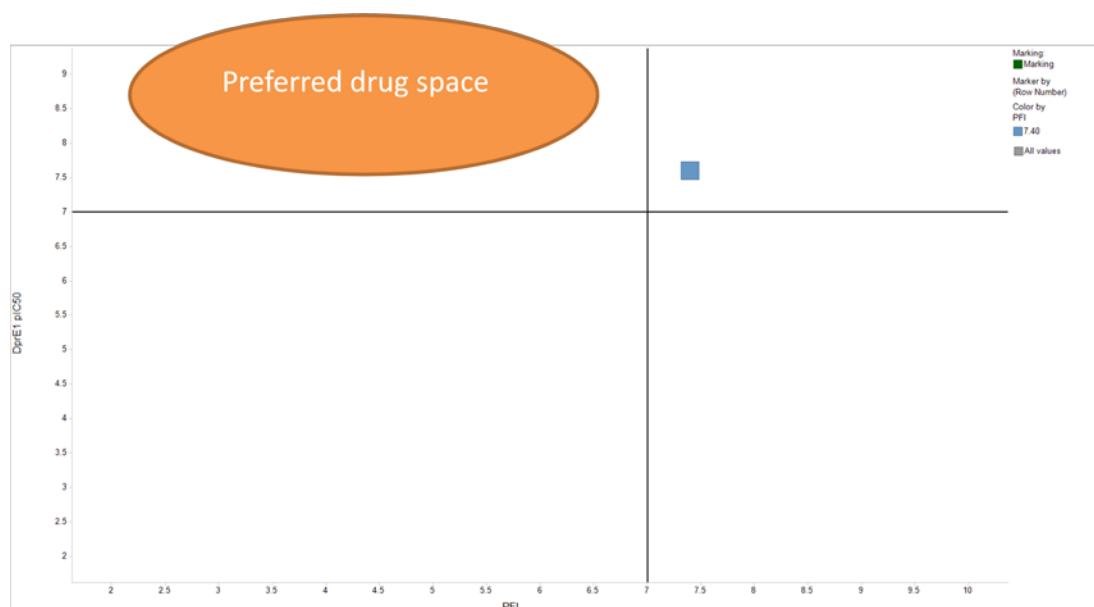
*Figure 4.7: Plot of DprE1 pIC50 vs PFI for compound **4.50** showing position relative to preferred drug space*

*Figure 4.*7 shows how compound **4.50** compares to the preferred drug profile. This compound represented an important step forward as it retained high

potency, and moved closer a desirable PFI space. Compound **4.50** embodied many of the desired features of a lead molecule for DprE1, but further improvement of the physicochemical profile was desirable.

Optimisation of pyrimidine series – fragmentation of the structure

One approach to assess the potential to obtain a molecule with improved physicochemical properties and maintained DprE1 potency was to fragment **4.50** and **4.36** to try to identify which parts of the molecule contributed the most efficiently to binding. The surprising result with piperidine replacements being mostly inactive made it strategically important to deconstruct these molecules in an attempt to try and understand which parts of the structure were important for activity.
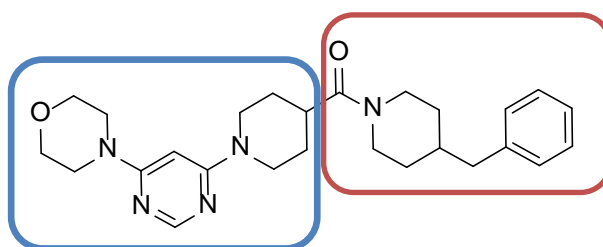
Figure 4.8: Proposed fragmentation strategy

Pyrimidine fragments were synthesised by sequential nucleophilic aromatic substitutions as previously described in *scheme 4.3*. The piperidine amide fragments were synthesised by reaction of the previously described intermediates **4.39** and **4.40** with acetic anhydride as shown in *scheme 4.5*.

4·39 R$_1$ = CH$_3$
4·40 R$_1$ = CH$_2$Ph

4·57 R$_1$ = CH$_3$
4·58 R$_1$ = CH$_2$Ph
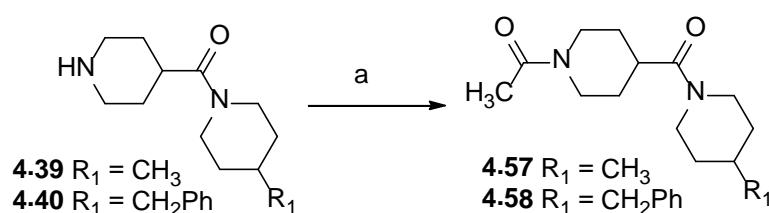
*Scheme 4.5: Synthesis of compounds **4.57** and **4.58**. Reagents and conditions: (a) Acetic anhydride, room temperature, 17 h 24 – 36 %.*

The results of screening the synthesised fragment compounds are presented in *table 4.7*. The pyrimidine-containing left hand side fragments had detectable activity and were thus shown to be binding in a ligand efficient

manner, whilst no activity could be detected for the right hand side bis-piperidine containing fragments. These results implied that it might be possible to grow from the morpholine pyrimidine fragment to find new compounds with more efficient right hand sides. Despite the lack of structural information, these empirical observations suggested there was potential to grow from these fragments to systematically explore potential growth vectors.
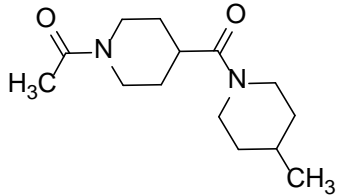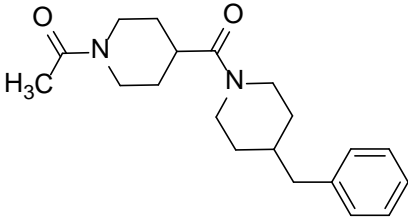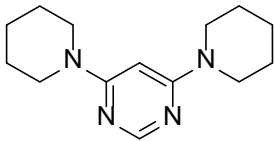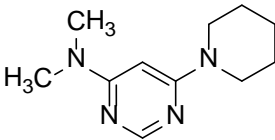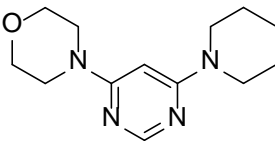
Compound	DprE1 pIC$_{50}$	LE, LLE$_{AT}$
4.57	<3.0*	
4.58	<4.0	
4.59	4.1	0.31, 0.21
4.60	3.9*	0.36, 0.27
4.61	4.1	0.31, 0.31

*Table 4.7: Compounds synthesised to identify efficient binding fragments. *FPR assay data.*
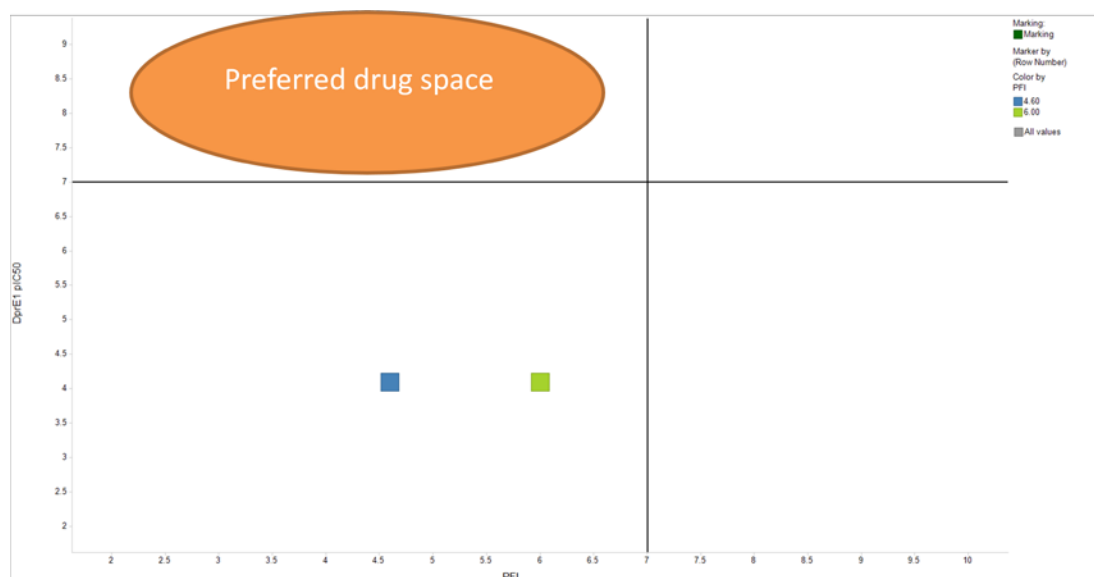
*Figure 4.9: DprE1 pIC50 vs PFI for fragments **4.59** and **4.61***

As illustrated in *figure 4.9*, the fragmentation excersize resulted in fragment molecules which could be considered as good starting points for fragment optimisation, having moderate potency and low PFI, along with good ligand efficiency. Growing from these fragments, especially the more polar **4.61**, could be envisaged to result in optimised leads in the preferred drug space area.

The fragment growing was initiated with the aim of exploring the question of whether or not the piperidine linker adjacent to the pyrimidine ring was optimal. Since measurable activity had been obtained for fragments **4.59**, **4.60** and **4.61** it was thus possible to explore replacements for and substituents on the central piperidine ring by synthesis of truncated morpholine-pyrimidine-amine fragments.This approach had the advantage of considerably simplifying the synthesis of these compounds, which could then be made in a single pot using the sequential $S_N Ar$ chemistry previously described. The crude products were purified after direct injection onto mass-directed preparative HPLC or in some cases precipitated from the reaction solution and were isolated in high purity by filtration. Another advantage of exploring this ring using a fragments approach was that groups which would not have an obvious linker to the benzyl piperidine could also be explored.

A selection of amines was made, which included a range of ring sizes as well as acyclic alkyl amines. Substituents in a range of positions were explored and electron-donating and electron-withdrawing substituents were used to investigate the effect of varying pK$_a$.

The results of the fragment exploration exercise are shown in Appendix 4.2, *table A4.2*. Disappointingly, the SAR in this region of the molecule appeared to be fairly restricted, with most of the synthesised compounds tested showing no quantifiable activity in the DprE1 assay. Only compounds with piperidine and pyrrolidine rings showed activity, with the substituent effects not able to be simply interpreted. The results of the fragment experiment were verified by synthesis of some representative larger compounds containing some of the rings investigated.
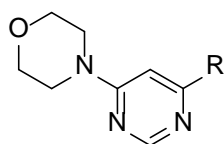
Compound	R	DprE1 pIC_{50}	LE, LLE_{AT}
4.50		7.6*	0.32*, 0.34*
4.106		5.9	0.25, 0.25
4.107		7.6*	0.31*, 0.33*
4.108		6.4	0.26, 0.21

*Table 4.8: Elaborated compounds with alternative central rings. *DprE1 pIC_{50} values above 7.3 are approaching tight binding limit of assay and should be treated with caution. Compound **4.107** was synthesised at GVK BioSciences at the request of Rob Young, GSK. Compound **4.108** was synthesised by Julia Castro-Pichel, GSK.*

Comparison of compound **4.106** with **4.50** showed that pyrrolidine was a less active ring connection than piperidine in the central region. Comparison of **4.107** with **4.108** shows that piperazine also conferred less activity and thus was less ligand efficient than piperidine. These compounds had a 4-fluoro substituent on the terminal benzyl ring. Benzyl substituents will be discussed in more detail later in this chapter.

In conclusion, the fragment work described established some confidence that the left hand portion of the molecule conferred the most effective and ligand efficient binding and that the morpholine and piperidine groups appeared to be optimal pyrimidine substituents.

Optimisation of pyrimidine series – alternative heterocycles

The final portion of the ligand efficient left hand side to be explored was the linking heterocyclic group. A small set of compounds was synthesised with different rings in place of pyrimidine. These had either morpholine or piperidine as the capping ring and either benzyl, methyl or isopropyl as the right hand side piperidine substituent.

The results of this investigation are given in *table 4.9*. Altering the ring was shown to have a drastic effect on the physicochemical properties of the molecules, with PFI values ranging between 5 and 10, due mostly to changes in the lipophilicity of the heterocyles. The thiadiazole ring found in the original hit molecule **4.33** was synthesised in this series (compound **4.109**) and found to maintain activity with an improved PFI value and lower intrinsic clearance relative to **4.33**. For all of the compounds containing more than one heteroatom in the ring (**4.109** – **4.117**), similar DprE1 potency to the pyrimidine core was observed, with pIC_{50} values around 7 for benzyl- and isopropyl-substituted compounds and 6 for methyl analogues (isopropyl substituent will be discussed in later sections). The one exception to this result is for pyridazine **4.113**, which presumably placed the terminal piperidine ring in the incorrect orientation to allow for binding with the protein. These data suggested that the heterocyclic ring could be acting as a spacer between the two cyclic amines, rather than contributing any specific polar interactions through its own heteroatoms. However, there were subtle caveats to this conclusion, revealed by the pyridine-core compounds **4.118 - 4.120**, which all showed substantially reduced activity compared to **4.117,** suggesting that a basic heterocycle was not well-tolerated, perhaps because a heteroatom in the active compounds may be acting as a hydrogen bond acceptor**.** There was a general trend observed for improving intrinsic clearance and hERG activity for lower PFI analogues. This was best exemplified by compound **4.116,** which had a PFI of just 5.6, low intrinsic clearance in human microsomes, moderate intrinsic clearance in mice and no measurable hERG binding in the barracuda assay.
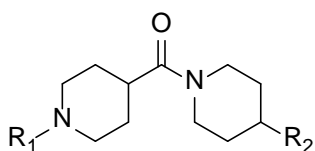
Compound	R1	R2	DprE1 pIC$_{50}$	LE, LLE$_{AT}$	PFI	MIC (μM)	Clint h/m (ml/min/g)	hERG pIC$_{50}$
4.109	morpholine-1,3,4-thiadiazolyl	CH$_2$Ph	7.4*	0.32* 0.34*	7.1	4.0	2.8, 3.1	4.4[a]
4.110	morpholine-pyrimidinyl	CH$_2$Ph	7.4*	0.31* 0.33*	8.0	3.0	5.4, 63.7	4.4
4.111	piperidine-pyrimidinyl	CH$_2$Ph	6.8	0.28 0.25	10.0	15.8		
4.112	morpholine-fluoropyrimidinyl	CH$_2$Ph	7.2	0.29 0.31	8.4	1.3	2.8, 8.3	4.9[b]
4.113	piperidine-pyridazinyl	CH$_3$	<4.0		6.1	>125		
4.114	piperidine-pyridazinyl	CH$_3$	5.9	0.30 0.31	5.3	54.8		
4.115	morpholine-aminopyrimidinyl	CH$_2$Ph	7.3*	0.29* 0.32*	7.1	3.5	3.4, 11.6	5.2
4.116	morpholine-oxopyrimidinyl	CH$_2$Ph	7.4*	0.30* 0.40*	5.6	3.0	<0.5, 4.9	<4.3
4.117	morpholine-pyrimidinyl	CH(CH$_3$)$_2$	7.1	0.34 0.37	6.2	3.0	3.3, 5.1	4.4[c]
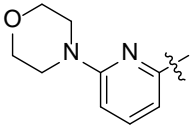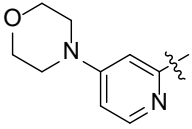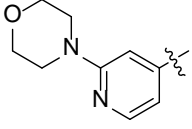
4.118		CH(CH₃)₂	5.0	0.24 0.25	8.3	>125
4.119		CH(CH₃)₂	5.2	0.25 0.25	5.6	>125
4.120		CH(CH₃)₂	5.1	0.24 0.25	5.6	>125

Table 4.9: Alternative heterocyclic cores. *DprE1 pIC$_{50}$ values above 7.3 are approaching tight binding limit of assay and should be treated with caution.
[a] Compound tested inactive (pIC50 < 4.3 on 2 out of 6 test occasions).
[b] Compound tested inactive (pIC50 < 4.3 on 3 out of 6 test occasions).
[c] Compound tested inactive (pIC50 < 4.3 on 1 out of 3 test occasions).
*Compound **4.109** was synthesised by Julia Castro-Pichel, GSK. Compounds **4.110** and **4.112** were synthesised by Rob Young, GSK. Compound **4.111** was synthesised by Maria Garcia-Palencar, GSK. Compounds **4.115** and **4.116** were synthesised by Ben Whitehurst, GSK/University of Strathclyde Industrial PhD student. Compound **4.117** was synthesised by chemists at GVK Bioscience at the request of Rob Young. Compounds **4.118, 4.119** and **4.120** were synthesised by chemists at Peakdale at the request of Rob Young.*
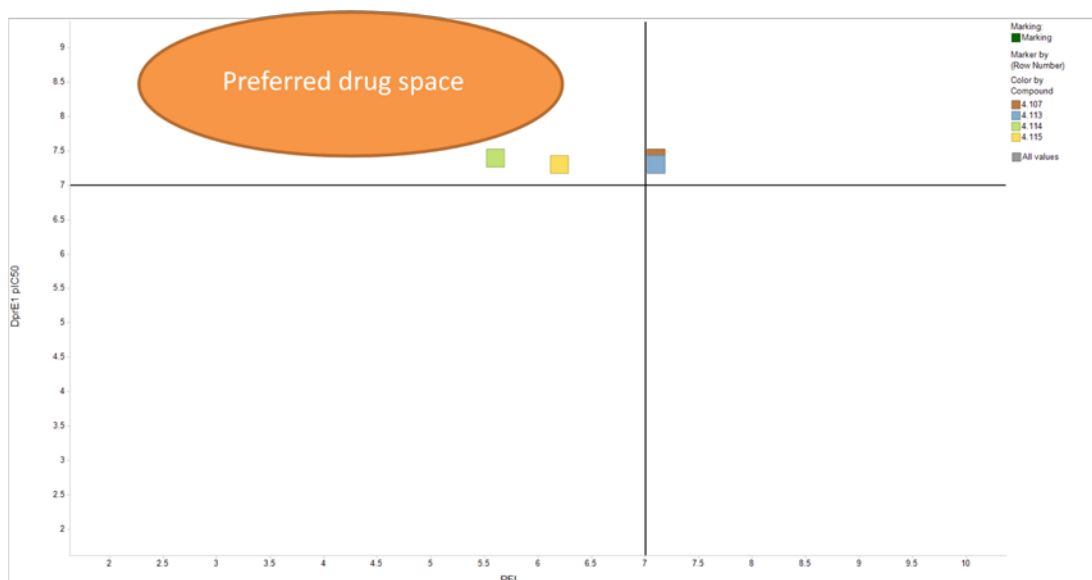
*Figure 4.10: Plot of DprE1 pIC$_{50}$ vs PFI for compounds **4.109, 4.115, 4.116** and **4.117** showing ideal drug space*

Figure 4.10 shows that for the first time, synthesised compounds (**4.115** and **4.116**) were beginning to enter the desired drug space quadrant of high pIC$_{50}$ and low PFI.

Compounds **4.113** and **4.114** were synthesised by me according to the route given in *scheme 4.6.*
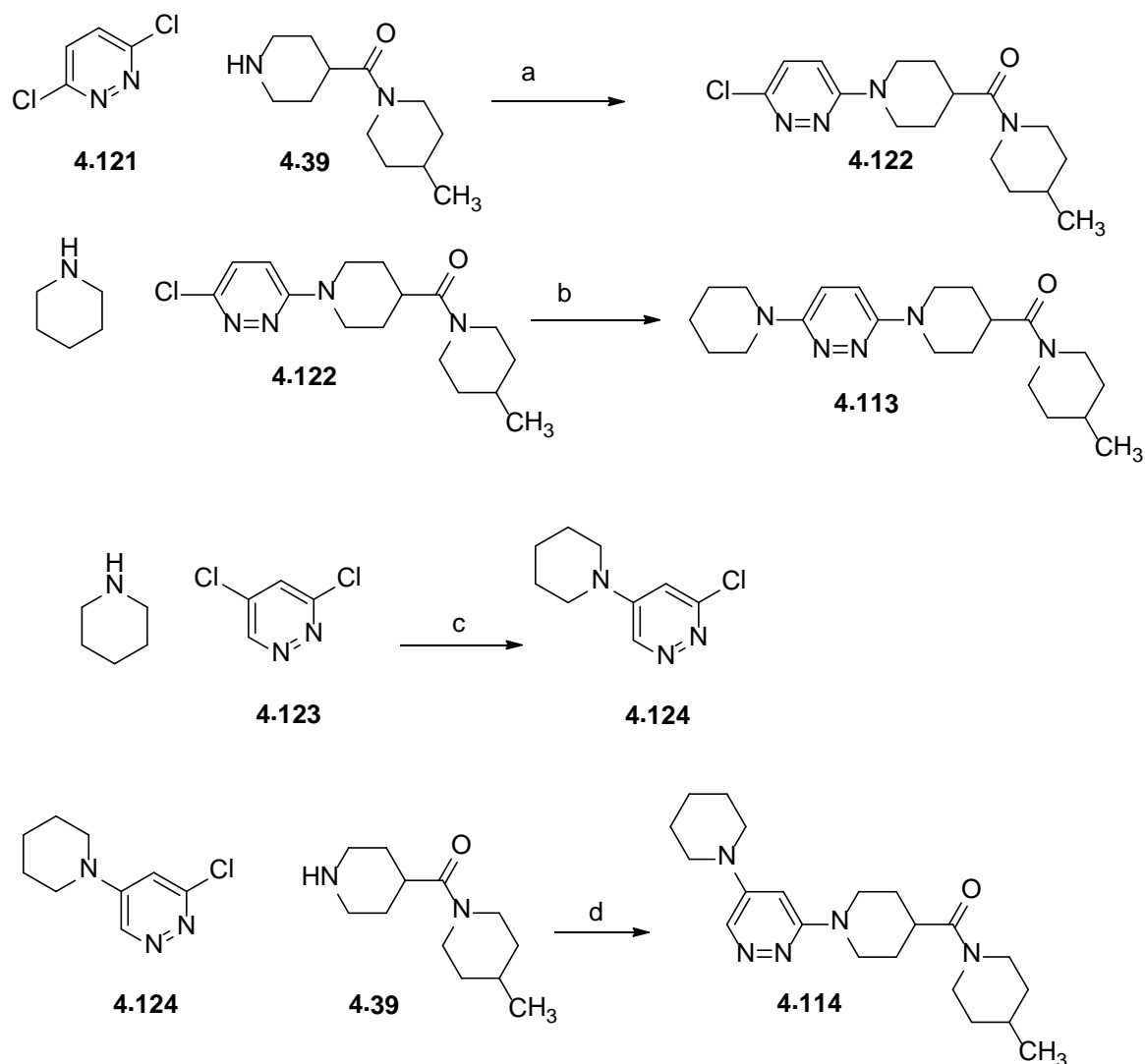
*Scheme 4.6: Synthesis of pyridazine containing compounds **4.113** and **4.114**. Reagents and conditions: (a) N,N-diisopropylethylamine (2 eq.), ethanol, microwave, 150 °C, 2 h; (b) N,N-diisopropylethylamine (2 eq.), ethanol, microwave, 150 °C, 12 h, 15 % over 2 steps; (c) N,N-diisopropylethylamine (2 eq.), ethanol, microwave, 150 °C, 5 min.; (d) N,N-diisopropylethylamine (2 eq.), ethanol, microwave, 150 °C, 2 h 2 % over 2 steps.*

The synthesis was carried out by sequential S_NAr chemistry, using a similar protocol as for the synthesis of the pyrimidine analogues. For the synthesis of compound **4.113**, the starting dichloropyridazine **4.121** was symmetrical and so tactically piperidine was added in the second step. This was because it was more convenient to use piperidine in excess in the second, less reactive step than it would be for the synthesised compound **4.39** for which less

material was available. For **4.114** the order of addition of the different amine groups was determined by precedented orders of reactivity of the two chlorines.[384]

The reaction was very low yielding for the synthesis of **4.114.** This was partially due a competing side-reaction in the first step, where the piperidine reacted twice with the dichloropyridazine **4.123** to form the undesired product **4.125** (molecular weight = 246), which eluted extremely closely with **4.114** and so was difficult to purify (see *figure 4.11*). Some pure product was obtained by normal phase column chromatography, but some desired product was discarded due to the difficulty of the separation.

4.125
Molecular weight = 246

4.114
Molecular weight = 371
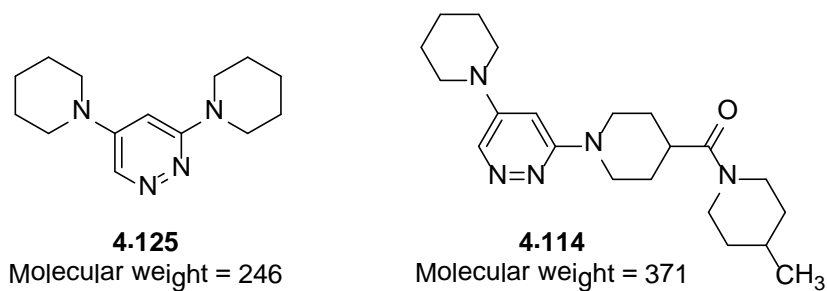
a
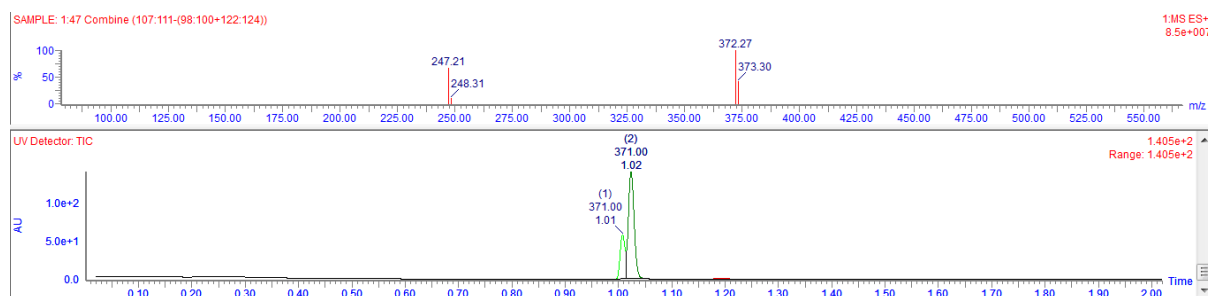
b
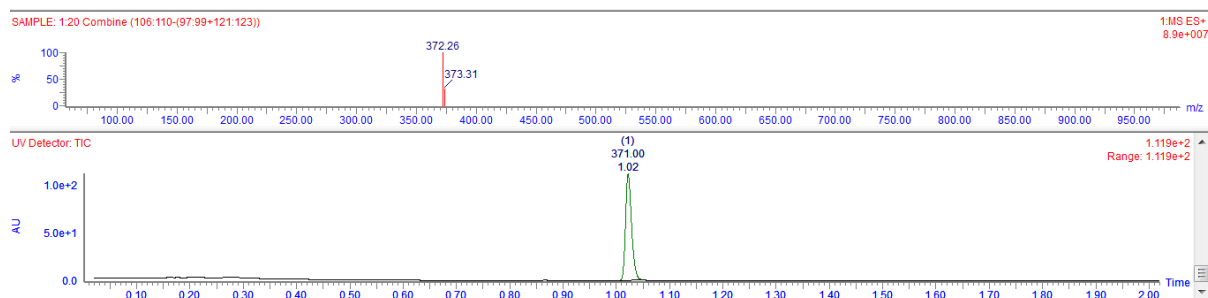
*Figure 4.11: Analysis of compound **4.114** by LCMS, showing (a) contamination with undesired side-product **4.125** and (b) after purification to remove **4.125***

The synthesis of **4.112** was also low-yielding, although this was more due to the sluggish nature of the S_NAr reactions on this 3,6-dichloropyridazine substrate **4.120** rather than over-reaction as had been observed for **4.113**. No evidence of disubstitution was seen in the first step, although interestingly some product with molecular weight of 246 was present after the second step, implying that unreacted starting dichloropyridazine **4.120** reacted twice with piperidine in the second step to form undesired **4.126**. This by-product was able to be separated by mass-directed preparative HPLC (*figure 4.12*).

4·126
Molecular weight = 246

4·113
Molecular weight = 371
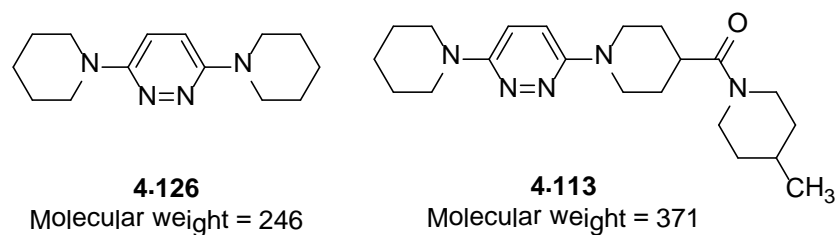
a
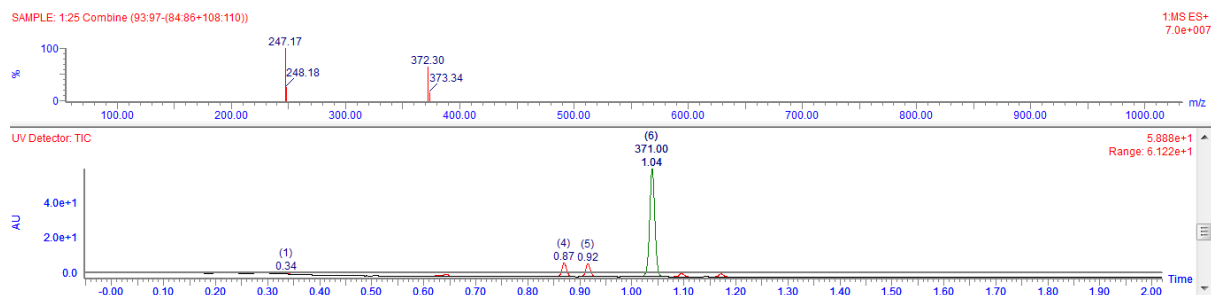
b
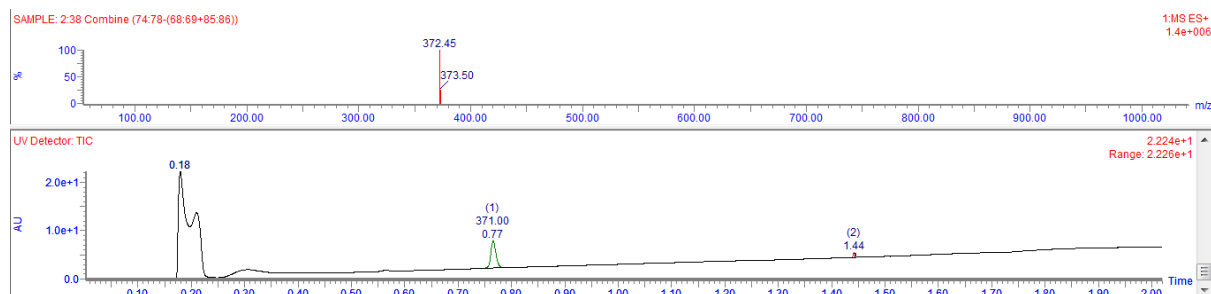
*Figure 4.12: Analysis of compound **4.113** by LCMS, showing (a) contamination with undesired side-product **4.126** (LCMS with ammonium bicarbonate modifier) and (b) after purification to remove **4.126** (LCMS with formic acid modifier).*

To confirm the expected regiochemistry of **4.114** as predicted by the literature[384] a rotating frame nuclear Overhauser effect spectroscopy (ROESY)[385] experiment was carried out to confirm which chlorine was substituted first. This experiment was carried out by Richard Upton, Chemical Sciences, GSK.

224
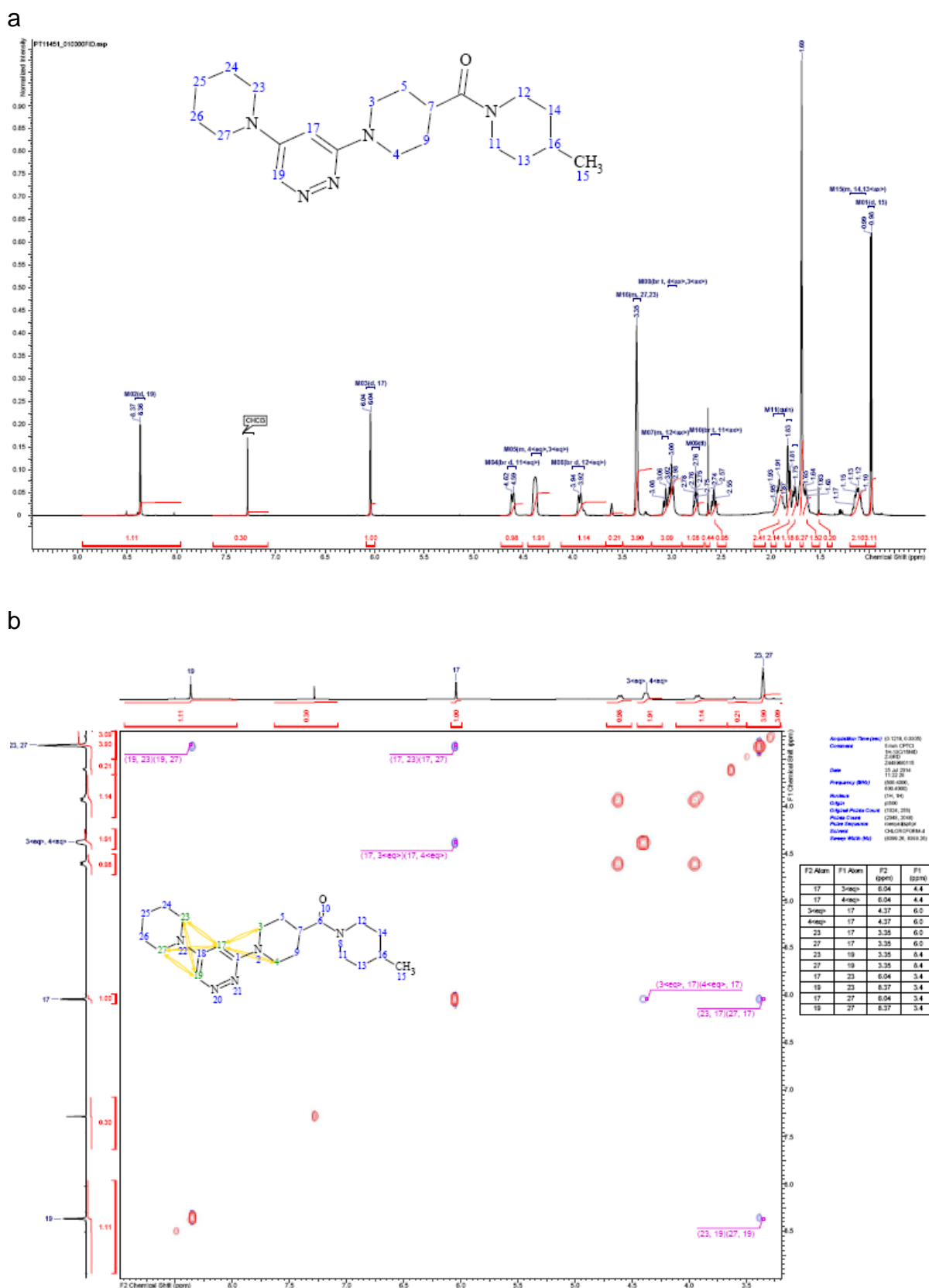
Figure 4.13: (a) ^{1}H NMR spectrum of **4.114**; (b) ROESY spectrum of **4.114**

The ^{1}H NMR spectrum shown in *figure 4.13* was used to assign the important signals needed to define regiochemistry; namely those marked as 23, 27, 17, 19, 3 and 4. The two heteroaromatic proton signals 17 and 19 could be easily differentiated from each other on the basis of their chemical shifts. Signals for protons 3 and 4 could be distinguished from 23 and 27 on the basis of their differing chemical environments as follows. The four protons in positions 23 and 27 were chemically equivalent to one another and so appeared as a broad singlet with an integral for four protons at δ = 3.3 Hz. In contrast to this, the four protons at position 3 and 4 were diastereotopic, as a result of the presence of the amide substituent at position 7 of the ring. Therefore, the signals for these protons were split into two different sets; one for equatorial protons and one for the axial ones. These could be assigned on the basis of their couplings. Axial protons show two large couplings as a result of coupling to their geminal proton and their adjacent axial proton; whilst equatorial protons only show one large coupling to their geminal proton. In this case, the equatorial protons appeared as a broad singlet, while the axial ones were a broad triplet. The results of the ROESY experiment shown in *figure 4.13* showed correlations between protons 17 and 19 with protons 23 and 27. A correlation was also observed from proton 17 only to the equatorial protons at positions 3 and 4. These data provided high confidence that the desired regiochemical outcome had been achieved.

With these results in hand, the left hand side of the molecule was fixed with morpholine, pyrimidine, piperidine as the preferred sequence of rings and attention turned to exploring SAR and modulating properties in the right hand side of the molecule.

Optimisation of pyrimidine series – modifying the right hand piperidine ring

Alternative rings to the right hand piperidine ring were synthesised in an effort to explore the SAR of this area of the molecule. The rings which were selected were small cyclic amines which had the closest structure to piperidine. The final products were synthesised in an analogous method to

the route used to synthesise the piperidine containing compounds depicted in *scheme 4.3*. The selected amines were coupled to 1-(6-morpholinopyrimidin-4-yl)piperidine-4-carboxylic acid (supplied in bulk by GVK Biosciences).
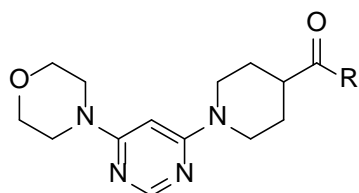
Compound	R	DprE1 pIC$_{50}$	LE, LLE$_{AT}$	PFI	MIC (µM)
4.127		5.4	0.22, 0.24	7.2	125
4.128		6.2	0.26, 0.28	7.6	32
4.129		5.8	0.23, 0.34	5.5	10
4.130		6.5	0.30, 0.37	6.3	10
4.131		5.2	0.22, 0.27	6.3	>125
4.132		6.2	0.26, 0.30	6.3	20
4.133		4.6	0.18, 0.26	4.9	>80
4.134		6.9	0.30, 0.34	6.6	4

*Table 4.10: Replacements for benzyl piperidine. Compounds **4.129**, **4.135** and **4.133** were synthesised by chemists at GVK Bioscience at the request of Rob Young, GSK*

Table 4.10 shows the results of the piperidine replacement experiment. Alternative regioisomers of benzyl piperidine were synthesised (**4.127** and **4.128**) and were shown to be less active than 4-substituted piperidine. Additional substituents such as hydroxyl in **4.129** were not well tolerated on the piperidine ring. The tetrahydroisoquinoline containing compound **4.130** was one of the more potent analogues, though it was still at least a log unit less active than the 4-benzyl piperidine compound **4.50** and it had no MIC. The morpholine-containing compound **4.131** was a log unit less active than the comparable piperidine **4.128**. Piperazine containing analogues, either directly linked to the phenyl or linked through an amide bond were less active than piperidine (**4.132** and **4.133**). Of all of the rings explored, pyrrolidine **4.134** gave the most promising profile. Although this compound had lower activity in the DprE1 and MIC assays than the lead molecule **4.50**, the level of activity was still within the range of the best compound. This compound is also less lipophilic than the piperidine containing compound, resulting in lower chromlogD$_{7.4}$ by almost 1 unit. This ring could perhaps be used as a viable lower PFI alternative to the piperidine ring during lead optimisation, especially if it could be found that the potency could be increased by optimisation in other areas of the molecule.
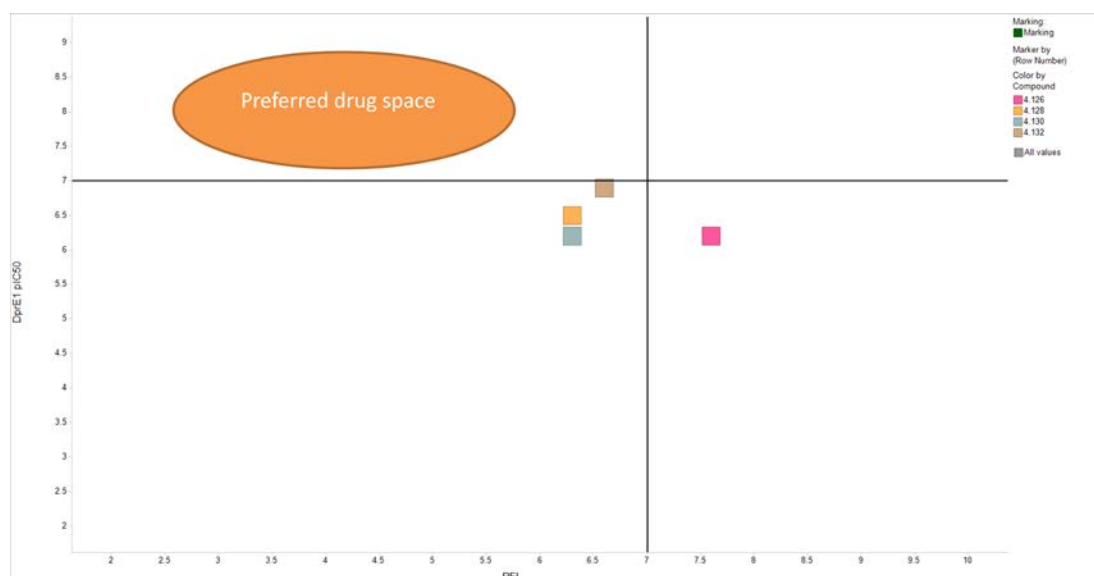
*Figure 4.14: Plot of DprE1 pIC$_{50}$ vs PFI for compounds **4.128**, **4.130**, **4.132** and **4.134** showing ideal drug space*

The replacements for the benzyl piperidine were close to reaching the preferred drug space in *figure 4.14*, but the potencies and MICS achieved were not quite good enough, although the lower PFIs were encouraging.

Optimisation of pyrimidine series – modifying the piperidine-phenyl linker

The aliphatic methylene carbon in a benzyl functional group is well known to be vulnerable to oxidative metabolism.[386] Therefore, alternative linkers between the piperidine and phenyl rings were explored, which might replace this potential liability and also improve the molecules' physicochemical profiles by reducing lipophilicity. Heteroatom containing linkers were used to reduce the lipophilicity of the molecules, and also to investigate whether additional polar interactions could provide improved binding in this region of the molecule. Additionally, heterocyclic replacements for the phenyl ring were also explored.
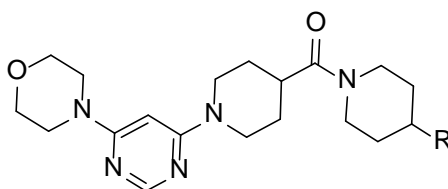
Compound	R	DprE1 pIC$_{50}$	LE, LLE$_{AT}$	PFI	MIC (μM)	Clint h/m (ml/min/g)	hERG pIC$_{50}$
4.135	NH-phenyl	6.4	0.27, 0.36	6.3	10		
4.136	O-phenyl	8.1*	0.34*, 0.41*	6.8	2	7.4, <0.5	4.6
4.137	C(O)-thiophene	6.2	0.26, 0.36	5.8	16		
4.138	C(O)-furan	5.2	0.22, 0.34	5.1	125		
4.139	C(O)-thiazole	5.2	0.22, 0.35	5.5	>125		
4.140	CH(OH)-thiophene	5.7	0.24, 0.35	5.2	125		
4.141	CH(OH)-furan	5.2	0.22, 0.35	4.7	125		
4.142	CH(OH)-thiazole	4.7	0.20, 0.36	4.2	>125		

*Table 4.11: Alternative linkers. *DprE1 pIC$_{50}$ values above 7.3 are approaching tight binding limit of assay and should be treated with caution. Compounds **4.135** and **4.136** were synthesised by chemists at GVK Bioscience at the request of Rob Young, GSK.*

Table 4.11 shows the results for the alternative linkers tested. The methylene carbon could be replaced with oxygen without loss of activity (**4.136**), although there was an approximately one log unit reduction when a nitrogen atom was used (**4.135**). The use of an oxygen linker reduced the PFI

compared to the parent benzyl compound **4.50** (PFI = 7.4) and this compound showed improved intrinsic clearance in mouse microsome preparations, but not human (**4.50** Clint h/m = 4.4/13.5 ml/min/g). Ketone and benzylic alcohol linkers were explored in a series of 5-membered heterocycles (**4.137** – **4.142**). In general, these showed a significant reduction in DprE1 potency and MICs.
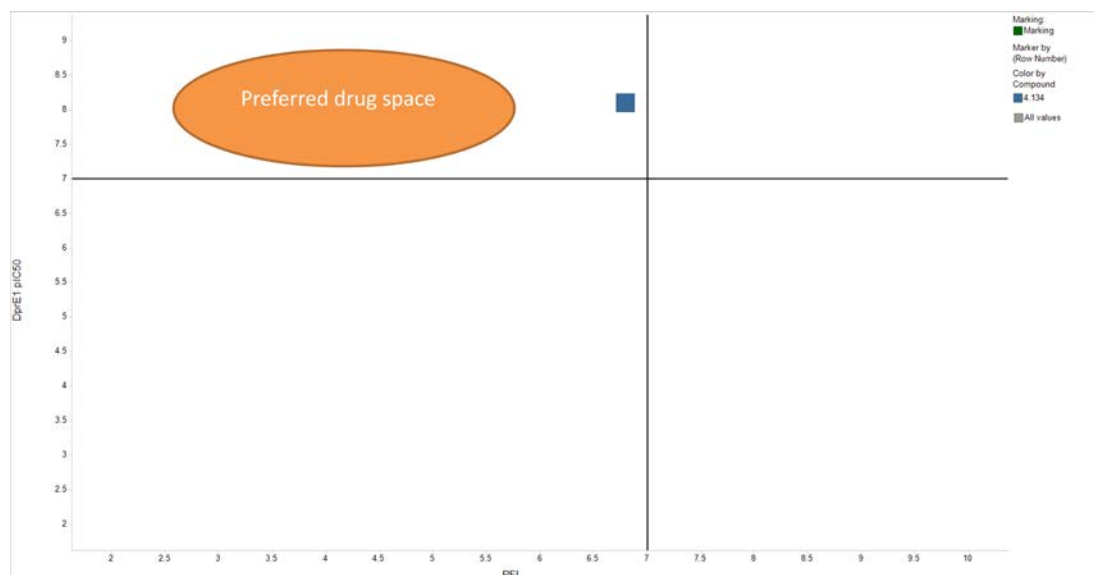
*Figure 4.15: Plot of DprE1 pIC_{50} vs PFI for compound **4.136**, showing ideal drug space.*

Compound **4.136** represented a significant step forward towards the goal of identifying compounds with high potency and low PFI (*figure 4.15*).
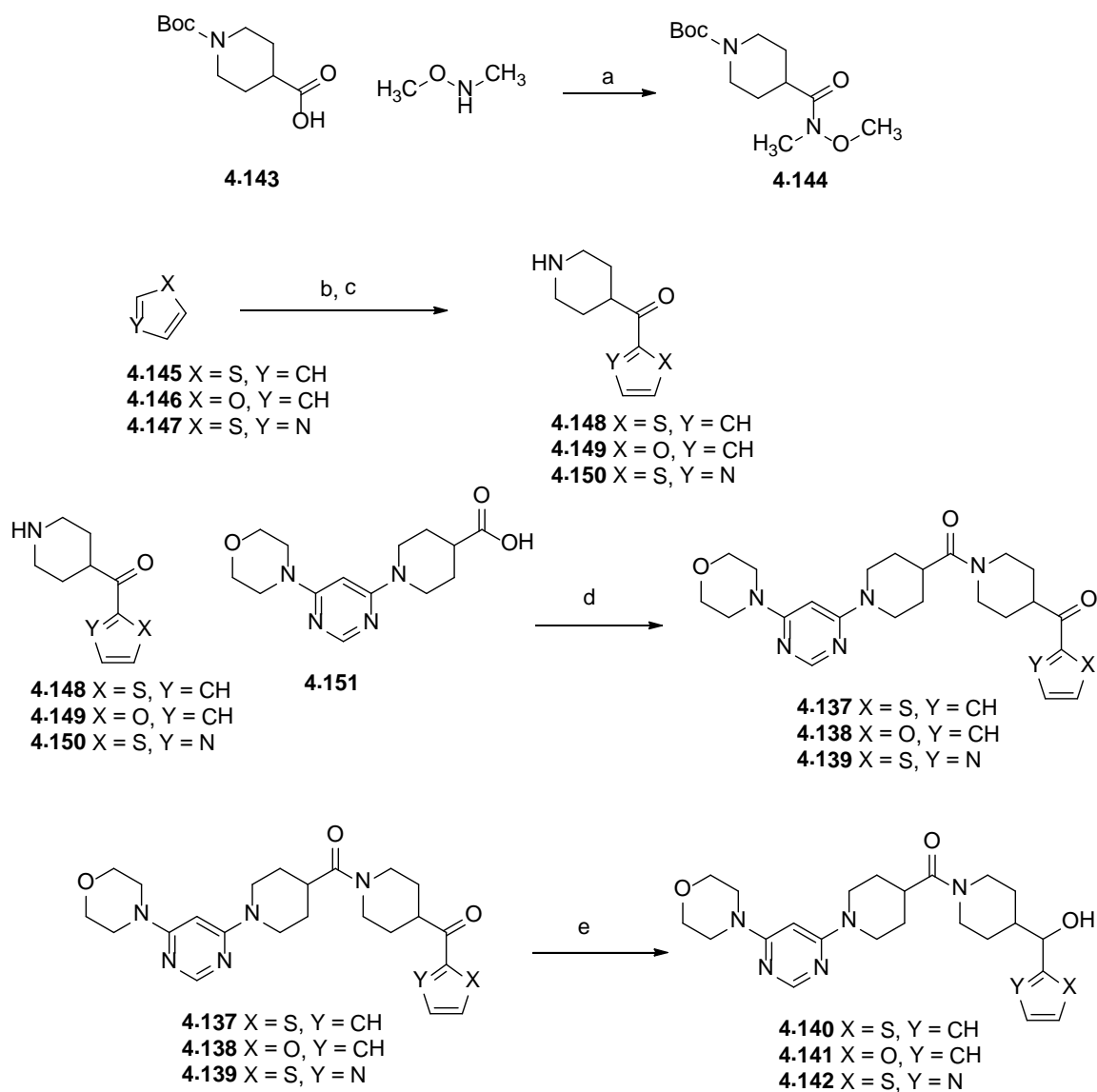
*Scheme 4.7: Synthesis of ketone linked compounds **4.137** - **4.139** and benzylic alcohol linked compounds **4.140** - **4.142**. Reagents and conditions: (a) Carbonyl diimidazole (1.2 eq.), triethylamine (2.2 eq.), dichloromethane, room temperature, 24 h, 73 %; (b) n-butyl lithium, tetrahydrofuran,**4.144**, -78 °C – room temperature overnight; (c) Concentrated HCl, tetrahydrofuran, room temperature, 3-4 h, 100 % over 2 steps; (d) COMU, N,N-diisopropylethylamine, N,N-dimethylformamide, room temperature, overnight 13–96 %; (e) Sodium borohydride, 2-methyl tetrahydrofuran, ethanol, room temperature 34-98%.*

The ketone and benzylic alcohol linked products **4.137** - **4.142** were synthesised as shown in scheme 4.7. The synthesis began with the conversion of the commercially available Boc-protected piperidine 4-

carboxylic acid into its corresponding Weinreb amide[387] using standard carbonyl diimidazole coupling conditions.[388] The ketone building blocks **4.148** - **4.150** were then synthesised by deprotonation of the appropriate heterocycle using *n*-butyllithium, followed by low-temperature addition to the Weinreb amide. Amide bond formation using COMU was carried out onto the piperidine acid intermediate **4.151**, which had been supplied by custom synthesis at GVK Biosciences to yield the ketone products **4.137** - **4.139**. Finally, reduction of these products with sodium borohydride resulted in the alcohols **4.139** - **4.142**.

Optimisation of pyrimidine series – modifying the terminal phenyl group

Phenyl rings are well known by medicinal chemists to be a likely site for oxidative metabolism[389,390] and so replacing or modifying this group was a desirable objective. A phenyl ring is a lipophilic, aromatic group, which itself has a calculated PFI value of 4 (1 aromatic ring and a chromlogD$_{7.4}$ of 3) and so replacing or modulating the phenyl ring with more polar or non-aromatic groups also represented an important opportunity to modulate the overall physical properties of the molecules.

The results of replacing the phenyl group are given in *table 4.12*. Blocking the most likely potential site of metabolism with a *para*-fluoro group (**4.107**) resulted in maintained activity in both the enzymatic and MIC assays, with the advantage of improved intrinsic clearance values in both species studied. This implied that oxidation of the ring in the 4-position was a likely route of metabolism for the parent compound **4.50**.

Heteroatoms were introduced into the pendant ring (**4.152 - 4.155)**. In the case of pyridine compounds **4.152** and **4.153**, activity at DprE1 was maintained, along with potent MICs. However, 5- and 6-membered rings containing more than one heteroatom (**4.154** and **4.155**) resulted in much-diminished potency. *Meta*-pyridyl compound **4.152** exhibited a very promising

overall profile, with improved intrinsic clearance values in both humans and mice, along with low hERG inhibition.

Importantly, it was demonstrated that the piperidine-substituent did not need to be aromatic and a range of aliphatic groups were synthesised to explore the SAR of non-aromatic substituents (**4.156** - **4.167**). Ethyl (**4.156**), isopropyl (**4.117**) and *tert*-butyl (**4.157**) groups all maintained DprE1 enzyme activity and showed good MICs. The isopropyl compound **4.117** was progressed to intrinsic clearance and hERG assays, were it was found to represent a likely improvement in both assays over the parent benzyl compound **4.50**.

Cyclic aliphatic groups, such as cyclopentyl (**4.159**) and (cyclopentyl)methyl (**4.160**) groups afforded high DprE1 potency and low MICs. These compounds were both very lipophilic and had higher than ideal PFI values. However, the (cyclopentyl)methyl compound **4.160** did demonstrate an improvement in intrinsic clearance compared to the phenyl-containing **4.50**, which again served to reinforce the hypothesis that the phenyl ring was a potential metabolic liability. A surprising result in the series of cyclic groups was the poor activity of cyclopropyl-containing **4.158**, as cyclopropyl is a commonly employed isostere for ethyl, propyl, isopropyl and *t*-butyl groups.[391] It is unclear from the established SAR why it should be that branched alkyl groups and larger rings are tolerated when cyclopropyl is not. An attempt to lower the lipophilicity of the cyclopentane-containing compounds was made by replacement of cyclopentyl group in **4.159** with both regio-isomers of tetrahydrofuran in compounds **4.161** and **4.162**. However, these changes were not well tolerated.

A series of spirocyclic rings was synthesised (**4.163** - **4.166**) and a similar trend to the pendant cyclic aliphatic series was observed. The carbocyclic ring of compound **4.163** was preferred to any of the heterocyclic rings in compounds **4.164** - **4.166**.

Finally, a range of basic susbtituents were explored (**4.166** - **4.168**), in order to dramatically reduce the PFI of the molecules and test the tolerance for basic groups. These compounds were all inactive.
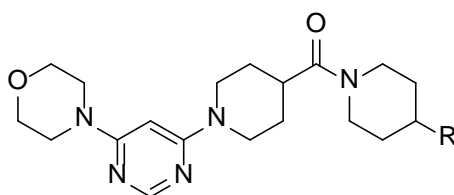
Compound	R	DprE1 pIC$_{50}$	LE, LLE$_{AT}$	PFI	MIC (µM)	Clint h/m (ml/min/g)	hERG pIC$_{50}$
4.50	benzyl	7.6*	0.32*, 0.34*	7.4	0.6	4.4, 13.5	4.9
4.107	4-fluorobenzyl	7.6*	0.31*, 0.33*	7.4	0.6	2.1, 8.4	5.0
4.152	3-pyridyl	7.0	0.29, 0.38	5.2	3.3	3.1, 7.2	5.6 [a]
4.153	2-pyridyl	6.6	0.27, 0.36	5.2	8.8		
4.154	pyrimidinyl	4.1	0.17, 0.30	4.2	>125		
4.155	imidazolyl	4.8	0.21, 0.33	3.4	>125		
4.156	CH$_3$	6.8	0.33, 0.38	5.6	8.0		
4.117	CH(CH$_3$)$_2$	7.1	0.34, 0.37	6.2	2.0	3.3, 5.1	4.4 [b]
4.157	C(CH$_3$)$_3$	6.9	0.32, 0.33	6.7	4.0		
4.158	cyclopropyl	<4.0 [c]		5.9	4.0		
4.159	cyclopentyl	7.1	0.31, 0.33	7.5	2.5	34.7, 6.6	
4.160	cyclopentylmethyl	7.6*	0.33*, 0.32*	7.9	3.0	2.1, 3.1	4.7 [d]
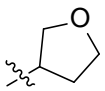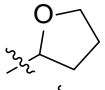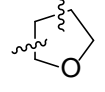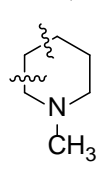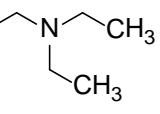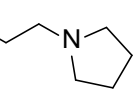
Compound	Structure				
4.161		4.7	0.21, 0.32	3.9	80
4.162		4.7	0.21, 0.32		80
4.163		6.4	0.29, 0.33	6.3	32.0
4.164		5.3	0.24, 0.38	3.5	>125
4.165		4.7	0.21, 0.36	4.0	>125
4.166		<4.0		2.2	>125
4.167		<4.0		2.2	>125
4.168		4.1	0.17, 0.25	2.1	>125

Table 4.12: Benzyl replacements. *DprE1 pIC_{50} values above 7.3 are approaching tight binding limit of assay and should be treated with caution.
[a] Compound tested inactive ($pIC_{50} < 4.3$) on 7 out of 9 test occasions.
[b] Compound tested inactive ($pIC_{50} < 4.3$) on 1 out of 3 test occasions.
[c] Compound tested active ($pIC_{50} = 4.3$) on 1 out of 3 test occasions.
[d] Compound tested inactive ($pIC_{50} < 4.3$) on 3 out of 6 test occasions.
Compounds 4.107, 4.117, 4152 - 4.155. and 4.160 were synthesised by chemists at GVK Bioscience at the request of Rob Young, GSK. Compounds 4.157 - 4.159 and 4.161 - 4.164 were synthesised by chemists at ChemPartner at the request of Rob Young, GSK. Compounds 4.156 and 4.165 - 4.168 were synthesised by chemists at Peakdale at my request.

Overall, some very promising results were obtained from altering the benzyl linker and the phenyl group, resulting in several compounds with excellent activity against DprE1 enzyme and potent MIC values, with improved developability properties. Several of these compounds were on the boundary of the preferred drug space (*figure 4.16*). A clear path forward for further optimisation was also established, by combining some of these improved

functional groups together into new molecules to try to further improve the overall profiles of the molecules.
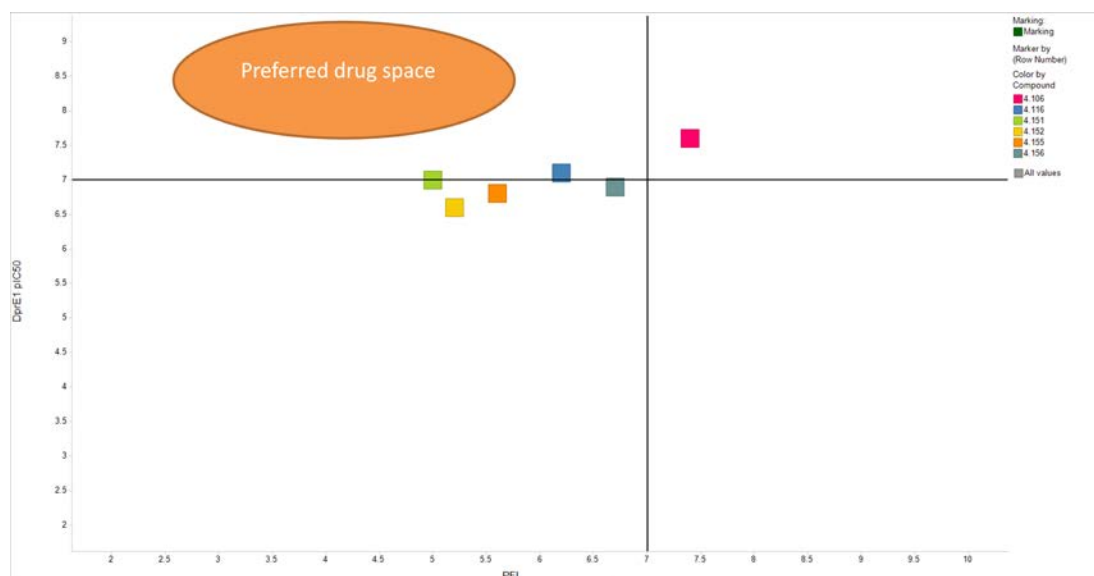
Figure 4.16: Plot of DprE1 pIC$_{50}$ vs PFI for compounds **4.107, 4.117, 4.152, 4.153, 4.156** and **4.157** showing ideal drug space.

Optimisation of pyrimidine series – combining improved right hand side groups

The results obtained by varying the linker with heteroatoms and substituting or replacing the phenyl group provided inspiration to carry out a further iteration of synthesis, focusing on combining the alternative linker groups with the phenyl replacements (*table 4.13*). The N- and O-linked 4-fluorophenyl substituents (**4.169** and **4.170**) confirmed the observed result from the phenyl series that oxygen linked compounds are more potent at DprE1 than nitrogen linked. Therefore, further modifications were carried out in the oxygen-linked series. The 4-fluorophenyl compound **4.170** and its close analogues with a chloro in the 4-position and/or an additional fluorine in the 2 position (**4.171 - 4.173**) all demonstrated an excellent overall profile. These compounds had very high activity in the DprE1 inhibition assay, which translated into very potent MIC values of around 1 micromolar. Despite PFI values at the edge of preferred space, the compounds nonetheless exhibited low levels of intrinsic

238

clearance in both species. Compound **4.170** was the only one of these tested for hERG inhibition and some moderate inhibition was observed.

A small set of heterocyclic compounds was explored (**4.174** - **4.176**). The thiazole containing compound, **4.174** maintained moderate DprE1 potency and MIC with an improved PFI value relative to the phenyl compounds. The methyl-pyridine compound **4.175** had a near identical profile in the *in vitro* assays, although it was a less attractive modification due to its higher PFI. As had been observed in the C-linked series, pyrimidine (**4.176**) had lower activity than pyridine.

A surprising and disappointing result was obtained when an oxygen-linker was inserted into the promising alkyl chain series. The resulting compounds **4.177** - **4.179** were consistently found to have weak activity against DprE1 and poor MICs. It was difficult to rationalise this result in the absence of any structural information.
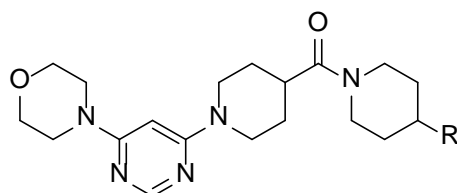
Compound	R	DprE1 pIC$_{50}$	LE, LLE$_{AT}$	PFI	MIC (µM)	Clint h/m (ml/min/g)	hERG pIC$_{50}$
4.169	NH-(4-F-phenyl)	6.4	0.26, 0.33	6.3	10.0		4.7
4.170	O-(4-F-phenyl)	7.3*	0.29*, 0.36*	6.7	1.7	< 0.5, 0.7	4.9
4.171	O-(4-Cl-phenyl)	7.5*	0.30*, 0.34*	7.6	1.5	0.9, 1.2	
4.172	O-(2,4-diF-phenyl)	7.5*	0.29*, 0.36*	6.9	1.0	0.8, 0.8	
4.173	O-(2-F-4-Cl-phenyl)	7.7*	0.30*, 0.34*	7.6	0.5	1.8, 2.9	
4.174	O-thiazol-2-yl	6.3	0.27, 0.37	5.6	16.0		
4.175	O-(5-CH$_3$-pyridin-2-yl)	6.2	0.25, 0.33	6.5	16.0		
4.176	O-(5-CH$_3$-pyrimidin-2-yl)	5.0	0.20, 0.31	5.1	125.0		
4.177	O-CH$_3$	4.7	0.23, 0.40	3.4	>125.0		
4.178	O-CH$_2$CH$_3$	5.3	0.25, 0.40	4.1	125.0		
4.179	O-CH(CH$_3$)$_2$	5.1	0.23, 0.37	4.6	62.0		

Table 4.13: Combined alternative linkers with phenyl replacements. *DprE1 pIC$_{50}$ values above 7.3 are approaching tight binding limit of assay and should be treated with caution. Compounds **4.169** and **4.170** were synthesised by chemists at GVK Bioscience at the request of Rob Young, GSK. Compound **4.179** was synthesised at ChemPartner at the request of Rob Young. Compounds **4.171** - **4.178** were synthesised at GVK Bioscience at my request.
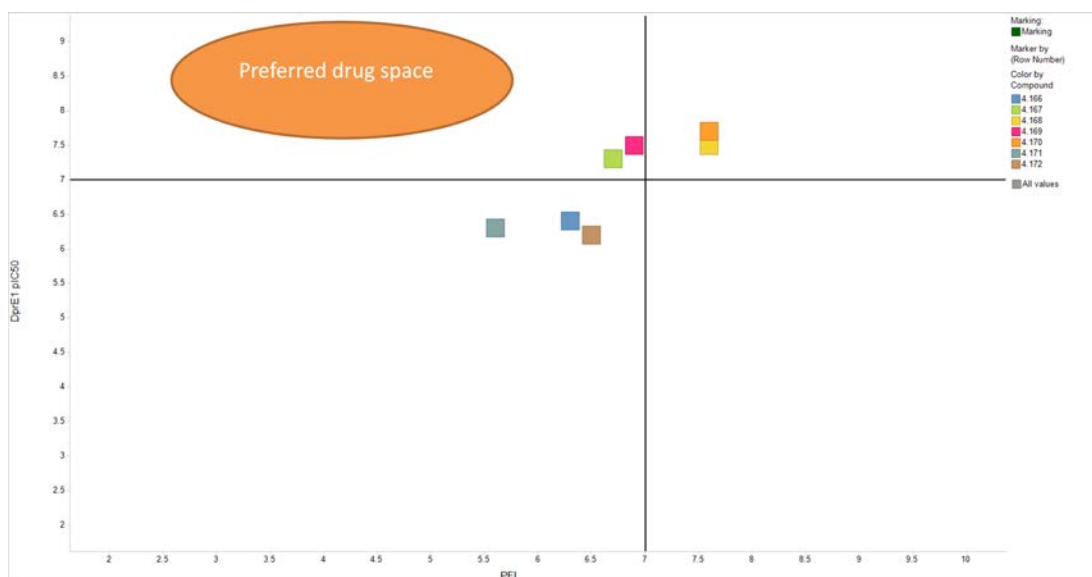
*Figure 4.17: Plot of DprE1 pIC$_{50}$ vs PFI for compounds **4.169 – 4.175**, showing ideal drug space.*

Once again, the replacements for the benzyl group led to compounds that were either just within, or on the edge of the desired drug space (*figure 4.17*). Varying the right hand side of the molecules had led to a series of molecules which represented a very high quality lead series for further optimisation. High potency in an enzyme and cellular system had been achieved and it had been demonstrated that through careful manipulation of physicochemical properties it was possible to ameliorate the potential hERG and clearance issues.

Further testing of optimised compounds

Two of the most promising molecules identified, the 4-fluorophenyl containing **4.107** and **4.170** were progressed for further evaluation both *in vitro* and *in vivo* to assess the progress made in this series towards the ultimate goal for the project of discovering a development candidate as a potential new medicine to treat tuberculosis.

Parameter	4.107	4.170
DprE1 pIC_{50}	7.6*	7.3*
LE, LLE_{AT}	0.31*, 0.33*	0.29*, 0.36*
PFI	7.4	6.7
clogP	2.2	1.1
MIC (µM)	0.6	1.7
Intracellular MIC (µM)	0.21	0.62
DprE1 Over-expressor MIC (µM)	15	62
Cytotoxicity HepG2 pIC_{50}	4.3[a]	4.5[b]
CLND solubility (µM)	160	≥364
FaSSIF solubility (µg/mL)	15	74
DMPK (mouse)	Clint h/m (ml/min/g) = 3.5, 5.1 CYP 3A4 pIC50 <4.4, low MDI risk $t_{1/2}$ (m) = 0.45 h, Clb (m) = 38.9 mL/min/kg, Vd_{ss} = 1.3 l/kg	Clint h/m (ml/min/g) < 0.5, = 0.7 CYP 3A4 pIC50 <4.4, low MDI risk $t_{1/2}$ (m) = 1 h, Clb (m) = 23.5 mL/min/kg, Vd_{ss} = 1.7 l/kg
Off-target effects	Phospholipidosis induction pMEC = 4.1[c] hERG pIC_{50} = 5.0 Panel of 44 undesirable targets, 1 target pIC_{50} > 5 (hERG pIC_{50} = 5.0)	Phospholipidosis induction pMEC ≤ 4 hERG pIC_{50} = 4.9 Panel of 44 undesirable targets, 1 target pIC_{50} > 5 (NET pIC_{50} = 5.6[d])

Table 4.14: Profiles of compounds **4.107** and **4.170** in a range of in vitro and in vivo assays. * DprE1 pIC_{50} values above 7.3 are approaching tight binding limit of assay and should be treated with caution. [a] Compound tested inactive (pIC50 = 4.0) on 6 out of 10 test occasions. [b] Compound tested inactive (pIC50 < 4.0) on 2 out of 4 test occasions. [c] Compound tested inactive (pIC50 < 4.0) on 2 out of 7 test occasions. [d] Compound tested inactive (pIC50 < 4.0) on 2 out of 4 test occasions.

Compounds **4.107** and **4.170** demonstrated very favourable overall profiles in assays designed to give early indications of developability (*table 4.14*), despite the observed lower FASSIF solubility and high-throughput hERG inhibition. It was particularly encouraging to note that the compounds showed good DMPK profiles and appeared very clean in a sentinel panel of toxicity assays.[392] These molecules were therefore progressed into a mouse model of tuberculosis infection to measure their efficacy in a disease-relevant model.

The mouse experiments were carried out by the therapeutic efficacy group, TB DPU GSK. Mice were subjected to an intratracheal infection of *M. tuberculosis* and then were treated every day for eight days beginning on the day after infection with either compound **4.107** or **4.170** at varying doses. A control compound was also included - the published AstraZeneca DprE1 inhibitor **4.31**. Since the authors noted[377] that **4.31** had better *in vivo* efficacy when administered along with 1-aminobenzotriazole (ABT), a CYP P450 inhibitor used to enhance the exposure of highly metabolised compounds in animal models, **4.31** was studied with and without co-administration of the ABT. At the end of the experiment, the animals were sacrificed and the number of colony forming units (CFUs) in the lungs were counted and compared with untreated animals.

Compound	ED_{99} (mg/kg)
4.31	164
4.31 + ABT	11
4.107	30
4.170	29

Table 4.15: Results of in vivo study of tuberculosis infection in mice.

The effective dose 99 % (ED_{99}), defined as the dose in mg/kg that reduced bacterial burden at day 9 after infection by 99 % (i.e. 2 log units) compared to untreated mice, was extrapolated for the test compounds (*table 4.15)*, and was found to show a very promising value of around 30 mg/kg for compounds **4.107** and **4.170**. For comparison, literature values for measured

ED$_{99}$ for a range of tuberculosis compounds in a similar experiment in mice are given in *table 4.16*.[393] Compounds **4.107** and **4.170** have ED$_{99}$ values of the same magnitude as several of the marketed TB drugs.

Compound	ED$_{99}$ (mg/kg)
Isoniazid **4.1**	0.95
Rifampin **4.2**	9.8
Pyrazinamide **4.6**	362
Ethambutol **4.4**	21.6
Moxifloxacin **4.11**	27.7
Linezolid	28

Table 4.16: Literature ED$_{99}$ values for a range of marketed TB drugs.[393]

Dose response curves for compounds **4.107** and **4.170** are shown in *figure 4.18*. It was important to observe that the compounds displayed well-shaped sigmoidal dose-response curves as these are consistent with a genuine pharmacological effect of the drug molecules on TB.
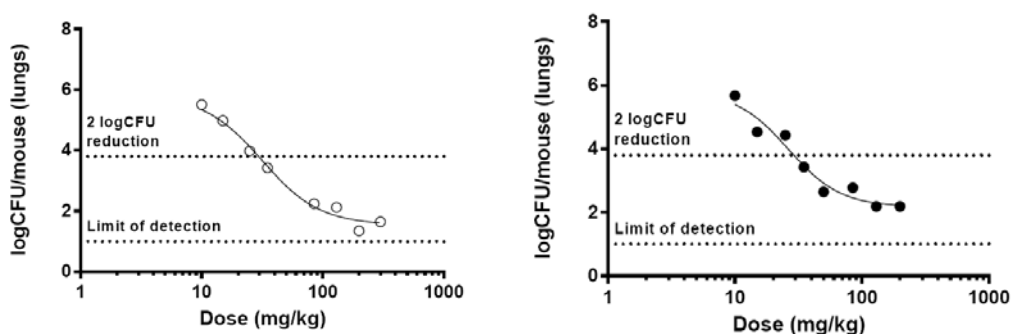
*Figure 4.18: Dose response curves for compounds **4.107** (○) and **4.170** (●).*

Overall, the *in vivo* experiments carried out on compounds **4.107** and **4.170** were extremely encouraging, as they demonstrated that this series of molecules could show efficacy against tuberculosis infection in mice at similar levels to marketed drugs. Therefore, the goal of identifying a high quality, developable series of DprE1 inhibitors suitable for further optimisation had more than been achieved. The lead series identified could be considered as being well-advanced in the path towards a development candidate, with

the *in vivo* efficacy demonstrated providing a high level of confidence in the likelihood of identifying a good candidate for development.

4.3 Conclusions and suggestions for further work

The main achievement of this work was the development of a phenotypic HTS hit with a far from ideal physicochemical profile into a lead series of molecules with improved properties, well-defined SAR, improved DMPK and hERG binding and demonstrable *in vivo* efficacy at a level suitable for a development candidate. This substantial improvement during the hit to lead journey was made possible through a rigorous and disciplined focus on improving physicochemical properties. The strategy to achieve this was to apply the FBDD philosophy of design, asking questions through compound design of how critical each atom or unit of lipophilicity was to the binding of the molecules.
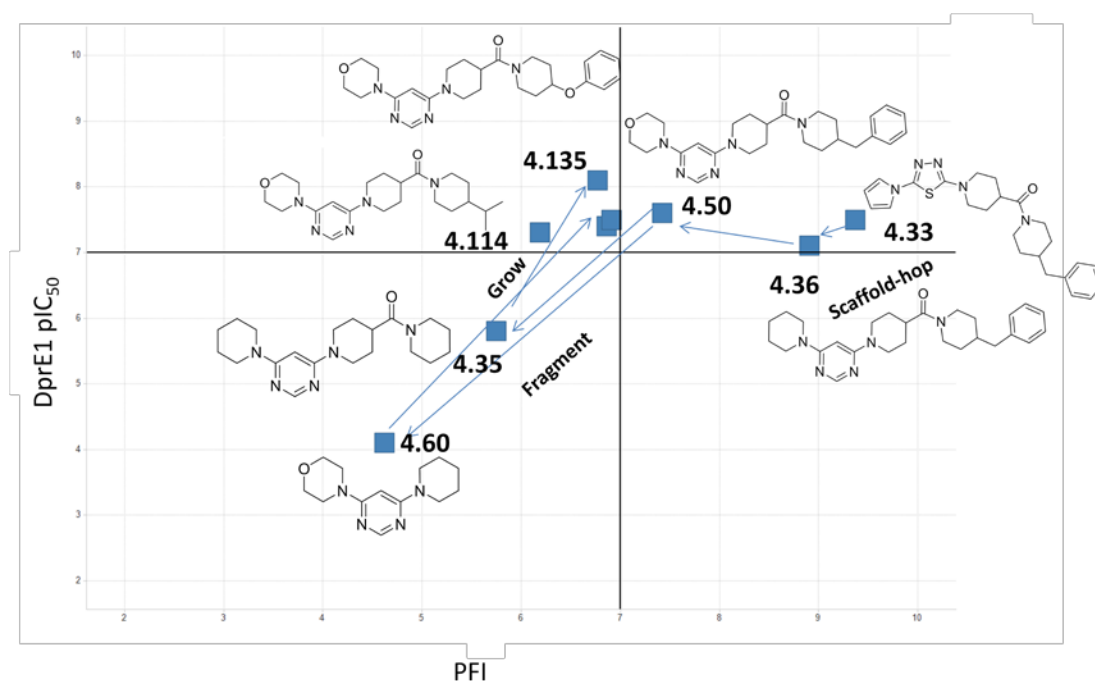
Figure 4.19: Schematic of optimisation journey for pyrimidine series

Considering the journey taken in the optimisation of the hit (*figure 4.19*), there were two important strategic insights in the discovery of optimised lead compounds: scaffold-hopping from thiadiazole pyrrole to the better pyrimidine morpholine and fragmenting the molecules to discover their most ligand

efficient constituents. Although neither of these steps initially seemed to offer an improvement on the hit in terms of potency, they were very important stepping stones to result in optimised compounds in the desired area of physicochemical space with maintained potency. The promise of these stepping-stone molecules was signalled by their retained ligand efficiency relative to the hit. An important learning from this work is that fragmenting larger molecules with unattractive physicochemical properties can be a very powerful tool in optimising towards better space. It is worth taking the extra time and effort in completing this step as it allows informed design of molecules with the minimum number of atoms and/or lipophilicity required for the desired level of activity. It is noteworthy that the optimised compounds are mostly on the very edge of the preferred limit of PFI of 7. It seems that the DprE1 enzyme and the tuberculosis cells require fairly lipophilic molecules to exert the desired effect; there could also be a compromise between size and shape of these molecules too, such that increased lipophilicity may be required to meet activity requirements. Nonetheless, the lead compounds have reasonable solubility and of course demostrable *in vivo* efficacy. The pyrimidinone core is a noteworthy exception to this observation, and will require further exploration. Defining the limits for activity is an area which should be explored more thoroughly during the lead optimisation of these molecules.

A high priority area for the next step of lead optimisation would be to combine the more polar cores discovered, such as pyrimidinone, with the optimised alkyl and phenoxy benzyl replacements. This will allow further exploration of the question of how much lipophilicity is required for activity and may lead to molecules with further improved physicochemical profiles and similar levels of efficacy.

Another area for future work arising from these results is to test the design philosophy used in other targets. In other words, to take unattractive starting points against a range of proteins and attempt the fragment then grow methodology described here to explore how generally this technique can be

successfully applied. It would be especially interesting to attempt this in targets which have structural information available to aid design, as it would be possible to develop and test hypotheses about which kinds of ligand-protein interactions are important to provide ligand efficient binding.

Given the origin of the hit, the work described here would appear to give strong support to a phenotypic approach to antituberculosis (or indeed antibacterial) compounds and a measurable MIC was the impetus for further investigation. Antibacterial research in general and anti-tuberculosis in particular are littered with target based programmes where potent activity has not led to measureable or useful MIC levels.[394,395] The approach of systematic fragmentation and reconconstruction using fragment based thinking is a strong learning that should pay dividends in the future.

Overall, this work has had significant impact in the high quality DprE1 inhibitors discovered, but also in the more general lessons learned for design in medicinal chemistry.

Appendix 4.1: Format of DprE1 Assay

The biochemical assay to detect inhibitors of DprE1 was developed and run by Archie Argyrou, GSK. The endogenous substrate of DprE1, decaprenylphosphoryl-β-D-ribose (DPR) was not commercially available and was difficult to synthesise, so a simpler substrate, 2E,6E,10E-Geranylgeranylphosphoryl-β-D-ribose (E-GGPR) was used in the assay (*figure A4.1*).
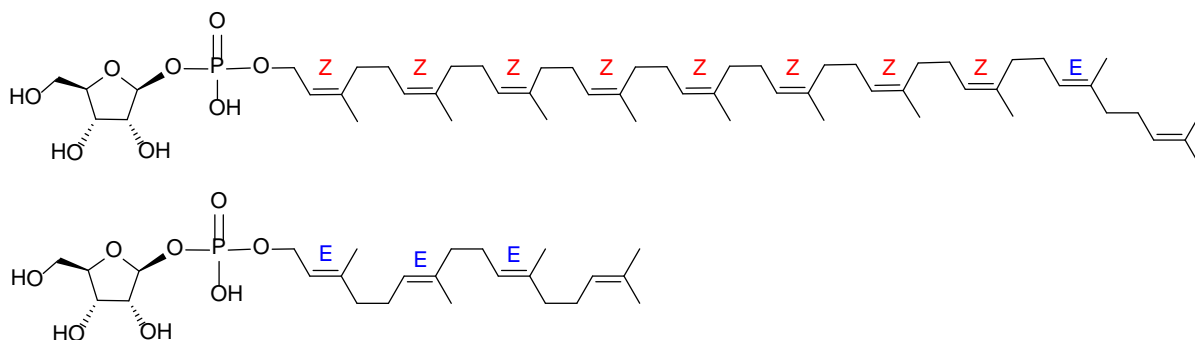
Figure A4.1: Structures of substrates of DprE1. Top: DPR; bottom: E-GGPR.

The enzyme was able to convert the shortened E-GGPR substrate to the corresponding ketone, 2E,6E,10E-geranylgeranylphosphoryl-b-D-2'-keto-erythro-pentafuranose (E-GGPX), using the FAD co-factor as the oxidant (*scheme A4.1*). In the assay, resazurin was added as an oxidant to regenerate the FAD from the $FADH_2$ formed. This resulted in the formation of the highly fluorescent reduction product resorufin, which could be quantified on a plate-based fluorescent reader 45 minutes after the reaction was initiated. Compounds which acted as inhibitors of DprE1 caused a lower fluorescent read-out to be observed.

Early in this project, Farnesylphosphoryl-β-D-ribose (FPR) was used in this assay in place of E-GGPR. Most compounds were re-screened in the E-GGPR assay when it became available, but some had only FPR assay data. These data were included and highlighted as from the FPR assay.
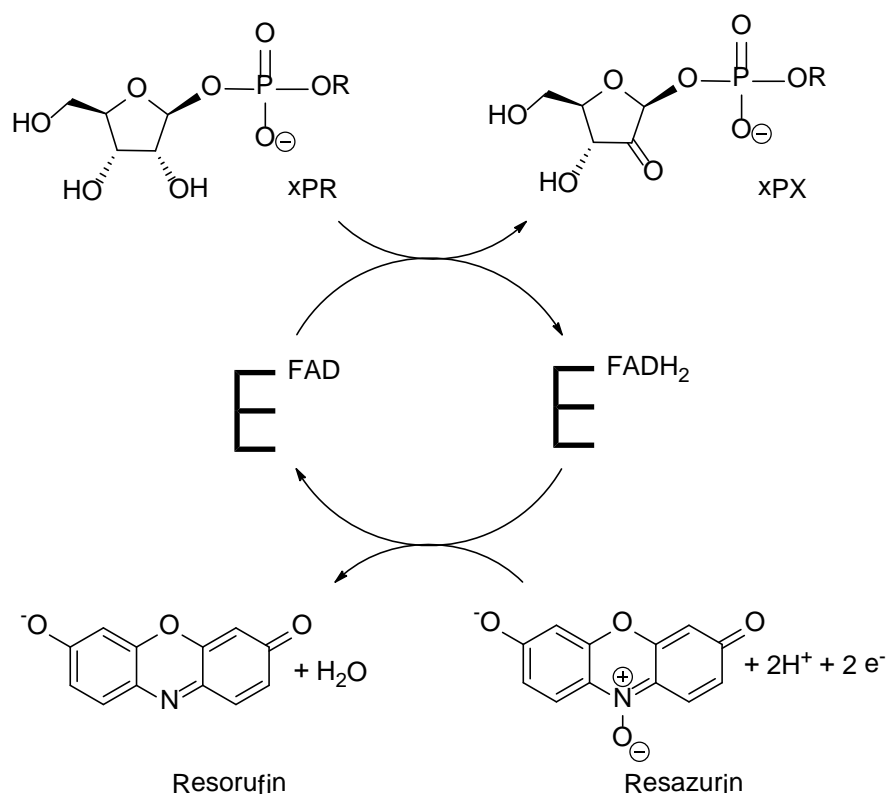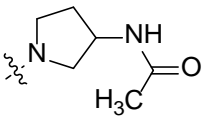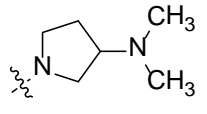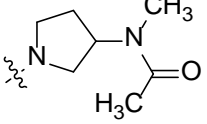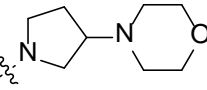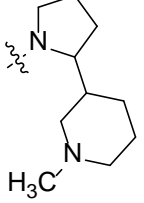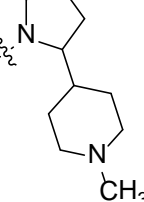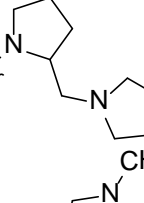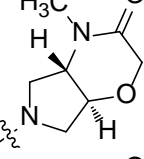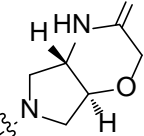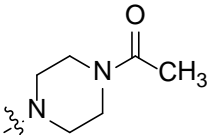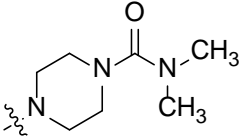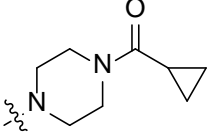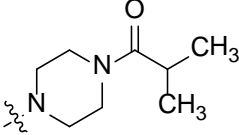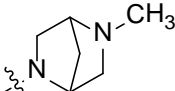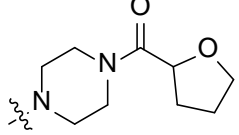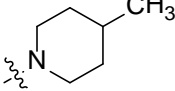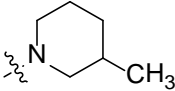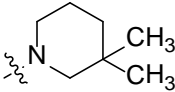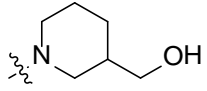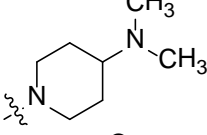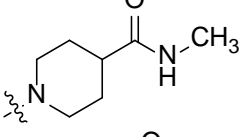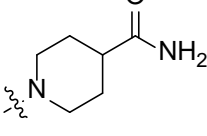
Scheme A4.1: Format of DprE1 assay

Appendix 4.2: SAR Tables

Compound	R	DprE1 pIC_{50}	LE, LLE_{AT}
4.62	$\begin{array}{c}CH_3\\ N{-}CH(CH_3)\\ CH_3\end{array}$	<4.0	
4.63	N,N-diethyl	<4.0	
4.64	N,N-dimethyl	<4.0	
4.65	N(CH$_3$)(ethyl)	4.3	0.37, 0.36
4.66	azetidine	<4.0	
4.67	pyrrolidine	<4.0	
4.68	2-methyl-1-methylpyrrolidine	4.1	0.31, 0.31
4.69	pyrrolidinone-methylamine	<4.0	
4.70	3,3-difluoropyrrolidine	4.1	0.30, 0.32
4.71	2-ethylpyrrolidine	<4.0	
4.72	3-(methylsulfonyl)pyrrolidine	4.1	0.27, 0.43

4.73		<4.0
4.74		<4.0
4.75		<4.0
4.76		<4.0
4.77		<4.0
4.78		<4.0
4.79		<4.0
4.80		<4.0
4.81		<4.0
4.82		<4.0

251

4.83		<4.0	
4.84		<4.0	
4.85		<4.0	
4.86		<4.0	
4.87		<4.0	
4.88		<4.0	
4.89		4.2	0.30, 0.27
4.90		<4.0	
4.91		4.6	0.32, 0.35
4.92		<4.0	
4.93		<4.0	
4.94		<4.0	
4.95		<4.0	
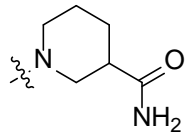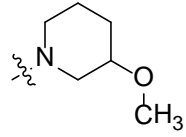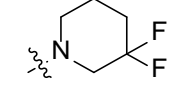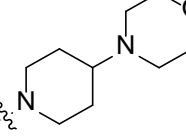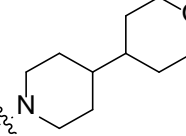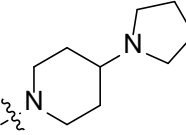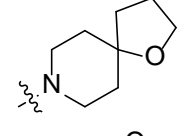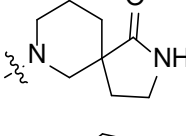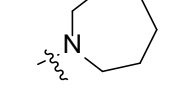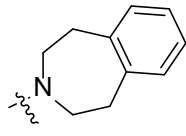
4.96		<4.0	
4.97		<4.0	
4.98		<4.0	
4.99		<4.0	
4.100		4.4	0.25, 0.27
4.101		<4.0	
4.102		4.1	0.26, 0.33
4.103		<4.0	
4.104		<4.0	
4.105		4.6	0.27, 0.23

*Table A4.2: Results of fragments tested to explore SAR of central piperidine ring. Compounds **4.62 – 4.66, 4.91 – 4.92,** and **4.104 – 4.105** were synthesised by chemists at GVK BioSciences at my request.*

5 Experimental

5.1: Materials and Instrumentation

Unless stated otherwise all reagents were used as obtained from commercial sources. All solvents and compounds were of analytical grade and used as supplied.

Liquid Chromatography Mass Spectrometry (LCMS)

Liquid Chromatography-Mass Spectrometry (LCMS) was conducted on an Acquity UPLC BEH C18 column (50 mm x 2.1 mm i.d. 1.7 μm packing diameter) at 40 °C, eluting with either 10 mM ammonium bicarbonate in water adjusted to pH 10 with ammonia solution (solvent A) and acetonitrile (solvent B) or 0.1 % v/v solution of formic acid in water (solvent A) and 0.1 % v/v solution of formic acid in acetonitrile (solvent B). The UV detection is a summed signal from wavelength of 210 nm to 350 nm. The mass spectra were recorded on a Waters ZQ spectrometer using electrospray positive and negative mode, scanning from 100-1000 AMU. Data are reported as Rt (retention time), $[M+H]^+$ (observed ionisation in positive mode for parent molecular ion plus a proton reported to the nearest integer), purity (relative integration of the UV peak area).

The following elution gradients were used:

Ammonium bicarbonate:

Time (min)	Flow rate (ml/min)	% A	% B
0	1	99	1
1.5	1	3	97
1.9	1	3	97
2	1	99	1

Formic:

Time (min)	Flow rate (ml/min)	% A	% B
0	1	97	3
1.5	1	0	100
1.9	1	0	100
2	1	97	3

High Resolution Mass Spectrometry (HRMS)

An Agilent 1100 Liquid Chromatograph equipped with a model G1367A autosampler, a model G1312A binary pump and a HP1100 model G1315B diode array detector was used. All separations were achieved using a Phenomenex Luna C18 (2) reversed phase column (100 x 2.1 mm, 3 μm particle size). ESI (+) high resolution mass spectra (HRMS) were obtained on a Micromass Q-Tof 2 hybrid quadrupole time-of-flight mass spectrometer, equipped with a Z-spray interface, over a mass range of 100 – 1100 Da, with a scan time of 0.9 s and an interscan delay of 0.1 s. Reserpine was used as the external mass calibrant ([M+H]+ = 609.2812 Da). The elemental composition was calculated using MassLynx v4.1 for the [M+H]+. All measured masses are accurate to within 5 ppm of the calculated mass

Preparative mass directed HPLC (MDAP)

Preparative mass directed HPLC was conducted on a Waters MassLynx system comprising of a Waters 515 pump with extended pump heads, Waters 2767 autosampler, Waters 996 photodiode array detector and Gilson 202 fraction collector on a XBridge or Sunfire C18 column (30 mm x 150 mm i.d. 5 μm packing diameter) at ambient temperature. The mobile phase was 0.1% formic acid in water or 10 mM ammonium bicarbonate in water adjusted to pH 10 with ammonia solution (solvent A) and 0.1% formic acid in acetonitrile or acetonitrile (solvent B). The UV detection is a summed signal from wavelength of 210 nm to 350 nm. Mass spectra were recorded on Waters ZQ mass spectrometer using alternate-scan positive and negative

electrospray ionization. The software used was MassLynx 3.5 with FractionLynx option or using equivalent alternative systems.

The elution gradients used were at a flow rate of 40 mL/min over 10 or 20 min (extended run):

Gradient A   5-30% B

Gradient B   15-55% B

Gradient C   30-85% B

Gradient D   50-99% B

Gradient E   80-99% B

Nuclear Magnetic Resonance (NMR) Spectroscopy

^{1}H NMR spectra were obtained on a Bruker AVI II (600 MHz) spectrometer or Bruker DPX400 (400 MHz) spectrometer. ^{13}C NMR spectra were obtained on a Bruker AVI500 (125 MHz) spectrometer or Bruker DPX400 (100 MHz) spectrometer. Chemical shifts are reported in parts per million (ppm) and referenced to tetramethylsilane. Coupling constants (*J*) in Hz, and are reported to the nearest 0.5 Hz for ^{1}H NMR and 1 Hz for ^{13}C NMR. The following abbreviations are used for multiplicities: s = singlet; br s = broad singlet; d = doublet; t = triplet; m = multiplet; dd = doublet of doublets; ddd = double double doublet; q = quartet; quin = quintet; sext = sextet. The following abbreviations are used to assign ^{13}C spectra: Ar = aryl; C=O = carbonyl.

Infrared (IR) Spectroscopy

IR spectra were recorded from solid samples using a Perkin Elmer Spectrum One FTIR spectrometer fitted with a Perkin Elmer Universal ATR (attenuated total reflectance) sampling accessory. Absorption frequencies of the higher intensity peaks are reported in wavenumbers (cm^{-1}).

Melting Points (mp)

Melting points were measured on a Stuart SMP40 automatic melting point apparatus. The melting points quoted are those observed by eye rather than the automatically generated values and are quoted in °C.

Flash Chromatography

Column chromatography was conducted on a Combiflash® Rf, automated flash chromatography system, from Teledyne Isco using disposable, normal or reverse phase, SPE Redisep® cartridges (4 g to 330 g). The CombiFlash® Rf uses RFID (Radio Frequency Identification) technology to automate setting the parameters for purification runs and fraction collection. The system is equipped with a UV variable dual-wavelength and a Foxy® fraction collector enabling automated peak cutting, collection and tracking.

Phase Separations

Isolute phase separators sold by Whatman were used for separation of DCM from a DCM/aqueous mixture in aqueous work-ups. This technique also effectively dries the organic layer, removing the need to add additional drying agents.

Biotage 103 cartridges were also used to extract organic material from aqueous solution. These cartridges are packed with a hydroxylated polystyrene-divinylbenzene co-polymer which allows catch and release of organic material.

Microwave Reactions

All microwave reactions were carried out in a Biotage Initiator® system in specialist microwave vials supplied by Biotage.

5.2: Experimental Procedures

All compounds which have experimental details described were synthesised by me.

4-Hydroxy-6-phenoxy-2*H*-chromen-2-one (2.30)
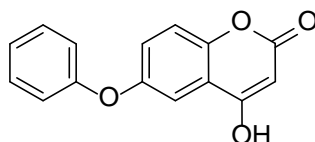
2-30

A mixture of 6-bromo-4-hydroxy-2H-chromen-2-one (1.94 g, 8.05 mmol), phenol (0.76 g, 8.05 mmol), potassium iodide (1.34 g, 8.05 mmol), cesium carbonate (2.62 g, 8.05 mmol), 3,4,7,8-tetramethyl-1,10-phenanthroline (0.95 g, 4.02 mmol) and copper(I) iodide (2.30 g,12.07 mmol) were suspended in DMF (15 mL) and heated in a microwave reactor at 150 °C for 2.5 hours. The solvent was removed by nitrogen blow-down to yield an orange solid. The crude product was purified by Andy Hobbs, GSK on an 80 g silica column, eluting with a gradient of 35 – 100 % TBME in cyclohexane. The product was further purified on a 50g C18 Aq Gold® column, eluting with a gradient of 0 - 30 % acetonitrile in 10 mM ammonium bicarbonate (aq) to afford the title compound (**2.30**) as an off-white solid (75 mg, 0.29 mmol, 4 %). LCMS (ammonium bicarbonate): Rt = 0.72 min, [M+H]$^+$ = 255, purity = 100 %. ^{1}H NMR (400 MHz, DMSO-d_6) δ ppm 7.34 - 7.40 (m, 2 H); 7.27 (d, J = 2.5 Hz, 1 H); 7.08 - 7.15 (m, 4 H); 6.97 - 7.01 (m, 2 H); 4.61 (s, 1 H).

General Procedure A: Synthesis of benzisoxazole-3-acetic acids

The appropriate 4-hydroxycoumarin was dissolved in hydroxylamine (50% solution in water) and heated at 70 °C for 24 hours. The solution was cooled and basified with saturated Na$_2$CO$_3$ (aq) and then washed twice with DCM. The aqueous layer was acidified with 2M HCl and the solid which formed was isolated by filtration, washed with water and dried in a vacuum oven (45 °C, 1 mBar) to yield the desired product.

2-(5-Phenoxybenzo[*d*]isoxazol-3-yl)acetic acid (2.27)
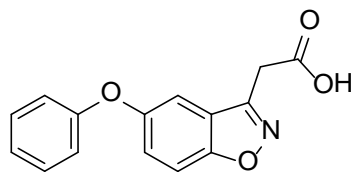
2·27

4-Hydroxy-6-phenoxy-2*H*-chromen-2-one (**2.30**) *(*75 mg, 0.30 mmol*)* was reacted with hydroxylamine (50 % solution in water) (2 mL) according to general procedure A to afford the title compound (**2.27**) as an orange solid (36 mg, 0.13 mmol, 45 %). Mp 109-111 °C. LCMS (formic): Rt = 0.98 min, $[M+H]^+$ = 270, purity = 100 %. ^{1}H NMR (DMSO-d_6) δ ppm 7.77 (d, J = 9.0 Hz, 1 H); 7.47 (d, J = 2.5 Hz, 1 H); 7.34 - 7.44 (m, 3 H); 7.10 - 7.17 (m, 1 H); 7.01 (d, J = 8.0 Hz, 2 H); 4.04 (s, 2 H). Carboxylic acid proton not visible. ^{13}C NMR (DMSO-d_6) δ ppm 169.8 (C=O); 159.1 (Ar C); 157.3 (Ar C); 153.9 (Ar C); 152.4 (Ar C); 130.0 (2 Ar CH); 123.3 (Ar C); 123.2 (Ar CH); 122.4 (Ar CH); 117.9 (2 Ar CH); 111.4 (Ar CH); 111.0 (Ar CH); 30.8 (CH_2). IR (ATR) cm^{-1} 3061; 2925; 1705; 1442; 1232; 1211; 893; 751.

1-(2-Hydroxy-5-phenoxyphenyl)ethanone (2.29)
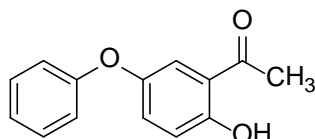
2·29

4-Phenoxyphenol (1.37 g, 7.36 mmol) was dissolved in acetic acid (10 mL) and treated with boron trifluoride diethyl etherate (1 mL, 8.13 mmol). The resulting yellow suspension was heated at 80 °C for 2 days. The heating temperature was increased to 110 °C and the solution was stirred for a further 24 hours. The solution was cooled and poured onto water (50 mL). DCM (50 mL) was added and the layers were separated using a phase separation cartridge. The aqueous layer was extracted with additional DCM (50 mL). The combined organic layers were concentrated to yield the ester

intermediate, which was purified by Andy Hobbs, GSK. Purification was carried out on a Redisep silica 24 g column eluting with a gradient of 0-10% TBME in cyclohexane. Appropriate fractions were combined and concentrated. The intermediate was dissolved in chlorobenzene (5 mL), treated with aluminium chloride (0.98 g, 7.4 mmol) and stirred at 130 °C for 4 hours. The solution was cooled to room temperature and poured onto ice (50 g). DCM (50 mL) was added and the layers were separated using a phase separation cartridge. The aqueous layer was extracted with DCM (2 X 50 mL) and the combined organic layers were concentrated to afford the title compound (**2.29**) as an orange solid (608 mg, 2.67 mmol, 36 %). LCMS (ammonium bicarbonate) Rt = 0.92 min, $[M+H]^+$ = 229, purity = 80%.

An additional batch of compound **2.29** was synthesised using similar conditions and then purified by Andy Hobbs, GSK on a Redisep® 100 g C18 GOLD® column, eluting with a gradient of 5 – 60 % acetonitrile in 10 mM ammonium bicarbonate (aq.) to afford the title compound (**30**) as an off-white solid (736 mg, 3.23 mmol, 30 %). LCMS (ammonium bicarbonate) Rt = 0.92 min, $[M+H]^+$ = 229, purity = 100%. ^{1}H NMR (DMSO-d_6) δ ppm 9.43 (br. s, 1 H); 7.92 (d, J = 9.0 Hz, 2 H); 6.88 - 7.03 (m, 4 H); 6.76 - 6.85 (m, 2 H); 3.28 (s, 3 H).

4-Hydroxy-6-phenoxy-2*H***-chromen-2-one (2.30)**

2.30
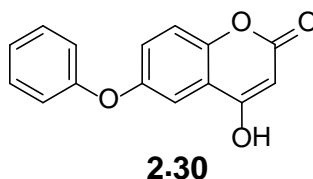
6-Bromo-4-hydroxy-2*H*-chromen-2-one (1.94 g, 8.05 mmol), phenol (0.76 g, 8.05 mmol), cesium carbonate (2.62 g, 8.05 mmol), potassium iodide (1.34 g, 8.05 mmol), 3,4,7,8-tetramethyl-1,10-phenanthroline (0.95 g, 4.02 mmol), and copper(I) iodide (2.30 g, 12.07 mmol) were suspended in DMF (15 mL) and heated in a microwave reactor at 150 °C for 2.5 hours. The solvent was removed by nitrogen blow-down and the crude product was purified by Andy Hobbs, GSK on an 80 g silica column, eluting with a gradient of 40-100%

TBME in cyclohexane. The fractions containing desired product were combined and concentrated to yield an orange solid. This material was further purified on a 50 g C18 column, eluting with a gradient of 0-30% acetonitrile in 10 mM ammonium bicarbonate solution. The appropriate fractions were combined and concentrated to afford the title compound (**2.30**) as a pink solid (75 mg, 0.30 mmol, 4%). LCMS (ammonium bicarbonate): Rt = 0.72 min, [M+H]$^+$ = 255, purity = 100 %. ^{1}H NMR (DMSO-d_6) δ ppm 7.33 - 7.42 (m, 2 H); 7.27 (d, J = 2.5 Hz, 1 H); 7.05 - 7.17 (m, 4 H); 6.97 (d, J = 8.0 Hz, 2 H); 4.62 (s, 1 H).

(5-Bromo-1,2-benzisoxazol-3-yl)acetic acid (2.33)

2·33
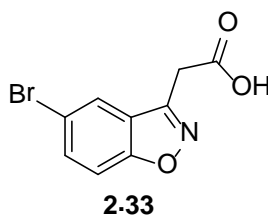
6-Bromo-4-hydroxy-2H-chromen-2-one (1.17 g, 4.87 mmol) was reacted with hydroxylamine (50 % solution in water) (20 mL) according to general procedure A to afford the title compound (**2.33**) as a white solid (827 mg, 3.24 mmol, 66%). Mp 174-177 °C. LCMS (formic): Rt = 0.84 min, [M+H]$^+$ = 255, 257, purity = 96%. ^{1}H NMR (DMSO-d_6) δ ppm 12.95 (br s, 1 H); 8.14 (d, J = 1.5 Hz, 1 H); 7.78 - 7.85 (m, 1 H); 7.72 - 7.77 (m, 1 H); 4.12 (s, 2 H). ^{13}C NMR (DMSO-d_6) δ ppm 169.7 (C=O); 161.3 (Ar C); 153.3 (Ar C); 133.0 (Ar CH); 125.2 (Ar CH); 123.6 (Ar C); 115.6 (Ar C); 111.7 (Ar CH); 30.6 (CH$_2$). IR (ATR) cm^{-1} 2969; 1712; 1427; 1399; 1228; 872; 804; 702.

2-(5,6-Dimethylbenzo[*d*]isoxazol-3-yl)acetic acid (2.25)
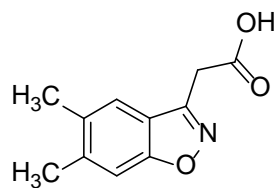
2.25

4-hydroxy-6,7-dimethyl-2H-chromen-2-one (2.09 g, 10.97 mmol) was reacted with hydroxylamine (30 mL) according to general procedure A to afford the title compound (**2.25**) as an off-white solid (1.90 g, 9.21 mmol, 84%). LCMS (formic): Rt = 0.84 min, $[M+H]^+$ = 206, purity = 98%. ^{1}H NMR (400 MHz, DMSO-d_6) δ ppm 12.83 (br. s., 1 H); 7.55 (s, 1 H); 7.52 (s, 1 H); 4.01 (s, 2 H); 2.38 (s, 3 H); 2.33 (s, 3 H).

General Procedure B: Amide Formations

The appropriate acid (1 eq.) was dissolved in DCM (1- 3 mL) and treated with HATU (2 eq.) and DIPEA (3 eq.) followed by the appropriate amine (1.5 eq.). The resulting solution was stirred at room temperature for 24 hours. The solution was diluted with additional DCM and water and the layers were separated using a phase separation cartridge. The aqueous layer was extracted with additional DCM and the combined organic layers were concentrated to yield the crude product. The product was purified by preparative mass-directed HPLC.

2-(5,6-Dimethyl-1,2-benzisoxazol-3-yl)-*N*-[(6-methyl-2-pyridinyl)methyl]acetamide (2.48)

2.48
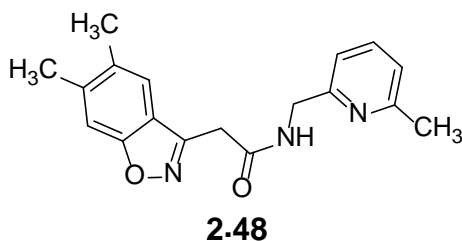
2-(5,6-Dimethylbenzo[*d*]isoxazol-3-yl)acetic acid (**2.25**, 50 mg, 0.24 mmol) was reacted with [(6-methyl-2-pyridinyl)methyl]amine hydroiodide (obtained from the GSK compound collection) according to general procedure B to afford the title compound (**2.48**) as a yellow oil (19 mg, 0.06 mmol, 25 %). LCMS (formic): Rt = 0.64 min, [M+H]$^+$ = 310, purity = 96%. ^{1}H NMR (CDCl$_3$) δ ppm 7.46 - 7.55 (m, 2 H); 7.36 (s, 2 H); 6.96 - 7.04 (m, 2 H); 4.51 (d, *J* = 5.0 Hz, 2 H); 4.00 (s, 2 H); 2.45 (s, 3 H); 2.40 (s, 3 H); 2.34 (s, 3 H).

2-(5,6-Dimethylbenzo[*d*]isoxazol-3-yl)-*N*-(4-isopropoxybenzyl)acetamide (2.49)

2.49
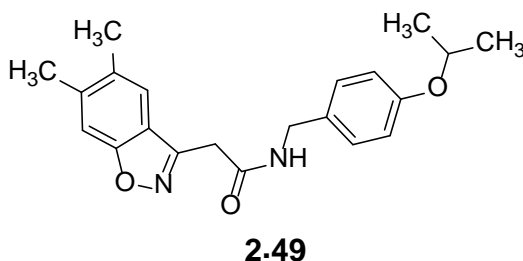
2-(5,6-Dimethylbenzo[*d*]isoxazol-3-yl)acetic acid (**2.25**, 50 mg, 0.24 mmol) was reacted with (4-isopropoxyphenyl)methanamine hydrochloride (obtained from the GSK compound collection) according to general procedure B to afford the title compound (**2.49**) as a yellow solid (23 mg, 0.06 mmol, 26 %). LCMS (formic): Rt = 1.16 min, [M+H]$^+$ = 353, purity = 100%. ^{1}H NMR (CDCl$_3$) δ ppm 7.48 (s, 1 H); 7.34 (s, 1 H); 7.11 (d, *J* = 8.5 Hz, 2 H); 6.79 (d, *J* = 8.5 Hz, 2 H); 6.48 (br. s, 1 H); 4.44 - 4.56 (m, 1 H); 4.36 (d, *J* = 5.5 Hz, 2 H); 3.94 (s, 2 H); 2.41 (s, 3 H); 2.36 (s, 3 H); 1.32 (d, *J* = 6.0 Hz, 6 H).

(S)-2-(5,6-Dimethylbenzo[d]isoxazol-3-yl)-N-(pyrrolidin-2-ylmethyl)acetamide 2,2,2-trifluoroacetate (2.50)

2·50
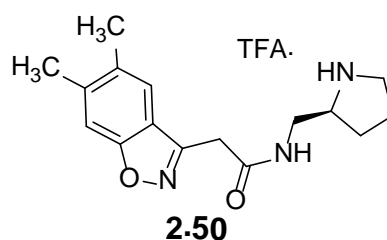
2-(5,6-Dimethylbenzo[d]isoxazol-3-yl)acetic acid (**2.25**, 50 mg, 0.24 mmol) was reacted with (S)-tert-butyl 2-(aminomethyl)pyrrolidine-1-carboxylate (obtained from the GSK compound collection) according to general procedure B. After purification, the BOC-protected product was dissolved in DCM (1 mL) and treated with TFA (0.2 mL) and stirred at room temperature for 48 hours. The solvents were removed by evaporation to afford the title compound (**2.50**) as a yellow solid (59 mg, 0.15 mmol, 61 %). LCMS (formic): Rt = 0.60 min, [M+H]$^+$ = 288, purity = 95%. ^{1}H NMR (CDCl$_3$) δ ppm 9.82 (br s, 1 H); 8.92 (br s, 1 H); 8.73 (br s, 1 H); 7.41 (s, 1 H); 7.24 (s, 1 H); 3.87 (br s, 2 H); 3.50 - 3.67 (m, 2 H); 3.31 (d, J = 5.5 Hz, 2 H); 2.36 (s, 3 H); 2.31 (s, 3 H); 1.95 - 2.20 (m, 4 H); 1.67 - 1.80 (m, 1 H).

2-(5,6-Dimethylbenzo[d]isoxazol-3-yl)-N-((tetrahydrofuran-2-yl)methyl)acetamide (2.51)

2·51
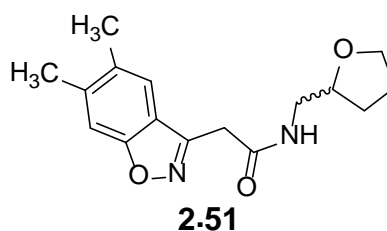
2-(5,6-Dimethylbenzo[d]isoxazol-3-yl)acetic acid (**2.25**, 50 mg, 0.24 mmol) was reacted with (tetrahydrofuran-2-yl)methanamine according to general procedure B to afford the title compound (**2.51**) as a white solid (36 mg, 0.13 mmol, 52 %). Mp 106 - 109 °C. LCMS (formic): Rt = 0.88 min, [M+H]$^+$ = 289, purity = 96%. ^{1}H NMR (CDCl$_3$) δ ppm 7.50 (s, 1 H); 7.35 (s, 1 H); 6.45 (br s.,

1 H); 3.89 - 3.99 (m, 3 H); 3.64 – 3.79 (m, 2 H); 3.47 - 3.56 (m, 1 H); 3.23 (dd, J = 13.0, 6.5 Hz, 1 H); 2.41 (s, 3 H); 2.36 (s, 3 H); 1.65 - 1.98 (m, 3 H); 1.37 - 1.54 (m, 1 H). ^{13}C NMR (DMSO-d_6) δ ppm 167.0 (C=O); 161.6 (Ar C); 153.8 (Ar C); 140.1 (Ar C); 132.2 (Ar C); 121.7 (Ar CH); 119.4 (Ar C); 109.4 (Ar CH); 77.0 (CH); 67.1 (CH$_2$); 42.9 (CH$_2$); 32.1 (CH$_2$); 28.4 (CH$_2$); 25.1 (CH$_2$); 20.3 (CH$_3$); 19.4 (CH$_3$). IR (ATR) cm^{-1} 3292; 2973; 2868; 1643; 1548; 1079; 861; 817; 688.

2-(5,6-Dimethylbenzo[*d*]isoxazol-3-yl)-*N*-((1-ethyl-1*H*-pyrazol-4-yl)methyl)acetamide (2.52)
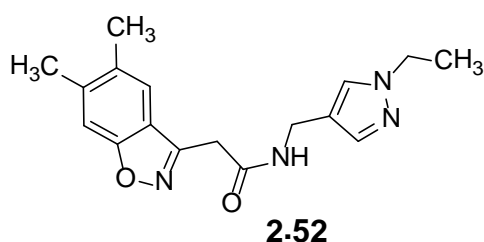
2.52

2-(5,6-Dimethylbenzo[*d*]isoxazol-3-yl)acetic acid (**2.25**, 50 mg, 0.24 mmol) was reacted with (1-ethyl-1*H*-pyrazol-4-yl)methanamine (obtained from the GSK compound collection) according to general procedure B to afford the title compound (**2.52**) as a yellow solid (52 mg, 0.17 mmol, 68 %). Mp 148-150 °C. LCMS (formic): Rt= 0.87 min, [M+H]$^+$ = 313, purity = 100%. ^{1}H NMR (chloroform-*d*) δ ppm 7.47 (s, 1 H); 7.33 (d, J = 2.0 Hz, 2 H); 7.28 (s, 1 H); 6.56 (br s, 1 H); 4.28 (d, J = 5.5 Hz, 2 H); 4.07 (q, J = 7.0 Hz, 2 H); 3.90 (s, 2 H); 2.40 (s, 3 H); 2.35 (s, 3 H); 1.41 (t, J = 7.0 Hz, 3 H). ^{13}C NMR (DMSO-d_6) δ ppm 166.5 (C=O); 161.6 (Ar C); 153.7 (Ar C); 140.1 (Ar C); 137.7 (Ar CH); 132.2 (Ar C); 127.8 (Ar CH); 121.7 (Ar CH); 119.4 (Ar C); 118.0 (Ar C); 109.4 (Ar CH); 46.0 (CH$_2$); 33.3 (CH$_2$); 32.2 (CH$_2$); 20.3 (CH$_3$); 19.4 (CH$_3$); 15.5 (CH$_3$). IR (ATR) cm^{-1} 3279; 2983; 2927; 1648; 1537; 1447; 1228; 995; 819; 676.

N-(2-(1H-Imidazol-1-yl)ethyl)-2-(5,6-dimethylbenzo[d]isoxazol-3-yl)acetamide (2.53)

2·53
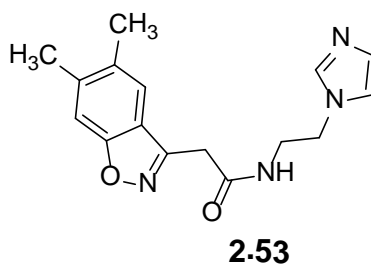
2-(5,6-Dimethylbenzo[d]isoxazol-3-yl)acetic acid (**2.25**, 50 mg, 0.24 mmol) was reacted with 2-(1H-imidazol-1-yl)ethanamine hydrobromide (obtained from the GSK compound collection) according to general procedure B to afford the title compound (**2.53**) as a yellow solid (8 mg, 0.03 mmol, 11%). LCMS (ammonium bicarbonate): Rt = 0.78 min, $[M+H]^+$ = 299, purity = 86%. ^{1}H NMR (CDCl$_3$) δ ppm 7.47 (s, 1 H); 7.36 (s, 1 H); 7.32 (s, 1 H); 7.15 (br s, 1 H); 6.95 (s, 1 H); 6.77 (s, 1 H); 4.06 (t, J = 6.0 Hz, 2 H); 3.91 (s, 2 H); 3.54 – 3.61 (m, 2 H); 2.41 (s, 3 H); 2.37 (s, 3 H).

N-(Cyclopentylmethyl)-2-(5,6-dimethylbenzo[d]isoxazol-3-yl)acetamide (2.69)

2·69
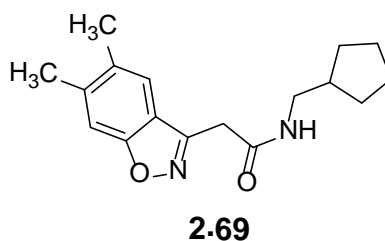
2-(5,6-Dimethylbenzo[d]isoxazol-3-yl)acetic acid (**2.25**, 50 mg, 0.24 mmol) was reacted with cyclopentylmethanamine (obtained from the GSK compound collection) according to general procedure B to afford the title compound (**2.69**) (14 mg, 0.05 mmol, 20 %). LCMS (formic): Rt = 1.11 min, $[M+H]^+$ = 287, purity = 100%. ^{1}H NMR (DMSO-d_6) δ ppm 8.25 - 8.40 (m, 1 H); 7.56 (s, 1 H); 7.50 (s, 1 H); 3.82 (s, 2 H); 2.99 - 3.08 (m, 2 H); 2.37 (s, 3 H); 2.31 (s, 3 H); 1.93 - 2.09 (m, 1 H); 1.60 - 1.72 (m, 2 H); 1.40 - 1.60 (m, 4 H); 1.11 - 1.25 (m, 2 H).

2-(5,6-Dimethylbenzo[*d*]isoxazol-3-yl)-*N*-(2-(methylamino)-2-oxoethyl)acetamide (2.70)

2.70
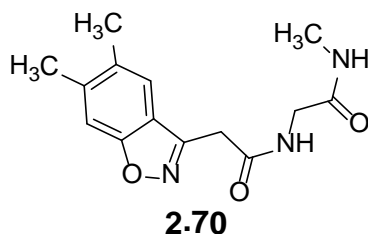
2-(5,6-Dimethylbenzo[*d*]isoxazol-3-yl)acetic acid (**2.25**, 50 mg, 0.24 mmol) was reacted with 2-amino-*N*-methylacetamide according to general procedure B to afford the title compound (**2.70**) as a yellow solid (7 mg, 0.03 mmol, 10 %). LCMS (formic): Rt = 0.72 min, [M+H]$^+$ = 276, purity = 100%. ^{1}H NMR (DMSO-d_6) δ ppm 8.56 - 8.63 (m, 1 H); 7.80 - 7.88 (m, 1 H); 7.63 (s, 1 H); 7.49 (s, 1 H); 3.91 (s, 3 H); 3.71 (d, *J* = 6.0 Hz, 2 H); 2.61 (d, *J* = 5.0 Hz, 2 H); 2.37 (s, 3 H); 2.32 (s, 3 H).

2-(5,6-Dimethylbenzo[*d*]isoxazol-3-yl)-*N*-((1,3-dimethylpyrrolidin-3-yl)methyl)acetamide (2.71)

2.71
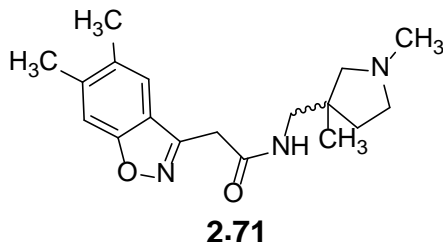
2-(5,6-Dimethylbenzo[*d*]isoxazol-3-yl)acetic acid (**2.25**, 50 mg, 0.24 mmol) was reacted with (1,3-dimethylpyrrolidin-3-yl)methanamine (obtained from the GSK compound collection) according to general procedure B to afford the title compound (**2.71**) as a yellow oil (41 mg, 0.13 mmol, 54 %). LCMS (formic): Rt = 0.65 min, [M+H]$^+$ = 316, purity = 99%. ^{1}H NMR (CDCl$_3$) δ ppm 7.85 (br s., 1 H); 7.46 (s, 1 H); 7.34 (s, 1 H); 3.90 (d, *J* = 6.5 Hz, 2 H); 3.20 (dq, *J* = 6.0, 1.3 Hz, 1 H); 2.98 (dd, *J* = 13.0, 3.0 Hz, 1 H); 2.45 (d, *J* = 9.0 Hz, 1 H); 2.39 (s, 3 H); 2.34 (s, 3 H); 2.26 (dt, *J* = 9.0, 3.0 Hz, 1 H); 1.90 - 2.03

(m, 4 H); 1.85 (dd, *J* = 9.0, 1.0 Hz, 1 H); 1.48 - 1.59 (m, 1 H); 1.37 – 1.45 (m, 1 H); 0.99 (s, 3 H).

N-((1*H*-Imidazol-2-yl)methyl)-2-(5,6-dimethylbenzo[*d*]isoxazol-3-yl)acetamide (2.72)

2.72
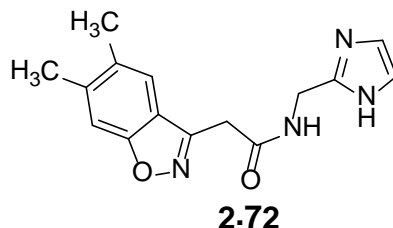
2-(5,6-Dimethylbenzo[*d*]isoxazol-3-yl)acetic acid (**2.25**, 50 mg, 0.24 mmol) was reacted with (1*H*-imidazol-2-yl)methanamine dihydrochloride (obtained from the GSK compound collection) according to general procedure B to afford the title compound (**2.72**) as a white solid (11 mg, 0.04 mmol, 15 %). LCMS (formic): Rt = 0.59 min, [M+H]$^+$ = 285, purity = 94%. ^{1}H NMR (DMSO-*d*$_6$) δ ppm 11.83 (br s, 1 H); 8.83 (br s, 1 H); 7.59 (s, 1 H); 7.49 (s, 1 H); 7.03 (s, 1 H); 6.84 (s, 1 H); 4.32 (d, *J* = 5.5 Hz, 2 H); 3.90 (s, 2 H); 2.37 (s, 3 H); 2.31 (s, 3 H). The identity of this isomer was confirmed by HMBC experiment showing a correlation from the carbonyl C (163 ppm) to both methylene group proton signals (4.32 and 3.90 ppm)
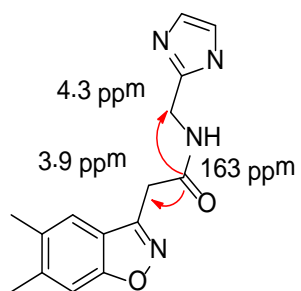
Observed correlations confirming structure
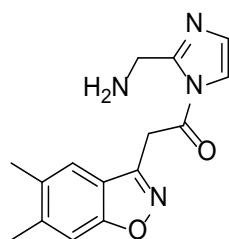
Correlation with 4.3 ppm would not
be observed for this alternative product

2-(5,6-Dimethylbenzo[*d*]isoxazol-3-yl)-*N*-(2-(furan-2-yl)ethyl)acetamide (2.73)

2·73
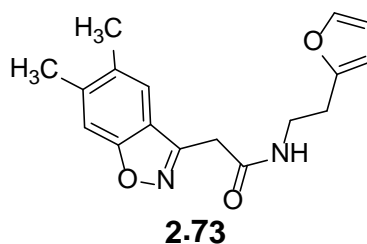
2-(5,6-Dimethylbenzo[*d*]isoxazol-3-yl)acetic acid (**2.25**, 50 mg, 0.24 mmol) was reacted with 2-(furan-2-yl)ethanamine (obtained from the GSK compound collection) according to general procedure B to afford the title compound (**2.73**) (13 mg, 0.04 mmol, 18 %). LCMS (formic): Rt = 1.01 min, [M+H]$^+$ = 299, purity = 100%.^{1}H NMR (DMSO-d_6) δ ppm 8.40 - 8.52 (m, 1 H); 7.47 - 7.55 (m, 3 H); 6.31 - 6.38 (m, 1 H); 6.09 - 6.16 (m, 1 H); 3.82 (s, 2 H); 3.31 - 3.42 (m, 2 H); 2.77 (t, *J* = 7.0 Hz, 2 H); 2.38 (s, 3 H); 2.31 (s, 3 H).

2-(5,6-Dimethylbenzo[*d*]isoxazol-3-yl)-*N*-((1-ethyl-1*H*-pyrazol-3-yl)methyl)acetamide (2.74)
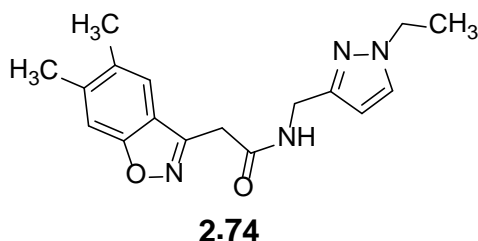
2·74

2-(5,6-Dimethylbenzo[*d*]isoxazol-3-yl)acetic acid (**2.25**, 50 mg, 0.24 mmol) was reacted with (1-ethyl-1*H*-pyrazol-3-yl)methanamine (obtained from the GSK compound collection) according to general procedure B to afford the title compound (**2.74**) as a white solid (39 mg, 0.13 mmol, 51 %). LCMS (ammonium bicarbonate): Rt = 0.91 min, [M+H]$^+$ = 313, purity = 100%. ^{1}H NMR (CDCl$_3$) δ ppm 7.50 (s, 1 H); 7.30 - 7.36 (m, 1 H); 7.23 - 7.30 (m, 1 H); 6.63 (br s, 1 H); 6.09 (d, *J* = 2.0 Hz, 1 H); 4.43 (d, *J* = 5.5 Hz, 2 H); 4.08 (q, *J* = 7.5 Hz, 2 H); 3.95 (s, 2 H); 2.40 (s, 3 H); 2.35 (s, 3 H); 1.43 (t, *J* = 7.5 Hz, 3 H).

N-(2-(1H-1,2,4-Triazol-1-yl)ethyl)-2-(5,6-dimethylbenzo[d]isoxazol-3-yl)acetamide (2.75)

2.75
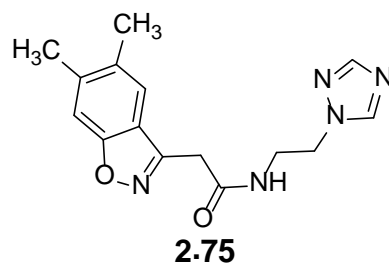
2-(5,6-Dimethylbenzo[d]isoxazol-3-yl)acetic acid (**2.25**, 50 mg, 0.24 mmol) was reacted with 2-(1H-1,2,4-triazol-1-yl)ethanamine (obtained from the GSK compound collection) according to general procedure B to afford the title compound (**2.75**) as a white solid (55 mg, 0.18 mmol, 75 %). LCMS (ammonium bicarbonate): Rt = 0.75 min, [M+H]$^+$ = 300, purity = 96%. ^{1}H NMR (DMSO-d_6) δ ppm 8.44 (br. s, 2 H); 7.96 (s, 1 H); 7.50 (br. s, 2 H); 4.26 (t, J = 6.0 Hz, 2 H); 3.81 (s, 2 H); 3.51 (dd, J = 12.0, 5.5 Hz, 2 H); 2.38 (s, 3 H); 2.33 (s, 3 H).

2-(5,6-Dimethylbenzo[d]isoxazol-3-yl)-N-((1-hydroxycyclopentyl)methyl)acetamide (2.76)

2.76
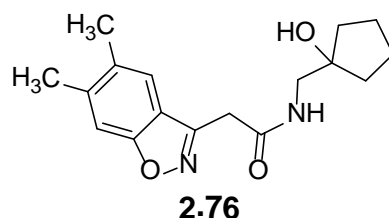
2-(5,6-Dimethylbenzo[d]isoxazol-3-yl)acetic acid (**2.25**, 50 mg, 0.24 mmol) was reacted with 1-(aminomethyl)cyclopentanol hydrochloride according to general procedure B to afford the title compound (**2.76**) as a white solid (58 mg, 0.19 mmol, 79 %). LCMS (ammonium bicarbonate): Rt = 0.92 min, [M+H]$^+$ = 303, purity = 100%. ^{1}H NMR (CDCl$_3$) δ ppm 7.50 (s, 1 H); 7.33 (s, 1 H); 6.84 (br s, 1 H); 3.93 (s, 2 H); 3.38 (d, J = 6.0 Hz, 2 H); 2.50 - 2.68 (m, 1 H); 2.40 (s, 3 H); 2.35 (s, 3 H); 1.91 (br. s, 1 H); 1.69 - 1.83 (m, 2 H); 1.52 - 1.67 (m, 6 H).

2-(5-Methylbenzo[d]isoxazol-3-yl)acetic acid (2.24)

2.24
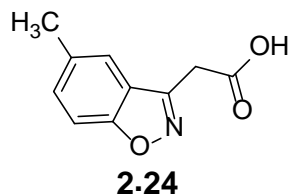
4-Hydroxy-6-methyl-2H-chromen-2-one (500 mg, 2.84 mmol) was reacted with hydroxylamine (10 mL) according to general procedure A to afford the title compound (**2.24**) as a white solid (408 mg, 2.14 mmol, 75%). LCMS (formic): Rt = 0.75 min, $[M+H]^+$ = 192, purity = 99 %. ^{1}H NMR (400 MHz, DMSO-d_6) δ ppm 12.86 (br. s., 1 H); 7.63 (s, 1H); 7.61 (s, 1 H); 7.47 (dd, J = 8.5, 1.5 Hz, 1 H); 4.05 (s, 2 H); 2.44 (s, 3 H).

2-(5-Methylbenzo[*d*]isoxazol-3-yl)-*N*-((6-methylpyridin-2-yl)methyl)acetamide (2.77)

2.77
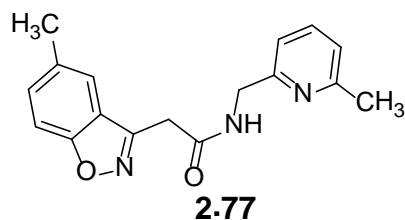
2-(5-Methylbenzo[d]isoxazol-3-yl)acetic acid (**2.24**, 54 mg, 0.28 mmol) was reacted with (6-methylpyridin-2-yl)methanamine according to general procedure B to afford the title compound (**2.77**) as a white solid (29 mg, 0.10 mmol, 35 %). LCMS (ammonium bicarbonate): Rt = 0.89 min, $[M+H]^+$ = 296, purity = 99%. ^{1}H NMR (CDCl$_3$) δ ppm 7.56 (s, 1 H); 7.44 - 7.54 (m, 2 H); 7.38 (dd, J = 8.5, 1.0 Hz, 1 H); 7.32 (br s, 1 H); 6.97 – 7.04 (m, 2 H); 4.52 (d, J = 5.0 Hz, 2 H); 4.03 (s, 2 H); 2.46 (s, 6 H).

2-(Benzo[*d*]isoxazol-3-yl)-*N*-((6-methylpyridin-2-yl)methyl)acetamide (2.78)

2·78
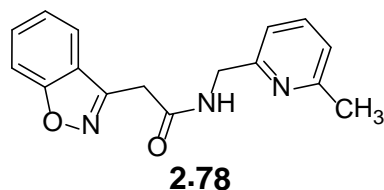
2-(Benzo[d]isoxazol-3-yl)acetic acid (50 mg, 0.28 mmol) (obtained from the GSK compound collection) was reacted with (6-methylpyridin-2-yl)methanamine according to general procedure B to afford the title compound (**2.78**) as a white solid (46 mg, 0.16 mmol, 58 %). LCMS (ammonium bicarbonate): Rt = 0.81 min, [M+H]$^+$ = 282, purity = 100%. ^{1}H NMR (400 MHz, CDCl$_3$) δ ppm 7.81 (d, *J* = 8.0 Hz, 1 H) 7.54 - 7.63 (m, 2 H); 7.46 – 7.53 (m, 1 H); 7.36 - 7.42 (m, 1 H); 7.33 (ddd, *J* = 8.0, 6.0, 2.0 Hz, 1 H); 6.95 – 7.04 (m, 2H); 4.52 (d, *J* = 5.0 Hz, 2 H); 4.06 (s, 2 H); 2.46 (s, 3 H).

2-(Cyanomethyl)-7-oxo-5-propyl-4,7-dihydropyrazolo[1,5-*a*]pyrimidine-3-carbonitrile (2.90)

2·90
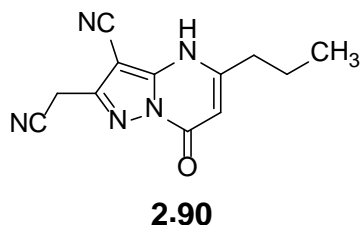
5-Amino-3-(cyanomethyl)-1*H*-pyrazole-4-carbonitrile (4.03 g, 27.4 mmol) was dissolved in acetic acid (40 mL) and water (20mL). Ethyl 3-oxohexanoate (5.73 mL, 35.6 mmol) was added and the resulting solution was heated at 120 ºC for 2 days. The solution was cooled to room temperature and the solvents were removed under reduced pressure Purification by Andy Hobbs, GSK in three batches, each of these on a 100 g C18 column, eluting with a gradient of 0 - 40 % methanol in 10 mM ammonium bicarbonate to afford the title compound (**2.90**) as an off-white solid (2.21 g, 9.2 mmol, 33%). LCMS (ammonium bicarbonate): Rt = 0.65 min, [M+H]$^+$ = 242, purity = 79 %.

Ethyl 2-(3-cyano-7-oxo-5-propyl-4,7-dihydropyrazolo[1,5-*a*]pyrimidin-2-yl)acetate (2.91)

2.91
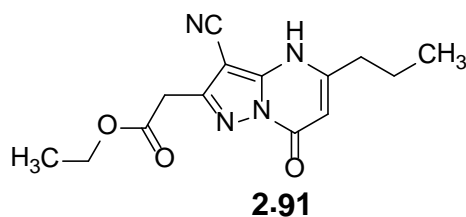
2-(Cyanomethyl)-7-oxo-5-propyl-4,7-dihydropyrazolo[1,5-*a*]pyrimidine-3-carbonitrile (**2.90**, 273 mg, 1.13 mmol) was suspended in a mixture of 1,4-dioxane (10 mL) and ethanol (10 mL) and heated at 60 ⁰C until complete dissolution had taken place. The solution was allowed to cool to 25 ⁰C and then placed into an ice bath at the same time as hydrochloric acid (g) was started bubbling through the solution (exothermic reaction). The gas was bubbled through the solution in an ice bath for 2.5 hours, maintaining the reaction temperature below 30 °C. The solvents were removed by evaporation and the residue was dissolved in water (20 mL) and stirred at 60 ⁰C for 10 minutes. The solution was cooled to room temperature and the precipitate formed was isolated by filtration, washed with water and dried in a vacuum oven (45 °C, 1 mBar) to afford the title compound (**2.91**) as a yellow solid (110 mg, 0.38 mmol, 34 %). LCMS (ammonium bicarbonate): Rt = 0.61 min, [M+H]$^+$ = 289, purity = 89 %. ^{1}H NMR (DMSO-*d*6) δ ppm 13.18 (s, 1H); 5.84 (s, 1 H); 4.14 (q, *J* = 7.0 Hz, 2 H); 3.90 (s, 2 H); 2.57 (t, *J* = 8.0 Hz, 2 H); 1.68 (m, 2 H); 1.22 (t, *J* = 7.0 Hz, 3 H); 0.94 (t, *J* = 8.0 Hz, 3 H). The filtrate was concentrated and purified by MDAP (formic acid, gradient B) to afford the title compound (**2.91**) as a white solid (38 mg, 0.13 mmol, 12 %). LCMS (ammonium bicarbonate): Rt = 0.60 min, [M+H]$^+$ = 289, purity = 100 %. ^{1}H NMR (DMSO-*d*6) as above.

2-(3-Cyano-7-oxo-5-propyl-4,7-dihydropyrazolo[1,5-*a*]pyrimidin-2-yl)acetic acid (2.92)
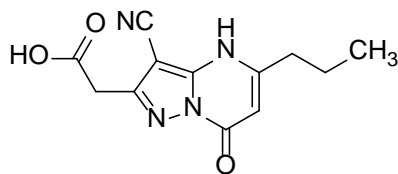
2·92

Ethyl 2-(3-cyano-7-oxo-5-propyl-4,7-dihydropyrazolo[1,5-*a*]pyrimidin-2-yl)acetate (**2.91**, 38 mg, 0.13 mmol) was dissovled in 2-methyltetrahydrofuran (1 mL), methanol (0.5 mL) and water (0.2 mL). Lithium hydroxide (32 mg, 1.32 mmol) was added and the resulting yellow solution was stirred at room temperature for 24 hours. The solvents were removed under reduced pressure and purified by MDAP (formic acid, gradient A) to afford the title compound (**2.92**) as a colourless oil (19 mg, 0.07 mmol, 55%). LCMS (formic): Rt = 0.53 min, [M+H]$^+$ = 261, purity = 93 %. ^{1}H NMR (CDCl$_3$) δ ppm 13.19 (br. s, 1H); 5.94 (s, 1 H); 3.63 (s, 2 H); 2.80 (t, *J* = 7.5 Hz, 2 H); 1.03 (t, *J* = 7.5 Hz, 3 H). Additional 3 H masked by water peak at 1.96 ppm.

7-Oxo-2-(2-oxo-2-(pyrrolidin-1-yl)ethyl)-5-propyl-4,7-dihydropyrazolo[1,5-*a*]pyrimidine-3-carbonitrile (2.87)
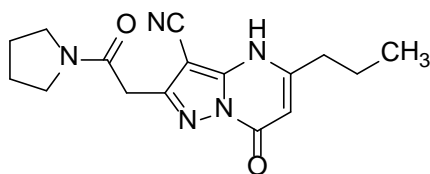
2·87

2-(3-Cyano-7-oxo-5-propyl-4,7-dihydropyrazolo[1,5-*a*]pyrimidin-2-yl)acetic acid (**2.92**, 19 mg, 0.07 mmol) was dissolved in DMF (0.5 mL) and HATU (33 mg, 0.09 mmol) was added, followed by DIPEA (0.03 mL, 0.15 mmol) and finally pyrrolidine (0.01 mL, 0.15 mmol). The resulting yellow solution was stirred at room temperature for 17 hours. Additional HATU (33 mg, 0.09 mmol), DIPEA (0.03 mL, 0.15 mmol) and pyrrolidine (0.01 mL, 0.15 mmol) were added and the solution was stirred at room temperature for a further 2

hours. The solvents were removed under reduced pressure and purified by MDAP (formic acid, gradient A) to afford the title compound (**2.87**) as an orange solid (13 mg, 0.04 mmol, 57 %). LCMS (ammonium bicarbonate): Rt = 0.57 min, [M+H]$^+$ = 314, purity = 100 %. ^{1}H NMR (CDCl$_3$) δ ppm 12.14 (br s, 1H); 5.65 (s, 1 H); 3.94 (s, 2 H); 3.68 (t, *J* = 7.0 Hz, 2 H); 3.63 (t, *J* = 7.0 Hz, 2 H); 2.59 (t, *J* = 8.0 Hz, 2 H); 2.04 – 2.14 (m, 2 H); 1.92 – 2.01 (m, 2 H); 1.63 – 1.74 (m, 2 H); 0.97 (t, *J* = 8.0 Hz, 3 H).

2-(2-Morpholino-2-oxoethyl)-7-oxo-5-propyl-4,7-dihydropyrazolo[1,5-*a*]pyrimidine-3-carbonitrile (2.93)

2.93
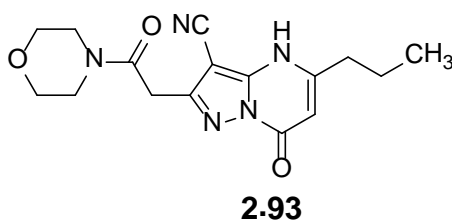
2-(3-Cyano-7-oxo-5-propyl-4,7-dihydropyrazolo[1,5-*a*]pyrimidin-2-yl)acetic acid (**2.92**, 47 mg, 0.18 mmol) was dissolved in DMF (0.5 mL) and HATU (82 mg, 0.22 mmol) was added, followed by DIPEA (0.06 mL, 0.36 mmol) and finally morpholine (0.02 mL, 0.22 mmol). The resulting yellow solution was stirred at room temperature for 17 h. Additional HATU (82 mg, 0.22 mmol), DIPEA (0.06 mL, 0.36 mmol) and morpholine (0.02 mL, 0.22 mmo) were added and the solution was stirred for 24 h at room temperature. The solvents were removed under reduced pressure and purified by MDAP (formic acid, gradient A) to afford the title compound (**2.93**) as a white solid (38 mg, 0.115 mmol, 64 %). Mp 185-188 °C. LCMS (formic): Rt = 0.55 min, [M+H]$^+$ = 330, purity = 100 %. ^{1}H NMR (DMSO-*d$_6$*) δ ppm 13.12 (br. s., 1 H); 5.83 (s, 1 H); 3.93 (s, 2 H); 3.60 – 3.65 (m, 2 H); 3.53 - 3.60 (m, 4 H); 3.43 - 3.52 (m, 2 H); 2.57 (t, *J* = 7.5 Hz, 2 H); 1.62 – 1.73 (m, 2 H); 0.94 (t, *J* = 7.5 Hz, 3 H). ^{13}C NMR (DMSO-*d$_6$*) δ ppm 166.1 (Ar C); 155.2 (C=O); 154.9 (Ar C); 152.5 (Ar C); 145.5 (C=O) 112.7 (CN); 97.6 (CH); 75.5 (Ar C); 66.0 (2 CH$_2$); 45.8 (CH$_2$); 41.8 (CH$_2$); 34.0 (CH$_2$); 32.3 (CH$_2$); 21.3 (CH$_2$); 13.2 (CH$_3$).

IR (ATR) cm^{-1} 3409; 3181; 3085; 2964; 2857; 2235; 1703; 1623; 1581; 1409; 1235; 1111; 1037; 813.

General Procedure C: Piperidine Amide Formation

1-(tert-butoxycarbonyl)piperidine-4-carboxylic acid (1 eq.) was dissolved in DMF (2 – 10 mL) and treated with COMU (2 eq.) and DIPEA (3 eq.), followed by the appropriately substituted amine (1.2 eq.). The resulting solutions were stirred at room temperature overnight. The intermediates were worked-up as described and then treated with hydrochloric acid (5-10 eq) and the solutions were stirred at room temperature until reactions were complete. The crude products were worked-up and purified as described.

Piperidin-1-yl(piperidin-4-yl)methanone (4.38)
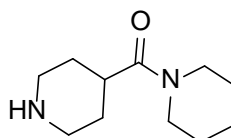
4.38

Piperidine (0.24 mL, 2.41 mmol) was reacted according to general procedure C. The intermediate was not worked up, and the reaction solution was treated directly with HCl (2M, 10 mL). After the deprotection was complete, the solution was basified by addition of saturated aqueous sodium bicarbonate (100 mL) and was then extracted with DCM (3 X 100 mL). The combined organic layers were passed through a hydrophobic frit and concentrated. LCMS analysis showed the product remained in the aqueous layer. The aqueous solution was loaded onto a 2 g Biotage® 103 column, which was washed with water and then eluted with methanol. The methanol washings were concentrated and purified by MDAP (ammonium bicarbonate method A) to afford the title compound (**4.38**) as an orange oil (196 mg, 0.99 mmol, 50 %). LCMS (formic): Clear [M+H]$^+$ = 197 at solvent front, indeterminate UV trace with poor chromophore. ^{1}H NMR (CDCl$_3$) δ ppm 3.50 – 3.59 (m, 2 H); 3.46 (s, 1 H); 3.38 – 3.45 (m, 2 H); 3.11 - 3.19 (m, 2 H); 2.58

- 2.71 (m, 3 H); 1.69 - 1.87 (m, 3 H); 1.60 - 1.69 (m, 6 H). N.B no impurities were visible by NMR.

(4-Methylpiperidin-1-yl)(piperidin-4-yl)methanone (4.39)

4.39
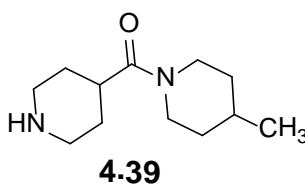
4-Methylpiperidine (0.63 mL, 5.34 mmol) was reacted according to general procedure C. The intermediate was worked up by removing the solvent by evaporation and partitioning the residue between ethyl acetate (20 mL) and water (20 mL). The aqueous layer was extracted with additional ethyl acetate (2 X 20mL) and the combined organic layers were dried by passing through a hydrophobic frit and concentrated to yield a red oil. The residue was treated with hydrochloric acid (4 M in dioxane) (5.56 mL, 22.2 mmol). When the deprotection was complete, the solution was basified by addition of saturated aqueous sodium bicarbonate (100 mL) and was then extracted with DCM (2 X 100 mL). The combined organic layers were passed through a hydrophobic frit and concentrated. This material was purified by Andy Hobbs, GSK on a 150 g C18 GOLD® Aq column, eluting with a gradient of 5 - 85 % acetonitrile in 10 mM ammonium bicarbonate (aq.) to afford the title compound (**4.39**) in multiple batches of varying purity, all of which were used as intermediates in following steps. Batch 1 as a brown gum (68 mg, 0.32 mmol, 7 %). LCMS (ammonium bicarbonate): Rt = 0.71 min, $[M+H]^+$ = 211, purity = 100 %. ^{1}H NMR (400 MHz, CDCl$_3$) δ ppm 4.57 (d, J = 12.5 Hz, 1 H); 3.87 (d, J = 12.5 Hz, 1 H); 3.17 (d, J = 11.7 Hz, 2 H); 2.93 − 3.06 (m, 2 H); 2.59 - 2.76 (m, 3 H); 2.46 − 2.61 (m, 2 H); 1.25 (s, 3 H); 1.01 − 1.14 (m, 3 H); 0.95 (d, J = 6.5 Hz, 4 H), purity by NMR approx. 90 %. Batch 2 as a brown gum (80 mg, 0.38 mmol, 9 %). LCMS (ammonium bicarbonate): Rt = 0.71 min, $[M+H]^+$ = 211, purity = 33 %. NMR consistent with batch 1, purity by NMR approx. 80 %. Batch 3 as a brown gum (254 mg, 1.21 mmol, 27 %). LCMS (ammonium bicarbonate): Rt = 0.69 min, $[M+H]^+$ = 211., purity = 75 %. NMR consistent

with batch 1, purity by NMR approx. 70 %. Batch 4 as a brown gum (540 mg, 2.57 mmol, 58 %). LCMS (ammonium bicarbonate): Rt = 0.67 min, [M+H]⁺ not visible, purity = 100 %. NMR consistent with batch 1, purity by NMR < 50 %.

(4-Benzylpiperidin-1-yl)(piperidin-4-yl)methanone (4.40)

4.40
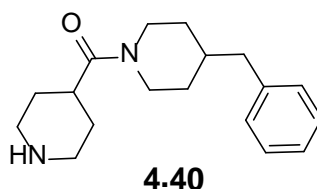
4-Benzylpiperidine (0.516 mL, 2.94 mmol) was reacted according to general procedure C. The intermediate was worked up by removing the solvent by evaporation and partitioning the residue between ethyl acetate (20 mL) and water (20 mL). The aqueous layer was extracted with additional ethyl acetate (2 X 20mL) and the combined organic layers were dried by passing through a hydrophobic frit and concentrated. The residue was treated with hydrochloric acid (4 M in dioxane) (3.1 mL, 12.2 mmol). When the deprotection was complete, the solution was basified by addition of saturated aqueous sodium bicarbonate (100 mL) and was then extracted with DCM (2 X 100 mL). The combined organic layers were passed through a hydrophobic frit and concentrated. The crude residue was purified on a 150 g Redisep C18 GOLD® column, eluting with a gradient of 20-60 % acetonitrile in 10 mM ammonium bicarbonate to afford the title compound (**4.40**) as an orange oil (637 mg, 2.22 mmol, 91 %). LCMS (ammonium bicarbonate): Rt = 1.00 min (broad peak), [M+H]⁺ = 287, purity = 100 %. (NB. Additional ion in peak for M+ = 316.21). NMR was broad and could not be assigned, even with heating to 120 °C.

General Procedure D: Nucleophilic Aromatic Substitutions

4,6-Dichloropyrimidine (1 eq.) was dissolved in ethanol and then treated with an amine (1 eq.) and DIPEA (2.5 eq.). The resulting solutions were heated in a microwave reactor at 150 °C for 5 minutes. A second amine (2 - 5 eq.) was

then added and the solutions were heated in a microwave reactor at 150 °C for 1 hour. Unless otherwise stated, the products were purified by direct injection of the reaction solution onto MDAP purification.

Piperidin-1-yl(1-(6-(piperidin-1-yl)pyrimidin-4-yl)piperidin-4-yl)methanone (4.35)

4.35
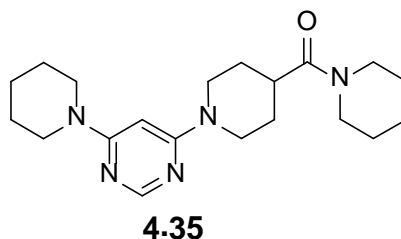
Piperidin-1-yl(piperidin-4-yl)methanone (**4.38**, 196 mg, 0.99 mmol), followed by piperidine (0.49 mL, 4.99 mmol, 5 eq.) were reacted according to general procedure D. Precipitation was observed in the reaction vial. The sample was dissolved with DMSO and then purified by Andy Hobbs, GSK on a 100g Redisep C18 GOLD column, eluting with a gradient of 20 – 80 % acetonitrile in 10 mM ammonium bicarbonate (aq.) to afford the title compound (**4.35**) as an off-white solid (239 mg, 0.67 mmol, 67 %). Mp 145-146 °C. LCMS (ammonium bicarbonate): Rt = 1.01 min, $[M+H]^+$ = 358, purity = 100 %. HRMS $C_{20}H_{32}N_5O$ required 358.2601 found 358.2599. ^{1}H NMR (DMSO-d_6) δ ppm 8.03 (s, 1 H); 5.85 (s, 1 H); 4.34 (d, J = 13.0 Hz, 2 H); 3.50 – 3.56 (m, 5 H); 3.48 (br. s., 1 H); 3.41 (br. s., 2 H); 2.80 - 2.96 (m, 3 H); 1.56 - 1.67 (m, 6 H); 1.37 - 1.55 (m, 10 H). ^{13}C NMR (DMSO-d_6) δ ppm 172.0 (C=O); 162.5 (2 Ar C); 156.9 (Ar CH); 80.9 (Ar CH); 45.7 (CH_2); 44.6 (2 CH_2); 43.3 (2 CH_2); 42.0 (CH_2); 37.3 (CH); 27.8 (2 CH_2); 26.4 (CH_2); 25.3 (CH_2); 25.0 (2 CH_2); 24.3 (CH_2); 24.1 (CH_2). IR (ATR) cm^{-1} 2928; 2847; 1623; 1582; 1489; 1306; 1294; 1202; 1005; 978; 971; 850; 811.

(4-Benzylpiperidin-1-yl)(1-(6-(piperidin-1-yl)pyrimidin-4-yl)piperidin-4-yl)methanone (4.36)

4·36
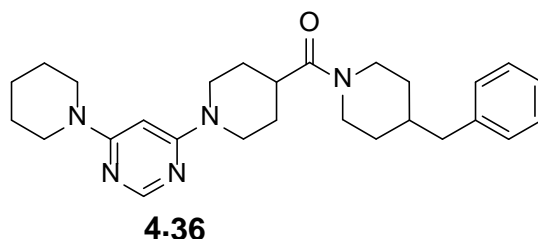
(4-Benzylpiperidin-1-yl)(piperidin-4-yl)methanone (**4.40**, 77 mg, 0.27 mmol), followed by piperidine (0.13 mL, 1.34 mmol, 5 eq.) were reacted according to general procedure D. Purification by MDAP (ammonium bicarbonate gradient C,) afforded the title compound (**4.36**) as an orange oil (44 mg, 0.10 mmol, 37 %). LCMS (formic): Rt = 0.99 min, $[M+H]^+$ = 448, purity = 100 %. ^{1}H NMR (DMSO-d_6) δ ppm 8.03 (s, 1 H); 7.25 – 7.31 (m, 2 H); 7.15 – 7.21 (m, 3 H); 5.85 (br. s, 1 H); 4.29 – 4.39 (m, 3 H); 3.95 – 4.02 (m, 1 H); 3.53 (t, *J* = 5.5 Hz, 4 H); 2.80 - 3.02 (m, 4 H); 1.70 - 1.83 (m, 1 H); 1.54 - 1.67 (m, 7 H); 1.39 - 1.54 (m, 7 H); 1.05 - 1.13 (m, 2 H); 0.91 - 1.02 (m, 1 H).

(4-Methylpiperidin-1-yl)(1-(6-morpholinopyrimidin-4-yl)piperidin-4-yl)methanone (4.44)
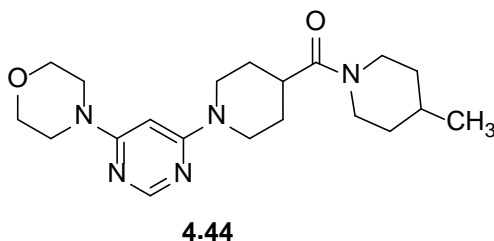
4.44

(4-Methylpiperidin-1-yl)(piperidin-4-yl)methanone (**4.39** 40 mg, 0.19 mmol) followed by morpholine (0.08 mL, 0.95 mmol, 5 eq.) were reacted according to general procedure D. Purification by MDAP (ammonium bicarbonate gradient B,) afforded the title compound (**4.44**) as a yellow oil (20 mg, 0.05 mmol, 28 %). LCMS (formic): Rt = 0.67 min, $[M+H]^+$ = 374, purity = 100 %. HRMS $C_{20}H_{32}N_5O_2$ required 374.2551, found 374.2550. ^{1}H NMR (400 MHz, CDCl$_3$) δ ppm 8.23 (s, 1 H); 5.59 (s, 1 H); 4.58 (d, *J* = 13.0 Hz, 1 H); 4.34 (d,

J = 13.0 Hz, 2 H); 3.90 (d, *J* = 13.2 Hz, 1 H); 3.74 – 3.80 (m, 4 H); 3.50 – 3.56 (m, 4 H); 3.04 (t, *J* = 12.0 Hz, 1 H); 2.89 – 2.99 (m, 2 H); 2.71 - 2.83 (m, 1 H); 2.50 – 2.60 (m, 1 H); 1.56 - 1.93 (m, 7 H); 1.05 - 1.19 (m, 2 H); 0.98 (d, *J* = 6.4 Hz, 3 H). ^{13}C NMR (101 MHz, DMSO-d_6) δ ppm 172.0 (C=O); 163.1 (Ar C); 162.4 (Ar C); 156.9 (Ar CH); 81.4 (Ar CH); 65.8 (2 CH$_2$); 44.9 (CH$_2$); 44.1 (2 CH$_2$); 43.3 (2 CH$_2$); 41.3 (CH$_2$); 37.3 (CH); 34.6 (CH$_2$); 33.6 (CH$_2$); 30.5 (CH); 27.8 (CH$_2$); 27.7 (CH$_2$); 21.6 (CH$_3$).

(1-(6-(Dimethylamino)pyrimidin-4-yl)piperidin-4-yl)(4-methylpiperidin-1-yl)methanone (4.45)

4.45
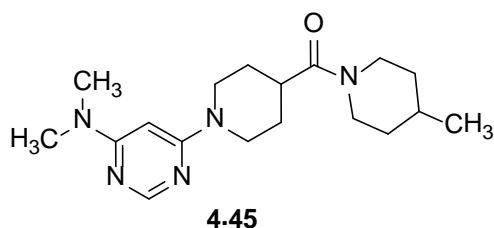
(4-Methylpiperidin-1-yl)(piperidin-4-yl)methanone (**4.39**, 68 mg, 0.32 mmol) followed by dimethylamine (2.0M in THF) (0.54 mL, 1.07 mmol, 5 eq.) were reacted according to general procedure D. Purification by MDAP (ammonium bicarbonate gradient B,) afforded the title compound (**4.45**) as an orange oil (19 mg, 0.06 mmol, 26 %). LCMS (formic): Rt = 0.67 min, [M+H]$^+$ = 332, purity = 100 %. ^{1}H NMR (400 MHz, CDCl$_3$) δ ppm 8.23 (s, 1 H); 5.48 (s, 1 H); 4.59 (d, J = 13.5 Hz, 1 H); 4.35 (d, J = 13.0 Hz, 2 H); 3.91 (d, J = 14.0, 1 H); 3.06 (s, 6 H); 3.00 - 3.05 (m, 1 H); 2.86 – 2.97 (m, 3 H); 2.70 - 2.79 (m, 1 H); 2.55 (t, J = 13.0 Hz, 1 H); 1.56 - 1.91 (m, 6 H); 1.04 - 1.18 (m, 2 H); 0.97 (d, J = 6.5 Hz, 3 H).

4-Methylpiperidin-1-yl)(1-(6-(pyrrolidin-1-yl)pyrimidin-4-yl)piperidin-4-yl)methanone (4.46)
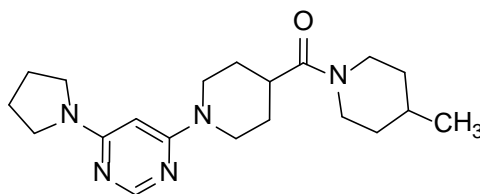
4.46

(4-Methylpiperidin-1-yl)(piperidin-4-yl)methanone (**4.39**, 40 mg, 0.19 mmol) followed by pyrrolidine (0.079 mL, 0.951 mmol, 5 eq.) were reacted according to general procedure D. Purification by MDAP (ammonium bicarbonate gradient C) afforded the title compound (**4.46**) as a yellow oil (22 mg, 0.06 mmol, 33 %) . LCMS (formic): Rt = 0.75 min, $[M+H]^+$ = 358, purity = 100 %. HRMS $C_{20}H_{32}N_5O$ required 358.2601, found 358.2595. ^{1}H NMR (400 MHz, DMSO-d_6) δ ppm 8.20 (d, J = 0.5 Hz, 1 H); 5.33 (s, 1 H); 4.56 (d, J = 13.0 Hz, 1 H); 4.32 (d, J = 13.0 Hz, 2 H); 3.89 (d, J = 13.0 Hz, 1 H); 3.35 - 3.48 (m, 4 H); 3.02 (t, J = 12.0 Hz, 1 H); 2.89 (t, J = 12.0 Hz, 2 H); 2.68 - 2.78 (m, 1 H); 2.53 (t, J = 12.0 Hz, 1 H); 1.94 - 2.00 (m, 4 H); 1.53 - 1.88 (m, 7 H); 1.01 - 1.17 (m, 2 H); 0.95 (d, J = 6.5 Hz, 3 H). ^{13}C NMR (101 MHz, DMSO-d_6) δ ppm 172.0 (C=O); 161.8 (Ar C); 160.7 (Ar C); 156.9 (Ar CH); 81.0 (Ar CH); 45.9 (2 CH_2); 44.9 (CH_2); 43.2 (2 CH_2); 41.3 (CH_2); 37.3 (CH_2); 34.7 (CH_2); 33.5 (CH); 30.5 (CH_2); 27.8 (CH_2); 27.6 (CH); 24.7 (2 CH_2); 21.5 (CH_3).

(1-(6-(4-Methylpiperazin-1-yl)pyrimidin-4-yl)piperidin-4-yl)(4-methylpiperidin-1-yl)methanone (4.47)
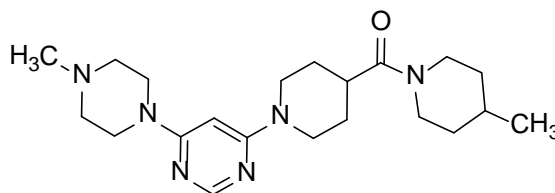
4.47

(4-Methylpiperidin-1-yl)(piperidin-4-yl)methanone (**4.39**, 50. mg, 0.24 mmol) followed by 1-methylpiperazine (0.13 mL, 1.19 mmol, 5 eq.) were reacted

according to general procedure D. Purification by MDAP (ammonium bicarbonate gradient B) afforded the title compound (**4.47**) as an orange oil (32 mg, 0.08 mmol, 35 %). LCMS (ammonium bicarbonate): Rt = 0.88 min, [M+H]$^+$ = 387, purity = 100 %. ^{1}H NMR (400 MHz, CDCl$_3$) δ ppm 8.22 (s, 1 H); 5.60 (s, 1 H); 4.56 (d, J = 13.0 Hz, 1 H); 4.33 (d, J = 13.0 Hz, 2 H); 3.89 (d, J = 13.0 Hz, 1 H); 3.55 – 3.61 (m, 4 H); 3.46 (s, 1 H); 3.03 (t, J = 12.0 Hz, 1 H); 2.92 (t, J = 12.0 Hz, 2 H); 2.69 - 2.79 (m, 2 H); 2.52 – 2.58 (m, 1H); 2.44 – 2.50 (m, 3 H); 2.33 (s, 3 H); 1.55 - 1.90 (m, 6 H); 1.00 - 1.16 (m, 2 H); 0.97 (d, J = 6.5 Hz, 3 H).

(1-(6-(Cyclopentylamino)pyrimidin-4-yl)piperidin-4-yl)(4-methylpiperidin-1-yl)methanone (4.48)

4.48
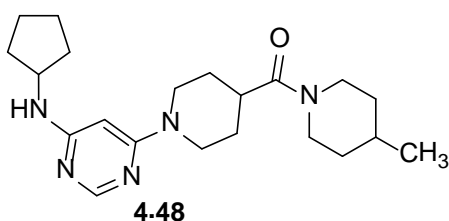
(4-Methylpiperidin-1-yl)(piperidin-4-yl)methanone (**4.39**, 50 mg, 0.24mmol) followed by cyclopentanamine (0.12 mL, 1.19 mmol, 5 eq.) were reacted according to general procedure D. After the second amine addition the reaction was heated at 150 °C for 9 hours. Purification by MDAP (ammonium bicarbonate gradient C extended run) afforded the title compound (**4.48**) as a yellow oil (29 mg, 0.08 mmol, 33 %). LCMS (formic): Rt = 0.86 min, [M+H]$^+$ = 372, purity = 93 %. ^{1}H NMR (400 MHz, CDCl$_3$) δ ppm 8.12 (s, 1 H); 5.43 (s, 1 H); 4.76 (d, J = 6.5 Hz, 1 H); 4.59 (d, J = 13.0 Hz, 1 H); 4.34 (d, J = 13.0 Hz, 2 H); 3.85 – 3.96 (m, 2 H); 3.04 (t, J = 12.0 Hz, 1 H); 2.93 (t, J = 12.0 Hz, 2 H); 2.70 - 2.80 (m, 1 H); 2.55 (t, J = 12.0 Hz, 1 H); 1.96 - 2.07 (m, 2 H); 1.56 - 1.92 (m, 11 H); 1.44 - 1.55 (m, 2 H); 1.01 - 1.18 (m, 2 H) 0.97 (d, J = 6.5 Hz, 3 H).

(1-(6-(Cyclohexylamino)pyrimidin-4-yl)piperidin-4-yl)(4-methylpiperidin-1-yl)methanone (4.49)

4.49
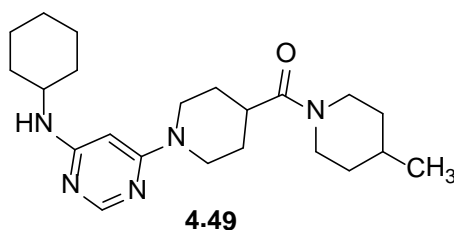
4-Methylpiperidin-1-yl)(piperidin-4-yl)methanone (**4.39**, 50 mg, 0.24 mmol) followed by cyclohexanamine (0.14 mL, 1.19 mmol, 5 eq.) were reacted according to general procedure D. After the second amine addition the reaction was heated at 150 °C for 9 hours. Purification by MDAP (ammonium bicarbonate gradient C extended run) afforded the title compound (**4.49**) as a yellow oil (18 mg, 0.05 mmol, 19 %). LCMS (formic): Rt = 0.90 min, $[M+H]^+$ = 386, purity = 98 %.^{1}H NMR (400 MHz, CDCl$_3$) δ ppm 8.12 (s, 1 H); 5.40 (s, 1 H); 4.86 (d, J = 6.5 Hz, 1 H); 4.58 (d, J = 13.0 Hz, 1 H); 4.32 (d, J = 13.2 Hz, 2 H); 3.90 (d, J = 13.2 Hz, 1 H); 3.40 - 3.48 (m, 2 H); 3.04 (t, J = 12.0 Hz, 1 H); 2.92 (t, J = 12.0 Hz, 2 H); 2.69 - 2.80 (m, 1 H); 2.55 (t, J = 12.1 Hz, 1 H); 2.13 (br. s., 2 H); 1.96 - 2.05 (m, 2 H); 1.57 - 1.91 (m, 7 H); 1.32 - 1.46 (m, 2 H); 1.17 - 1.30 (m, 3 H); 1.10 (t, J = 11.5 Hz, 2 H); 0.98 (d, J = 6.5 Hz, 3 H).

(4-Benzylpiperidin-1-yl)(1-(6-morpholinopyrimidin-4-yl)piperidin-4-yl)methanone (4.50)

4.50
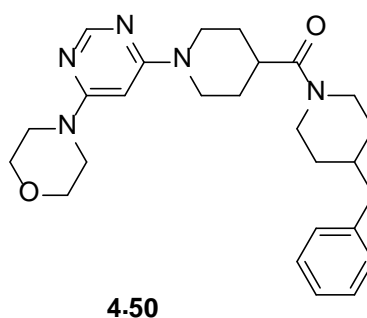
(4-Benzylpiperidin-1-yl)(piperidin-4-yl)methanone (**4.40**, 1.0 g, 3.49 mmol) followed by morpholine (1.5 mL, 17.45 mmol, 5 eq.) were reacted according to general procedure D. The solvents were removed by evaporation and then

purified by Andy Hobbs, Chemical Sciences, GSK. The product was purified on a 80g Redisep Gold® silica column, eluting with a gradient of 10-95 % ethyl acetate in cyclohexane, followed by 95 – 100 % (10 % methanol in ethyl acetate) in cyclohexane. The appropriate fractions were combined and concentrated to yield the title compound (**4.50**) as an off-white solid (1.32 g, 2.94 mmol, 84 %). Mp 153-155 °C. LCMS (formic): Rt = 0.84 min, $[M+H]^+$ = 450, purity = 100 %. HRMS $C_{26}H_{36}N_5O_2$ required 450.2864, found 450.2855. ^{1}H NMR (400 MHz, DMSO-d_6) δ ppm 8.07 (s, 1 H); 7.24 - 7.30 (m, 2 H); 7.14 - 7.20 (m, 3 H); 5.88 (s, 1 H); 4.34 (br. d, J = 13.0 Hz, 3 H); 3.98 (d, J = 13.0 Hz, 1 H); 3.61 - 3.66 (m, 4 H); 3.45 - 3.51 (m, 4 H); 2.81 - 3.00 (m, 4 H); 2.41 – 2.54 (m, 3 H); 1.69 - 1.82 (m, 1 H); 1.53 – 1.66 (m, 4 H); 1.38 - 1.51 (m, 2 H); 0.88 - 1.15 (m, 2 H). ^{13}C NMR (101 MHz, DMSO-d_6) δ ppm 178.8 (C=O); 171.9 (Ar C); 163.0 (Ar C); 162.4 (Ar CH); 156.9 (Ar CH); 140.0 (Ar C); 128.9 (2 Ar CH); 128.0 (Ar CH); 125.7 (Ar CH); 81.4 (Ar CH); 65.8 (2 CH_2); 44.8 (CH_2); 44.1 (2 CH_2); 43.2 (CH_2); 42.0 (CH_2); 41.2 (CH_2); 37.5 (CH_2); 37.3 (CH); 32.6 (CH_2); 31.4 (CH_2); 30.3 (CH); 27.8 (CH_2); 27.7 (CH_2). IR (ATR) cm^{-1} 3024; 2920; 2852; 1628; 1578; 1446; 1200; 1121; 973; 800; 695.

The HCl salt of this product was formed by dissolving 640 mg of the product in methanol (2 mL) and treating the solution with 4M HCl in dioxane (10 mL). The vial was sonicated to fully dissolve the material and then the solvents were removed by nitrogen blow-down to yield (4-benzylpiperidin-1-yl)(1-(6-morpholinopyrimidin-4-yl)piperidin-4-yl)methanone hydrogen chloride as a yellow solid (649 mg, 1.34 mmol). LCMS (ammonium bicarbonate): Rt = 1.11 min, $[M+H]^+$ = 450, purity = 99 %. ^{1}H NMR peaks were too broad to assign.

(4-Benzylpiperidin-1-yl)(1-(6-(4-methylpiperazin-1-yl)pyrimidin-4-yl)piperidin-4-yl)methanone (4.51)

4-51
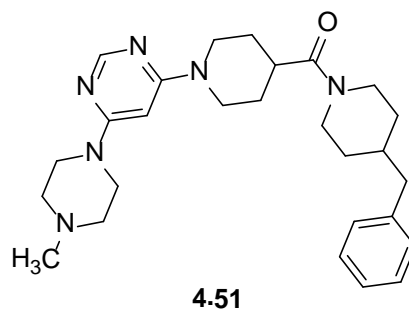
(4-Benzylpiperidin-1-yl)(piperidin-4-yl)methanone (**4.40**, 100 mg, 0.35 mmol) followed by 1-methylpiperazine (0.19 mL, 1.75 mmol, 5 eq.) were reacted according to general procedure D. Purification by MDAP (ammonium bicarbonate gradient C extended run) afforded the title compound (**4.51**) as a yellow oil (70 mg, 0.15 mmol, 43 %). LCMS (formic): Rt = 0.75 min, [M+H]$^+$ = 463, purity = 100 %. ^{1}H NMR (400 MHz, DMSO-d_6) δ ppm 8.05 (s, 1 H); 7.28 (t, J = 7.0 Hz, 2 H); 7.15 – 7.21 (m, 3 H); 5.88 (s, 1 H); 4.34 (d, J = 12.0 Hz, 3 H); 3.98 (d, J = 13.0 Hz, 1 H); 3.49 - 3.55 (m, 4 H) 2.79 – 3.01 (m, 4 H); 2.40 - 2.54 (m, 3 H); 2.33 (t, J = 4.9 Hz, 4 H); 2.19 (s, 3 H); 1.69 - 1.82 (m, 1 H); 1.53 – 1.66 (m, 4 H); 1.37 - 1.54 (m, 2 H); 0.88 - 1.18 (m, 2 H).

General Procedure E: Nucleophilic Aromatic Substitutions

An amine (1 eq.) was dissolved in ethanol (0.5 – 1 mL) and then treated with a chloropyrimidine (0.9 eq.) and DIPEA (2 eq.). The resulting solutions were heated in a microwave reactor at 150 °C until the reaction was complete by LCMS. The products were purified by direct injection of the reaction solution onto MDAP.

(4-Methylpiperidin-1-yl)(1-(6-methylpyrimidin-4-yl)piperidin-4-yl)methanone (4.52)

4.52
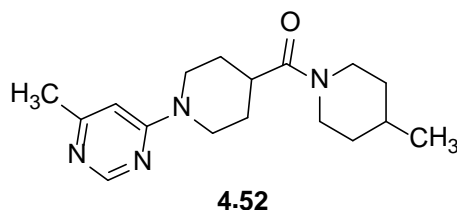
(4-Methylpiperidin-1-yl)(piperidin-4-yl)methanone (**4.39**, 20mg, 0.10 mmol) and 4-chloro-6-methylpyrimidine (11mg, 0.09 mmol) were reacted according to general procedure E with a heating time of 2 h. Purification by MDAP (ammonium bicarbonate gradient B) afforded the title compound (**4.52**) as a yellow oil (11 mg, 0.04 mmol, 37 %). LCMS (formic): Rt = 0.63 min, [M+H]$^+$ = 303, purity = 100 %. ^{1}H NMR (400 MHz, CDCl$_3$) δ ppm 8.49 (s, 1 H); 6.38 (s, 1 H); 4.57 (d, *J* = 13.0 Hz, 1 H); 4.40 (d, *J* = 12.0 Hz, 2 H); 3.90 (d, *J* = 13.0 Hz, 1 H); 2.92 - 3.10 (m, 3 H); 2.79 (dt, *J* = 9.5, 4.5 Hz, 1 H); 2.55 (t, *J* = 12.0 Hz, 1 H); 2.35 (s, 3 H) 2.09 (br. s., 2 H) 1.56 - 1.90 (m, 5 H); 1.01 – 1.18 (m, 2 H); 0.96 (d, *J* = 6.6 Hz, 3 H).

(4-Methylpiperidin-1-yl)(1-(pyrimidin-4-yl)piperidin-4-yl)methanone (4.53)

4.53
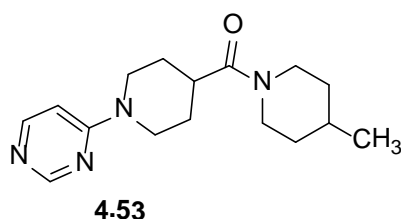
(4-Methylpiperidin-1-yl)(piperidin-4-yl)methanone (**4.39**, 20 mg, 0.10 mmol) and 4-chloropyrimidine (10 mg, 0.09 mmol) were reacted according to general procedure E with a heating time of 1 h. Purification by MDAP (ammonium bicarbonate gradient B) afforded the title compound (**4.53**) as a yellow oil (6 mg, 0.02 mmol, 22 %). LCMS (formic): Rt = 0.60 min, [M+H]$^+$ = 289, purity = 100 %. ^{1}H NMR (400 MHz, CDCl$_3$) δ ppm 8.59 (s, 1 H); 8.18 (d, *J* = 6.5 Hz, 1 H); 6.52 (dd, *J* = 6.5, 1.0 Hz, 1 H); 4.58 (d, *J* = 13.0 Hz, 1 H);

4.41 (d, J = 12.5 Hz, 2 H); 3.90 (d, J = 13.0 Hz, 1 H); 2.97 - 3.10 (m, 3 H); 2.81 (ddd, J = 14.5, 9.5, 5.5 Hz, 1 H); 2.56 (t, J = 12.0 Hz, 1 H); 1.57 - 1.92 (m, 7 H); 1.11 (t, J = 12.0 Hz, 2 H); 0.97 (d, J = 6.5 Hz, 3 H).

(4-Benzylpiperidin-1-yl)(1-(pyrimidin-4-yl)piperidin-4-yl)methanone (4.54)

4.54
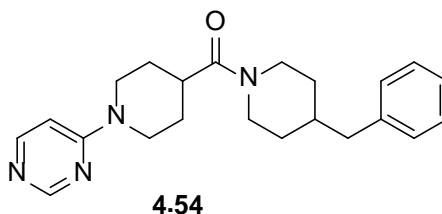
(4-Benzylpiperidin-1-yl)(piperidin-4-yl)methanone (**4.40**, 100 mg, 0.35 mmol) and 4-chloropyrimidine (40 mg, 0.35 mmol) were reacted according to general procedure E with a heating time of 1 h. Purification by MDAP (ammonium bicarbonate gradient C extended run) in 2 injections afforded the title compound (**4.54**) as a yellow oil (45 mg, 0.12 mmol, 35 %). LCMS (ammonium bicarbonate): Rt = 1.04 min, [M+H]$^+$ = 365, purity = 100 %. ^{1}H NMR (400 MHz, CDCl$_3$) δ ppm 8.59 (s, 1 H); 8.18 (d, J = 6.4 Hz, 1 H); 7.27 - 7.35 (m, 2 H); 7.19 - 7.25 (m, 1 H); 7.11 - 7.18 (m, 2 H); 6.52 (dd, J = 6.4, 1.0 Hz, 1 H); 4.62 (d, J = 13.2 Hz, 1 H); 4.41 (br. s., 2 H); 3.92 (d, J = 13.2 Hz, 1 H); 2.95 - 3.07 (m, 3 H); 2.75 - 2.86 (m, 1 H); 2.45 - 2.65 (m, 4 H); 1.63 - 1.91 (m, 6 H); 1.06 - 1.29 (m, 2 H).

1-(6-(4-(4-Methylpiperidine-1-carbonyl)piperidin-1-yl)pyrimidin-4-yl)pyrrolidin-2-one (4.56)

4.56
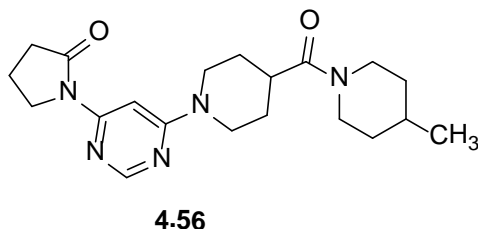
(4-Methylpiperidin-1-yl)(piperidin-4-yl)methanone (**4.39**, 200 mg, 0.95 mmol) and 6-chloropyrimidin-4-amine (123 mg, 0.95 mmol) were reacted according

to general procedure E with a heating time of 5 min. This intermediate ((1-(6-aminopyrimidin-4-yl)piperidin-4-yl)(4-methylpiperidin-1-yl)methanone, **4.55**) was used in the subsequent step without work-up or purification. Half of the solution **4.55**, (144 mg, 0.48 mmol) in Ethanol (1 mL) was treated with potassium carbonate (197 mg, 1.43 mmol) and 4-bromobutanoyl chloride (0.055 mL, 0.48 mmol). The resulting suspension was stirred at room temperature for 6 days.The solution was partitioned between DCM (10 mL) and water (10 ml) and the layers were separated using a hydrophobic frit. The aqueous layer was re-extracted with DCM (10 mL X 2) and the combined organic layers were concentrated to yield the crude product. The product was purified by MDAP (ammonium bicarbonate gradient C) to afford the title compound (**4.56**) as an orange oil (3.0 mg, 8.1 µmol, 2 %). LCMS (ammonium bicarbonate): Rt = 0.92 min, $[M+H]^+$ = 372.23, purity = 100 %. ^{1}H NMR (400 MHz, CDCl$_3$) δ ppm 8.40 (d, J = 1.0 Hz, 1 H); 7.70 (d, J = 1.0 Hz, 1 H); 4.58 (d, J = 13.0 Hz, 1 H); 4.44 (d, J = 13.0 Hz, 1 H); 4.07 (dt, J = 7.0, 1.0 Hz, 1 H); 3.91 (d, J = 13.5 Hz, 1 H); 2.93 - 3.10 (m, 3 H); 2.79 (td, J = 10.0, 5.0 Hz, 1 H); 2.64 (t, J = 8.0 Hz, 1 H); 2.55 (t, J = 12.0 Hz, 1 H); 2.36 (q, J = 7.0 Hz, 1 H); 2.03 - 2.16 (m, 2 H); 1.75 – 2.03 (m, 6 H); 1.56 - 1.75 (m, 2 H); 1.23 - 1.32 (m, 1 H); 1.02 - 1.18 (m, 2 H); 0.97 (d, J = 6.5 Hz, 3 H).

General Procedure F: Acetylations

The appropriate amine (20 mg) was dissolved in acetic anhydride (250 µL) and the solution was stirred at room temperature for 17 h. The solvent was removed by evaporation and the crude products were purified.

1-(4-(4-Methylpiperidine-1-carbonyl)piperidin-1-yl)ethanone (4.57)

4.57
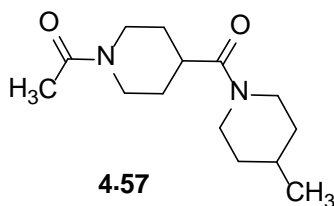
(4-Methylpiperidin-1-yl)(piperidin-4-yl)methanone (**4.39**, 20mg, 0.10 mmol) was reacted according to general procedure F. The product was purified by MDAP (ammonium bicarbonate gradient B). The product was repurified by Andy Hobbs, Chemical Sciences, GSK on a Redisep® silica 4g column, eluting with a gradient of 0 - 95 % (0.1 % triethylamine in 10 % methanol/DCM) in 0.1 % triethylamine in DCM. The appropriate fractions were combined and concentrated to afford the title compound (**4.57**) as a colourless gum (9 mg, 0.03 mmol, 36 %). LCMS (formic): Rt = 0.70 min, [M+H]$^+$ = 253, purity = 97 %. ^{1}H NMR (400 MHz, CDCl$_3$) δ ppm 4.58 (d, J = 13.0 Hz, 2 H); 3.88 (d, J = 13.0 Hz, 2 H); 2.99 - 3.16 (m, 2 H); 2.65 - 2.77 (m, 2 H); 2.55 (t, J = 13.0 Hz, 1 H); 2.10 (s, 3 H); 1.79 - 1.90 (m, 1 H); 1.59 - 1.78 (m, 6 H); 1.02 - 1.16 (m, 2 H); 0.97 (d, J = 6.5 Hz, 3 H).

1-(4-(4-Benzylpiperidine-1-carbonyl)piperidin-1-yl)ethanone (4.58)

4.58
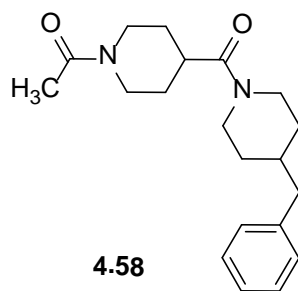
(4-Benzylpiperidin-1-yl)(piperidin-4-yl)methanone (**4.40**, 20 mg, 0.07 mmol) was reacted according to general procedure F. The product was purified by MDAP (formic method B) to afford the title compound (**4.58**) as a colourless oil (7 mg, 0.02 mmol, 24 %). LCMS (ammonium bicarbonate): Rt = 0.97 min, [M+H]$^+$ = 329, purity = 98 %. ^{1}H NMR (400 MHz, CD$_3$OD) δ ppm 7.23 - 7.39 (m, 2 H); 7.13 - 7.20 (m, 3 H); 4.45 - 4.58 (m, 2 H); 4.06 (d, J = 13.0 Hz, 1 H);

3.89 – 3.99 (m, 1 H); 3.12 - 3.24 (m, 1 H); 3.01 - 3.10 (m, 1 H); 2.91 - 3.01 (m, 1 H); 2.66 - 2.78 (m, 1 H); 2.59 - 2.62 (m, 1 H); 2.56 (dd, J = 7.0, 3.0 Hz, 3 H); 2.09 (d, J = 1.5 Hz, 3 H); 1.80 - 1.90 (m, 1 H); 1.64 - 1.79 (m, 4 H); 1.45 - 1.64 (m, 1 H); 1.04 - 1.25 (m, 2 H).

4,6-Di(piperidin-1-yl)pyrimidine (4.59)
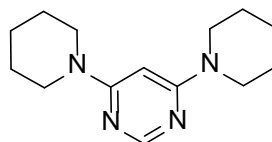
4.59

4,6-Dichloropyrimidine (100 mg, 0.67 mmol) was dissolved in Ethanol (0.5 mL) and added to piperidine (0.66 mL, 6.7 mmol). The resulting solution was heated in a microwave reactor at 150 °C for 1 h. A few drops of DMSO was added to the solution to ensure complete dissolution then the solution was directly injected onto MDAP purification (ammonium bicarbonate gradient C) in 2 injections. The appropriate fraction from each run was combined and concentrated to afford the title compound (**4.59**) as a white solid (130 mg, 0.53 mmol, 79 %). Mp 103 - 106 °C. LCMS (ammonium bicarbonate): Rt = 1.13 min, $[M+H]^+$ = 247, purity = 100 %. HRMS $C_{14}H_{23}N_4$ required 247.1917, found 247.1921. ^{1}H NMR (400 MHz, DMSO-d_6) δ ppm 8.01 (d, J = 0.5 Hz, 1 H); 5.82 (s, 1 H); 3.52 (t, J = 6.0 Hz, 8 H); 1.56 - 1.63 (m, 4 H); 1.44 - 1.51 (m, 8 H). ^{13}C NMR (101 MHz, DMSO-d_6) δ ppm 163.5 (Ar CH); 156.9 (2 Ar C); 80.7 (Ar CH); 44.6 (4 CH_2); 25.0 (4 CH_2); 24.3 (2 CH_2). IR (ATR) cm^{-1} 2923; 2849; 1577; 1490; 1437; 1348; 1215; 1018; 970; 800.

N,N-dimethyl-6-(piperidin-1-yl)pyrimidin-4-amine (4.60)

4·60
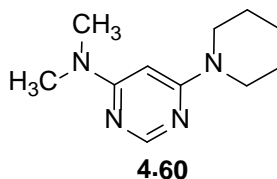
Dimethylamine (2.0M in THF) (0.34 mL, 0.67 mmol) followed by piperidine (0.33 mL, 3.4 mmol, 5 eq.) were reacted according to general procedure D. A few drops of DMSO was added to the solution to ensure complete dissolution then purification by MDAP (ammonium bicarbonate gradient B) in 2 injections was carried out. Only one injection collected product. The appropriate fraction from this run was concentrated to afford the title compound (**4.60**) as a yellow oil (36 mg, 0.18 mmol, 26 %). LCMS (formic): Rt = 0.58 min, [M+H]$^+$ = 207, purity = 98 %. HRMS C$_{11}$H$_{19}$N$_4$ required 207.1604, found 207.1608. ^{1}H NMR (400 MHz, DMSO-d_6) δ ppm 8.02 (d, J = 0.5 Hz, 1 H); 5.64 (s, 1 H); 3.52 (t, J = 5.0 Hz, 4 H); 2.98 (s, 6 H); 1.56 - 1.64 (m, 2 H); 1.44 - 1.52 (m, 4 H). ^{13}C NMR (101 MHz, DMSO-d_6) δ ppm 162.9 (Ar C); 162.2 (Ar C); 156.7 (Ar CH); 80.1 (Ar CH)l 44.6 (2 CH$_2$); 36.8 (2 CH$_3$); 25.0 (2 CH$_2$); 24.3 (CH$_2$). IR (ATR) cm^{-1} 3375; 2929; 2852; 1581; 1489; 1428; 1335; 1247; 975; 798.

4-(6-(Piperidin-1-yl)pyrimidin-4-yl)morpholine (4.61)

4·61
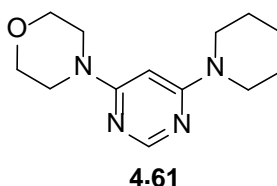
Morpholine (0.059 mL, 0.67 mmol) followed by piperidine (0.332 mL, 3.36 mmol, 5 eq.) were reacted according to general procedure D. Methanol (2 mL) was added to the solution to ensure complete dissolution then purification by MDAP (ammonium bicarbonate gradient B) in 3 injections was carried out. The appropriate fractions from each run were combined and concentrated to afford the title compound (**4.61**) as a white solid (96 mg, 0.39 mmol, 58 %). Mp 100 - 102 °C. LCMS (formic): Rt = 0.52 min, [M+H]$^+$ = 249,

purity = 100 %. HRMS $C_{13}H_{21}N_4O$ required 249.1710, found 249.1712. ^{1}H NMR (400 MHz, CDCl$_3$) δ ppm 8.25 (s, 1 H); 5.58 (s, 1 H); 3.77 – 3.81 (m, 4 H); 3.51 - 3.59 (m, 8 H); 1.59 - 1.72 (m, 6 H). ^{13}C NMR (101 MHz, DMSO-d_6) δ ppm 163.1 (Ar C); 162.4 (Ar C); 156.7 (Ar CH); 81.1 (Ar CH); 65.8 (2 CH$_2$); 44.6 (2 CH$_2$); 44.1 (2 CH$_2$); 25.0 (2 CH$_2$); 24.3 (CH$_2$). IR (ATR) cm^{-1} 2938; 2856; 2826; 1574; 1466; 1440; 1211; 1119; 991; 971; 804; 796.

4-(6-(Pyrrolidin-1-yl)pyrimidin-4-yl)morpholine (4.67)
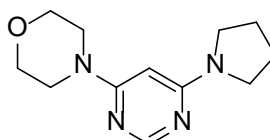
4.67

Morpholine (0.029 mL, 0.34 mmol) followed by pyrrolidine (0.055 mL, 0.67 mmol, 2 eq.) were reacted according to general procedure D. Purification by MDAP (ammonium bicarbonate gradient B) afforded the title compound (**4.67**) as a yellow solid (51 mg, 0.22 mmol, 65 %). LCMS (ammonium bicarbonate): Rt = 0.73 min, [M+H]$^+$ = 235, purity = 100 %. ^{1}H NMR (400 MHz, DMSO-d_6) δ ppm 8.04 (d, J = 0.5 Hz, 1 H); 5.53 (s, 1 H); 3.62 – 3.67 (m, 4 H); 3.43 – 3.48 (m, 4 H); 3.35 (br. s., 4 H); 1.86 – 1.93 (m, 4 H).

4-(6-(2-Methylpyrrolidin-1-yl)pyrimidin-4-yl)morpholine (4.68)
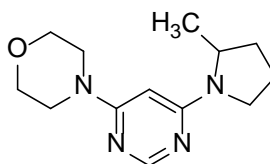
4.68

Morpholine (0.029 mL, 0.34 mmol) followed by 2-methylpyrrolidine (obtained from GSK compound collection, 57 mg, 0.67 mmol, 2 eq.) were reacted according to general procedure D. Purification by MDAP (ammonium bicarbonate gradient B) afforded the title compound (**4.68**) as a yellow gum (41.2 mg, 0.17 mmol, 44 %). LCMS (ammonium bicarbonate): Rt = 0.82 min, [M+H]$^+$ = 249, purity = 100 %. ^{1}H NMR (400 MHz, DMSO-d_6) δ ppm 8.04 (s,

1 H); 5.51 (s, 1 H); 4.16 (br. s., 1 H); 3.62 – 3.66 (m, 4 H); 3.38 - 3.48 (m, 5 H); 3.13 - 3.29 (m, 1 H); 1.86 - 2.06 (m, 3 H); 1.60 - 1.66 (m, 1 H); 1.12 (d, *J* = 6.5 Hz, 3 H).

5-(((6-Morpholinopyrimidin-4-yl)amino)methyl)pyrrolidin-2-one (4.69)

4.69

Morpholine (0.029 mL, 0.34 mmol) followed by 5-(aminomethyl)pyrrolidin-2-one (obtained from GSK compound collection, 76 mg, 0.67 mmol, 2 eq.) were reacted according to general procedure D. Purification by MDAP (ammonium bicarbonate gradient A) afforded the title compound (**4.69**) as a yellow solid (15 mg, 0.06 mmol, 17 %). LCMS (ammonium bicarbonate): Rt = 0.51 min, [M+H]$^+$ = 278, purity = 100 %. ^{1}H NMR (400 MHz, DMSO-d_6) δ ppm 8.24 (s, 1 H); 8.01 (s, 1 H); 7.61 (s, 1 H); 6.78 - 6.83 (m, 1 H); 5.64 (s, 1 H); 3.61 - 3.69 (m, 4 H); 3.38 - 3.44 (m, 4 H); 3.16 - 3.25 (m, 1 H); 2.00 - 2.2- (m, 2 H); 1.67 - 1.77 (m, 1 H); 0.99 (d, *J* = 6.5 Hz, 2 H).

4-(6-(3,3-Difluoropyrrolidin-1-yl)pyrimidin-4-yl)morpholine (4.70)
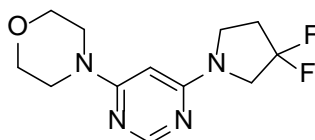
4.70

Morpholine (0.029 mL, 0.34 mmol), followed by 3,3-difluoropyrrolidine (96 mg, 0.67 mmol, 2 eq.) were reacted according to general procedure D. Purification by MDAP (ammonium bicarbonate gradient B) afforded the title compound (**4.70**) as an off-white solid (51 mg, 0.19 mmol, 56 %). Mp 140 - 142 °C. LCMS (ammonium bicarbonate): Rt = 0.77 min, [M+H]$^+$ = 271, purity = 100 %. HRMS C$_{12}$H$_{17}$F$_2$N$_4$O required 271.1365, found 271.1370. ^{1}H NMR

(400 MHz, DMSO-d_6) δ ppm 8.10 (d, J = 0.5 Hz, 1 H); 5.67 (s, 1 H); 3.81 (t, J = 13.5 Hz, 2 H); 3.58 - 3.67 (m, 6 H); 3.48 – 3.53 (m, 4 H); additional 2H masked by DMSO peak. ^{13}C NMR (101 MHz, DMSO-d_6) δ ppm 162.4 (Ar C); 160.7 (Ar C); 156.9 (Ar CH); 128.2 (t, J = 247 Hz, CF_2); 81.5 (Ar CH); 65.8 (2 CH_2); 52.8 (t, J = 32 Hz, CH_2); 44.1 (2 CH_2); 43.6 (t, J = 4.0 Hz, CH_2); 32.8 (t, J = 24 Hz, CH_2). IR (ATR) cm^{-1} 2960; 2874; 2838; 1582; 1481; 1310; 1237; 1114; 974; 927; 800.

4-(6-(2-Ethylpyrrolidin-1-yl)pyrimidin-4-yl)morpholine (4.71)

4.71
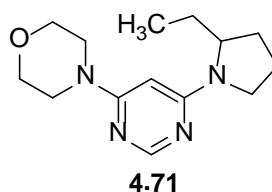
Morpholine (0.029 mL, 0.335 mmol), followed by 2-ethylpyrrolidine (66 mg, 0.67 mmol, 2 eq.) were reacted according to general procedure D. Purification by MDAP (ammonium bicarbonate gradient B extended) afforded the title compound (**4.71**) as a colourless gum (22 mg, 0.08 mmol, 25 %). LCMS (ammonium bicarbonate): Rt = 0.93 min, [M+H]$^+$ = 263, purity = 100 %. ^{1}H NMR (400 MHz, DMSO-d_6) δ ppm 8.04 (s, 1 H); 5.50 (s, 1 H); 3.94 (br. s., 1 H); 3.61 – 3.67 (m, 4 H); 3.42 – 3.48 (m, 4 H); 3.16 - 3.42 (m, 2 H); 1.82 - 2.01 (m, 3 H); 1.66 - 1.82 (m, 2 H); 1.22 - 1.35 (m, 1 H); 0.84 (t, J = 7.5 Hz, 3 H).

4-(6-(3-(Methylsulfonyl)pyrrolidin-1-yl)pyrimidin-4-yl)morpholine (4.72)

4.72
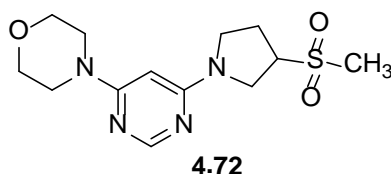
Morpholine (0.029 mL, 0.34 mmol), followed by 3-(methylsulfonyl)pyrrolidine (100 mg, 0.67 mmol, 2 eq.) were reacted according to general procedure D. Purification by MDAP (ammonium bicarbonate gradient A) afforded the title compound (**4.72**) as an off-white solid (60 mg, 0.19 mmol, 57 %). LCMS

(ammonium bicarbonate): Rt = 0.56 min, $[M+H]^+$ = 313, purity = 100 %. ^{1}H NMR (400 MHz, DMSO-d_6) δ ppm 8.08 (s, 1 H); 5.65 (s, 1 H); 4.01 - 4.10 (m, 1 H); 3.69 - 3.82 (m, 2 H); 3.61 – 3.67 (m, 4 H); 3.52 - 3.61 (m, 1 H); 3.47 – 3.52 (m, 4 H); 3.30 - 3.47 (m, 1 H); 3.05 (s, 3 H); 2.30 – 2.40 (m, 2 H).

N-(1-(6-morpholinopyrimidin-4-yl)pyrrolidin-3-yl)acetamide (4.73)

4.73
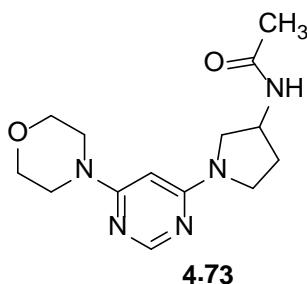
Morpholine (0.029 mL, 0.34 mmol), followed by *N*-(pyrrolidin-3-yl)acetamide (86 mg, 0.67 mmol, 2 eq.) were reacted according to general procedure D. Purification by MDAP (ammonium bicarbonate gradient A) afforded the title compound (**4.73**) as an off-white solid (59 mg, 0.20 mmol, 60 %). LCMS (ammonium bicarbonate): Rt = 0.54 min, $[M+H]^+$ = 292, purity = 100 %. ^{1}H NMR (400 MHz, DMSO-d_6) δ ppm 8.10 (d, *J* = 7.0 Hz, 1 H); 8.05 (d, *J* = 1.0 Hz, 1 H); 5.54 (s, 1 H); 4.25 - 4.34 (m, 1 H); 3.61 – 3.67 (m, 4 H); 3.53 - 3.59 (m, 2 H); 3.45 - 3.49 (m, 4 H); 3.21 (br. s., 2 H); 2.05 – 2.15 (m, 1 H); 1.82 - 1.88 (m, 1 H); 1.81 (s, 3 H).

N,N-dimethyl-1-(6-morpholinopyrimidin-4-yl)pyrrolidin-3-amine (4.74)

4.74
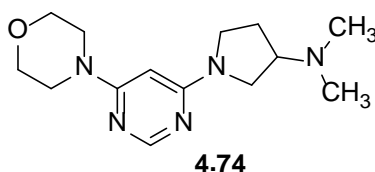
Morpholine (0.029 mL, 0.34 mmol), followed by *N,N*-dimethylpyrrolidin-3-amine (obtained from GSK compound collection, 77 mg, 0.67 mmol, 2 eq.) were reacted according to general procedure D. Purification by MDAP (ammonium bicarbonate gradient B extended) afforded the title compound (**4.74**) as an off-white solid (62 mg, 0.22 mmol, 67 %). LCMS (ammonium

bicarbonate): Rt = 0.65 min, $[M+H]^+$ = 278, purity = 100 %. ^{1}H NMR (400 MHz, DMSO-d_6) δ ppm 8.04 (s, 1 H); 5.56 (s, 1 H); 3.61 – 3.68 (m, 4 H); 3.52 - 3.59 (m, 2 H); 3.44 – 3.50 (m, 4 H); 3.23 - 3.32 (m, 1 H); 3.02 - 3.10 (m, 1 H); 2.66 – 2.77 (m, 1 H); 2.19 (s, 6 H); 2.06 - 2.15 (m, 1 H); 1.68 - 1.81 (m, 1 H).

N-methyl-N-(1-(6-morpholinopyrimidin-4-yl)pyrrolidin-3-yl)acetamide (4.75)

4.75
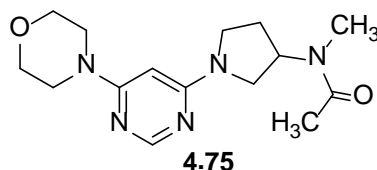
Morpholine (0.029 mL, 0.335 mmol), followed by *N*-methyl-*N*-(pyrrolidin-3-yl)acetamide (95 mg, 0.67 mmol, 2 eq.) were reacted according to general procedure D. Purification by MDAP (formic gradient A extended) afforded the formate salt of the title compound (**4.75**) as a yellow gum (68 mg, 0.22 mmol, 67 %). LCMS (formic): Rt = 0.39 min, $[M+H]^+$ = 306, purity = 100 %. ^{1}H NMR (400 MHz, DMSO-d_6) shows evidence of rotameric forms δ ppm 8.14 (s, 0.4 H); 8.06 (br. s, 0.6 H); 5.60 (s, 0.4 H); 5.58 (s, 0.6 H); 5.05 - 5.14 (m, 0.6 H); 4.56 - 4.67 (m, 0.4 H); 3.58 – 3.67 (m, 4 H); 3.45 - 3.52 (m, 4 H); 3.22 – 3.38 (m, 4.6 H); 3.17 (s, 1 H); 2.86 (s, 1.4 H); 2.72 (s, 1 H); 2.08 – 2.16 (m, 1.6 H); 1.98 – 2.06 (m, 2.4 H).

4-(1-(6-Morpholinopyrimidin-4-yl)pyrrolidin-3-yl)morpholine (4.76)

4.76
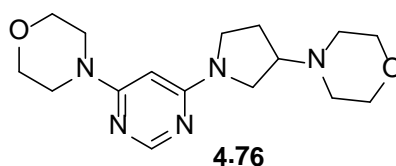
Morpholine (0.029 mL, 0.34 mmol), followed by 4-(pyrrolidin-3-yl)morpholine (obtained from GSK compound collection, 105 mg, 0.67 mmol, 2 eq.) were reacted according to general procedure D. Purification by MDAP (ammonium bicarbonate gradient A) afforded the title compound (**4.76**) with an impurity

present. The crude product was partitioned between water (2 mL) and DCM (2 mL) and the layers were separated using a phase separation cartridge. The aqueous layer was extracted with additional DCM (2 X 2 mL). The combined organic layers were concentrated to yield the title compound (**4.76**) as a white solid (9 mg, 0.03 mmol, 8 %). LCMS (ammonium bicarbonate): Rt = 0.62 min, [M+H]$^+$ = 320, purity = 97 %. ^{1}H NMR (400 MHz, DMSO-d_6) δ ppm 8.04 (s, 1 H); 5.57 (s, 1 H); 3.61 – 3.66 (m, 4 H); 3.57 – 3.61 (m, 4 H); 3.43 - 3.52 (m, 8 H); 3.28 (s, 2 H) 3.04 - 3.12 (m, 1 H); 2.79 - 2.89 (m, 1 H); 2.39 - 2.47 (m, 1 H); 2.09 - 2.18 (m, 1 H); 1.68 - 1.81 (m, 1 H).

4-(6-(2-(1-Methylpiperidin-3-yl)pyrrolidin-1-yl)pyrimidin-4-yl)morpholine (4.77)

4.77
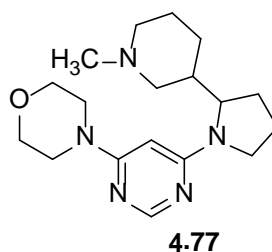
Morpholine (0.029 mL, 0.34 mmol), followed by 1-methyl-3-(pyrrolidin-2-yl)piperidine (obtained from GSK compound collection, 113 mg, 0.67 mmol, 2 eq.) were reacted according to general procedure D. Purification by MDAP (ammoniun bicarbonate gradient B extended) afforded the title compound (**4.77**) as a yellow gum (38 mg, 0.12 mmol, 34 %). LCMS (ammonium bicarbonate): Rt = 0.80 min, [M+H]$^+$ = 332, purity = 100 %. ^{1}H NMR (400 MHz, DMSO-d_6) δ ppm 8.06 (d, J = 2.0 Hz, 1 H); 5.53 - 5.63 (m, 1 H); 4.02 - 4.15 (m, 1 H); 3.62 – 3.67 (m, 4 H); 3.43 – 3.48 (m, 4 H); 3.23 - 3.40 (m, 1 H); 2.63 – 2.71 (m, 1 H); 2.53 – 2.60 (m, 1 H); 2.11 (d, J = 3.5 Hz, 3 H); 1.83 - 1.93 (m, 4 H); 1.67 - 1.80 (m, 3 H); 1.56 - 1.66 (m, 2 H); 1.46 – 1.55 (m, 1H); 1.28 - 1.44 (m, 1H); 0.91 - 1.06 (m, 1H).

4-(6-(2-(1-Methylpiperidin-4-yl)pyrrolidin-1-yl)pyrimidin-4-yl)morpholine (4.78)

4.78
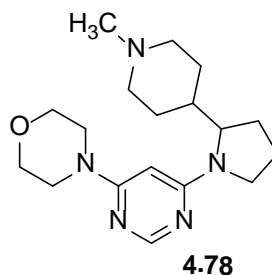
Morpholine (0.029 mL, 0.34 mmol), followed by 1-methyl-4-(pyrrolidin-2-yl)piperidine (obtained from GSK compound collection, 113 mg, 0.67 mmol, 2 eq.) were reacted according to general procedure D. Purification by MDAP (ammoniun bicarbonate gradient B) afforded the title compound (**4.78**) as a yellow gum (37 mg, 0.11 mmol, 33 %). LCMS (ammonium bicarbonate): Rt = 0.74 min, [M+H]$^+$ = 332, purity = 100 %. ^{1}H NMR (400 MHz, DMSO-d_6) δ ppm 8.05 (s, 1 H); 5.55 (s, 1 H); 4.08 (br. s, 1 H); 3.61 – 2.37 (m, 4 H); 3.42 – 3.48 (m, 4 H); 3.23 - 3.40 (m, 2 H); 2.78 (d, J = 11.0 Hz, 2 H); 2.12 (s, 3 H); 1.66 - 1.96 (m, 7 H); 1.20 - 1.48 (m, 4H).

4-(6-(2-(Pyrrolidin-1-ylmethyl)pyrrolidin-1-yl)pyrimidin-4-yl)morpholine (4.79)

4.79
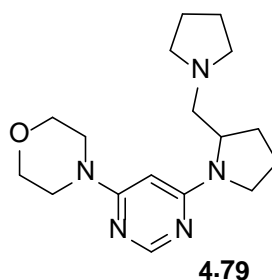
Morpholine (0.029 mL, 0.34 mmol), followed by 1-(pyrrolidin-2-ylmethyl)pyrrolidine (obtained from GSK compound collection, 103 mg, 0.67 mmol, 2 eq.) were reacted according to general procedure D. Purification by MDAP (ammoniun bicarbonate gradient B) afforded the title compound (**4.79**) as a yellow gum (63 mg, 0.20 mmol, 59 %). LCMS (ammonium bicarbonate): Rt = 0.79 min, [M+H]$^+$ = 318, purity = 100 %. ^{1}H NMR (400 MHz, DMSO-d_6) δ

ppm 8.05 (s, 1 H); 5.54 (s, 1 H); 4.02 - 4.22 (m, 1 H); 3.61 – 3.68 (m, 4 H); 3.42 – 3.48 (m, 4 H); 3.15 - 3.34 (m, 4 H); 2.52 - 2.59 (m, 1 H); 2.41 - 2.48 (m, 3 H); 1.80 - 2.04 (m, 4 H); 1.62 - 1.71 (m, 4 H).

4-(6-(7-Methyl-2,7-diazaspiro[4.4]nonan-2-yl)pyrimidin-4-yl)morpholine (4.80)

4.80
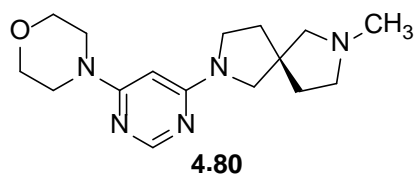
Morpholine (0.029 mL, 0.34 mmol), followed by 2-methyl-2,7-diazaspiro[4.4]nonane hydrochloride (obtained from GSK compound collection, 143 mg, 0.67 mmol, 2 eq.) were reacted according to general procedure D. Purification by MDAP (ammoniun bicarbonate gradient B extended) afforded the title compound (**4.80**) as a colourless gum (36 mg, 0.12 mmol, 35 %). LCMS (ammonium bicarbonate): Rt = 0.69 min, $[M+H]^+$ = 304, purity = 100 %. ^{1}H NMR (400 MHz, DMSO-d_6) δ ppm 8.03 (s, 1 H); 5.52 (s, 1 H); 3.60 – 3.66 (m, 4 H); 3.43 – 3.49 (m, 4 H); 3.22 – 3.40 (m, 4 H) 2.53 - 2.59 (m, 2 H); 2.31 - 2.47 (m, 2 H); 2.23 (s, 3 H); 1.81 – 1.96 (m, 2 H); 1.74 (t, J = 7.0 Hz, 2 H).

(4a,7a)-4-Methyl-6-(6-morpholinopyrimidin-4-yl)hexahydropyrrolo[3,4-b][1,4]oxazin-3(2H)-one (4.81)

4.81
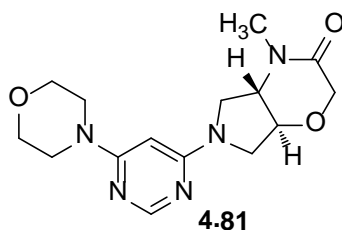
Morpholine (0.029 mL, 0.34 mmol), followed by (4a,7a)-4-methylhexahydropyrrolo[3,4-b][1,4]oxazin-3(2H)-one (obtained from GSK compound collection, 105 mg, 0.67 mmol, 2 eq.) were reacted according to general procedure D. Purification by MDAP (formic gradient A extended)

afforded the title compound (**4.81**) as an off-white solid (8 mg, 0.03 mmol, 7 %). LCMS (formic): Rt = 0.39 min, [M+H]$^+$ = 320, purity = 95 %. ^{1}H NMR (400 MHz, DMSO-d_6) δ ppm 8.08 (s, 1 H); 5.65 (s, 1 H); 4.30 (s, 2 H); 4.13 - 4.26 (m, 2 H); 3.75 – 3.89 (m, 2 H); 3.61 – 3.67 (m, 4 H); 3.46 - 3.53 (m, 4 H); 3.14 - 3.26 (m, 2 H); 2.87 (s, 3 H).

(4a,7a)-6-(6-Morpholinopyrimidin-4-yl)hexahydropyrrolo[3,4-b][1,4]oxazin-3(2H)-one (4.82)

4.82
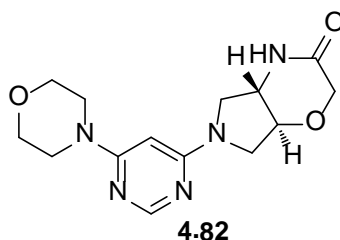
Morpholine (0.029 mL, 0.34 mmol), followed by (4a,7a)-hexahydropyrrolo[3,4-b][1,4]oxazin-3(2H)-one hydrochloride (obtained from GSK compound collection, 120 mg, 0.67 mmol, 2 eq.) were reacted according to general procedure D. Purification by MDAP (ammonium bicarbonate gradient A) afforded the title compound (**4.82**) as a white solid (18 mg, 0.06 mmol, 17 %). LCMS (ammonium bicarbonate): Rt = 0.54 min, [M+H]$^+$ = 306, purity = 97 %. ^{1}H NMR (400 MHz, DMSO-d_6) δ ppm 8.63 (br. s, 1 H); 8.07 (s, 1 H); 5.60 (s, 1 H); 4.16 – 4.31 (m, 2 H); 3.98 - 4.09 (m, 1 H); 3.67 - 3.75 (m, 2 H); 3.61 – 3.66 (m, 4 H); 3.46 - 3.51 (m, 4 H); 3.28 (br. s., 1 H); 3.12 - 3.19 (m, 1 H); 3.01 (t, *J* = 10.5 Hz, 1 H).

1-(4-(6-Morpholinopyrimidin-4-yl)piperazin-1-yl)ethanone (4.83)

4.83
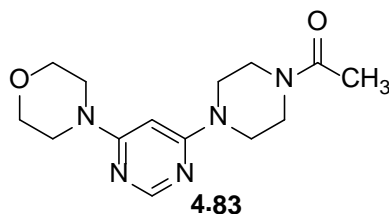
Morpholine (0.029 mL, 0.34 mmol), followed by 1-(piperazin-1-yl)ethanone (86 mg, 0.67 mmol, 2 eq.) were reacted according to general procedure D.

Purification by MDAP (ammonium bicarbonate gradient A) afforded the title compound (**4.83**) as a white solid (59 mg, 0.20 mmol, 60 %). Mp = 165-166 °C. LCMS (ammonium bicarbonate): Rt = 0.58 min, [M+H]$^+$ = 292, purity = 100 %. HRMS C$_{14}$H$_{22}$N$_5$O$_2$ required 292.1768 found 292.1780. ^{1}H NMR (400 MHz, DMSO-d_6) δ ppm 8.10 (s, 1 H); 5.92 (s, 1 H); 3.59 - 3.67 (m, 6 H); 3.46 - 3.55 (m, 10 H); 2.03 (s, 3 H). ^{13}C NMR (101 MHz, DMSO-d_6) δ ppm 178.7 (C=O); 163.0 (Ar C); 162.5 (Ar C); 156.9 (Ar CH); 81.6 (Ar CH); 65.8 (2 CH$_2$); 45.1 (CH$_2$); 44.1 (2 CH$_2$); 43.6 (CH$_2$); 43.4(CH$_2$); 40.4 (CH$_2$); 21.0 (CH$_3$). IR (ATR) cm^{-1} 2967; 2859; 1645; 1591; 1491; 1446; 1420; 1246; 1227; 1206; 1117; 992; 976; 806.

N,N-dimethyl-4-(6-morpholinopyrimidin-4-yl)piperazine-1-carboxamide (4.84)

4.84
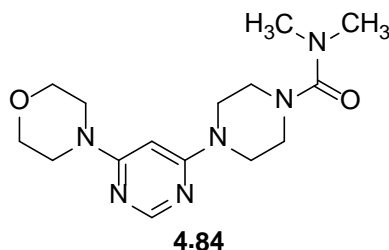
Morpholine (0.029 mL, 0.34 mmol), followed by *N,N*-dimethylpiperazine-1-carboxamide hydrochloride (130 mg, 0.67 mmol, 2 eq.) were reacted according to general procedure D. Purification by MDAP (ammonium bicarbonate gradient B extended) afforded the title compound (**4.84**) as a white solid (59 mg, 0.18 mmol, 55%). LCMS (ammonium bicarbonate): Rt = 0.66 min, [M+H]$^+$ = 321, purity = 100 %. ^{1}H NMR (400 MHz, DMSO-d_6) δ ppm 8.09 (s, 1 H); 5.92 (s, 1 H); 3.61 - 3.66 (m, 4 H); 3.53 - 3.58 (m, 4 H); 3.48 - 3.52 (m, 4 H); 3.13 - 3.17 (m, 4 H); 2.77 (s, 6 H).

Cyclopropyl(4-(6-morpholinopyrimidin-4-yl)piperazin-1-yl)methanone (4.85)

4.85
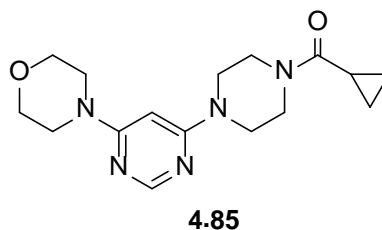
Morpholine (0.029 mL, 0.34 mmol), followed by cyclopropyl(piperazin-1-yl)methanone hydrochloride (128 mg, 0.67 mmol, 2 eq.) were reacted according to general procedure D. Filtration of the precipitate which formed, followed by washing with water and drying in a vacuum oven (40 °C) afforded the title compound (**4.85**) as a white solid (21 mg, 0.06 mmol, 18 %). LCMS (ammonium bicarbonate): Rt = 0.68 min, [M+H]$^+$ = 318, purity = 100 %. ^{1}H NMR (400 MHz, DMSO-d_6) δ ppm 8.11 (s, 1 H); 5.94 (s, 1 H); 3.74 (br. s, 2 H); 3.62 - 3.68 (m, 6 H); 3.49 – 3.55 (m, 8 H); 1.97 - 2.04 (m, 1 H); 0.69 - 0.78 (m, 4 H).

2-Methyl-1-(4-(6-morpholinopyrimidin-4-yl)piperazin-1-yl)propan-1-one (4.86)

4.86
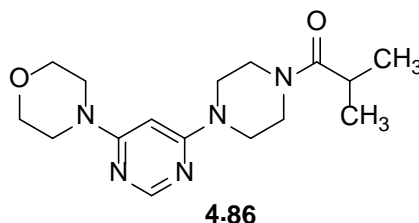
Morpholine (0.029 mL, 0.34 mmol), followed by 2-methyl-1-(piperazin-1-yl)propan-1-one (obtained from GSK compound collection, 105 mg, 0.67 mmol, 2 eq.) were reacted according to general procedure D. Purification by MDAP (ammonium bicarbonate gradient B extended) afforded the title compound (**4.86**) as a white solid (67 mg, 0.21 mmol, 63 %). LCMS (ammonium bicarbonate): Rt = 0.71 min, [M+H]$^+$ = 320, purity = 100 %. ^{1}H NMR (400 MHz, DMSO-d_6) δ ppm 8.10 (s, 1 H); 5.93 (s, 1 H); 3.62 - 3.66 (m,

8 H); 3.54 – 3.61 (m, 2 H); 3.48 - 3.54 (m, 6 H); 2.90 (sept, J = 6.5 Hz, 1 H); 1.01 (d, J = 6.5 Hz, 6 H).

4-(6-(5-Methyl-2,5-diazabicyclo[2.2.1]heptan-2-yl)pyrimidin-4-yl)morpholine (4.87)

4.87
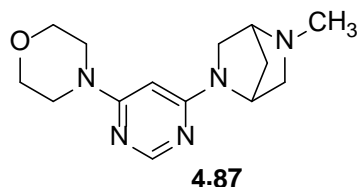
Morpholine (0.029 mL, 0.34 mmol), followed by 2-methyl-2,5-diazabicyclo[2.2.1]heptane hydrochloride (obtained from GSK compound collection, 100 mg, 0.67 mmol, 2 eq.) were reacted according to general procedure D. Purification by MDAP (ammonium bicarbonate gradient A) afforded the title compound (**4.87**) as a yellow oil (11 mg, 0.04 mmol, 12 %). LCMS (formic): Rt = 0.26 min, [M+H]$^+$ = 276, purity = 100 %. ^{1}H NMR (400 MHz, DMSO-d_6) δ ppm 8.16 (s, 1 H); 8.02 (s, 1 H); 5.59 (br. s, 1 H); 4.65 (br. s, 1 H); 3.61 – 3.67 (m, 4 H); 3.44 - 3.49 (m, 4 H); 3.18 - 3.24 (m, 2 H); 2.80 (dd, J = 9.5, 2.0 Hz, 1 H); 2.43 (d, J = 10.0 Hz, 1 H); 2.29 (s, 3 H); 1.85 (d, J = 9.0 Hz, 1 H); 1.68 (d, J = 9.3 Hz, 1 H).

(4-(6-Morpholinopyrimidin-4-yl)piperazin-1-yl)(tetrahydrofuran-2-yl)methanone (4.88)

4.88
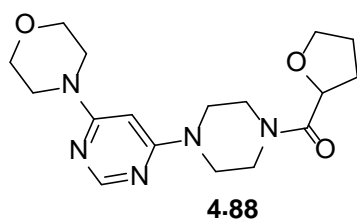
Morpholine (0.029 mL, 0.34 mmol), followed by piperazin-1-yl(tetrahydrofuran-2-yl)methanone (obtained from GSK collection, 123 mg, 0.67 mmol, 2 eq.) were reacted according to general procedure D. Purification by MDAP (formic gradient A extended) afforded the title compound (**4.88**) as a formic acid salt as a white solid (38 mg, 0.10 mmol, 29

%). LCMS (formic): Rt = 0.43 min, $[M+H]^+$ = 348, purity = 99 %. ^{1}H NMR (400 MHz, DMSO-d_6) δ ppm 8.36 (br. s., 1 H); 8.10 (s, 1 H); 5.94 (s, 1 H); 4.67 – 4.73 (m, 1 H); 3.70 – 3.82 (m, 2 H); 3.58 - 3.67 (m, 4 H); 3.54 – 3.58 (m, 2 H); 3.45 - 3.54 (m, 9 H); 3.17 (s, 1 H); 1.94 - 2.12 (m, 2 H); 1.78 - 1.90 (m, 2 H).

4-(6-(4-Methylpiperidin-1-yl)pyrimidin-4-yl)morpholine (4.89)

4.89
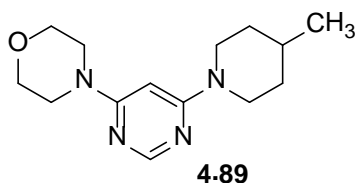
Morpholine (0.029 mL, 0.34 mmol), followed by 4-methylpiperidine (66 mg, 0.67 mmol, 2 eq.) were reacted according to general procedure D. Purification by MDAP (ammonium bicarbonate gradient C extended) afforded the title compound (**4.89**) as a white solid (43 mg, 0.16 mmol, 48 %). Mp = 81-83 °C. LCMS (ammonium bicarbonate): Rt = 0.97 min, $[M+H]^+$ = 263, purity = 99 %. HRMS $C_{14}H_{23}N_4O$ required 263.1866 found 263.1874. ^{1}H NMR (400 MHz, DMSO-d_6) δ ppm 8.06 (s, 1 H); 5.87 (s, 1 H); 4.33 (d, J = 13.0 Hz, 2 H); 3.59 – 3.66 (m, 4 H); 3.44 – 3.51 (m, 4 H); 2.71 - 2.80 (m, 2 H); 1.55 - 1.66 (m, 3 H); 0.95 - 1.08 (m, 2 H); 0.90 (d, J = 6.0 Hz, 3 H). ^{13}C NMR (101 MHz, DMSO-d_6) δ ppm 163.0 (Ar C); 162.4 (Ar C); 156.8 (Ar CH); 81.2 (Ar CH); 65.8 (2 CH_2); 44.1 (2 CH_2); 43.9 (2 CH_2); 33.2 (2 CH_2); 30.6 (CH); 21.7 (CH_3). IR (ATR) cm^{-1} 2946; 2924; 2869; 2837; 1579; 1440; 1216; 1114; 966; 806; 705.

4-(6-(3-methylpiperidin-1-yl)pyrimidin-4-yl)morpholine (4.90)

4.90
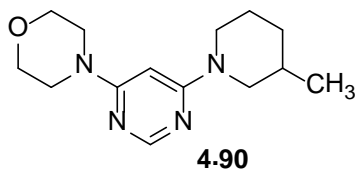
Morpholine (0.029 mL, 0.34 mmol), followed by 3-methylpiperidine (66 mg, 0.67 mmol, 2 eq.) were reacted according to general procedure D. Purification by MDAP (ammonium bicarbonate gradient C) afforded the title

compound (**4.90**) as a yellow solid (43 mg, 0.16 mmol, 49 %). LCMS (formic): Rt = 0.59 min, [M+H]$^+$ = 263, purity = 100 %. ^{1}H NMR (400 MHz, DMSO-d_6) δ ppm 8.05 (s, 1 H); 5.87 (s, 1 H); 4.24 (d, *J* = 13.0 Hz, 2 H); 3.60 – 3.66 (m, 4 H); 3.45 – 3.51 (m, 4 H); 2.71 - 2.79 (m, 1 H); 2.44 (dd, *J* = 13.0, 10.5 Hz, 1 H); 1.73 – 1.80 (m, 1 H); 1.59 - 1.67 (m, 1 H); 1.44 – 1.55 (m, 1 H); 1.30 – 1.43 (m, 1 H); 1.07 – 1.18 (m, 1 H); 0.88 (d, *J* = 6.5 Hz, 3 H).

### *N,N*-dimethyl-1-(6-morpholinopyrimidin-4-yl)piperidin-4-amine (4.93)

4.93
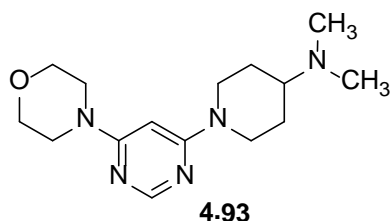
Morpholine (0.029 mL, 0.34 mmol), followed by *N,N*-dimethylpiperidin-4-amine (86 mg, 0.67 mmol, 2 eq.) were reacted according to general procedure D. Purification by MDAP (ammonium bicarbonate gradient B extended) afforded the title compound (**4.93**) as a yellow gum (70 mg, 0.24 mmol, 71 %). LCMS (ammonium bicarbonate): Rt = 0.67 min, [M+H]$^+$ = 292, purity = 99 %. ^{1}H NMR (400 MHz, DMSO-d_6) δ ppm 8.07 (s, 1 H); 5.90 (s, 1 H); 4.36 (d, *J* = 13.0 Hz, 2 H); 3.61 – 3.66 (m, 4 H); 3.46 – 3.51 (m, 4 H); 3.17 (s, 1 H); 2.74 - 2.82 (m, 1 H); 2.34 – 2.43 (m, 1 H); 2.20 (s, 6 H); 1.77 (d, *J* = 11.0 Hz, 2 H); 1.27 (dd, *J* = 11.5, 3.5 Hz, 2 H).

N-methyl-1-(6-morpholinopyrimidin-4-yl)piperidine-4-carboxamide (4.94)

4.94
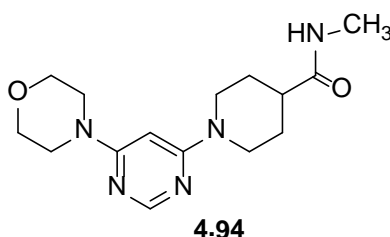
Morpholine (0.029 mL, 0.34 mmol), followed by *N*-methylpiperidine-4-carboxamide (95 mg, 0.67 mmol, 2 eq.) were reacted according to general procedure D. Filtration of the precipitate which formed, followed by washing

with water and drying in a vacuum oven (40 °C) afforded the title compound (**4.94**) as a white solid (78 mg, 0.26 mmol, 72 %). LCMS (ammonium bicarbonate): Rt = 0.57 min, $[M+H]^+$ = 306, purity = 95 %. ^{1}H NMR (400 MHz, DMSO-d_6) δ ppm 8.07 (s, 1 H); 7.73 (d, J = 4.5 Hz, 1 H); 5.90 (s, 1 H); 4.36 (d, J = 13.0 Hz, 2 H); 3.61 – 3.67 (m, 4 H); 3.46 – 3.53 (m, 4 H); 2.80 (td, J = 12.5, 2.0 Hz, 2 H); 2.56 (d, J = 4.5 Hz, 3 H); 2.31 – 2.40 (m, 1 H); 1.64 - 1.72 (m, 2 H); 1.38 – 1.51 (m, 2 H).

1-(6-Morpholinopyrimidin-4-yl)piperidine-4-carboxamide (4.95)

4.95
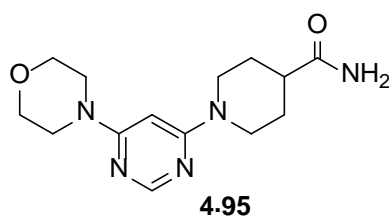
Morpholine (0.029 mL, 0.34 mmol), followed by piperidine-4-carboxamide (obtained from the GSK compound collection, 86 mg, 0.67 mmol, 2 eq.) were reacted according to general procedure D. Filtration of the precipitate which formed, followed by washing with water and drying in a vacuum oven (40 °C) afforded the title compound (**4.95**) as a white solid (39 mg, 0.13 mmol, 39 %). Mp 232 - 234 °C. LCMS (ammonium bicarbonate): Rt = 0.54 min, $[M+H]^+$ = 292, purity = 98 %. HRMS $C_{14}H_{22}N_5O_2$ required 292.1768 found 292.1768. ^{1}H NMR (400 MHz, DMSO-d_6) δ ppm 8.07 (s, 1 H); 7.25 (br. s., 1 H); 6.75 (br. s., 1 H); 5.89 (s, 1 H); 4.34 (d, J = 13.0 Hz, 2 H); 3.61 – 3.66 (m, 4 H); 3.46 – 3.52 (m, 4 H); 2.77 - 2.86 (m, 2 H); 2.31 – 2.40 (m, 1 H) 1.71 (dd, J = 13.0, 2.5 Hz, 2 H); 1.38 – 1.50 (m, 2 H). ^{13}C NMR (101 MHz, DMSO-d_6) δ ppm 176.1 (C=O); 163.1 (Ar C); 162.4 (Ar C); 156.8 (Ar CH); 81.4 (Ar CH); 65.8 (2 CH_2); 44.1 (2 CH_2); 43.4 (2 CH_2); 41.7 (CH); 27.8 (2 CH_2). IR (ATR) cm^{-1} 3390; 3197; 2956; 2854; 1667; 1585; 1502; 1204; 1115; 990; 796.

1-(6-Morpholinopyrimidin-4-yl)piperidine-3-carboxamide (4.96)

4.96
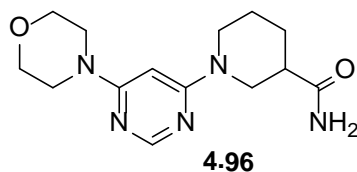
Morpholine (0.029 mL, 0.34 mmol), followed by piperidine-3-carboxamide (86 mg, 0.67 mmol, 2 eq.) were reacted according to general procedure D. Filtration of the precipitate which formed, followed by washing with water and drying in a vacuum oven (40 °C) afforded the title compound (**4.96**) as a white solid (30 mg, 0.10 mmol, 30 %). Mp 216-217 °C. LCMS (ammonium bicarbonate): Rt = 0.57 min, $[M+H]^+$ = 292, purity = 97 %. HRMS $C_{14}H_{22}N_5O_2$ required 292.1768 found 292.1771. ^{1}H NMR (400 MHz, DMSO-d_6) δ ppm 8.07 (s, 1 H); 7.32 (br. s., 1 H); 6.83 (br. s., 1 H); 5.91 (s, 1 H); 4.37 (d, J = 12.5 Hz, 1 H); 4.29 (d, J = 12.5 Hz, 1 H); 3.61 − 3.66 (m, 4 H); 3.47 − 3.51 (m, 4 H); 2.81 − 2.88 (m Hz, 1 H); 2.71 - 2.80 (m, 1 H); 2.19 − 2.28 (m, 1 H); 1.84 - 1.91 (m, 1 H); 1.63 - 1.70 (m, 1 H); 1.54 - 1.62 (m, 1 H); 1.29 - 1.41 (m, 1 H). ^{13}C NMR (101 MHz, DMSO-d_6) δ ppm 175.0 (C=O); 163.1 (Ar C); 162.4 (Ar C); 156.9 (Ar CH); 81.4 (Ar CH); 65.8 (2 CH_2); 46.4 (CH_2); 44.1 (2 CH_2); 44.0 (CH_2); 41.5 (CH); 27.9 (CH_2); 23.8 (CH_2). IR (ATR) cm^{-1} 3369; 3191; 2932; 2865; 1663; 1591; 1478; 1445; 1222; 1208; 1114; 974; 795.

4-(6-(3-Methoxypiperidin-1-yl)pyrimidin-4-yl)morpholine (4.97)

4.97
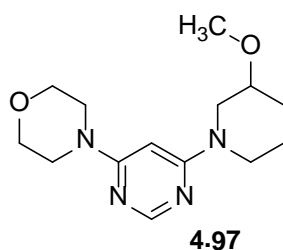
Morpholine (0.029 mL, 0.34 mmol), followed by 3-methoxypiperidine hydrochloride (obtained from the GSK compound collection, 102 mg, 0.67 mmol, 2 eq.) were reacted according to general procedure D. Filtration of the precipitate which formed, followed by washing with water and drying in a

vacuum oven (40 °C) afforded the title compound (**4.97**) as a white solid (46 mg, 0.17 mmol, 49 %). LCMS (ammonium bicarbonate): Rt = 0.76 min, [M+H]$^+$ = 279, purity = 100 %. ^{1}H NMR (400 MHz, DMSO-d_6) δ ppm 8.06 (s, 1 H); 5.89 (s, 1 H); 4.00 (d, J = 11.0 Hz, 1 H); 3.70 - 3.77 (m, 1 H); 3.61 - 3.65 (m, 4 H); 3.46 – 3.51 (m, 4 H); 3.27 (s, 3 H); 3.16 - 3.26 (m, 3 H); 1.89 - 1.97 (m, 1 H); 1.62 - 1.72 (m, 1 H); 1.43 - 1.53 (m, 1H); 1.32 - 1.43 (m, 1 H).

4-(6-(3,3-Difluoropiperidin-1-yl)pyrimidin-4-yl)morpholine (4.98)

4.98
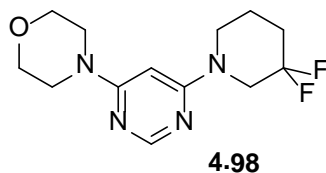
Morpholine (0.029 mL, 0.335 mmol), followed by 3,3-difluoropiperidine hydrochloride (obtained from the GSK compound collection, 106 mg, 0.67 mmol, 2 eq.) were reacted according to general procedure D. Filtration of the precipitate which formed, followed by washing with water and drying in a vacuum oven (40 °C) afforded the crude product with impurities present. Purification by MDAP (ammonium bicarbonate gradient B) afforded the title compound (**4.98**) as a yellow solid (13 mg, 0.05 mmol, 14 %). Mp 121 °C. HRMS C$_{13}$H$_{19}$F$_2$N$_4$O required 285.1521 found 285.1523. LCMS (ammonium bicarbonate): Rt = 0.85 min, [M+H]$^+$ = 285, purity = 100 %. ^{1}H NMR (400 MHz, DMSO-d_6) δ ppm 8.09 (d, J = 0.5 Hz, 1 H); 6.00 (s, 1 H); 3.95 (t, J = 12.0 Hz, 2 H); 3.58 - 3.66 (m, 6 H); 3.49 - 3.54 (m, 4 H); 2.01 – 2.13 (m, 2 H); 1.64 – 1.71 (m, 2 H). ^{13}C NMR (101 MHz, DMSO-d_6) δ ppm 163.0 (Ar C); 162.4 (Ar C); 156.8 (Ar CH); 81.5 (Ar CH); 65.8 (2 CH$_2$); 48.6 (CH$_2$); 44.1 (2 CH$_2$); 42.4 (CH$_2$); 32.0 (CH$_2$); 21.4 (CH$_2$) CF$_2$ carbon not visible. IR (ATR) cm^{-1} 2966; 2857; 1587; 1492; 1478; 1441; 1209; 1119; 1095; 973; 895; 797.

4-(6-(4-Morpholinopiperidin-1-yl)pyrimidin-4-yl)morpholine (4.99)
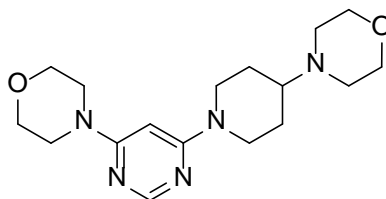
4.99

Morpholine (0.029 mL, 0.34 mmol), followed by 4-(piperidin-4-yl)morpholine (obtained from the GSK compound collection, 114 mg, 0.67 mmol, 2 eq.) were reacted according to general procedure D. Purification by MDAP (ammonium bicarbonate gradient B extended) afforded the title compound (**4.99**) as a yellow gum (91 mg, 0.27 mmol, 80 %). LCMS (ammonium bicarbonate): Rt = 0.66 min, [M+H]$^+$ = 334, purity = 100 %. ^{1}H NMR (400 MHz, DMSO-d_6) δ ppm 8.06 (s, 1 H); 5.90 (s, 1 H); 4.36 (d, J = 13.0 Hz, 2 H); 3.61 – 3.66 (m, 4 H); 3.53 – 3.58 (m, 4 H); 3.46 – 3.50 (m, 4 H); 3.17 (s, 1 H); 2.74 – 2.82 (m, 2 H); 2.31 - 2.48 (m, 4H); 1.79 (d, J = 11.5 Hz, 2 H); 1.21 - 1.34 (m, 2 H).

4-(6-(4-(Tetrahydro-2H-pyran-4-yl)piperidin-1-yl)pyrimidin-4-yl)morpholine (4.100)
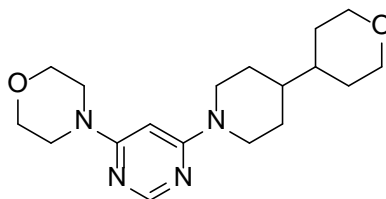
4.100

Morpholine (0.029 mL, 0.34 mmol), followed by 4-(tetrahydro-2H-pyran-4-yl)piperidine (obtained from the GSK compound collection, 113 mg, 0.67 mmol, 2 eq.) were reacted according to general procedure D. Purification by MDAP (ammonium bicarbonate gradient C extended) afforded the title compound (**4.100**) as a white solid (58 mg, 0.17 mmol, 52 %). Mp 148-149 °C. LCMS (ammonium bicarbonate): Rt = 0.90 min, [M+H]$^+$ = 333, purity = 100 %. HRMS C$_{18}$H$_{29}$N$_4$O$_2$ required 333.2285 found 333.2288. ^{1}H NMR

(400 MHz, DMSO-d_6) δ ppm 8.06 (s, 1 H); 5.87 (s, 1 H); 4.40 (d, J = 13.0 Hz, 2 H); 3.85 (dd, J = 11.0, 3.5 Hz, 2 H); 3.60 -3.66 (m, 4 H); 3.46 - 3.50 (m, 4 H); 3.19 - 3.27 (m, 2 H); 2.65 – 2.75 (m, 2 H); 1.70 (d, J = 12.0 Hz, 2 H); 1.56 (d, J = 12.5 Hz, 2 H); 1.12 - 1.35 (m, 4 H); 0.99 – 1.11 (m, 2 H). ^{13}C NMR (101 MHz, DMSO-d_6) δ ppm 163.6 (Ar C); 162.9 (Ar C); 157.4 (Ar CH); 81.7 (Ar CH); 67.8 (2 CH_2); 66.4 (2 CH_2); 44.6 (2 CH_2); 44.5 (2 CH_2); 41.3 (CH); 40.7 (CH); 30.3 (2 CH_2); 28.8 (2 CH_2). IR (ATR) cm^{-1} 2988; 2950; 2840; 1574; 1481; 1448; 1227; 1200; 1119; 997; 970; 876; 795.

## 4-(6-(4-(Pyrrolidin-1-yl)piperidin-1-yl)pyrimidin-4-yl)morpholine (4.101)

4.101
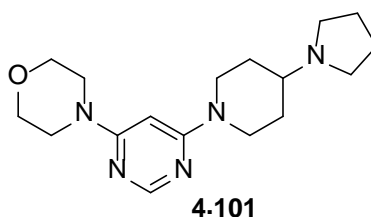
Morpholine (0.029 mL, 0.34 mmol), followed by 4-(pyrrolidin-1-yl)piperidine (obtained from the GSK compound collection, 103 mg, 0.67 mmol, 2 eq.) were reacted according to general procedure D. Filtration of the precipitate which formed, followed by washing with water and drying in a vacuum oven (40 °C) afforded (**4.101**) as a yellow solid (85 mg, 0.27 mmol, 80 %). LCMS (ammonium bicarbonate): Rt = 0.76 min, [M+H]$^+$ = 318, purity = 100 %. ^{1}H NMR (400 MHz, DMSO-d_6) δ ppm 8.07 (s, 1 H); 5.89 (s, 1 H); 4.22 (d, J = 13.5 Hz, 2 H); 3.61 – 3.66 (m, 4 H); 3.45 – 3.51 (m, 4 H); 3.36 (br. s 3 H); 3.17 (s, 1 H); 2.86 - 2.94 (m, 2 H); 2.20 - 2.29 (m, 1 H); 1.85 (dd, J = 12.5, 3.0 Hz, 2 H); 1.64 – 1.70 (m, 4 H); 1.25 - 1.36 (m, 2 H).

8-(6-Morpholinopyrimidin-4-yl)-1-oxa-8-azaspiro[4.5]decane (4.102)

4.102
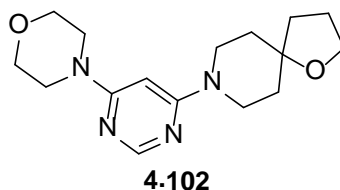
Morpholine (0.029 mL, 0.34 mmol), followed by 1-oxa-8-azaspiro[4.5]decane hydrochloride (obtained from the GSK compound collection, 119 mg, 0.67 mmol, 2 eq.) were reacted according to general procedure D. Purification by MDAP (ammonium bicarbonate gradient B) afforded the title compound (**4.102**) as a white gum (48 mg, 0.16 mmol, 46 %). LCMS (ammonium bicarbonate): Rt = 0.82 min, [M+H]$^+$ = 305, purity = 100 %. ^{1}H NMR (400 MHz, DMSO-d_6) δ ppm 8.06 (s, 1 H); 5.90 (s, 1 H); 3.71 - 3.79 (m, 4 H); 3.61 - 3.66 (m, 4 H); 3.39 - 3.51 (m, 6 H); 1.83 - 1.93 (m, 2 H); 1.64 - 1.71 (m, 2 H); 1.44 - 1.57 (m, 4 H).

7-(6-Morpholinopyrimidin-4-yl)-2,7-diazaspiro[4.5]decan-1-one (4.103)

4.103
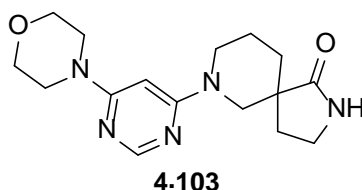
Morpholine (0.029 mL, 0.34 mmol), followed by 2,7-diazaspiro[4.5]decan-1-one (obtained from the GSK compound collection, 103 mg, 0.67 mmol, 2 eq.) were reacted according to general procedure D. Purification by MDAP (formic gradient A extended) afforded the title compound (**4.103**) as a white solid (75 mg, 0.24 mmol, 69 %). LCMS (formic): Rt = 0.43 min, [M+H]$^+$ = 318, purity = 100 %. ^{1}H NMR (400 MHz, DMSO-d_6) δ ppm 8.04 (s, 1 H); 7.65 (s, 1 H); 5.93 (s, 1 H); 4.34 - 4.42 (m, 1 H); 4.25 (d, J = 13.0 Hz, 1 H); 3.60 - 3.66 (m, 4 H); 3.46 - 3.52 (m, 4 H); 3.09 - 3.24 (m, 2 H); 2.65 - 2.83 (m, 2 H); 1.85 − 1.93 (m, 1 H); 1.62 - 1.79 (m, 3 H); 1.38-1.58 (m 2 H).

(4-Benzylpiperidin-1-yl)(1-(6-morpholinopyrimidin-4-yl)pyrrolidin-3-yl)methanone (4.106)
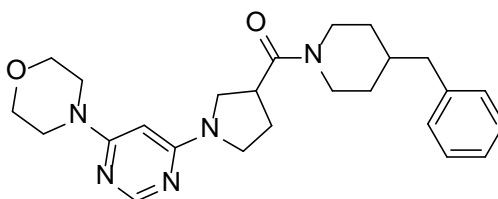
4.106

(4-Benzylpiperidin-1-yl)(pyrrolidin-3-yl)methanone (0.029 mL, 0.092 mmol), followed by morpholine (0.040 mL, 0.46 mmol, 5 eq) were reacted according to general procedure D. Purification by MDAP (ammonium bicarbonate gradient C) afforded the title compound (**4.106**) as an off-white solid (11 mg, 0.03 mmol, 28 %). LCMS (formic): Rt = 0.86 min, $[M+H]^+$ = 436, purity = 100 %. ^{1}H NMR (400 MHz, DMSO-d_6) δ ppm 8.04 (d, J = 5.5 Hz, 1 H); 7.26 - 7.31 (m, 2 H); 7.16 – 7.21 (m, 3 H); 5.54 (d, J = 3.5 Hz, 1 H); 4.33 - 4.40 (m, 1 H); 3.95 - 4.02 (m, 1 H); 3.61 - 3.66 (m, 6 H); 3.43-3.49 (m, 6 H); 3.28 (s, 2 H); 2.94 - 3.04 (m, 1 H); 2.53-2.55 (m, 2 H); 1.95 - 2.15 (m, 2 H); 1.71 - 1.82 (m, 1 H); 1.54 - 1.67 (m, 2 H); 0.94 - 1.17 (m, 2 H).

**(4-Methylpiperidin-1-yl)(1-(6-(piperidin-1-yl)pyridazin-3-yl)piperidin-4-yl)methanone (4.113)**
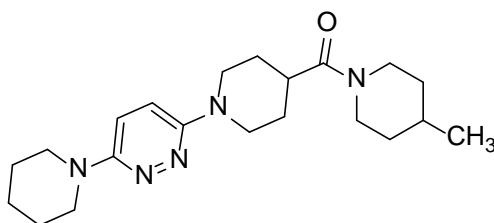
4.113

(4-Methylpiperidin-1-yl)(piperidin-4-yl)methanone (40 mg, 0.19 mmol) was dissolved in Ethanol (1 mL) and then treated with 3,6-dichloropyridazine (26 mg, 0.17 mmol) and DIPEA (0.07 mL, 0.38 mmol). The resulting solution was heated in a microwave reactor at 150 ºC for 2 hours. Piperidine (0.038 mL, 0.38 mmol) and DIPEA (0.066 mL, 0.38 mmol) were added and the solution was heated at 150 ºC for 2 hours. Additional piperidine (0.038 mL, 0.38

mmol) was added and the solution was heated at 150 °C for a further 10 hours. Purification by MDAP (ammonium bicarbonate gradient C) afforded the title compound (**4.113**) as an off-white solid (11 mg, 0.03 mmol, 15 %). Mp 97-99 °C. LCMS (formic): Rt = 0.77 min, [M+H]$^+$ = 372, purity = 91 %. HRMS C$_{21}$H$_{34}$N$_5$O required 372.2758 found 372.2765. ^{1}H NMR (400 MHz, DMSO-d_6) δ ppm 7.18 (s, 2 H); 4.35 (d, J = 12.5 Hz, 1 H); 4.10 (d, J = 13.0 Hz, 2 H); 3.97 (d, J = 12.5 Hz, 1 H); 3.36 - 3.41 (m, 4 H); 3.00 (t, J = 12.5 Hz, 1 H); 2.77 - 2.89 (m, 3 H); 1.53 - 1.72 (m, 14 H); 1.02 (m, 2 H); 0.91 (d, J = 6.5 Hz, 3 H). ^{13}C NMR (101 MHz, DMSO-d_6) δ ppm 178.2 (Ar CH); 172.1 (C=O); 155.8 (Ar C); 155.4 (Ar C); 117.2 (Ar CH); 46.8 (2 CH$_2$); 45.5 (CH$_2$); 44.9 (CH$_2$); 41.3 (CH$_2$); 37.3 (CH); 34.7 (CH$_2$); 33.6 (CH$_2$); 30.5 (CH); 27.7 (CH$_2$); 27.6 (CH$_2$); 24.8 (2 CH$_2$); 24.1 (2 CH$_2$); 21.5 (CH$_3$). IR (ATR) cm^{-1} 2925; 2852; 2808; 1628; 1442; 1248; 1215; 931; 831.

(4-Methylpiperidin-1-yl)(1-(5-(piperidin-1-yl)pyridazin-3-yl)piperidin-4-yl)methanone (4.114)
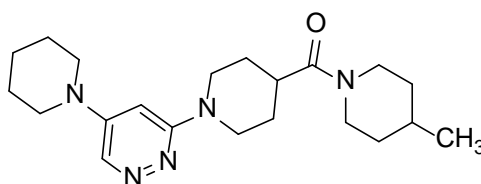
4.114

3,5-Dichloropyridazine (64 mg, 0.43 mmol) was dissolved in Ethanol (0.5 mL) and treated with piperidine (0.052 mL, 0.52 mmol) and DIPEA (0.17 mL, 0.95 mmol). The resulting solution was heated in a microwave reactor at 150 °C for five minutes. (4-Methylpiperidin-1-yl)(piperidin-4-yl)methanone (100 mg, 0.48 mmol) and DIPEA (0.17 mL, 0.95 mmol) dissolved in Ethanol (0.5 mL) were added to the solution and it was heated in a microwave reactor at 150 °C for 2 hours. Purification by MDAP (ammonium bicarbonate gradient C extended) afforded impure product. Purification by Andy Hobbs on a 4 g silica column, eluting with a gradient of 0-50 % methanol in TBME afforded the title compound (**4.114**) as a colourless gum (3 mg, 8 μmol, 2 %). LCMS (ammonium bicarbonate): Rt = 1.02 min, [M+H]$^+$ = 372, purity = 100 %. ^{1}H

NMR (400 MHz, CDCl$_3$) δ ppm 8.37 (d, J = 2.5 Hz, 1 H); 6.03 (d, J = 2.5 Hz, 1 H); 4.60 (d, J = 13.5 Hz, 1 H); 4.37 (d, J = 12.0 Hz, 2 H); 3.92 (d, J = 13.0 Hz, 1 H); 3.33 (br. s., 4 H); 2.92 - 3.10 (m, 3 H); 2.69 - 2.79 (m, 1 H); 2.51 - 2.60 (m, 1 H); 1.72 - 1.97 (m, 12 H); 1.59 – 1.71 (m, 1H) 1.03 – 1.19 (m, 2 H); 0.97 (d, J = 6.5 Hz, 3 H).

General Procedure G: Amide formations

1-(6-Morpholinopyrimidin-4-yl)piperidine-4-carboxylic acid (**4.151** 1 eq.) was dissolved in DMF (1 – 2 mL) and treated with COMU (3 eq.), DIPEA (2 – 4 eq.) and then the appropriate amine (1.2 – 1.5 eq.). The solutions were stirred at room temperature until reactions were complete by LCMS analysis. The solutions were partitioned between DCM and water and the layers were separated using hydrophobic frits and the aqueous layers were re-extracted with additional DCM. The combined organic layers were concentrated to yield crude products, which were purified by MDAP.

(2-Benzylpiperidin-1-yl)(1-(6-morpholinopyrimidin-4-yl)piperidin-4-yl)methanone (4.127)
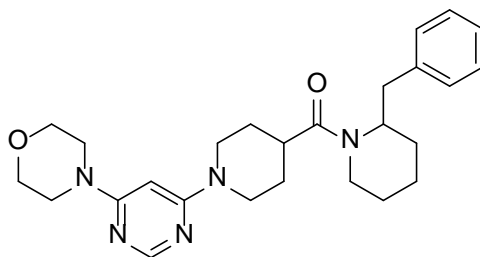
4.127

2-Benzylpiperidine (36 mg, 0.21 mmol, 1.2 eq.) was reacted according to general procedure G. Purification by MDAP (ammonium bicarbonate gradient C) afforded the title compound (**4.127**) as a yellow gum (20 mg, 0.04 mmol, 26 %). LCMS (formic): Rt = 1.04 min, [M+H]$^+$ = 450, purity = 100 %. HRMS C$_{26}$H$_{36}$N$_5$O$_2$ required 450.2864 found 450.2860. ^{1}H NMR (400 MHz, DMSO-d_6) δ ppm 7.99 – 8.11 (m, 1 H); 7.12 - 7.33 (m, 5 H); 5.79 – 5.92 (m, 1 H); 4.09 - 4.43 (m, 3 H); 3.59 – 3.67 (m, 4 H); 3.44 – 3.51 (m, 4 H); 3.09 - 3.26 (m, 1 H); 2.66 - 2.92 (m, 4 H); 2.39 – 2.48 (m, 1 H); 2.24 – 2.34 (m, 1 H); 1.63

- 1.83 (m, 2 H); 1.43 - 1.63 (m, 4 H); 1.30 - 1.43 (m, 2 H); 1.13 - 1.29 (m, 2 H).

(3-Benzylpiperidin-1-yl)(1-(6-morpholinopyrimidin-4-yl)piperidin-4-yl)methanone (4.128)
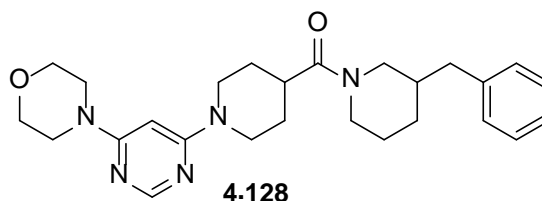
4.128

3-Benzyl piperidine (36 mg, 0.21 mmol, 1.2 eq.) was reacted according to general procedure G. Purification by MDAP (ammonium bicarbonate gradient C) afforded the title compound (**4.128**) as an orange solid (18 mg, 0.04 mmol, 24 %). Mp 65 – 68 °C. LCMS (ammonium bicarbonate): Rt = 1.18 min, $[M+H]^+$ = 450, purity = 99 %. HRMS $C_{26}H_{36}N_5O_2$ required 450.2864 found 450.2858. ^{1}H NMR (400 MHz, DMSO-d_6) δ ppm 8.07 (s, 1 H); 7.25 - 7.35 (m, 2 H); 7.14 - 7.24 (m, 3 H); 5.88 (d, J = 3.5 Hz, 1 H); 4.25 - 4.38 (m, 2 H); 4.13 - 4.24 (m, 1 H); 3.69 – 3.92 (m, 1 H); 3.61 – 3.66 (m, 4 H); 3.46 – 3.51 (m, 4 H); 2.97 - 3.10 (m, 1 H); 2.82 - 2.95 (m, 2 H); 2.64 - 2.82 (m, 1 H); 2.52 - 2.63 (m, 1 H); 2.45 - 2.48 (m, 1 H); 2.34 - 2.44 (m, 1 H); 1.66 – 1.76 (m, 2 H); 1.53 - 1.65 (m, 2 H); 1.38 - 1.52 (m, 3 H); 1.28 – 1.38 (m, 1 H); 1.14 - 1.26 (m, 1 H). ^{13}C NMR (101 MHz, DMSO-d_6) δ ppm 171.7 (C=O); 163.0 (Ar C); 162.4 (Ar C); 156.9 (Ar CH); 139.8 (Ar C); 128.9 (2 Ar CH); 128.2 (2 Ar CH); 125.9 (Ar CH); 81.4 (Ar CH); 65.8 (CH$_2$); 50.2 (CH$_2$); 46.6 (CH$_2$); 45.4 (CH$_2$); 44.1 (CH$_2$); 43.3 (CH$_2$); 41.8 (CH$_2$); 37.6 (CH$_2$); 37.4 (CH); 37.3 (CH); 30.4 (CH$_2$); 27.7 (CH$_2$); 27.5 (CH$_2$); 25.6 (CH$_2$); 24.5 (CH$_2$).

(3,4-Dihydroisoquinolin-2(1H)-yl)(1-(6-morpholinopyrimidin-4-yl)piperidin-4-yl)methanone (4.130)
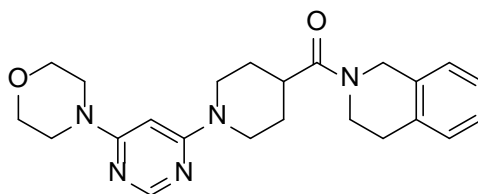
4.130

1,2,3,4-Tetrahydroisoquinoline (0.067 mL, 0.54 mmol, 1.5 eq.) was reacted according to general procedure G. Purification by MDAP (ammonium bicarbonate gradient B) afforded the title compound (**4.130**) as a yellow gum (113 mg, 0.28 mmol, 77 %). LCMS (formic): Rt = 0.63 min, $[M+H]^+$ = 408.14, purity = 100 %. HRMS $C_{23}H_{30}N_5O_2$ required 408.2394 found 408.2390. ^1H NMR (400 MHz, DMSO-d_6) δ ppm 8.08 (s, 1 H); 7.13 - 7.26 (m, 4 H); 5.90 (s, 1 H); 4.76 (s, 1 H); 4.60 (s, 1 H); 4.32 – 4.42 (m, 2 H); 3.78 (t, J = 5.5 Hz, 1 H); 3.60 - 3.70 (m, 5 H); 3.45 - 3.54 (m, 4 H); 3.04 (br. s., 1 H); 2.84 - 2.98 (m, 3 H); 2.72 – 2.78 (m, 1 H); 1.60 – 1.72 (m, 2 H); 1.42 - 1.58 (m, 2 H). ^{13}C NMR (101 MHz, DMSO-d_6) δ ppm 178.7 (C=O); 163.0 (Ar C); 162.4 (Ar C); 156.8 (Ar CH); 133.6 (Ar C); 128.5 (Ar CH); 128.3 (Ar CH); 126.4 (Ar CH); 126.2 (Ar CH); 126.1 (Ar C); 81.4 (Ar CH); 65.8 (2 CH_2); 44.1 (2 CH_2); 43.7 (CH_2); 43.3 (CH_2); 42.4 (CH_2); 37.6 (CH); 29.1 (CH_2); 27.8 (CH_2); 27.7 (CH_2); 27.5 (CH_2). IR (ATR) cm^{-1} 2922; 2851; 1632; 1578; 1440; 1197; 1114; 986; 974; 799; 749.

(2-Benzylmorpholino)(1-(6-morpholinopyrimidin-4-yl)piperidin-4-yl)methanone (4.131)
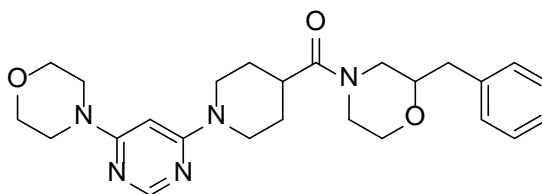
4.131

2-Benzylmorpholine (36 mg, 0.21 mmol,1.2 eq.) was reacted according to general procedure G. Purification by MDAP (ammonium bicarbonate gradient B) afforded the title compound (**4.131**) as an orange solid (42 mg, 0.09 mmol, 55 %). Mp 82 – 84 °C. LCMS (ammonium bicarbonate): Rt = 1.03 min, $[M+H]^+$ = 452, purity = 100 %. HRMS $C_{25}H_{34}N_5O_3$ required 452.2656 found 452.2668. ^1H NMR (400 MHz, DMSO-d_6) δ ppm 8.07 (s, 1 H); 7.16 - 7.37 (m, 5 H); 5.89 (s, 1 H); 4.34 (d, J = 13.0 Hz, 2 H); 4.11 - 4.23 (m, 1 H); 3.78 - 3.94 (m, 2 H); 3.60 - 3.66 (m, 4 H); 3.38 - 3.55 (m, 5 H); 3.10 – 3.22 (m, 1 H); 2.62 - 3.00 (m, 6 H); 2.39 - 2.48 (m, 1 H); 1.56 – 1.66 (m, 2 H); 1.36 - 1.55 (m, 2 H). ^{13}C NMR data not shown – restricted rotation caused line broadening so that some signals not visible. IR (ATR) cm^{-1} 2853; 1635; 1579; 1487; 1441; 1199; 1113; 987; 973; 799; 752; 670.

(3-Benzylpyrrolidin-1-yl)(1-(6-morpholinopyrimidin-4-yl)piperidin-4-yl)methanone (4.134)
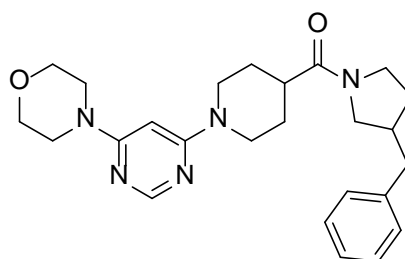
4.134

3-Benzylpyrrolidine (33 mg, 0.21 mmol, 1.2 eq.) was reacted according to general procedure G. Purification by MDAP (ammonium bicarbonate gradient C) afforded the title compound (**4.134**) as a yellow gum (34 mg, 0.08 mmol,

45 %). LCMS (formic): Rt = 0.98 min, [M+H]$^+$ = 436, purity = 99 %. HRMS C$_{25}$H$_{34}$N$_5$O$_2$ required 436.2707 found 436.2704. ^{1}H NMR (400 MHz, DMSO-d_6) δ ppm 8.07 (s, 1 H); 7.26 - 7.33 (m, 2 H); 7.17- 7.25 (m, 3 H); 5.89 (s, 1 H); 4.31 − 4.41 (m, 2 H); 3.61 - 3.69 (m, 5 H); 3.46 - 3.51 (m, 4 H); 3.35 − 3.46 (m, 1 H); 3.14 - 3.22 (m, 1 H); 2.80 - 2.95 (m, 3 H); 2.61 - 2.76 (m, 3 H); 1.78 − 1.99 (m, 1 H); 1.59 - 1.70 (m, 3 H); 1.38 - 1.56 (m, 3 H). ^{13}C NMR (101 MHz, DMSO-d_6) δ ppm 172.7 (C=O); 163.6 (Ar C); 162.9 (Ar C); 157.4 (Ar CH); 140.9 (Ar C); 129.1 (Ar CH); 128.8 (Ar CH); 128.8 (Ar CH); 126.5 (Ar CH); 126.4 (Ar CH); 81.9 (Ar CH); 66.4 (CH$_2$); 51.4 (CH$_2$); 51.0 (CH$_2$); 45.8 (CH$_2$); 45.4 (CH$_2$); 44.6 (CH$_2$); 43.8 (CH$_2$); 43.8 (CH$_2$); 39.0 (CH); 38.7 (CH); 31.6 (CH$_2$); 29.8 (CH$_2$); 27.7 (CH$_2$); 27.7 (CH$_2$). IR (ATR) cm^{-1} 3459; 2949; 2852; 1628; 1577; 1494; 1437; 1337; 1201; 1115; 972; 799; 751; 700.

Tert-butyl4-(methoxy(methyl)carbamoyl)piperidine-1-carboxylate (4.144)

4.144
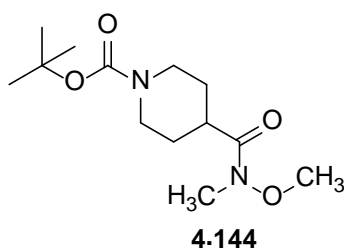
1-(_Tert_-butoxycarbonyl)piperidine-4-carboxylic acid (5.00 g, 21.8 mmol) was dissolved in Dichloromethane (DCM) (50 mL) and treated with CDI (4.24 g, 26.2 mmol). The solution was stirred at room temperature for 10 minutes then N,O-dimethylhydroxylamine hydrochloride (2.13 g, 21.8 mmol) and triethylamine (6.69 mL, 48.0 mmol) were added and the solution was stirred at room temperature for 24 h. The solution was diluted with saturated sodium carbonate (50 mL). The layers were separated using a hydrophobic frit and the aqueous layer was re-extracted with additional DCM (2 X 50 mL). The combined organic layers were concentrated to yield an orange oil. Purification on a 130 g C18 column, eluting with a gradient of 15-55 % acetonitrile in 10 mM ammonium bicarbonate solution afforded title compound (**4.144**) an orange oil (4.35 g, 16.0 mmol, 73 %). LCMS (ammonium bicarbonate): Rt = 0.96 min, [M+H]$^+$ = 237, purity = 97 %. ^{1}H

NMR (400 MHz, DMSO-d_6) δ ppm 3.94 (d, J = 13.5 Hz, 2 H); 3.68 (s, 3 H); 3.09 (s, 3 H); 2.69 - 2.93 (m, 3 H); 1.62 (dd, J = 13.5, 2.0 Hz, 2 H); 1.39 (s, 9 H); 1.34 (dd, J = 12.5, 4.5 Hz, 2 H).

General Procedure H: Ketone formations

A solution of the appropriate heterocycle (1.5 eq.) in THF (2 mL) was cooled to -78 °C and then n-butyllithium (2.5 M in hexanes) (1.8 eq.) was added dropwise, keeping the temperature below -70 °C. This solution was warmed to 0 C and stirred at 0 °C for 30 minutes. The solution was then added via cannula to a flask containing *tert*-butyl 4-(methoxy(methyl)carbamoyl)piperidine-1-carboxylate (**4.144**, 1 eq) dissolved in THF (2 mL) at -78 °C. The resulting solution was allowed to warm to room temperature overnight. The reaction was then quenched by addition of saturated ammonium chloride (50 mL). The aqueous layer was extracted with ethyl acetate (3 X 50 mL) and the combined organic layers were dried by passing through a hydrophobic frit and concentrated. The intermediate was dissolved in THF (2 mL) and treated with HCl (conc.) (2 mL) and stirred at room temperature for 3- 4 h. The solvents were evaporated to yield crude product, which was used in subsequent steps without purification.

Piperidin-4-yl(thiophen-2-yl)methanone (4.148)
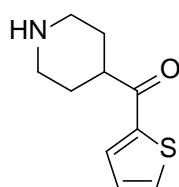
4·148

Thiophene (0.23 mL, 2.85 mmol) was reacted according to general procedure H to afford the title compound (**4.148**) as a brown oil. LCMS (ammonium bicarbonate): Rt = 0.64 min, [M+H]$^+$ = 196, purity = 100 %.

Furan-2-yl(piperidin-4-yl)methanone (4.149)
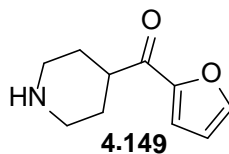
4.149

Furan (0.21 mL, 2.94 mmol) was reacted according to general procedure H to afford the title compound (**4.149**) as a brown solid. LCMS (ammonium bicarbonate): Rt = 0.54 min, [M+H]$^+$ = 180, purity = 100 %.

Piperidin-4-yl(thiazol-2-yl)methanone (4.150)
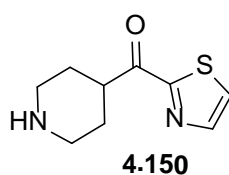
4.150

Thiazole (0.21 mL, 2.94 mmol) was reacted according to general procedure H to afford the title compound (**4.150**) as a brown solid. LCMS (ammonium bicarbonate): Rt = 0.61 min, [M+H]$^+$ = 197, purity = 96 %.

(1-(6-Morpholinopyrimidin-4-yl)piperidin-4-yl)(4-(thiophene-2-carbonyl)piperidin-1-yl)methanone (4.137)
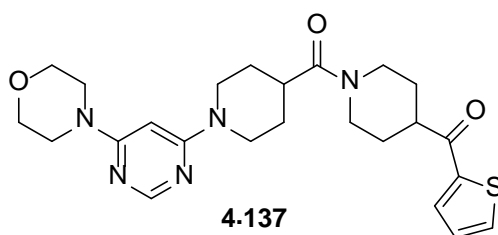
4.137

Piperidin-4-yl(thiophen-2-yl)methanone hydrochloride (119 mg, 0.51 mmol, 1.5 eq.) was reacted according to general procedure G. Purification by MDAP (ammonium bicarbonate gradient C extended) afforded the title compound (**4.137**) as a beige solid (155 mg, 0.33 mmol, 96 %). LCMS (TFA): Rt = 0.67 min, [M+H]$^+$ = 470, purity = 100 %. ^{1}H NMR (400 MHz, DMSO-d_6) δ ppm 8.07 - 8.10 (m, 2 H); 8.02 - 8.05 (m, 1 H); 7.26 - 7.30 (m, 1 H); 5.90 (s, 1 H); 4.31 - 4.47 (m, 3 H); 4.06 - 4.13 (m, 1 H); 3.62 − 3.66 (m, 4 H); 3.56 - 3.62

(m, 1 H); 3.46 – 3.52 (m, 4 H); 3.15 - 3.26 (m, 1 H); 2.84 - 3.00 (m, 3 H); 2.67 - 2.77 (m, 1 H); 1.79 - 1.91 (m, 2 H); 1.59 - 1.68 (m, 2 H); 1.31 - 1.58 (m, 4 H).

(4-(Furan-2-carbonyl)piperidin-1-yl)(1-(6-morpholinopyrimidin-4-yl)piperidin-4-yl)methanone (4.138)
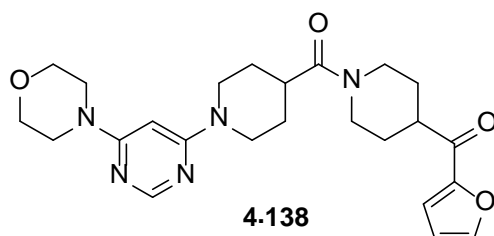
4.138

Furan-2-yl(piperidin-4-yl)methanone hydrochloride (111 mg, 0.51 mmol, 1.5 eq.) was reacted according to general procedure G. Purification by MDAP (ammonium bicarbonate gradient B) afforded the title compound (**4.138**) as a beige solid (67 mg, 0.15 mmol, 43 %). LCMS (TFA): Rt = 0.60 min, $[M+H]^+$ = 454, purity = 94 %. ^{1}H NMR (400 MHz, DMSO-d_6) δ ppm 8.08 (s, 1 H); 8.02 (s, 1 H); 7.55 – 7.59 (m, 1 H) 6.73 – 6,76 (m, 1 H); 5.91 (s, 1 H); 4.31 - 4.46 (m, 3 H); 4.05 - 4.14 (m, 1 H); 3.61 – 3.67 (m, 4 H); 3.47 – 3.52 (m, 4 H); 3.38 - 3.46 (m, 2 H); 3.13 - 3.24 (m, 1 H); 2.84 - 3.01 (m, 2 H); 2.65 - 2.75 (m, 1 H); 1.75 - 1.89 (m, 2 H); 1.64 (d, J = 12.5 Hz, 2 H); 1.30 - 1.57 (m, 4 H).

(1-(6-Morpholinopyrimidin-4-yl)piperidin-4-yl)(4-(thiazole-2-carbonyl)piperidin-1-yl)methanone (4.139)

4.139
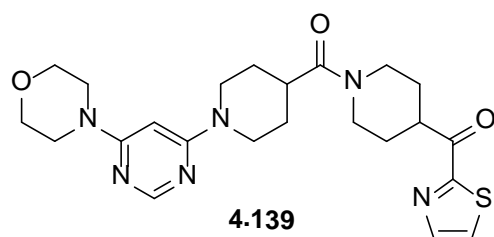
Piperidin-4-yl(thiazol-2-yl)methanone hydrochloride (456 mg, 1.96 mmol, 1.5 eq.) was reacted according to general procedure G. Purification on a 150 g C18 Redisep GOLD column, eluting with a gradient of 20-60 % acetonitrile in 10 mM ammonium bicarbonate (aq.) afforded the title compound (**4.139**) as

an orange oil (78 mg, 0.17 mmol, 13 %). LCMS (formic): Rt = 0.57 min, [M+H]$^+$ = 471, purity = 100 %. ^{1}H NMR (400 MHz, DMSO-d_6) δ ppm 8.24 (d, J = 3.0 Hz, 1 H); 8.18 (d, J = 3.0 Hz, 1 H); 8.07 (s, 1 H); 5.90 (s, 1 H); 4.32 - 4.46 (m, 3 H); 4.05 - 4.15 (m, 1 H); 3.78 - 3.88 (m, 1 H); 3.62 – 3.67 (m, 4 H); 3.47 – 3.52 (m, 4 H); 3.15 - 3.29 (m, 1 H); 2.85 - 3.00 (m, 3 H); 2.65 - 2.79 (m, 1 H); 1.92 - 2.03 (m, 2 H); 1.58 - 1.68 (m, 3 H); 1.33 - 1.58 (m, 3 H).

General Procedure J: Ketone reductions

The appropriate ketone was dissolved in 2-MeTHF (1 mL) and ethanol (0.25 mL) and treated with sodium borohydride (2 eq.). The resulting solution was stirred at room temperature until reaction was complete. The reaction was quenched by addition of water (30 mL) and then extracted with DCM (3 X 30 mL). The layers were separated using a hydrophobic frit and the combined organic layers were concentrated to yield the product.

(4-(Hydroxy(thiophen-2-yl)methyl)piperidin-1-yl)(1-(6-morpholinopyrimidin-4-yl)piperidin-4-yl)methanone (4.140)
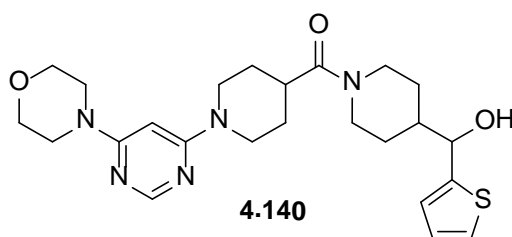
4.140

(1-(6-Morpholinopyrimidin-4-yl)piperidin-4-yl)(4-(thiophene-2-carbonyl)piperidin-1-yl)methanone (**4.137**, 68 mg, 0.15 mmol) was reacted according to general procedure J to afford the title compound (**4.140**) as a colourless gum (67 mg, 0.14 mmol, 98 %). LCMS (ammonium bicarbonate): Rt = 0.89 min, [M+H]$^+$ = 472, purity = 95 %. ^{1}H NMR (400 MHz, DMSO-d_6) δ ppm 8.07 (s, 1 H); 7.39 (d, J = 5.0 Hz, 1 H); 6.95 – 6.98 (m, 1 H); 6.92 (d, J = 3.0 Hz, 1 H); 5.89 (s, 1 H); 5.60 - 5.63 (m, 1 H); 4.55 - 4.60 (m, 1 H); 4.30 - 4.44 (m, 3 H); 3.95 - 4.09 (m, 1 H); 3.61 - 3.66 (m, 4 H); 3.46 - 3.51 (m, 4 H); 3.28 (s, 1 H); 2.81 - 3.01 (m, 4 H); 2.36 - 2.46 (m, 1 H); 1.55 - 1.63 (m, 2 H); 1.36 - 1.51 (m, 3 H); 1.14 - 1.25 (m, 1 H); 0.97 - 1.10 (m, 2 H).

(4-(Furan-2-yl(hydroxy)methyl)piperidin-1-yl)(1-(6-morpholinopyrimidin-4-yl)piperidin-4-yl)methanone (4.141)
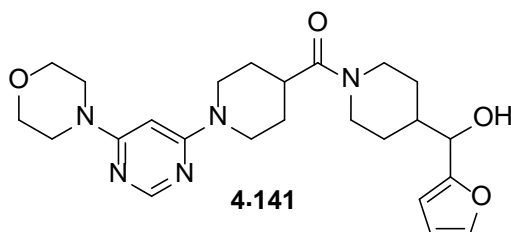
4.141

(4-(Furan-2-carbonyl)piperidin-1-yl)(1-(6-morpholinopyrimidin-4-yl)piperidin-4-yl)methanone (**4.138**, 49 mg, 0.11 mmol) was reacted according to general procedure J to afford the title compound (**4.141**) as a colourless gum (45 mg, 0.10 mmol, 91 %). LCMS (ammonium bicarbonate): Rt = 0.83 min, [M+H]$^+$ = 456, purity = 100 %. ^{1}H NMR (400 MHz, DMSO-d_6) δ ppm 8.07 (s, 1 H); 7.56 (d, J = 1.0 Hz, 1 H); 6.37 – 6.40 (m, 1 H); 6.23 (d, J = 3.0 Hz, 1 H); 5.89 (s, 1 H); 5.29 (d, J = 5.0 Hz, 1 H); 4.26 - 4.45 (m, 4 H); 3.95 - 4.08 (m, 1 H); 3.61 – 3.66 (m, 4 H); 3.46 – 3.51 (m, 4 H); 3.29 (s, 1 H); 2.81 – 3.03 (m, 4 H); 2.40 - 2.48 (m, 1 H); 1.59 (d, J = 11.0 Hz, 2 H); 1.37 - 1.53 (m, 4 H); 0.93 - 1.06 (m, 2 H).

(4-(Hydroxy(thiazol-2-yl)methyl)piperidin-1-yl)(1-(6-morpholinopyrimidin-4-yl)piperidin-4-yl)methanone (4.142)
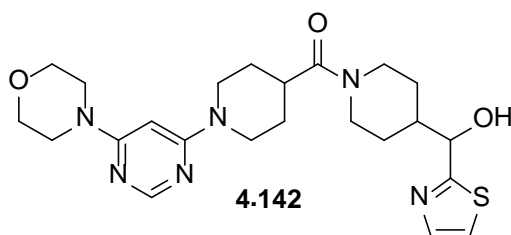
4.142

(1-(6-morpholinopyrimidin-4-yl)piperidin-4-yl)(4-(thiazole-2-carbonyl)piperidin-1-yl)methanone (**4.138**, 18 mg, 0.04 mmol) was reacted according to general procedure J. Purification by MDAP (ammonium bicarbonate gradient B) followed by MDAP (formic gradient A) afforded the title compound (**4.142**) as a formic acid salt as a colourless gum (6 mg, 0.01 mmol, 34 %). LCMS (ammonium bicarbonate): Rt = 0.78 min, [M+H]$^+$ = 473, purity = 100 %. ^{1}H NMR (400 MHz, CDCl$_3$) δ ppm 8.25 (s, 1 H); 8.13 (s, 1 H); 7.76 (br. s., 1 H);

7.34 (d, *J* = 3.0 Hz, 1 H); 5.58 (s, 1 H); 4.88 (d, *J* = 5.5 Hz, 1 H); 4.68 (d, *J* = 13.0 Hz, 1 H); 4.31 (d, *J* = 13.0 Hz, 2 H); 3.88 – 4.04 (m., 5 H); 3.75 – 3.81 (m, 4 H); 3.51 – 3.57 (m, 4 H); 3.01 - 3.11 (m, 1 H); 2.90 - 3.01 (m, 2 H); 2.71 - 2.81 (m, 1 H); 2.47 - 2.59 (m, 1 H); 2.06 – 2.21 (m, 1 H) 1.61 - 1.89 (m, 3 H); 1.31 - 1.53 (m, 2 H).

6. Conclusions

This thesis has aimed to explore how medicinal chemistry can be more successful in identifying high quality lead molecules. Two major questions were investigated: how important is the quality of the starting point and how important is what the medicinal chemist does to the starting hit.

Fragment-based screening has been proposed as a method to identify very high quality starting points for optimisation, as the hits are believed to contain the minimal structural motif required for binding. In this work, FBDD was used to identify starting hits for the anti-obesity enzyme target BCATm. The fragment screening cascade selected was shown to be successful in identifying a set of hits which were chemically diverse from one another andoccupied distinct binding sites on the enzyme. A number of different pockets discovered, which could be induced by the presence of a binding ligand. This work was the first description of these binding pockets and so provided new information on the structure of BCATm and potential approaches medicinal chemists could use to design and discover new inhibitors.

The optimisation of two of the hits generated was described in chapter 2. Optimisation of the benzisoxazole acid compound **2.3** (*figure 6.1*) was attempted by substitution of the aryl core and growing from the carboxylic acid. Ultimately, although some increases in potency were observed, it was found that ligand efficient increases could not be achieved, nor could the required levels of potency be reached. This result showed that a ligand efficient hit will not necessarily result in a potent, ligand efficient lead.
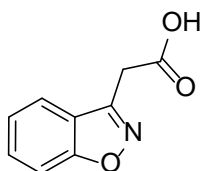
*Figure 6.1: Comppound **2.3***

The cyanopyrazole lead series derived from compound **2.14** exemplified by compound **2.85** (*figure 6.2*), was quickly identified from the starting hit, by incorporating knowledge gained from high throughput screening and paying close attention to metrics such as ligand efficiency and PFI during the optimisation. These molecules are the first known potent BCATm inhibitors and demonstrated *in vivo* activity in acute animal models of BCATm inhibition for the first time. This achievement was extended by the introduction of a polar, non-aromatic replacement for the benzylamino substituent in compound **2.85**, resulting in compound **2.87**. This molecule retained high BCATm potency and represented a new series suitable for further optimisation, which would allow more lipophilic potency enhancing groups to be added elsewhere in the molecule.

2·14   **2·85**   **2·87**
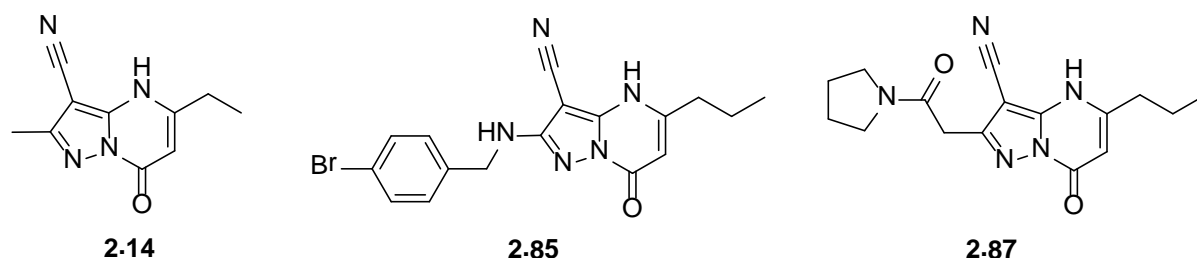
*Figure 6.2: Cyanopyrazole compounds **2.14**, **2.85** and **2.87**.*

The cyanopyrazole lead series represented by compound **2.85** was compared to other lead series generated for BCATm at GSK using alternative screening methods in chapter 3. The FBDD-derived cyanopyrazole series had definite advantages over the HTS and ELT derived leads in terms of its *in vivo* DMPK profile. When the physicochemical properties of many compounds were compared by hit finding method for the BCATm project, it became clear that the ELT compounds consistently had poorer physicochemical properties than the HTS and FBDD compounds. The HTS and FBDD derived compounds tended to have similar properties, and it was difficult to find any statistically significant differences between these. These results showed that in this case, there was definitely a quality advantage to be had from generating a lead from a high quality hit, but that

FBDD was not the only method to generate a high quality hit, and HTS could do a very good job in identifying high quality hits also.

The generality of this result was explored by comparing clinical candidates against multiple targets that had been identified by a range of screening technologies. Only weak trends towards better physicochemical properties were identified for FBDD molecules over other hit finding techniques and, if these trends are real, they have not yet led to improved outcomes for FBDD derived compounds in the clinic. There were, of course, caveats to these conclusions, mainly that FBDD is a new technology in the timescales of drug discovery, and so its advantages may not yet be apparent in clinical candidates. However, it seems from these initial analyses that the more evangelical proponents of FBDD may be over-stating the advantages that can be gained from the methodology. A question still remaining from this work is whether FBDD hits have the potential to become better candidates but medicinal chemistry practice is overly focussed on improving potency by adding lipophilic interactions and the advantages inherent in FBDD hits are lost during optimisation.

When seeking new lead series for the tuberculosis enzyme DprE1, compound **4.33**, an HTS hit initially seemed a relatively poor prospect as a starting point (*figure 6.3*). Despite its high enzyme potency, the compound had major disadvantages of high PFI, poor solubility and a poor DMPK profile. However, by paying close attention to the physicochemical properties of analogues tested and synthesised, the much improved analogue **4.35** and optimised leads such as **4.107** were rapidly discovered (*figure 6.3*).
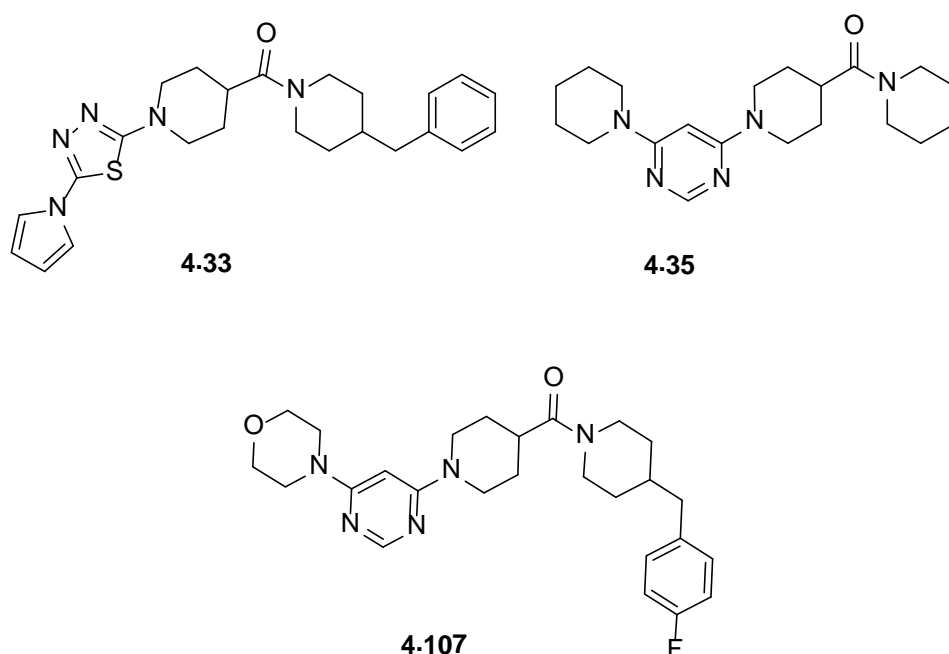
*Figure 6.3: DprE1 compounds: HTS hit **4.33** and optimised compounds **4.35** and **4.107**.*

The lead series exemplified by compound **4.107** had excellent enzyme and cellular potency, low PFI, high solubility, good DMPK and showed good levels of activity in *in vivo* models of tuberculosis. This result represented a major step forward in the field of tuberculosis research in general, and DprE1 inhibitors in particular.

Some of the medicinal chemistry practices which helped to achieve these results were borrowed from the field of FBDD research. In particular, close attention was paid to LE and LLE_{AT} metrics during optimisation; this approach helped to avoid the trap of adding lipophilicity to improve activity and allowed the optimised compounds to have much improved physicochemical properties from the hit. The exercise of fragmenting potent molecules into smaller fragments and assessing their efficiencies of binding was also a useful and helpful one. Applying a fragments philosophy to the optimisation of an HTS hit allowed the medicinal chemistry to focus on keeping constant the parts of the molecule known to contain efficient binding and optimising where the binding was shown to be less favourable.

The overall conclusions gained from examining the work in this thesis as a whole, are that the physicochemical properties of a lead or candidate molecule are very important for the likely success of the molecule, and that there are a number of strategies which must be employed to result in a molecule with a favourable profile. It is definitely true that beginning optimisation with a high quality hit can confer an advantage in the properties of the molecule resulting from that optimisation. It is less clear that FBDD is the only, or even the most important, method to identify a high quality hit. What happens to the properties of a hit during optimisation is in the hands of the medicinal chemist and it is very possible to squander the advantages of a high quality hit, or to vastly improve the properties of an unattractive hit during this phase. The consequences of these conclusions for medicinal chemists are that they can, and should, adopt a more disciplined approach in optimisation. Where fragments based research has made a major contribution to the field of drug discovery, and what its lasting legacy may be, is the philosophy of efficient optimisation to guide medicinal chemistry. Use of some FBDD methodology (for example, ligand efficiency metrics) can be applied outside of traditional fragments programmes and can provide medicinal chemists with a framework in which to carry out disciplined optimisation. The technique of fragmenting an HTS hit to identify where efficient binding resides is an example of a shift in traditional medicinal chemistry practice, which has the potential to focus optimisation activities towards identifying compounds with the best physicochemical profile possible. These philosophies and learnings are now being applied in medicinal chemistry projects by myself and colleagues at GSK.

7. References

1.   Chao, P.; Uss, A. S.; Cheng, K. C. Use of intrinsic clearance for prediction of human hepatic clearance. *Expert Opin. Drug Metab. Toxicol.* **2010**, *6* (2), 189-198.

2.   Kestranek, A.; Chervenak, A.; Longenberger, J.; Placko, S. Chemiluminescent Nitrogen Detection (CLND) to Measure Kinetic Aqueous Solubility. In *Current Protocols in Chemical Biology*, John Wiley & Sons, Inc.: **2009**.

3.   Kostewicz, E.; Brauns, U.; Becker, R.; Dressman, J. Forecasting the Oral Absorption Behavior of Poorly Soluble Weak Bases Using Solubility and Dissolution Studies in Biorelevant Media. *Pharm. Res.* **2002**, *19* (3), 345-349.

4.   Schoonen, W. G. E. J.; de Roos, J. A. D. M.; Westerink, W. M. A.; Débiton, E. Cytotoxic effects of 110 reference compounds on HepG2 cells and for 60 compounds on HeLa, ECC-1 and CHO cells.: II Mechanistic assays on NAD(P)H, ATP and DNA contents. *Toxicol. in Vitro* **2005**, *19* (4), 491-503.

5.   Fishman, M. C.; Porter, J. A. Pharmaceuticals: A new grammar for drug discovery. *Nature* **2005**, *437* (7058), 491-493.

6.   Paul, S. M.; Mytelka, D. S.; Dunwiddie, C. T.; Persinger, C. C.; Munos, B. H.; Lindborg, S. R.; Schacht, A. L. How to improve R&D productivity: the pharmaceutical industry's grand challenge. *Nat. Rev. Drug Discov.* **2010**, *9* (3), 203-214.

7.   Kola, I.; Landis, J. Can the pharmaceutical industry reduce attrition rates? *Nat. Rev. Drug Discov.* **2004**, *3* (8), 711-716.

8.   Scannell, J. W.; Blanckley, A.; Boldon, H.; Warrington, B. Diagnosing the decline in pharmaceutical R&D efficiency. *Nat. Rev. Drug Discov.* **2012**, *11* (3), 191-200.

9.   Knowles, J.; Gromo, G. Target selection in drug discovery. *Nat. Rev. Drug Discov.* **2003**, *2* (1), 63-69.

10.   Smith, C. Drug target validation: Hitting the target. *Nature* **2003**, *422* (6929), 341-347.

11.   Scannell, J. W.; Bosley, J. When Quality Beats Quantity: Decision Theory, Drug Discovery, and the Reproducibility Crisis. *PLoS ONE* **2016**, *11* (2), e0147215.

12.   Makley, L. N.; Gestwicki, J. E. Expanding the Number of 'Druggable' Targets: Non-Enzymes and Protein-Protein Interactions. *Chem. Biol. Drug Des.* **2013**, *81* (1), 22-32.

13.   Owens, J. Determining druggability. *Nat. Rev. Drug Discov.* **2007**, *6* (3), 187.

14.   Zhang, J. H.; Chung, T. D. Y.; Oldenburg, K. R. A Simple Statistical Parameter for Use in Evaluation and Validation of High Throughput Screening Assays. *J.Biomol. Screen.* **1999**, *4* (2), 67-73.

15.   Robert, A. Hit and lead identification: Integrated technology-based approaches. *Drug Discov.Today: Technologies* **2006**, *3* (4), 367-375.

16.   Hughes, J. P.; Rees, S.; Kalindjian, S. B.; Philpott, K. L. Principles of early drug discovery. *Brit. J.Pharmacol.* **2011**, *162* (6), 1239-1249.

17.   Balani, S. K.; Miwa, G. T.; Gan, L. S.; Wu, J. T.; Lee, F. W. Strategy of Utilizing In Vitro and In Vivo ADME Tools for Lead Optimization and Drug Candidate Selection. *Curr. Top. Med. Chem.* **2005** 5[11], 1033-1038.

18.   Lombardino, J. G.; Lowe, J. A. The role of the medicinal chemist in drug discovery - then and now. *Nat. Rev. Drug Discov.* **2004**, *3* (10), 853-862.

19.   Karaman, M. W.; Herrgard, S.; Treiber, D. K.; Gallant, P.; Atteridge, C. E.; Campbell, B. T.; Chan, K. W.; Ciceri, P.; Davis, M. I.; Edeen, P. T.; Faraoni, R.; Floyd, M.; Hunt, J. P.; Lockhart, D. J.; Milanov, Z. V.; Morrison, M. J.; Pallares, G.; Patel, H. K.; Pritchard, S.; Wodicka, L. M.; Zarrinkar, P. P. A quantitative analysis of kinase inhibitor selectivity. *Nat. Biotech.* **2008**, *26* (1), 127-132.

20.   Sanguinetti, M. C.; Tristani-Firouzi, M. hERG potassium channels and cardiac arrhythmia. *Nature* **2006**, *440* (7083), 463-469.

21.   De Bruin, M. L.; Pettersson, M.; Meyboom, R. H. B.; Hoes, A. W.; Leufkens, H. G. M. Anti-HERG activity and the risk of drug-induced arrhythmias and sudden death. *Eur. Heart J.* **2005**, *26* (6), 590-597.

22.   Kramer, J. A.; Sagartz, J. E.; Morris, D. L. The application of discovery toxicology and pathology towards the design of safer pharmaceutical lead candidates. *Nat. Rev. Drug Discov.* **2007**, *6* (8), 636-649.

23.   Carey, J. S.; Laffan, D.; Thomson, C.; Williams, M. T. Analysis of the reactions used for the preparation of drug candidate molecules. *Org. Biomol. Chem.* **2006**, *4* (12), 2337-2347.

24.   Steinmetz, K.; Spack, E. The basics of preclinical drug development for neurodegenerative disease indications. *BMC Neurology* **2009**, *9* (Suppl 1), S2.

25.   DiMasi, J. A.; Hansen, R. W.; Grabowski, H. G. The price of innovation: new estimates of drug development costs. *J.Health Econ.* **2003**, *22* (2), 151-185.

26.   Leo, A.; Hansch, C.; Elkins, D. Partition coefficients and their uses. *Chem.Rev.* **1971**, *71* (6), 525-616.

27.   Ghose, A. K.; Viswanadhan, V. N.; Wendoloski, J. J. Prediction of Hydrophobic (Lipophilic) Properties of Small Organic Molecules Using Fragmental Methods: An Analysis of ALOGP and CLOGP Methods. *J. Phys. Chem. A* **1998**, *102* (21), 3762-3772.

28.   Manners, C. N.; Payling, D. W.; Smith, D. A. Distribution coefficient, a convenient term for the relation of predictable physico-chemical properties to metabolic processes. *Xenobiotica* **1988**, *18* (3), 331-350.

29.   Kaufman, J. J.; Semo, N. M.; Koski, W. S. Microelectrometric titration measurement of the pKa's and partition and drug distribution coefficients of narcotics and narcotic antagonists and their pH and temperature dependence. *J. Med. Chem.* **1975**, *18* (7), 647-655.

30.   Tetko, I. V.; Poda, G. I. Application of ALOGPS 2.1 to Predict logD Distribution Coefficient for Pfizer Proprietary Compounds. *J. Med. Chem.* **2004**, *47* (23), 5601-5604.

31.   Young, R. J.; Green, D. V. S.; Luscombe, C. N.; Hill, A. P. Getting physical in drug discovery II: the impact of chromatographic hydrophobicity measurements and aromaticity. *Drug Discov. Today* **2011**, *16* (17-18), 822-830.

32.   Lipinski, C. A.; Lombardo, F.; Dominy, B. W.; Feeney, P. J. Experimental and computational approaches to estimate solubility and permeability in drug discovery and development settings. *Adv. Drug Deliv. Rev.* **1997**, *23* (1-3), 3-25.

33.   Waring, M. J. Lipophilicity in drug discovery. *Expert Opin. Drug Discov.* **2010**, *5* (3), 235-248.

34.   Gleeson, M. P. Generation of a Set of Simple, Interpretable ADMET Rules of Thumb. *J. Med. Chem.* **2008**, *51* (4), 817-834.

35.   Hughes, J. D.; Blagg, J.; Price, D. A.; Bailey, S.; DeCrescenzo, G. A.; Devraj, R. V.; Ellsworth, E.; Fobian, Y. M.; Gibbs, M. E.; Gilles, R. W.; Greene, N.; Huang, E.; Krieger-Burke, T.; Loesel, J.; Wager, T.; Whiteley, L.; Zhang, Y. Physiochemical drug properties associated with in vivo toxicological outcomes. *Bioorg.Med. Chem. Lett.* **2008**, *18* (17), 4872-4875.

36.   Lovering, F.; Bikker, J.; Humblet, C. Escape from Flatland: Increasing Saturation as an Approach to Improving Clinical Success. *J. Med. Chem.* **2009**, *52* (21), 6752-6756.

37.   Ritchie, T. J.; Macdonald, S. J. F. The impact of aromatic ring count on compound developability - are too many aromatic rings a liability in drug design? *Drug Discov. Today* **2009**, *14* (21-22), 1011-1020.

38.   Ritchie, T. J.; Macdonald, S. J. F.; Young, R. J.; Pickett, S. D. The impact of aromatic ring count on compound developability: further insights by examining carbo- and hetero-aromatic and -aliphatic ring types. *Drug Discov. Today* **2011**, *16* (3-4), 164-171.

39.   Hill, A. P.; Young, R. J. Getting physical in drug discovery: a contemporary perspective on solubility and hydrophobicity. *Drug Discov. Today* **2010**, *15* (15-16), 648-655.

40.   Kenny, P.; Montanari, C. Inflation of correlation in the pursuit of drug-likeness. *J Comput Aided Mol Des* **2013**, *27* (1), 1-13.

41.   Bickerton, G. R.; Paolini, G. V.; Besnard, J.; Muresan, S.; Hopkins, A. L. Quantifying the chemical beauty of drugs. *Nat. Chem.* **2012**, *4* (2), 90-98.

42.   Leeson, P. D.; Springthorpe, B. The influence of drug-like concepts on decision-making in medicinal chemistry. *Nat. Rev. Drug Discov.* **2007**, *6* (11), 881-890.

43.   Hann, M. M. Molecular obesity, potency and other addictions in drug discovery. *Med. Chem. Commun.* **2011**, *2* (5), 349-355.

44.   Gleeson, M. P.; Hersey, A.; Montanari, D.; Overington, J. Probing the links between in vitro potency, ADMET and physicochemical parameters. *Nat. Rev. Drug Discov.* **2011**, *10* (3), 197-208.

45.   Morphy, R. The Influence of Target Family and Functional Activity on the Physicochemical Properties of Pre-Clinical Compounds. *J. Med. Chem.* **2006**, *49* (10), 2969-2978.

46.   Hann, M. M.; Keserü, G. M. Finding the sweet spot: the role of nature and nurture in medicinal chemistry. *Nat. Rev. Drug Discov.* **2012**, *11* (5), 355-365.

47.   Nadin, A.; Hattotuwagama, C.; Churcher, I. Lead-Oriented Synthesis: A New Opportunity for Synthetic Chemistry. *Angew. Chem. Int. Ed.* **2012**, *51* (5), 1114-1122.

48.   Leeson, P. D.; St-Gallay, S. A. The influence of the 'organizational factor' on compound quality in drug discovery. *Nat. Rev. Drug Discov.* **2011**, *10* (10), 749-765.

49.   Fox, S.; Farr-Jones, S.; Sopchak, L.; Boggs, A.; Nicely, H. W.; Khoury, R.; Biros, M. High-Throughput Screening: Update on Practices and Success. *J.Biomol. Screen.* **2006**, *11* (7), 864-869.

50.   Macarron, R.; Banks, M. N.; Bojanic, D.; Burns, D. J.; Cirovic, D. A.; Garyantes, T.; Green, D. V. S.; Hertzberg, R. P.; Janzen, W. P.; Paslay, J. W.; Schopfer, U.; Sittampalam, G. S. Impact of high-throughput screening in biomedical research. *Nat. Rev. Drug Discov.* **2011**, *10* (3), 188-195.

51.   Villar, H. O.; Hansen, M. R. Design of chemical libraries for screening. *Expert Opin. Drug Discov.* **2009**, *4* (12), 1215-1220.

52.   Baell, J. B. Broad Coverage of Commercially Available Lead-like Screening Space with Fewer than 350,000 Compounds. *J. Chem. Inf. Model.* **2012**, *53* (1), 39-55.

53.   Mok, N. Y.; Maxe, S.; Brenk, R. Locating Sweet Spots for Screening Hits and Evaluating Pan-Assay Interference Filters from the Performance Analysis of Two Lead-like Libraries. *J. Chem. Inf. Model.* **2013**, *53* (3), 534-544.

54.   Brenk, R.; Schipani, A.; James, D.; Krasowski, A.; Gilbert, I. H.; Frearson, J.; Wyatt, P. G. Lessons Learnt from Assembling Screening Libraries for Drug Discovery for Neglected Diseases. *ChemMedChem* **2008**, *3* (3), 435-444.

55.   Baell, J. B.; Holloway, G. A. New Substructure Filters for Removal of Pan Assay Interference Compounds (PAINS) from Screening Libraries and for Their Exclusion in Bioassays. *J. Med. Chem.* **2010**, *53* (7), 2719-2740.

56.   Kogej, T.; Blomberg, N.; Greasley, P. J.; Mundt, S.; Vainio, M. J.; Schamberger, J.; Schmidt, G.; Hüser, J. Big pharma screening collections: more of the same or unique libraries? The AstraZeneca-Bayer Pharma AG case. *Drug Discov. Today* **2012**, *18* (19-20) 1014-1024.

57.   http://nihsmr.evotec.com/evotec/

58.   Sundberg, S. A. High-throughput and ultra-high-throughput screening: solution- and cell-based approaches. *Curr.Opin. Biotech.* **2000**, *11* (1), 47-53.

59.   Malo, N.; Hanley, J. A.; Cerquozzi, S.; Pelletier, J.; Nadon, R. Statistical practice in high-throughput screening data analysis. *Nat. Biotech.* **2006**, *24* (2), 167-175.

60.   Owen, S. C.; Doak, A. K.; Wassam, P.; Shoichet, M. S.; Shoichet, B. K. Colloidal Aggregation Affects the Efficacy of Anticancer Drugs in Cell Culture. *ACS Chem. Biol.* **2012**, *7* (8), 1429-1435.

61.   Clark, M. A.; Acharya, R. A.; rico-Muendel, C. C.; Belyanskaya, S. L.; Benjamin, D. R.; Carlson, N. R.; Centrella, P. A.; Chiu, C. H.; Creaser, S. P.; Cuozzo, J. W.; Davie, C. P.; Ding, Y.; Franklin, G. J.; Franzen, K. D.; Gefter, M. L.; Hale, S. P.; Hansen, N. J. V.; Israel, D. I.; Jiang, J.; Kavarana, M. J.; Kelley, M. S.; Kollmann, C. S.; Li, F.; Lind, K.; Mataruse, S.; Medeiros, P. F.; Messer, J. A.; Myers, P.; O'Keefe, H.; Oliff, M. C.; Rise, C. E.; Satz, A. L.; Skinner, S. R.; Svendsen, J. L.; Tang, L.; van Vloten, K.; Wagner, R. W.; Yao, G.; Zhao, B.; Morgan, B. A. Design, synthesis and selection of DNA-encoded small-molecule libraries. *Nat. Chem. Biol.* **2009**, *5* (9), 647-654.

62.   Disch, J. S.; Evindar, G.; Chiu, C. H.; Blum, C. A.; Dai, H.; Jin, L.; Schuman, E.; Lind, K. E.; Belyanskaya, S. L.; Deng, J.; Coppo, F.; Aquilani, L.; Graybill, T. L.; Cuozzo, J. W.; Lavu, S.; Mao, C.; Vlasuk, G. P.; Perni, R. B. Discovery of Thieno[3,2-*d*]pyrimidine-6-carboxamides as Potent Inhibitors of SIRT1, SIRT2, and SIRT3. *J. Med. Chem.* **2013**, *56* (9), 3666-3679.

63.   Weisinger, R. M.; Wrenn, S. J.; Harbury, P. B. Highly Parallel Translation of DNA Sequences into Small Molecules. *PLoS ONE* **2012**, *7* (3), e28056.

64.   Kleiner, R. E.; Dumelin, C. E.; Tiu, G. C.; Sakurai, K.; Liu, D. R. *In Vitro* Selection of a DNA-Templated Small-Molecule Library Reveals a Class of Macrocyclic Kinase Inhibitors. *J. Am. Chem. Soc.* **2010**, *132* (33), 11779-11791.

65.   Mannocci, L.; Melkko, S.; Buller, F.; Molnàr, I.; Gapian Bianké, J. P.; Dumelin, C. E.; Scheuermann, J.; Neri, D. Isolation of Potent and Specific Trypsin Inhibitors from a DNA-Encoded Chemical Library. *Bioconjugate Chem.* **2010**, *21* (10), 1836-1841.

66.   Hann, M. M.; Leach, A. R.; Harper, G. Molecular complexity and its impact on the probability of finding leads for drug discovery. *J. Chem. Inf. Comp. Sci.* **2001**, *41* (3), 856-864.

67.   Leach, A. R.; Hann, M. M. Molecular complexity and fragment-based drug discovery: ten years on. *Curr.Opin. Chem. Biol.* **2011**, *15* (4), 489-496.

68.   Schuffenhauer, A.; Ruedisser, S.; Marzinzik, A. L.; Jahnke, W.; Blommers, M.; Selzer, P.; Jacoby, E. Library design for fragment based screening. *Curr. Top. Med. Chem.* **2005**, *5* (8), 751-762.

69.   Fink, T.; Reymond, J. L. Virtual Exploration of the Chemical Universe up to 11 Atoms of C, N, O, F: Assembly of 26.4 Million Structures (110.9 Million Stereoisomers) and Analysis

for New Ring Systems, Stereochemistry, Physicochemical Properties, Compound Classes, and Drug Discovery. *J. Chem. Inf. Model.* **2007**, *47* (2), 342-353.

70.   Lipinski, C.; Hopkins, A. Navigating chemical space for biology and medicine. *Nature* **2004**, *432* (7019), 855-861.

71.   Ruddigkeit, L.; van Deursen, R.; Blum, L. C.; Reymond, J. L. Enumeration of 166 Billion Organic Small Molecules in the Chemical Universe Database GDB-17. *J. Chem. Inf. Model.* **2012**, *52* (11), 2864-2875.

72.   Rees, D. C.; Congreve, M.; Murray, C. W.; Carr, R. Fragment-based lead discovery. *Nat. Rev. Drug Discov.* **2004**, *3* (8), 660-672.

73.   Keserü, G. M.; Makara, G. M. The influence of lead discovery strategies on the properties of drug candidates. *Nat. Rev. Drug Discov.* **2009**, *8* (3), 203-212.

74.   Albert, J. S.; Blomberg, N.; Breeze, A. L.; Brown, A. J. H.; Burrows, J. N.; Edwards, P. D.; Folmer, R. H. A.; Geschwindner, S.; Griffen, E. J.; Kenny, P. W.; Nowak, T.; Olsson, L. L.; Sanganee, H.; Shapiro, A. B. An Integrated Approach to Fragment-Based Lead Generation:Philosophy, Strategy and Case Studies from AstraZeneca's Drug Discovery Programmes. *Curr.Top. Med. Chem.* **2007**, *7* (16), 1600-1629..

75.   Ludwig, C.; Guenther, U. L. Ligand based NMR methods for drug discovery. *Front Biosci.* **2009**, *14*, 4565-4574.

76.   Gozalbes, R.; Carbajo, R. J.; Pineda-Lucena, A. Contributions of computational chemistry and biophysical techniques to fragment-based drug discovery. *Curr. Med. Chem.* **2010**, *17* (17), 1769-1794.

77.   Orita, M.; Warizaya, M.; Amano, Y.; Ohno, K.; Niimi, T. Advances in fragment-based drug discovery platforms. *Expert Opin. Drug Discov.* **2009**, *4* (11), 1125-1144.

78.   Murray, C. W.; Rees, D. C. The rise of fragment-based drug discovery. *Nat. Chem.* **2009**, *1* (3), 187-192.

79.   Hajduk, P. J.; Greer, J. A decade of fragment-based drug design: strategic advances and lessons learned. *Nat. Rev. Drug Discov.* **2007**, *6* (3), 211-219.

80.   Congreve, M.; Chessari, G.; Tisi, D.; Woodhead, A. J. Recent developments in fragment-based drug discovery. *J. Med. Chem.* **2008**, *51* (13), 3661-3680.

81.   Oltersdorf, T.; Elmore, S. W.; Shoemaker, A. R.; Armstrong, R. C.; Augeri, D. J.; Belli, B. A.; Bruncko, M.; Deckwerth, T. L.; Dinges, J.; Hajduk, P. J.; Joseph, M. K.; Kitada, S.; Korsmeyer, S. J.; Kunzer, A. R.; Letai, A.; Li, C.; Mitten, M. J.; Nettesheim, D. G.; Ng, S. C.; Nimmer, P. M.; O'Connor, J. M.; Oleksijew, A.; Petros, A. M.; Reed, J. C.; Shen, W.; Tahir, S. K.; Thompson, C. B.; Tomaselli, K. J.; Wang, B.; Wendt, M. D.; Zhang, H.; Fesik, S. W.; Rosenberg, S. H. An inhibitor of Bcl-2 family proteins induces regression of solid tumours. *Nature* **2005**, *435* (7042), 677-681.

82.   Howard, N.; Abell, C.; Blakemore, W.; Chessari, G.; Congreve, M.; Howard, S.; Jhoti, H.; Murray, C. W.; Seavers, L. C. A.; Van, M. Application of Fragment Screening and

Fragment Linking to the Discovery of Novel Thrombin Inhibitors. *J. Med. Chem.* **2006**, *49* (4), 1346-1355.

83.   Fischer, M.; Hubbard, R. E. Fragment-based ligand discovery. *Mol.Interv.* **2009**, *9* (1), 22-30.

84.   Hopkins, A. L.; Groom, C. R.; Alex, A. Ligand efficiency: a useful metric for lead selection. *Drug Discov.Today* **2004**, *9* (10), 430-431.

85.   bad-Zapatero, C.; Metz, J. T. Ligand efficiency indices as guideposts for drug discovery. *Drug Discov. Today* **2005**, *10* (7), 464-469.

86.   Edwards, M. P.; Price, D. A. Role of Physicochemical Properties and Ligand Lipophilicity Efficiency in Addressing Drug Safety Risks. In *Annual Reports in Medicinal Chemistry*, Volume 45 ed.; John E.Macor, Ed.; Academic Press: **2010**; pp 380-391.

87.   Mortenson, P.; Murray, C. Assessing the lipophilicity of fragments and early hits. *J. Comput. Aid. Mol. Des.* **2011**, *25* (7), 663-667.

88.   Alex, A. A.; Flocco, M. M. Fragment-Based Drug Discovery: What has it Achieved so Far? *Curr. Top. Med. Chem.* **2007**, *7* (16), 1544-1567.

89.   Chessari, G.; Woodhead, A. J. From fragment to clinical candidate - a historical perspective. *Drug Discov.Today* **2009**, *14* (13-14), 668-675.

90.   Whittaker, M.; Law, R. J.; Ichihara, O.; Hesterkamp, T.; Hallett, D. Fragments: past, present and future. *Drug Discov. Today: Technologies* **2010**, *7* (3), e163-e171.

91.   Artis, D. R.; Lin, J. J.; Zhang, C.; Wang, W.; Mehra, U.; Perreault, M.; Erbe, D.; Krupka, H. I.; England, B. P.; Arnold, J.; Plotnikov, A. N.; Marimuthu, A.; Nguyen, H.; Will, S.; Signaevsky, M.; Kral, J.; Cantwell, J.; Settachatgull, C.; Yan, D. S.; Fong, D.; Oh, A.; Shi, S.; Womack, P.; Powell, B.; Habets, G.; West, B. L.; Zhang, K. Y. J.; Milburn, M. V.; Vlasuk, G. P.; Hirth, K. P.; Nolop, K.; Bollag, G.; Ibrahim, P. N.; Tobin, J. F. Scaffold-based discovery of indeglitazar, a PPAR pan-active anti-diabetic agent. *P.Natl. Acad. Sci.* **2008** *106* (1) 262-267.

92.   Bénardeau, A.; Benz, J.; Binggeli, A.; Blum, D.; Boehringer, M.; Grether, U.; Hilpert, H.; Kuhn, B.; Märki, H. P.; Meyer, M.; Püntener, K.; Raab, S.; Ruf, A.; Schlatter, D.; Mohr, P. Aleglitazar, a new, potent, and balanced dual PPARα/ɣ agonist for the treatment of type II diabetes. *Bioorg.Med. Chem. Lett.* **2009**, *19* (9), 2468-2473.

93.   Harrity, T.; Farrelly, D.; Tieman, A.; Chu, C.; Kunselman, L.; Gu, L.; Ponticiello, R.; Cap, M.; Qu, F.; Shao, C.; Wang, W.; Zhang, H.; Fenderson, W.; Chen, S.; Devasthale, P.; Jeon, Y.; Seethala, R.; Yang, W. P.; Ren, J.; Zhou, M.; Ryono, D.; Biller, S.; Mookhtiar, K. A.; Wetterau, J.; Gregg, R.; Cheng, P. T.; Hariharan, N. Muraglitazar, a Novel Dual (α/ɣ) Peroxisome Proliferator-Activated Receptor Activator, Improves Diabetes and Other Metabolic Abnormalities and Preserves b-Cell Function in db/db Mice. *Diabetes* **2006**, *55* (1), 240-248.

94.   Gambhire, D.; Jani, R. H.; Pandey, B.; Sata, K.; Kothari, H.; Patel, P. R. Treatment for lipodystrophy. WO2012104869A1, Aug 9, **2012**.

95.   Bollag, G.; Tsai, J.; Zhang, J.; Zhang, C.; Ibrahim, P.; Nolop, K.; Hirth, P. Vemurafenib: the first drug approved for BRAF-mutant cancer. *Nat. Rev. Drug Discov.* **2012**, *11* (11), 873-886.

96.   Stellwagen, J. C.; Adjabeng, G. M.; Arnone, M. R.; Dickerson, S. H.; Han, C.; Hornberger, K. R.; King, A. J.; Mook, J.; Petrov, K. G.; Rheault, T. R.; Rominger, C. M.; Rossanese, O. W.; Smitheman, K. N.; Waterson, A. G.; Uehling, D. E. Development of potent B-RafV600E inhibitors containing an arylsulfonamide headgroup. *Bioorg.Med. Chem. Lett.* **2011**, *21* (15), 4436-4440.

97.   Caceres, R. A.; Pauli, I.; Timmers, L. F. S. M.; Filgueira, d. A. W., Jr. Molecular recognition models: a challenge to overcome. *Curr. Drug Targets* **2008**, *9* (12), 1077-1083.

98.   Leach, A. R.; Shoichet, B. K.; Peishoff, C. E. Prediction of Protein-Ligand Interactions. Docking and Scoring: Successes and Gaps. *J. Med. Chem.* **2006**, *49* (20), 5851-5855.

99.   Fischer, E. Einfluss der Configuration auf die Wirkung der Enzyme. *Ber. Dtsch. Chem. Ges.* **1894**, *27* (3), 2985-2993.

100.   Koshland, D. E. Application of a Theory of Enzyme Specificity to Protein Synthesis. *P.Natl. Acad. Sci.* **1958**, *44* (2), 98-104.

101.   Shan, Y.; Seeliger, M. A.; Eastwood, M. P.; Frank, F.; Xu, H.; Jensen, M. Ø.; Dror, R. O.; Kuriyan, J.; Shaw, D. E. A conserved protonation-dependent switch controls drug binding in the Abl kinase. *P.Natl. Acad. Sci.* **2009**, *106* (1), 139-144.

102.   Weikl, T. R.; von Deuster, C. Selected-fit versus induced-fit protein binding: Kinetic differences and mutational analysis. *Proteins* **2009**, *75* (1), 104-110.

103.   Williams, D. H.; Cox, J. P. L.; Doig, A. J.; Gardner, M.; Gerhard, U.; Kaye, P. T.; Lal, A. R.; Nicholls, I. A.; Salter, C. J.; Mitchell, R. C. Toward the semiquantitative estimation of binding constants. Guides for peptide-peptide binding in aqueous solution. *J. Am. Chem. Soc.* **1991**, *113* (18), 7020-7030.

104.   Page, M. I.; Jencks, W. P. Entropic Contributions to Rate Accelerations in Enzymic and Intramolecular Reactions and the Chelate Effect. *P.Natl. Acad. Sci.* **1971**, *68* (8), 1678-1683.

105.   Searle, M. S.; Williams, D. H. The cost of conformational order: entropy changes in molecular associations. *J. Am. Chem. Soc.* **1992**, *114* (27), 10690-10697.

106.   Boström, J.; Norrby, P. O.; Liljefors, T. Conformational energy penalties of protein-bound ligands. *J. Comput. Aid. Mol. Des.* **1998**, *12* (4), 383.

107.   Martin, S. F. Preorganization in biological systems: are conformational constraints worth the energy? *Pure Appl. Chem.* **2007**, *79* (2), 193-200.

108.   Murray, C. W.; Verdonk, M. L. The consequences of translational and rotational entropy lost by small molecules on binding to proteins. *J. Comput. Aid. Mol. Des.* **2002**, *16* (10), 741-753.

109.   Bissantz, C.; Kuhn, B.; Stahl, M. A Medicinal Chemist's Guide to Molecular Interactions. *J. Med. Chem.* **2010**, *53* (14), 5061-5084.

110.   Laurence, C.; Brameld, K. A.; Graton, J.; Le Questel, J. Y.; Renault, E. The pK_{BHX} Database: Toward a Better Understanding of Hydrogen-Bond Basicity for Medicinal Chemists. *J. Med. Chem.* **2009**, *52* (14), 4073-4086.

111.   Böhm, H. J.; Klebe, G. What Can We Learn from Molecular Recognition in Protein-Ligand Complexes for the Design of New Drugs? *Angew. Chem. Int. Ed. Engl.* **1996**, *35* (22), 2588-2614.

112.   Klebe, G.; Böhm, H. J. Energetic and entropic factors determining binding affinity in protein-ligand complexes. *J. Recept. Signal Tr. R..* **1997**, *17* (1-3), 459-473.

113.   Morgan, B.; Scholtz, J. M.; Ballinger, M. D.; Zipkin, I. D.; Bartlett, P. A. Differential binding energy: a detailed evaluation of the influence of hydrogen-bonding and hydrophobic groups on the inhibition of thermolysin by phosphorus-containing inhibitors. *J. Am. Chem. Soc.* **1991**, *113* (1), 297-307.

114.   Fersht, A. R. Dissection of the structure and activity of the tyrosyl-tRNA synthetase by site-directed mutagenesis. *Biochemistry* **1987**, *26* (25), 8031-8037.

115.   Zhou, P.; Tian, F.; Zou, J.; Shang, Z. Rediscovery of halogen bonds in protein-ligand complexes. *Mini-Rev. Med. Chem.* **2010**, *10* (4), 309-314.

116.   Voth, A. R.; Ho, P. S. The role of halogen bonding in inhibitor recognition and binding by protein kinases. *Curr. Top. Med. Chem.* **2007**, *7* (14), 1336-1348.

117.   Ma, J. C.; Dougherty, D. A. The Cation-p Interaction. *Chem. Rev.* **1997**, *97* (5), 1303-1324.

118.   Meyer, E. A.; Castellano, R. K.; Diederich, F. Interactions with Aromatic Rings in Chemical and Biological Recognition. *Angew. Chem. Int. Ed.* **2003**, *42* (11), 1210-1250.

119.   Toth, G.; Bowers, S. G.; Truong, A. P.; Probst, G. The role and significance of unconventional hydrogen bonds in small molecule recognition by biological receptors of pharmaceutical relevance. *Curr. Pharm. Des.* **2007**, *13* (34), 3476-3493.

120.   Homans, S. W. Dynamics and thermodynamics of ligand-protein interactions. *Top. Curr. Chem.* **2007**, *272* (Bioactive Conformation I), 51-82.

121.   Barillari, C.; Taylor, J.; Viner, R.; Essex, J. W. Classification of Water Molecules in Protein Binding Sites. *J. Am. Chem. Soc.* **2007**, *129* (9), 2577-2587.

122.   Beattie, J. F.; Breault, G. A.; Ellston, R. P. A.; Green, S.; Jewsbury, P. J.; Midgley, C. J.; Naven, R. T.; Minshull, C. A.; Pauptit, R. A.; Tucker, J. A.; Pease, J. E. Cyclin-dependent kinase 4 inhibitors as a treatment for cancer. Part 1: identification and optimisation of substituted 4,6-Bis anilino pyrimidines. *Bioorg. Med. Chem. Lett.* **2003**, *13* (18), 2955-2960.

123.   Vidler, L. R.; Filippakopoulos, P.; Fedorov, O.; Picaud, S.; Martin, S.; Tomsett, M.; Woodward, H.; Brown, N.; Knapp, S.; Hoelder, S. Discovery of Novel Small-Molecule

Inhibitors of BRD4 Using Structure-Based Virtual Screening. *J. Med. Chem.* **2013**, *56* (20), 8073-8088.

124.   Mikol, V.; Papageorgiou, C.; Borer, X. The Role of Water Molecules in the Structure-Based Design of (5-Hydroxynorvaline)-2-cyclosporin: Synthesis, Biological Activity, and Crystallographic Analysis with Cyclophilin A. *J. Med. Chem.* **1995**, *38* (17), 3361-3367.

125.   Guimarães, C. R. W.; Mathiowetz, A. M. Addressing Limitations with the MM-GB/SA Scoring Procedure using the WaterMap Method and Free Energy Perturbation Calculations. *J. Chem. Inf. Model.* **2010**, *50* (4), 547-559.

126.   Higgs, C.; Beuming, T.; Sherman, W. Hydration Site Thermodynamics Explain SARs for Triazolylpurines Analogues Binding to the A2A Receptor. *ACS Med. Chem. Lett.* **2010**, *1* (4), 160-164.

127.   Beuming, T.; Farid, R.; Sherman, W. High-energy water sites determine peptide binding affinity and specificity of PDZ domains. *Protein Sci.* **2009**, *18* (8), 1609-1619.

128.   Robinson, D. D.; Sherman, W.; Farid, R. Understanding Kinase Selectivity Through Energetic Analysis of Binding Site Waters. *ChemMedChem* **2010**, *5* (4), 618-627.

129.   Kawasaki, Y.; Chufan, E. E.; Lafont, V.; Hidaka, K.; Kiso, Y.; Mario Amzel, L.; Freire, E. How Much Binding Affinity Can be Gained by Filling a Cavity? *Chem. Biol. Drug Des.* **2010**, *75* (2), 143-151.

130.   Whitesides, G. M.; Krishnamurthy, V. M. Designing ligands to bind proteins. *Q. R. Biophys.* **2005**, *38* (04), 385-395.

131.   Freire, E. Do enthalpy and entropy distinguish first in class from best in class? *Drug Discov. Today* **2008**, *13* (19-20), 869-874.

132.   Ferenczy, G. G.; Keserü, G. M. Thermodynamics guided lead discovery and optimization. *Drug Discov. Today* **2010**, *15* (21-22), 919-932.

133.   Mohan, V.; Gibbs, A. C.; Cummings, M. D.; Jaeger, E. P.; DesJarlais, R. L. Docking: Successes and Challenges. Curr. Pharm. Design **2005** *11* (3), 323-333.

134.   de Kloe, G. E.; Bailey, D.; Leurs, R.; de Esch, I. J. P. Transforming fragments into candidates: small becomes big in medicinal chemistry. *Drug Discov. Today* **2009**, *14* (13-14), 630-646.

135.   Goodford, P. J. A computational procedure for determining energetically favorable binding sites on biologically important macromolecules. *J. Med. Chem.* **1985**, *28* (7), 849-857.

136.   She, P.; Reid, T. M.; Bronson, S. K.; Vary, T. C.; Hajnal, A.; Lynch, C. J.; Hutson, S. M. Disruption of BCATm in Mice Leads to Increased Energy Expenditure Associated with the Activation of a Futile Protein Turnover Cycle. *Cell Metab.* **2007**, *6* (3), 181-194.

137.   She, P.; Zhou, Y.; Zhang, Z.; Griffin, K.; Gowda, K.; Lynch, C. J. Disruption of BCAA metabolism in mice impairs exercise metabolism and endurance. *J. Appl. Physiol.* **2010**, *108* (4), 941-949.

138.   Yennawar, N.; Dunbar, J.; Conway, M.; Hutson, S.; Farber, G. The structure of human mitochondrial branched--chain aminotransferase. *Acta Cryst. D* **2001**, *57* (4), 506-515.

139.   Susan, H. Structure and function of branched chain aminotransferases. *Prog. Nucleic Acid Res.* **2001**, *70*, 175-206.

140.   Yennawar, N. H.; Conway, M. E.; Yennawar, H. P.; Farber, G. K.; Hutson, S. M. Crystal Structures of Human Mitochondrial Branched Chain Aminotransferase Reaction Intermediates: Ketimine and Pyridoxamine Phosphate Forms. *Biochemistry* **2002**, *41* (39), 11592-11601.

141.   Davoodi, J.; Drown, P. M.; Bledsoe, R. K.; Wallin, R.; Reinhart, G. D.; Hutson, S. M. Overexpression and Characterization of the Human Mitochondrial and Cytosolic Branched-chain Aminotransferases. *J.Biol. Chem.* **1998**, *273* (9), 4982-4989.

142.   Sweatt, A. J.; Wood, M.; Suryawan, A.; Wallin, R.; Willingham, M. C.; Hutson, S. M. Branched-chain amino acid catabolism: unique segregation of pathway enzymes in organ systems and peripheral nerves. *Am. J. Physiol. -Endoc. M.* **2004**, *286* (1), E64-E76.

143.   Sweatt, A. J.; Garcia-Espinosa, M. A.; Wallin, R.; Hutson, S. M. Branched-chain amino acids and neurotransmitter metabolism: Expression of cytosolic branched-chain aminotransferase (BCATc) in the cerebellum and hippocampus. *J. Comp. Neurol.* **2004**, *477* (4), 360-370.

144.   García-Espinosa, M. A.; Wallin, R.; Hutson, S. M.; Sweatt, A. J. Widespread neuronal expression of branched-chain aminotransferase in the CNS: implications for leucine/glutamate metabolism and for signaling by amino acids. *J. Neurochem.* **2007**, *100* (6), 1458-1468.

145.   Hutson, S. M.; Berkich, D.; Drown, P.; Xu, B.; Aschner, M.; LaNoue, K. F. Role of branched-chain aminotransferase isoenzymes and gabapentin in neurotransmitter metabolism. *J. Neurochem.* **1998**, *71* (2), 863-874.

146.   Hu, L. Y.; Boxer, P. A.; Kesten, S. R.; Lei, H. J.; Wustrow, D. J.; Moreland, D. W.; Zhang, L.; Ahn, K.; Ryder, T. R.; Liu, X.; Rubin, J. R.; Fahnoe, K.; Carroll, R. T.; Dutta, S.; Fahnoe, D. C.; Probert, A. W.; Roof, R. L.; Rafferty, M. F.; Kostlan, C. R.; Scholten, J. D.; Hood, M.; Ren, X. D.; Schielke, G. P.; Su, T. Z.; Taylor, C. P.; Mistry, A.; McConnell, P.; Hasemann, C.; Ohren, J. The design and synthesis of human branched-chain amino acid aminotransferase inhibitors for treatment of neurodegenerative diseases. *Bioorg. Med. Chem. Lett.* **2006**, *16* (9), 2337-2340.

147.   Mendoza, R.; Petros, A. M.; Liu, Y.; Thimmapaya, R.; Surowy, C. S.; Leise, W. F.; Pereda-Lopez, A.; Panchal, S. C.; Sun, C. Cracking the molecular weight barrier: Fragment screening of an aminotransferase using an NMR-based functional assay. *Bioorg. Med. Chem. Lett.* **2011**, *21* (18), 5248-5250.

148.   Meyer, B.; Peters, T. NMR Spectroscopy Techniques for Screening and Identifying Ligand Binding to Protein Receptors. *Angew. Chem. Int. Ed.* **2003**, *42* (8), 864-890.

149. Schiebel, J.; Radeva, N.; Köster, H.; Metz, A.; Krotzky, T.; Kuhnert, M.; Diederich, W. E.; Heine, A.; Neumann, L.; Atmanene, C.; Roecklin, D.; Vivat-Hannah, V.; Renaud, J. P.; Meinecke, R.; Schlinck, N.; Sitte, A.; Popp, F.; Zeeb, M.; Klebe, G. One Question, Multiple Answers: Biochemical and Biophysical Screening Methods Retrieve Deviating Fragment Hit Lists. *ChemMedChem* **2015**, *10* (9), 1511-1521.

150. Baldi, P.; Nasr, R. When is Chemical Similarity Significant? The Statistical Distribution of Chemical Similarity Scores and Its Extreme Values. *J. Chem. Inf. Model.* **2010**, *50* (7), 1205-1222.

151. Borthwick, J. A.; Ancellin, N.; Bertrand, S. M.; Bingham, R. P.; Carter, P. S.; Chung, C. w.; Churcher, I.; Dodic, N.; Fournier, C. n.; Francis, P. L.; Hobbs, A.; Jamieson, C.; Pickett, S. D.; Smith, S. E.; Somers, D. O.; Spitzfaden, C.; Suckling, C. J.; Young, R. J. Structurally Diverse Mitochondrial Branched Chain Aminotransferase (BCATm) Leads with Varying Binding Modes Identified by Fragment Screening. *J. Med. Chem.* **2016**, *59* (6), 2452-2467.

152. Anandan, S. K.; Do, Z. N.; Webb, H. K.; Patel, D. V.; Gless, R. D. Non-urea functionality as the primary pharmacophore in soluble epoxide hydrolase inhibitors. *Bioorg.Med. Chem. Lett.* **2009**, *19* (4), 1066-1070.

153. Bertrand, S. M.; Ancellin, N.; Beaufils, B.; Bingham, R. P.; Borthwick, J. A.; Boullay, A. B.; Boursier, E.; Carter, P. S.; Chung, C. w.; Churcher, I.; Dodic, N.; Fouchet, M. H.; Fournier, C.; Francis, P. L.; Gummer, L. A.; Herry, K.; Hobbs, A.; Hobbs, C. I.; Homes, P.; Jamieson, C.; Nicodeme, E.; Pickett, S. D.; Reid, I. H.; Simpson, G. L.; Sloan, L. A.; Smith, S. E.; Somers, D. O.; Spitzfaden, C.; Suckling, C. J.; Valko, K.; Washio, Y.; Young, R. J. The Discovery of in Vivo Active Mitochondrial Branched-Chain Aminotransferase (BCATm) Inhibitors by Hybridizing Fragment and HTS Hits. *J. Med. Chem.* **2015**, *58* (18), 7140-7163.

154. Scanlon, M. Inhibitors of BCATm: A Tough Nut To Crack. *J. Med. Chem.* **2015**, *58* (18), 7138-7139.

155. Giannella, M.; Gualtieri, F.; Melchiorre, C. Benzisoxazole and benzisothiazole analogs of auxin. *Phytochemistry* **1971**, *10* (3), 539-544.

156. Zhao, P. L.; Wang, L.; Zhu, X. L.; Huang, X.; Zhan, C. G.; Wu, J. W.; Yang, G. F. Subnanomolar Inhibitor of Cytochrome bc1 Complex Designed by Optimizing Interaction with Conformationally Flexible Residues. *J. Am. Chem. Soc.* **2009**, *132* (1), 185-194.

157. Jung, J. C.; Jung, Y. J.; Park, O. S. A convenient one-pot synthesis of 4-hydroxycoumarin, 4-hydroxythiocoumarin and 4-hydroxyquinolin-2-one. *Synthetic Commun.* **2001**, *31* (8), 1195-1200.

158. Nolan, K. A.; Doncaster, J. R.; Dunstan, M. S.; Scott, K. A.; Frenkel, A. D.; Siegel, D.; Ross, D.; Barnes, J.; Levy, C.; Leys, D.; Whitehead, R. C.; Stratford, I. J.; Bryce, R. A. Synthesis and Biological Evaluation of Coumarin-Based Inhibitors of NAD(P)H: Quinone Oxidoreductase-1 (NQO1). *J. Med. Chem.* **2009**, *52* (22), 7142-7156.

159. Roma, G.; Braccio, M. D.; Carrieri, A.; Grossi, G.; Leoncini, G.; Grazia Signorello, M.; Carotti, A. Coumarin, chromone, and 4(3H)-pyrimidinone novel bicyclic and tricyclic

derivatives as antiplatelet agents: synthesis, biological evaluation, and comparative molecular field analysis. *Bioorg. Med. Chem.* **2003**, *11* (1), 123-138.

160.   Humbert, D.; Clemence, F.; Dagnaux, M. Substituted derivatives of [4H]-1,3-benzodioxin-2-carboxylic acids. DE2917902A1, Nov 15, **1979**.

161.   Ogawa, A.; Kambe, N.; Murai, S.; Sonoda, N. Selenium assisted carbonylation of alkyl aryl ketones with carbon monoxide. *Tetrahedron* **1985**, *41* (21), 4813-4819.

162.   Kalinin, A. V.; da Silva, A. J. M.; Lopes, C. C.; Lopes, R. S. C.; Snieckus, V. Directed ortho Metalation - Cross Coupling Links. Carbamoyl Rendition of the Baker-Venkataraman Rearrangement. Regiospecific Route to Substituted 4-Hydroxycoumarins. *Tetrahedron Lett.* **1998**, *39* (28), 4995-4998.

163.   Dittmer, D. C.; Li, Q.; Avilov, D. V. Synthesis of Coumarins, 4-Hydroxycoumarins, and 4-Hydroxyquinolinones by Tellurium-Triggered Cyclizations1. *J. Org. Chem.* **2005**, *70* (12), 4682-4686.

164.   Gao, W. T.; Hou, W. D.; Zheng, M. R.; Tang, L. J. Clean and Convenient One-Pot Synthesis of 4-Hydroxycoumarin and 4-Hydroxy-2-quinolinone Derivatives. *Synthetic Commun.* **2010**, *40* (5), 732-738.

165.   Monnier, F.; Taillefer, M. Catalytic C-C, C-N, and C-O Ullmann-Type Coupling Reactions. *Angew. Chem. Int. Ed.* **2009**, *48* (38), 6954-6971.

166.   Beletskaya, I. P.; Cheprakov, A. V. Copper in cross-coupling reactions: The post-Ullmann chemistry. *Coordin. Chem. Rev.* **2004**, *248* (21-24), 2337-2364.

167.   Soula, G. Tris(polyoxaalkyl)amines (trident), a new class of solid-liquid phase-transfer catalysts. *J. Org. Chem.* **1985**, *50* (20), 3717-3721.

168.   Ouali, A.; Spindler, J. F.; Jutand, A.; Taillefer, M. Nitrogen Ligands in Copper-Catalyzed Arylation of Phenols: Structure/Activity Relationships and Applications. *Adv. Synth. Catal.* **2007**, *349* (11-12), 1906-1916.

169.   Taylor, E. C.; Hartke, K. S. The Reaction of Malononitrile with Substituted Hydrazines: New Routes to 4-Aminopyrazolo[3,4-*d*]pyrimidines1,2. *J. Am. Chem. Soc.* **1959**, *81* (10), 2456-2464.

170.   Hopkins, A. L.; Keseru, G. M.; Leeson, P. D.; Rees, D. C.; Reynolds, C. H. The role of ligand efficiency metrics in drug discovery. *Nat. Rev. Drug Discov.* **2014**, *13* (2), 105-121.

171.   Oprea, T. I.; Davis, A. M.; Teague, S. J.; Leeson, P. D. Is There a Difference between Leads and Drugs? A Historical Perspective. *J. Chem. Inf. Comp. Sci.* **2001**, *41* (5), 1308-1315.

172.   Proudfoot, J. R. Drugs, leads, and drug-likeness: an analysis of some recently launched drugs. *Bioorg. Med. Chem. Lett.* **2002**, *12* (12), 1647-1650.

173.   Perola, E. An Analysis of the Binding Efficiencies of Drugs and Their Leads in Successful Drug Discovery Programs. *J.Med. Chem.* **2010**, *53* (7), 2986-2997.

174. Hann, M. M.; Oprea, T. I. Pursuing the leadlikeness concept in pharmaceutical research. *Curr. Opin. Chem. Biol.* **2004**, *8* (3), 255-263.

175. Congreve, M.; Carr, R.; Murray, C.; Jhoti, H. A Rule of Three for fragment-based lead discovery? *Drug Discov. Today* **2003**, *8* (19), 876-877.

176. Tarcsay, Á.; Nyíri, K.; Keserü, G. M. Impact of Lipophilic Efficiency on Compound Quality. *J. Med. Chem.* **2012**, *55* (3), 1252-1260.

177. http://www.daylight.com/dayhtml/doc/theory/theory.smarts.html

178. Weininger, D. SMILES, a chemical language and information system. 1. Introduction to methodology and encoding rules. *J.Chem. Inform. Comp. Sci.* **1988**, *28* (1), 31-36.

179. http://spotfire.tibco.com/

180. Hajduk, P. J. Fragment-Based Drug Design: How Big Is Too Big? *J. Med. Chem.* **2006**, *49* (24), 6972-6976.

181. Erlanson, D. A. Introduction to Fragment-Based Drug Discovery. In *Fragment-Based Drug Discovery and X-Ray Crystallography*, 317 ed.; Davies, T. G., Hyvönen, M., Eds.; Springer Berlin Heidelberg: **2012**; pp 1-32.

182. http://www.citeline.com/products/pharmaprojects/.

183. http://www.cas.org/products/scifinder.

184. Acton, J. J.; Akiyama, T. E.; Chang, C. H.; Colwell, L.; Debenham, S.; Doebber, T.; Einstein, M.; Liu, K.; McCann, M. E.; Moller, D. E.; Muise, E. S.; Tan, Y.; Thompson, J. R.; Wong, K. K.; Wu, M.; Xu, L.; Meinke, P. T.; Berger, J. P.; Wood, H. B. Discovery of (2R)-2-(3-{3-[(4-Methoxyphenyl)carbonyl]-2-methyl-6-(trifluoromethoxy)-1H-indol-1-yl}phenoxy)butanoic Acid (MK-0533): A Novel Selective Peroxisome Proliferator-Activated Receptor g Modulator for the Treatment of Type 2 Diabetes Mellitus with a Reduced Potential to Increase Plasma and Extracellular Fluid Volume. *J. Med. Chem.* **2009**, *52* (13), 3846-3854.

185. Anselm, L.; Banner, D. W.; Benz, J.; Groebke Zbinden, K.; Himber, J.; Hilpert, H.; Huber, W.; Kuhn, B.; Mary, J. L.; Otteneder, M. B.; Panday, N.; Ricklin, F.; Stahl, M.; Thomi, S.; Haap, W. Discovery of a factor Xa inhibitor (3R,4R)-1-(2,2-difluoro-ethyl)-pyrrolidine-3,4-dicarboxylic acid 3-[(5-chloro-pyridin-2-yl)-amide] 4-{[2-fluoro-4-(2-oxo-2H-pyridin-1-yl)-phenyl]-amide} as a clinical candidate. *Bioorg. Med. Chem. Lett.* **2010**, *20* (17), 5313-5319.

186. Artis, D. R.; Lin, J. J.; Zhang, C.; Wang, W.; Mehra, U.; Perreault, M.; Erbe, D.; Krupka, H. I.; England, B. P.; Arnold, J.; Plotnikov, A. N.; Marimuthu, A.; Nguyen, H.; Will, S.; Signaevsky, M.; Kral, J.; Cantwell, J.; Settachatgull, C.; Yan, D. S.; Fong, D.; Oh, A.; Shi, S.; Womack, P.; Powell, B.; Habets, G.; West, B. L.; Zhang, K. Y. J.; Milburn, M. V.; Vlasuk, G. P.; Hirth, K. P.; Nolop, K.; Bollag, G.; Ibrahim, P. N.; Tobin, J. F. Scaffold-based discovery of indeglitazar, a PPAR pan-active anti-diabetic agent. *Proc. Natl. Acad. Sci.* **2009**, *106* (1), 262-267.

187.   Bebbington, D.; Binch, H.; Charrier, J. D.; Everitt, S.; Fraysse, D.; Golec, J.; Kay, D.; Knegtel, R.; Mak, C.; Mazzei, F.; Miller, A.; Mortimore, M.; O'Donnell, M.; Patel, S.; Pierard, F.; Pinder, J.; Pollard, J.; Ramaya, S.; Robinson, D.; Rutherford, A.; Studley, J.; Westcott, J. The discovery of the potent aurora inhibitor MK-0457 (VX-680). *Bioorg. Med. Chem. Lett.* **2009**, *19* (13), 3586-3592.

188.   Bold, G.; Altmann, K. H.; Frei, J.; Lang, M.; Manley, P. W.; Traxler, P.; Wietfeld, B.; Brüggen, J.; Buchdunger, E.; Cozens, R.; Ferrari, S.; Furet, P.; Hofmann, F.; Martiny-Baron, G.; Mestan, J.; Rösel, J.; Sills, M.; Stover, D.; Acemoglu, F.; Boss, E.; Emmenegger, R.; Lässer, L.; Masso, E.; Roth, R.; Schlachter, C.; Vetterli, W.; Wyss, D.; Wood, J. M. New Anilinophthalazines as Potent and Orally Well Absorbed Inhibitors of the VEGF Receptor Tyrosine Kinases Useful as Antagonists of Tumor-Driven Angiogenesis. *J. Med. Chem.* **2000**, *43* (12), 2310-2323.

189.   Brasca, M. G.; Amboldi, N.; Ballinari, D.; Cameron, A.; Casale, E.; Cervi, G.; Colombo, M.; Colotta, F.; Croci, V.; D'Alessio, R.; Fiorentini, F.; Isacchi, A.; Mercurio, C.; Moretti, W.; Panzeri, A.; Pastori, W.; Pevarello, P.; Quartieri, F.; Roletto, F.; Traquandi, G.; Vianello, P.; Vulpetti, A.; Ciomei, M. Identification of N,1,4,4-Tetramethyl-8-[189]-4,5-dihydro-1H-pyrazolo[4,3-h]quinazoline-3-carboxamide (PHA-848125), a Potent, Orally Available Cyclin Dependent Kinase Inhibitor. *J. Med. Chem.* **2009**, *52* (16), 5152-5163.

190.   Brough, P. A.; Aherne, W.; Barril, X.; Borgognoni, J.; Boxall, K.; Cansfield, J. E.; Cheung, K. M.; Collins, I.; Davies, N. G. M.; Drysdale, M. J.; Dymock, B.; Eccles, S. A.; Finch, H.; Fink, A.; Hayes, A.; Howes, R.; Hubbard, R. E.; James, K.; Jordan, A. M.; Lockie, A.; Martins, V.; Massey, A.; Matthews, T. P.; McDonald, E.; Northfield, C. J.; Pearl, L. H.; Prodromou, C.; Ray, S.; Raynaud, F. I.; Roughley, S. D.; Sharp, S. Y.; Surgenor, A.; Walmsley, D. L.; Webb, P.; Wood, M.; Workman, P.; Wright, L. 4,5-Diarylisoxazole Hsp90 Chaperone Inhibitors: Potential Therapeutic Agents for the Treatment of Cancer. *J. Med. Chem.* **2007**, *51* (2), 196-218.

191.   Cai, Z. w.; Zhang, Y.; Borzilleri, R. M.; Qian, L.; Barbosa, S.; Wei, D.; Zheng, X.; Wu, L.; Fan, J.; Shi, Z.; Wautlet, B. S.; Mortillo, S.; Jeyaseelan, R.; Kukral, D. W.; Kamath, A.; Marathe, P.; D'Arienzo, C.; Derbin, G.; Barrish, J. C.; Robl, J. A.; Hunt, J. T.; Lombardo, L. J.; Fargnoli, J.; Bhide, R. S. Discovery of Brivanib Alaninate ((S)-((R)-1-(4-(4-Fluoro-2-methyl-1H-indol-5-yloxy)-5-methylpyrrolo[2,1-f][1,2,4]triazin-6-yloxy)propan-2-yl)2-aminopropanoate), A Novel Prodrug of Dual Vascular Endothelial Growth Factor Receptor-2 and Fibroblast Growth Factor Receptor-1 Kinase Inhibitor (BMS-540215). *J. Med. Chem.* **2008**, *51* (6), 1976-1980.

192.   Cantello, B. C. C.; Cawthorne, M. A.; Cottam, G. P.; Duff, P. T.; Haigh, D.; Hindley, R. M.; Lister, C. A.; Smith, S. A.; Thurlby, P. L. [[w.-(Heterocyclylamino)alkoxy]benzyl]-2,4-thiazolidinediones as potent antihyperglycemic agents. *J. Med. Chem.* **1994**, *37* (23), 3977-3985.

193.   Claridge, S.; Raeppel, F.; Granger, M. C.; Bernstein, N.; Saavedra, O.; Zhan, L.; Llewellyn, D.; Wahhab, A.; Deziel, R.; Rahil, J.; Beaulieu, N.; Nguyen, H.; Dupont, I.; Barsalou, A.; Beaulieu, C.; Chute, I.; Gravel, S.; Robert, M. F.; Lefebvre, S.; Dubay, M.; Pascal, R.; Gillespie, J.; Jin, Z.; Wang, J.; Besterman, J. M.; MacLeod, A. R.; Vaisburg, A. Discovery of a novel and potent series of thieno[3,2-b]pyridine-based inhibitors of c-Met and VEGFR2 tyrosine kinases. *Bioorg. Med. Chem. Lett.* **2008**, *18* (9), 2793-2798.

194.   Dai, Y.; Hartandi, K.; Ji, Z.; Ahmed, A. A.; Albert, D. H.; Bauch, J. L.; Bouska, J. J.; Bousquet, P. F.; Cunha, G. A.; Glaser, K. B.; Harris, C. M.; Hickman, D.; Guo, J.; Li, J.; Marcotte, P. A.; Marsh, K. C.; Moskey, M. D.; Martin, R. L.; Olson, A. M.; Osterling, D. J.; Pease, L. J.; Soni, N. B.; Stewart, K. D.; Stoll, V. S.; Tapang, P.; Reuter, D. R.; Davidsen, S. K.; Michaelides, M. R. Discovery of N-(4-(3-Amino-1H-indazol-4-yl)phenyl)-N'-(2-fluoro-5-methylphenyl)urea (ABT-869), a 3-Aminoindazole-Based Orally Active Multitargeted Receptor Tyrosine Kinase Inhibitor. *J. Med. Chem.* **2007**, *50* (7), 1584-1597.

195.   Fancelli, D.; Moll, J.; Varasi, M.; Bravo, R.; Artico, R.; Berta, D.; Bindi, S.; Cameron, A.; Candiani, I.; Cappella, P.; Carpinelli, P.; Croci, W.; Forte, B.; Giorgini, M. L.; Klapwijk, J.; Marsiglio, A.; Pesenti, E.; Rocchetti, M.; Roletto, F.; Severino, D.; Soncini, C.; Storici, P.; Tonani, R.; Zugnoni, P.; Vianello, P. 1,4,5,6-Tetrahydropyrrolo[3,4-c]pyrazoles:Identification of a Potent Aurora Kinase Inhibitor with a Favorable Antitumor Kinase Inhibition Profile. *J. Med. Chem.* **2006**, *49* (24), 7247-7251.

196.   Fujimoto, T.; Imaeda, Y.; Konishi, N.; Hiroe, K.; Kawamura, M.; Textor, G. P.; Aertgeerts, K.; Kubo, K. Discovery of a Tetrahydropyrimidin-2(1H)-one Derivative (TAK-442) as a Potent, Selective, and Orally Active Factor Xa Inhibitor. *J. Med. Chem.* **2010**, *53* (9), 3517-3531.

197.   Gingrich, D. E.; Reddy, D. R.; Iqbal, M. A.; Singh, J.; Aimone, L. D.; Angeles, T. S.; Albom, M.; Yang, S.; Ator, M. A.; Meyer, S. L.; Robinson, C.; Ruggeri, B. A.; Dionne, C. A.; Vaught, J. L.; Mallamo, J. P.; Hudkins, R. L. A New Class of Potent Vascular Endothelial Growth Factor Receptor Tyrosine Kinase Inhibitors: Structure-Activity Relationships for a Series of 9-Alkoxymethyl-12-(3-hydroxypropyl)indeno[2,1-a]pyrrolo[3,4-c]carbazole-5-ones and the Identification of CEP-5214 and Its Dimethylglycine Ester Prodrug Clinical Candidate CEP-7055. *J. Med. Chem.* **2003**, *46* (25), 5375-5388.

198.   Guertin, K. R.; Gardner, C. J.; Klein, S. I.; Zulli, A. L.; Czekaj, M.; Gong, Y.; Spada, A. P.; Cheney, D. L.; Maignan, S.; Guilloteau, J. P.; Brown, K. D.; Colussi, D. J.; Chu, V.; Heran, C. L.; Morgan, S. R.; Bentley, R. G.; Dunwiddie, C. T.; Leadley, R. J.; Pauls, H. W. Optimization of the b-Aminoester class of factor Xa inhibitors. part 2: Identification of FXV673 as a potent and selective inhibitor with excellent In vivo anticoagulant activity. *Bioorg. Med. Chem. Lett.* **2002**, *12* (12), 1671-1674.

199.   Harris, P. A.; Boloor, A.; Cheung, M.; Kumar, R.; Crosby, R. M.; Davis-Ward, R. G.; Epperly, A. H.; Hinkle, K. W.; Hunter, R. N.; Johnson, J. H.; Knick, V. B.; Laudeman, C. P.; Luttrell, D. K.; Mook, R. A.; Nolte, R. T.; Rudolph, S. K.; Szewczyk, J. R.; Truesdale, A. T.; Veal, J. M.; Wang, L.; Stafford, J. A. Discovery of 5-[[4-[(2,3-Dimethyl-2H-indazol-6-yl)methylamino]-2-pyrimidinyl]amino]-2-methyl-benzenesulfonamide (Pazopanib), a Novel and Potent Vascular Endothelial Growth Factor Receptor Inhibitor. *J. Med. Chem.* **2008**, *51* (15), 4632-4640.

200.   Hennequin, L. F.; Thomas, A. P.; Johnstone, C.; Stokes, E. S. E.; Plé, P. A.; Lohmann, J. J.; Ogilvie, D. J.; Dukes, M.; Wedge, S. R.; Curwen, J. O.; Kendrew, J.; Lambert-van der Brempt, C. Design and Structure-Activity Relationship of a New Class of Potent VEGF Receptor Tyrosine Kinase Inhibitors. *J. Med. Chem.* **1999**, *42* (26), 5369-5389.

201.   Hirayama, F.; Koshio, H.; Ishihara, T.; Hachiya, S.; Sugasawa, K.; Koga, Y.; Seki, N.; Shiraki, R.; Shigenaga, T.; Iwatsuki, Y.; Moritani, Y.; Mori, K.; Kadokura, T.; Kawasaki, T.; Matsumoto, Y.; Sakamoto, S.; Tsukamoto, S. i. Discovery of N-[2-Hydroxy-6-(4-

methoxybenzamido)phenyl]-4- (4-methyl-1,4-diazepan-1-yl)benzamide (Darexaban, YM150) as a Potent and Orally Available Factor Xa Inhibitor. *J. Med. Chem.* **2011**, *54* (23), 8051-8065.

202.   Howard, S.; Berdini, V.; Boulstridge, J. A.; Carr, M. G.; Cross, D. M.; Curry, J.; Devine, L. A.; Early, T. R.; Fazal, L.; Gill, A. L.; Heathcote, M.; Maman, S.; Matthews, J. E.; McMenamin, R. L.; Navarro, E. F.; O'Brien, M. A.; O'Reilly, M.; Rees, D. C.; Reule, M.; Tisi, D.; Williams, G.; Vinkovic, M.; Wyatt, P. G. Fragment-Based Discovery of the Pyrazol-4-yl Urea (AT9283), a Multitargeted Kinase Inhibitor with Potent Aurora Kinase Activity. *J. Med. Chem.* **2008**, *52* (2), 379-388.

203.   Kohrt, J. T.; Bigge, C. F.; Bryant, J. W.; Casimiro-Garcia, A.; Chi, L.; Cody, W. L.; Dahring, T.; Dudley, D. A.; Filipski, K. J.; Haarer, S.; Heemstra, R.; Janiczek, N.; Narasimhan, L.; McClanahan, T.; Peterson, J. T.; Sahasrabudhe, V.; Schaum, R.; Van Huis, C. A.; Welch, K. M.; Zhang, E.; Leadley, R. J.; Edmunds, J. J. The Discovery of (2R,4R)-N- (4-chlorophenyl)-N- (2-fluoro-4-(2-oxopyridin-1(2H)-yl)phenyl)-4-methoxypyrrolidine-1,2-dicarboxamide (PD 0348292), an Orally Efficacious Factor Xa Inhibitor. *Chem. Biol. Drug Des.* **2007**, *70* (2), 100-112.

204.   Lee, H. W.; Kim, B. Y.; Ahn, J. B.; Kang, S. K.; Lee, J. H.; Shin, J. S.; Ahn, S. K.; Lee, S. J.; Yoon, S. S. Molecular design, synthesis, and hypoglycemic and hypolipidemic activities of novel pyrimidine derivatives having thiazolidinedione. *Eur. J. Med. Chem.* **2005**, *40* (9), 862-874.

205.   Lohray, B. B.; Lohray, V. B.; Bajji, A. C.; Kalchar, S.; Poondra, R. R.; Padakanti, S.; Chakrabarti, R.; Vikramadithyan, R. K.; Misra, P.; Juluri, S.; Mamidi, N. V. S. R.; Rajagopalan, R. (-)3-[4-[2-(Phenoxazin-10-yl)ethoxy]phenyl]-2-ethoxypropanoic Acid [(-)DRF 2725]: A Dual PPAR Agonist with Potent Antihyperglycemic and Lipid Modulating Activity. *J. Med. Chem.* **2001**, *44* (16), 2675-2678.

206.   Miyachi, H.; Nomura, M.; Tanase, T.; Takahashi, Y.; Ide, T.; Tsunoda, M.; Murakami, K.; Awano, K. Design, synthesis and evaluation of substituted phenylpropanoic acid derivatives as peroxisome proliferator-activated receptor (PPAR) activators: novel human PPARα-selective activators. *Bioorg. Med. Chem. Lett.* **2002**, *12* (1), 77-80.

207.   Mortlock, A. A.; Foote, K. M.; Heron, N. M.; Jung, F. H.; Pasquet, G.; Lohmann, J. J.; Warin, N.; Renaud, F.; De Savi, C.; Roberts, N. J.; Johnson, T.; Dousson, C. B.; Hill, G. B.; Perkins, D.; Hatter, G.; Wilkinson, R. W.; Wedge, S. R.; Heaton, S. P.; Odedra, R.; Keen, N. J.; Crafter, C.; Brown, E.; Thompson, K.; Brightwell, S.; Khatri, L.; Brady, M. C.; Kearney, S.; McKillop, D.; Rhead, S.; Parry, T.; Green, S. Discovery, Synthesis, and in Vivo Activity of a New Class of Pyrazoloquinazolines as Selective Inhibitors of Aurora B Kinase. *J. Med. Chem.* **2007**, *50* (9), 2213-2224.

208.   Nomura, M.; Yumoto, K.; Shinozaki, T.; Isogai, S.; Takano, Y.; Murakami, K. Discovery of cyclic amine-substituted benzoic acids as PPARα agonists. *Bioorg. Med. Chem. Lett.* **2012**, *22* (1), 334-338.

209.   Oslob, J. D.; Romanowski, M. J.; Allen, D. A.; Baskaran, S.; Bui, M.; Elling, R. A.; Flanagan, W. M.; Fung, A. D.; Hanan, E. J.; Harris, S.; Heumann, S. A.; Hoch, U.; Jacobs, J. W.; Lam, J.; Lawrence, C. E.; McDowell, R. S.; Nannini, M. A.; Shen, W.; Silverman, J. A.; Sopko, M. M.; Tangonan, B. T.; Teague, J.; Yoburn, J. C.; Yu, C. H.; Zhong, M.;

Zimmerman, K. M.; O'Brien, T.; Lew, W. Discovery of a potent and selective Aurora kinase inhibitor. *Bioorg. Med. Chem. Lett.* **2008**, *18* (17), 4880-4884.

210.   Park, C. M.; Bruncko, M.; Adickes, J.; Bauch, J.; Ding, H.; Kunzer, A.; Marsh, K. C.; Nimmer, P.; Shoemaker, A. R.; Song, X.; Tahir, S. K.; Tse, C.; Wang, X.; Wendt, M. D.; Yang, X.; Zhang, H.; Fesik, S. W.; Rosenberg, S. H.; Elmore, S. W. Discovery of an Orally Bioavailable Small Molecule Inhibitor of Prosurvival B-Cell Lymphoma 2 Proteins. *J. Med. Chem.* **2008**, *51* (21), 6902-6915.

211.   Pinto, D. J. P.; Orwat, M. J.; Koch, S.; Rossi, K. A.; Alexander, R. S.; Smallwood, A.; Wong, P. C.; Rendina, A. R.; Luettgen, J. M.; Knabb, R. M.; He, K.; Xin, B.; Wexler, R. R.; Lam, P. Y. S. Discovery of 1-(4-Methoxyphenyl)-7-oxo-6-(4-(2-oxopiperidin-1-yl)phenyl)-4,5,6,7-tetrahydro- 1H-pyrazolo[3,4-c]pyridine-3-carboxamide (Apixaban, BMS-562247), a Highly Potent, Selective, Efficacious, and Orally Bioavailable Inhibitor of Blood Coagulation Factor Xa. *J. Med. Chem.* **2007**, *50* (22), 5339-5356.

212.   Renhowe, P. A.; Pecchi, S.; Shafer, C. M.; Machajewski, T. D.; Jazan, E. M.; Taylor, C.; Antonios-McCrea, W.; McBride, C. M.; Frazier, K.; Wiesmann, M.; Lapointe, G. R.; Feucht, P. H.; Warne, R. L.; Heise, C. C.; Menezes, D.; Aardalen, K.; Ye, H.; He, M.; Le, V.; Vora, J.; Jansen, J. M.; Wernette-Hammond, M. E.; Harris, A. L. Design, Structure-Activity Relationships and in Vivo Characterization of 4-Amino-3-benzimidazol-2-ylhydroquinolin-2-ones: A Novel Class of Receptor Tyrosine Kinase Inhibitors. *J. Med. Chem.* **2008**, *52* (2), 278-292.

213.   Rheault, T. R.; Stellwagen, J. C.; Adjabeng, G. M.; Hornberger, K. R.; Petrov, K. G.; Waterson, A. G.; Dickerson, S. H.; Mook, R. A.; Laquerre, S. G.; King, A. J.; Rossanese, O. W.; Arnone, M. R.; Smitheman, K. N.; Kane-Carson, L. S.; Han, C.; Moorthy, G. S.; Moss, K. G.; Uehling, D. E. Discovery of Dabrafenib: A Selective Inhibitor of Raf Kinases with Antitumor Activity against B-Raf-Driven Tumors. *ACS Med. Chem. Lett.* **2013**, *4* (3), 358-362.

214.   Roehrig, S.; Straub, A.; Pohlmann, J.; Lampe, T.; Pernerstorfer, J.; Schlemmer, K. H.; Reinemer, P.; Perzborn, E. Discovery of the Novel Antithrombotic Agent 5-Chloro-N-([214]methyl)thiophene- 2-carboxamide (BAY 59-7939):An Oral, Direct Factor Xa Inhibitor. *J. Med. Chem.* **2005**, *48* (19), 5900-5908.

215.   Roth, G. J.; Heckel, A.; Colbatzky, F.; Handschuh, S.; Kley, J.; Lehmann-Lintz, T.; Lotz, R.; Tontsch-Grunt, U.; Walter, R.; Hilberg, F. Design, Synthesis, and Evaluation of Indolinones as Triple Angiokinase Inhibitors and the Discovery of a Highly Specific 6-Methoxycarbonyl-Substituted Indolinone (BIBF 1120). *J. Med. Chem.* **2009**, *52* (14), 4466-4480.

216.   Rowbottom, M. W.; Faraoni, R.; Chao, Q.; Campbell, B. T.; Lai, A. G.; Setti, E.; Ezawa, M.; Sprankle, K. G.; Abraham, S.; Tran, L.; Struss, B.; Gibney, M.; Armstrong, R. C.; Gunawardane, R. N.; Nepomuceno, R. R.; Valenta, I.; Hua, H.; Gardner, M. F.; Cramer, M. D.; Gitnick, D.; Insko, D. E.; Apuy, J. L.; Jones-Bolin, S.; Ghose, A. K.; Herbertz, T.; Ator, M. A.; Dorsey, B. D.; Ruggeri, B.; Williams, M.; Bhagwat, S.; James, J.; Holladay, M. W. Identification of 1-(3-(6,7-Dimethoxyquinazolin-4-yloxy)phenyl)-3-(5-(1,1,1-trifluoro-2-methylpropan-2-yl)isoxazol-3-yl)urea Hydrochloride (CEP-32496), a Highly Potent and Orally Efficacious Inhibitor of V-RAF Murine Sarcoma Viral Oncogene Homologue B1 (BRAF) V600E. *J. Med. Chem.* **2011**, *55* (3), 1082-1105.

217.   Shinkai, H.; Onogi, S.; Tanaka, M.; Shibata, T.; Iwao, M.; Wakitani, K.; Uchida, I. Isoxazolidine-3,5-dione and Noncyclic 1,3-Dicarbonyl Compounds as Hypoglycemic Agents. *J. Med. Chem.* **1998**, *41* (11), 1927-1933.

218.   Sohda, T.; Mizuno, K.; Momose, Y.; Ikeda, H.; Fujita, T.; Meguro, K. Studies on antidiabetic agents. 11. Novel thiazolidinedione derivatives as potent hypoglycemic and hypolipidemic agents. *J. Med. Chem.* **1992**, *35* (14), 2617-2626.

219.   Souers, A. J.; Leverson, J. D.; Boghaert, E. R.; Ackler, S. L.; Catron, N. D.; Chen, J.; Dayton, B. D.; Ding, H.; Enschede, S. H.; Fairbrother, W. J.; Huang, D. C. S.; Hymowitz, S. G.; Jin, S.; Khaw, S. L.; Kovar, P. J.; Lam, L. T.; Lee, J.; Maecker, H. L.; Marsh, K. C.; Mason, K. D.; Mitten, M. J.; Nimmer, P. M.; Oleksijew, A.; Park, C. H.; Park, C. M.; Phillips, D. C.; Roberts, A. W.; Sampath, D.; Seymour, J. F.; Smith, M. L.; Sullivan, G. M.; Tahir, S. K.; Tse, C.; Wendt, M. D.; Xiao, Y.; Xue, J. C.; Zhang, H.; Humerickhouse, R. A.; Rosenberg, S. H.; Elmore, S. W. ABT-199, a potent and selective BCL-2 inhibitor, achieves antitumor activity while sparing platelets. *Nat. Med.* **2013**, *19* (2), 202-208.

220.   Sun, L.; Liang, C.; Shirazian, S.; Zhou, Y.; Miller, T.; Cui, J.; Fukuda, J. Y.; Chu, J. Y.; Nematalla, A.; Wang, X.; Chen, H.; Sistla, A.; Luu, T. C.; Tang, F.; Wei, J.; Tang, C. Discovery of 5-[5-Fluoro-2-oxo-1,2- dihydroindol-(3Z)-ylidenemethyl]-2,4- dimethyl-1H-pyrrole-3-carboxylic Acid (2-Diethylaminoethyl)amide, a Novel Tyrosine Kinase Inhibitor Targeting Vascular Endothelial and Platelet-Derived Growth Factor Receptor Tyrosine Kinase. *J. Med. Chem.* **2003**, *46* (7), 1116-1119.

221.   Tang, P. C.; Su, Y. D.; Feng, J.; Fu, J. H.; Yang, J. L.; Xiao, L.; Peng, J. H.; Li, Y. L.; Zhang, L.; Hu, B.; Zhou, Y.; Li, F. Q.; Fu, B. B.; Lou, L. G.; Gong, A. S.; She, G. H.; Sun, W. H.; Mong, X. T. Novel Potent Orally Active Multitargeted Receptor Tyrosine Kinase Inhibitors: Synthesis, Structure-Activity Relationships, and Antitumor Activities of 2-Indolinone Derivatives. *J. Med. Chem.* **2010**, *53* (22), 8140-8149.

222.   Taygerly, J. P.; McGee, L. R.; Rubenstein, S. M.; Houze, J. B.; Cushing, T. D.; Li, Y.; Motani, A.; Chen, J. L.; Frankmoelle, W.; Ye, G.; Learned, M. R.; Jaen, J.; Miao, S.; Timmermans, P. B.; Thoolen, M.; Kearney, P.; Flygare, J.; Beckmann, H.; Weiszmann, J.; Lindstrom, M.; Walker, N.; Liu, J.; Biermann, D.; Wang, Z.; Hagiwara, A.; Iida, T.; Aramaki, H.; Kitao, Y.; Shinkai, H.; Furukawa, N.; Nishiu, J.; Nakamura, M. Discovery of INT131: A selective PPARɣ modulator that enhances insulin sensitivity. *Bioorg. Med. Chem.* **2013**, *21* (4), 979-992.

223.   Toogood, P. L.; Harvey, P. J.; Repine, J. T.; Sheehan, D. J.; VanderWel, S. N.; Zhou, H.; Keller, P. R.; McNamara, D. J.; Sherry, D.; Zhu, T.; Brodfuehrer, J.; Choi, C.; Barvian, M. R.; Fry, D. W. Discovery of a Potent and Selective Inhibitor of Cyclin-Dependent Kinase 4/6. *J. Med. Chem.* **2005**, *48* (7), 2388-2406.

224.   Tsai, J.; Lee, J. T.; Wang, W.; Zhang, J.; Cho, H.; Mamo, S.; Bremer, R.; Gillette, S.; Kong, J.; Haass, N. K.; Sproesser, K.; Li, L.; Smalley, K. S. M.; Fong, D.; Zhu, Y. L.; Marimuthu, A.; Nguyen, H.; Lam, B.; Liu, J.; Cheung, I.; Rice, J.; Suzuki, Y.; Luu, C.; Settachatgul, C.; Shellooe, R.; Cantwell, J.; Kim, S. H.; Schlessinger, J.; Zhang, K. Y. J.; West, B. L.; Powell, B.; Habets, G.; Zhang, C.; Ibrahim, P. N.; Hirth, P.; Artis, D. R.; Herlyn, M.; Bollag, G. Discovery of a selective inhibitor of oncogenic B-Raf kinase with potent antimelanoma activity. *Proc.Natl. Acad. Sci.* **2008**, *105* (8), 3041-3046.

225. Ueno, H.; Yokota, K.; Hoshi, J. i.; Yasue, K.; Hayashi, M.; Hase, Y.; Uchida, I.; Aisaka, K.; Katoh, S.; Cho, H. Synthesis and Structure-Activity Relationships of Novel Selective Factor Xa Inhibitors with a Tetrahydroisoquinoline Ring. *J. Med. Chem.* **2005**, *48* (10), 3586-3604.

226. Wang, S.; Midgley, C. A.; Scaërou, F.; Grabarek, J. B.; Griffiths, G.; Jackson, W.; Kontopidis, G.; McClue, S. J.; McInnes, C.; Meades, C.; Mezna, M.; Plater, A.; Stuart, I.; Thomas, M. P.; Wood, G.; Clarke, R. G.; Blake, D. G.; Zheleva, D. I.; Lane, D. P.; Jackson, R. C.; Glover, D. M.; Fischer, P. M. Discovery of N-Phenyl-4-(thiazol-5-yl)pyrimidin-2-amine Aurora Kinase Inhibitors. *J. Med. Chem.* **2010**, *53* (11), 4367-4378.

227. William, A. D.; Lee, A. C. H.; Goh, K. C.; Blanchard, S.; Poulsen, A.; Teo, E. L.; Nagaraj, H.; Lee, C. P.; Wang, H.; Williams, M.; Sun, E. T.; Hu, C.; Jayaraman, R.; Pasha, M. K.; Ethirajulu, K.; Wood, J. M.; Dymock, B. W. Discovery of Kinase Spectrum Selective Macrocycle (16E)-14-Methyl-20-oxa-5,7,14,26-tetraazatetracyclo[19.3.1.1(2,6).1(8,12)]heptacosa-1(25),2(26),3,5,8(27),9,11,16,21,23-decaene (SB1317/TG02), a Potent Inhibitor of Cyclin Dependent Kinases (CDKs), Janus Kinase 2 (JAK2), and Fms-like Tyrosine Kinase-3 (FLT3) for the Treatment of Cancer. *J. Med. Chem.* **2011**, *55* (1), 169-196.

228. Woodhead, A. J.; Angove, H.; Carr, M. G.; Chessari, G.; Congreve, M.; Coyle, J. E.; Cosme, J.; Graham, B.; Day, P. J.; Downham, R.; Fazal, L.; Feltell, R.; Figueroa, E.; Frederickson, M.; Lewis, J.; McMenamin, R.; Murray, C. W.; O'Brien, M. A.; Parra, L.; Patel, S.; Phillips, T.; Rees, D. C.; Rich, S.; Smith, D. M.; Trewartha, G.; Vinkovic, M.; Williams, B.; Woolford, A. J. A. Discovery of (2,4-Dihydroxy-5-isopropylphenyl)-[5-(4-methylpiperazin-1-ylmethyl)-1,3-dihydroisoindol-2-yl]methanone (AT13387), a Novel Inhibitor of the Molecular Chaperone Hsp90 by Fragment Based Drug Design. *J. Med. Chem.* **2010**, *53* (16), 5956-5969.

229. Xu, Y.; Mayhugh, D.; Saeed, A.; Wang, X.; Thompson, R. C.; Dominianni, S. J.; Kauffman, R. F.; Singh, J.; Bean, J. S.; Bensch, W. R.; Barr, R. J.; Osborne, J.; Montrose-Rafizadeh, C.; Zink, R. W.; Yumibe, N. P.; Huang, N.; Luffer-Atlas, D.; Rungta, D.; Maise, D. E.; Mantlo, N. B. Design and Synthesis of a Potent and Selective Triazolone-Based Peroxisome Proliferator-Activated Receptor a Agonist. *J. Med. Chem.* **2003**, *46* (24), 5121-5124.

230. Yamazaki, Y.; Abe, K.; Toma, T.; Nishikawa, M.; Ozawa, H.; Okuda, A.; Araki, T.; Oda, S.; Inoue, K.; Shibuya, K.; Staels, B.; Fruchart, J. C. Design and synthesis of highly potent and selective human peroxisome proliferator-activated receptor a-agonists. *Bioorg. Med. Chem. Lett.* **2007**, *17* (16), 4689-4693.

231. Zhang, P.; Huang, W.; Wang, L.; Bao, L.; Jia, Z. J.; Bauer, S. M.; Goldman, E. A.; Probst, G. D.; Song, Y.; Su, T.; Fan, J.; Wu, Y.; Li, W.; Woolfrey, J.; Sinha, U.; Wong, P. W.; Edwards, S. T.; Arfsten, A. E.; Clizbe, L. A.; Kanter, J.; Pandey, A.; Park, G.; Hutchaleelaha, A.; Lambing, J. L.; Hollenbach, S. J.; Scarborough, R. M.; Zhu, B. Y. Discovery of betrixaban (PRT054021), N-(5-chloropyridin-2-yl)-2-(4-(N,N-dimethylcarbamimidoyl)benzamido)-5-methoxybenzamide, a highly potent, selective, and orally efficacious factor Xa inhibitor. *Bioorg. Med. Chem. Lett.* **2009**, *19* (8), 2179-2185.

232. Ge, J.; Normant, E.; Porter, J. R.; Ali, J. A.; Dembski, M. S.; Gao, Y.; Georges, A. T.; Grenier, L.; Pak, R. H.; Patterson, J.; Sydor, J. R.; Tibbitts, T. T.; Tong, J. K.; Adams, J.;

Palombella, V. J. Design, Synthesis, and Biological Evaluation of Hydroquinone Derivatives of 17-Amino-17-demethoxygeldanamycin as Potent, Water-Soluble Inhibitors of Hsp90. *J. Med. Chem.* **2006**, *49* (15), 4606-4615.

233.   Wada, C. K.; Holms, J. H.; Curtin, M. L.; Dai, Y.; Florjancic, A. S.; Garland, R. B.; Guo, Y.; Heyman, H. R.; Stacey, J. R.; Steinman, D. H.; Albert, D. H.; Bouska, J. J.; Elmore, I. N.; Goodfellow, C. L.; Marcotte, P. A.; Tapang, P.; Morgan, D. W.; Michaelides, M. R.; Davidsen, S. K. Phenoxyphenyl Sulfone N-Formylhydroxylamines (Retrohydroxamates) as Potent, Selective, Orally Bioavailable Matrix Metalloproteinase Inhibitors. *J. Med. Chem.* **2001**, *45* (1), 219-232.

234.   MacPherson, L. J.; Bayburt, E. K.; Capparelli, M. P.; Carroll, B. J.; Goldstein, R.; Justice, M. R.; Zhu, L.; Hu, S. i.; Melton, R. A.; Fryer, L.; Goldberg, R. L.; Doughty, J. R.; Spirito, S.; Blancuzzi, V.; Wilson, D.; O'Byrne, E. M.; Ganu, V.; Parker, D. T. Discovery of CGS 27023A, a Non-Peptidic, Potent, and Orally Active Stromelysin Inhibitor That Blocks Cartilage Degradation in Rabbits. *J. Med. Chem.* **1997**, *40* (16), 2525-2532.

235.   Sandanayaka, V.; Mamat, B.; Mishra, R. K.; Winger, J.; Krohn, M.; Zhou, L. M.; Keyvan, M.; Enache, L.; Sullins, D.; Onua, E.; Zhang, J.; Halldorsdottir, G.; Sigthorsdottir, H.; Thorlaksdottir, A.; Sigthorsson, G.; Thorsteinnsdottir, M.; Davies, D. R.; Stewart, L. J.; Zembower, D. E.; Andresson, T.; Kiselyov, A. S.; Singh, J.; Gurney, M. E. Discovery of 4-[(2S)-2-{[4-(4-Chlorophenoxy)phenoxy]methyl}-1-pyrrolidinyl]butanoic Acid (DG-051) as a Novel Leukotriene A4 Hydrolase Inhibitor of Leukotriene B4 Biosynthesis. *J. Med. Chem.* **2009**, *53* (2), 573-585.

236.   Liu, G.; Link, J. T.; Pei, Z.; Reilly, E. B.; Leitza, S.; Nguyen, B.; Marsh, K. C.; Okasinski, G. F.; von Geldern, T. W.; Ormes, M.; Fowler, K.; Gallatin, M. Discovery of Novel p-Arylthio Cinnamides as Antagonists of Leukocyte Function-Associated Antigen-1/Intracellular Adhesion Molecule-1 Interaction. 1. Identification of an Additional Binding Pocket Based on an Anilino Diaryl Sulfide Lead. *J. Med. Chem.* **2000**, *43* (21), 4025-4040.

237.   Zhong, M.; Gadek, T. R.; Bui, M.; Shen, W.; Burnier, J.; Barr, K. J.; Hanan, E. J.; Oslob, J. D.; Yu, C. H.; Zhu, J.; Arkin, M. R.; Evanchik, M. J.; Flanagan, W. M.; Hoch, U.; Hyde, J.; Prabhu, S.; Silverman, J. A.; Wright, J. Discovery and Development of Potent LFA-1/ICAM-1 Antagonist SAR 1118 as an Ophthalmic Solution for Treating Dry Eye. *ACS Med. Chem. Lett.* **2012**, *3* (3), 203-206.

238.   Shetty, R. S.; Lee, Y.; Liu, B.; Husain, A.; Joseph, R. W.; Lu, Y.; Nelson, D.; Mihelcic, J.; Chao, W.; Moffett, K. K.; Schumacher, A.; Flubacher, D.; Stojanovic, A.; Bukhtiyarova, M.; Williams, K.; Lee, K. J.; Ochman, A. R.; Saporito, M. S.; Moore, W. R.; Flynn, G. A.; Dorsey, B. D.; Springman, E. B.; Fujimoto, T.; Kelly, M. J. Synthesis and Pharmacological Evaluation of N-(3-(1H-Indol-4-yl)-5-(2-methoxyisonicotinoyl)phenyl)methanesulfonamide (LP-261), a Potent Antimitotic Agent. *J. Med. Chem.* **2010**, *54* (1), 179-200.

239.   Schroeder, G. M.; An, Y.; Cai, Z. w.; Chen, X. T.; Clark, C.; Cornelius, L. A. M.; Dai, J.; Gullo-Brown, J.; Gupta, A.; Henley, B.; Hunt, J. T.; Jeyaseelan, R.; Kamath, A.; Kim, K.; Lippy, J.; Lombardo, L. J.; Manne, V.; Oppenheimer, S.; Sack, J. S.; Schmidt, R. J.; Shen, G.; Stefanski, K.; Tokarski, J. S.; Trainor, G. L.; Wautlet, B. S.; Wei, D.; Williams, D. K.; Zhang, Y.; Zhang, Y.; Fargnoli, J.; Borzilleri, R. M. Discovery of N-(4-(2-Amino-3-chloropyridin-4-yloxy)-3-fluorophenyl)-4-ethoxy-1-(4-fluorophenyl)-2-oxo-1,2-dihydropyridine-

3-carboxamide (BMS-777607), a Selective and Orally Efficacious Inhibitor of the Met Kinase Superfamily. *J. Med. Chem.* **2009**, *52* (5), 1251-1254.

240. Albrecht, B. K.; Harmange, J. C.; Bauer, D.; Berry, L.; Bode, C.; Boezio, A. A.; Chen, A.; Choquette, D.; Dussault, I.; Fridrich, C.; Hirai, S.; Hoffman, D.; Larrow, J. F.; Kaplan-Lefko, P.; Lin, J.; Lohman, J.; Long, A. M.; Moriguchi, J.; O'Connor, A.; Potashman, M. H.; Reese, M.; Rex, K.; Siegmund, A.; Shah, K.; Shimanovich, R.; Springer, S. K.; Teffera, Y.; Yang, Y.; Zhang, Y.; Bellon, S. F. Discovery and Optimization of Triazolopyridazines as Potent and Selective Inhibitors of the c-Met Kinase. *J. Med. Chem.* **2008**, *51* (10), 2879-2882.

241. Cui, J. J.; McTigue, M.; Nambu, M.; Tran-Dubé, M.; Pairish, M.; Shen, H.; Jia, L.; Cheng, H.; Hoffman, J.; Le, P.; Jalaie, M.; Goetz, G. H.; Ryan, K.; Grodsky, N.; Deng, Y. l.; Parker, M.; Timofeevski, S.; Murray, B. W.; Yamazaki, S.; Aguirre, S.; Li, Q.; Zou, H.; Christensen, J. Discovery of a Novel Class of Exquisitely Selective Mesenchymal-Epithelial Transition Factor (c-MET) Protein Kinase Inhibitors and Identification of the Clinical Candidate 2-(4-(1-(Quinolin-6-ylmethyl)-1H-[1,2,3]triazolo[4,5-b]pyrazin-6-yl)-1H-pyrazol-1-yl)ethanol (PF-04217903) for the Treatment of Cancer. *J. Med. Chem.* **2012**, *55* (18), 8091-8109.

242. http://www.aureus-sciences.com/

243. Huang, S.; Jin, X.; Liu, Z.; Poon, D.; Tellew, J.; Wan, Y.; Wang, X.; Xie, Y. Preparation of sulfonamidophenylimidazolylpyrimidine derivatives and analogs for use as protein kinase inhibitors. WO2011025927A1, Mar 3, **2011**.

244. Bruncko, M.; Ding, H.; Doherty, G.; Elmore, S.; Hasvold, L.; Hexamer, L.; Kunzer, A. R.; Song, X.; Souers, A. J.; Sullivan, G.; Tao, Z. F.; Wang, G. T.; Wang, L.; Wang, X.; Wendt, M.; Mantei, R.; Hansen, T. M. Preparation of N-(phenylsulfonyl)benzamides and N-(3-pyridylsulfonyl)benzamides as apoptosis-inducing agents for the treatment of cancer and immune diseases and autoimmune diseases. WO2010138588A2, Dec 2, **2010**.

245. Adams, J. L.; Dickerson, S. H.; Johnson, N. W.; Kuntz, K.; Petrov, K.; Ralph, J. M.; Rheault, T. R.; Schaaf, G.; Stellwagen, J.; Tian, X.; Uehling, D. E.; Waterson, A. G.; Wilson, B. Preparation of benzenesulfonamidethiazole derivatives and analogs for use as B-Raf protein kinase inhibitors. WO2009137391A2, Nov 12, **2009**.

246. Dimitroff, M.; Miller, B. R.; Stillwell, B. S.; Siesel, D. A.; Swiftney, T.; Diaz, B.; Gu, D.; Van Dyck, J. P.; Ryckman, D.; Poon, D. J.; Pick, T. E. Method for the preparation of benzimidazoles. US20070049622A1, Mar 1, **2007**.

247. Bruncko, M.; Ding, H.; Elmore, S. W.; Kunzer, A. R.; Lynch, C. L.; McClellan, W. J.; Park, C. M.; Song, X.; Wang, X. Benzoyl aminoarylsulfonamide as apoptosis promoters and their preparation, pharmaceutical compositions and use in the treatment of cancers. US20070027135A1, Feb 1, **2007**.

248. Ibrahim, P. N.; Artis, D. R.; Bremer, R.; Mamo, S.; Nespi, M.; Zhang, C.; Zhang, J.; Zhu, Y. L.; Tsai, J.; Hirth, K. P.; Bollag, G.; Spevak, W.; Cho, H.; Gillette, S. J.; Wu, G.; Zhu, H.; Shi, S. Pyrrolo[2,3-b]pyridine derivatives as protein kinase inhibitors and their preparation, pharmaceutical compositions and use in the treatment of diseases. WO2007002325A1, Jan 4, **2007**.

249. Vaisburg, A.; William, S.; Raeppel, F.; Saavedra, O. M.; Berstein, N.; Granger, M. C.; Zhan, L. Thienopyridine and thienopyrimidine derivatives and their preparation, pharmaceutical compositions, and use as inhibitors of VEGF receptor and HGF receptor signaling for treatment of proliferative diseases. WO2006010264A1, Feb 2, **2006**.

250. Fink, B. E.; Gavai, A. V.; Vite, G. D.; Chen, P.; Mastalerz, H.; Norris, D. J.; Tokarski, J. S.; Zhao, Y.; Han, W. C. Preparation of pyrrolo[2,1-f][1,2,4]triazine derivatives as HER1, HER2, and HER4 kinase inhibitors, and antiproliferative agents. WO2005066176A1, Jul 21, **2005**.

251. Bannen, L. C.; Chan, D. S.; Chen, J.; Dalrymple, L. E.; Forsyth, T. P.; Huynh, T. P.; Jammalamadaka, V.; Khoury, R. G.; Leahy, J. W.; Mac, M. B.; Mann, G.; Mann, L. W.; Nuss, J. M.; Parks, J. J.; Takeuchi, C. S.; Wang, Y.; Xu, W. Preparation of quinolines and quinazolines as inhibitors of c-Met and other tyrosine kinases and therapeutic uses against proliferative diseases. WO2005030140A2, Apr 7, **2005**.

252. Dai, Y.; Davidsen, S. K.; Ericsson, A. M.; Hartandi, K.; Ji, Z.; Michaelides, M. R. Preparation of (indazolylphenyl), (benzisoxazolylphenyl), (benzisothiazolylphenyl) ureas and related compounds as protein tyrosine kinase inhibitors for treatment of cancer. WO2004113304A1, Dec 29, **2004**.

253. Attardo, G.; Dairi, K.; Lavallee, J. F.; Rioux, E.; Tripathy, S. Preparation of nitrogen triheterocyclic compounds for treating cancer or viral diseases. WO2004106328A1, Dec 9, **2004**.

254. Dai, Y.; Davidsen, S. K.; Ericsson, A. M.; Hartandi, K.; Ji, Z.; Michaelides, M. R. Preparation of (indazolylphenyl) and (benzisoxazolylphenyl) ureas and related compounds as protein tyrosine kinase inhibitors for treatment of cancer. US20040235892A1, Nov 25, **2004**.

255. Kubo, K.; Sakai, T.; Nagao, R.; Fujiwara, Y.; Isoe, T.; Hasegawa, K. Preparation of quinoline derivatives having azolyl group and quinazoline derivatives as antitumor agents. WO2002088110A1, Nov 7, **2002**.

256. Chen, G.; Adams, J.; Bemis, J.; Booker, S.; Cai, G.; Croghan, M.; DiPietro, L.; Dominguez, C.; Elbaum, D.; Germain, J.; Geuns-Meyer, S.; Handley, M.; Huang, Q.; Kim, J. L.; Kim, T. s.; Kiselyov, A.; Ouyang, X.; Patel, V. F.; Smith, L. M.; Stec, M.; Tasker, A.; Xi, N.; Xu, S.; Yuan, C. C. Preparation of heterocyclylalkylamine derivatives as remedies for angiogenesis mediated diseases. WO2002066470A1, Aug 29, **2002**.

257. Boloor, A.; Cheung, M.; Davis, R.; Harris, P. A.; Hinkle, K.; Mook, R. A.; Stafford, J. A.; Veal, J. M. Preparation of pyrimidinamines as angiogenesis modulators. WO2002059110A1, Aug 1, **2002**.

258. Renhowe, P.; Pecchi, S.; Machajewski, T.; Shafer, C.; Taylor, C.; McCrea, B.; McBride, C.; Jazan, E.; Wernette-Hammond, M. E.; Harris, A. Benzimidazolyl-substituted quinolinone derivatives and analogs, with inhibitory action against vascular endothelial growth factor receptor tyrosine kinase, and useful as anticancer agents. WO2002022598A1, Mar 21, **2002**.

259. Tang, P. C.; Miller, T.; Li, X.; Sun, L.; Wei, C. C.; Shirazian, S.; Liang, C.; Vojkovsky, T.; Nematalla, A. S. Preparation of pyrrole substituted 2-indolinone protein kinase inhibitors for treatment of cancer. WO2001060814A2, Aug 23, **2001**.

260. Hennequin, L. F. A.; Stokes, E. S. E.; Thomas, A. P. Preparation of 4-anilino-7-piperidinyloxyquinazolines as vascular endothelial growth factor inhibitors. WO2001032651A1, May 10, **2001**.

261. Heckel, A.; Roth, G. J.; Walter, R.; Van Meel, J.; Redemann, N.; Tontsch-Grunt, U.; Spevak, W.; Hilberg, F. Preparation of substituted aminomethyleneindolinone inhibitors of tyrosine receptor kinases and CDK/cyclin kinases as antitumor agents and inhibitors of cell proliferation. WO2001027081A1, Apr 19, **2001**.

262. Dumas, J. P.; Joe, T. K.; Kluender, H. C. E.; Lee, W.; Nagarathnam, D.; Sibley, R. N.; Su, N.; Boyer, S. J.; Dixon, J. A. Preparation of substituted pyridines and pyridazines with angiogenesis inhibiting activity for pharmaceutical use as antitumor agents. WO2001023375A2, Apr 5, **2001**.

263. Kania, R. S.; Bender, S. L.; Borchardt, A. J.; Braganza, J. F.; Cripps, S. J.; Hua, Y.; Johnson, M. D.; Johnson, T. O., Jr.; Luu, H. T.; Palmer, C. L.; Reich, S. H.; Tempczyk-russell, A. M.; Teng, M.; Thomas, C.; Varney, M. D.; Wallace, M. B. Indazole compounds and pharmaceutical compositions for inhibiting protein kinases, and methods for their use. WO2001002369A2, Jan 11, **2001**.

264. Hennequin, L. F. A.; Ple, P.; Stokes, E. S. E.; Mckerrecher, D. Preparation of quinazoline derivatives as angiogenesis inhibitors. WO2000047212A1, Aug 17, **2000**.

265. Michaelides, M. R. Preparation of pyrazolylthienopyridinylphenylureas as kinase inhibitors with improved safety profile due to low CYP3A4 inhibition. WO2010065825A2, Jun 10, **2010**.

266. Cee, V. J.; Nguyen, H. N.; Romero, K. Preparation of substituted phthalazinamines as Aurora kinase modulators. US7560551B2, Jul 14, **2009**.

267. Hubert, M. D.; Tremel, J. D.; Frischknecht, K. D.; Truong, N. Flat plate encapsulation assembly for electronic devices. WO2009086228A1, Jul 9, **2009**.

268. Tang, P. C.; Su, Y.; Li, Y.; Zhang, L.; Zhao, F.; Yang, J.; Zhou, Y.; Bie, P.; Qian, G.; Ju, M. Preparation of pyrrolo[3,2-c]azepine-4(1H)-one derivatives as protein kinase inhibitors. WO2008138232A1, Nov 20, **2008**.

269. Claiborne, C. F.; Sells, T. B.; Stroud, S. G. Preparation of [(phenylpyrimidobenzazepinyl)amino]methoxybenzoic acid derivatives for us as antitumor agents. WO2008063525A1, May 29, **2008**.

270. Guzi, T. J.; Paruch, K.; Dwyer, M. P.; Doll, R. J.; Girijavallabhan, V. M.; Mallams, A.; Alvarez, C. S.; Keertikar, K. M.; Rivera, J.; Chan, T. Y.; Madison, V. S.; Fischmann, T. O.; Dillard, L. W.; Tran, V. D.; He, Z.; James, R. A.; Park, H.; Paradkar, V. M.; Hobbs, D. W.; Kirschmeier, P.; Bannerji, R. Preparation of pyrazolopyrimidines as cyclin-dependent kinase inhibitors. US20080050384A1, Feb 28, **2008**.

271.   Cee, V. J.; Deak, H. L.; Du, B.; Geuns-Meyer, S. D.; Hodous, B. L.; Nguyen, H. N.; Olivieri, P. R.; Patel, V. F.; Romero, K.; Schenkel, L. Preparation of substituted phthalazinamines as Aurora kinase modulators. WO2007087276A1, Aug 2, **2007**.

272.   Deng, B.; Su, Y.; Zhang, L.; Xiao, L. Pyrrolo[3,2-c]pyridine-4-one 2-indolinone as protein kinase inhibitors and their preparation, pharmaceutical compositions and use in the treatment of diseases. WO2007085188A1, Aug 2, **2007**.

273.   Arcari, J. T.; Bhattacharya, S. K.; Brosius, A. D.; Luzzio, M. J.; Nelson, K. L.; Pan, G.; Southers, J. A., Jr.; Wishka, D. G.; Xiao, J. Pyrimidine derivatives for the treatment of abnormal cell growth and their preparation. WO2007072158A2, Jun 28, **2007**.

274.   Xiao, X. Y.; Patel, D. V.; Ward, J. S.; Bray, M. R.; Agoston, G. E.; Treston, A. M. Preparation of substituted pyrazole compounds as protein kinase inhibitors. WO2007041358A2, Apr 12, **2007**.

275.   Lal, B.; Joshi, K.; Kulkarni, S.; Mascarenhas, M.; Kamble, S.; Rathos, M. J.; Joshi, R.; Sivakumar, M. Preparation of pyrrolidinylchromenones as inhibitors of cyclin-dependent kinases. US20070015802A1, Jan 18, **2007**.

276.   Berdini, V.; Carr, M. G.; Gill, A. L.; Howard, S.; Navarro, E. F.; Trewartha, G.; Rees, D. C.; Vinkovic, M.; Wyatt, P. G. Preparation of benzimidazolylpyrazole compounds that modulate the activity of cdk, gsk and aurora kinasis. WO2006070195A1, Jul 6, **2006**.

277.   Guzi, T. J.; Paruch, K.; Dwyer, M. P.; Labroli, M.; Keertikar, K. M. Preparation of pyrazolopyrimidines as cyclin-dependent kinase inhibitors. US20060128725A1, Jun 15, **2006**.

278.   Lew, W.; Baskaran, S.; Oslob, J. D.; Yoburn, J. C.; Zhong, M. Thienopyrimidines useful as Aurora kinase inhibitors and their preparation, pharmaceutical compositions, and their use for treatment of Aurora kinase-mediated diseases. US20060035908A1, Feb 16, **2006**.

279.   Claiborne, C. F.; Payne, L. J.; Boyce, R. J.; Sells, T. B.; Stroud, S. G.; Travers, S.; Vos, T. J.; Weatherhead, G. S. Preparation of pyrimidoazepine derivatives and methods for inhibiting mitotic progression. US20050256102A1, Nov 17, **2005**.

280.   Berdini, V.; O'Brien, M. A.; Carr, M. G.; Early, T. R.; Navarro, E. F.; Gill, A. L.; Trewartha, G.; Woolford, A. J.-A.; Woodhead, A. J.; Wyatt, P. G. Preparation of 3,4-disubstituted 1h-pyrazole compounds and their use as cyclin dependent kinases (cdk) and glycogen synthase kinase-3 (gsk-3) modulators. WO2005012256A1, Feb 10, **2005**.

281.   Fancelli, D.; Forte, B.; Moll, J.; Varasi, M.; Vianello, P. Preparation of pyrrolo[3,4-c]pyrazole derivatives active as kinase inhibitors. WO2005005427A1, Jan 20, **2005**.

282.   Guzi, T. J.; Paruch, K.; Dwyer, M. P.; Doll, R. J.; Girijavallabhan, V. M.; Mallams, A.; Alvarez, C. S.; Keertikar, K. M.; Rivera, J.; Chan, T. Y.; Madison, V.; Fischmann, T. O.; Dillard, L. W.; Tran, V. D.; He, Z. M.; James, R. A.; Park, H.; Paradkar, V. M.; Hobbs, D. W. Preparation of pyrazolopyrimidines as cyclin-dependent kinase inhibitors. US20040209878A1, Oct 21, **2004**.

283. Heron, N. M.; Jung, F. H.; Pasquet, G. R.; Mortlock, A. A. Preparation of phosphonooxy quinazoline derivatives and their pharmaceutical use. WO2004058781A1, Jul 15, **2004**.

284. Wang, S.; Meades, C.; Wood, G.; O'Boyle, J.; McInnes, C.; Fischer, P. Preparation of pyrimidine derivs. as inhibitors of cyclin-dependent kinases. WO2004043953A1, May 27, **2004**.

285. Bhide, R.; Cai, Z. w.; Qian, L.; Barbosa, S. Pyrrolotriazine inhibitors of kinases for use in treatment of diseases associated with growth factor receptor signal transduction. WO2004009784A2, Jan 29, **2004**.

286. Charrier, J. D.; Mazzei, F.; Kay, D.; Miller, A. Processes for preparing 6-pyrazolylpyrimidines as inhibitors of protein kinase, in particular Aurora kinases, by nucleophilic substitution. WO2004000833A1, Dec 31, **2003**.

287. Jin, Q.; Mauragis, M. A.; May, P. D. Process for preparing aminocarbonylpyrrolylmethylideneindolinones from indolinones, imidazolcarbonylpyrrolecarboxaldehydes, and amines. WO2003070725A2, Aug 28, **2003**.

288. Barvian, M. R.; Booth, R. J.; Quin, J., III; Repine, J. T.; Sheehan, D. J.; Toogood, P. L.; Vanderwel, S. N.; Zhou, H. Preparation of pyrido[2,3-d]pyrimidin-7-ones as cdk4 inhibitors. WO2003062236A1, Jul 31, **2003**.

289. Guan, H.; Liang, C.; Sun, L.; Tang, P. C.; Wei, C. C.; Mauragis, M. A.; Vojkovsky, T.; Jin, Q.; Herrinton, P. M. 3-(4-Amidopyrrol-2-ylmethylidene)-2-indolinone derivatives as protein kinase inhibitors. WO2002066463A1, Aug 29, **2002**.

290. Gingrich, D. E.; Hudkins, R. L. Preparation of fused pyrrolocarbazoles as novel agents for treating or preventing angiogenic, neurodegenerative, or pathological disorders. WO2002017914A2, Mar 7, **2002**.

291. Bold, G.; Frei, J.; Traxler, P.; Altmann, K. H.; Mett, H.; Stover, D. R.; Wood, J. Preparation of 1-arylamino-4-pyridylmethylphthalazines and analogs as VEGF receptor inhibitors. WO9835958A1, Aug 20, **1998**.

292. Naik, R. G.; Lal, B.; Rupp, R. H.; Sedlacek, H. H.; Dickneite, G.; Czech, J. Preparation and use of 4H-1-benzopyran-4-one derivatives as antitumor agents. DE3836676A1, May 3, **1990**.

293. Delmedico, M. K. Methods of treating or preventing cognitive impairment using indaneacetic acid derivatives and their preparation. US20140370011A1, Dec 18, **2014**.

294. Cai, X.; Qian, C.; Zhai, H. Preparation of imidazo[4,5-c]pyridine derivatives as HSP90 inhibitors. WO2008115719A1, Sep 25, **2008**.

295. Machajewski, T. D.; Shafer, C. M.; McBride, C.; Antonios-McCrea, W.; Doughan, B. M.; Levine, B. H.; Xia, Y.; McKenna, M.; Wang, X. M.; Mendenhall, K.; Zhou, Y.; Gong, B.; Gu, D.; Dolan, J.; Tulinsky, J.; Brinner, K.; Gao, Z. Preparation of 2-amino-7,8-dihydro-6H-pyrido[4,3-d]pyrimidin-5-ones as inhibitors of HSP90 for treating cellular proliferative, viral, autoimmune, cardiovascular, and central nervous system diseases. WO2007041362A1, Apr 12, **2007**.

296. Delhomel, J. F.; Caumont-Bertrand, K. Combinations of substituted 1,3-diphenylprop-2-en-1-one derivatives with other therapeutically active ingredients and their preparation, and use in the treatment of diseases. US20070032543A1, Feb 8, **2007**.

297. Chessari, G.; Congreve, M. S.; Figueroa Navarro, E.; Frederickson, M.; Murray, C.; Woolford, A. J.-A.; Carr, M. G.; Downham, R.; O'Brien, M. A.; Phillips, T. R.; Woodhead, A. J. Preparation of hydroxybenzamides as Hsp90 inhibitors. WO2006109085A1, Oct 19, **2006**.

298. Ying, W.; James, D.; Zhang, S.; Przewloka, T.; Chae, J.; Chimmanamada, D. U.; Lee, C. W.; Kostik, E.; Ng, H. P.; Foley, K.; Du, Z.; Barsoum, J. Preparation of triazoles as Hsp90 inhibitors for treating cancer. WO2006055760A1, May 26, **2006**.

299. Nomura, M.; Takano, Y.; Yumoto, K.; Shinozaki, T.; Isogai, S.; Murakami, K. Preparation of cyclic aminobenzoic acid derivatives as PPARα agonists. WO2006016637A1, Feb 16, **2006**.

300. Zhu, Y.; Ma, J.; Cheng, P.; Zhao, Z.; Gregoire, F. M.; Rakhmanova, V. A. Preparation of triazoles as modulators of peroxisome proliferator activated receptors (PPAR). WO2005115383A2, Dec 8, **2005**.

301. Xie, Q.; Wenkert, D.; Shen, Y.; Vande Woude, G. F.; Hay, R. Preparation of geldanamycin and derivatives to inhibit cancer invasion and identify novel targets. WO2005095347A1, Oct 13, **2005**.

302. Nara, S.; Nakagawa, H.; Kanda, Y.; Nakashima, T.; Soga, S.; Kajita, J.; Saito, J. i.; Shiotsu, Y.; Akinaga, S. Preparation of benzophenone derivatives as HSP90 inhibitors for treatment of tumor. WO2005000778A1, Jan 6, **2005**.

303. Drysdale, M. J.; Dymock, B. W.; Finch, H.; Webb, P.; McDonald, E.; James, K. E.; Cheung, K. M.; Mathews, T. P. Preparation of isoxazoles as inhibitors of heat shock proteins. WO2004072051A1, Aug 26, **2004**.

304. Acton, J. J., III; Debenham, S. D.; Liu, K.; Meinke, P. T.; Wood, H. B.; Black, R. M. Preparation of indoles having aryloxyalkanoic or arylalkanoic acid substituents as PPARγ agonists or partial agonists having anti-diabetic activity. WO2004020408A1, Mar 11, **2004**.

305. Najib, J.; Caumont Bertrand, K. Preparation of 1,3-diphenylprop-2-en-1-one as PPAR agonists and as antioxidants for treating cerebral ischemia and related diseases. FR2841900A1, Jan 9, **2004**.

306. Bach, A. T.; Kapa, P. K.; Lee, G. T.-S.; Loeser, E. M.; Sabio, M. L.; Stanton, J. L.; Vedananda, T. R. Preparation of arylsulfonyl-azetidine/pyrrolidine derivatives as agonists of peroxisome proliferator-activated receptors. WO2003043985A1, May 30, **2003**.

307. Mantlo, N. B.; Collado Cano, I.; Dominianni, S. J.; Etgen, G. J., Jr.; Garcia-Paredes, C.; Johnston, R. D.; Letourneau, M. E.; Martinelli, M. J.; Mayhugh, D. R.; Saeed, A.; Thompson, R. C.; Wang, X.; Coffey, D. S.; Schmid, C. R.; Vicenzi, J. T.; Xu, Y. Preparation of (phenylalkyl)-1H-[1,2,4]triazolones as PPARγ agonists for treatment of cardiovascular disease associated with Syndrome X and related conditions. WO2002038553A2, May 16, **2002**.

308. Cheng, P. T. W.; Devasthale, P.; Jeon, Y. T.; Chen, S.; Zhang, H. Preparation of oxazolyl- and thiazolylalkoxybenzylglycines and related compounds as antidiabetic and antiobesity agents. WO2001021602A1, Mar 29, **2001**.

309. Nomura, M.; Takahashi, Y.; Tanase, T.; Miyachi, H.; Tsunoda, M.; Ide, T.; Murakami, K. Preparation of phenylmethylcarbamoylphenylpropionic acid derivatives as human peroxisome proliferator-activated receptor-α (PPAR-α) agonists. WO2000075103A1, Dec 14, **2000**.

310. Brunet, M.; Zeiller, J. J.; Berthelon, J. J.; Contard, F.; Augert, G.; Guerrier, D. Preparation of benzopyrans and benzoxepines and their hypolipidemic and antidiabetic activity. WO2000039113A1, Jul 6, **2000**.

311. Andersson, K. Preparation of new 3-aryl-2-hydroxypropionic acid derivative for treatment of insulin resistance. WO9962872A1, Dec 9, **1999**.

312. Lohray, B. B.; Lohray, V. B.; Bajji, A. C.; Kalchar, S.; Ramanujam, R.; Chakrabarti, R. Preparation of 2-alkoxy-3-arylalken- and -anoates and analogs as peroxisome proliferator-activated receptor agonists. WO9919313A1, Apr 22, **1999**.

313. Fujita, T.; Wada, K.; Fujiwara, T. Preparation of substituted fused heterocyclic compounds as pharmaceuticals. WO9918081A1, Apr 15, **1999**.

314. Shinkai, H. Preparation of isoxazolidinedione derivatives as antidiabetics and antilipemics. WO9518125A1, Jul 6, **1995**.

315. Thiazolidine derivatives for lowering blood lipids and sugar. JP60051189A, Mar 22, **1985**.

316. Sasaki, K.; Inoue, Y. Geldanamycin derivative and antitumor agent containing it. DE3006097A1, Aug 28, **1980**.

317. Kauramatsu, Y.; Fujita, T. Thiazolidine derivatives, and pharmaceutical compositions comprising them. EP8203A1, Feb 20, **1980**.

318. Borzilleri, R. M.; Schroeder, G. M.; Cai, Z. w. Preparation of pyridinone compound as MET kinase inhibitor. WO2008058229A1, May 15, **2008**.

319. Bounaud, P. Y.; Smith, C. R.; Jefferson, E. A. Preparation of bicyclic triazoles as protein kinase modulators. WO2008051808A2, May 2, **2008**.

320. Albrecht, B.; Bauer, D.; Bellon, S.; Bode, C.; Booker, S.; Boezio, A.; Choquette, D.; D'Amico, D.; Harmange, J. C.; Hirai, S.; Hungate, R.; Kim, T. s.; Lewis, R.; Liu, L.; Lohman, J.; Norman, M.; Potashman, M.; Siegmund, A.; Springer, S.; Stec, M.; Xi, N.; Yang, K. Preparation of fused heterocyclic derivatives for treating HGF mediated diseases. WO2008008539A2, Jan 17, **2008**.

321. Cheng, H.; Cui, J. J.; Hoffman, J. E.; Jia, L.; Johnson, M. C.; Kania, R. S.; Le, P. T. Q.; Nambu, M. D.; Pairish, M. A.; Shen, H.; Tran-Dube, M. B. Preparation of triazolopyrazine derivatives for treating hyperproliferative disorders. US20070265272A1, Nov 15, **2007**.

322.   Sandanayaka, V.; Singh, J.; Gurney, M.; Mamat, B.; Yu, P.; Bedel, L.; Zhao, L. Preparation of heterocyclic compounds containing biaryl moiety as LTA4H inhibitors. US20070066820A1, Mar 22, **2007**.

323.   Kelly, M.; Lee, Y.; Liu, B.; Fujimoto, T.; Freundlich, J.; Dorsey, B. D.; Flynn, G. A.; Husain, A. Preparation of heterocyclic anticancer agents and uses thereof. US20060270686A1, Nov 30, **2006**.

324.   Gadek, T.; Burnier, J. Compositions and methods for treatment of eye disorders. WO2006125119A1, Nov 23, **2006**.

325.   Li, C. J.; Ashwell, M. A.; Hill, J.; Moussa, M. M.; Munshi, N. Preparation of maleimide derivatives, pharmaceutical compositions and methods for treatment of cancer. WO2006086484A1, Aug 17, **2006**.

326.   Lapierre, J. M.; Rotstein, D. M.; Sjogren, E. B. Preparation of new retinoids for the treatment of emphysema, cancer and dermatological disorders. WO2002028810A2, Apr 11, **2002**.

327.   Curtin, M. L.; Dai, Y.; Davidsen, S. K.; Heyman, H. R.; Holmes, J. H.; Michaelides, M. R.; Steinman, D. H. Preparation of reverse hydroxamate inhibitors of matrix metalloproteinases. WO2000044739A1, Aug 3, **2000**.

328.   Link, J.; Liu, G.; Pei, Z.; Von Geldern, T.; Winn, M.; Xin, Z.; Boyd, S. A.; Jae, H. S.; Lynch, J. K.; Zhu, G. D.; Freeman, J. C.; Gunawardana, I. W.; Staeger, M. A. Cell adhesion-inhibiting antiinflammatory and immune-suppressive compounds. WO2000039081A2, Jul 6, **2000**.

329.   Kluender, H. C. E.; Benz, G. H. H. H.; Brittelli, D. R.; Bullock, W. H.; Combs, K. J.; Dixon, B. R.; Schneider, S.; Wood, J. E.; Vanzandt, M. C.; et, a. Substituted 4-biarylbutyric or 5-biarylpentanoic acids and derivatives as matrix metalloprotease inhibitors. WO9615096A1, May 23, **1996**.

330.   MacPherson, L. J.; Parker, D. T. Arylsulfonamido-substituted hydroxamic acid antiinflammatory agents. EP606046A1, Jul 13, **1994**.

331.   Chandraratna, R. A. S. Preparation of disubstituted acetylenes bearing heteroaromatic and heterobicyclic groups having retinoid-like activity. EP284288A1, Sep 28, **1988**.

332.   Student The Probable Error of A Mean. *Biometrika* **1908**, *6* (1), 1-25.

333.   Hutchinson, T. P. *Essentials of statistical methods, in 41 pages;* Rumsby Scientific Pub.: **1993**.

334.   Paulson, T. Epidemiology: A mortal foe. *Nature* **2013**, *502* (7470), S2-S3.

335.   Zumla, A.; Raviglione, M.; Hafner, R.; Fordham von Reyn, C. Tuberculosis. *N. Engl. J. Med.* **2013**, *368* (8), 745-755.

336.   Humphries, C. Latency: A sleeping giant. *Nature* **2013**, *502* (7470), S14-S15.

337.   Lawn, S. D.; Zumla, A. I. Tuberculosis. *The Lancet* **2002**, *378* (9785), 57-72.

338.   Russell, D. G. Who puts the tubercle in tuberculosis? *Nat. Rev. Microbiol.* **2007**, *5* (1), 39-47.

339.   Ernst, J. D. The immunological life cycle of tuberculosis. *Nat. Rev. Immunol.* **2012**, *12* (8), 581-591.

340.   Brennan, P. J. Structure, function, and biogenesis of the cell wall of *Mycobacterium tuberculosis. Tuberculosis* **2003**, *83* (1-3), 91-97.

341.   Cook, G. M.; Berney, M.; Gebhard, S.; Heinemann, M.; Cox, R. A.; Danilchanka, O.; Niederweis, M. Physiology of Mycobacteria. In *Advances in Microbial Physiology*, Volume 55 ed.; Robert, K. P., Ed.; Academic Press: **2009**; 81-319.

342.   Maxmen, A. Drug development: A combined effort. *Nature* **2013**, *502* (7470), S4-S6.

343.   Grassi, C. New drugs for tuberculosis. *Expert Opin. Investig. Drugs* **1997**, *6* (9), 1211-1226.

344.   Zhang, Y. The Magic Bullets and Tuberculosis Drug Targets. *Annu. Rev. Pharmacol. Toxicol.* **2004**, *45* (1), 529-564.

345.   Sacchettini, J. C.; Rubin, E. J.; Freundlich, J. S. Drugs versus bugs: in pursuit of the persistent predator *Mycobacterium tuberculosis. Nat. Rev. Microbiol.* **2008**, *6* (1), 41-52.

346.   van den Boogaard, J.; Kibiki, G. S.; Kisanga, E. R.; Boeree, M. J.; Aarnoutse, R. E. New Drugs against Tuberculosis: Problems, Progress, and Evaluation of Agents in Clinical Development. *Antimicrob. Agents Ch.* **2009**, *53* (3), 849-862.

347.   Zumla, A.; Nahid, P.; Cole, S. T. Advances in the development of new tuberculosis drugs and treatment regimens. *Nat. Rev. Drug Discov.* **2013**, *12* (5), 388-404.

348.   http://www.accessdata.fda.gov/Scripts/cder/drugsatfda/index.cfm.

349.   http://www.micromedexsolutions.com/.

350.   Matsumoto, M.; Hashizume, H.; Tomishige, T.; Kawasaki, M.; Tsubouchi, H.; Sasaki, H.; Shimokawa, Y.; Komatsu, M. OPC-67683, a Nitro-Dihydro-Imidazooxazole Derivative with Promising Action against Tuberculosis In Vitro and In Mice. *PLoS Med.* **2006**, *3* (11), e466.

351.   Gler, M. T.; Skripconoka, V.; Sanchez-Garavito, E.; Xiao, H.; Cabrera-Rivero, J. L.; Vargas-Vasquez, D. E.; Gao, M.; Awad, M.; Park, S. K.; Shim, T. S.; Suh, G. Y.; Danilovits, M.; Ogata, H.; Kurve, A.; Chang, J.; Suzuki, K.; Tupasi, T.; Koh, W. J.; Seaworth, B.; Geiter, L. J.; Wells, C. D. Delamanid for Multidrug-Resistant Pulmonary Tuberculosis. *N. Engl. J. Med.* **2012**, *366* (23), 2151-2160.

352.   Snell, N. J. C. The treatment of tuberculosis: current status and future prospects. *Expert Opin. Investig. Drugs* **1998**, *7* (4), 545-552.

353. Diacon, A. H.; Pym, A.; Grobusch, M.; Patientia, R.; Rustomjee, R.; Page-Shipp, L.; Pistorius, C.; Krause, R.; Bogoshi, M.; Churchyard, G.; Venter, A.; Allen, J.; Palomino, J. C.; De Marez, T.; van Heeswijk, R. P. G.; Lounis, N.; Meyvisch, P.; Verbeeck, J.; Parys, W.; de Beule, K.; Andries, K.; Neeley, D. F. M. The Diarylquinoline TMC207 for Multidrug-Resistant Tuberculosis. *N. Engl. J. Med.* **2009**, *360* (23), 2397-2405.

354. Chahine, E. B.; Karaoui, L. R.; Mansour, H. Bedaquiline: A Novel Diarylquinoline for Multidrug-Resistant Tuberculosis. *Ann. Pharmacother.* **2014**, *48* (1), 107-115.

355. Makarov, V.; Manina, G.; Mikusova, K.; Möllmann, U.; Ryabova, O.; Saint-Joanis, B.; Dhar, N.; Pasca, M. R.; Buroni, S.; Lucarelli, A. P.; Milano, A.; De Rossi, E.; Belanova, M.; Bobovska, A.; Dianiskova, P.; Kordulakova, J.; Sala, C.; Fullam, E.; Schneider, P.; McKinney, J. D.; Brodin, P.; Christophe, T.; Waddell, S.; Butcher, P.; Albrethsen, J.; Rosenkrands, I.; Brosch, R.; Nandi, V.; Bharath, S.; Gaonkar, S.; Shandil, R. K.; Balasubramanian, V.; Balganesh, T.; Tyagi, S.; Grosset, J.; Riccardi, G.; Cole, S. T. Benzothiazinones Kill *Mycobacterium tuberculosis* by Blocking Arabinan Synthesis. *Science* **2009**, *324* (5928), 801-804.

356. Christophe, T.; Jackson, M.; Jeon, H. K.; Fenistein, D.; Contreras-Dominguez, M.; Kim, J.; Genovesio, A.; Carralot, J. P.; Ewann, F.; Kim, E. H.; Lee, S. Y.; Kang, S.; Seo, M. J.; Park, E. J.; Škovierová, H.; Pham, H.; Riccardi, G.; Nam, J. Y.; Marsollier, L.; Kempf, M.; Joly-Guillou, M. L.; Oh, T.; Shin, W. K.; No, Z.; Nehrbass, U.; Brosch, R.; Cole, S. T.; Brodin, P. High Content Screening Identifies Decaprenyl-Phosphoribose 2' Epimerase as a Target for Intracellular Antimycobacterial Inhibitors. *PLoS Pathog.* **2009**, *5* (10), e1000645.

357. Crellin, P. K.; Brammananth, R.; Coppel, R. L. Decaprenylphosphoryl-b-D-Ribose 2'-Epimerase, the Target of Benzothiazinones and Dinitrobenzamides, Is an Essential Enzyme in *Mycobacterium smegmatis. PLoS ONE* **2011**, *6* (2), e16869.

358. Li, H.; Jogl, G. Crystal structure of decaprenylphosphoryl-b-D-ribose 2'-epimerase from *Mycobacterium smegmatis. Proteins* **2013**, *81* (3), 538-543.

359. Neres, J.; Pojer, F.; Molteni, E.; Chiarelli, L. R.; Dhar, N.; Boy-Röttger, S.; Buroni, S.; Fullam, E.; Degiacomi, G.; Lucarelli, A. P.; Read, R. J.; Zanoni, G.; Edmondson, D. E.; De Rossi, E.; Pasca, M. R.; McKinney, J. D.; Dyson, P. J.; Riccardi, G.; Mattevi, A.; Cole, S. T.; Binda, C. Structural Basis for Benzothiazinone-Mediated Killing of *Mycobacterium tuberculosis. Science Transl.Med.* **2012**, *4* (150), 150ra121.

360. Carroll, P.; Faray-Kele, M. C.; Parish, T. Identifying Vulnerable Pathways in *Mycobacterium tuberculosis* by Using a Knockdown Approach. *Appl. Environ. Microb.* **2011**, *77* (14), 5040-5043.

361. Kolly, G. S.; Boldrin, F.; Sala, C.; Dhar, N.; Hartkoorn, R. C.; Ventura, M.; Serafini, A.; McKinney, J. D.; Manganelli, R.; Cole, S. T. Assessing the essentiality of the decaprenyl-phospho-d-arabinofuranose pathway in *Mycobacterium tuberculosis* using conditional mutants. *Mol. Microbiol.* **2014**, *92* (1), 194-211.

362. Manina, G.; Pasca, R.; Buroni, S.; De Rossi, E.; Riccardi, G. Decaprenylphosphoryl-b-D-Ribose 2'-Epimerase from *Mycobacterium tuberculosis* is a Magic Drug Target. *Curr. Med. Chem.* **2010** *17*(27), 3099-3108.

363.   Brecik, M.; Centárová, I.; Mukherjee, R.; Kolly, G. S.; Huszár, S.; Bobovská, A.; Kilacsková, E.; Mokošová, V.; Svetlíková, Z.; Šarkan, M.; Neres, J.; Korduláková, J.; Cole, S. T.; Mikušová, K. DprE1 Is a Vulnerable Tuberculosis Drug Target Due to Its Cell Wall Localization. *ACS Chem. Biol.* **2015**, *10* (7), 1631-1636.

364.   Gao, C.; Ye, T. H.; Wang, N. Y.; Zeng, X. X.; Zhang, L. D.; Xiong, Y.; You, X. Y.; Xia, Y.; Xu, Y.; Peng, C. T.; Zuo, W. Q.; Wei, Y.; Yu, L. T. Synthesis and structure activity relationships evaluation of benzothiazinone derivatives as potential anti-tubercular agents. *Bioorg. Med. Chem. Lett.* **2013**, *23* (17), 4919-4922.

365.   Makarov, V.; Lechartier, B.; Zhang, M.; Neres, J.; van der Sar, A. M.; Raadsen, S. A.; Hartkoorn, R. C.; Ryabova, O. B.; Vocat, A.; Decosterd, L. A.; Widmer, N.; Buclin, T.; Bitter, W.; Andries, K.; Pojer, F.; Dyson, P. J.; Cole, S. T. Towards a new combination therapy for tuberculosis with next generation benzothiazinones. *EMBO Mol. Med.* **2014**, emmm.201303575

366.   Andrews, J. M. Determination of minimum inhibitory concentrations. *J. Antimicrob. Chem.* **2001**, *48* (suppl 1), 5-16.

367.   Magnet, S.; Hartkoorn, R. C.; Székely, R.; Pató, J.; Triccas, J. A.; Schneider, P.; Szántai-Kis, C.; Órfi, L.; Chambon, M.; Banfi, D.; Bueno, M.; Turcatti, G.; Kéri, G.; Cole, S. T. Leads for antitubercular compounds from kinase inhibitor library screens. *Tuberculosis* **2010**, *90* (6), 354-360.

368.   Stanley, S. A.; Grant, S. S.; Kawate, T.; Iwase, N.; Shimizu, M.; Wivagg, C.; Silvis, M.; Kazyanskaya, E.; Aquadro, J.; Golas, A.; Fitzgerald, M.; Dai, H.; Zhang, L.; Hung, D. T. Identification of Novel Inhibitors of *M. tuberculosi*s Growth Using Whole Cell Based High-Throughput Screening. *ACS Chem. Biol.* **2012**, *7* (8), 1377-1384.

369.   De Jesus Lopes Ribeiro, A. L.; Degiacomi, G.; Ewann, F.; Buroni, S.; Incandela, M. L.; Chiarelli, L. R.; Mori, G.; Kim, J.; Contreras-Dominguez, M.; Park, Y. S.; Han, S. J.; Brodin, P.; Valentini, G.; Rizzi, M.; Riccardi, G.; Pasca, M. R. Analogous Mechanisms of Resistance to Benzothiazinones and Dinitrobenzamides in *Mycobacterium smegmatis*. *PLoS ONE* **2011**, *6* (11), e26675.

370.   Trefzer, C.; Rengifo-Gonzalez, M.; Hinner, M. J.; Schneider, P.; Makarov, V.; Cole, S. T.; Johnsson, K. Benzothiazinones: Prodrugs That Covalently Modify the Decaprenylphosphoryl-b-ribose 2'-epimerase DprE1 of *Mycobacterium tuberculosis*. *J. Am. Chem. Soc.* **2010**, *132* (39), 13663-13665.

371.   Trefzer, C.; Škovierová, H.; Buroni, S.; Bobovská, A.; Nenci, S.; Molteni, E.; Pojer, F.; Pasca, M. R.; Makarov, V.; Cole, S. T.; Riccardi, G.; Mikušová, K.; Johnsson, K. Benzothiazinones Are Suicide Inhibitors of Mycobacterial Decaprenylphosphoryl-b-d-ribofuranose 2'-Oxidase DprE1. *J. Am. Chem. Soc.* **2011**, *134* (2), 912-915.

372. Tiwari, R.; Moraski, G. C.; Krchňák, V.; Miller, P. A.; Colon-Martinez, M.; Herrero, E.; Oliver, A. G.; Miller, M. J. Thiolates Chemically Induce Redox Activation of BTZ043 and Related Potent Nitroaromatic Anti-Tuberculosis Agents. *J. Am. Chem. Soc.* **2013**, *135* (9), 3539-3549.

373. Singh, J.; Petter, R. C.; Baillie, T. A.; Whitty, A. The resurgence of covalent drugs. *Nat. Rev. Drug Discov.* **2011**, *10* (4), 307-317.

374. Kalgutkar, A. S.; Gardner, I.; Obach, R. S.; Shaffer, C. L.; Callegari, E.; Henne, K. R.; Mutlib, A. E.; Dalvie, D. K.; Lee, J. S.; Nakai, Y.; O'Donnell, J. P.; Boer, J.; Harriman, S. P. A Comprehensive Listing of Bioactivation Pathways of Organic Functional Groups. *Curr. Drug Metab.* **2005** *6(*3), 161-225.

375. Naik, M.; Humnabadkar, V.; Tantry, S. J.; Panda, M.; Narayan, A.; Guptha, S.; Panduga, V.; Manjrekar, P.; Jena, L. k.; Koushik, K.; Shanbhag, G.; Jatheendranath, S.; Manjunatha, M. R.; Gorai, G.; Bathula, C.; Rudrapatna, S.; Achar, V.; Sharma, S.; Ambady, A.; Hegde, N.; Mahadevaswamy, J.; Kaur, P.; Sambandamurthy, V. K.; Awasthy, D.; Narayan, C.; Ravishankar, S.; Madhavapeddi, P.; Reddy, J.; Prabhakar, K. R.; Saralaya, R.; Chatterji, M.; Whiteaker, J.; McLaughlin, B.; Chiarelli, L. R.; Riccardi, G.; Pasca, M. R.; Binda, C.; Neres, J.; Dhar, N.; Signorino-Gelo, F.; McKinney, J. D.; Ramachandran, V.; Shandil, R.; Tommasi, R.; Iyer, P. S.; Narayanan, S.; Hosagrahara, V.; Kavanagh, S.; Dinesh, N.; Ghorpade, S. R. 4-Aminoquinolone Piperidine Amides: Noncovalent Inhibitors of DprE1 with Long Residence Time and Potent Antimycobacterial Activity. *J. Med. Chem.* **2014**, *57* (12), 5419-5434.

376. Panda, M.; Ramachandran, S.; Ramachandran, V.; Shirude, P. S.; Humnabadkar, V.; Nagalapur, K.; Sharma, S.; Kaur, P.; Guptha, S.; Narayan, A.; Mahadevaswamy, J.; Ambady, A.; Hegde, N.; Rudrapatna, S. S.; Hosagrahara, V. P.; Sambandamurthy, V. K.; Raichurkar, A. Discovery of Pyrazolopyridones as a Novel Class of Noncovalent DprE1 Inhibitor with Potent Anti-Mycobacterial Activity. *J. Med. Chem.* **2014**, *57* (11), 4761-4771.

377. Shirude, P. S.; Shandil, R.; Sadler, C.; Naik, M.; Hosagrahara, V.; Hameed, S.; Shinde, V.; Bathula, C.; Humnabadkar, V.; Kumar, N.; Reddy, J.; Panduga, V.; Sharma, S.; Ambady, A.; Hegde, N.; Whiteaker, J.; McLaughlin, R. E.; Gardner, H.; Madhavapeddi, P.; Ramachandran, V.; Kaur, P.; Narayan, A.; Guptha, S.; Awasthy, D.; Narayan, C.; Mahadevaswamy, J.; Vishwas, K. G.; Ahuja, V.; Srivastava, A.; Prabhakar, K. R.; Bharath, S.; Kale, R.; Ramaiah, M.; Choudhury, N. R.; Sambandamurthy, V. K.; Solapure, S.; Iyer, P. S.; Narayanan, S.; Chatterji, M. Azaindoles: Noncovalent DprE1 Inhibitors from Scaffold Morphing Efforts, Kill Mycobacterium tuberculosis and Are Efficacious in Vivo. *J. Med. Chem.* **2013**, *56* (23), 9701-9708.

378. Wang, F.; Sambandan, D.; Halder, R.; Wang, J.; Batt, S. M.; Weinrick, B.; Ahmad, I.; Yang, P.; Zhang, Y.; Kim, J.; Hassani, M.; Huszar, S.; Trefzer, C.; Ma, Z.; Kaneko, T.; Mdluli, K. E.; Franzblau, S.; Chatterjee, A. K.; Johnsson, K.; Mikusova, K.; Besra, G. S.; Fütterer, K.; Robbins, S. H.; Barnes, S. W.; Walker, J. R.; Jacobs, W. R.; Schultz, P. G. Identification of a small molecule with activity against drug-resistant and persistent tuberculosis. *Proc. Natl. Acad. Sci.* **2013**, *110* (27), E2510-E2517.

379. Shirude, P. S.; Shandil, R. K.; Manjunatha, M. R.; Sadler, C.; Panda, M.; Panduga, V.; Reddy, J.; Saralaya, R.; Nanduri, R.; Ambady, A.; Ravishankar, S.; Sambandamurthy, V. K.; Humnabadkar, V.; Jena, L. K.; Suresh, R. S.; Srivastava, A.; Prabhakar, K. R.; Whiteaker, J.; McLaughlin, R. E.; Sharma, S.; Cooper, C. B.; Mdluli, K.; Butler, S.; Iyer, P. S.; Narayanan, S.; Chatterji, M. Lead Optimization of 1,4-Azaindoles as Antimycobacterial Agents. *J. Med. Chem.* **2014**, *57* (13), 5728-5737.

380. Ballell, L.; Bates, R. H.; Young, R. J.; Alvarez-Gomez, D.; Alvarez-Ruiz, E.; Barroso, V.; Blanco, D.; Crespo, B.; Escribano, J.; González, R.; Lozano, S.; Huss, S.; Santos-Villarejo, A.; Martín-Plaza, J. J.; Mendoza, A.; Rebollo-Lopez, M. J.; Remuiñan-Blanco, M.; Lavandera, J. L.; Pérez-Herran, E.; Gamo-Benito, F. J.; García-Bustos, J. F.; Barros, D.; Castro, J. P.; Cammack, N. Fueling Open-Source Drug Discovery: 177 Small-Molecule Leads against Tuberculosis. *ChemMedChem* **2013**, *8* (2), 313-321.

381. Batt, S. M.; Cacho Izquierdo, M.; Castro Pichel, J.; Stubbs, C. J.; Vela-Glez Del Peral, L.; Pérez-Herrán, E.; Dhar, N.; Mouzon, B.; Rees, M.; Hutchinson, J. P.; Young, R. J.; McKinney, J. D.; Barros Aguirre, D.; Ballell, L.; Besra, G. S.; Argyrou, A. Whole Cell Target Engagement Identifies Novel Inhibitors of Mycobacterium tuberculosis Decaprenylphosphoryl-b-d-ribose Oxidase. *ACS Infect. Dis.* **2015**, *1* (12), 615-626.

382. El-Faham, A.; Albericio, F. COMU: A third generation of uronium-type coupling reagents. *J. Peptide Sci.* **2010**, *16* (1), 6-9.

383. Rastogi, N.; Labrousse, V. r.; Goh, K. S. In Vitro Activities of Fourteen Antimicrobial Agents Against Drug Susceptible and Resistant Clinical Isolates of Mycobacterium tuberculosis and Comparative Intracellular Activities Against the Virulent H37Rv Strain in Human Macrophages. *Curr. Microbio.l* **1996**, *33* (3), 167-175.

384. Cai, H.; Chavez, F.; Dunford, P. J.; Greenspan, A. J.; Meduna, S. P.; Quiroz, J. A.; Savall, B. M.; Tays, K. L.; Thurmond, R. L.; Wei, J. Diamino-pyridine, pyrimidine, and pyrazine modulators of the histamine H4 receptor. U.S. 2/997,567, Jun 11, **2009**.

385. Hwang, T. L.; Shaka, A. J. Cross relaxation without TOCSY: transverse rotating-frame Overhauser effect spectroscopy. *J. Am. Chem. Soc.* **1992**, *114* (8), 3157-3159.

386. Nassar, A. E.; Kamel, A. M.; Clarimont, C. Improving the decision-making process in the structural modification of drug candidates: enhancing metabolic stability. *Drug Discov.Today* **2004**, *9* (23), 1020-1028.

387. Nahm, S.; Weinreb, S. M. N-methoxy-n-methylamides as effective acylating agents. *Tet. Lett.* **1981**, *22* (39), 3815-3818.

388. Li, J.; Zhang, X.; Zhang, Z.; Padakanti, P. K.; Jin, H.; Cui, J.; Li, A.; Zeng, D.; Rath, N. P.; Flores, H.; Perlmutter, J. S.; Parsons, S. M.; Tu, Z. Heteroaromatic and Aniline Derivatives of Piperidines As Potent Ligands for Vesicular Acetylcholine Transporter. *J. Med. Chem.* **2013**, *56* (15), 6216-6233.

389. Billings, R. E.; McMahon, R. E. Microsomal Biphenyl Hydroxylation: the Formation of 3-Hydroxybiphenyl and Biphenyl Catechol. *Mol. Pharmacol.* **1978**, *14* (1), 145-154.

390. Azouz, W.; Parke, D.; Williams, R. Studies in detoxication, 42. Fluorobenzene: Spectrophotometric determination of the elimination of unchanged halogenobenzenes by rabbits; a comparison of the oxidation in vivo of fluorobenzene and of benzene. *Biochem. J.* **1952**, *50* (5), 702-0.

391. Meanwell, N. A. Synopsis of Some Recent Tactical Application of Bioisosteres in Drug Design. *J. Med. Chem.* **2011**, *54* (8), 2529-2591.

392.   Bowes, J.; Brown, A. J.; Hamon, J.; Jarolimek, W.; Sridhar, A.; Waldron, G.; Whitebread, S. Reducing safety-related drug attrition: the use of in vitro pharmacological profiling. *Nat. Rev. Drug Discov.* **2012**, *11* (12), 909-922.

393.   Rullas, J.; García, J. I.; Beltrán, M.; Cardona, P. J.; Cáceres, N.; García-Bustos, J. F.; Angulo-Barturen, I. Fast Standardized Therapeutic-Efficacy Assay for Drug Discovery against Tuberculosis. *Antimicrob. Agents Ch.* **2010**, *54* (5), 2262-2264.

394.   Manjunatha, U. H.; Smith, P. W. Perspective: Challenges and opportunities in TB drug discovery from phenotypic screening. *Bioorg. Med. Chem.* **2015**, *23* (16), 5087-5097.

395.   Payne, D. J.; Gwynn, M. N.; Holmes, D. J.; Pompliano, D. L. Drugs for bad bugs: confronting the challenges of antibacterial discovery. *Nat. Rev. Drug Discov.* **2007**, *6* (1), 29-40.

8. Publications Of Work Contained in Thesis

The Discovery of in Vivo Active Mitochondrial Branched-Chain Aminotransferase (BCATm) Inhibitors by Hybridizing Fragment and HTS Hits

Sophie M. Bertrand,*[†,§] Nicolas Ancellin,[‡] Benjamin Beaufils,[‡] Ryan P. Bingham,[†] Jennifer A. Borthwick,[†,§] Anne-Bénédicte Boullay,[‡] Eric Boursier,[‡] Paul S. Carter,[†] Chun-wa Chung,[†] Ian Churcher,[†] Nerina Dodic,[‡] Marie-Hélène Fouchet,[‡] Charlène Fournier,[†] Peter L. Francis,[†] Laura A. Gummer,[†] Kenny Herry,[‡] Andrew Hobbs,[†] Clare I. Hobbs,[†] Paul Homes,[†] Craig Jamieson,[§] Edwige Nicodeme,[‡] Stephen D. Pickett,[†] Iain H. Reid,[†] Graham L. Simpson,[†] Lisa A. Sloan,[†] Sarah E. Smith,[†] Donald O'N. Somers,[†] Claus Spitzfaden,[†] Colin J. Suckling,[§] Klara Valko,[†] Yoshiaki Washio,[†] and Robert J. Young[†]

[†]GlaxoSmithKline R&D, Medicines Research Centre, Gunnels Wood Road, Stevenage, Hertfordshire SG1 2NY, U.K.
[‡]Centre de Recherche, GlaxoSmithKline R&D, Les Ulis, 25, 27 Avenue du Québec, 91140 Villebon sur Yvette, France
[§]Department of Pure and Applied Chemistry, University of Strathclyde, 295 Cathedral Street, Glasgow, G1 1XL, U.K.

Ⓢ *Supporting Information*

ABSTRACT: The hybridization of hits, identified by complementary fragment and high throughput screens, enabled the discovery of the first series of potent inhibitors of mitochondrial branched-chain amino-transferase (BCATm) based on a 2-benzylamino-pyrazolo[1,5-a]-pyrimidinone-3-carbonitrile template. Structure-guided growth enabled rapid optimization of potency with maintenance of ligand efficiency, while the focus on physicochemical properties delivered compounds with excellent pharmacokinetic exposure that enabled a proof of concept experiment in mice. Oral administration of 2-((4-chloro-2,6-difluorobenzyl)amino)-7-oxo-5-propyl-4,7-dihydropyrazolo[1,5-a]-pyrimidine-3-carbonitrile **61** significantly raised the circulating levels of the branched-chain amino acids leucine, isoleucine, and valine in this acute study.

1
BCATm pIC$_{50}$ **3.3**

61
BCATm pIC$_{50}$ = **7.3**, chromlogD$_{7.4}$ = 3.12
LE = 0.39, LLE$_{AT}$ = 0.33
cell pIC$_{50}$ = **6.8**
solid sol. 500 μg/mL
Cl$_b$ 0.3 mL/min/kg; T$_{1/2}$ 9 h; F% 100
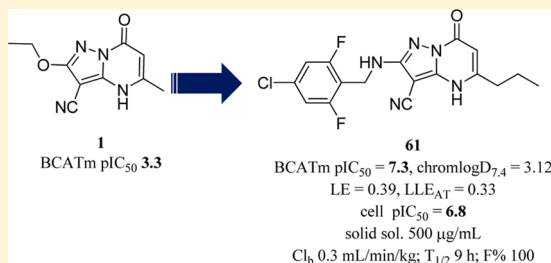
■ INTRODUCTION

Branched-chain aminotransferases (BCATs) are pyridoxal-phosphate driven enzymes that catalyze the transamination of branched-chain amino acids (BCAAs: Leu, Ile, and Val) into their corresponding α-keto acids.[1] In mammals, BCAT exists in two isoforms; a cytosolic form (BCATc) that is mainly expressed in neuronal tissues and a mitochondrial form (BCATm) that is ubiquitously expressed in the body, with the notable exception of the liver.[2−5] Elevated levels of BCAAs, especially leucine, which are involved in increased protein synthesis and inhibition of protein degradation are believed to increase energy expenditure and induce satiety, resulting in weight loss as observed with high protein diets.[6−8] It was hypothesized that increasing levels of BCAAs via inhibition of BCATm might have similar effects to a high protein diet; therefore, inhibitors of BCATm may have therapeutic potential in diseases such as obesity and dislipidema. Interestingly, BCATm knockout mice appear healthy and viable and exhibit a beneficial metabolic phenotype.[8] When fed a high-fat diet, these mice consume more food but weigh less and have lower levels of body fat than wild-type mice; they also display improved insulin sensitivity and glucose tolerance. However, a full understanding of this pathway and its regulation appears incomplete, as studies in genetically modified obese rodents (ob/ob mice and Zucker rats) and diet-induced obese mice and humans have shown that individuals with these characteristics have higher BCAA levels than lean animals and have lower levels of expression of BCATm.[9] To better understand BCATm pharmacology and its potential link with weight loss, the in vivo evaluation of small molecule inhibitors of this enzyme was an attractive prospect. To date, only inhibitors of the related cytosolic form, BCATc have been reported and these have only been evaluated in an in vitro context.[10−13] Selective BCATm inhibitors have thus far not been described.

The focus of the current study was initially to identify a tool molecule, which was suitable for investigating the biological role of BCATm in vivo and understand the associated metabolic pathway. The candidate molecule needed to combine good cellular potency (cell pIC$_{50}$ ≥ 6.5), selectivity over
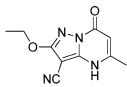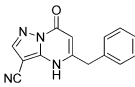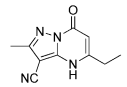
BCATc, and/or be a nonbrain penetrant inhibitor for BCATm (BCATc is mainly expressed in the brain) and suitable physicochemical properties for an oral drug (chromlogD$_{7.4}$ < 4; Ar ring ≤3; CLND solubility >100 μg/mL),[14−17] alongside a suitable pharmacokinetic profile for a once or twice daily dosing. ChromlogD$_{7.4}$ (chromatographic log D at pH 7.4)[14] is a new parameter developed at GSK to assess lipophilicity of compounds. The chemiluminescent nitrogen detection (CLND) solubility[15] is a high throughput method used in our laboratory, which provides a good measure of the kinetic solubility of compounds.

The practices of fragment-based drug discovery[16−19] are firmly established as powerful tools in the drug discovery process;[20,21] they complement the focus on the physical quality of molecules,[22−27] whereby lipophilicity[28,29] and aromaticity[30,31] are kept in check during the optimization trajectory. It has been recognized that the most effective pharmacological tools possess both high ligand efficiency and good physical properties.[32−34] Herein, the key efficiency parameters employed are ligand efficiency[35,36] (defined by LE = −ln RT(pIC$_{50}$)/heavy atom count) and the Astex ligand lipophilicity efficiency[37] (LLE$_{AT}$ − essentially LE corrected for the lipophilic contribution, estimated by clogP). Typically, LE values should be at least 0.3 and an LLE$_{AT}$ value at a similar level to LE indicates that the binding is not overly influenced by lipophilicity.

A fragment screening of our fragment library (1056 compounds) was carried out using saturation transfer difference NMR (STD-NMR), thermal shift (T_m), and an enzymatic biochemical assay to identify a diverse set of BCATm inhibitors.[38] From this exercice, several fragment hits were identified including the ethoxypyrazolopyrimidinone 1 (Table 1). Although this compound failed to generate a crystal
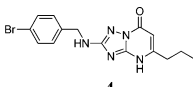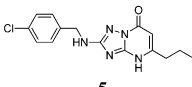
Table 1. Fragment Hit and Close Analogues

Structure	1	2	3
BCATm pIC$_{50}$	3.3[a]	4.6	< 3.2[b]
LE; LLE$_{AT}$	0.28; 0.41	0.33; 0.38	< 0.29; < 0.39
chromlogD$_{7.4}$	0.38	1.43	0.21
CLND sol. (μg/mL)	96	123	92
STD-NMR	hit	hit	hit
T_m	hit	ND	ND

[a]Compound reported inactive (pIC$_{50}$ < 2.9) in one out of the two test occasions. [b]Compound reported active (pIC$_{50}$ = 4.4) in one out of three test occasions.

Table 2. HTS Hits

Structure	4	5
BCATm pIC$_{50}$	6.2	5.7
LE; LLE$_{AT}$	0.39; 0.35	0.36; 0.32
chromlogD$_{7.4}$	2.92	2.86
CLND sol. (μg/mL)	54	37
Cell pIC$_{50}$	6.1	5.9

In this paper, the growth and optimization of a ligand efficient fragment hit 1, hybridized with a series identified by HTS, into a novel series of efficient and cell active BCATm inhibitors is described alongside in vivo pharmacokinetic and pharmacodynamic studies.

RESULTS AND DISCUSSION

To guide the optimization of 1 repeated attempts were made to elucidate the binding mode of this compound by X-ray crystallography, but these experiments did not deliver a liganded structure. Subsequently, a number of close analogues of 1, which were available in our company library, were screened by STD-NMR in order to identify the more effective binders. In doing so, this aided the selection of compounds for progression to X-ray crystallography. Two fragment hits identified in this manner gave liganded crystal structures (compounds 2 and 3, Table 1). The LE, LLE$_{AT}$, chromlogD$_{7.4}$, and CLND solubility are included for all tested compounds.

Crystal structures of 2 (in magenta) and 3 (in cyan) showed that the ethyl and benzyl substituents bound in a lipophilic pocket that was occupied by several fragment hits identified during our fragment screen[38] (Figure 1); this region is where
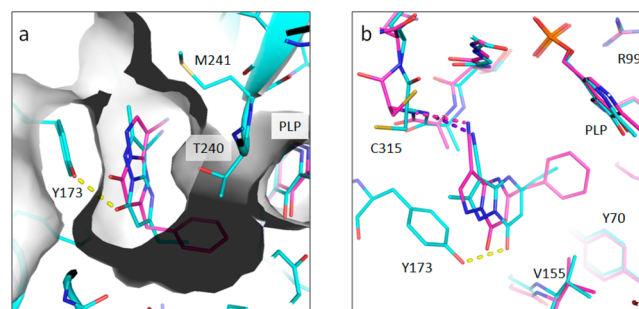
Figure 1. Overlay of compounds 2 (in magenta, 5BWR) and 3 (in cyan, 5BWT) crystal structures in BCATm, showing (a) the hydrogen bond (yellow dotted line) to Tyr-173 and protein surface of compound 3, and (b) the interaction of nitrile with Cys-315 (dotted lines, colored magenta and blue accordingly).

structure, it was consistently detected by all three primary assays employed given us confidence it was genuinely binding to the protein. In addition, a concurrent high throughput screening (HTS) of our chemical library (1.7 million compounds) was conducted and identified a series of triazolopyrimidinones (4 and 5, Table 2) as analogues to the fragment hit 1. Therefore, it was decided to pursue this fragment hit further.

the side chains of the BCAA substrates bind in proximity to the pyridoxal (PLP, cofactor) binding site. In terms of interactions with the protein, the carbonyl made a hydrogen-bond with Tyr-173 (Figure 1a), and the nitrile appeared to interact with the backbone NH of Cys-315 (Figure 1b), although the angle appeared not to be optimal.[39] To accommodate the benzyl group of 2 in the lipophilic pocket, the core shifts significantly and the activated loop (residues 172−178) containing Tyr-173

was disordered but the interaction with Cys-315 was maintained.

Elaboration of the fragments, while preserving good ligand efficiency (LE and LLE$_{AT}$), could be achieved by the exploration of adjacent pockets in order to gain productive interactions and contacts that improve binding affinity. The concurrent HTS campaign carried out in our laboratory identified compounds **4** and **5** as efficient hits that displayed encouraging cellular potency against BCATm (Table 2). A crystal structure of compound **4** bound into BCATm (in orange, Figure 2) confirmed a similar binding mode to the
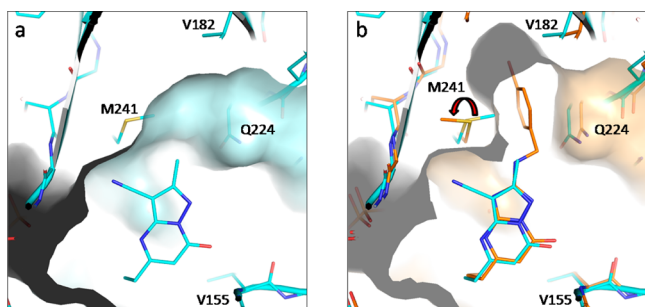
Figure 2. Movement of Met-241 enlarges inhibitor binding site. (a) Structure of compound **3** (in cyan, 5BWT), protein surface (in light cyan), illustrates Met-241 forms the top of the methyl pocket for this compound. (b) Overlay of crystal structures of compounds **3** and **4** (in orange, 5BWU) with protein surface of compound **4** (orange) shown. Rotation of Met-241 now creates a new pocket that accommodates the benzylic substituent of of **4**.

fragment hits (e.g., **3**, in cyan) and revealed access to a novel induced pocket that accommodated the bromobenzyl substituent. This pocket is blocked by a methionine side chain (Met-241) in the protein crystal structure of **3** (in cyan, Figure 2a), however, rotation of the thioether side chain through 180° facilitated binding of the larger substituent (Figure 2). This movement had not previously been observed in any other BCATm protein structures identified in our screening[38] or described in the literature;[11,12] in the absence of this information, traditional fragment optimization techniques may

not have identified this induced pocket from fragment hits **2** and **3**.

The initial medicinal chemistry strategy was to synthesize hybrids of the fragments (**2** and **3**) and HTS derived molecules (**4** and **5**) in order to confirm that SAR between the series was transferable and to further understand the role of the 3-cyano substituent (Table 3). The pertinent point changes were thus incorporated in compounds **6–8**, which were synthesized using the methods described in Scheme 1 and Scheme 9. Biological data showed a consistent 10-fold increase in potency and improvement in solubility by replacing the triazole 3-nitrogen with the 3-cyano motif of the pyrazolo fragments. The bromo analogue **7** showed a slight increase in potency compared to its chloro analogue **6**, a trend that also translated into the cellular assay. In contrast, the combination of a 5-benzyl substituent with a chlorobenzylamine (**8**), while showing similar potency, engendered reduced efficiency and solubility and was not pursued further.

A crystal structure of compound **6** (in green, Figure 3) was obtained and confirmed that the binding mode of the hybrid
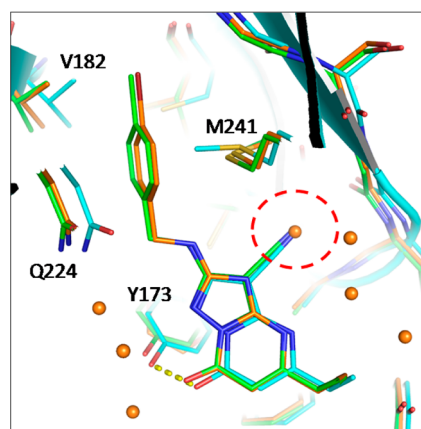
Figure 3. Crystal structure of compounds **3** (in cyan, 5BWT) and **4** (in orange, 5BWU) overlaid with compound **6** (in green, 5BWV) illustrating the water displaced by the nitrile **3** and **6**.

Table 3. Initial SAR of Hybrid Compounds

Cmpd	Structure	BCATm pIC$_{50}$	LE	LLE$_{AT}$	Chrom logD$_{7.4}$	CLND sol. (μg/mL)	Cell pIC$_{50}$
4		6.2	0.39	0.35	2.92	54	6.1
5		5.7	0.36	0.32	2.86	37	5.9
6		7.1	0.41	0.36	2.90	144	6.2
7		7.6	0.43	0.38	3.02	≥ 163	6.6
8		7.0	0.34	0.30	3.23	26	5.9

compound was as designed. Comparison with compound **4** (in orange, Figure 4) suggested the nitrile group of **6** displaced a
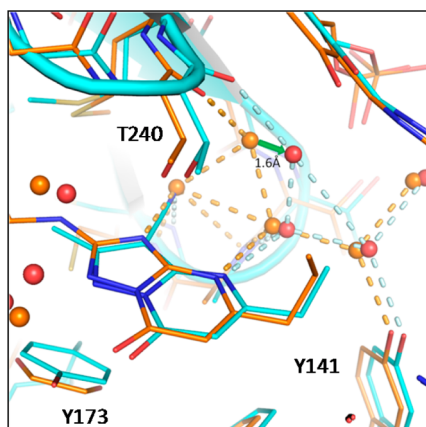
Figure 4. Crystal structure of compounds **3** (in cyan, 5BWT) and **4** (in orange, 5BWU) showing the change in the water network on changing the triazole (**4**, in orange) for the nitrile (**3**, in red).

water molecule observed in the structure with **4**. Displacing this water may account for the 10-fold increase in affinity, suggesting that this may be energetically favorable. The displaced water is at the end of a network of water molecules, and while it has multiple polar contacts, the geometry is nonideal.[39] When the nitrile group is present, the water network rearranges, one water molecule moved 1.6 Å, presumably providing a more optimal arrangement of the waters (Figure 4).

From these initial data, further SAR exploration focused on investigating three key areas, as highlighted in Figure 5: the
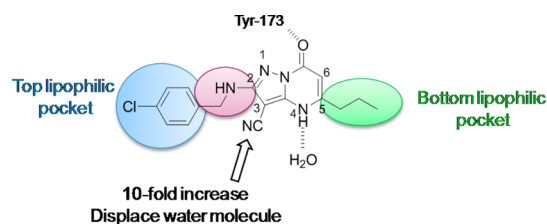
Figure 5. SAR exploration strategy.

lipophilic pocket (in green), the linker (in pink), and the chlorobenzyl substituent in the induced lipophilic pocket (in blue). The nitrile showed a consistent 10-fold increase in potency as described above. From crystal structure of compound **6** (in green, Figure 6), both the pyrimidinone carbonyl and 4-NH motif were believed to be important for potency (hydrogen bond to Tyr-173).

Exploring the Lipophilic Pocket from the 5-Position. Through analysis of the crystal structure of compound **6** (in green, Figure 6), it was observed that the propyl chain did not optimally fill the volume of the lipophilic pocket, thus longer and branched chains were investigated. To mitigate the increasing lipophilicity associated with such changes, heteroatoms were also introduced into the chain.

Compounds **9**−**14** were obtained rapidly from reaction of the key benzyldiaminopyrazole **18a** with the desired β-keto ester **19a**−**h** (Scheme 1). Reaction of 4-chlorobenzylamine **15a** with 2-(bis(methylthio)methylene)malononitrile **16** in ethanol at reflux gave intermediate **17a**, which was reacted immediately
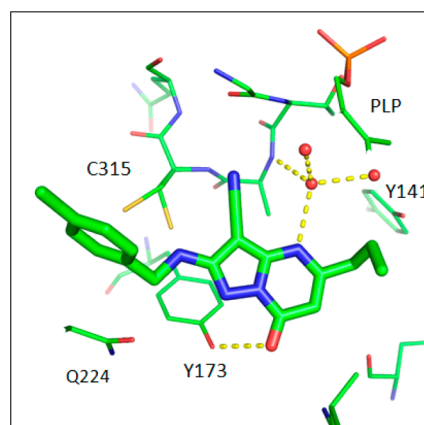
Figure 6. Crystal structure of compound **6** (in green, 5BWV) illustrating the key interactions with Tyr-173 and water molecules.

with hydrazine hydrate to provide the desired benzyldiaminopyrazole **18a**. Reaction of **18a** with the desired β-ketoester **19a**−**h** in a mixture of acetic acid/water at 120 °C gave the final products in reasonable yields (16−70%), with most products collected by filtration on cooling.[40] The β-ketoester **19h** was prepared following procedures described by Brooks et al. (Scheme 2).[41] The carboxylic acid **20** was converted to the activated imidazolide using CDI and was then treated without isolation with the magnesium salt of malonic acid to give **19h**.

The ethyl analogue **9** showed a significant drop (>10-fold) in enzyme potency, suggesting that the extra length of the propyl chain (**6**) was enabling more significant interactions with the protein (Table 4). Addition of an extra carbon in the butyl analogue **10** maintained good potency with the same ligand efficiency. Branched compounds, e.g., isobutyl **11** and isopentyl **12**, gave somewhat reduced potency and efficiency, while the incorporation of oxygen in the chain, e.g., **13**, was not well tolerated. These results confirmed the hypothesis made from the crystal structure, which showed mainly lipophilic residues in this region, favoring hydrophobic contacts with little accommodation for polar motifs. Most significantly from these data, propyl and butyl substituents (**6** and **10**) were shown to be the most efficient. Interestingly, introduction of a furan ring (**14**) maintained good enzyme potency and good LE and LLE$_{AT}$, however, this activity did not translate into the cellular assay. Although in this case, addition of a fourth aromatic ring to the structure was not favorable in terms of cellular activity, it offered a potentially interesting substituent in molecules with nonaromatic groups at the 2-position.

Exploring the Linker at the 2-Position. From consideration of the crystal structure, the linker NH did not appear to make any polar interactions with the protein; therefore, a systematic set of elongated (**23**), isosteric, and isomeric linkers were investigated including exemplars with oxygen and carbon (**24**−**27**). The crystal structure of compound **6** (in green, Figure 7) also suggested that an additional interaction could be accessed via the amide linkers in this region of the protein. The backbone NH and the side chain hydroxyl of Thr-240 were within an appropriate distance to target a new hydrogen-bonding interaction. On the basis of this, compounds (**28** and **29**) were selected for synthesis to test these hypotheses.

The phenethyl analogue **23** was synthesized by incorporating 4-chlorophenylethylamine **15b** into the route, described in Scheme 1.

Scheme 1. General Procedure of Alternative Derivatives of Pyrazolopyrimidinone[a]
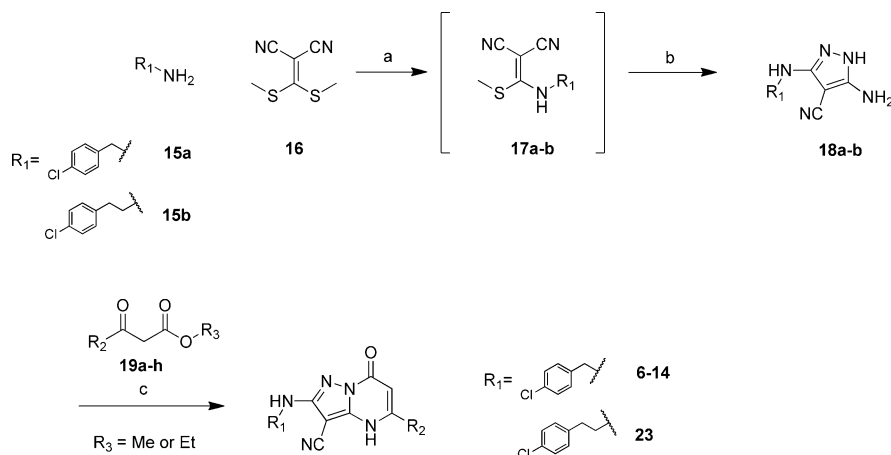
[a]Reagents and conditions: (a) EtOH, reflux, 3 h; (b) NH$_2$NH$_2$·H$_2$O, reflux, 1 h, 62−82%; (c) AcOH/H$_2$O, 120 °C, overnight, 16−70%.

Scheme 2. Synthesis of β-Ketoester 19h[a]
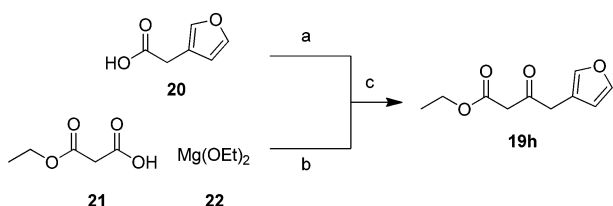
[a]Reagents and conditions: (a) CDI, THF, overnight; (b) THF, rt, 5 h then evaporated and redissolved in THF; (c) rt, 5 h, crude.

The methylene aryl amine **24** and ether **25** were prepared following Scheme 3, whereby malonitrile **30** was reacted with ethyl oxalate and subsequently treated with phosphorus oxychloride and methanol to give the vinyl ether **31**. Subsequent reaction with hydrazine hydrate generated aminopyrazole **32**, which was reacted with ethyl 3-oxohexanoate to give the ester **33**. This was reduced to the alcohol **34** in good yield using lithium borohydride and converted to the bromide **35** using the Appel reaction.[42,43] Finally, alkylation of 4-chloroaniline with **35** gave the final product **24** and alkylation of 4-chlorophenol with **35** was mediated by sodium hydride to give the final product **25**.

The benzyloxy analogue **26** was prepared following Scheme 4. The commercially available methylthioaminopyrazole **36** was reacted with ethyl 3-oxohexanoate to give methylthioether **37**, which was oxidized using mCPBA to the sulfone analogue **38**.

Table 4. SAR of the Alkyl Side Chain at Position 5 of the Pyrazolopyrimidinone

Cmpd	R$_2$	pIC$_{50}$	LE	LLE$_{AT}$	Chrom logD$_{7.4}$	CLND sol. (μg/mL)	Cell pIC$_{50}$
6		7.1	0.41	0.36	2.90	144	6.2
8		7.0	0.34	0.30	3.23	26	5.9
9		5.9	0.35	0.33	2.34	≤ 144	ND
10		7.4	0.41	0.34	3.38	109	6.7
11		6.6	0.36	0.30	3.26	≤ 133	5.7
12		6.9	0.36	0.28	3.87	75	6.2
13		5.4	0.31	0.36	1.94	162	ND
14		7.5	0.38	0.37	2.86	149	5.8
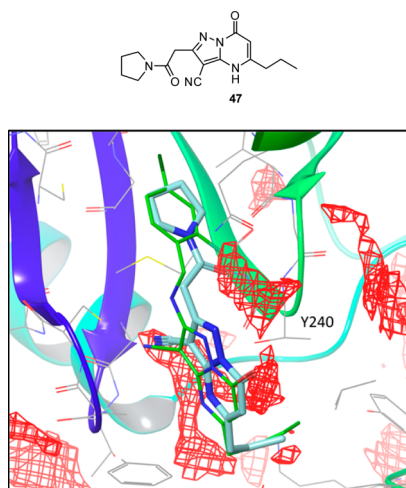
Figure 7. Designed pyrrolidine amide analogue **47** (in cyan) docked into the BCATm pocket showing potential hydrogen bond with Thr-240 and planar access to the lipophilic pocket as observed with the phenyl ring in compound **6** (in green).

Scheme 4. Preparation of Benzylic *O*-Linked Analogue 26[a]
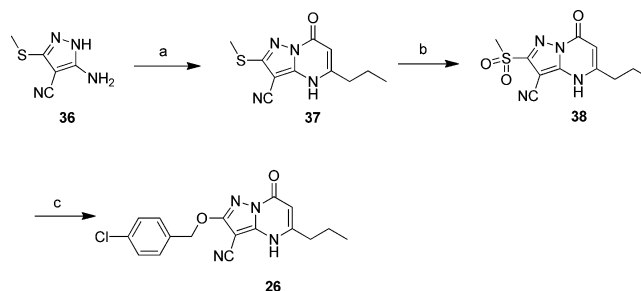
[a]Reagents and conditions: (a) ethyl 3-oxohexanoate, AcOH/H$_2$O (2:1), 120 °C, 3 days, 53%; (b) mCPBA, rt, 4 days, 85%; (c) NaH, 4-chlorobenzylalcohol, THF, 90 °C, microwave, 12%.

The sulfone was displaced with 4-chlorobenzylalcohol in THF at 90 °C to give the target compound **26**.

The all-carbon linked **27** was prepared following Scheme 5. The first step in this synthesis involved the preparation of morpholinethioamide **40** from the ketone **39** using the Willgerodt−Kindler reaction.[44,45] The enamine intermediate **42** was prepared by reaction of thioamide **40** with tetracyanoethylene oxide **41** in excellent yield by following the procedure of Taminoga and co-workers.[46,47] Subsequent reaction with hydrazine hydrate gave the desired phenethylpyrazole **43**, which was converted to the product **27** using the previously reported procedure.[47]

The amide **28** was prepared following Scheme 6. The aminopyrazolopyrimidinone intermediate **45** was prepared using the standard methods; conversion to the targeted amide **28** was achieved using 4-chlorobenzoyl chloride in the presence of DMAP and pyridine. The reversed amide **29** was prepared following Scheme 7, exploiting the ester intermediate **33** (Scheme 3) via hydrolysis to the corresponding carboxylic

acid **46** using sodium hydroxide, then HATU mediated amide coupling with 4-chloroaniline gave the desired final product **29**.

In efforts to further modulate the physicochemical properties of the compounds, which could positively impact on the DMPK profile of the series, the feasibility of replacing the aromatic ring in the top pocket with an aliphatic ring was investigated. The existing *N*-alkyl or *O*-alkyl linkers did not appear to present suitable geometry to enable good contacts within the pocket by an aliphatic ring as confirmed by compound **56**, so alternative linkers were sought. A GRID analysis[48,49] was performed using probe atoms with different hydrogen bond donating and accepting abilities (see Experimental Section). Inspection of the carbonyl O GRID map revealed an acceptor region formed by the backbone NH and side chain hydroxyl of Thr-240 that could be accessible from an appropriate donating motif on the linker. Several alternative linkers and ring variations were constructed in silico and docked using GLIDE (see Experimental Section) to determine the potential for interacting with this region. The best candidate was the methyl carbonyl linker with a pyrrolidine ring (**47**, in cyan, Figure 7).

The target pyrrolidine amide **47** was prepared following the procedure described in Scheme 8. The condensation reaction between ethyl 3-oxohexanoate and commercial aminopyrazole **48** generated the desired pyrazolopyrimidinone **49**. Selective hydrolysis of the alkyl nitrile to the corresponding ethyl ester

Scheme 3. Preparation of Analogues 24 and 25[a]
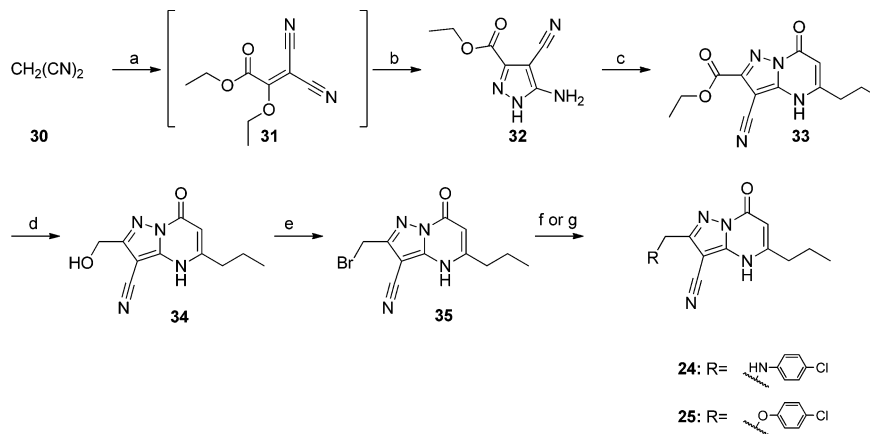
[a]Reagents and conditions: (a) (1) ethyl oxalate, NaOEt, EtOH, (2) POCl$_3$, (3) MeOH; (b) NH$_2$NH$_2$·H$_2$O, EtOH, 42% over the two steps; (c) ethyl 3-oxohexanoate, AcOH, 52%; (d) LiBH$_4$, THF, 84%; (e) CBr$_4$, Ph$_3$P, DCM, 44%; (f) 4-chloroaniline, THF, 140 °C, microwave, 30 min, 67%; (g) NaH, 4-chlorophenol, THF, 88%.

Scheme 5. Preparation of C-Linked Analogue 27[a]
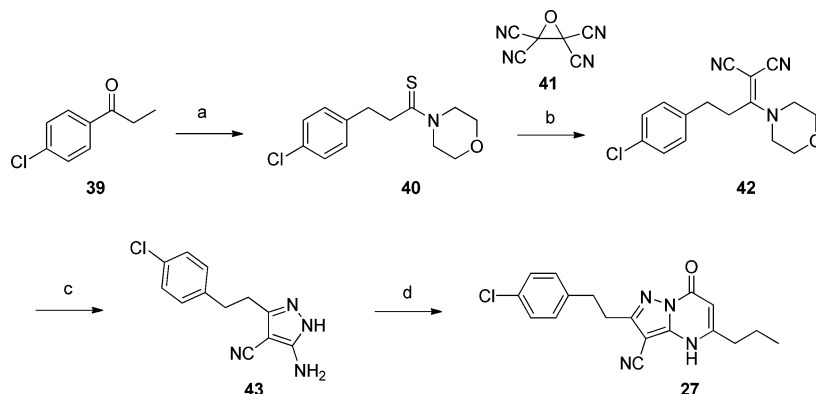
[a]Reagents and conditions: (a) morpholine, sulfur powder, 130 °C, 24 h, 62%; (b) toluene, rt, 14 h, 90%; (c) NH$_2$NH$_2$·H$_2$O, EtOH, reflux, 5 h, 73%; (d) ethyl 3-oxohexanoate, AcOH, reflux, 20 h, 59%.

Scheme 6. Preparation of Amide-Linked Analogue 28[a]
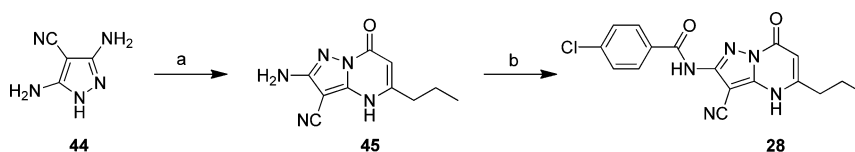
[a]Reagents and conditions: (a) ethyl 3-oxohexanoate, AcOH, reflux, 24 h, 98%; (b) 4-chlorobenzoyl chloride, DMAP, pyridine, DCM, rt, 4 days, 41%.

Scheme 7. Preparation of Reversed Amide-Linked Analogue 29[a]
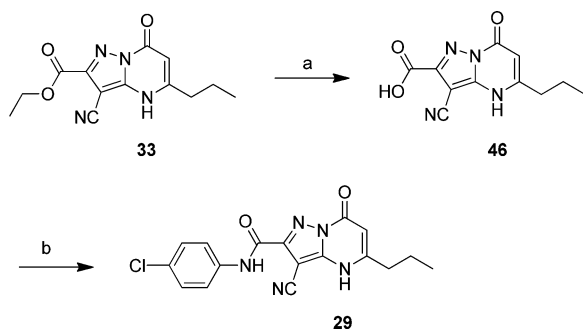
[a]Reagents and conditions: (a) NaOH, EtOH, 2 h, quantitative; (b) 4-chloroaniline, HATU, DIPEA, DCM, rt, 14 h, 62%.

50 in the presence of the aryl nitrile was achieved using a saturated solution of HCl in ethanol.[50] The identity of the

product formed (50) was confirmed by an HMBC signal from the ester carbonyl carbon (168.8 ppm) to both the ester CH$_2$ protons (4.14 ppm) and the methylene protons adjacent to the ring (3.9 ppm). No hydrolysis of the aryl nitrile was observed. The synthesis of the final compound 47 was achieved after ester hydrolysis and HATU-mediated coupling with pyrrolidine.

Phenethyl analogue 23 showed that extension of the chain was not as efficient as its analogue 6 and therefore offered no real advantage. From the crystal structure of compound 6 (in green, Figure 8), it appeared that the chloro substituent fit the pocket well; extension of the chain might have pushed the phenyl ring too far into this space, resulting in a clash with the protein (Table 5). Reversing the connectivity, with the NH in an aniline linkage (24) significantly reduced the potency. Similarly, the amide analogues (28−29) and C-linked compound 27 showed significantly decreased activity. The O-linked compounds (25−26) showed reasonable potency while maintaining good efficiencies, but when analogues were synthesized they tended to show poor cellular potency

Scheme 8. Preparation of Pyrrolidine Amide Derivative 47[a]
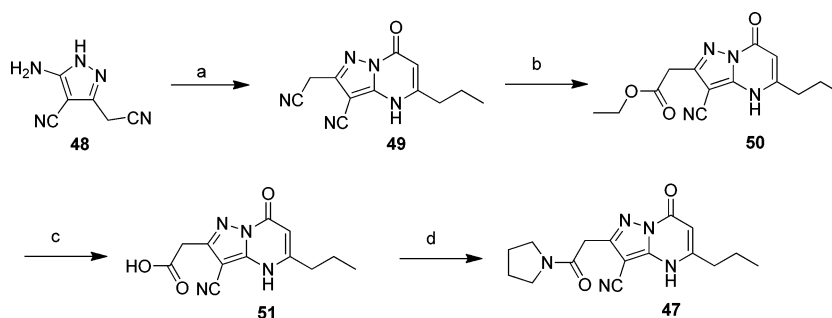
[a]Reagents and conditions: (a) ethyl 3-oxohexanoate, AcOH, H$_2$O, 120 °C, 2 days, 33%; (b) HCl(g), EtOH, <30 °C, 2.5 h, 46%; (c) LiOH, 2Me-THF/MeOH/H$_2$O, rt, 24 h, 55%; (d) pyrrolidine, HATU, DIPEA, DMF, 19 h, rt, 57%.
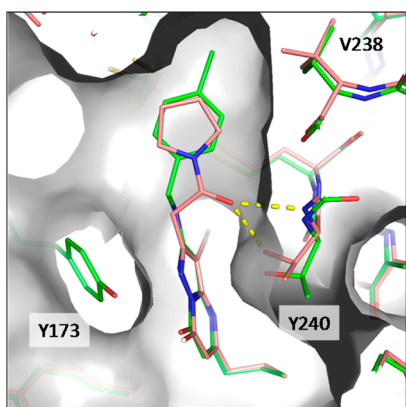
Figure 8. Crystal structure of compound **47** (in pink, 5BWW) overlaid with compound **6** (in green, 5BWV) showing the key hydrogen bonds from the carbonyl to Thr-240. Protein surface of compound **6** is shown.

compared to the *N*-linker (data not shown) and poor solubility for analogues of **26**. The outcome of this exercise was that the *N*-linker, directly attached to the core (e.g., **6**) remained the most potent and efficient with aryl substitution.

On the other hand, the pyrrolidine amide **47** showed very encouraging data, showing reasonable potency while improving LE, LLE$_{AT}$, and physicochemical properties compared with the benzylic analogues. A liganded structure of **47** was solved (in pink, Figure 8) and, gratifyingly, showed a binding pose very close to that predicted. In this structure, the carbonyl of **47** is within H-bonding distance (2.9 Å) to both the backbone NH and side chain OH of Thr-240, with better geometry to the NH, however, the density of residues 172−178, including Tyr-173, are disordered. The compound showed no activity in the cellular assay (the compound is rather hydrophilic with chromlogD$_{7.4}$ 0.98), but the benefit of an aliphatic substituent in this position was proven and could enable the incorporation of more lipophilic groups elsewhere in the molecule.

Table 5. SAR of the Linkers

X = O, NH, C
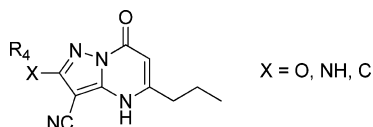
Cmpd	Linker -XR$_4$	pIC$_{50}$	LE	LLE$_{AT}$	chromlogD$_{7.4}$	CLND sol. (µg/mL)	Cell pIC$_{50}$
6		7.1	0.41	0.36	2.90	144	6.2
23		6.6	0.36	0.29	3.32	130	6.0
24		5.9 (n=1)	0.34	0.31	2.85	191	ND
25		6.7	0.38	0.32	3.16	162	5.3[a]
26		6.6	0.38	0.33	3.49	16	ND
27		6.2	0.35	0.27	3.26	34	5.3[a]
28		6.0	0.33	0.36	2.28	≤202	ND
29		6.1	0.33	0.34	3.08	100	ND
47		6.3	0.38	0.49	0.98	147	<5.0

[a]Compound reported pIC$_{50}$ < 5.5 in 1 out of the 2 test occasions.

Exploring the Induced Lipophilic Pocket. Substitution of the pendant benzyl ring was also explored with the aim of improving enzyme and cellular inhibition by targeting additional residues, especially Thr-240. The crystal structure had revealed a small pocket at the *para*-position of the phenyl ring, which was occupied by the chlorine substituent (Figure 9).
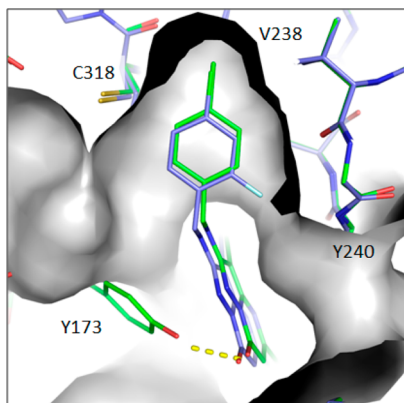
Figure 9. Crystal structure of compound **66** (in blue, 5BWX) overlaid with compound **6** (in green, 5BWV). Protein surface of compound **6** is shown.

Compounds **52−57** were synthesized via reductive amination (Scheme 9, route A) and compounds **58−64** by an adaptation of Scheme 1 with appropriate benzyl amines (Scheme 9, route B). The reductive amination of aminopyrazolopyrimidnone **43** (route A), which allowed introduction of the desired diversity at the final step, was an attractive option; however, the reactions were slow and low-yielding (11−29%, with compounds **52−57** synthesized in this way). Route B (with compounds **58−64**) was high yielding and ultimately as fast; in addition, it offered opportunities to vary substituents on the 5-position with each aryl halide analogue.

The impact of substituents on the phenyl ring showed some clear positive contributions to the potency, which could be rationalized by observed interactions in the crystal structure. Reduced potency and ligand efficiency of the phenyl analogue (**52**) confirmed that the *para*-substituent made a positive contribution to binding, which reached deeply into a narrow hydrophobic well, formed largely by valine residues at the end of the pocket (Table 6). The chlorine of **6** could be replaced by a bromine (**7**), with similar potency, but other substituents were less well tolerated (e.g., methyl **53**). Exploration of substituents around the ring revealed that *meta*-substitution was, perhaps not unexpectedly, less well tolerated (**54** and **59**), while fluorination at the *ortho*-position maintained good potency and efficiencies (**60**). This observation was attributed to a likely fluorine−H-bonding interaction with Thr-240.[51] The *ortho* fluorinated compounds also showed improved potency in the cellular assay. Other *ortho*-substituents were less well tolerated and resulted in a decrease in potency. Heteroaromatic rings (e.g., **57−58**) were also synthesized in order to explore reduced lipophilicity; the 2-pyridyl (**58**) was tolerated for enzyme potency, but its lower lipophilicity perhaps accounted for reduced cellular potency. Attempts to saturate the ring resulted in compounds with reduced potency (e.g., **56**) as suggested by the geometry of the pocket.

Combination of Best Groups. Gratifyingly, combining the optimized benzyl substituents of the induced lipophilic pocket with the more potent butyl chain, occupying the bottom pocket gave an additive improvement in potency in both the enzyme and cellular assays (Table 7). In general, 4-chloro substituted compounds (**66**, **69**) were slightly more soluble than the corresponding 4-bromo analogues (**67**, **70**). The methyl substituted linker (**68**) increased lipophilicity with no real advantage when compared to the nonsubstituted analogues (e.g., **67**). Compounds **66−70** were synthesized according to the synthetic route B described in Scheme 9.

A crystal structure of compound **66** (in blue) was obtained and confirmed a conserved binding mode (Figure 9) and also indicated the proximity of the *ortho*-fluorine to Thr-240 seemed beneficial.

Scheme 9. Preparation of Alternative Benzyl Derivatives[a]
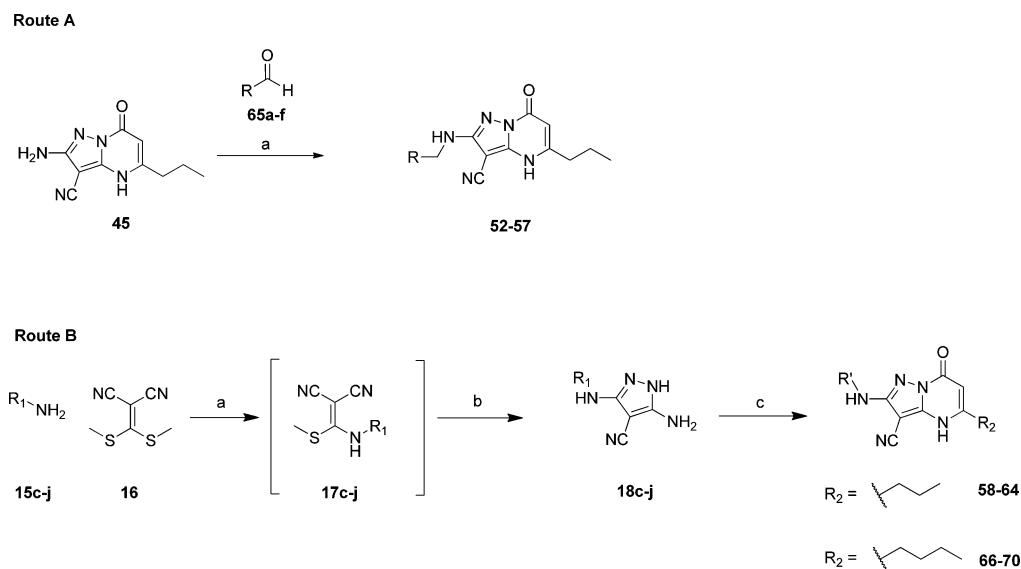
[a]Reagents and conditions. Route A: (a) NaBH(OAc)$_3$, AcOH, DCM, rt −50 °C, 1−2 days, 11−29%. Route B: (a) EtOH, reflux; (b) NH$_2$NH$_2$·H$_2$O, reflux, 1 h, 67−96%; (c) methyl 3-oxohexanoate (**58−64**) or methyl 3-oxoheptanoate (**66−70**), AcOH/H$_2$O, 120 °C, overnight, 22−76%.

Table 6. SAR of the Benzyl Substituents
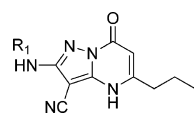
Cmpd	R$_1$	pIC$_{50}$	LE	LLE$_{AT}$	Chrom logD$_{7.4}$	CLND sol. (µg/mL)	Cell pIC$_{50}$
6	(4-Cl-benzyl)	7.1	0.41	0.36	2.90	144	6.2
7	(4-Br-benzyl)	7.6	0.43	0.38	3.02	163	6.6
45	H	5.0	0.43	0.56	ND	ND	ND
52	(benzyl)	5.9	0.35	0.34	2.15	145	ND
53	(4-Me-benzyl)	6.6	0.38	0.34	2.60	93	5.7
54	(3-Me-4-Cl-benzyl)	6.7	0.37	0.30	3.32	119	6.0
55	(2-OMe-5-Cl-benzyl)	6.2	0.33	0.29	3.13	39	ND
56	(tetrahydropyran-4-yl-methyl)	5.2	0.31	0.37	1.23	185	ND
57	(6-Cl-pyridin-3-yl-methyl)	5.6	0.32	0.36	1.66	167	ND
58	(5-Br-pyridin-2-yl-methyl)	6.8	0.39	0.42	2.01	310	5.7
59	(3-F-4-Cl-benzyl)	6.5	0.36	0.31	2.98	167	ND
60	(2-F-4-Cl-benzyl)	7.3	0.40	0.35	2.91	155	6.5
61	(2,6-diF-4-Cl-benzyl)	7.3	0.39	0.33	3.12	164	6.8
62	(2-F-4-Br-benzyl)	7.6	0.42	0.36	3.10	157	6.8
63	(2-F-4-Br-α-methyl-benzyl)	7.7	0.41	0.34	3.69	142	7.2
64	(2-F-4-Br-α-methyl-benzyl)	5.8	0.31	0.24	3.55	136	ND

Table 7. SAR of Optimized Compounds 66−70

Cmpd	Structure	pIC$_{50}$	LE	LLE$_{AT}$	Chrom logD$_{7.4}$	CLND sol. (µg/mL)	Cell pIC$_{50}$
66		7.8	0.41	0.34	3.56	101	**7.1**
67		7.9	0.42	0.34	3.58	60	**7.3**
68		7.9	0.40	0.32	4.06	74	**7.3**
69		7.8	0.40	0.33	3.48	163	**7.5**
70		8.0	0.41	0.33	3.67	142	**7.2**

Pharmacokinetic Studies. As the optimized compounds were progressed into downstream assays, it was observed that the solubility of the solid samples, dissolved in neutral buffer, was significantly poorer than had been measured in a high throughput precipitation experiment from DMSO solution using chemiluminescent nitrogen detection (CLND, Table 8).

Table 8. Solubility, Oral Bioavailability, and Exposure for Different pH Formulations for Compounds 6 and 60[a]

	6		60	
	pH 7	**pH 10**	**pH 7**	**pH 10**
Solid sol. (µg/mL)	37*	>500	43	402
AUC (0-t) (µg·h/mL)	38*	54	26	113
F (%)	56*	100	23	91

[a]Studies carried out using *n* = 2 C57−B6 mice per route of administration (*n* = 4). Dose: 5 mg/kg: solid solubility assay.

As the pK_a of the pyrimidinone NH of compound **6** was measured to be 6.3, the compounds were subsequently progressed into pharmacokinetic (PK) experiments dissolved in buffer at pH 10, which produced a dramatic improvement in both solubility and overall pharmacokinetic exposure (Table 8).

Once the dissolution issue had been addressed, it was clear that a focus on the physicochemical properties of the compounds during optimization delivered entities with consistently good pharmacokinetic profiles. The compounds typically had low clearance, high bioavailability, and long half-lives, as exemplified by **61** and **69** in Table 9, although the

Table 9. Physicochemical Properties and Mouse PK Profile of Compounds 61 and 69

	61	69
BCATm pIC$_{50}$ (LE, LLE$_{AT}$)	7.3 (0.39; 0.33)	7.8 (0.40; 0.33)
Human differentiated adipocyte cell BCATm pIC$_{50}$	6.5	7.5
BCATc pIC$_{50}$	6.6	7.2
Ratio brain/blood (10 mg/kg)	0.03	ND
chromlogD$_{7.4}$	3.12	3.48
Solid sol. (µg/mL) pH 10	>500	326
AUC (0-t) (µg·h/mL)	306	65
t$_{1/2}$ (h)	9.2	6.8
Cl$_b$ (mL/min/kg)	0.3	0.63
F (%)	100	50
PPB (%)	97	96.5

generally more potent bromo compounds showed poorer pharmacokinetic profiles than their chloro analogues (e.g., **68** Cl$_b$ 2.4 mL/min/kg, t$_{1/2}$ 2.5 h, F% 23). A similar trend was apparent for compounds with butyl versus propyl substituents. Although the optimized compounds showed limited selectivity over BCATc, their measured low brain exposure suggested engagement with BCATc in vivo would likely be minimal.

Taking potency and pharmacokinetic data into consideration, compounds **61** and **69**, both with potent cellular inhibition of BCATm and excellent PK profiles, thus represented attractive
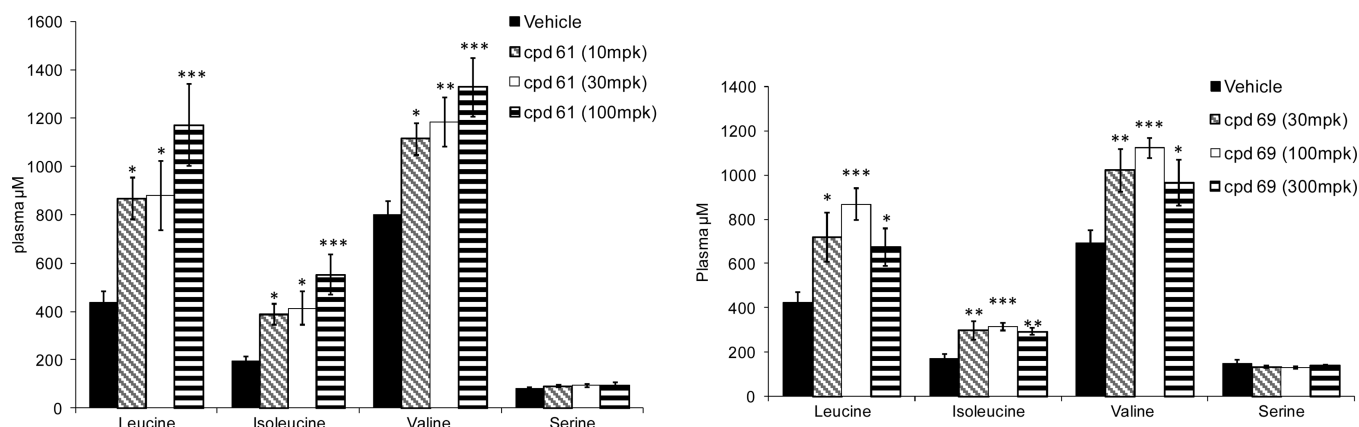
Figure 10. BCAA levels after treatment with compounds **61** and **69**. Statistical posthoc analysis using least significant difference (LSD) test was used to compare group. *** $P < 0.001$; ** $0.001 < P < 0.01$; * $P < 0.05$.

molecules for in vivo pharmacology experiments to investigate the impact of inhibiting the target.

In Vivo Studies. The effect of compounds **61** and **69** on BCAA catabolism in vivo was evaluated. A murine assay using a bolus amino acid "meal", given 5 h after compound administration, was designed to monitor the modulation of BCAA levels by BCATm in vivo. As shown in Figure 10, mice treated with compounds **61** or **69** demonstrated higher levels of all three BCAAs in their serum compared to those given the vehicle only. Serine and tyrosine concentrations were used as control, and no effects on their levels was observed in treated mice (data shown for serine only). Compound **61** demonstrated a good dose response, with leucine increasing from 473 μM (basal level) to 1.2 mM in 100 mg/kg treated mice. In comparison, compound **69** appeared to plateau above an effective dose of 30 mg/kg.

CONCLUSIONS

A rapid optimization of weak, yet efficient fragment hits into potent BCATm inhibitors (cell $pIC_{50} > 7$) was achieved by incorporating information from high throughput screening hits and intensive use of structure-based design. The optimization was carried out with a focus on physicochemical properties, which resulted in optimized molecules with excellent pharmacokinetic profiles for in vivo studies (F% > 50% and high exposure). The high quality compounds developed clearly demonstrated in vivo engagement of the target thus establishing them as valuable pharmacological tools, which can be used to further understand the biological role of BCATm.

EXPERIMENTAL SECTION

Chemistry. *General.* All solvents and reagents, unless otherwise stated, were commercially available from regular suppliers such as Sigma-Aldrich and Fluorochem and were used as purchased without further purification. Proton and carbon nuclear magnetic resonance (^{1}H NMR and ^{13}C NMR) spectra were recorded on a Bruker AVI (400 MHz), Bruker Nano (400 MHz), or Bruker AVII+ (600 MHz) spectrometer (with cryoprobe) in the indicated solvent. Chemical shifts δ are reported in parts per million (ppm) relative to tetramethylsilane and are internally referenced to the residual solvent peak. Coupling constants (J) are given in hertz (Hz) to the nearest 0.5 Hz. Liquid chromatography—mass spectroscopy (LC—MS) analyses were conducted on either system A, a Waters Acquity UPLC BEH C_{18} column (50 mm × 2.1 mm i.d., 1.7 μm packing diameter) at 40 °C eluting with 0.1% v/v solution of formic acid in water (solvent A) and 0.1% v/v solution of formic acid in acetonitrile (solvent B), using the

following elution gradient 0.0−1.5 min 3−100% B, 1.5−1.9 min 100% B, 1.9−2.0 min 3% B, at a flow rate of 1 mL/min; or system B, a Waters Acquity UPLC BEH C_{18} column (50 mm × 2.1 mm i.d., 1.7 μm packing diameter) at 40 °C eluting with 10 mM ammonium bicarbonate in water adjusted to pH 10 with ammonia solution (solvent A) and acetonitrile (solvent B), using the following elution gradient 0.0−1.5 min 1−97% B, 1.5−1.9 min 97% B, 1.9−2.0 min 100% B, at a flow rate of 1 mL/min. The UV detection was based on an average signal from wavelength of 210 to 350 nm. The mass spectra were recorded on a Waters ZQ mass spectrometer using alternate-scan positive and negative mode electrospray ionization. Preparative HPLC using a mass directed auto purification (MDAP) were conducted on a Waters FractionLynx system comprising a Waters 515 pump with extended pump heads, Waters 2767 autosampler, Waters 996 photodiode array detector, and Gilson 202 fraction collector on a XBridge or Sunfire C_{18} column (30 mm × 150 mm i.d., 5 μm packing diameter) at ambient temperature. The mobile phase was 0.1% v/v solution formic acid in water or 10 mM ammonium bicarbonate in water adjusted to pH 10 with ammonia solution (solvent A) and 0.1% v/v solution formic acid in acetonitrile or acetonitrile (solvent B), respectively. The UV detection is a summed signal from wavelength of 210−350 nm. The mass spectra were recorded on a Waters ZQ mass spectrometer using alternate-scan positive and negative electrospray ionization. The software used was MassLynx 3.5 with OpenLynx and FractionLynx options. High resolution mass spectra (HRMS) were obtained on a Micromass Q-Tof Ultima hybrid quadrupole time-of-flight mass spectrometer, equipped with a Z-spray interface (ESI), over a mass range of 100−1100 Da, with a scan time of 0.9 s and an interscan delay of 0.1 s. Reserpine was used as the external mass calibrant ([M + H]$^+$ = 609.2812 Da). The Q-Tof Ultima mass spectrometer was operated in W reflectron mode to give a resolution (fwhm) of 16000−20000. Ionization was achieved with a spray voltage of 3.2 kV, a cone voltage of 50 V, with cone and desolvation gas flows of 10−20 and 600 L/h, respectively. The source block and desolvation temperatures were maintained at 120 and 250 °C, respectively. The elemental composition was calculated using MassLynx v4.1 for the [M + H]$^+$ and the mass error quoted as ppm. Flash column chromatography was conducted on a Combiflash Rf, automated flash chromatography system, from Teledyne Isco using disposable, normal or reverse phase, SPE Redisep cartridges (4 to 330 g). The CombiFlash Rf used radio frequency identification detector (RFID) technology to automate setting the parameters for purification runs and fraction collection. The system was equipped with a UV variable dual-wavelength and a Foxy fraction collector enabling automated peak cutting, collection, and tracking. Isolute 103 cartridges from Biotage are hydroxylated polystyrene—divinylbenzene copolymer resin and were used to extract organic compounds from aqueous solution using a catch and release protocol. The purity of all compounds screened in the biological assays was examined by LC—MS analysis and was found to be ≥95% unless otherwise specified. All animal

studies were ethically reviewed and carried out in accordance with Animals (Scientific Procedures) Act 1986 and the GSK Policy on the Care, Welfare, and Treatment of Laboratory Animals. The human biological samples were sourced ethically, and their research use was in accord with the terms of the informed consents.

5-Benzyl-7-oxo-4,7-dihydropyrazolo[1,5-a]pyrimidine-3-carbonitrile (2). 3-Amino-1*H*-pyrazole-4-carbonitrile (100 mg, 0.925 mmol) and methyl-3-oxo-4-phenylbutanoate (196 mg, 1.018 mmol) in acetic acid (1 mL) and water (2 mL) were heated at reflux for 48 h. The resulting solution was cooled to room temperature and concentrated under reduced pressure. The resulting crude mixture was diluted with EtOAc. The solid formed was filtered, washed with EtOAc, and dried in a vacuum oven overnight. The aqueous layer collected was concentrated under reduced pressure, and the solid obtained was combined with the solid from EtOAc wash. The resulting crude product was purified by reverse phase chromatography (43 g C$_{18}$ column, 5−30% 0.1% formic acid in acetonitrile in 0.1% formic acid in water over 27 CV) to give the title product **2** as a white solid (23 mg, 10%). ^{1}H NMR (400 MHz, chloroform-*d*) δ 8.02 (s, 1H), 7.33−7.47 (m, 3H), 7.25−7.32 (m, 2H), 5.89 (s, 1H), 4.00 (s, 2H). LC−MS (ESI, formic) *m/z* 251 [M + H]$^+$, R_t = 0.69 min.

2-((4-Bromobenzyl)amino)-5-propyl-[1,2,4]triazolo[1,5-a]-pyrimidin-7(4H)-one (4). Compound made following Reiter et al.[52]

2-((4-Chlorobenzyl)amino)-5-propyl-[1,2,4]triazolo[1,5-a]-pyrimidin-7(4H)-one (5). Compound made following Reiter et al.[52]

5-Amino-3-((4-chlorobenzyl)amino)-1H-pyrazole-4-carbonitrile (18a). A mixture of 2-(bis(methylthio)methylene)malononitrile (2.6 g, 15 mmol) and (4-chlorophenyl)methanamine (1.9 mL, 15 mmol) in EtOH (50 mL) was heated at reflux with a bleach scrubber on a stream of nitrogen for 3 h. Hydrazine (50 wt % in water, 1 mL, 15 mmol) was added dropwise over 1 min, and the reaction mixture was refluxed under nitrogen for 1 h. After this time, further hydrazine (50 wt % in water, 0.5 mL, 8 mmol) was added and the reaction mixture was refluxed for 4 h. The reaction mixture was cooled, and all volatile components were removed under reduced pressure. The oily residue was triturated with water, and a yellowish solid formed. The solid was collected by filtration under vacuum. The resulting crude product was purified by reverse phase chromatography (150 g C$_{18}$ Gold column, 15−35% 0.1% formic acid in acetonitrile in 0.1% formic acid in water over 30 min) to give the title product **18** as a white solid (2.3 g, 62%). ^{1}H NMR (400 MHz, DMSO-*d$_6$*) δ 10.92 (br s, 1H), 10.59 (br s, 1H), 7.33 (s, 4H), 6.03 (br s, 2H), 4.21 (d, *J* = 5.8 Hz, 2H). LC−MS (ESI, formic) *m/z* 248 [M + H]$^+$, R_t = 0.73 min. HRMS (ESI) calcd for C$_{11}$H$_{10}$ClN$_5$ + H$^+$, 248.0697; found, 248.0698.

3-Amino-5-((4-chlorophenethyl)amino)-1H-pyrazole-4-carbonitrile (18b). A mixture of 2-(bis(methylthio)methylene)malononitrile (1.12 g, 6.55 mmol) and 2-(4-chlorophenyl)ethanamine (1.02 g, 6.55 mmol) in EtOH (20 mL) was heated at reflux with a bleach scrubber on a nitrogen stream for 3 h. The mixture was cooled, and the resulting crude solution treated with hydrazine (50 wt % in water, 0.41 mL, 6.55 mmol). The mixture was heated at reflux with a bleach scrubber on a nitrogen stream for 1 h. The reaction was cooled, and all volatile components were removed under reduced pressure. The resulting residue was triturated with water, depositing a yellowish solid that was collected by filtration, washed with water, and dried in vacuum oven to give the title product **18b** (1.48 g, 82%). ^{1}H NMR (400 MHz, DMSO-*d$_6$*) δ 10.71 (br s, 1H), 7.33 (d, *J* = 8.3 Hz, 2H), 7.24 (d, *J* = 8.3 Hz, 2H), 5.86 (br s, 3H), 3.20−3.28 (m, 2H), 2.80 (t, *J* = 7.4 Hz, 2H). LC−MS (ESI, formic) *m/z* 262 [M + H]$^+$, R_t = 0.79 min.

2-((4-Chlorobenzyl)amino)-7-oxo-5-propyl-4,7-dihydropyrazolo-[1,5-a]pyrimidine-3-carbonitrile (6). Ethyl 3-oxohexanoate (415 mg, 2.62 mmol) was added to a suspension of 5-amino-3-((4-chlorobenzyl)amino)-1*H*-pyrazole-4-carbonitrile **18a** (500 mg, 2.02 mmol) in acetic acid (10 mL) and water (5 mL). The mixture was heated at 120 °C for 16 h. Additional ethyl 3-oxohexanoate (160 mg, 1.01 mmol) was added, and the mixture was heated at 120 °C for 4 h before the mixture was left to cool to room temperature. The solid formed was filtered and dried in a vacuum oven overnight to give the title product **6** as a white solid (481 mg, 70%); mp 278−280 °C. [1]H

NMR (400 MHz, DMSO-*d$_6$*) δ 12.77 (s, 1H), 7.37 (s, 4H), 7.23 (t, *J* = 6.3 Hz, 1H), 5.69 (s, 1H), 4.41 (d, *J* = 6.0 Hz, 2H), 2.49−2.53 (m under DMSO, 2H), 1.64 (sxt, *J* = 7.4 Hz, 2H), 0.92 (t, *J* = 7.3 Hz, 3H). LC−MS (ESI, formic) *m/z* 342 [M + H]$^+$, R_t = 0.91 min. HRMS (ESI) calcd for C$_{17}$H$_{16}$ClN$_5$O + H$^+$, 342.1121; found, 342.1116.

2-((4-Bromobenzyl)amino)-7-oxo-5-propyl-4,7-dihydropyrazolo-[1,5-a]pyrimidine-3-carbonitrile (7). 4-Bromobenzaldehyde (511 mg, 2.76 mmol) and 2-amino-7-oxo-5-propyl-4,7-dihydropyrazolo[1,5-a]-pyrimidine-3-carbonitrile **45** (300 mg, 1.38 mmol) were mixed in DCM (9 mL) and acetic acid (0.15 mL) under nitrogen and left to stir for 1 h. Then tetramethylammonium diacetoxy(formyloxy)-hydroborate (1.38 g, 5.52 mmol) was added. The mixture was stirred overnight at room temperature. Sodium triacetoxyborohydride (292 mg, 1.38 mmol) was added, and the mixture was stirred for 2 h. The mixture was quenched with saturated aqueous sodium bicarbonate (1 mL), and the phases were separated. The organic layer was then washed with water (×3) and then brine. The organic layer was passed through a hydrophobic frit and concentrated under reduced pressure. The resulting crude product was purified by reverse phase choromotgrapy using MDAP (formic acid, 30−85% solvent B over 15 min) to give the title product **7** (74 mg, 14%). ^{1}H NMR (400 MHz, DMSO-*d$_6$*) δ 12.77 (s, 1H), 7.50 (d, *J* = 8.3 Hz, 2H), 7.30 (d, *J* = 8.3 Hz, 2H), 7.22 (br s, 1H), 5.67 (br s, 1H), 4.38 (d, *J* = 6.3 Hz, 2H), 2.46−2.55 (m, 2H), 1.56−1.70 (m, 2H), 0.91 (t, *J* = 7.4 Hz, 3H). LC−MS (ESI, formic) *m/z* 386, 388 [M + H]$^+$, R_t = 0.94 min.

5-Benzyl-2-((4-chlorobenzyl)amino)-7-oxo-4,7-dihydropyrazolo-[1,5-a]pyrimidine-3-carbonitrile (8). Methyl 3-oxo-4-phenylbutanoate (excess) was added to a suspension of 5-amino-3-((4-chlorobenzyl)-amino)-1*H*-pyrazole-4-carbonitrile **18a** (200 mg, 0.807 mmol) in acetic acid (3 mL). The mixture was heated at reflux for 24 h. Volatile components were removed under reduced pressure. The resulting crude product was purified by reverse phase chromatography using MDAP (formic acid, 15−55% solvent B) to give the title product **8** as a white solid (53 mg, 17%). ^{1}H NMR (400 MHz, DMSO-*d$_6$*) δ 13.01 (br s, 1H), 7.22−7.40 (m, 9H), 7.13 (br s, 1H), 5.56 (s, 1H), 4.39 (d, *J* = 6.0 Hz, 2H), 3.86 (s, 2H). LC−MS (ESI, formic) *m/z* 390 [M + H]$^+$, R_t = 1.00 min.

2-((4-Chlorobenzyl)amino)-5-ethyl-7-oxo-4,7-dihydropyrazolo-[1,5-a]pyrimidine-3-carbonitrile (9). Methyl 3-oxopentanoate (0.051 mL, 0.404 mmol) was added to a suspension of 5-amino-3-((4-chlorobenzyl)amino)-1*H*-pyrazole-4-carbonitrile **18a** (100 mg, 0.404 mmol) in acetic acid (2 mL) and water (1 mL). The mixture was heated at reflux for 16 h. The mixture was cooled to room temperature, and a fine off-white solid was deposited, collected by filtration, washed with water, and dried in a vacuum oven to give the title product **9** as an off-white solid (91 mg, 67%). ^{1}H NMR (400 MHz, DMSO-*d$_6$*) δ 12.79 (br s, 1H), 7.36 (s, 4H), 7.23 (t, *J* = 6.1 Hz, 1H), 5.68 (s, 1H), 4.40 (d, *J* = 6.0 Hz, 2H), 2.54 (q, *J* = 7.5 Hz, 2H), 1.18 (t, *J* = 7.4 Hz, 3H). LC−MS (ESI, formic) *m/z* 328 [M + H]$^+$, R_t = 0.86 min.

5-Butyl-2-((4-chlorobenzyl)amino)-7-oxo-4,7-dihydropyrazolo-[1,5-a]pyrimidine-3-carbonitrile (10). The synthesis of this compound was used to assess the impact of variations in solvent ratios on the yield of the condensation reaction. Thus, portions of methyl 3-oxoheptanoate (48 μL, 0.30 mmol) were added to a suspension of 3-amino-5-((4-chlorobenzyl)amino)-1*H*-pyrazole-4-carbonitrile **18a** (75 mg, 0.30 mmol) in the solvent mixtures listed in Table 10. The reaction mixtures were heated at reflux for 16 h.

The conditions with the highest level of conversion, as assessed by analysis of the LC−MS traces of the reactions, corresponded to entry

Table 10. Solvent Mixtures

entry	acetic acid (mL)	water (mL)	toluene (mL)
1	3	0	0
2	2	1	0
3	1	2	0
4	1	0	2
5	0.5	0.5	2

2. To maximize compound recovery, the reaction mixtures of entries 2, 4, and 5 were combined and concentrated under reduced pressure. The resulting crude product was purified by reverse phase chromatography (30 g C_{18} Gold column, 15−65% 0.1% formic acid in acetonitrile in 0.1% formic acid in water over 30 min) to give the title product **10** as a white solid (115 mg, 36%). ^1H NMR (400 MHz, DMSO-d_6) δ 12.77 (br s, 1H), 7.36 (s, 4H), 7.19 (t, J = 6.0 Hz, 1H), 5.66 (s, 1H), 4.39 (d, J = 6.3 Hz, 2H), 2.44−2.55 (m, 2H), 1.58 (quin, J = 7.5 Hz, 2H), 1.32 (sxt, J = 7.4 Hz, 2H), 0.89 (t, J = 7.3 Hz, 3H). LC−MS (ESI, formic) m/z 356 [M + H]$^+$, R_t = 1.00 min.

2-((4-Chlorobenzyl)amino)-5-isobutyl-7-oxo-4,7-dihydropyrazolo[1,5-a]pyrimidine-3-carbonitrile (11). Ethyl 5-methyl-3-oxohexanoate (153 mg, 0.888 mmol) was added to a suspension of 5-amino-3-((4-chlorobenzyl)amino)-1H-pyrazole-4-carbonitrile **18a** (200 mg, 0.807 mmol) in acetic acid (2 mL). The reaction mixture was heated at reflux for 18 h. The mixture was diluted with water (15 mL) and extracted with EtOAc (2 × 10 mL). The aqueous layer was saturated by addition of brine (5 mL) and extracted again with EtOAc (10 mL). The combined organic extracts were washed with brine, dried over $MgSO_4$, and concentrated under reduced pressure. The resulting crude product was purified by reverse phase chromatography using MDAP (formic acid, 15−55% solvent B) to give the title product **11** as a white solid (53 mg, 18%). ^1H NMR (400 MHz, DMSO-d_6) δ 12.74 (br s, 1H), 7.37 (s, 4H), 7.21 (br s, 1H), 5.65 (s, 1H), 4.40 (d, J = 6.0 Hz, 2H), 2.38 (d, J = 7.3 Hz, 2H), 1.98 (spt, J = 6.8 Hz, 1H), 0.91 (d, J = 6.8 Hz, 6H). LC−MS (ESI, formic) m/z 356 [M + H]$^+$, R_t = 0.98 min.

3-Cyano-7-oxo-5-propyl-4,7-dihydropyrazolo[1,5-a]pyrimidine-2-carboxylic Acid (12). Ethyl 6-methyl-3-oxoheptanoate (61 mg, 0.33 mmol) was added to a suspension of 5-amino-3-((4-chlorobenzyl)amino)-1H-pyrazole-4-carbonitrile **18a** (60 mg, 0.24 mmol) in acetic acid (1.2 mL) and water (0.6 mL). The mixture was heated at 120 °C for 24 h. Volatile components were evaporated under reduced pressure. The resulting crude product was purified by reverse phase chromatography using MDAP (formic acid, 30−85% solvent B) to give the title product **12** (46 mg, 51%). ^1H NMR (400 MHz, DMSO-d_6) δ 12.77 (s, 1H), 7.36 (s, 4H), 7.21 (br s, 1H), 5.68 (s, 1H), 4.40 (d, J = 6.3 Hz, 2H), 2.53 (br s, 2H), 1.54−1.63 (spt, J = 6.5 Hz, 1H), 1.44−1.53 (m, 2H), 0.91 (d, J = 6.5 Hz, 6H). LC−MS (ESI, formic) m/z 370 [M + H]$^+$, R_t = 1.06 min.

2-((4-Chlorobenzyl)amino)-5-(methoxymethyl)-7-oxo-4,7-dihydropyrazolo[1,5-a]pyrimidine-3-carbonitrile (13). Methyl 4-methoxy-3-oxobutanoate (47 µL, 0.36 mmol) was added to a suspension of 5-amino-3-((4-chlorobenzyl)amino)-1H-pyrazole-4-carbonitrile **18a** (60 mg, 0.24 mmol) in acetic acid (1.2 mL) and water (0.6 mL). The reaction mixture was heated at 120 °C for 24 h. Volatile components were removed under reduced pressure. The resulting crude product was purified by reverse phase chromatography using MDAP (formic acid, 15−55% solvent B over 15 min) to give the title product **13** as a white solid (37 mg, 44%). ^1H NMR (400 MHz, DMSO-d_6) δ 13.07 (br s, 1H), 7.37 (s, 4H), 7.24 (br s, 1H), 5.80 (s, 1H), 4.40 (d, J = 6.0 Hz, 2H), 4.31 (s, 2H), 3.34 (s, 3H). LC−MS (ESI, formic) m/z 344 [M + H]$^+$, R_t = 0.82 min. HRMS (ESI) calcd for $C_{16}H_{14}ClN_5O_2$ + H$^+$, 344.0910; found, 344.0909.

Ethyl 4-(Furan-3-yl)-3-oxobutanoate (19h). CDI (355 mg, 2.2 mmol) was added to a stirred solution of 2-(furan-3-yl)acetic acid (250 mg, 2 mmol) in THF (7 mL) at room temperature under nitrogen. The mixture was stirred at room temperature for 20 h. During this time, in a separate round-bottom flask, magnesium ethoxide (250 mg, 2.2 mmol) was added to a stirred solution of 3-ethoxy-3-oxopropanoic acid (576 mg, 4.4 mmol) in THF (7 mL) at rt under nitrogen. The mixture was stirred at room temperature for 5 h. Solvent was removed under reduced pressure. The resulting solid was then suspended in THF (4 mL) and added dropwise over 1 min to previously stirred CDI furanylacetate suspension. The resulting mixture was stirred at room temperature for 6 h. A saturated aqueous solution of sodium bicarbonate (20 mL) and EtOAc (20 mL) was added, and the phases were separated. The aqueous phase was extracted with EtOAc (2 × 20 mL). The combined organic phases were passed through a hydrophobic frit and evaporated under reduced pressure to give the crude product, ethyl 4-(furan-3-yl)-3-oxobutanoate as brown liquid (215 mg, 55%). LC−MS (ESI, formic) m/z 197 [M + H]$^+$, R_t = 0.80 min, 57% by area.

2-((4-Chlorobenzyl)amino)-5-(furan-3-ylmethyl)-7-oxo-4,7-dihydropyrazolo[1,5-a]pyrimidine-3-carbonitrile (14). Crude ethyl 4-(furan-3-yl)-3-oxobutanoate **19h** (160 mg, 0.815 mmol, 57% area by LC−MS) was added to a suspension of 5-amino-3-((4-chlorobenzyl)amino)-1H-pyrazole-4-carbonitrile **18a** (60 mg, 0.2 mmol) in acetic acid (1.2 mL) and water (0.6 mL). The reaction mixture was heated at 120 °C for 16 h. Solvent was removed under reduced pressure. The resulting crude product was purified by reverse phase chromatography using MDAP (formic acid, 30−85% solvent B over 15 min) to give the title product **14** as an orange solid (41 mg, 45%). ^1H NMR (400 MHz, DMSO-d_6) δ 12.99 (br s, 1H), 7.57−7.65 (m, 2H), 7.36 (s, 4H), 7.22 (t, J = 5.9 Hz, 1H), 6.47 (s, 1H), 5.61 (s, 1H), 4.40 (d, J = 6.3 Hz, 2H), 3.69 (s, 2H). ^{13}C NMR (101 MHz, DMSO-d_6) δ 157.2 (C), 154.5 (C), 143.5 (Ar-CH), 140.6 (Ar-CH), 138.9 (C), 131.1 (C), 129.0 (2C, Ar-CH), 128.0 (2C, Ar-CH), 119.9 (C), 113.1 (C), 111.2 (CH), 98.3 (CH), 62.6 (C), 44.8 (CH$_2$), 27.4 (CH$_2$), two carbons not observed. LC−MS (ESI, formic) m/z 380 [M + H]$^+$, R_t = 0.93 min. HRMS (ESI) calcd for $C_{19}H_{18}ClN_5O_2$ + H$^+$, 380.0909; found, 380.0905. IR (ATR) cm^{-1} 3395, 2821, 2209, 1664, 1625, 1593, 1571.

2-((4-Chlorophenethyl)amino)-7-oxo-5-propyl-4,7-dihydropyrazolo[1,5-a]pyrimidine-3-carbonitrile (23). Ethyl 3-oxohexanoate (0.135 mL, 0.841 mmol) was added to a suspension of 3-amino-5-((4-chlorophenethyl)amino)-1H-pyrazole-4-carbonitrile **18b** (200 mg, 0.764 mmol) in acetic acid (3 mL). The mixture was heated at reflux for 24 h. Volatile components were removed under reduced pressure. The resulting crude product was purified by reverse phase chromatography (43 g C_{18} column, 20−70% 0.1% formic acid in acetonitrile in 0.1% formic acid in water) to give the title product **23** as a cream solid (88 mg, 32%). ^1H NMR (400 MHz, methanol-d_4) δ 7.27 (s, 4H), 5.77 (s, 1H), 3.57 (t, J = 7.3 Hz, 2H), 2.93 (t, J = 7.3 Hz, 2H), 2.58 (t, J = 7.3 Hz, 2H), 1.73 (sxt, J = 7.5 Hz, 2H), 1.02 (t, J = 7.3 Hz, 3H). LC−MS (ESI, formic) m/z 356 [M + H]$^+$, R_t = 0.97 min.

Ethyl 3,3-Dicyano-2-methoxyacrylate (31). NaOEt in EtOH (21% w/w) (225 mL) was added dropwise to a solution of malononitrile (39.6 g, 600 mmol) and diethyl oxalate (88 g, 600 mmol) in EtOH (900 mL). The mixture was stirred at room temperature for 1 h. The mixture was then concentrated, and the resulting residue was dissolved in EtOAc. The mixture was then stirred at room temperature for 1 h. The solid formed was removed by filtration. The EtOAc solution was concentrated under reduced pressure, and 200 mL of EtOH was added. Then 1.5 L of diethyl ether was added to the solution. The ether layer was removed by decantation, and then the residue was washed twice with ether. The remaining gum was dried under reduced pressure to give brownish amorphous solid.

The amorphous intermediate was added portionwise to $POCl_3$ (250 mL, 2.68 mol) at 0 °C, and the mixture was stirred at room temperature for 10 min. The dark-red solution was then heated at 110 °C for 1 h. Excess $POCl_3$ was removed, and MeOH was added very slowly (exothermic) at 0 °C until no more heat was generated (ca. 1 L). The insoluble material was removed by filtration. The resulting filtrate was concentrated, and the residue was dissolved in DCM/EtOAc (1:1) and passed through SiO_2 cartridge to remove inorganic material. Solvents were removed under reduced pressure. The residue obtained was separated into three batches, and each batch was purified by normal phase chromatography (330 g silica column, DCM/EtOAc = 20:1). Fractions including the desired product were collected and concentrated under reduced pressure. The residue was repurified by normal phase chromatography (330 g silica column, cyclohexane/EtOAc 20:1−1:1) to give the title product **31** as a light-brown oil (17.1 g). The material was used in next step without further purification.

Ethyl 5-Amino-4-cyano-1H-pyrazole-3-carboxylate (32). Crude ethyl 3,3-dicyano-2-methoxyacrylate **31** (10.7 g, 59.6 mmol) in EtOH (50 mL) was added to a solution of hydrazine monohydrate (2.9 mL, 59.6 mmol) in EtOH (400 mL). The mixture was stirred at room temperature for 30 min. The solid formed was collected by filtration and washed with EtOH. The solid was then recrystallized from EtOH to give the title product **32** (2.34 g, 42%, 78% area by LC−MS). ^1H

NMR (400 MHz, DMSO-d_6) δ 12.64 (br s, 1H), 6.56 (s, 2H), 4.26 (q, J = 7.1 Hz, 2H), 1.28 (t, J = 7.0 Hz, 3H). ^{13}C NMR (101 MHz, DMSO-d_6) δ 161.2 (C=O), 155.2 (Ar-C), 143.4 (Ar-C), 114.8 (CN), 73.9 (Ar-C), 61.5 (CH$_2$), 14.9 (CH$_3$). LC–MS (ESI, formic) m/z 181 [M + H]$^+$, R_t = 0.50 min (78% by area).

Ethyl 3-Cyano-7-oxo-5-propyl-4,7-dihydropyrazolo[1,5-a]-pyrimidine-2-carboxylate (33). A mixture of ethyl 3-oxohexanoate (6.4 mL, 40 mmol) and ethyl 5-amino-4-cyano-1*H*-pyrazole-3-carboxylate 32 (6.0 g, 33.3 mmol) in acetic acid (200 mL) was stirred at 100 °C for 3 days. The mixture was cooled to room temperature. The solid formed was collected by filtration and washed with EtOH three times to give the title product 33 (4.7 g, 52%, 91% area by LC–MS). The material was used in the next step without further purification. ^{1}H NMR (400 MHz, DMSO-d_6) δ 13.38 (br s, 1H), 5.95 (s, 1H), 4.41 (q, J = 7.1 Hz, 2H), 2.60 (t, J = 7.5 Hz, 2H), 1.69 (sxt, J = 7.4 Hz, 2H), 1.36 (t, J = 7.0 Hz, 3H), 0.95 (t, J = 7.3 Hz, 3H). LC–MS (ESI, formic) m/z 275 [M + H]$^+$, R_t = 0.73 min (91% by area).

2-(Hydroxymethyl)-7-oxo-5-propyl-4,7-dihydropyrazolo[1,5-a]-pyrimidine-3-carbonitrile (34). LiBH$_4$ (4.3 g, 198 mmol) was added to a suspension of ethyl 3-cyano-7-oxo-5-propyl-4,7-dihydropyrazolo-[1,5-a]pyrimidine-2-carboxylate 33 (2.7 g, 9.9 mmol) in THF (150 mL), and the mixture was stirred at room temperature for 2 h. The reaction was quenched with saturated aqueous NH$_4$Cl solution. The pH of the solution was adjusted to pH = 3 with aqueous HCl solution. The mixture was extracted with EtOAc/EtOH (5:1) until no more product was detected in the aqueous layer by LC–MS. The combined organic layers were dried over Na$_2$SO$_4$ and concentrated under reduced pressure. The resulting residue was purified by normal phase chromatography (80 g silica column, 1:5−1:3 MeOH/EtOAc). Fractions including the desired product were collected and concentrated. The residue was repurified by normal phase chromatography (120 g silica column, 1/20−1/5 MeOH/EtOAc) to give the title product 34 as a white solid (1.92 g, 84%). ^{1}H NMR (400 MHz, DMSO-d_6) δ 13.19 (br s, 1H), 5.76 (s, 1H), 5.54 (br s, 1H), 4.56 (br d, J = 3.8 Hz, 2H), 2.53−2.58 (overlapped with DMSO, 2H), 1.67 (sxt, J = 7.5 Hz, 2H), 0.93 (t, J = 7.3 Hz, 3H). LC–MS (ESI, formic) m/z 233 [M + H]$^+$, R_t = 0.50 min.

2-(Bromomethyl)-7-oxo-5-propyl-4,7-dihydropyrazolo[1,5-a]-pyrimidine-3-carbonitrile (35). Triphenylphosphine (1.92 g, 7.32 mmol) and carbon tetrabromide (2.43 g, 7.33 mmol) were added to a suspension of 2-(hydroxymethyl)-7-oxo-5-propyl-4,7-dihydropyrazolo-[1,5-a]pyrimidine-3-carbonitrile 25 (1.0 g, 4.3 mmol) in DCM (50 mL). The mixture was stirred at room temperature for 4 days. The mixture was loaded directly on to a silica column and purified by normal phase chromatography (120 g silica column, 1:1−2:1 EtOAc/cyclohexane). The product containing were collected and concentrated under reduced pressure. The resulting product was washed with EtOAc (3 × 1 mL) to give the title product 35 (562 mg, 44%). The less pure fractions were combined and concentrated under reduced pressure. The resulting crude product was purified by reverse phase chromatography using MDAP (formic acid, 30−85% solvent B) to give additional title product 35 (225 mg, 18%). ^{1}H NMR (400 MHz, DMSO-d_6) δ 13.25 (br s, 1H), 5.88 (s, 1H), 4.74 (s, 2H), 2.57 (t, J = 7.7 Hz, 2H), 1.68 (sxt, J = 7.4 Hz, 2H), 0.95 (t, J = 7.3 Hz, 3H). LC–MS (ESI, formic) m/z 295, 297 [M + H]$^+$, R_t = 0.72 min.

2-(((4-Chlorophenyl)amino)methyl)-7-oxo-5-propyl-4,7-dihydropyrazolo[1,5-a]pyrimidine-3-carbonitrile (24). A mixture of 4-chloroaniline (60.5 mg, 0.474 mmol) and 2-(bromomethyl)-7-oxo-5-propyl-4,7-dihydropyrazolo[1,5-a]pyrimidine-3-carbonitrile 35 (35 mg, 0.119 mmol) in THF (2 mL) was heated at 140 °C for 30 min in a microwave reactor. Solvent was removed by evaporation. The resulting crude product was purified by reverse phase chromatography using MDAP (formic acid, 30−85%). The product obtained was washed with MeOH to give the title product 24 as a white solid (27 mg, 67%). ^{1}H NMR (400 MHz, DMSO-d_6) δ 13.13 (br s, 1H), 7.09 (d, J = 8.8 Hz, 2H), 6.63 (d, J = 8.8 Hz, 2H), 6.50 (br s, 1H), 5.83 (s, 1H), 4.39 (br s, 2H), 2.55 (t, J = 7.5 Hz, 2H), 1.66 (sxt, J = 7.4 Hz, 2H), 0.92 (t, J = 7.3 Hz, 3H). LC–MS (ESI, formic) m/z 342 [M + H]$^+$, R_t = 0.95 min.

2-((4-Chlorophenoxy)methyl)-7-oxo-5-propyl-4,7-dihydropyrazolo[1,5-a]pyrimidine-3-carbonitrile (25). 4-Chlorophenol (46 mg, 0.36 mmol) in THF (1 mL) was added to a suspension of sodium hydride (60% dispersion in mineral oil, 16 mg, 0.39 mmol) in THF (1.5 mL). The mixture was stirred at room temperature for 5 min. 2-(Bromomethyl)-7-oxo-5-propyl-4,7-dihydropyrazolo[1,5-a]-pyrimidine-3-carbonitrile 35 (35 mg, 0.12 mmol) in THF (1.5 mL) was then added, and the mixture was stirred at room temperature for 5 min, then heated at 50 °C for 1 h. The mixture was quenched with MeOH (0.5 mL) then concentrated under a stream of nitrogen. The residue was purified by reverse phase chromatography using the MDAP (formic acid, 30−85% solvent B over 15 min) to give the title product 25 as a white solid (36 mg, 88%). ^{1}H NMR (400 MHz, DMSO-d_6) δ 13.23 (br s, 1H), 7.37 (d, J = 8.8 Hz, 2H), 7.09 (d, J = 9.0 Hz, 2H), 5.85 (s, 1H), 5.28 (s, 2H), 2.56 (t, J = 7.5 Hz, 2H), 1.67 (sxt, J = 7.4 Hz, 2H), 0.94 (t, J = 7.3 Hz, 3H). LC–MS (ESI, formic) m/z 343 [M + H]$^+$, R_t = 0.99 min.

5-Amino-3-methylthiopyrazole-4-carbonitrile (36). Compound prepared following procedure from Tominaga et al.[53]

2-(Methylthio)-7-oxo-5-propyl-4,7-dihydropyrazolo[1,5-a]-pyrimidine-3-carbonitrile (37). Ethyl 3-oxohexanoate (770 mg, 4.9 mmol) was added to a suspension of 5-amino-3-(methylthio)-1*H*-pyrazole-4-carbonitrile 36 (500 mg, 3.3 mmol) in acetic acid (15 mL) and water (7.5 mL). The mixture was heated at 120 °C for 20 h. Due to incomplete reaction, further ethyl 3-oxohexanoate (385 mg, 2.43 mmol) was added and the reaction mixture was heated at 120 °C for 66 h. The reaction was left to cool to room temperature, and a few drops of water were added. The solid formed was collected by filtration and dried in a vacuum oven for 4 h to give the title product 37 as an off-white solid (365 mg, 45%). The filtrate collected was evaporated under reduced pressure. The resulting crude product was purified by reverse phase chromatography using the MDAP (formic acid, 15−55% solvent B over 15 min) to give additional title product 37 as a white solid (67 mg, 8%). ^{1}H NMR (400 MHz, DMSO-d_6) δ 13.12 (br s, 1H), 5.82 (s, 1H), 2.62 (s, 3H), 2.54 (t, J = 7.3 Hz, 2H), 1.66 (sxt, J = 7.4 Hz, 2H), 0.93 (t, J = 7.4 Hz, 3H). LC–MS (ESI, formic) m/z 249.13 [M + H]$^+$, R_t = 0.72 min (94% by area).

2-(Methylsulfonyl)-7-oxo-5-propyl-4,7-dihydropyrazolo[1,5-a]-pyrimidine-3-carbonitrile (38). A solution of 2-(methylthio)-7-oxo-5-propyl-4,7-dihydropyrazolo[1,5-a]pyrimidine-3-carbonitrile 37 (365 mg, 1.47 mmol) in DCM (15 mL) was cooled to 0 °C under nitrogen. mCPBA (805 mg, 3.73 mmol) was added, and the mixture was left to warm up to room temperature and then stirred for 4 days. Saturated aqueous sodium sulfite solution (10 mL) and saturated aqueous sodium bicarbonate solution (10 mL) were added to the mixture, and the mixture was extracted with DCM (2 × 40 mL). LC–MS showed desired product only in the aqueous layer. The aqueous layer was passed through an isolute 103 SPE cartridge (packed with a hydroxylated polystyrene−divinylbenzene copolymer) to remove inorganics. The desired product was eluted with MeOH (2 column volume). The methanol fraction was evaporated under reduced pressure to give the title product 38 as a white solid (349 mg, 85%, 92% area by LC–MS). ^{1}H NMR (400 MHz, DMSO-d_6) δ 13.54 (br s, 1H), 6.00 (s, 1H), 3.44 (s, 3H), 2.60 (t, J = 7.5 Hz, 2H), 1.68 (sxt, J = 7.4 Hz, 2H), 0.94 (t, J = 7.4 Hz, 3H). LC–MS (ESI, formic) m/z 281 [M + H]$^+$, R_t = 0.61 min, (92% area by LC–MS).

2-((4-Chlorobenzyl)oxy)-7-oxo-5-propyl-4,7-dihydropyrazolo[1,5-a]pyrimidine-3-carbonitrile (26). Sodium hydride (60% dispersion in mineral oil, 14 mg, 0.35 mmol) was suspended in THF (0.5 mL) in a microwave vial under nitrogen. (4-Chlorophenyl)methanol (34 mg, 0.24 mmol) was added, and the mixture was stirred at room temperature under nitrogen for 1 h. 2-(Methylsulfonyl)-7-oxo-5-propyl-4,7-dihydropyrazolo[1,5-a]pyrimidine-3-carbonitrile 38 (50 mg, 0.18 mmol) was then added, and the reaction mixture was heated at 90 °C for 1 h in a microwave reactor. Water was added, and the mixture was extracted with DCM (2 × 10 mL). LC–MS showed product mainly in the aqueous layer. The aqueous layer was evaporated under reduced pressure. The resulting crude product was purified by reverse phase chromatography using MDAP (formic acid, 30−85% solvent B over 15 min) to give the title product 26 as a beige

solid (7.6 mg, 12%). ^{1}H NMR (400 MHz, DMSO-d_6) δ 13.10 (br s, 1H), 7.42−7.56 (m, 4H), 5.81 (s, 1H), 5.40 (s, 2H), 2.52 (t, J = 7.3 Hz, 2H), 1.64 (sxt, J = 7.4 Hz, 2H), 0.93 (t, J = 7.3 Hz, 3H). LC−MS (ESI, formic) m/z 343 [M + H]$^+$, R_t = 1.01 min. Structural assigment was confirmed by HMBC (see Supporting Information).

3-(4-Chlorophenyl)-1-morpholinopropane-1-thione (40). A mixture of 1-(4-chlorophenyl)propan-1-one **39** (2 g, 12 mmol), morpholine (4 mL, 46 mmol), and sulfur (0.77 g, 23.9 mmol) was heated at 130 °C for 24 h under nitrogen with a bleach scrubber. After cooling to room temperature, the reaction mixture was poured into CHCl$_3$ (50 mL) and stirred with activated charcoal for 15 min. The mixture was filtered through Celite and concentrated under reduced pressure. The resulting product was recrystallized from EtOH. The precipitate formed was collected by filtration and dried in a vacuum oven for 3 h to give the title product **40** as a green solid (2.0 g, 62%). ^{1}H NMR (400 MHz, DMSO-d_6) δ 7.26−7.36 (m, 4H), 4.19 (t, J = 4.8 Hz, 2H), 3.74 (t, J = 4.7 Hz, 2H), 3.63 (t, J = 5.0 Hz, 2H), 3.51 (t, J = 4.7 Hz, 2H), 3.03−3.08 (m, 2H), 2.92−2.98 (m, 2H). LC−MS (ESI, formic) m/z 270 [M + H]$^+$, R_t = 1.08 min.

2-(3-(4-Chlorophenyl)-1-morpholinopropylidene)malononitrile (42). Tetracyanoethylene oxide **41** (0.96 g, 6.7 mmol) in toluene (20 mL) was added dropwise to a solution of 3-(4-chlorophenyl)-1-morpholinopropane-1-thione **39** (1.5 g, 5.6 mmol) in toluene (20 mL) and cooled to 0 °C under nitrogen. After complete addition, the reaction mixture was stirred at room temperature overnight under nitrogen. Additional toluene was added, and the organic phase was washed with saturated aqueous sodium carbonate solution. After several washes (×10), a Merckoquant test still showed a trace of cyanide. The toluene phase was washed with aqueous copper sulfate solution followed by brine. The brine wash showed no trace of cyanide. The organic phase was separated, passed through a hydrophobic frit, and evaporated under reduced pressure. The resulting residue was triturated with a minimum volume of MeOH. The solid was collected by filtration and dried in a vacuum oven overnight to give the title product as a beige solid (688 mg, 41%, 94% area by LC−MS). The MeOH filtrate was evaporated under reduced pressure. The resulting crude product was purified by normal phase chromatography (40 g silica column, 20−100% *tert*-butylmethyl ether in cyclohexane over 58 min) to give additional title product **42** as light-brown solid (829 mg, 49%). ^{1}H NMR (400 MHz, DMSO-d_6) δ 7.39 (d, J = 8.3 Hz, 2H), 7.31 (d, J = 8.3 Hz, 2H), 3.75 (br s, 4H), 3.65−3.71 (m, 4H), 2.77−2.91 (m, 4H). LC−MS (ESI, formic) m/z 302 [[M + H]$^+$, R_t = 1.03 min.

5-Amino-3-(4-chlorophenethyl)-1H-pyrazole-4-carbonitrile (43). Hydrazine monohydrate (0.53 mL, 6.9 mmol) was added to a solution of 2-(3-(4-chlorophenyl)-1-morpholinopropylidene)-malononitrile **42** (1.4 g, 4.6 mmol) in EtOH (10 mL). The reaction mixture was refluxed for 5 h under nitrogen. The mixture was left to cool overnight. Solvent was removed under reduced pressure, and the resulting residue was triturated with water. The solid was collected by filtration and dried in a vacuum oven to give the title product **43** as a pale-brown solid (836 mg, 73%, 84% area by LC−MS). ^{1}H NMR (400 MHz, DMSO-d_6) δ 12.08−11.57 (2 br s, 1H, two pyrazole isomers visible), 7.32 (d, J = 8.0 Hz, 2H), 7.21 (d, J = 8.0 Hz, 2H), 6.21 + 5.29 (2 br s, 2H), 2.67−2.98 (m, 4H). LC−MS (ESI, formic) m/z 247 [M + H]$^+$, R_t = 0.87 min (84% by area).

5-Benzyl-2-(4-chlorophenethyl)-7-oxo-4,7-dihydropyrazolo[1,5-a]pyrimidine-3-carbonitrile (27). A solution of 5-amino-3-(4-chlorophenethyl)-1H-pyrazole-4-carbonitrile **43** (90 mg, 0.37 mmol) and methyl 3-oxo-4-phenylbutanoate (62 μL, 0.40 mmol) in acetic acid (1.5 mL) was heated at reflux for 20 h. After cooling to ambient temperature, and solvent was removed under reduced pressure. The resulting crude product was purified by reverse phase chromatography using MDAP (formic acid, 30−85% solvent B over 15 min) to give the title product **27** as a white solid (73 mg, 59%); mp 264−267 °C. ^{1}H NMR (400 MHz, DMSO-d_6) δ 13.09 (br s, 1H), 7.32−7.36 (m, 2H), 7.26−7.30 (m, 2H), 5.81 (s, 1H), 3.03 (s, 4H), 2.55 (t, J = 7.3 Hz, 2H), 1.66 (apparent sxt, J = 7.5 Hz, 2H), 0.93 (t, J = 7.4 Hz, 3H). ^{13}C NMR (101 MHz, DMSO-d_6) δ 156.4 (C), 154.9 (C), 145.3 (C), 139.5 (C), 130.7 (C), 130.2 (2C, Ar-CH), 128.3 (2C, Ar-CH), 112.8 (C),

97.8 (CH), 74.0 (C), 33.9 (CH$_2$), 32.5 (CH$_2$), 28.8 (CH$_2$), 21.3 (CH$_2$), 13.3 (CH$_3$). LC−MS (ESI, formic) m/z 341 [M + H]$^+$, R_t = 1.03 min. HRMS (ESI) calcd for C$_{18}$H$_{17}$ClN$_4$O + H$^+$, 341.1164; found, 341.1165. IR (ATR) cm^{-1} 3158, 3073, 2964, 2224, 1663, 1626, 1581.

2-Amino-7-oxo-5-propyl-4,7-dihydropyrazolo[1,5-a]pyrimidine-3-carbonitrile (45). A mixture of 3,5-diamino-1H-pyrazole-4-carbonitrile **44** (2.0 g, 16.24 mmol) and ethyl 3-oxohexanoate (2.87 mL, 17.8 mmol) in acetic acid (8 mL) and water (16 mL) was heated at reflux for 24 h. Volatile components were removed under reduced pressure to give the title product **45** (3.4 g, 98%). ^{1}H NMR (400 MHz, DMSO-d_6) d 12.72 (br s, 1H), 6.12 (br s, 2H), 5.66 (s, 1H), 2.45−2.53 (m, 2H), 1.64 (sxt, J = 7.4 Hz, 2H), 0.92 (t, J = 7.4 Hz, 3H). LC−MS (ESI, formic) m/z 218 [M + H]$^+$, R_t = 0.50 min.

4-Chloro-N-(3-cyano-7-oxo-5-propyl-4,7-dihydropyrazolo[1,5-a]-pyrimidin-2-yl)benzamide (28). A mixture of 2-amino-7-oxo-5-propyl-4,7-dihydropyrazolo[1,5-a]pyrimidine-3-carbonitrile **45** (100 mg, 0.460 mmol) and pyridine (0.074 mL, 0.92 mmol) in DCM (3 mL) was stirred for 10 min under nitrogen. 4-Chlorobenzoyl chloride (89 mg, 0.51 mmol) was then added, and the mixture was stirred at room temperature overnight. Portions of DMAP (5.6 mg, 0.046 mmol) and DMAP (51 mg, 0.17 mmol) were added, and the reaction was left to stir at room temperature for 2 days. Additional 4-chlorobenzoyl chloride (40 mg, 0.23 mmol) and DMAP (28 mg, 0.29 mmol) were again added. The reaction mixture was stirred at room temperature for a further day. The mixture was partioned between 2 M aqueous HCl solution (5 mL) and DCM (5 mL). A solid formed was filtered and dried in a vacuum oven to give the title product **40** (68 mg, 42%, 88% area by LC−MS). ^{1}H NMR (400 MHz, DMSO-d_6) δ 13.17 (br s, 1H), 11.47 (br s, 1H), 8.06 (d, J = 8.6 Hz, 2H), 7.63 (d, J = 8.8 Hz, 2H), 5.85 (br s, 1H), 4.05 (br s, 2H), 1.63−1.74 (m, 2H), 0.95 (t, J = 7.3 Hz, 3H). LC−MS (ESI, formic) m/z 356 [M + H]$^+$, R_t = 0.84 min (88% by area).

3-Cyano-7-oxo-5-propyl-4,7-dihydropyrazolo[1,5-a]pyrimidine-2-carboxylic acid (46). Sodium hydroxide (2 M aqueous solution, 3 mL, 6 mmol) was added to a suspension of ethyl 3-cyano-7-oxo-5-propyl-4,7-dihydropyrazolo[1,5-a]pyrimidine-2-carboxylate **33** (200 mg, 0.729 mmol) in EtOH (3 mL). The mixture was stirred at room temperature for 2 h. Solvent was removed under a stream of nitrogen. Water (10 mL) was added, and the solution was acidified with 2 N aqueous HCl solution. The suspension was charged onto isolute 103 SPE cartridge (2 g), washed with water (50 mL), then eluted with DCM−MeOH (3:1, 200 mL). The organic fractions were concentrated under reduced pressure to give the title product **46** (189 mg, quantitative). ^{1}H NMR (400 MHz, DMSO-d_6) δ 13.36 (br s, 1H), 5.90 (s, 1H), 4.02 (br s, 1H), 2.58 (t, J = 7.6 Hz, 2H), 1.68 (sxt, J = 7.5 Hz, 2H), 0.94 (t, J = 7.4 Hz, 3H). LC−MS (ESI, formic) m/z 247 [M + H]$^+$, R_t = 0.49.

N-(4-Chlorophenyl)-3-cyano-7-oxo-5-propyl-4,7-dihydropyrazolo[1,5-a]pyrimidine-2-carboxamide (29). HATU (97 mg, 0.26 mmol) and DIPEA (80 μL, 0.46 mmol) were added to a suspension of 3-cyano-7-oxo-5-propyl-4,7-dihydropyrazolo[1,5-a]-pyrimidine-2-carboxylic acid **46** (37 mg, 0.15 mmol) in DCM (3 mL), and the mixture was stirred at room temperature for 2 min. 4-Chloroaniline (25 μL, 0.23 mmol) was then added, and the mixture was stirred at room temperature overnight. Volatile components were removed under reduced pressure. The resulting residue was purified by reverse phase chromatography using MDAP (formic acid, 30−85% solvent B) to give the title product **29** (33 mg, 63%). ^{1}H NMR (400 MHz, DMSO-d_6) δ 10.80 (s, 1H), 7.87 (d, J = 8.8 Hz, 2H), 7.42 (d, J = 8.8 Hz, 2H), 5.94 (s, 1H), 2.60 (overlapped with DMSO, 2H), 1.69 (sxt, J = 7.4 Hz, 2H), 0.95 (t, J = 7.3 Hz, 3H), 1 H not visible. LC−MS (ESI, formic) m/z 356 [M + H]$^+$, R_t = 0.99.

2-(Cyanomethyl)-7-oxo-5-propyl-4,7-dihydropyrazolo[1,5-a]-pyrimidine-3-carbonitrile (49). Ethyl 3-oxohexanoate (5.73 mL, 35.6 mmol) was added to a suspension of 5-amino-3-(cyanomethyl)-1H-pyrazole-4-carbonitrile **48** (4.03 g, 27.4 mmol) in acetic acid (40 mL) and water (20 mL). The mixture was heated at 120 °C for 2 days. The solution was cooled to room temperature, and solvents were removed under reduced pressure. The crude material was purified by reverse

phase chromatography (3 × 100 g C$_{18}$ column, 0−40% MeOH in 10 mM ammonium bicarbonate) to give the title product **49** as an off-white solid (2.2 g, 33%, 79% area by LC−MS). ^{1}H NMR (400 MHz, DMSO-d_6) δ 5.74 (s, 1H), 4.20 (s, 2H), 2.44 (t, J = 7.5 Hz, 2H), 1.64 (q, J = 7.6 Hz, 2H), 0.92 (t, J = 7.5 Hz, 3H), 1 H not visible. LC−MS (ESI, high pH) m/z 242 [M + H]$^+$, R_t = 0.65 (79% by area).

Ethyl 2-(3-Cyano-7-oxo-5-propyl-4,7-dihydropyrazolo[1,5-a]-pyrimidin-2-yl)acetate (50). 2-(Cyanomethyl)-7-oxo-5-propyl-4,7-dihydropyrazolo[1,5-a]pyrimidine-3-carbonitrile **49** (273 mg, 1.132 mmol) was suspended in a mixture of 1,4-dioxane (10 mL) and EtOH (10 mL) and heated at 60 °C until complete dissolution had taken place. The solution was allowed to cool to 25 °C and then placed into an ice bath. Hydrochloric acid gas was bubbled through the solution in an ice bath for 2.5 h, maintaining the reaction temperature below 30 °C. The solvents were removed under reduced pressure. The residue was dissolved in water (20 mL) and stirred at 60 °C for 10 min. The solution was cooled to room temperature, and the precipitate formed was isolated by filtration, washed with water, and dried in a vacuum oven to give the title product **50** as a yellow solid (110 mg, 34%). ^{1}H NMR (400 MHz, DMSO-d_6) δ ppm 13.20 (br s, 1H), 5.84 (s, 1 H), 4.14 (q, J = 7.1 Hz, 2H), 3.90 (s, 2H), 2.57 (t, J = 7.6 Hz, 2H), 1.61−1.74 (q, J = 7.6 Hz, 2H), 1.22 (t, J = 7.1 Hz, 3H), 0.94 (t, J = 7.6 Hz, 3H). LC−MS (ESI, high pH) m/z 289 [M + H]$^+$, R_t = 0.61. The product structure was confirmed by HMBC (see Supporting Information).

The filtrate was concentrated and the yellow solid obtained was purified by reverse phase chromatography using MDAP (formic acid, 15−55% solvent B) to give the title product **50** as a white solid (38 mg, 12%). LC−MS and NMR in accordance with reported spectra.

2-(3-Cyano-7-oxo-5-propyl-4,7-dihydropyrazolo[1,5-a]pyrimidin-2-yl)acetic Acid (51). Ethyl 2-(3-cyano-7-oxo-5-propyl-4,7-dihydropyrazolo[1,5-a]pyrimidin-2-yl)acetate **50** (38 mg, 0.132 mmol) was dissolved in 2-MeTHF (1 mL), MeOH (0.5 mL) and water (0.2 mL). Lithium hydroxide (32 mg, 1.32 mmol) was added, and the resulting yellow solution was stirred at room temperature for 24 h. The solvents were removed under reduced pressure. The crude product was purified by reverse phase chromatography using MDAP (formic acid, 5−30% solvent B over 15 min) to give the title product **51** as a colorless oil (19 mg, 55%, 93% area by LC−MS). ^{1}H NMR (400 MHz, CDCl$_3$) δ 13.33 (br s, 1H), 5.94 (s, 1H), 3.63 (s, 2H), 2.80 (t, J = 7.5 Hz, 2H), 1.83−1.98 (overlapped with water, 2H), 1.03 (t, J = 7.3 Hz, 3H), 1H not visible. LC−MS (ESI, formic) m/z 261 [M + H]$^+$, R_t = 0.53 (93% by area).

7-Oxo-2-(2-oxo-2-(pyrrolidin-1-yl)ethyl)-5-propyl-4,7-dihydropyrazolo[1,5-a]pyrimidine-3-carbonitrile (47). 2-(3-Cyano-7-oxo-5-propyl-4,7-dihydropyrazolo[1,5-a]pyrimidin-2-yl)acetic acid **51** (19 mg, 0.073 mmol) was dissolved in DMF (0.5 mL). HATU (33 mg, 0.088 mmol) was added, followed by DIPEA (0.026 mL, 0.146 mmol) and finally pyrrolidine (0.012 mL, 0.146 mmol). The resulting yellow solution was stirred at room temperature for 17 h. Additional HATU (33 mg, 0.088 mmol), DIPEA (0.026 mL, 0.146 mmol), and pyrrolidine (0.012 mL, 0.146 mmol) were added, and the solution was stirred at room temperature for a further 2 h. The solvents were removed under reduced pressure. The crude product was purified by reverse phase chromatography using MDAP (formic acid, 5−30% solvent B over 15 min) to give the title product **47** as an orange solid (13 mg, 57%). ^{1}H NMR (400 MHz, CDCl$_3$) δ 12.14 (br s, 1H), 5.65 (s, 1H), 3.94 (s, 2H), 3.66 (dt, J = 18.5, 6.9 Hz, 4H), 2.59 (t, J = 7.8 Hz, 2H), 2.09 (apparent qn, J = 6.7 Hz, 2H), 1.90−2.01 (apparent qn, J = 7.1 Hz, 2H), 1.69 (apparent sx, J = 7.8 Hz, 2H), 0.97 (t, J = 7.8 Hz, 3H), 1H not visible. LC−MS (ESI, high pH) m/z 314 [M + H]$^+$, R_t = 0.57.

2-(Benzylamino)-7-oxo-5-propyl-4,7-dihydropyrazolo[1,5-a]-pyrimidine-3-carbonitrile (52). 2-Amino-7-oxo-5-propyl-4,7-dihydropyrazolo[1,5-a]pyrimidine-3-carbonitrile **45** (100 mg, 0.460 mmol) and benzaldehyde (0.094 mL, 0.921 mmol) were dissolved in DCM (3 mL) and acetic acid (0.05 mL), and the mixture was heated at 50 °C for 1 h. Sodium triacetoxyborohydride (459 mg, 2.16 mmol) was then added, and the mixture was stirred overnight. Another equivalent of aldehyde (0.047 mL) was added, the mixture was left to

stir for 10 min, and then another equivalent of sodium triacetoxyborohydride (115 mg) was added and the mixture was stirred for 2 h. Saturated aqueous sodium bicarbonate solution was added, and the mixture was passed through a hydrophobic frit. The organic layer was collected and concentrated under reduced pressure. The resulting crude product was purified by reverse phase chromatography using MDAP (formic acid, 15−55% solvent B) to give the title product **52** as a white solid (31 mg, 22%). ^{1}H NMR (400 MHz, methanol-d_4) δ 7.40 (d, J = 7.3 Hz, 2H), 7.30 (t, J = 7.5 Hz, 2H), 7.17−7.26 (m, 1H), 5.76 (s, 1H), 4.55 (s, 2H), 2.58 (t, J = 7.3 Hz, 2H), 1.73 (sxt, J = 7.5 Hz, 2H), 1.02 (t, J = 7.4 Hz, 3H). LC−MS (ESI, formic) m/z 308 [M + H]$^+$, R_t = 0.82.

2-((4-Methylbenzyl)amino)-7-oxo-5-propyl-4,7-dihydropyrazolo-[1,5-a]pyrimidine-3-carbonitrile (53). 2-Amino-7-oxo-5-propyl-4,7-dihydropyrazolo[1,5-a]pyrimidine-3-carbonitrile **45** (100 mg, 0.460 mmol) and 4-methylbenzaldehyde (0.11 mL, 0.92 mmol) were dissolved in DCM (3 mL) and acetic acid (0.05 mL) under nitrogen and stirred at room temperature for 1 h. Sodium triacetoxyborohydride (484 mg, 2.28 mmol) was then added, and the mixture was stirred at room temperature overnight. Another equivalent of aldehyde and sodium triacetoxyborohydride were added, and the mixture was left to stir at room temperature overnight. The reaction was quenched with 1 mL of saturated aqueous bicarbonate solution. The mixture was diluted with DCM and water. The organic layer was separated. The aqueous was extracted with DCM (2×). The combined organic layers were washed with brine and passed through a hydrophobic frit. Solvent was removed under reduced pressure. The resulting crude product was purified by reverse phase chromatography using MDAP (formic acid, 15−55% solvent B) to give the title product **53** as a white solid (29 mg, 20%). ^{1}H NMR (400 MHz, DMSO-d_6) δ 12.75 (s, 1H), 7.23 (d, J = 7.8 Hz, 2H), 7.11 (d, J = 7.8 Hz, 2H), 5.66 (br s, 1H), 4.36 (d, J = 6.0 Hz, 2H), 2.44−2.57 (m, 2H), 2.26 (s, 3H), 1.63 (sx, J = 7.3 Hz, 2H), 0.91 (t, J = 7.3 Hz, 3H), 1 NH not visible. LC−MS (ESI, formic) m/z 322 [M + H]$^+$, R_t = 0.90.

2-((4-Chloro-3-methylbenzyl)amino)-7-oxo-5-propyl-4,7-dihydropyrazolo[1,5-a]pyrimidine-3-carbonitrile (54). A mixture of 4-chloro-3-methylbenzaldehyde (142 mg, 0.921 mmol) and 2-amino-7-oxo-5-propyl-4,7-dihydropyrazolo[1,5-a]pyrimidine-3-carbonitrile **45** (100 mg, 0.460 mmol) in DCM (3 mL) and acetic acid (0.05 mL) was stirred for 30 min under nitrogen. Sodium triacetoxyborohydride (459 mg, 2.17 mmol) was added, and the mixture was left to stir overnight. Additional equivalents of sodium triacetoxyborohydride (115 mg) and aldehyde (71 mg) were added. The mixture was stirred at room temperature overnight. The mixture was quenched with 1 mL of saturated aqueous sodium bicarbonate solution. The mixture was extracted using DCM/water (×3) and then brine. The combined organic layers were passed through a hydrophobic frit and concentrated under reduced pressure. The resulting crude product was purified by reverse phase chromatography using MDAP (formic acid, 15−55% solvent B over 15 min) to give the title product **54** as a white solid (30 mg, 18%). ^{1}H NMR (400 MHz, methanol-d_4) δ 7.15−7.34 (m, 3H), 5.76 (s, 1H), 4.50 (br s, 2H), 2.54−2.61 (m, 2H), 2.28−2.38 (m, 3H), 1.66−1.79 (m, 2H), 1.02 (t, J = 7.4 Hz, 3H). LC−MS (ESI, formic) m/z 356 [M + H]$^+$, R_t = 0.99.

2-((4-Chloro-2-methoxybenzyl)amino)-7-oxo-5-propyl-4,7-dihydropyrazolo[1,5-a]pyrimidine-3-carbonitrile (55). A mixture of 2-amino-7-oxo-5-propyl-4,7-dihydropyrazolo[1,5-a]pyrimidine-3-car-bonitrile **45** (128 mg, 0.589 mmol) and 4-chloro-2-methoxybenzalde-hyde (201 mg, 1.18 mmol) in DCM (3 mL) and acetic acid (0.05 mL) was stirred at room temperature for 1 h. Sodium triacetoxyborohy-dride (587 mg, 2.77 mmol) was then added, and the mixture was stirred overnight. The mixture was quenched with 1 mL of saturated aqueous sodium bicarbonate solution. The mixture was extracted with DCM/water (×3). The combined organic layers were passed through a hydrophobic frit and concentrated under reduced pressure. The resulting crude product was purified by reverse phase choromatog-raphy using MDAP (formic acid, 15−55% solvent B over 15 min) to give the title product **55** as a white solid (25 mg, 11%). ^{1}H NMR (400 MHz, DMSO-d_6) δ 12.78 (s, 1H), 7.20 (d, J = 8.3 Hz, 1H), 7.05 (d, J = 1.8 Hz, 1H), 7.00−7.09 (br s, 1H), 6.95 (dd, J = 8.0, 2.0 Hz, 1H),

5.66 (br s, 1H), 4.34 (d, J = 6.0 Hz, 2H), 3.85 (s, 3H), 2.43−2.55 (m, 2H under DMSO), 1.63 (sxt, J = 7.5 Hz, 2H), 0.92 (t, J = 7.3 Hz, 3H). LC−MS (ESI, formic) m/z 372 [M + H]$^+$, R_t = 0.96.

7-Oxo-5-propyl-2-(((tetrahydro-2H-pyran-4-yl)methyl)amino)-4,7-dihydropyrazolo[1,5-a]pyrimidine-3-carbonitrile (56). A mixture of 2-amino-7-oxo-5-propyl-4,7-dihydropyrazolo[1,5-*a*]pyrimidine-3-carbonitrile **45** (100 mg, 0.460 mmol) and tetrahydro-2*H*-pyran-4-carbaldehyde (105 mg, 0.921 mmol) in DCM (3 mL) and acetic acid (0.05 mL) was stirred at room temperature for 1.5 h. Sodium triacetoxyborohydride (459 mg, 1.84 mmol) was then added, and the mixture was stirred at room temperature overnight. Additional sodium triacetoxyborohydride (115 mg, 0.54 mmol) was added, and the mixture was left to stir at room temperature for few hours. The mixture was quenched with 1 mL of saturated aqueous bicarbonate. DCM was added, and the organic layer was washed with water (×3) and then brine. The organic layer was passed through a hydrophobic frit and concentrated under reduced pressure. The resulting crude was purified by reverse phase chromatography using MDAP (formic acid, 15−55% solvent B over 15 min) to give the title product **56** as a white solid (42 mg, 29%). ^{1}H NMR (400 MHz, DMSO-d_6) δ 12.71 (s, 1H), 6.62 (br s, 1H), 5.67 (s, 1H), 3.84 (br dd, J = 11.2, 2.6 Hz, 2H), 3.21−3.32 (m, 2H overlap with water), 3.08 (t, J = 6.4 Hz, 2H), 2.44−2.54 (m, 2H overlap with DMSO), 1.82−1.95 (m, 1H), 1.57−1.68 (m, 4H), 1.11−1.24 (m, 2H), 0.92 (t, J = 7.3 Hz, 3H). LC−MS (ESI, formic) m/z 316 [M + H]$^+$, R_t = 0.66.

3-Amino-5-(((6-chloropyridin-3-yl)methyl)amino)-1H-pyrazole-4-carbonitrile (18c). A mixture of 2-(bis(methylthio)methylene)-malononitrile (2.4 g, 14 mmol) and (6-chloropyridin-3-yl)-methanamine (2.0 g, 14 mmol) in EtOH (45 mL) was heated under reflux with a bleach scrubber under nitrogen for 1 h. The crude solution was then treated with hydrazine (50 wt % in water, 0.88 mL, 14 mmol), and the mixture was heated under reflux for 30 min. The mixture was cooled, and 40 mL of water were added. The volatiles were partially removed under reduced pressure to favor precipitation of the product. Only a small amount of solid was obtained, and thus the solid collected was recombined with the filtrate and concentrated under reduced pressure to give the crude title product **18c** (2.8 g, 79%). ^{1}H NMR (400 MHz, methanol-d_4) δ 8.33 (d, J = 2.3 Hz, 1H), 7.80 (dd, J = 8.3, 2.5 Hz, 1H), 7.40 (d, J = 8.3 Hz, 1H), 4.38 (s, 2H), 4H not visible (exchangeable). LC−MS (ESI, formic) m/z 249 [M + H]$^+$, R_t = 0.54 (92% by area).

2-(((6-Chloropyridin-3-yl)methyl)amino)-7-oxo-5-propyl-4,7-dihydropyrazolo[1,5-a]pyrimidine-3-carbonitrile (57). 3-Amino-5-(((6-chloropyridin-3-yl)methyl)amino)-1*H*-pyrazole-4-carbonitrile **18c** (100 mg, 0.40 mmol) and methyl 3-oxohexanoate (84 μL, 0.52 mmol) in acetic acid (2 mL) and water (1 mL) was heated at reflux for 24 h. The mixture was left to cool and concentrated under reduced pressure. The resulting crude product was purified by reverse phase chromatography using MDAP (formic acid, 15−55% solvent B) to give the title product **57** as a white solid (39 mg, 28%). ^{1}H NMR (400 MHz, DMSO-d_6) δ 12.77 (br s, 1H), 8.38 (d, J = 2.3 Hz, 1H), 7.82 (dd, J = 8.3, 2.3 Hz, 1H), 7.46 (d, J = 8.3 Hz, 1H), 7.24 (br s, 1H), 5.66 (br s, 1H), 4.41 (d, J = 6.0 Hz, 2H), 2.44−2.53 (m, 2H overlap with DMSO), 1.62 (sx, J = 7.3 Hz, 2H), 0.90 (t, J = 7.3 Hz, 3H). LC−MS (ESI, formic) m/z 343 [M + H]$^+$, R_t = 0.74.

3-Amino-5-(((5-bromopyridin-2-yl)methyl)amino)-1H-pyrazole-4-carbonitrile (18d). A mixture of 2-(bis(methylthio)methylene)-malononitrile (710 mg, 4.17 mmol) and (5-bromopyridin-2-yl)-methanamine (780 mg, 4.17 mmol) in EtOH (25 mL) was heated under reflux with a bleach scrubber under nitrogen for 1 h. The crude solution was then treated with hydrazine (50 wt % in water, 0.26 mL), and the mixture was heated at reflux for 1.5 h. A further 80 μL of hydrazine was added, and the mixture was heated at reflux for a further 3 h. The mixture was concentrated under reduced pressure. The residue was triturated with water (10 mL). The solid was collected by filtration and dried in a vacuum oven to give the title product **18d** (935 mg, 73%). LC−MS (ESI, formic) m/z 293, 295 [M + H]$^+$, R_t = 0.59 (94% by area).

2-(((5-Bromopyridin-2-yl)methyl)amino)-7-oxo-5-propyl-4,7-dihydropyrazolo[1,5-a]pyrimidine-3-carbonitrile, Acetic Acid Salt

(58). A mixture of 3-amino-5-(((5-bromopyridin-2-yl)methyl)amino)-1*H*-pyrazole-4-carbonitrile **18d** (100 mg, 0.341 mmol) and ethyl 3-oxohexanoate (55 μL, 0.34 mmol) in acetic acid (2 mL) and water (1 mL) was heated at reflux overnight. The mixture was cooled. The solid formed was collected by filtration, washed with water, and dried in a vacuum oven to give the title product **58** as the acetate salt (94 mg, 61%). ^{1}H NMR (400 MHz, DMSO-d_6) δ 12.82 (s, 1H), 11.92 (br s, 1H), 8.63 (d, J = 2.0 Hz, 1H), 7.99 (dd, J = 8.5, 2.4 Hz, 1H), 7.26−7.36 (m, 2H), 5.68 (s, 1H), 4.48 (d, J = 5.8 Hz, 2H), 2.45−2.54 (m, 2H overlap with DMSO), 1.91 (s, 3H), 1.63 (sx, J = 7.4 Hz, 2H), 0.92 (t, J = 7.5 Hz, 3H). LC−MS (ESI, formic) m/z 387, 389 [M + H]$^+$, R_t = 0.79.

3-Amino-5-((4-chloro-3-fluorobenzyl)amino)-1H-pyrazole-4-carbonitrile (18e). A mixture of 2-(bis(methylthio)methylene)-malononitrile (2.1 g, 12.5 mmol) and (4-chloro-3-fluorophenyl)-methanamine (2.0 g, 12.5 mmol) in EtOH (40 mL) was heated at reflux with a bleach scrubber under nitrogen for 1 h. The crude solution was then treated with hydrazine (50 wt % in water, 0.83 mL, 13.2 mmol), and the mixture was heated at reflux for 2.5 h. The mixture was cooled, and ca. 40 mL of water added. The volatile components were substantially removed under reduced pressure until an off-white solid was deposited. The solid was collected by filtration, washed with water, and dried in vacuum oven to give the title product **18e** as an off-white solid (2.97 g, 85%). LC−MS (ESI, formic) m/z 266 [M + H]$^+$, R_t = 0.78 (92% by area).

2-((4-Chloro-3-fluorobenzyl)amino)-7-oxo-5-propyl-4,7-dihydropyrazolo[1,5-a]pyrimidine-3-carbonitrile (59). A mixture of 3-amino-5-((4-chloro-3-fluorobenzyl)amino)-1*H*-pyrazole-4-carbonitrile **18e** (100 mg, 0.376 mmol) and ethyl 3-oxohexanoate (0.061 mL, 0.376 mmol) in acetic acid (2 mL) and water (1 mL) was heated at reflux overnight. All volatile components were removed, and the resulting crude product was purified by reverse phase chromatography using MDAP (formic acid, 30−85% solvent B over 15 min) to give the title product **59** as a white solid (34 mg, 25%). ^{1}H NMR (400 MHz, DMSO-d_6) δ 12.79 (br s, 1H), 7.52 (t, J = 7.9 Hz, 1H), 7.35 (dd, J = 10.6, 1.8 Hz, 1H), 7.26 (t, J = 6.2 Hz, 1H), 7.21 (dd, J = 8.3, 1.3 Hz, 1H), 5.67 (s, 1H), 4.41 (d, J = 6.0 Hz, 2H), 2.44−2.52 (overlapped with DMSO, 2H), 1.63 (sx, J = 7.5 Hz, 2H), 0.91 (t, J = 7.3 Hz, 3H). LC−MS (ESI, formic) m/z 360 [M + H]$^+$, R_t = 0.94.

3-Amino-5-((4-chloro-2-fluorobenzyl)amino)-1H-pyrazole-4-carbonitrile (18f). A mixture of 2-(bis(methylthio)methylene)-malononitrile (2.17 g, 12.8 mmol) and (4-chloro-2-fluorophenyl)-methanamine, hydrochloride (2.5 g, 12.8 mmol) in EtOH (40 mL) was heated under reflux with a bleach scrubber for 2 h under nitrogen. The crude solution was then treated with hydrazine (50 wt % in water, 0.8 mL, 12.8 mmol), and the mixture was heated at reflux for 1 h. The mixture was cooled, and 40 mL of water were added. Volatile components were partially removed under reduced pressure until a solid formed. The solid was collected by filtration, washed with water, and dried in a vacuum oven to give the title product **18f** as an off-white solid (2.6 g, 75%). ^{1}H NMR (400 MHz, DMSO-d_6) δ 10.61 (br s, 1H), 7.28−7.47 (m, 2H), 7.23 (d, J = 7.8 Hz, 1H), 5.97−6.20 (m, 2H), 4.25 (br s, 2H). LC−MS (ESI, formic) m/z 266 [M + H]$^+$, R_t = 0.78.

2-((4-Chloro-2-fluorobenzyl)amino)-7-oxo-5-propyl-4,7-dihydropyrazolo[1,5-a]pyrimidine-3-carbonitrile (60). A mixture of 3-amino-5-((4-chloro-2-fluorobenzyl)amino)-1*H*-pyrazole-4-carbonitrile **18f** (100 mg, 0.376 mmol) and ethyl 3-oxohexanoate (61 μL, 0.38 mmol) in acetic acid (2 mL) and water (1 mL) was heated at reflux overnight. All volatile components were removed under reduced pressure. The resulting solid was triturated with ether. The solid was collected, washed with ether, and dried in a vacuum oven to give the title product **60** (85 mg, 60%, 93% area by LC−MS). ^{1}H NMR (400 MHz, DMSO-d_6) δ 12.80 (br s, 1H), 7.35−7.46 (m, 2H), 7.19−7.28 (m, 2H), 5.69 (s, 1H), 4.43 (d, J = 6.0 Hz, 2H), 2.45−2.52 (overlapped with DMSO, 2H), 1.63 (sxt, J = 7.4 Hz, 2H), 0.92 (t, J = 7.3 Hz, 3H). LC−MS (ESI, formic) m/z 360 [M + H]$^+$, R_t = 0.95 (93% by area).

3-Amino-5-((4-chloro-2,6-difluorobenzyl)amino)-1H-pyrazole-4-carbonitrile (18g). A mixture of 2-(bis(methylthio)methylene)-

malononitrile (1.917 g, 11.26 mmol) and (4-chloro-2,6-difluorophenyl)methanamine (2.0 g, 11.3 mmol) in EtOH (40 mL) was heated under reflux with a bleach scrubber under nitrogen for 1 h. Hydrazine (50 wt % in water, 0.92 mL, 14.6 mmol) was added, and the mixture was heated at reflux for 1 h. Then 40 mL of water was added and volatile components were removed under reduced pressure until a solid appeared. The solid was collected by filtration to give the title product **18g** (3.1 g, 87%, 91% area by LC−MS). ^{1}H NMR (400 MHz, DMSO-d_6) δ 10.69 (br s, 1H), 7.29 (apparent d, J = 5.3 Hz, 2H), 6.03 (br s, 2H), 5.85 (br s, 1H), 4.22 (d, J = 4.3 Hz, 2H). LC−MS (ESI, formic) m/z 284 [M + H]$^+$, R_t = 0.80.

2-((4-Chloro-2,6-difluorobenzyl)amino)-7-oxo-5-propyl-4,7-dihydropyrazolo[1,5-a]pyrimidine-3-carbonitrile (61). A mixture of 3-amino-5-((4-chloro-2,6-difluorobenzyl)amino)-1H-pyrazole-4-carbonitrile **18g** (100 mg, 0.353 mmol) and methyl 3-oxohexanoate (67 μL, 0.46 mmol) was heated under reflux in acetic acid (2 mL) and water (1 mL) for 24 h. The mixture was cooled, and water was added. The mixture was left to stand until solid crashed out. The solid was collected by filtration, washed with water, and dried in a vacuum oven to give the title product **61** as an off-white solid (50 mg, 38%, 93% area by LC−MS). ^{1}H NMR (400 MHz, DMSO-d_6) δ 12.76 (s, 1H), 7.30−7.39 (m, 2H), 7.06 (br s, 1H), 5.70 (s, 1H), 4.39 (d, J = 5.0 Hz, 2H), 2.46−2.53 (m, 2H), 1.64 (sx, J = 7.4 Hz, 2H), 0.92 (t, J = 7.3 Hz, 3H). LC−MS (ESI, formic) m/z 378 [M + H]$^+$, R_t = 0.97 (93% by area).

3-Amino-5-((4-bromo-2-fluorobenzyl)amino)-1H-pyrazole-4-carbonitrile (18h). A mixture of 2-(bis(methylthio)methylene)-malononitrile (0.835 g, 4.91 mmol) and (4-bromo-2-fluorophenyl)-methanamine, hydrochloride (1.18 g, 4.91 mmol) and sodium hydrogen carbonate (0.412 g, 4.91 mmol) in EtOH (25 mL) was heated at reflux with a bleach scrubber under nitrogen for 2 h. Hydrazine (0.4 mL, 6.4 mmol) was added, and the mixture was heated at reflux for 1 h. The mixture was cooled, and water (10 mL) was added. The volatile components were removed under reduced pressure. Water and EtOAc were added. The aqueous layer was extracted with EtOAc (2×). The combined organic layers were washed with brine (×2). The organic layer was passed through a hydrophobic frit and concentrated under reduced pressure to give the title product **18h** (1.4 g, 93%, 85% area by LC−MS). ^{1}H NMR (400 MHz, DMSO-d_6) δ 10.60 (br s, 1H), 7.26−7.51 (m, 3H), 6.05 (br s, 3H), 4.23 (d, J = 5.3 Hz, 2H). LC−MS (ESI, formic) m/z 310, 312 [M + H]$^+$, R_t = 0.81 (85% by area).

2-((4-Bromo-2-fluorobenzyl)amino)-7-oxo-5-propyl-4,7-dihydropyrazolo[1,5-a]pyrimidine-3-carbonitrile (62). A mixture of 3-amino-5-((4-bromo-2-fluorobenzyl)amino)-1H-pyrazole-4-carbonitrile **18h** (100 mg, 0.322 mmol) and methyl 3-oxohexanoate (0.061 mL, 0.419 mmol) in acetic acid (2 mL) and water (1 mL) were heated at reflux for 24 h. The mixture was left to cool; a solid formed which was collected by filtration and dried in a vacuum oven. The resulting crude product was purified by reverse phase chromatography using MDAP (formic acid, 15−55% solvent B over 15 min) to give the title product **62** as a white solid (37 mg, 28%). ^{1}H NMR (400 MHz, DMSO-d_6) δ 12.79 (s, 1H), 7.47−7.54 (m, 1H), 7.31−7.41 (m, 2H), 7.22 (br s, 1H), 5.68 (s, 1H), 4.41 (d, J = 6.0 Hz, 2H), 2.46−2.53 (m, 2H overlap with DMSO), 1.63 (sxt, J = 7.5 Hz, 2H), 0.92 (t, J = 7.3 Hz, 3H). LC−MS (ESI, formic) m/z 404, 406 [M + H]$^+$, R_t = 0.99.

(R)-3-Amino-5-((1-(4-bromo-2-fluorophenyl)ethyl)amino)-1H-pyrazole-4-carbonitrile (18i). A mixture of 2-(bis(methylthio)-methylene)malononitrile (0.390 g, 2.29 mmol) and (R)-1-(4-bromo-2-fluorophenyl)ethanamine (0.5 g, 2.29 mmol) in EtOH (20 mL) was heated under reflux with a bleach scrubber under nitrogen for 2 h. Hydrazine (0.19 mL, 2.98 mmol) was added, and the mixture was heated at reflux for 1 h. The mixture was cooled and concentrated under reduced pressure. The resulting crude product was purified by reverse phase chromatography (43 g Redisep C18 GOLD column, 10−50% 0.1% formic acid in acetonitrile in 0.1% formic acid in water gradient) to give the title product **18i** (415 mg, 55%). ^{1}H NMR (400 MHz, methanol-d_4) δ 7.22−7.36 (m, 3H), 4.94 (q, J = 6.8 Hz, 1H), 1.48 (d, J = 6.8 Hz, 3H), 4H not visible (exchangeable). LC−MS (ESI, formic) m/z 324, 326 [M + H]$^+$, R_t = 0.85.

(R)-2-((1-(4-Bromo-2-fluorophenyl)ethyl)amino)-7-oxo-5-propyl-4,7-dihydropyrazolo[1,5-a]pyrimidine-3-carbonitrile (63). A mixture of (R)-3-amino-5-((1-(4-bromo-2-fluorophenyl)ethyl)amino)-1H-pyrazole-4-carbonitrile **18i** (135 mg, 0.416 mmol) and ethyl 3-oxohexanoate (67 μL, 0.416 mmol) in acetic acid (2 mL) and water (1 mL) was heated at reflux for 5 h. The mixture was cooled and diluted with water (5 mL). The solid formed was collected by filtration and washed with water and dried in a vacuum oven to give the title product **63** as a white solid (129 mg, 70%). ^{1}H NMR (400 MHz, DMSO-d_6) δ 12.76 (s, 1H), 7.35−7.51 (m, 3H), 7.25 (d, J = 7.8 Hz, 1H), 5.66 (s, 1H), 5.06−5.15 (m, 1H), 2.44−2.53 (m, 2H), 1.56−1.67 (m, 2H), 1.45 (d, J = 6.8 Hz, 3H), 0.90 (t, J = 7.3 Hz, 3H). LC−MS (ESI, formic) m/z 418 [M + H]$^+$, R_t = 1.01.

(S)-3-Amino-5-((1-(4-bromo-2-fluorophenyl)ethyl)amino)-1H-pyrazole-4-carbonitrile (18j). A mixture of 2-(bis(methylthio)-methylene)malononitrile (0.781 g, 4.59 mmol) and (S)-1-(4-bromo-2-fluorophenyl)ethanamine (1.0 g, 4.59 mmol) and sodium bicarbonate (0.385 g, 4.59 mmol) in EtOH (25 mL) was heated under reflux with a bleach scrubber under nitrogen for 3 h. A further 0.3 equiv of sodium bicarbonate (116 mg) was added, and the mixture was heated at reflux for 1 h. Hydrazine (0.374 mL, 5.96 mmol) was then added, and the mixture was heated at reflux for 30 min. The mixture was cooled, and 5 mL of water was added. The mixture was then concentrated under reduced pressure. The resulting crude product was worked up with EtOAc and water (×3) followed by brine (×2). The organic layer was separated and concentrated under reduced pressure. The resulting crude product was purified by reverse phase chromatography (150 g Redisep C$_{18}$ GOLD column, 10−50% 0.1% formic acid in acetonitrile in 0.1% formic acid in water gradient) to give the title product **18j** as an off-white solid (554 mg, 37%). ^{1}H NMR (400 MHz, DMSO-d_6) δ 10.67 (br s, 1H), 7.29−7.48 (m, 3H), 6.17 (br s, 1H), 5.91 (br s, 2H), 4.73−4.90 (m, 1H), 1.36 (d, J = 6.8 Hz, 3H). LC−MS (ESI, formic) m/z 324, 326 [M + H]$^+$, R_t = 0.85.

(S)-2-((1-(4-Bromo-2-fluorophenyl)ethyl)amino)-7-oxo-5-propyl-4,7-dihydropyrazolo[1,5-a]pyrimidine-3-carbonitrile (64). A mixture of (S)-3-amino-5-((1-(4-bromo-2-fluorophenyl)ethyl)amino)-1H-pyrazole-4-carbonitrile **18j** (100 mg, 0.308 mmol) and methyl 3-oxohexanoate (0.06 mL, 0.40 mmol) in acetic acid (2 mL) and water (1 mL) was heated under reflux for 24 h. The mixture was cooled, and water (2 mL) was added. The solid formed was collected by filtration and dried in a vacuum oven to give the title product **64** as a white solid (28 mg, 22%, 89% area by LC−MS). ^{1}H NMR (400 MHz, DMSO-d_6) δ 12.75 (s, 1H), 7.34−7.51 (m, 3H), 7.23 (d, J = 8.0 Hz, 1H), 5.66 (s, 1H), 5.04−5.16 (m, 1H), 2.44−2.53 (m, 2H), 1.61 (apparent sx, J = 7.4 Hz, 2H), 1.44 (d, J = 7.0 Hz, 3H), 0.90 (t, J = 7.3 Hz, 3H). LC−MS (ESI, formic) m/z 418, 420 [M + H]$^+$, R_t = 1.01 (89% by area).

5-Butyl-2-((4-chloro-2-fluorobenzyl)amino)-7-oxo-4,7-dihydropyrazolo[1,5-a]pyrimidine-3-carbonitrile (66). A mixture of 3-amino-5-((4-chloro-2-fluorobenzyl)amino)-1H-pyrazole-4-carbonitrile **18f** (100 mg, 0.376 mmol) and methyl 3-oxoheptanoate (0.060 mL, 0.376 mmol) in acetic acid (2 mL) and water (1 mL) was heated at reflux overnight. All volatiles were removed under reduced pressure. The resulting crude product was triturated with ether. The solid was collected by filtration, washed with ether, and dried in a vacuum oven to give the title product **66** as a white solid (113 mg, 76%, 91% area by LC−MS). ^{1}H NMR (400 MHz, DMSO-d_6) δ 12.79 (br s, 1H), 7.34−7.46 (m, 2H), 7.18−7.29 (m, 2H), 5.69 (s, 1H), 4.43 (d, J = 5.8 Hz, 2H), 2.43−2.57 (m, 2H), 1.59 (quin, J = 7.6 Hz, 2H), 1.33 (sxt, J = 7.4 Hz, 2H), 0.90 (t, J = 7.3 Hz, 3H). LC−MS (ESI, formic) m/z 374 [M + H]$^+$, R_t = 1.02 (91% by area).

2-((4-Bromo-2-fluorobenzyl)amino)-5-butyl-7-oxo-4,7-dihydropyrazolo[1,5-a]pyrimidine-3-carbonitrile (67). A mixture of 3-amino-5-((4-bromo-2-fluorobenzyl)amino)-1H-pyrazole-4-carbonitrile **18h** (100 mg, 0.322 mmol) and methyl 3-oxoheptanoate (0.067 mL, 0.419 mmol) in acetic acid (1 mL) and water (0.5 mL) was heated at reflux for 24 h. The mixture was cooled to room temperature. The solid formed was collected by filtration and dried in a vacuum oven. The resulting crude product was purified by reverse phase chromatography using MDAP (formic acid, 15−55% solvent B

over 15 min) to give the title product **67** as a white solid (43 mg, 32%). ^{1}H NMR (400 MHz, DMSO-d_6) δ 12.78 (s, 1H), 7.46−7.53 (m, 1H), 7.31−7.41 (m, 2H), 7.22 (br s, 1H), 5.68 (br s, 1H), 4.41 (d, J = 5.8 Hz, 2H), 2.46−2.54 (m, 2H overlap with DMSO), 1.59 (qn, J = 7.5 Hz, 2H), 1.26−1.39 (m, 2H), 0.90 (t, J = 7.3 Hz, 3H). LC−MS (ESI, formic) m/z 418, 420 [M + H]+, R_t = 1.06.

(R)-2-((1-(4-Bromo-2-fluorophenyl)ethyl)amino)-5-butyl-7-oxo-4,7-dihydropyrazolo[1,5-a]pyrimidine-3-carbonitrile (68). A mixture of (R)-3-amino-5-((1-(4-bromo-2-fluorophenyl)ethyl)amino)-1H-pyrazole-4-carbonitrile **18i** (135 mg, 0.416 mmol) and methyl 3-oxoheptanoate (66 μL, 0.416 mmol) in acetic acid (2 mL) and water (1 mL) was heated at reflux for 5 h. The mixture was left to cool to room temperature. Water (5 mL) was added, and the solid formed was collected by filtration, washed with water, and dried in a vacuum oven to give the title product **68** as a white solid (102 mg, 56%). ^{1}H NMR (400 MHz, DMSO-d_6) δ 12.76 (s, 1H), 7.34−7.51 (m, 3H), 7.25 (d, J = 8.1 Hz, 1H), 5.66 (s, 1H), 5.10 (qn, J = 7.2 Hz, 1H), 2.44−2.54 (m, 2H), 1.57 (qn, J = 7.6 Hz, 2H), 1.44 (d, J = 6.8 Hz, 3H), 1.32 (sx, J = 7.3 Hz, 2H), 0.89 (t, J = 7.3 Hz, 3H). LC−MS (ESI, formic) m/z 432, 434 [M + H]+, R_t = 1.07.

5-Butyl-2-((4-chloro-2,6-difluorobenzyl)amino)-7-oxo-4,7-dihydropyrazolo[1,5-a]pyrimidine-3-carbonitrile (69). A mixture of 5-amino-3-((4-chloro-2,6-difluorobenzyl)amino)-1H-pyrazole-4-carbonitrile **18g** (800 mg, 2.82 mmol) and ethyl 3-oxoheptanoate (0.59 mL, 3.38 mmol) in acetic acid (12 mL) and water (6 mL) was heated at reflux for 22 h. Additional ethyl-3-oxoheptanoate (0.1 mL, 0.577 mmol) was added, and the mixture was heated at reflux for 3 h. The mixture was left to cool to room temperature. The solid formed was collected by filtration, washed with water, and dried in a vacuum oven. The product obtained was recrystallized in EtOH to give the title product **69** as a white solid (530 mg, 48%). ^{1}H NMR (400 MHz, DMSO-d_6) δ 12.75 (br s, 1H), 7.31−7.38 (m, 2H), 7.05 (t, J = 5.0 Hz, 1H), 5.70 (s, 1H), 4.39 (d, J = 5.0 Hz, 2H), 2.50−2.56 (m, 2H), 1.59 (m, 2H), 1.34 (dq, J = 14.8, 7.4 Hz, 2H), 0.91 (t, J = 7.4 Hz, 3H). LC−MS (ESI, formic) m/z 392 [M + H]+, R_t = 1.01 min. The filtrate was concentrated under reduced pressure and purified by reverse phase chromatography using MDAP (formic acid, 30−85% solvent B) to give additionnal product **69** (122 mg, 11%).

3-Amino-5-((4-bromo-2,6-difluorobenzyl)amino)- 1H-pyrazole-4-carbonitrile (18h). A mixture of (4-bromo-2,6-difluorophenyl)-methanamine (360 mg, 1.62 mmol) and 2-(bis(methylthio)-methylene)malononitrile (276 mg, 1.62 mmol) in EtOH (6 mL) was heated under reflux with a bleach scrubber under nitrogen for 1 h. Hydrazine (0.10 mL, 1.62 mmol) was then added, and the mixture was left to stir for 4 h. The mixture was cooled, and 10 mL of water was added. Solvent was partially removed under reduced pressure to favor precipitation of the desired product. The solid formed was collected by filtration and dried in a vacuum oven to give the title product **18h** as an orange solid (365 mg, 69%). ^{1}H NMR (400 MHz, DMSO-d_6) δ 10.69 (br s, 1H), 7.40 (br s, 2H), 6.03 (br s, 2H), 5.84 (br s, 1H), 4.20 (br s, 2H). LC−MS (ESI, formic) m/z 328, 330 [M + H]+, R_t = 0.80 min.

2-((4-Bromo-2,6-difluorobenzyl)amino)-5-butyl-7-oxo-4,7-dihydropyrazolo[1,5-a]pyrimidine-3-carbonitrile (70). A mixture of 3-amino-5-((4-bromo-2,6-difluorobenzyl)amino)-1H-pyrazole-4-carbonitrile **18h** (100 mg, 0.305 mmol) and ethyl 3-oxoheptanoate (69 μL, 0.40 mmol) in acetic acid (2 mL) and water (1 mL) was heated at reflux over the weekend. The mixture was cooled to room temperature, and water (2 mL) was added. The solid formed was collected by filtration and dried in a vacuum oven to give the title product **70** as an orange solid (53 mg, 36%, 94% area by LC−MS). ^{1}H NMR (400 MHz, DMSO-d_6) δ 12.75 (s, 1H), 7.40−7.50 (m, 2H), 7.05 (t, J = 5.0 Hz, 1H), 5.70 (s, 1H), 4.38 (d, J = 4.8 Hz, 2H), 2.47−2.56 (m, 2H), 1.59 (qn, J = 7.5 Hz, 2H), 1.34 (sx, J = 7.3 Hz, 2H), 0.91 (t, J = 7.4 Hz, 3H). LC−MS (ESI, formic) m/z 436, 438 [M + H]+, R_t = 1.03 min (94% by area).

Physicochemical Properties. *Chemi-Luminescent Nitrogen Detection (CLND) Solubility Determination.* GSK in-house kinetic solubility assay: 5 mL of 10 mM DMSO stock solution diluted to 100 μL with pH 7.4 phosphate buffered saline, equilibrated for 1 h at room temperature, filtered through Millipore Multiscreen$_{HTS}$-PCF filter plates (MSSL BPC). The filtrate was quantified by suitably calibrated flow injection chemiluminescent nitrogen detection.[15] The standard error of the CLND solubility determination was ±30 μM, and the upper limit of the solubility is 500 μM when working from 10 mM DMSO stock solution.

ChromlogD$_{7.4}$ Determination. The Chromatographic Hydrophobicity Index (CHI)[14] values were measured using reversed phase HPLC column (50 mm × 2 mm 3 μM Gemini NX C18, Phenomenex, UK) with fast acetonitrile gradient at starting mobile phase of pH = 7.4. CHI values were derived directly from the gradient retention times by using a calibration line obtained for standard compounds. The CHI value approximates to the volume % organic concentration when the compound eluted. CHI was linearly transformed into ChromlogD by least-squares fitting of experimental CHI values to calculated clogP values for over 20K research compounds using the following formula: ChromlogD = 0.0857CHI − 2.00. The average error of the assay was ±3 CHI unit or ±0.25 ChromlogD.

pK$_a$ Determination. The pK$_a$ was measured using Sirius T3 Fast UV pK$_a$ method. The sample was run under the spectrophotometric (UV-metric) method on a Sirius T3 instrument covering the pH range 2−12. Then 5 μL of 10 mM DMSO stock solution was used in the cosolvent method utilizing MeOH as cosolvent. Data were refined using the Yasuda−Shedlovsky extrapolation.

Computational Chemistry. *Docking.* Docking studies were performed with the program GLIDE [Glide, version 5.7, Schrödinger, LLC, New York, NY, 2011].[54−56] Protein structures were prepared using the Protein Preparation Wizard in Maestro [Maestro, version 9.2, Schrödinger, LLC, New York, NY, 2011] with default options at each stage except for the addition of "Cap termini" at the preprocess stage. By default Maestro generates an alternative mesomer for the PLP, shifting the double bonds to give a carbonyl in place of the phenolate. This was corrected by the use of a custom file: common_mesomers.dat in the users $HOME/.schrodinger/mmshare directory as supplied by Schrodinger support. GLIDE grids were generated using standard settings and standard precision docking was run saving 5 poses per ligand.

GRID Analysis. Protein preparation on the in-house structure of GSK2854414A was run within Maestro as above and a PDB file written. The PLP coordinates were moved from HETATM to ATOM records in a text editor, adding to Lys 202, and renaming to PLP as this residue is specifically encoded in GRID. All other HETATM records were removed prior to running GRID. A number of GRID probes were run on the active site within a 33 × 33 × 26 Å³ box within the active site with 0.5 Å grid spacing. The following probes were used: methyl (C3), DRY, amide NH (N1), water (OH2), carbonyl O (O), phenolate O (O−).

Biology. *Human BCATm Cloning and Expression.* hBCATm (GenBank: NM_001190) was PCR amplified lacking the N-terminal signal sequence (amino acids 28−392), with flanking NdeI/XhoI restriction endonuclease sites using two oligonucleotides 5′-AGC__CATATG__GCCTCCTCCAGTTTCAAGGCT-3′ and 5′-GCC__CTCGAG__TTACACCGGGAACATCCACTCG-3′. The fragment was cloned into pET28a (MERCK) containing an N-terminal 6 Histidine purification tag and thrombin protease cleavage recognition site. Expression of 6His thrombin hBCATm was performed using *Escherichia coli* BL21 Star (DE3) (Invitrogen). The cells were transformed using standard heat shock protocols and then seeded onto LB plates containing kanamycin (50 μg/mL). Colonies were grown up and used to seed Turbo media supplemented with glucose and kanamycin (50 μg/mL) and 1% glucose. Shake flask cultures were grown at 37 °C induced with 0.5 mM IPTG at OD$_{600\,nm}$ 2.0 and then incubated at 25 °C for 20 h prior to harvesting by centrifugation.

Human BCATm Protein Production. Purification of hBCATm (either Holo- or Apo-) used a modified version of the method described by Conway and Huston.

I. Holo-hBCATm. Frozen cell pellets were thawed in buffer (25 mM HEPES, pH 7.5, 500 mM NaCl, 4 M urea, 1 mM DTT, 20 mM imidazole, Protease Inhibitor Cocktail III (Merck)) containing 0.1 mM

pyridoxal phosphate, 0.2 mg/mL lysozyme, and 10 U/mL benzonase (MERCK) and mixed for 30 min at room temperature. The cell suspension was sonicated, and the cell debris removed by centrifugation at 100000g for 90 min. The supernatant was loaded onto a 5 mL HisTrap HP column (GE Healthcare), washed with 10 bed volumes (Bv) of buffer before running a gradient to 0 M urea in buffer over 10 Bv at 5 mL/min. The column was eluted using a series of Imidazole steps 25, 50, 100, 200, and 500 mM in buffer (10 Bv for each at 5 mL/min). The hBCATm containing fractions (generally eluted following the 100 mM imidazole step) were pooled and concentrated using an Amicon Ultra (Millipore) and further purified using a Superdex 200 column (GE Healthcare). Dimeric hBCATm was pooled and buffer exchanged into thrombin cleavage buffer (50 mM HEPES, pH 7.5, 150 mM NaCl, 2 mM CaCl) and incubated for 2 h at room temp with 10 U/mL of thrombin (LeeBio). After cleavage, DTT and $(NH_4)_2SO_4$ was added at 1 mM and 1.5 M, respectively, and the thrombin removed by purification on a butyl sepharose HP column (GE Healthcare). hBCATm was eluted using a gradient to 0 M $(NH_4)_2SO_4$ over 20 Bv. The hBCATm was pooled, buffer exchanged into storage buffer (25 mM HEPES pH 7.5, 25 mM NaCl, 20 mM DTT, 20 mM EDTA, 2.5% glycerol), concentrated to 10 mg/mL, and snap frozen at −80 °C.

ii. Apo-hBCATm. Frozen cell pellets were thawed in buffer (0.1 M sodium phosphate, 0.01 M Tris, 0.5 M NaCl, 5 mM β-mercaptoethanol, protease inhibitor cocktail (Merck)), sonicated, and centrifuged at 100000g for 90 min. As described for the generation of Holo-enzyme, the clarified lysate was loaded onto a 5 mL HisTrap HP column and bound protein eluted using a series of imidazole steps. hBCATm containing fractions were pooled and dialyzed overnight versus 5 L of 25 mM HEPES pH 7.5, 5 mM EDTA, 25 mM NaCl, 5 mM DTT, and 5% glycerol then stored in aliquots at −80 °C.

Cloning, Expression, and Purification of Streptomyces L-glutamine Oxidase (LGOX). The coding sequence for Streptomyces L-glutamine oxidase (LGOX) was PCR amplified from Streptomyces sp. X119-6 (ATTC 39343) genomic DNA and subcloned into pENTR/D. The signal sequence was removed by PCR of the LGOX gene from the pENTER/D construct at the same time a Tev cleavage site was added at the N-terminal of the protein along the AttB1 and AttB2 sites at the 5′ and 3′ ends of the PCR product, respectively. The PCR product was gel purified and Gateway cloned into pDEST7 (N-6His) to yield a construct that expressed 6His-Tev−LGOX.

The pDEST 6His-Tev−LGOX construct was transformed into *E. coli* BL21 (DE3) for expression. Expression was performed using Terrific Broth by using a 2% inoculum, the cells were grown for 3 h at 37 °C before induction with 0.5 mM IPTG and a temperature shift to 25 °C for 16 h. The cells were collected by centrifugation.

The cell pellet (42 g) was resuspended in 300 mL of buffer (25 mM HEPES, pH 8.0, 500 mM NaCl, 20 mM imidazole, Protease Inhibitor Cocktail 3) and lysozyme added to 0.5 mg/mL along with 10K units of benzonase, this was incubated at room temp for 20 min prior to sonication for 10 min to disrupt the cells. The insoluble material was removed by centrifugation at 108800g, 90 min at 4 °C, and the supernatant loaded on to a 5 mL HisTrapHP column (GH Healthcare) at 5 mL/min. The column was washed with 10 column volumes of buffer and eluted using imidazole steps 100 mM, 250 mM, and 500 mM, 10 column volumes of each collecting fractions. The fractions were Bradford assayed to determine the protein concentration and analyzed by SDS PAGE and LC-MS. Then 450 mg of LGOX was recovered at 9 mg/mL. LC-MS analysis confirmed the identity of the protein, the LGOX was missing the N-terminal methionine, and around half the material had an α-N-D-gluconoyl modification of the His tag (+178 Da larger that the Des Met protein).

BCATm Fluorescent Assay. All reagents were purchased from Sigma-Aldrich Ltd. (Gillingham, Dorset, UK) unless otherwise stated. Assay buffer was 50 mM HEPES (pH 7.5), 50 mM NaCl, and 1 mM CHAPS. Horseradish peroxidase was initially diluted to 500 units/mL in water. 4-Methyl-2-oxovalerate was initially diluted to 10 mM in assay buffer. L-Leucine and α-ketogluterate were both initially diluted to 100 mM in 50 mM HEPES (pH 7.5) with pyridoxal phosphate (PLP) initially diluted to 10 mM in 50 mM HEPES (pH 7.5). Amplex

Red (Invitrogen, Paisley, UK) was initially diluted to 20 mM in DMSO. BCATm and L-GOX proteins were cloned, expressed, and isolated in-house (GSK, Stevenage, UK) as described above.

The assay monitors the production of L-glutamate from branch chain amino acids and α-ketoglutarate through the coupling of hBCATm activity to two additional enzymes, L-glutamate oxidase (L-GOx) and horseradish peroxidase (HRP). L-GOx catabolizes L-glutamate to generate a-ketoglutarate and hydrogen peroxide, the later being utilized by HRP and leading to the formation of fluorescent resorufin from the redox sensitive dye Amplex Red.

The BCATm fluorescent assay was carried out in low volume 384-well plates (Greiner Bio-one, Stonehouse, UK) at a final volume of 10 μL per well. Test compounds were added to plates as 50 nL solution in DMSO using an Echo 555 acoustic dispenser (Labcyte, Sunnyvale, CA) prior to the addition of assay components. Additionally, 50 nL of DMSO or a control inhibitor compound at a suitable concentration to give 100% inhibition in the assay or something to that effect was included in two columns each to give 100% activity and 100% inhibition controls, respectively. Single-concentration testing was at 10 μM compound concentration. For pIC$_{50}$ determination, compounds were tested using an 11-point, 3-fold dilution series from either 625 or 6.25 μM prepared using a Biomek FX (Beckman Coulter, Wycombe, UK).

To these compound plates, 4 μL of an enzyme−PLP solution containing 20 nM BCATm and 40 nM PLP in assay buffer was added. Following this, 4 μL of a coupling solution containing 3 mM L-leucine, 0.5 mM α-ketogluterate, 10 units/mL HRP, and 80 μM Amplex red in assay buffer was added to initiate the reaction. The coupling solution was incubated on a roller at room temperature in a 15 mL tube with 1 mL of agarose immobilized catalase (Sigma-Aldrich Ltd.) per 10 mL of coupling solution to "scrub" the coupling solution prior to addition of Amplex Red and remove background levels of hydrogen peroxide. After a 10 min incubation, 2 μL of 100 mM 4-methyl-2-oxovalerate was added to stop the reaction.

Final assay concentrations were 10 nM BCATm, 20 nM PLP, 5 units per mL HRP, 1.5 mM L-leucine, 0.25 mM α-ketoglutarate and 40 μM Amplex Red. All additions were performed using a Multidrop Combi (Thermo Fisher Scientific, Waltham, MA). Plates were transferred to an EnVision reader (PerkinElmer) (excitation filter 525/20 nm; emission filter 598/25 nm).

BCATm Cellular Assay. Differentiated primary human adipocyte (Zenbio) were challenged overnight using compounds dissolved in HBSS (Gibco 1g/L glucose) complemented with HEPES 10 mM, L-serine 50 μM, and L-leucine 150 μM. Next day, cell supernatant was subjected to amino acid determinations using HPLC analysis essentially as previously described [ref agilent]. The method is based on automated, online derivatization using o-phthalaldehyde (OPA) for primary amino acids and 9-fluorenylmethyl chloroformate (FMOC) for secondary amino acids, using an Eclipse Plus C18 3 mm × 10 mm 3.5 μm column to perform reversed phase HPLC (all chemicals and hardware from Agilent Technologies, Inc.). The percentage of inhibition was calculated on leucine concentration remaining compared to vehicle treated cells.

Pharmacokinetic Studies. All animal studies were ethically reviewed and carried out in accordance with the GSK Policy on the Care, Welfare, and Treatment of Animals and European Directive 86/609. The mouse PK studies were performed at Les Ulis, France. For all studies, the temperature and humidity were nominally maintained at 21 °C ± 2 °C and 55% ± 10%, respectively. Male BalbC mice (20−25 g, Charles River, France) were used. For the intravenous route, one animal was used, while for the oral route, two animals were used, in both cases in a serial bleeding design with blood samples taken at the tail vein up to 24 h. The animals had free access to food and water throughout. For the IV route, the compound was formulated in DMSO and hydroxypropyl-β cyclodextrin 20% in phosphate buffer 60 mM pH 7 (5%:95%), which was filtered and then administered as an intravenous bolus at 10 mL/kg to achieve a target dose of 1 mg/kg. For the oral route, the compound was formulated as a suspension of HPMC K100 0.5%/Tween 80 0.1% in phosphate buffer 60 mM pH 7 and then administered by gavage at 10 mL/kg to achieve a target dose

of 5 mg/kg. Diluted blood samples (1:1 with water) were extracted using protein precipitation with acetonitrile containing an analytical internal standard. An aliquot of the supernatant was analyzed by reverse phase LC−MS/MS using a heat assisted electrospray interface in positive ion mode. Samples were assayed against calibration standards prepared in control blood. PK parameters were obtained from the blood concentration−time profiles using noncompartmental analysis with WinNonlin Professional 4.1a (Pharsight, Mountain View, CA).

In Vivo Experimental Methods. Male, C57Black/6J mice (from Charles River Laboratories, L'Arbresle, France) were used in all experiments. Animals were housed under controlled conditions of temperature and humidity, in a 12 h light/12 h dark cycle and provided with food and water ad libitum.

Oral administration of vehicle (0.5% HPMC K100 + 0.1% Tween 80 pH = 10.0) or indicated doses of compound as suspensions were typically administered in the morning. Five hours after compound oral gavages, animals were fasted. Then 1 h after, each animal was challenged with a mix of amino acid 1.5 g AA/20 mL/kg mice. Amino acid mix was prepared in 0.5% HPMC/0.1% Tween pH 7 and composed of L-cysteine 114 mg, L-histidine 114 mg, L-isoleucine 468 mg, L-leucine 939 mg, L-lysine 486 mg, L-methionine 39 mg, L-phenylalanine 75 mg, L-threonine 264 mg, L-tryptophan 15 mg, L-tyrosine 21 mg, and L-valine 468 mg (all amino acids from Sigma). One hour after amino acid challenge, blood samples were taken by intracardiac puncture. Sera were collected and frozen at −20 °C until use.

Sera amino acid analyses were performed by HPLC as described in the in vitro cell assay methods.

Crystallization and Crystallography Material and Methods. *BCATm/PLP Protein Production and Crystallization.* Human branched-chain amino acid aminotransferase mitochondrial (BCATm) (residues 28−392) deleted of the N-terminal mitochondria signal peptide (residues 1−27) was cloned into kanamycin resistant pET28a via NdeI/XhoI restriction endonuclease sites with an n-terminal 6His-thrombin cleavage site. The protein was expressed in *Escherichia coli* in inclusion bodies. Purification required 4 M urea lysis, followed by refolding and elution by NiSephHP ultrafiltration (UF). HiPrep desalting was then performed using Superdex 200 prep grade column followed by thrombin cleavage to remove the tag and final clarification by UF on a butyl sepharose HP-HiPrep desalting column. The purified protein was stored in buffer (25 mM HEPES, pH7.5, 25 mM NaCl, 20 mM DTT, 20 mM EDTA, 2.5% glycerol) and concentrated to at least 7.6 mg/mL for crystallography. Crystal of BCATm were grown by hanging drop vapor diffusion at 20 °C with microseeding using MDL Morpheus screen condition B2 supplemented with 10 mM DTT in a protein to microseed solution of drop ratio of 1:1. The Hampton Research seed-bead method was used to generate microseeds. The crystals had a yellow hue suggestive of bound PLP cofactor despite none being added during purification or crystallization.

To Obtain Crystal Structures of BCATm/PLP Complexed with Inhibitors. Holocrystals were transferred to soaking buffer comprising MDL Morpheus screen condition B2 supplemented with 10 mM or 20 mM DTT and the compound of interest (from a stock solution dissolved in DMSO) at the soaking concentration given in the X-ray summary table (Supporting Information). Crystals were harvested in a cryo-loop and plunge-frozen into liquid nitrogen before loading in a puck for mounting with a sample collector. Data from single crystals were collected at 100 K either at the European Synchrotron Radiation Facility (Grenoble) or on an in-house Rigaku FR-E⁺ SUPER-BRIGHT/Saturn A200 detector/ACTOR robotic system. Data processing was achieve using DENZO[57] or MOSFLM[58] and scaled using either SCALEPACK[57] or SCALA[59] within the CCP4 programming suite,[60] respectively. Structures were solved by Fourier synthesis using REFMAC[61] (via CCP4) starting from a previously determined in-house structure, model-building was performed using COOT[62] and refined using REFMAC via CCP4. The statistics for the data collection and refined coordinates are given in the table in the Supporting Information.

■ ASSOCIATED CONTENT

Ⓢ Supporting Information

HMBC spectra for compounds **26** and **50**; X-ray crystallography table of statistics for compounds **2, 3, 4, 6, 47**, and **66** (PDF). SMILES data (CSV). The Supporting Information is available free of charge on the ACS Publications website at DOI: 10.1021/acs.jmedchem.5b00313.

Accession Codes

The final crystal structures are deposited in the Protein Data Bank under the accession codes 5BWR (**2**), 5BWT (**3**), 5BWU (**4**), 5BWV (**6**), 5BWW (**47**), and 5BWX (**66**).

■ AUTHOR INFORMATION

Corresponding Author

*Phone: 00441438 551180. E-mail: sophie.x.bertrand@gsk.com.

Notes

The authors declare no competing financial interest.

■ ACKNOWLEDGMENTS

■ ABBREVIATIONS USED

BCAT, branched-chain aminotransferase; BCATc, cytosolic branched-chain aminotransferase; BCATm, mitochondrial branched-chain aminotransferase; BCAA, branched-chain amino acids; CDI, 1,1′-carbonyldiimidazole; CLND, chemiluminescent nitrogen detection; FBDD, fragment-based drug discovery; HATU, 1-[bis(dimethylamino)methylene]-1*H*-1,2,3-triazolo[4,5-*b*]pyridinium 3-oxid hexafluorophosphate); HTS, high throughput screening; LE, ligand efficiency; LLE$_{AT}$, lipophilic ligand efficiency defined by Astex; PK, pharmacokinetic; SAR, structure−activity relationship; STD-NMR, saturation-transfer difference nuclear magnetic resonance; T_m, thermal shift

■ REFERENCES

(1) Hutson, S. Structure and function of branched chain amino-transferases. *Prog. Nucleic Acid Res. Mol. Biol.* **2001**, *70*, 175−206.

(2) Hall, T. R.; Wallin, R.; Reinhart, G. D.; Hutson, S. M. Branched chain aminotransferase isoenzymes. Purification and characterization of the rat brain isoenzyme. *J. Biol. Chem.* **1993**, *268*, 3092−3098.

(3) Harper, A. E. Thoughts on the role of branched-chain alpha-keto acid dehydrogenase complex in nitrogen metabolism. *Ann. N. Y. Acad. Sci.* **1989**, *573*, 267−273.

(4) Hutson, S. M.; Wallin, R.; Hall, T. R. Identification of mitochondrial branched chain aminotransferase and its isoforms in rat tissues. *J. Biol. Chem.* **1992**, *267*, 15681−15686.

(5) Hutson, S. M.; Fenstermacher, D.; Mahar, C. Role of mitochondrial transamination in branched chain amino acid metabolism. *J. Biol. Chem.* **1988**, *263*, 3618−3625.

(6) Halton, T. L.; Hu, F. B. The effects of high protein diets on thermogenesis, satiety and weight loss: a critical review. *J. Am. Coll. Nutr.* **2004**, *23*, 373−385.

(7) Layman, D. K.; Walker, D. A. Potential importance of leucine in treatment of obesity and the metabolic syndrome. *J. Nutr.* **2006**, *136*, 319S−323S.

(8) She, P.; Reid, T. M.; Bronson, S. K.; Vary, T. C.; Hajnal, A.; Lynch, C. J.; Hutson, S. M. Disruption of BCATm in mice leads to increased energy expenditure associated with the activation of a futile protein turnover cycle. *Cell Metab.* **2007**, *6*, 181−194.

(9) She, P.; Zhou, Y.; Zhang, Z.; Griffin, K.; Gowda, K.; Lynch, C. J. Disruption of BCAA metabolism in mice impairs exercise metabolism and endurance. *J. Appl. Physiol.* **2010**, *108*, 941−949.

(10) Goto, M.; Miyahara, I.; Hirotsu, K.; Conway, M.; Yennawar, N.; Islam, M. M.; Hutson, S. M. Structural determinants for branched-chain aminotransferase isozyme-specific inhibition by the anticonvulsant drug gabapentin. *J. Biol. Chem.* **2005**, *280*, 37246−37256.

(11) Hu, L. Y.; Boxer, P. A.; Kesten, S. R.; Lei, H. J.; Wustrow, D. J.; Moreland, D. W.; Zhang, L.; Ahn, K.; Ryder, T. R.; Liu, X.; Rubin, J. R.; Fahnoe, K.; Carroll, R. T.; Dutta, S.; Fahnoe, D. C.; Probert, A. W.; Roof, R. L.; Rafferty, M. F.; Kostlan, C. R.; Scholten, J. D.; Hood, M.; Ren, X. D.; Schielke, G. P.; Su, T. Z.; Taylor, C. P.; Mistry, A.; McConnell, P.; Hasemann, C.; Ohren, J. The design and synthesis of human branched-chain amino acid aminotransferase inhibitors for treatment of neurodegenerative diseases. *Bioorg. Med. Chem. Lett.* **2006**, *16*, 2337−2340.

(12) Hutson, S. M.; Berkich, D.; Drown, P.; Xu, B.; Aschner, M.; LaNoue, K. F. Role of branched-chain aminotransferase isoenzymes and gabapentin in neurotransmitter metabolism. *J. Neurochem.* **1998**, *71*, 863−874.

(13) Mendoza, R.; Petros, A. M.; Liu, Y.; Thimmapaya, R.; Surowy, C. S.; Leise, W. F.; Pereda-Lopez, A.; Panchal, S. C.; Sun, C. Cracking the molecular weight barrier: fragment screening of an aminotransferase using an NMR-based functional assay. *Bioorg. Med. Chem. Lett.* **2011**, *21*, 5248−5250.

(14) Valko, K.; Bevan, C.; Reynolds, D. Chromatographic Hydrophobicity Index by Fast-Gradient RP-HPLC: A High-Throughput Alternative to Log *P*/log *D*. *Anal. Chem.* **1997**, *69*, 2022−2029.

(15) Bhattachar, S. N.; Wesley, J. A.; Seadeek, C. Evaluation of the chemiluminescent nitrogen detector for solubility determinations to support drug discovery. *J. Pharm. Biomed. Anal.* **2006**, *41*, 152−157.

(16) Carr, R. A. E.; Congreve, M.; Murray, C. W.; Rees, D. C. Fragment-based lead discovery: leads by design. *Drug Discovery Today* **2005**, *10*, 987−992.

(17) Congreve, M.; Murray, C. W.; Carr, R.; Rees, D. C. Fragment-based lead discovery. *Annu. Rep. Med. Chem.* **2007**, *42*, 431−448.

(18) Joseph-McCarthy, D.; Campbell, A. J.; Kern, G.; Moustakas, D. Fragment-Based Lead Discovery and Design. *J. Chem. Inf. Model.* **2014**, *54*, 693−704.

(19) Murray, C. W.; Rees, D. C. The rise of fragment-based drug discovery. *Nature Chem.* **2009**, *1*, 187−192.

(20) Chessari, G.; Woodhead, A. J. From fragment to clinical candidate—a historical perspective. *Drug Discovery Today* **2009**, *14*, 668−675.

(21) Murray, C. W.; Verdonk, M. L.; Rees, D. C. Experiences in fragment-based drug discovery. *Trends Pharmacol. Sci.* **2012**, *33*, 224−232.

(22) Gleeson, M. P. Generation of a Set of Simple, Interpretable ADMET Rules of Thumb. *J. Med. Chem.* **2008**, *51*, 817−834.

(23) Hughes, J. D.; Blagg, J.; Price, D. A.; Bailey, S.; DeCrescenzo, G. A.; Devraj, R. V.; Ellsworth, E.; Fobian, Y. M.; Gibbs, M. E.; Gilles, R. W.; Greene, N.; Huang, E.; Krieger-Burke, T.; Loesel, J.; Wager, T.; Whiteley, L.; Zhang, Y. Physiochemical drug properties associated with in vivo toxicological outcomes. *Bioorg. Med. Chem. Lett.* **2008**, *18*, 4872−4875.

(24) Leeson, P. D.; Springthorpe, B. The influence of drug-like concepts on decision-making in medicinal chemistry. *Nature Rev. Drug Discovery* **2007**, *6*, 881−890.

(25) Leeson, P. D.; Empfield, J. R. Reducing the risk of drug attrition associated with physicochemical properties. *Annu. Rep. Med. Chem.* **2010**, *45*, 393−407.

(26) Price, D. A.; Blagg, J.; Jones, L.; Greene, N.; Wager, T. Physicochemical drug properties associated with in vivo toxicological outcomes: a review. *Expert Opin. Drug Metab. Toxicol.* **2009**, *5*, 921−931.

(27) Waring, M. J. Lipophilicity in drug discovery. *Expert Opin. Drug Discovery* **2010**, *5*, 235−248.

(28) Hill, A. P.; Young, R. J. Getting physical in drug discovery: a contemporary perspective on solubility and hydrophobicity. *Drug Discovery Today* **2010**, *15*, 648−655.

(29) Young, R. J.; Green, D. V. S.; Luscombe, C. N.; Hill, A. P. Getting physical in drug discovery II: the impact of chromatographic hydrophobicity measurements and aromaticity. *Drug Discovery Today* **2011**, *16*, 822−830.

(30) Ritchie, T. J.; MacDonald, S. J. F. The impact of aromatic ring count on compound developability: are too many aromatic rings a liability in drug design? *Drug Discovery Today* **2009**, *14*, 1011−1020.

(31) Ritchie, T. J.; MacDonald, S. J. F.; Young, R. J.; Pickett, S. D. The impact of aromatic ring count on compound developability: further insights by examining carbo- and hetero-aromatic and -aliphatic ring types. *Drug Discovery Today* **2011**, *16*, 164−171.

(32) Hopkins, A. L.; Keserue, G. M.; Leeson, P. D.; Rees, D. C.; Reynolds, C. H. The role of ligand efficiency metrics in drug discovery. *Nature Rev. Drug Discovery* **2014**, *13*, 105−121.

(33) Young, R. J. Physical Properties in Drug Design. In *Topics in Medicinal Chemistry*; Springer: Berlin Heidelberg, 2014.

(34) Shultz, M. D. Setting expectations in molecular optimizations: strengths and limitations of commonly used composite parameters. *Bioorg. Med. Chem. Lett.* **2013**, *23*, 5980−5991.

(35) Hopkins, A. L.; Groom, C. R.; Alex, A. Ligand efficiency: a useful metric for lead selection. *Drug Discovery Today* **2004**, *9*, 430−431.

(36) Kuntz, I. D.; Chen, K.; Sharp, K. A.; Kollman, P. A. The maximal affinity of ligands. *Proc. Natl. Acad. Sci. U. S. A.* **1999**, *96*, 9997−10002.

(37) Mortenson, P. N.; Murray, C. W. Assessing the lipophilicity of fragments and early hits. *J. Comput.-Aided Mol. Des.* **2011**, *25*, 663−667.

(38) Borthwick, J. A.; Ancellin, N.; Bertrand, S. M.; Bingham, R. P.; Carter, P. S.; Chung, C.-W.; Churcher, I.; Dodic, N.; Fournier, C.; Francis, P. L.; Hobbs, A.; Jamieson, C.; Pickett, S. D.; Smith, S.; Somers, D. O'N.; Spitzfaden, C.; Young, R. J. Structurally Diverse Mitochondrial Branched Chain Aminotransferase (BCATm) Leads With Varying Binding Modes Identified by Fragment Screening. *J. Med. Chem.* **2015**.

(39) Legon, A. C.; Millen, D. J. Angular geometries and other properties of hydrogen-bonded dimers: a simple electrostatic interpretation of the success of the electron-pair model. *Chem. Soc. Rev.* **1987**, *16*, 467−498.

(40) Mukaiyama, H.; Nishimura, T.; Shiohara, H.; Kobayashi, S.; Komatsu, Y.; Kikuchi, S.; Tsuji, E.; Kamada, N.; Ohnota, H.; Kusama, H. Discovery of novel 2-anilinopyrazolo[1,5-*a*]pyrimidine derivatives as c-Src kinase inhibitors for the treatment of acute ischemic stroke. *Chem. Pharm. Bull.* **2007**, *55*, 881−889.

(41) Brooks, D. W.; Lu, L. D. L.; Masamune, S. C-Acylation under virtually neutral conditions. *Angew. Chem., Int. Ed. Engl.* **1979**, *18*, 72−74.

(42) Denton, R. M.; An, J.; Adeniran, B.; Blake, A. J.; Lewis, W.; Poulton, A. M. Catalytic Phosphorus(V)-Mediated Nucleophilic Substitution Reactions: Development of a Catalytic Appel Reaction. *J. Org. Chem.* **2011**, *76*, 6749−6767.

(43) Appel, R. Tertiary phosphane/tetrachloromethane, a versatile reagent for chlorination, dehydration, and phosphorus−nitrogen linking. *Angew. Chem.* **1975**, *87*, 863−874.

(44) Brown, E. V. Willgerodt reaction. *Synthesis* **1975**, 358−375.

(45) Moghaddam, F. M.; Ghaffarzadeh, M. Microwave-assisted rapid hydrolysis and preparation of thioamides by Willgerodt−Kindler reaction. *Synth. Commun.* **2001**, *31*, 317−321.

(46) Tominaga, Y.; Matsuoka, Y.; Kohra, S.; Hosomi, A. A novel preparation of polarized ethylenes by the reaction of thioamides or dithiocarboxylates with tetracyanoethylene oxide. Synthesis of pyrazoles and pyrimidines. *Heterocycles* **1987**, *26*, 613−616.

(47) Tominaga, Y.; Matsuoka, Y.; Oniyama, Y.; Uchimura, Y.; Komiya, H.; Hirayama, M.; Kohra, S.; Hosomi, A. Polarized ethylenes. IV. Synthesis of polarized ethylene using thioamides and methyl dithiocarboxylates and their application to syntheses of pyrazoles,

pyrimidines, pyrazolo[3,4-*d*]pyrimidines and 5-aza[2.2.3]cyclazines. *J. Heterocycl. Chem.* **1990**, *27*, 647−660.

(48) Goodford, P. J. A computational procedure for determining energetically favorable binding sites on biologically important macromolecules. *J. Med. Chem.* **1985**, *28*, 849−857.

(49) Carosati, E.; Sciabola, S.; Cruciani, G. Hydrogen Bonding Interactions of Covalently Bonded Fluorine Atoms: From Crystallographic Data to a New Angular Function in the GRID Force Field. *J. Med. Chem.* **2004**, *47*, 5114−5125.

(50) Taylor, E. C.; Hartke, K. S. The Reaction of Malononitrile with Substituted Hydrazines: New Routes to 4-Aminopyrazolo[3,4-*d*]-pyrimidines1,2. *J. Am. Chem. Soc.* **1959**, *81*, 2456−2464.

(51) Howard, J. A. K.; Hoy, V. J.; O'Hagan, D.; Smith, G. T. How good is fluorine as a hydrogen bond acceptor? *Tetrahedron* **1996**, *52*, 12613−12622.

(52) Berecz, G.; Reiter, J.; Csaszar, J. On triazoles. Part 40. Non-catalytic dehalogenation of some 5-chloro-1,2,4-triazolo[1,5-*a*]-pyrimidine derivatives. *J. Heterocycl. Chem.* **1999**, *36*, 1199−1212.

(53) Tominaga, Y.; Honkawa, Y.; Hara, M.; Hosomi, A. Synthesis of pyrazolo[3,4-*d*]pyrimidine derivatives using ketene dithioacetals. *J. Heterocycl. Chem.* **1990**, *27*, 775−783.

(54) Friesner, R. A.; Murphy, R. B.; Repasky, M. P.; Frye, L. L.; Greenwood, J. R.; Halgren, T. A.; Sanschagrin, P. C.; Mainz, D. T. Extra Precision Glide: Docking and Scoring Incorporating a Model of Hydrophobic Enclosure for Protein-Ligand Complexes. *J. Med. Chem.* **2006**, *49*, 6177−6196.

(55) Halgren, T. A.; Murphy, R. B.; Friesner, R. A.; Beard, H. S.; Frye, L. L.; Pollard, W. T.; Banks, J. L. Glide: A new approach for rapid, accurate docking and scoring. 2. Enrichment factors in database screening. *J. Med. Chem.* **2004**, *47*, 1750−1759.

(56) Friesner, R. A.; Banks, J. L.; Murphy, R. B.; Halgren, T. A.; Klicic, J. J.; Mainz, D. T.; Repasky, M. P.; Knoll, E. H.; Shelley, M.; Perry, J. K.; Shaw, D. E.; Francis, P.; Shenkin, P. S. Glide: A new approach for rapid, accurate docking and scoring. 1. method and assessment of docking accuracy. *J. Med. Chem.* **2004**, *47*, 1739−1749.

(57) Otwinowski, Z.; Minor, W. Processing of X-ray diffraction data collected in oscillation mode. *Methods Enzymol.* **1997**, *276*, 307−326.

(58) Leslie, A. G. W.; Powell, H. R. *Evolving Methods for Macromolecular Crystallography*; Springer Press: New York, 2007; pp 41−51.

(59) Evans, P. Scaling and assessment of data quality. *Acta Crystallogr., Sect. D: Biol. Crystallogr.* **2006**, *D62*, 72−82.

(60) Bailey, S. The CCP4 suite: programs for protein crystallography. *Acta Crystallogr., Sect. D: Biol. Crystallogr.* **1994**, *D50*, 760−763.

(61) Murshudov, G. N.; Vagin, A. A.; Dodson, E. J. Refinement of macromolecular structures by the maximum-likelihood method. *Acta Crystallogr., Sect. D: Biol. Crystallogr.* **1997**, *D53*, 240−255.

(62) Emsley, P.; Cowtan, K. Coot: model-building tools for molecular graphics. *Acta Crystallogr., Sect. D: Biol. Crystallogr.* **2004**, *D60*, 2126−2132.

Structurally Diverse Mitochondrial Branched Chain Aminotransferase (BCATm) Leads with Varying Binding Modes Identified by Fragment Screening

Jennifer A. Borthwick,[*,†,§] Nicolas Ancellin,[‡] Sophie M. Bertrand,[†,§] Ryan P. Bingham,[†] Paul S. Carter,[†] Chun-wa Chung,[†] Ian Churcher,[†] Nerina Dodic,[‡] Charlène Fournier,[†] Peter L. Francis,[†] Andrew Hobbs,[†] Craig Jamieson,[§] Stephen D. Pickett,[†] Sarah E. Smith,[†] Donald O'N. Somers,[†] Claus Spitzfaden,[†] Colin J. Suckling,[§] and Robert J. Young[†]

[†]Medicines Research Centre, GlaxoSmithKline R&D, Gunnels Wood Road, Stevenage, Hertfordshire, SG1 2NY, U.K.
[‡]Les Ulis, Centre de Recherche, GlaxoSmithKline R&D, 25,27 Avenue du Québec, 91140 Villebon sur Yvette, France
[§]Department of Pure and Applied Chemistry, University of Strathclyde, 295 Cathedral Street, Glasgow, G1 1XL, U.K.

S *Supporting Information*

ABSTRACT: Inhibitors of mitochondrial branched chain aminotransferase (BCATm), identified using fragment screening, are described. This was carried out using a combination of STD-NMR, thermal melt (T_m), and biochemical assays to identify compounds that bound to BCATm, which were subsequently progressed to X-ray crystallography, where a number of exemplars showed significant diversity in their binding modes. The hits identified were supplemented by searching and screening of additional analogues, which enabled the gathering of further X-ray data where the original hits had not produced liganded structures. The fragment hits were optimized using structure-based design, with some transfer of information between series, which enabled the identification of ligand efficient lead molecules with micromolar levels of inhibition, cellular activity, and good solubility.
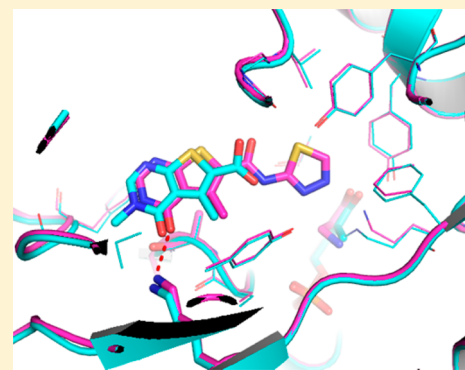
■ INTRODUCTION

Mitochondrial branched chain aminotransferase (BCATm) is a metabolic enzyme that converts the branched chain amino acids (BCAAs) leucine, isoleucine, and valine into their corresponding α-keto acids. Over the past few years, evidence has appeared linking this enzyme to obesity in animals and humans; accordingly inhibition of this enzyme has potential as a treatment for obesity and related diseases. The BCATm isoform is expressed ubiquitously, with very high levels in the stomach, pancreas, and salivary glands, consistent with its role in protein metabolism.[1] Interestingly, BCATm knockout mice are resistant to high-fat diet induced obesity and diabetes;[2] these effects are believed to be caused by the establishment of an energy consuming cycle of protein synthesis and degradation. This phenotype is similar to that observed in humans who consume high protein diets or BCAA supplements and experience increased energy expenditure, lower appetite, and ultimately, lower body weights.[2] The role of BCATm and BCAAs in the etiology of obesity is complex and not fully understood; knockout and dietary studies discussed above, where high levels of BCAA appear to be associated with reduced risk of becoming obese, are complicated by studies of obese animals. Genetically mutated obese rodents and diet-induced obese mice and humans have all been shown to have reduced BCATm expression, resulting in higher BCAA levels than lean animals.[3]

The search for inhibitors of BCATm at GSK was pursued using three complementary methods: fragment screening, high throughput screening (HTS), and encoded library technology. This paper describes the diversity of chemical matter, displaying distinct binding modes discovered by fragment screening. Hybridization of one of these hits with an HTS hit led to a potent in vivo active series,[4] and a further series was identified by encoded library technology.[5] Together, this package of work has shed much light on the variable binding modes observed with BCATm and is beginning to shed some light on the effects of specific pharmacological inhibition of BCATm by small molecules and the role of this enzyme in disease.

In a commentary[6] on our fragment assisted drug design[7] paper, the difficulty of the target was highlighted, as was the importance of having diverse chemical matter with appropriate in vivo activities to interrogate a target; this paper illustrates structural information describing diverse binding modes observed. In fragment screening, the lack of overlap between screening methods has been acknowledged;[8] this was observed in the progression of hits identified by the various methods in

Scheme 1. Reaction Cycle Catalyzed by BCATm
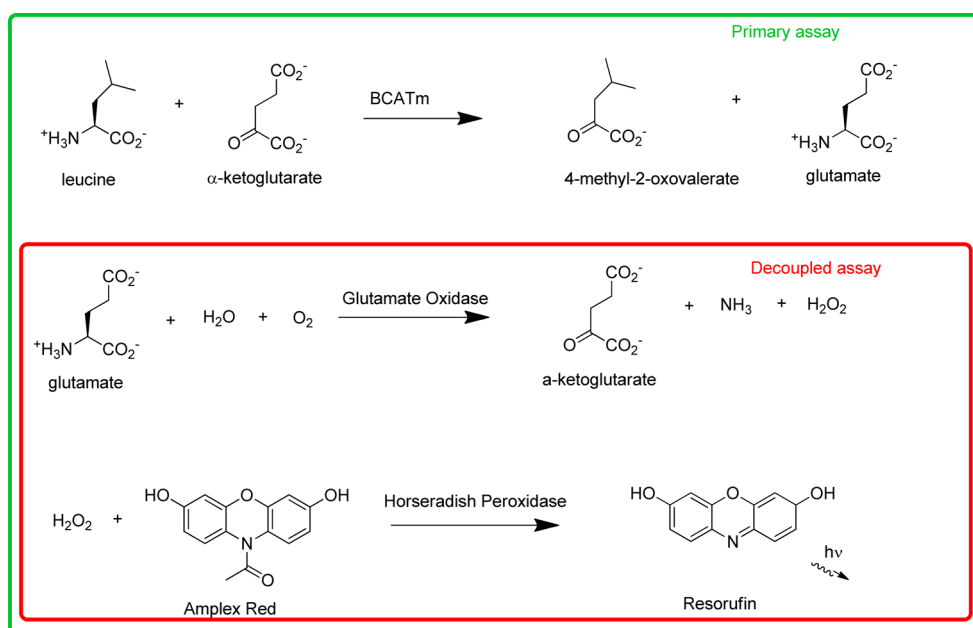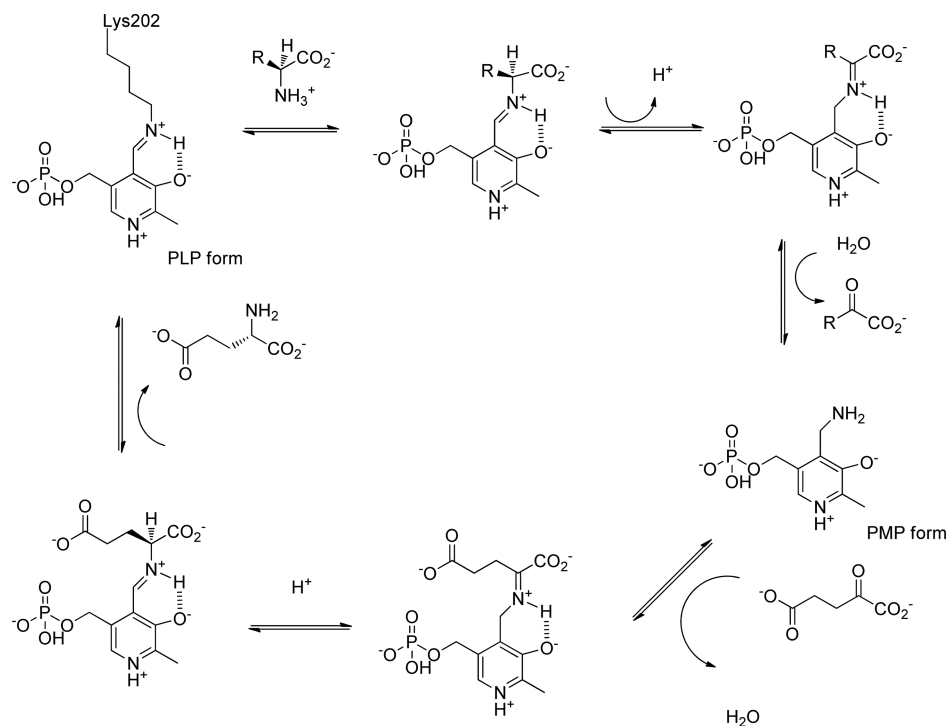
Figure 1. Biochemical assay format.

this fragment screen, perhaps compounded by the diversity of binding modes.

The fragment hits were clustered according to their distinct binding modes. Importantly, this study provides new structural understanding of this enzyme, with several binding pockets identified by the fragment screen, which were not occupied by either of the other series.[4,5] Additionally, further optimization efforts on two of the fragment hit series are described, which represent useful starting points and give important structural pointers to enable the identification of structurally novel tools for further pharmacological studies.

■ RESULTS AND DISCUSSION

Fragment Screening. FBDD techniques have become an integral part of the drug discovery process during the past decade.[7,9,10] Standard components of the FBDD methodology include the use of biophysical screening and X-ray crystallography to enable the identification, optimization, and designed growth of inherently weakly binding ligands into potent lead molecules.[11] Commonly, these methods have used a single form of the protein, for example, the apo or a cofactor bound state.

However, during enzyme turnover in solution, the dynamic changes in protein conformation and biochemical state present a number of potential binding opportunities. The use of a single form for screening in a binding assay may restrict the type of compounds that can be detected and characterized. In the extreme case, this arbitrary choice may preclude sampling the most tractable form of the enzyme. During the catalytic cycle (Scheme 1) PLP and PMP cofactor bound forms of BCATm are sampled. Pragmatically we therefore used both PLP and PMP forms in our studies where possible, as these can both be stably isolated.

At the start of the cycle, the cofactor pyridoxal phosphate (PLP) is covalently bound to the enzyme via a lysine residue (Lys-202) (Scheme 1).[12] This lysine is then displaced by the α-amine of an incoming BCAA substrate. The imine formed is hydrolyzed to the corresponding α-keto acid. In the course of the reaction, the cofactor is released from its covalent bond to the enzyme as pyridoxamine phosphate (PMP). A complementary half-reaction occurs to complete the cycle, whereby α-ketoglutarate is transaminated to glutamate and the PLP form of the enzyme is regenerated. It was possible to characterize both the PLP and PMP forms of the enzyme (e.g., spectroscopically or by mass spectrometry) and to interconvert between these using an excess of either leucine or α-keto glutarate as appropriate.

A functional biochemical assay was designed to detect inhibitors of this pathway, making use of a coupled sequence of enzymes (Figure 1), whereby the glutamate product of BCATm activity was reoxidized to α-keto glutarate along with hydrogen peroxide by the enzyme glutamate oxidase. The peroxide thus generated was detected by reaction with 1-(3,7-dihydroxy-10H-phenoxazin-10-yl)ethanone to form resorufin, catalyzed by the enzyme horseradish peroxidase. Decoupled parallel control wells without the BCATm initiated step were added to detect any inhibitors of the coupled processes. A potential risk of carrying out fragment screening using such a coupled enzyme system was that genuine inhibitors of BCATm could be discarded as nonspecific in nature due the higher chances of fragments interacting with more than one enzyme. Theoretical reasoning based on complexity,[13] on which much of FBDD methodology is predicated, suggests that there is a higher probability of smaller molecules binding to any given protein than for larger molecules. Therefore, it is more likely that fragments binding to BCATm may also bind to the coupled enzyme glutamate oxidase than would be the case if this assay was used for a traditional HTS campaign with larger, more complex molecules. However, using this functional biochemical assay had the advantage that all biochemical forms of the protein necessary for reaction could be sampled, permitting the detection of inhibitors that inhibited only one of these forms.

As is common in fragment screening campaigns, complementary biophysical screening was also carried out to detect compounds that bound to BCATm; in this case NMR and thermal shift techniques were used. The saturation transfer difference (STD) NMR assay[14] used a mixture of the PLP and PMP forms of the enzyme. Hits identified may interact with either, or potentially both, the PLP and PMP forms of the protein. However, as both forms are catalytically relevant, the precise binding profile was not initially determined as all hits had the potential to yield functional inhibitors. The STD-NMR approach was complemented by a thermal shift screen (T_m),[15] where both forms of the enzyme were independently assayed. This was necessary because of the very different denaturation

temperatures of the PLP(E) and PMP(F) bound proteins, 73 and 54 °C, respectively.

The GSK core fragment library of 1056 compounds was screened in parallel through all three assays, and hit rates are shown in Figure 2. The crystallography was carried out by
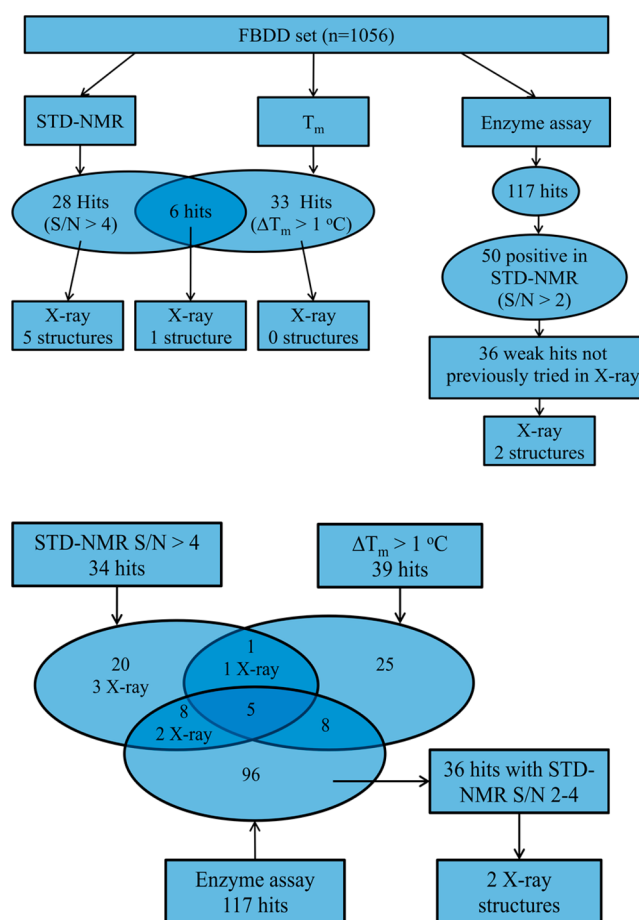
Figure 2. Flow and Venn diagrams illustrating the output of the fragment screening campaign, showing number of hits identified by each screening technique and the logic employed for X-ray prioritization, plus the distribution of those which yielded X-ray crystal structures.

soaking high concentration solutions (40−60 mM) of the ligand of interest into preformed crystals of both PMP and PLP forms of the protein for 1−14 days, sometimes yielding liganded crystals that gave data sets sufficient to unambiguously determine binding modes (resolutions in the range 1.8−2.4 Å). Although crystals of both the PLP and PMP forms of the BCATm were tried, the initial hits only yielded complexes with the more stable PLP protein. We therefore took the pragmatic decision to prioritize inhibitors for which crystal structures could be elucidated, thereby concentrating efforts on inhibitors of the PLP form of BCATm.

The output of the fragment screening is summarized in Figure 2. The different screening techniques produced different sets of hits, which is a common observation in FBDD campaigns,[8] as screening is carried out close to the limits of detection for the assays and different experimental conditions may favor a particular target conformation. All of the hits from either of the biophysical assays were progressed to X-ray crystallography. The STD-NMR experiment gave the better

Table 1. Summary of Fragment Hits Identified

Compound Number	Structure	pIC$_{50}$	clogP	Heavy Atoms	LE	LLE$_{AT}$	Source	Binding Mode
1		<2.9	0.78	13			STD-NMR	PLP lipophilic pocket, Hydrogen bond acceptor to Ala-314
2		<2.9	1.25	15			T$_m$ and STD-NMR	PLP lipophilic pocket, Hydrogen bond acceptor to Ala-314
3		<2.9	1.57	15			STD-NMR	PLP lipophilic pocket, Hydrogen bond acceptor to Ala-314
4		4.2^a	0.62	15	0.38	0.43	STD-NMR and biochemical	π- stacking to Phe-30, Hydrogen bond acceptor to Lys-79
5		3.0^b	1.31	15	0.27	0.26	STD-NMR and biochemical	π- stacking to Phe-30, PLP lipophilic pocket
6		<2.9	1.96	11			STD-NMR	Interface between protein dimers (no functional effect)
7		3.1	-0.2	13	0.33	0.45	STD-NMR and biochemical	PLP lipophilic pocket, Hydrogen bond acceptor to Ala-314, Displacement of water adjacent to Cys-315
8		3.9	1.6	14	0.38	0.33	STD-NMR and biochemical	π- stacking to Phe-30, PLP lipophilic pocket
9		6.6	3.8	18	0.48	0.30	HTS hit with similarity to fragment hits	Hydrogen bond acceptor to Ala-314
10		5.1	2.69	18	0.39	0.29	HTS hit with similarity to fragment hits	π- stacking to Phe-30
11		3.3^c	0.21	16	0.28	0.41	T$_m$, STD-NMR and biochemical	No crystal structure obtained
12		<3.2^d	0.14	15	0.40	0.50	Analogue of 11	PLP lipophilic pocket, Displacement of water adjacent to Cys-315
13		4.6	0.77	19	0.44	0.45	Analogue of 11	PLP lipophilic pocket, Displacement of water adjacent to Cys-315
14		3.8	1.9	14	0.37	0.29	T$_m$, STD-NMR and biochemical	No crystal structure obtained
15		3.8	2.08	15	0.35	0.26	Analogue of 14	PLP lipophilic pocket, Hydrogen bond acceptor to Ala-314

^{a}Compound reported inactive (pIC$_{50}$ < 4.2) on 3 out of 35 test occasions. ^{b}Compound reported inactive (pIC$_{50}$ < 2.9) on 1 out of 2 test occasions. ^{c}Compound reported inactive (pIC$_{50}$ < 2.9) on 1 out of 3 test occasions. ^{d}Compound reported inactive (pIC$_{50}$ < 3.2) on 2 out of 4 test occasions.

success rate in identifying apparent binders that led to liganded X-ray structures, with the orthogonal thermal shift experiment showing a relatively poor prediction of success. The biochemical assay had yielded a high number of specific hits, which could not all be progressed to crystallography, so the STD-NMR data were used to triage these hits, using a lower cutoff (2 × signal-to-noise versus 4 × signal-to-noise) than was used in the initial selection of NMR hits.

Additional activities were carried out in an effort to increase the number of liganded X-ray structures as potential starting points for chemical optimization. Five compounds identified were hits in both T_m and NMR assays but failed to produce crystal structures. Given reasonable confidence that these compounds were genuinely binding to BCATm, structural analogues were sourced from the GSK compound collection and screened in the STD-NMR and biochemical assays. Analogue searching was performed by focused substructure searching complemented by a GSK-developed workflow, FindAnalogues, specifically designed for fragment follow-up. FindAnalogues combines substructure and similarity searching methods with different descriptors and constraints on compound properties to identify suitable fragment-like analogues from both in-house and external vendors (see Experimental Section for details). 80 compounds were selected from this exercise and screened. 32 compounds were identified with activity in one of the two assays, from which three yielded liganded structures where the original fragment hit had not (12, 13, 15). An additional 120 similarly selected analogues were

subsequently screened and yielded valuable SAR for compounds 4 and 5 as described below.

Concurrent with this fragment screen, a high throughput screen of the GSK HTS compound collection (1.7 million compounds) had been conducted. The single-shot percentage inhibition data and subsequent XC$_{50}$ data were interrogated for compounds that were identified by the FindAnalogues search. Four analogues of 1 were identified with micromolar activity in the HTS and were submitted to crystallography, yielding additional liganded structures 9 and 10.

Fragment Hits. Table 1 summarizes the fragment hits identified that yielded liganded crystal structures, along with their calculated ligand efficiency (LE)[16] and modified lipophilic ligand efficiency (LLE$_{AT}$) as defined by researchers at Astex.[17] The crystal structures obtained for the hits showed occupation of a range of positions in the BCATm binding site and that significant movement in the protein was induced by the compounds. Some of the most important features for binding are summarized in the X-ray crystal structures shown in Figure 3.

Benzo[d]isoxazole 1 (Figure 3a) occupied a binding pocket defined by a lipophilic region adjacent to the PLP cofactor, which is confined by a closed "gate" between residues Phe-30 and Tyr-173. The carboxylic acid carbonyl group acted as a hydrogen bond acceptor to the backbone NH of Ala-314.

The crystal structure of thienopyrimidine 4 (Figure 3b) showed occupation of a distinct binding site. The site adjacent to the cofactor was occupied only by ethylene glycol (present in crystallography medium) and the Phe-30 Tyr-173 "gate" had
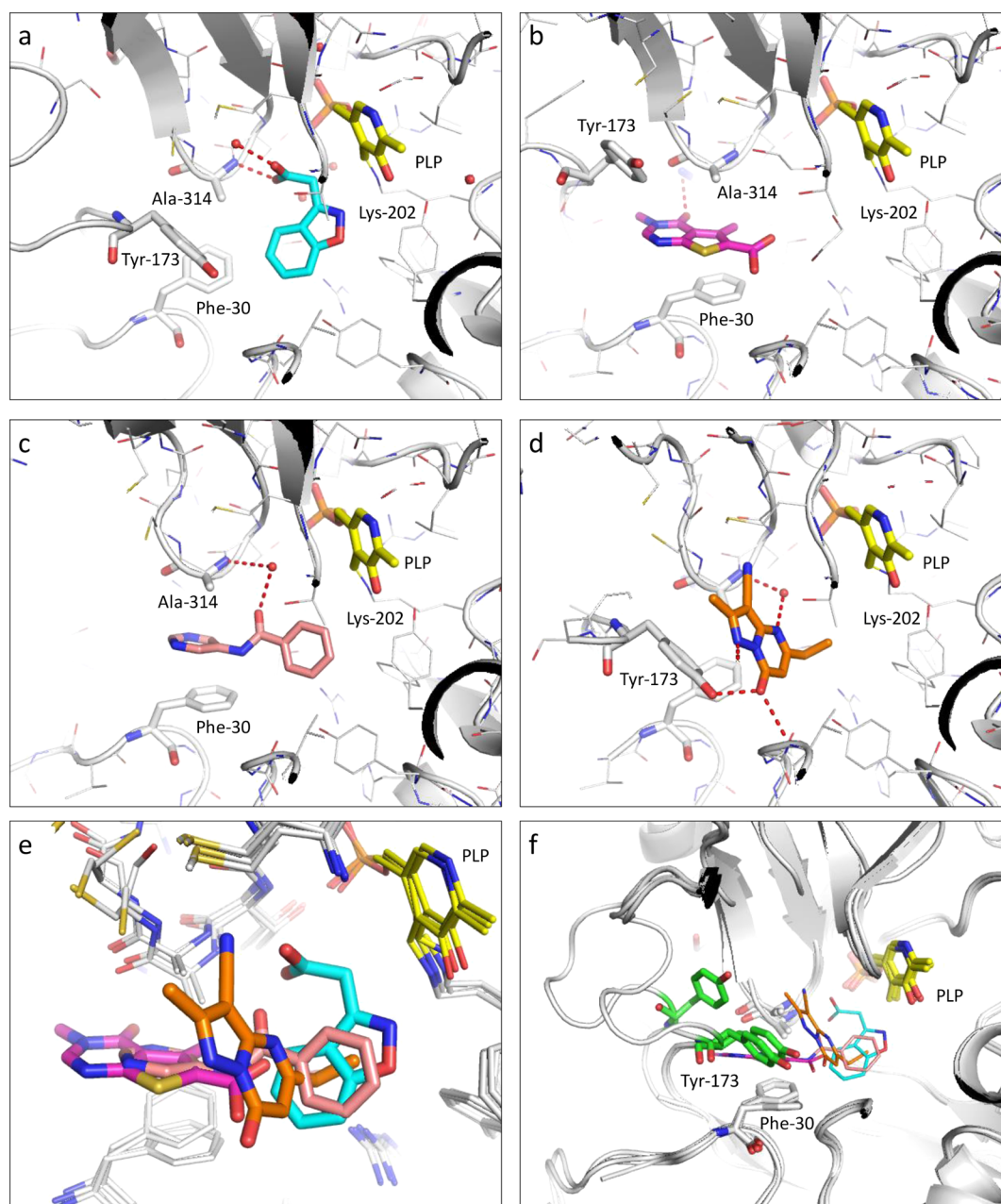
Figure 3. X-ray crystal structures of compounds **1** (cyan, PDB entry 5I5S), **4** (magenta PDB entry 5I5V), **5** (pink PDB entry 5I5W), and **12** (orange PDB entry 5BWT[4]) in the BCATm binding site in panels a, b, c and d, respectively. Panel e shows an overlay of all these compounds within the binding site. Panel f shows the same overlay but with Tyr-173 in green stick format, highlighting the mobility of the 170−180 loop region.

opened to allow the formation of a π-stacking interaction between Phe-30 and the heterocyclic core. The opening of the gate involved significant conformational rearrangement, with Phe-30 moving by around 2 Å, while Tyr-173 moved by approximately 6 Å. Additionally, the amide carbonyl acted as a hydrogen bond acceptor to a lysine NH (Lys-79).

The pyrimidine ring of the biarylamide **5** (Figure 3c) formed a similar π-stacking interaction with Phe-30 to thienopyrimidine **4**, while the phenyl ring occupied a similar lipophilic aromatic pocket to benzo[*d*]isoxazole **1**. The tyrosine residue, which moved to open the induced pocket in the structure of **4** (Tyr-173) was completely disordered in this structure. There are no direct hydrogen bonding interactions between the heteroatoms of the fragment and the protein, which may explain the poor ligand efficiency observed. However, the

amide carbonyl is well solvated and there is a water mediated hydrogen bond to the hydroxyl of Tyr-141. Biarylamide **5** was an effective bridge between the two binding sites identified and demonstrated that it is possible to have both sites occupied simultaneously.

Pyrazolopyrimidine **12** (Figure 3d, PDB entry 5BWT[4]) displayed an additional distinct binding mode. The pendent ethyl group was close to the lipophilic site occupied by aromatic groups for compounds **1** and **5**, and the "gate" was closed. The heterocyclic core was positioned in a site that was unoccupied in the other structures, with the nitrile substituent displacing a water molecule, which formed a hydrogen bonding interaction with the NH of Cys-315 in other structures. The pyridone carbonyl forms hydrogen bonds with Tyr-173 and the

backbone of Val-155. The pyridone NH and pyrazole N are both involved in water networks.

When all of these liganded crystal structures of the fragment hits were considered together (Figure 3e and Figure 3f), it was clear that the BCATm protein has considerable flexibility to accommodate a range of ligand binding modes. However, there were several binding "hot spots" identified, which appeared to act as anchors for the fragments. The most notable of these was the lipophilic pocket adjacent to the PLP, hydrogen bonding with Ala-314, π-stacking with Phe-30, and displacement of the water molecule adjacent to Cys-315. All of the hits identified satisfied at least one of these interactions (see Table 1). This flexibility in the protein would thus have caused difficulties in attempting to predict the binding modes of hits using docking methods alone. Therefore, to enable structure based fragment growth, it was important to generate multiple X-ray crystal structures (as is common practice), even for compounds that appeared to be closely structurally related. The diversity of structural information obtained provided opportunities to grow the fragment hits in various ways.[18]

Hits to Leads Optimization. The fragment hits identified were grouped ("clustered") according to their binding modes in the BCATm active site. An example of this process is shown for compounds **1**, **2**, and **3**, which look dissimilar on the basis of their chemical structures but which all make similar binding interactions with the protein (Figure 4). One exemplar was
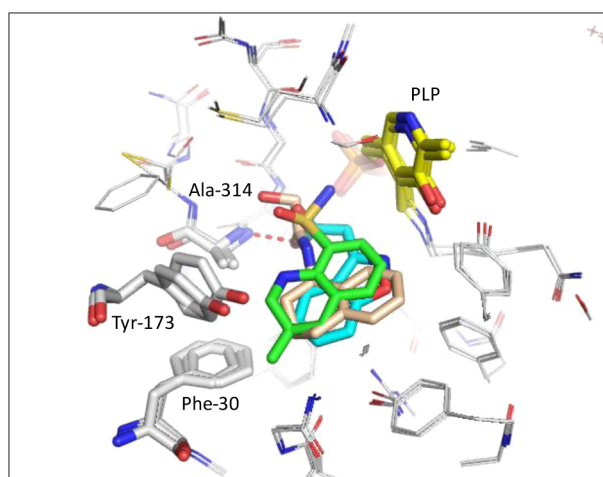

Figure 4. Example of vectorial clustering, showing an overlay of compounds **1** (cyan PDB entry 5I5S), **2** (green PDB entry 5I5T), and **3** (beige PDB entry 5I5U) with similar binding interactions.

chosen from each vectorial cluster, either because it demonstrated superior efficiency of binding or because it offered more flexible and tractable chemistry than other structures within the same cluster. The fragment growth and further optimization of the pyrazolopyrimidinone series represented by compounds **11−13** are described in the complementary paper;[4] a noteworthy feature of this series was that the original fragment hit (**11**) did not give a crystal structure, but analogue searching identified closely related compounds that did yield liganded crystal structures. Herein, the initial lead optimization efforts on two other series to illustrate the strategies employed are described.

Thienopyrimidine **4** had very favorable LE and LLE$_{AT}$ values and contained a tractable functional group (carboxylic acid), which could be used to grow toward the PLP pocket. The

crystal structure of biarylamide **5** provided further confidence in this approach because it showed that concomitant binding in both of these pockets could be achieved. With these aims in mind, initial optimization focused on a small array of amides, mostly containing lipophilic substituents, which were designed to fill the PLP pocket.

These compounds were synthesized using HATU-mediated coupling chemistry or via acylation using the appropriate acid chloride (Table 2). Due to monomer availability, some of the chemistry was carried out on the closely related des-methyl series, e.g., **16**, which showed similar activity to the initial hit **4**. Analogues **17** and **18** confirmed that activity with either of these two substituents was comparable. In general, aromatic amides were preferred to aliphatic substituents, as demonstrated by the comparisons between compounds **17** and **18** plus **19** and **20**. Substitution on the pendent phenyl ring was only tolerated in the ortho position (compounds **21**, **22**, **23**). Attempts to accommodate heteroaromatic rings in the lipophilic pocket were not productive (e.g., compounds **24** and **25**), with the exceptions of the lipophilic thiophene (**26**) and thiadiazole (**27**), both of which also maintained the highly favorable LE and LLE$_{AT}$ values of the hit.

The potency associated with compound **27** could not be rationalized by knowledge of the crystal structure of compound **4**. Soaking experiments failed to produce a crystal structure of compound **27**; however cocrystallization was successful, which yielded the first liganded structure of BCATm in the PMP form (Figure 5). The PMP form shows a few significant differences with respect to the PLP form. First, the Lys-202 side chain, now no longer covalently linked to cofactor, as in the PLP form, is free to shift slightly to optimally interact with one of the nitrogen atoms in the thiadiazole ring. Second, the PMP cofactor pyridine rotates by ∼11° from the PLP pyridine plane and Leu-266 adopts a lower energy rotamer conformation due to the additional space created by the rotation of the PMP pyridine ring. Due to its potent inhibition of BCATm, compound **27** was progressed to a cellular assay measuring BCATm inhibition and was found to have a cellular pIC$_{50}$ value of 5.4.
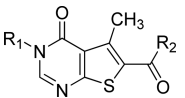
The next logical expansion was to grow toward Ala-314 to try to exploit a hydrogen-bonding opportunity, which had been identified from the fragment screening as a binding hot spot. A range of heteroatom-containing functional groups were introduced in the ortho-position of compound **18** (Table 3). From this effort, only the aryl acetate **29** showed any significant improvement in BCATm inhibition resulting in micromolar activity while maintaining good efficiencies. Crystallization of this compound in BCATm (Figure 5) confirmed that the acid carbonyl moiety was acting as a hydrogen bond acceptor to the backbone NH of Ala-314.
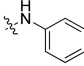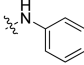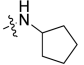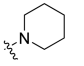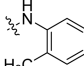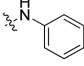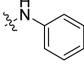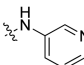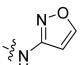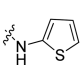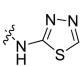
By using the structural information obtained from different fragment hits to identify binding hot spots, it was thus possible to grow weakly active fragment **4** into more potent analogues, with activity in a cellular assay.

Analysis of structures showed that biarylamide **5** offered potential vectors toward the Ala-314 NH donor and the Lys-79 NH$_2$ donor, to which the pyrimidinone carbonyl of **4** was hydrogen bonded. The biarylamide substructure is an abundant motif in the GSK compound collection, so the initial SAR was readily delineated (Table 4).

The pyrimidine ring was initially replaced with phenyl, as a greater number of analogues were available, and the crystal structure of **5** suggested that the pyrimidine nitrogens were not

Table 2. Activity and Efficiency Data for Amide Analogues of Compound 4

Compound Number	R1	R2	pIC$_{50}$	LE	LLE$_{AT}$
4	CH$_3$	OH	4.2[a]	0.38	0.44
16	H	OH	4.3	0.44	0.51
17	CH$_3$	–NH–phenyl	5.1	0.33	0.34
18	H	–NH–phenyl	5.1	0.36	0.37
19	CH$_3$	–NH–cyclopentyl	< 4.2		
20	CH$_3$	–piperidine	< 3.2		
21	H	–NH–(2-methylphenyl)	4.3[b]	0.28	0.30
22	H	–NH–(3-methylphenyl)	< 4.2		
23	H	–NH–(4-methylphenyl)	< 4.2		
24	H	–NH–pyridin-3-yl	3.6	0.25	0.33
25	H	–NH–isoxazol-3-yl	< 4.2		
26	H	–NH–thiophen-2-yl	5.8	0.48	0.45
27	H	–NH–(1,3,4-thiadiazol-2-yl)	6.7	0.48	0.63

[a] Compound reported inactive (pIC$_{50}$ < 4.2) on 3 out of 35 test occasions. [b] Compound reported inactive (pIC$_{50}$ < 4.2) on 2 out of 4 test occasions.

participating in any binding interactions. As with the optimization of **4**, it was found that adding hydrogen bond acceptors, which could interact with Ala-314, provided modest improvements in binding (**34** and **35**), with maintained ligand efficiency. A more dramatic improvement in enzyme inhibition was achieved when hydrogen bond acceptors, represented by carboxamide and pyrazole (**36** and **37**), enabled engagement with Lys-79. Carboxamide **36** also had additional lipophilic chlorine groups that enhanced binding in the PLP pocket, contributing to micromolar levels of activity, which represented a roughly 1000-fold increase in activity from the fragment hit. This compound also displayed a significant improvement in the efficiency measures relative to the hit compound **5**. Synthesis of compound **38**, which combined the acceptors targeting both Lys-79 and Ala-314, demonstrated that the effects on the activity could be additive, with good LE and LLE$_{AT}$ values achieved. The intent of this design was confirmed by the Xray structure of **38** within BCATm shown in Figure 6.

Once a good understanding of the SAR within this series had been established through screening of available analogues, attention was turned to improving the physicochemical profiles of the compounds. Biarylamides are notoriously insoluble, being highly planar and crystalline,[19] and indeed, the measured solubilities of these compounds were poor (Table 5, compounds **37** and **39**). Two strategies were adopted to improve the solubility within the series. The amide N–H was constrained in a tetrahydroisoquinoline ring to prevent intermolecular hydrogen bonding, which could contribute to the high crystallinity (**40** and **42**). Additionally, the pyrimidine ring from the initial hit was returned to the molecules in place of the phenyl ring to lower the lipophilicity (compound **41**). The targeted analogues were synthesized as shown in Scheme 2. Both of these strategies resulted in a modest improvement in enzyme inhibition and approximately 10-fold increased solubility. As in the optimization of thienopyrimidine **4**, the biarylamide series had been grown into a series of lead-like molecules through focused structure-based design combined with consideration of molecular properties.

CONCLUSIONS

When carrying out any diversity screening campaign but particularly when utilizing fragment-based approaches, it is important to realize that different biochemical and biophysical screening techniques can, and indeed do, identify different subsets of hits. Therefore, there could be an advantage to using multiple, complementary techniques for the initial screening phase. This is particularly important in FBDD, where the binding of hits will likely be near the limit of detection in some assays. This set of hits identified for BCATm, and the crystal structures generated have illustrated many aspects of the binding of small molecules to this enzyme for the first time. It was particularly interesting to observe such different conformations of the protein between different fragment hit, while gratifying to be able to identify several binding "hot spots" in the protein structure and confirm that these could be accessed simultaneously and from different structural types. The insights from multiple liganded crystal structures during both the screening and chemical optimization stages were invaluable in guiding progress, consistent with contemporary practice[11,20] in fragment based design. Another important aspect of this work
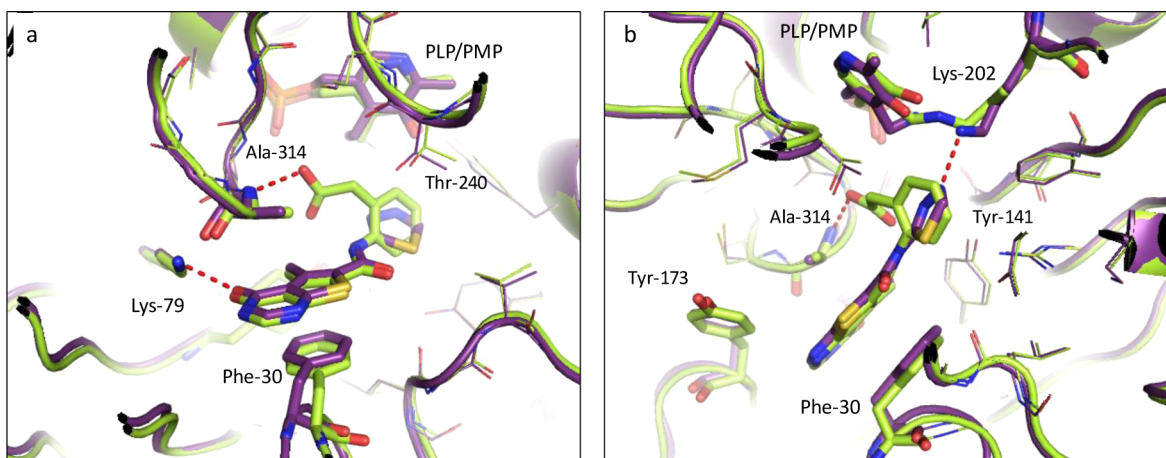
Figure 5. Overlay of compounds **27** (purple PDB entry 5I5X) and **29** (pale green PDB entry 5I5Y). Panel a shows the common interactions with Lys-79, Phe-30, and Ala-314. Panel b illustrates the difference in interactions around PLP/PMP for the two compounds.

Table 3. Results of Targeting Ala-314 through Growth from the Ortho-Position of 18

Compound Number	R	pIC$_{50}$	LE	LLE$_{AT}$
18	H	5.1	0.36	0.37
28	(ethyl ester)	< 4.2		
29	(carboxylic acid)	6.0	0.34	0.45
30	(OH)	5.0	0.31	0.44
31	(sulfonamide)	4.9	0.28	0.41
32	(methylsulfonyl)	< 4.2		

Table 4. Screening Results from Analogues of 5 Available in the GSK Collection

Compound	Structure	pIC$_{50}$	LE	LLE$_{AT}$	clogP
5		3.0	0.27	0.26	1.31
33		< 3.2			2.65
34		3.7	0.27	0.26	1.66
35		3.5[a]	0.25	0.25	1.58
36		5.6	0.39	0.31	2.86
37		5.3	0.36	0.26	3.00
38		5.7	0.33	0.32	1.94

was the use of analogue searching from an extensive collection. This was important both in the hit finding phase, where it was used to generate additional hits, and in fragment optimization and growth, where significant improvements in hit activities were obtained without recourse to synthesis. The chemical libraries are a major asset for large pharmaceutical companies,

[a]Compound reported inactive (pIC$_{50}$ < 4.2) on 2 out of 4 test occasions.

which allow scientists to rapidly explore SAR around fragment hits. The "SAR by catalogue" allowed expansion beyond the
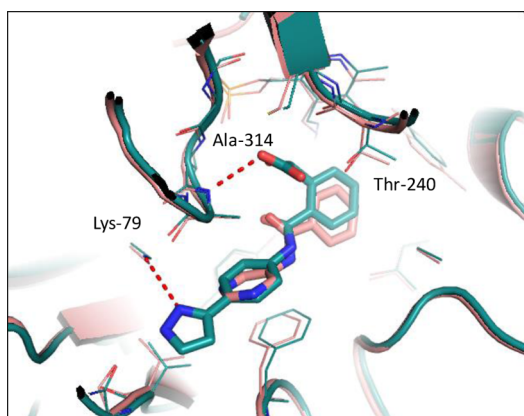
Figure 6. Overlay of compounds **38** (blue PDB entry 5I60) and **5** (pink PDB entry 5I5W) confirms **38** makes additional interactions with Lys-79 and Ala-314.

deliberately designed screening sets while continuing to exercise discipline with the molecular properties of compounds screened. Finally, micromolar inhibitors of BCATm have been identified, with characterized novel binding modes and measurable activities in a cellular assay. This represents a

major step forward toward the goal of establishing if pharmaceutical inhibition of BCATm using small molecules could provide a useful treatment for metabolic diseases; a previous paper[4] describes further progress achieved in one series.

■ EXPERIMENTAL SECTION

Chemistry. All solvents and reagents, unless otherwise stated, were commercially available from regular suppliers such as Sigma-Aldrich and Fluorochem and were used as purchased without further purification. Nuclear magnetic resonance (^{1}H NMR and ^{13}C NMR) spectra were recorded on a Bruker AVI (400 MHz), Bruker Nano (500 MHz), or Bruker AVII+ (600 MHz) spectrometer (with cryoprobe) in the indicated solvent. Chemical shifts δ are reported in parts per million (ppm) relative to tetramethylsilane and are internally referenced to the residual solvent peak. Coupling constants (J) are given in hertz (Hz) to the nearest 0.5 Hz. Liquid chromatography mass−spectroscopy (LCMS) analysis was conducted on either system A, a Waters Acquity UPLC BEH C$_{18}$ column (50 mm × 2.1 mm i.d., 1.7 μm packing diameter) at 40 °C eluting with 0.1% v/v solution of formic acid in water (solvent A) and 0.1% v/v solution of formic acid in acetonitrile (solvent B), using the following elution gradient 0.0−1.5 min 3−100% B, 1.5−1.9 min 100% B, 1.9−2.0 min 3% B, at a flow rate of 1 mL/min; or system B, a Waters Acquity UPLC BEH C$_{18}$ column (50 mm × 2.1 mm i.d., 1.7 μm packing diameter) at 40 °C eluting with 10 mM ammonium bicarbonate in

Table 5. Data from the Biarylamides Series, Illustrating Structural Modifications Designed To Improve Solubility

Compound	Structure	pIC$_{50}$	LE	LLE$_{AT}$	clogP	Sol(μg/ml)
39		4.3[a]	0.33	0.33	1.46	13
40		4.8	0.33	0.36	1.14	132
37		5.2	0.36	0.26	3.00	12
41		5.5	0.38	0.35	1.94	82
42		5.8	0.36	0.29	2.83	94

[a]Compound reported inactive (pIC$_{50}$ < 4.2) on 1 out of 4 test occasions.

Scheme 2. Synthesis of Analogues of Compound 5[a]

39 R$_1$ = CONH$_2$, X = CH, R$_2$ = H
43 R$_1$ = Br, X = CH, R$_2$ = H
44 R$_1$ = Br, X = CH, R$_2$ = CH$_2$CO$_2$CH$_3$
45 R$_1$ = Cl, X = N, R$_2$ = H

37 X = CH, R$_2$ = H
38 X = CH, R$_2$ = CH$_2$CO$_2$H
41 X = N, R$_2$ = H

46 R$_3$ = CN
47 R$_3$ = Br

40

42
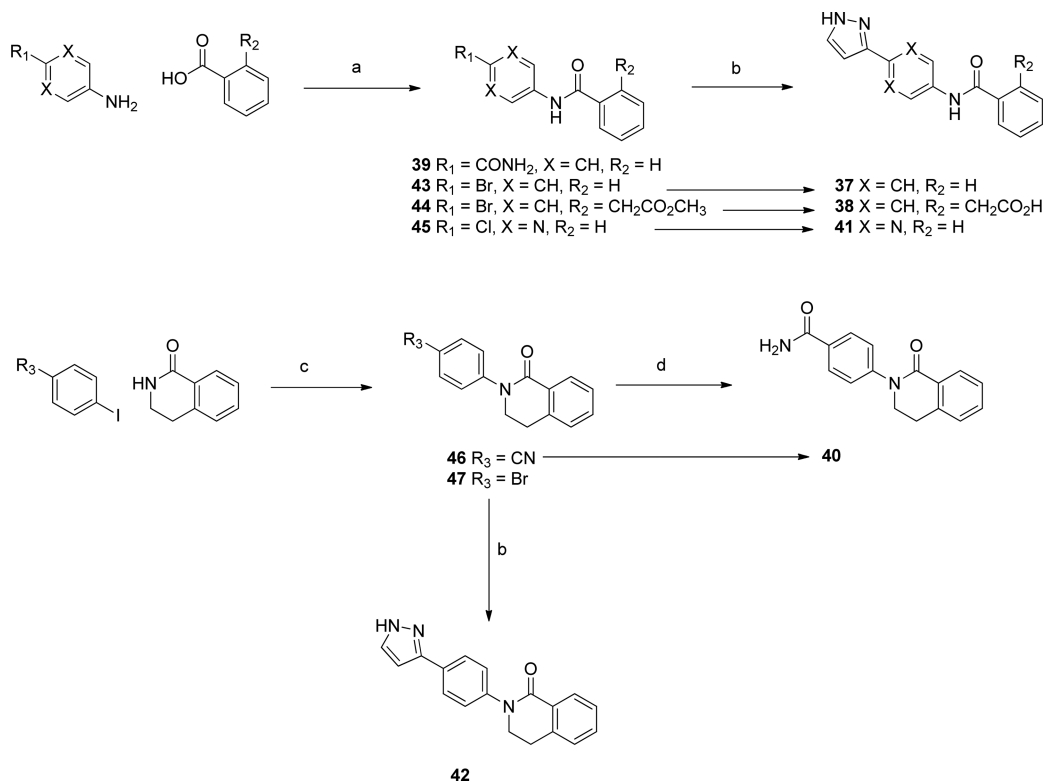
[a]Reagents and conditions: (a) HATU, DIPEA, DMF, 20−40 °C, 41−79%; (b) 1H-pyrazol-3-ylboronic acid, Pd(PPh$_3$)$_4$, Na$_2$CO$_3$ (sat. aq), 130 °C, microwave 20 min, 41−72%; (c) CuI, K$_2$CO$_3$, DMF, 160 °C, 18 h, 57−66%; (d) 2 M NaOH (aq), 30% H$_2$O$_2$ (aq), EtOH, 50 °C, 20 h, 19%.

water adjusted to pH 10 with ammonia solution (solvent A) and acetonitrile (solvent B), using the following elution gradient 0.0−1.5 min 1−97% B, 1.5−1.9 min 97% B, 1.9−2.0 min 100% B, at a flow rate of 1 mL/min. The UV detection was based on an average signal from wavelength of 210−350 nm. The mass spectra were recorded on a Waters ZQ mass spectrometer using alternate-scan positive and negative mode electrospray ionization. Preparative HPLC using a mass directed autopurification (MDAP) was conducted on a Waters FractionLynx system comprising a Waters 515 pump with extended pump heads, Waters 2767 autosampler, Waters 996 photodiode array detector, and Gilson 202 fraction collector on an XBridge or Sunfire C18 column (30 mm × 150 mm i.d., 5 μm packing diameter) at ambient temperature. The mobile phase was 0.1% v/v solution formic acid in water or 10 mM ammonium bicarbonate in water adjusted to pH 10 with ammonia solution (solvent A) and 0.1% v/v solution formic acid in acetonitrile or acetonitrile (solvent B). The UV detection is a summed signal from wavelength of 210 to 350 nm. The mass spectra were recorded on Waters ZQ mass spectrometer using alternate-scan positive and negative electrospray ionization. The software used was MassLynx 3.5 with OpenLynx and FractionLynx options. High resolution mass spectra (HRMS) were obtained on a Micromass Q-Tof Ultima hybrid quadrupole time-of-flight mass spectrometer, equipped with a Z-spray interface (ESI), over a mass range of 100−1100 Da, with a scan time of 0.9 s and an interscan delay of 0.1 s. Reserpine was used as the external mass calibrant ([M + H]$^+$ = 609.2812 Da). The Q-Tof Ultima mass spectrometer was operated in W reflectron mode to give a resolution (fwhm) of 16 000−20 000. Ionization was achieved with a spray voltage of 3.2 kV, a cone voltage of 50 V, with cone and desolvation gas flows of 10−20 and 600 L/h, respectively. The source block and desolvation temperatures were maintained at 120 and 250 °C, respectively. The elemental composition was calculated using MassLynx, version 4.1, for the [M + H]$^+$ and the mass error quoted as ppm. Flash column chromatography was conducted on a Combiflash Rf automated flash chromatography system (Teledyne Isco) using disposable normal or

reverse phase Redisep cartridges (4−330 g). The CombiFlash Rf used RFID (radiofrequency identification detector) technology to automate setting the parameters for purification runs and fraction collection. The system was equipped with a UV variable dual-wavelength and a Foxy fraction collector enabling automated peak cutting, collection, and tracking. The purity of all compounds screened in the biological assays was examined by LCMS analysis and was found to be ≥95% unless otherwise specified. The human biological samples were sourced ethically, and their research use was in accord with the terms of the informed consents.

Compounds **2**, **3**, and **14** were purchased from Enamine. Compound **12** was purchased from Vitas. Compound **18** was purchased from ChemDiv. Compounds **1**, **4**, **5**, **6**, **7**, **8**, **10**, **13**, **15**, **33**, and **34** were obtained from the GSK compound collection but are also available from commercial suppliers. Compound **35** was obtained from the GSK compound collection and may be synthesized according to the procedure described by Azizian and co-workers.[21]

2-Ethoxy-5-methyl-7-oxo-4,7-dihydropyrazolo[1,5-a]-pyrimidine-3-carbonitrile (11). 11 was obtained from the GSK compound collection. ^{1}H NMR (500 MHz, DMSO-d_6) δ ppm 5.78 (s, 1 H), 4.36 (q, J = 7.0 Hz, 2 H), 2.47−2.52 (m, 1 H), 2.27 (s, 3 H). 1.36 (t, J = 7.0 Hz, 3 H); LCMS (ESI, formic) m/z 219.01 [M + H]$^+$, t_R = 0.63 min.

5-Methyl-4-oxo-3,4-dihydrothieno[2,3-d]pyrimidine-6-carboxylic Acid (16). Lithium hydroxide, monohydrate (2.3 g, 55 mmol) was added to a solution of ethyl 5-methyl-4-oxo-3,4-dihydrothieno[2,3-d]pyrimidine-6-carboxylate (4.0 g, 17 mmol) in a mixture of THF (50 mL), MeOH (25 mL), and water (8 mL). The reaction mixture was stirred at room temperature for 16 h. Lithium hydroxide, monohydrate (1.0 g, 24 mmol) was added, and the reaction mixture was stirred for another 6 h. The reaction mixture was then heated at 40 °C for 24 h. Solvent was evaporated under reduced pressure. The resulting crude product was dissolved in water, and the mixture was acidified to pH 1 with 2 M aqueous HCl solution. The resulting precipitate was collected by filtration and dried in a vacuum

oven overnight to give the title product as a pale pink solid (3.5 g, 99%). ^{1}H NMR (400 MHz, DMSO-d_6) δ 13.31 (br s, 1H), 12.56 (br s, 1H), 8.17 (s, 1H), 2.80 (s, 3H); LCMS (ESI, formic) m/z 211.02 [M + H]$^+$, t_R = 0.45 min; HRMS (ESI) calcd for C$_8$H$_6$N$_2$O$_3$S + H$^+$ 211.0177, found 211.0172 (2.95 min).

General Procedure A for Amide Coupling. The appropriate amine (1.2 equiv), HATU (1.2 equiv), and DIPEA (2 equiv) were added to a solution of 3,5-dimethyl-4-oxo-3,4-dihydrothieno[2,3-d]pyrimidine-6-carboxylic acid (**4**) (1 equiv) in DMF (4−10 mL). The mixture was stirred at room temperature until reaction was complete by LCMS. Water (50 mL) and EtOAc (50 mL) were added. The aqueous phase was extracted with EtOAc (2 × 50 mL). The organic layers were combined, passed through a hydrophobic frit, and concentrated to dryness under reduced pressure. The resulting crude product was purified by reverse phase chromatography to give the desired final product.

General Procedure B for Amide Coupling. HATU (1.2 equiv) and DIPEA (2 equiv) were added to a solution of 5-methyl-4-oxo-3,4-dihydrothieno[2,3-d]pyrimidine-6-carboxylic acid (**16**) (1 equiv) in DMF (1.5−2.5 mL). The mixture was stirred at room temperature between 1 and 10 min. The appropriate amine (1.2 equiv) was then added, and the reaction mixture was stirred at room temperature until reaction was complete by LCMS. Solvent was then evaporated under reduced pressure. The resulting crude product was purified by reverse phase chromatography to give the desired final product.

3,5-Dimethyl-4-oxo-N-phenyl-3,4-dihydrothieno[2,3-d]-pyrimidine-6-carboxamide (17). **17** was prepared according to general procedure A using aniline (50 μL, 0.54 mmol). The resulting crude product was purified by reverse phase chromatography using the formic acid MDAP to give the title product as white solid (90 mg, 64%). ^{1}H NMR (400 MHz, DMSO-d_6) δ 10.25 (s, 1H), 8.50 (s, 1H), 7.68 (br d, J = 7.5 Hz, 2H), 7.36 (br t, J = 8.0 Hz, 2H), 7.07−7.16 (br t, J = 7.5 Hz, 1H), 3.49 (s, 3H), 2.74 (s, 3H); LCMS (ESI, high pH) m/z 300.04 [M + H]$^+$, t_R = 0.83 min.

5-Methyl-4-oxo-N-phenyl-3,4-dihydrothieno[2,3-d]-pyrimidine-6-carboxamide (18). **18** was prepared according to general procedure B using aniline (50 μL, 0.54 mmol). The crude product was purified by reverse phase chromatography (C18 column, 10−40% CH$_3$CN (B)/10 mM aqueous ammonium bicarbonate solution (A)) to give the title product as a pale yellow solid (87 mg, 64%). ^{1}H NMR (400 MHz, DMSO-d_6) δ 12.57 (br s, 1H), 10.20 (s, 1H), 8.18 (s, 1H), 7.68 (d, J = 7.5 Hz, 2H), 7.36 (t, J = 8.0 Hz, 2H), 7.03−7.18 (m, 1H), 2.73 (s, 3H); ^{13}C NMR (101 MHz, DMSO-d_6) δ 164.2 (C), 160.6 (C=O), 158.3 (C=O), 147.4 (Ar−CH), 138.5 (C), 136.4 (C), 128.7 (2C, Ar−CH), 127.9 (C), 124.0 (Ar−CH), 123.4 (C), 120.3 (2C, Ar−CH), 15.1 (CH$_3$); LCMS (ESI, high pH) m/z 286.01 [M + H]$^+$, t_R = 0.72 min; HRMS (ESI) calcd for C$_{14}$H$_{11}$N$_3$O$_2$S + H$^+$ 286.0650, found 286.0646 (4.08 min); IR (ATR) cm^{-1} 3294, 3062, 3020, 2929, 2866, 1656, 1634, 1595, 1580, 1529.

N-Cyclopentyl-3,5-dimethyl-4-oxo-3,4-dihydrothieno[2,3-d]-pyrimidine-6-carboxamide (19). **19** was prepared according to general procedure A using cyclopentanamine (0.026 mL, 0.268 mmol). Purification twice by reverse phase chromatography gave the title product as a white solid (20 mg, 28%). ^{1}H NMR (400 MHz, CDCl$_3$) δ 8.03 (s, 1H), 5.82 (d, J = 6.5 Hz, 1H), 4.39 (apparent sxt, J = 7.0 Hz, 1H), 3.58 (s, 3H), 2.86 (s, 3H), 2.05−2.17 (m, 2H), 1.62−1.81 (m, 4H), 1.45−1.57 (m, 2H); LCMS (ESI, formic) m/z 292.09 [M + H]$^+$, t_R = 0.78 min.

3,5-Dimethyl-6-(piperidine-1-carbonyl)thieno[2,3-d]-pyrimidin-4(3H)-one (20). **20** was prepared according to general procedure A using piperidine (0.04 mL, 0.43 mmol). Purification by reverse phase chromatography using the formic acid MDAP gave the title product as a white solid (70 mg, 64%). ^{1}H NMR (400 MHz, DMSO-d_6) δ 8.43 (s, 1H), 3.47 (br s, 7H), 2.43 (s, 3H), 1.56−1.67 (m, 2H), 1.55−1.44 (m, 4H); LCMS (ESI, formic) m/z 292.17 [M + H]$^+$, t_R = 0.74 min.

5-Methyl-4-oxo-N-(o-tolyl)-3,4-dihydrothieno[2,3-d]-pyrimidine-6-carboxamide (21). **21** was prepared according to general procedure B using o-toluidine (0.4 mL, 0.3 mmol). Purification by reverse phase chromatography using the formic acid MDAP gave

the title product as yellow solid (32 mg, 37%). ^{1}H NMR (400 MHz, DMSO-d_6) δ 12.55 (br s, 1H), 9.69 (s, 1H), 8.17 (s, 1H), 7.39 (br d, J = 7.5 Hz, 1H), 7.28 (br d, J = 7.0 Hz, 1H), 7.15−7.25 (m, 2H), 2.79 (s, 3H), 2.26 (s, 3H); LCMS (ESI, formic) m/z 300.04 [M + H]$^+$, t_R = 0.78 min, purity =94%.

5-Methyl-4-oxo-N-(m-tolyl)-3,4-dihydrothieno[2,3-d]-pyrimidine-6-carboxamide (22). **22** was prepared according to general procedure B using m-toluidine (60 μL, 0.57 mmol). Purification by reverse phase chromatography using the formic acid MDAP gave the title product as a white solid (39 mg, 46%). ^{1}H NMR (400 MHz, DMSO-d_6) δ 12.55 (br s, 1H), 10.12 (s, 1H), 8.17 (s, 1H), 7.51 (s, 1H), 7.47 (d, J = 8.5 Hz, 1H), 7.23 (t, J = 8.0 Hz, 1H), 6.94 (d, J = 7.5 Hz, 1H), 2.73 (s, 3H), 2.31 (s, 3H); ^{13}C NMR (101 MHz, DMSO-d_6) δ 164.2 (C), 160.5 (C=O), 158.3 (C=O), 147.3 (CH), 138.4 (C), 137.9 (C), 136.3 (C), 128.5 (C), 128.0 (CH), 124.7 (CH), 123.4 (C), 120.8 (CH), 117.5 (CH), 21.1 (CH$_3$), 15.0 (CH$_3$); LCMS (ESI, formic) m/z 300.11 [M + H]$^+$, t_R = 0.85 min; HRMS (ESI) calcd for C$_{15}$H$_{13}$N$_3$O$_2$S + H$^+$ 300.0801, found 300.0798 (4.21 min).

5-Methyl-4-oxo-N-(p-tolyl)-3,4-dihydrothieno[2,3-d]-pyrimidine-6-carboxamide (23). **23** was prepared according to general procedure B using p-toluidine (80 mg, 0.75 mmol). Purification by reverse phase chromatography using the formic acid MDAP gave the title product as a white solid (39 mg, 45%). ^{1}H NMR (400 MHz, DMSO-d_6) δ 12.54 (br s, 1H), 10.10 (s, 1H), 8.17 (s, 1H), 7.56 (d, J = 8.5 Hz, 2H), 7.16 (d, J = 8.5 Hz, 2H), 2.72 (s, 3H), 2.28 (s, 3H); ^{13}C NMR (101 MHz, DMSO-d_6) δ 164.1 (C), 160.4 (C=O), 158.3 (C=O), 147.3 (Ar−CH), 136.2 (C), 136.0 (C), 133.1 (C), 129.0 (2C, Ar−CH), 128.0 (C), 123.4 (C), 120.3 (2C, Ar−CH), 20.5 (CH$_3$), 15.0 (CH$_3$); LCMS (ESI, formic) m/z 300.11 [M + H]$^+$, t_R = 0.85 min; HRMS (ESI) calcd for C$_{15}$H$_{13}$N$_3$O$_2$S + H$^+$ 300.0801, found 300.0803 (4.19 min).

5-Methyl-4-oxo-N-(pyridin-3-yl)-3,4-dihydrothieno[2,3-d]-pyrimidine-6-carboxamide (24). **24** was prepared according to general procedure B using pyridin-3-amine (57 mg, 0.61 mmol). Purification was by reverse phase chromatography (5−20% acetonitrile (B)/10 mM aqueous ammonium bicarbonate solution (A)). The product was dissolved in MeOH and transferred in a vial for test to give the title product as MeOH solvate, yellow solid (70 mg, 46%). ^{1}H NMR (400 MHz, DMSO-d_6) δ 12.59 (br s, 1H), 10.39 (s, 1H), 8.84 (d, J = 2.5 Hz, 1H), 8.33 (dd, J = 5.0, 1.5 Hz, 1H), 8.19 (s, 1H), 8.07−8.14 (m, 1H), 7.40 (dd, J = 8.5, 5.0 Hz, 1H), 4.06 (d, J = 5.0 Hz, 1H, CH$_3$OH), 3.17 (d, J = 5.0 Hz, 3H, CH$_3$OH), 2.76 (s, 3H); LCMS (ESI, high pH) m/z 286.99 [M + H]$^+$, t_R = 0.52 min.

N-(Isoxazol-3-yl)-5-methyl-4-oxo-3,4-dihydrothieno[2,3-d]-pyrimidine-6-carboxamide (25). A solution of 5-methyl-4-oxo-3,4-dihydrothieno[2,3-d]pyrimidine-6-carboxylic acid **16** (100 mg, 0.48 mmol) in thionyl chloride (2 mL, 27 mmol) was heated at 80 °C for 3 days before the reaction mixture was concentrated to dryness under reduced pressure. A solution of isoxazol-3-amine (160 mg, 1.9 mmol) and DIPEA (0.2 mL, 1.2 mmol) in DMF (1.5 mL) dried over molecular sieves (4 Å) was added to the crude, and the reaction mixture was stirred at room temperature with molecular sieves for 24 h. The crude reaction mixture was purified by reverse phase chromatography using formic acid MDAP to give the title product as white solid (18 mg, 14%). ^{1}H NMR (400 MHz, DMSO-d_6) δ 11.98 (br s, 2H), 8.85 (d, J = 1.5 Hz, 1H), 8.19 (s, 1H), 6.97 (d, J = 2.0 Hz, 1H), 2.75 (s, 3H); LCMS (ESI, formic) m/z 277.06 [M + H]$^+$, t_R = 0.57 min.

5-Methyl-4-oxo-N-(thiophen-2-yl)-3,4-dihydrothieno[2,3-d]-pyrimidine-6-carboxamide (26). **26** was prepared according to general procedure B using thiophen-2-amine (64 mg, 0.65 mmol) at 40 °C. Purification by reverse phase chromatography using the formic acid MDAP gave the title product as a brown solid (21 mg, 15%). ^{1}H NMR (400 MHz, DMSO-d_6) δ 12.59 (br s, 1H), 11.42 (s, 1H), 8.19 (d, J = 4.0 Hz, 1H), 7.05 (t, J = 4.0 Hz, 1H), 6.90−6.93 (m, 2H), 2.76 (s, 3H); ^{13}C NMR (101 MHz, DMSO-d_6) δ 164.4 (C), 158.5 (C=O), 158.2 (C=O), 147.6 (Ar−CH), 139.2 (C), 138.0 (C), 125.4 (C), 124.1 (C), 123.5 (Ar−CH), 117.9 (Ar−CH), 112.8 (Ar−CH), 15.1 (CH$_3$); LCMS (ESI, formic) m/z 292.03 [M + H]$^+$, t_R = 0.74 min;

HRMS (ESI) calcd for C$_{12}$H$_9$N$_3$O$_3$S$_2$ + H$^+$ 292.0214, found 292.0214 (4.01 min).

5-Methyl-4-oxo-*N*-(1,3,4-thiadiazol-2-yl)-3,4-dihydrothieno-[2,3-*d*]pyrimidine-6-carboxamide (27). 27 was prepared according to general procedure B using 2-amino-1,3,4-thiadiazole (62 mg, 0.613 mmol) at 40 °C. DMSO (2 mL) was added to the reaction mixture and the whole solubilized with heating. After cooling a solid precipitated out which was collected by filtration and dried in a vacuum oven overnight to give the title product as yellow solid (70 mg, 50%). ^{1}H NMR (400 MHz, DMSO-d_6) δ 14.10 (br s, 1H), 12.54 (br s, 1H), 9.04 (br s, 1H), 8.18 (d, *J* = 3.5 Hz, 1H), 2.89 (s, 3H); ^{13}C NMR (126 MHz, DMSO-d_6) δ 167.6 (C), 166.7 (C=O), 158.5 (C= O), 146.2 (Ar−CH), 144.9 (Ar−CH), 135.6 (C), 134.2 (C), 124.2 (C), 109.5 (C), 14.8 (CH$_3$); LCMS (ESI, formic) *m/z* 294.03 [M + H]$^+$, t_R = 0.38 min; HRMS (ESI) calcd for C$_{10}$H$_7$N$_5$O$_2$S$_2$ + H$^+$ 294.0119, found 294.0115 (3.22 min); IR (ATR) cm^{-1} 3142, 3095, 3007, 2930, 1676, 1651, 1552.

Ethyl 2-(2-(5-Methyl-4-oxo-3,4-dihydrothieno[2,3-*d*]-pyrimidine-6-carboxamido)phenyl)acetate (28). 28 was prepared according to general procedure B using ethyl 2-(2-aminophenyl)acetate 48 (66 mg, 0.4 mmol). The crude product was purified by reverse phase chromatography using formic acid MDAP to give the title product as a yellow solid (46 mg, 40%). ^{1}H NMR (400 MHz, DMSO-d_6) δ 12.56 (br s, 1H), 9.75 (s, 1H), 8.17 (d, *J* = 4.0 Hz, 1H), 7.42 (br d, *J* = 8.0 Hz, 1H), 7.29−7.36 (m, 2H), 7.19−7.28 (m, 1H), 4.04 (q, *J* = 7.0 Hz, 2H), 3.73 (s, 2H), 2.76 (s, 3H), 1.13 (t, *J* = 7.0 Hz, 3H); LCMS (ESI, formic) *m/z* 372.07 [M + H]$^+$, t_R = 0.83 min.

2-(2-(5-Methyl-4-oxo-3,4-dihydrothieno[2,3-*d*]pyrimidine-6-carboxamido)phenyl)acetic Acid (29). A solution of ethyl 2-(2-(5-methyl-4-oxo-3,4-dihydrothieno[2,3-*d*]pyrimidine-6-carboxamido)-phenyl)acetate 28 (30 mg, 0.1 mmol) and lithium hydroxide (5.8 mg, 0.2 mmol) in a mixture of THF (0.4 mL), MeOH (0.2 mL), and water (0.1 mL) was stirred at room temperature for 2 h. Solvents were removed under a stream of nitrogen. The resulting crude product was dissolved in water (0.5 mL), and 2 M aqueous HCl solution was added. The resulting precipitate was collected by filtration and dried in a vacuum oven overnight to give the title product as a brown solid (16 mg, 58%). ^{1}H NMR (400 MHz, DMSO-d_6) δ 12.55 (br s, 1H), 12.41 (br s, 1H), 9.74 (s, 1H), 8.17 (d, *J* = 3.5 Hz, 1H), 7.46 (br d, *J* = 7.5 Hz, 1H), 7.28−7.36 (m, 2H), 7.18−7.25 (m, 1H), 3.66 (s, 2H), 2.77 (s, 3H); LCMS (ESI, formic) *m/z* 344.09 [M + H]$^+$, t_R = 0.64 min.

N-(2-(Hydroxymethyl)phenyl)-5-methyl-4-oxo-3,4-dihydrothieno[2,3-*d*]pyrimidine-6-carboxamide (30). TBAF (1 M in THF, 0.39 mL, 0.39 mmol) was added to a solution of *N*-(2-(((*tert*-butyldimethylsilyl)oxy)methyl)phenyl)-5-methyl-4-oxo-3,4-dihydrothieno[2,3-d]pyrimidine-6-carboxamide 50 (83 mg, 0.2 mmol) in THF (1 mL). The reaction mixture was stirred at room temperature for 3 h. Saturated aqueous NaHCO$_3$ solution (10 mL) and EtOAc (10 mL) were added. The organic layer was separated and the aqueous was extracted with EtOAc (2 × 10 mL). The combined organic layers were passed through a hydrophobic frit and concentrated under reduced pressure. The crude product was purified by reverse phase chromatography using the formic acid MDAP to give the title product as a white solid (36 mg, 59%). ^{1}H NMR (400 MHz, DMSO-d_6) δ 12.57 (br s, 1H), 9.87 (br s, 1H), 8.18 (s, 1H), 7.79 (br d, *J* = 8.0 Hz, 1H), 7.40 (br d, *J* = 7.5 Hz, 1H), 7.30 (br t, *J* = 8.0 Hz, 1H), 7.19 (br t, *J* = 7.5 Hz, 1H), 5.63 (br s, 1H), 4.61 (s, 2H), 2.83 (s, 3H); LCMS (ESI, formic) *m/z* 316.00 [M + H]$^+$, t_R = 0.67 min; HRMS (ESI) calcd for C$_{15}$H$_{13}$N$_3$O$_3$S + H$^+$ 316.0741, found 316.0756 (3.68 min).

5-Methyl-4-oxo-*N*-(2-sulfamoylphenyl)-3,4-dihydrothieno-[2,3-*d*]pyrimidine-6-carboxamide (31). A solution of 5-methyl-4-oxo-3,4-dihydrothieno[2,3-*d*]pyrimidine-6-carboxylic acid 16 (60 mg, 0.29 mmol) in thionyl chloride (2 mL, 27 mmol) was refluxed for 16 h before the reaction mixture was concentrated under reduced pressure. A solution of 2-aminobenzenesulfonamide (59.0 mg, 0.34 mmol) and DIPEA (0.1 mL, 0.6 mmol) in DMF (1.5 mL) was dried over molecular sieves (4 Å) and then added to the acid chloride intermediate under nitrogen. The reaction mixture was stirred at room temperature under nitrogen for 5 h. The crude product was

purified by reverse phase chromatography using the formic acid MDAP to give the title product as an orange solid (11 mg, 11%). ^{1}H NMR (400 MHz, DMSO-d_6) δ 12.56 (br s, 1H), 8.17 (d, *J* = 3.5 Hz, 1H), 7.67 (dd, *J* = 8.0, 1.5 Hz, 1H), 7.29−7.36 (m, 1H), 6.84 (d, *J* = 8.5 Hz, 1H), 6.68−6.74 (m, 1H), 2.69 (s, 3H), amide NH and NH$_2$ protons not visible; LCMS (ESI, formic) *m/z* 364.97 [M + H]$^+$, t_R = 0.62 min.

5-Methyl-*N*-(2-(methylsulfonyl)phenyl)-4-oxo-3,4-dihydrothieno[2,3-*d*]pyrimidine-6-carboxamide (32). 5-Methyl-4-oxo-3,4-dihydrothieno[2,3-*d*]pyrimidine-6-carboxylic acid 16 (100 mg, 0.48 mmol) in thionyl chloride (2 mL, 27 mmol) was heated at 50 °C for 2 days before the reaction mixture was concentrated under reduced pressure. A solution of DMF (1.5 mL) and DIPEA (0.2 mL, 1.1 mmol) dried over molecular sieves (4 Å) was added to the crude intermediate followed by 2-(methylsulfonyl)aniline (250 mg, 1.5 mmol). The reaction mixture was stirred at room temperature with molecular sieves under nitrogen for 16 h before being heated to 50 °C for a further 16 h. The crude mixture was purified by reverse phase chromatography using the formic acid MDAP to give the title product as a yellow solid (16 mg, 9%). ^{1}H NMR (400 MHz, DMSO-d_6) δ 8.19−8.24 (m, 2H), 7.96 (dd, *J* = 8.0, 1.5 Hz, 1H), 7.75−7.81 (m, 1H), 7.47 (td, *J* = 8.5, 1.0 Hz, 1H), 3.33 (s, 3H), 2.85 (s, 3H), amide NH protons not visible; LCMS (ESI, formic) *m/z* 364.11 [M + H]$^+$, t_R = 0.76 min.

N-(4-Carbamoylphenyl)-3,4-dichlorobenzamide (36). HATU (191 mg, 0.5 mmol), 4-aminobenzamide (68 mg, 0.5 mmol), and DIPEA (0.15 mL, 0.84 mmol) were added to a solution of 3,4-dichlorobenzoic acid (80 mg, 0.42 mmol) in DMF (1.5 mL), and the reaction mixture was stirred at room temperature for 3 h. Saturated aqueous sodium bicarbonate solution (25 mL) was added, and the aqueous phase was extracted with DCM (2 × 25 mL). Solid was present in both phases. The solid was collected by filtration under vacuum and dried in a vacuum oven to give the title product as a white solid (87 mg, 65%). ^{1}H NMR (400 MHz, DMSO-d_6) δ 10.55 (br s, 1H), 8.23 (d, *J* = 2.0 Hz, 1H), 7.95 (dd, *J* = 8.5, 2.0 Hz, 1H), 7.77−7.91 (m, 6H), 7.24 (br s, 1H); LCMS (ESI, formic) *m/z* 309.03 [M + H]$^+$, t_R = 0.92 min.

General Procedure C for Suzuki Coupling. A mixture of the appropriate aryl halide (1 equiv), (1*H*-pyrazol-3-yl)boronic acid·3H$_2$O (2 equiv), Pd(PPh$_3$)$_4$ (15 mol %), NMP, and saturated aqueous sodium carbonate solution (1 equiv) was heated at 130 °C for 20 min in a microwave reactor. The reaction mixture was filtered, and solvent was evaporated. The crude product was purified by reverse phase chromatography to give the desired final product

N-(4-(1*H*-Pyrazol-3-yl)phenyl)benzamide (37). 37 was prepared according to general procedure C using *N*-(4-bromophenyl)-benzamide 43 (55 mg, 0.2 mmol). The crude product was purified by reverse phase chromatography using the formic acid MDAP to give the title product as a white solid (35 mg, 67%). ^{1}H NMR (400 MHz, DMSO-d_6) δ 13.20−12.80 (2 br s, 1H, two pyrazole isomers visible), 10.27 (br s, 1H), 7.93−8.01 (m, 2H), 7.70−7.88 (m, 5H), 7.48−7.64 (m, 3H), 6.68 (br s, 1H); LCMS (ESI, formic) *m/z* 264.11 [M + H]$^+$, t_R = 0.82 min; HRMS (ESI) calcd for C$_{16}$H$_{13}$N$_3$O + H$^+$ 264.1131, found 264.1125 (3.99 min).

2-(2-((4-(1*H*-Pyrazol-3-yl)phenyl)carbamoyl)phenyl)acetic Acid (38). 38 was prepared according to general procedure C using methyl 2-(2-((4-bromophenyl)carbamoyl)phenyl)acetate 44 (60 mg, 0.172 mmol). The crude product was purified by reverse phase chromatography using the formic acid MDAP to give the title product as a white solid (33 mg, 60%). ^{1}H NMR (600 MHz, DMSO-d_6) δ 12.59 (br s, 1H), 10.47 (br s, 1H), 7.73−7.79 (m, 5H), 7.68 (br s, 1H), 7.60 (d, *J* = 7.5 Hz, 1H), 7.44−7.48 (m, 1H), 7.34−7.42 (m, 2H), 6.65 (d, *J* = 2.0 Hz, 1H), 3.84 (s, 2H); LCMS (ESI, formic) *m/z* 322.07 [M + H]$^+$, t_R = 0.72 min; HRMS (ESI) calcd for C$_{18}$H$_{15}$N$_3$O$_3$ + H$^+$ 322.1186, found 322.1187 (3.64 min).

N-(4-Carbamoylphenyl)benzamide (39). HATU (300 mg, 0.8 mmol), 4-aminobenzamide (107 mg, 0.8 mmol), and DIPEA (0.23 mL, 1.3 mmol) were added to a solution of benzoic acid (80 mg, 0.66 mmol) in DMF (1.5 mL), and the reaction mixture was stirred at room temperature overnight. Saturated aqueous sodium bicarbonate

solution (25 mL) was added, and the aqueous phase was extracted with DCM (2 × 25 mL). Some solid remained in the aqueous phase and was collected by filtration. LCMS of the solid and the organic phase showed desired product present in both. The organic phase was passed through a hydrophobic frit and concentrated under reduced pressure. The resulting crude product was combined with the solid isolated by filtration prior purification. The resulting crude was purified by reverse phase chromatography using the formic acid MDAP to give the title product as a white solid (67 mg, 41%). ¹H NMR (400 MHz, DMSO-d_6) δ 10.41 (s, 1H), 7.92−8.02 (m, 2H), 7.78−7.92 (m, 5H), 7.57−7.66 (m, 1H), 7.49−7.58 (m, 2H), 7.22 (br s, 1H); ¹³C NMR (101 MHz, DMSO-d_6) δ 167.3 (C=O), 165.8 (C=O), 141.8 (C), 134.7 (C), 131.7 (2C, Ar−CH), 129.1 (2C, Ar−CH), 128.4 (2C, Ar−CH), 128.2 (2C, Ar−CH), 127.7 (C), 119.3 (Ar−CH); LCMS (ESI, formic) m/z 241.11 [M + H]⁺, t_R = 0.66 min; HRMS (ESI) calcd for $C_{14}H_{12}N_2O_2$ + H⁺ 241.0972, found 241.0967 (3.29 min); IR (ATR) cm⁻¹ 3383, 3308, 3163, 1650, 1606, 1516.

4-(1-Oxo-3,4-dihydroisoquinolin-2(1H)-yl)benzamide (40). A mixture of 4-(1-oxo-3,4-dihydroisoquinolin-2(1H)-yl)benzonitrile **46** (40 mg, 0.16 mmol), 2 M aqueous NaOH solution (1.2 mL, 2.4 mmol), and 30% aqueous H₂O₂ solution (54 μL, 0.53 mmol) in EtOH (1 mL) was heated at 50 °C for 20 h. The reaction mixture was poured in saturated aqueous sodium sulfite solution and acidified to pH 1 with aqueous H₂SO₄ solution. The mixture was concentrated under reduced pressure. Water and DCM were added. The aqueous phase was extracted with DCM. The combined organic phases were passed through a hydrophobic frit and concentrated under reduced pressure. The resulting crude product was purified by reverse phase chromatography using the formic acid MDAP to give the title product as a white solid (8 mg, 19%). ¹H NMR (400 MHz, DMSO-d_6) δ 7.86−8.00 (m, 4H), 7.45−7.58 (m, 3H), 7.35−7.44 (m, 2H), 7.27−7.34 (m, 1H), 4.00 (t, J = 6.5 Hz, 2H), 3.14 (t, J = 6.5 Hz, 2H); LCMS (ESI, formic) m/z 267.07 [M + H]⁺, t_R = 0.71 min; HRMS (ESI) calcd for $C_{16}H_{15}N_2O_2$ + H⁺ 267.1128, found 267.1125 (3.56 min).

N-(2-(1H-Pyrazol-3-yl)pyrimidin-5-yl)benzamide (41). 41 was prepared according to general procedure C using N-(2-chloropyrimidin-5-yl)benzamide **45** (60 mg, 0.26 mmol). The resulting crude product was purified by reverse phase chromatography using the high pH MDAP to give the title product as a white solid (28 mg, 41%). ¹H NMR (400 MHz, DMSO-d_6) δ 13.02−13.79 (br d, 1H, two pyrazole isomers visible), 10.68 (br s, 1H), 9.23 (s, 2H), 8.00−8.05 (m, 2H), 7.62−7.68 (m, 2H), 7.55−7.61 (m, 2H), 6.90 (d, J = 1.5 Hz, 1H); ¹³C NMR (101 MHz, DMSO-d_6) δ 177.6 (Ar−CH), 165.9 (C=O), 148.5 (2C, Ar−CH), 133.7 (C), 132.6 (C), 132.2 (Ar−CH), 128.5 (2C, Ar−CH), 127.7 (2C, Ar−CH), 119.1 (C), 105.4 (Ar−CH), one carbon too weak to assign should be around 150 ppm; LCMS (ESI, high pH) m/z 266.04 [M + H]⁺, t_R = 0.74 min; HRMS (ESI) calcd for $C_{14}H_{11}N_5O$ + H⁺ 266.1029, found 266.1036 (3.47 min).

2-(4-(1H-Pyrazol-3-yl)phenyl)-3,4-dihydroisoquinolin-1(2H)-one (42). 42 was prepared according to general procedure C using 2-(4-bromophenyl)-3,4-dihydroisoquinolin-1(2H)-one **47** (100 mg, 0.331 mmol). The resulting crude product was purified by reverse phase chromatography using the formic acid MDAP (15−55% (B) over 15 min) to give the title product as a white solid (45 mg, 47%). ¹H NMR (400 MHz, DMSO-d_6) δ 13.31 + 12.89 (2 br s, 1H), 7.95 (dd, J = 7.5, 1.0 Hz, 1H), 7.75−7.88 (m, 3H), 7.54 (td, J = 7.5, 1.5 Hz, 1H), 7.46 (br s, 1H), 7.36−7.43 (m, 3H), 6.73 (br s, 1H), 3.99 (t, J = 6.5 Hz, 2H), 3.15 (t, J = 6.5 Hz, 2H); LCMS (ESI, high pH) m/z 290.23 [M + H]⁺, t_R = 0.89 min.

N-(4-Bromophenyl)benzamide (43). HATU (335 mg, 0.88 mmol) and DIPEA (0.26 mL, 1.5 mmol) were added to a solution of benzoic acid (90 mg, 0.74 mmol) in DMF (3 mL). The mixture was stirred at room temperature for 5 min. 4-Bromoaniline (152 mg, 0.88 mmol) was then added, and the reaction mixture was stirred at room temperature for 15 h. The crude reaction mixture was purified by reverse phase chromatography (30−85% CH₃CN + 0.01% formic acid (B)/H₂O + 0.01% formic acid (A), 43 g C18 column) to give the title product as a white solid (120 mg, 49%). ¹H NMR (400 MHz, DMSO-d_6) δ 10.34 (s, 1H), 7.94 (br d, J = 7.0 Hz, 2H), 7.77 (br d, J = 9.0 Hz,

2H), 7.59−7.62 (m, 1H), 7.50−7.56 (m, 4H); LCMS (ESI, formic) m/z 275.97 + 277.93 [M + H]⁺, t_R = 1.09 min.

Methyl 2-(2-((4-Bromophenyl)carbamoyl)phenyl)acetate (44). HATU (335 mg, 0.88 mmol) and DIPEA (0.26 mL, 1.49 mmol) were added to a solution of 2-(2-methoxy-2-oxoethyl)benzoic acid (135 mg, 0.69 mmol) in DMF (3 mL). The mixture was stirred at room temperature for 5 min. 4-Bromoaniline (152 mg, 0.88 mmol) was then added and the reaction mixture was stirred at room temperature for 15 h. The crude reaction mixture was purified by reverse phase chromatography (30−85% CH₃CN + 0.01% formic acid (B)/H₂O + 0.01% formic acid (A), 43 g C18 column) to give the title product as a beige solid (210 mg, 68%). ¹H NMR (400 MHz, DMSO-d_6) δ 10.44 (s, 1H), 7.69 (br d., J = 9.0 Hz, 2H), 7.60 (br d, J = 7.5 Hz, 1H), 7.34−7.54 (m, 5H), 3.90 (s, 2H), 3.53 (s, 3H); LCMS (ESI, formic) m/z 347.97, 349.93 [M + H]⁺, t_R = 1.08 min.

N-(2-Chloropyrimidin-5-yl)benzamide (45). HATU (747 mg, 1.96 mmol) and DIPEA (0.57 mL, 3.27 mmol) were added to a solution of benzoic acid (200 mg, 1.64 mmol) in DMF. The mixture was stirred at room temperature for 5 min. 2-Chloropyrimidin-5-amine (255 mg, 1.97 mmol) was then added, and the reaction mixture was stirred at room temperature for 3 h. The reaction mixture was then heated at 40 °C for 15 h. Additional 2-chloropyrimidin-5-amine (125 mg, 0.97 mmol) was added, and the reaction mixture was heated at 40 °C for 5 h. Solvent was evaporated under reduced pressure. The resulting crude product was purified by reverse phase chromatography (20−60% MeOH (B)/water + 0.1% formic acid (A), C18 GOLD column) to give the title product as a brown solid (175 mg, 46%). ¹H NMR (400 MHz, DMSO-d_6) δ 10.77 (br s, 1H), 9.14 (s, 2H), 7.98−8.02 (m, 2H), 7.62−7.69 (m, 1H), 7.58 (apparent triplet, J = 7.0, 8.0 Hz, 2H); LCMS (ESI, high pH) m/z 234.09 [M + H]⁺, t_R = 0.84 min.

4-(1-Oxo-3,4-dihydroisoquinolin-2(1H)-yl)benzonitrile (46). A mixture of 3,4-dihydroisoquinolin-1(2H)-one (62 mg, 0.42 mmol), 4-iodobenzonitrile (195 mg, 0.85 mmol), potassium carbonate (59 mg, 0.43 mmol), and copper(I) iodide (16 mg, 0.084 mmol) in DMF (1 mL) was heated at 160 °C overnight under nitrogen. The reaction mixture was cooled and poured into saturated aqueous NH₄OH solution and EtOAc. The phases were separated, and the aqueous phase was extracted with EtOAc. The combined organic phases were washed with brine, separated, passed through a hydrophobic frit, and concentrated under reduced pressure. The resulting crude product was then purified by reverse phase chromatography using the formic acid MDAP to give the title product as a white solid (69 mg, 66%). ¹H NMR (400 MHz, DMSO-d_6) δ 7.93−7.99 (m, 1H), 7.88 (d, J = 9.0 Hz, 2H), 7.66 (d, J = 9.0 Hz, 2H), 7.56 (td, J = 7.5, 1.5 Hz, 1H), 7.36−7.44 (m, 2H), 4.03 (t, J = 6.5 Hz, 2H), 3.15 (t, J = 6.5 Hz, 2H); LCMS (ESI, formic) m/z 249.12 [M + H]⁺, t_R = 0.94 min.

2-(4-Bromophenyl)-3,4-dihydroisoquinolin-1(2H)-one (47). A mixture of 3,4-dihydroisoquinolin-1(2H)-one (200 mg, 1.36 mmol), 1-bromo-4-iodobenzene (769 mg, 2.72 mmol), copper(I) iodide (52 mg, 0.27 mmol), and potassium carbonate (207 mg, 1.495 mmol) in DMF (3 mL) was heated at 160 °C overnight. The reaction mixture was cooled and poured into saturated aqueous NH₄OH solution and EtOAc. The two phases were separated, and the aqueous phase was extracted with EtOAc. The combined organic phases were washed with brine, separated, passed through a hydrophobic frit, and evaporated under reduced pressure. The resulting crude product was purified by reverse phase chromatography (Redisep C18 column GOLD, 50 g, 40−85% acetonitrile (B)/water + 0.1% formic acid (A) gradient) to give the title product as a white solid (242 mg, 59%). ¹H NMR (400 MHz, DMSO-d_6) δ 7.94 (d, J = 8.0 Hz, 1H), 7.58−7.63 (m, 2H), 7.54 (td, J = 7.5, 1.5 Hz, 1H), 7.34−7.42 (m, 4H), 3.95 (t, J = 6.5 Hz, 2H), 3.13 (t, J = 6.5 Hz, 2H); LCMS (ESI, high pH) m/z 301.77 + 303.75 [M + H]⁺, t_R = 1.09 min.

Ethyl 2-(2-Aminophenyl)acetate (48). A solution of ethyl 2-(2-nitrophenyl)acetate (200 mg, 0.96 mmol) in EtOH (40 mL) was pumped through an H-cube (10% Pd/C CatCart cartridge, 20 °C, full H₂). Solvent was evaporated under reduced pressure to give the title product as an orange gum (148 mg, 86%). ¹H NMR (400 MHz, DMSO-d_6) δ 6.90−6.99 (m, 2H), 6.65 (dd, J = 8.0, 1.0 Hz, 1H), 6.51

(apparent dt, J = 7.5, 1.5 Hz, 1H), 4.84 (br s, 2H), 4.07 (q, J = 7.0 Hz, 2H), 3.49 (s, 2H), 1.18 (t, J = 7.0 Hz, 3H); LCMS (ESI, formic) m/z 180.06 [M + H]$^+$, t_R = 0.70 min.

2-(((*tert*-Butyldimethylsilyl)oxy)methyl)aniline (49). *tert*-Butyl-dimethylsilyl chloride (673 mg, 4.47 mmol) and imidazole (553 mg, 8.12 mmol) were added to a solution of (2-aminophenyl)methanol (500 mg, 4.06 mmol) in CH$_2$Cl$_2$ (6 mL). The reaction mixture was stirred at room temperature for 14 h. CH$_2$Cl$_2$ (5 mL) and water (10 mL) were added and the organic layer was separated using a hydrophobic frit before being concentrated under reduced pressure to give the title product as an orange liquid (889 mg, 92%). ^{1}H NMR (400 MHz, DMSO-d_6) δ 7.07 (br d, J = 7.5 Hz, 1H), 6.96 (apparent dt, J = 7.5, 1.5 Hz, 1H), 6.62 (dd, J = 8.0, 1.0 Hz, 1H), 6.54 (apparent dt, J = 7.5, 1.0 Hz, 1H), 4.83 (br s, 2 H), 4.57 (s, 2H), 0.89 (s, 9H), 0.06 (s, 6H); LCMS (ESI, formic) m/z 238.14 [M + H]$^+$, t_R = 1.36 min.

N-(2-(((*tert*-Butyldimethylsilyl)oxy)methyl)phenyl)-5-methyl-4-oxo-3,4-dihydrothieno[2,3-*d*]pyrimidine-6-carboxamide (50). **50** was prepared according to general procedure B using 2-(((*tert*-butyldimethylsilyl)oxy)methyl)aniline **49** (140 mg, 0.59 mmol). The crude product was purified by reverse phase chromatography (43 g C18 column, 40−80% CH$_3$CN + 0.1% formic acid (B)/H$_2$O + 0.1% formic acid (A) over 25 min) to give the title product as a yellow solid (90 mg, 44%). ^{1}H NMR (400 MHz, DMSO-d_6) δ 12.57 (br s, 1H), 9.63 (s, 1H), 8.18 (s, 1H), 7.60 (dd, J = 8.0, 1.0 Hz, 1H), 7.46 (dd, J = 7.5, 1.0 Hz, 1H), 7.32 (apparent td, J = 8.0, 1.5 Hz, 1H), 7.26 (apparent td, J = 7.5, 1.0 Hz, 1H), 4.77 (s, 2H), 2.80 (s, 3H), 0.87 (s, 9H), 0.06 (s, 6H). LCMS (ESI, formic) m/z 430.14 [M + H]$^+$, t_R = 1.32 min.

Chemiluminescent Nitrogen Detection (CLND) Solubility Determination. For GSK in-house kinetic solubility assay, 5 μL of 10 mM DMSO stock solution was diluted to 100 μL with pH 7.4 phosphate buffered saline, equilibrated for 1 h at room temperature, and filtered through Millipore Multiscreen$_{HTS}$-PCF filter plates (MSSL BPC). The filtrate was quantified by suitably calibrated flow injection chemiluminescent nitrogen detection. The standard error of the CLND solubility determination is ±30 μM, and the upper limit of the solubility was 500 μM when working from 10 mM DMSO stock solution.

Calculated Properties. Calculated partition coefficient (clogP) was computed using the BioByte algorithm, version 5.4 (BioByte Corp., 201 W. Fourth Street, No. 204, Claremont, CA 91711-4707).

BCATm Fluorescent Assay. All reagents were purchased from Sigma-Aldrich Ltd. (Gillingham, Dorset, U.K.) unless otherwise stated. Assay buffer was 50 mM HEPES (pH 7.5), 50 mM NaCl, and 1 mM CHAPS. Horseradish peroxidase was initially diluted to 500 units/mL in water. 4-Methyl-2-oxovalerate was initially diluted to 10 mM in assay buffer. L-Leucine and α-ketoglutarate were both initially diluted to 100 mM in 50 mM HEPES (pH 7.5) with pyridoxal phosphate (PLP) initially diluted to 10 mM in 50 mM HEPES (pH 7.5). Amplex red (Invitrogen, Paisley, U.K.) was initially diluted to 20 mM in DMSO.

BCATm and L-GOX protein were cloned, expressed, and isolated in house (GSK, Stevenage, U.K.). The assay monitors the production of L-glutamate from branch chain amino acids and α-ketoglutarate through the coupling of hBCATm activity to two additional enzymes, L-glutamate oxidase (L-GOx) and horseradish peroxidase (HRP). L-GOx catabolizes L-glutamate to generate α-ketoglutarate and hydrogen peroxide, the latter being utilized by HRP and leading to the formation of fluorescent resorufin from the redox sensitive dye Amplex Red.

The BCATm fluorescent assay was carried out in low volume 384-well plates (Greiner Bio-one, Stonehouse, U.K.) at a final volume of 10 μL per well. Test compounds were added to plates as 50 nL solutions in DMSO using an Echo 555 acoustic dispenser (Labcyte, Sunnyvale, CA) prior to the addition of assay components. Additionally, 50 nL of DMSO or positive control (5-chloro-2-benzofurancarboxylic acid 2-[[2-(trifluoromethyl)phenyl]sulfonyl]hydrazide; eMolecules) was included in two columns each to give 100% activity and 100% inhibition controls, respectively. Single-concentration testing was at 10 μM compound concentration. For pIC$_{50}$ determination, compounds were

tested using an 11-point, 3-fold dilution series from either 625 μM or 6.25 μM prepared using a Biomek FX (Beckman Coulter, Wycombe, U.K.).

To these compound plates, 4 μL of an enzyme-PLP solution containing 20 nM BCATm and 40 nM PLP in assay buffer was added. Following this, 4 μL of a coupling solution containing 3 mM L-leucine, 0.5 mM α-ketoglutarate, 10 units/mL HRP, and 80 μM Amplex Red in assay buffer was added to initiate the reaction. The coupling solution was incubated on a roller at room temperature in a 15 mL tube with 1 mL of agarose immobilized catalase (Sigma-Aldrich Ltd.) per 10 mL of coupling solution to "scrub" the coupling solution prior to addition of Amplex Red and to remove background levels of hydrogen peroxide. After a 10 min incubation, 2 μL of 100 mM 4-methyl-2-oxovalerate was added to stop the reaction.

Final assay concentrations were 10 nM BCATm, 20 nM PLP, 5 units per mL HRP, 1.5 mM L-leucine, 0.25 mM α-ketoglutarate, and 40 μM Amplex Red. All additions were performed using a Multidrop Combi (Thermo Fisher Scientific, Waltham, MA). Plates were transferred to an EnVision reader (PerkinElmer) (excitation filter 525/20 nm; emission filter 598/25 nm).

BCAT Cellular Assay. Differentiated primary human adipocytes (Zenbio) were challenged overnight using compounds dissolved in HBSS (Gibco 1 g/L glucose) complemented with HEPES 10 mM, L-serine 50 μM, and L-leucine 150 μM. Next day cell supernatant was subjected to amino acids determinations using HPLC analysis essentially as previously described.[4] The method is based on automated, online derivatization using *o*-phthalaldehyde (OPA) for primary amino acids and 9-fluorenylmethyl chloroformate (FMOC) for secondary amino acids, using an Eclipse Plus C18, 3 mm × 10 mm, 3.5 μm column to perform reversed phase HPLC (all chemicals and hardware from Agilent Technologies, Inc.). The percentage of inhibition was calculated on leucine concentration remaining compared to vehicle treated cells.

Analogue Searching. FindAnalogues is an in-house developed PipelinePilot [Pipeline Pilot (2010) Accelrys Ltd., San Diego, CA] protocol developed to search for analogues of fragment compounds. The protocol used several search methods to retrieve analogues of fragment structures. The tautomers of the input molecule were enumerated prior to searching and core generation using the relevant PipelinePilot component. Tautomers were also enumerated for the core. A core was generated for each input query molecule by iteratively removing terminal chain atoms, stopping at O, N, S. An amide/sulfonamide/ester/acid was cleaved to leave either N or C=O/SO$_2$. Additional rules break N-linked piperidines to leave N. Terminal nitrogens are set to [#7], [nH] to n.

The core was used to conduct a substructure search on the relevant database. The JChem Cartridge was used for enabling chemical structure search and management within Oracle, JChem 5.3, ChemAxon (http://www.chemaxon.com).

Similarity searches were performed on the database using the full query molecule and the ChemAxon fingerprint. Several similarity search metrics[22] were used: Tversky searches[23] using the input molecule as both the target and the query with α = 0.9, β = 0.1, cutoff = 0.8; Tanimoto search with similarity cutoff of 0.8. Additionally a reduced graph[24] substructure search was performed with the reduced graph derived from the full query structure. Optionally, limits could be placed on the hit list according to the difference in heavy atom count or molecular weight difference between the query and the hit molecule. This was particularly significant for the substructure and Tversky searches to control the size of the hit molecules. The total number of hits from any single query could also be specified, defined as MaxHits in the following. For the SS and RG search, hits were ordered by molecular weight and the MaxHits lowest molecular weight compounds were returned. For the Tversky and Tanimoto search, the MaxHits most similar compounds were returned.

NMR Saturation Transfer Difference (STD). All NMR spectra were recorded in PBS buffer [pH 7.2], 100% D$_2$O, 300 K, and Bruker Avance 700 MHz spectrometer, equipped with a 5 mm cryoprobe and sample changer (Bruker-BioSpin). Sample volume was 180 μL in a 3

mm sample tube (Norrell). A set of reference ^{1}H NMR spectra for individual fragments was recorded in the absence of protein.

Fragments were tested for binding to BCAT in pools of typically 5 compounds per sample at a concentration of 1 mM each. The protein concentration was 10 μM. Saturation of protein ^{1}H resonances was achieved by continuous wave irradiation at 0.3 ppm for 2 s. A 30 ms spin-lock period was employed before acquisition to allow the residual protein signal to decay. STD spectra were processed and deconvoluted by comparison with the reference spectra of the individual compounds using the TOPSPIN program (Bruker BioSpin). Only STD signals to the left of the waterline (i.e., >5.5 ppm) were evaluated. The intensity of the largest resolved signal of each compound was determined and compared to the maximum noise level of the spectrum in the signal-free region between 11 and 12 ppm. STD signals with an intensity 4× above noise level were classified as hits.

T_m Methods. The protein was diluted to a final concentration 2.4 μM in buffer (25 mM HEPES pH 7.5 containing 25 mM NaCl, 20 mM DTT, 20 mM EDTA, 2.5% glycerol). The PLP (E) form of the enzyme was prepared by incubation with a 100-fold excess of α-ketoglutarate for 1 min at 20 °C. The PMP (F) form of the enzyme was prepared by incubation with a 100-fold excess of L-leucine for 1 min at 20 °C. The isoforms of the enzyme were purified by centrifugal ultrafiltration at 15 000g at 4 °C for 15 min using Vivaspin-6 10 kDa nominal molecular cutoff spin filters. The retentates were recovered and the volume was adjusted to give a final protein concentration of 2.4 μM. The purified enzymes were stored at 4 °C until used. Samples were prepared in 96-well plates. 0.5 μL of buffer (control), DMSO, or compound at 10 mM in DMSO was aliquoted into separate wells. To each well was added 50 μL of the required form of the enzyme containing a 1:1000 dilution of Sypro Orange (Invitrogen). The plate was incubated for 1 min at room temperature and centrifuged for 1 min at 1000g. 20 μL aliquots from each well were transferred to wells in sequential rows of a white 96-well plate (Abgene 0.2 mL semiskirted Thermo-Fast plate; AB-0900/w) and overlaid with 5 μL of silicon oil. Data were acquired on an Exicycler rt-pcr instrument (Bioneer Inc.). Fluorescence intensity was recorded at 0.5 °C intervals over a temperature range of 4–94 °C at a heating rate of 1 °C/min. The raw fluorescent intensity signals were exported into Excel csv format. The raw data were normalized using the formula: (cell value − min(column data range))/(max(column data range) − min(column data range)) where "cell value" is the raw fluorescence reading at each temperature point.

The normalized fluorescence intensities versus temperature data were fitted to a standard denaturation isotherm in Grafit5 (Erithacus software).

BCATm/PLP Protein Production and Crystallization. Human branched-chain amino acid aminotransferase mitochondrial (BCATm) (residues 28−392) deleted of the N-terminal mitochondria signal peptide (residues 1−27) was cloned into kanamycin resistant pET28a via NdeI/XhoI restriction endonuclease sites with an N-terminal 6-His-thrombin cleavage site. This was used to transform *E. coli* BL21 Star (DE3) (Invitrogen) cells. The transformed cells were grown in turbo media supplemented with glucose and kanamycin; after induction with IPTG 1 mM the temperature was reduced from 37 to 25 °C and the cells harvested 23 h later. The human BCATm was purified using a modification of the method described by Conway and Huston,[25] frozen cell pellets were thawed in buffer (25 mM HEPES, pH 7.5, 500 mM NaCl, 4 M urea, 1 mM DTT, 20 mM imidazole, protease inhibitor cocktail III (Merck) containing 0.1 mM pyridoxal phosphate, 0.2 mg/mL lysozyme, and 10 U/mL Benzonase (Merck) and mixed for 30 min at room temperature. The cell suspension was sonicated and the cell debris removed by centrifugation at 100 000g for 90 min. The supernatant was loaded onto a 5 mL HisTrap HP column (GE Healthcare), washed with 10 bed volumes (Bv) of buffer before running a gradient to 0 M urea in buffer over 10 Bv at 5 mL/min. The column was eluted using a series of imidazole steps 25, 50, 100, 200, and 500 mM in buffer (10 Bv of each at 5 mL/min). The human BCATm containing fractions (100 mM and 200 mM imidazole step) were pooled and concentrated using Amicon Ultra (Millipore) centrifugal ultrafilters with a 30 kDa MWCO and further purified

using a Superdex200 column (GE Healthcare). Dimeric human BCATm was pooled and buffer exchanged into thrombin cleavage buffer (50 mM HEPES, pH 7.5, 150 mM NaCl, 2 mM CaCl) and incubated for 2 h at room temp with 10 U/mL of thrombin (LeeBio). After cleavage, DTT and (NH$_4$)$_2$SO$_4$ were added at 1 mM and 1.5 M, respectively, and the thrombin was removed by purification on a butyl Sepharose HP column (GE Healthcare). Human BCATm was eluted using a gradient to 0 M (NH$_4$)$_2$SO$_4$ over 20 Bv. The human BCATm was pooled, buffer exchanged into storage buffer (25 mM HEPES, pH 7.5, 25 mM NaCl, 20 mM DTT, 20 mM EDTA, 2.5% glycerol), concentrated to ~10 mg/mL, and snap frozen at −80 °C. Functional competency was confirmed using the coupled biochemical assay. Structural integrity was confirmed using differential scanning fluorimetry measurements and protein crystallization.

The purified protein in 25 mM HEPES, pH 7.5, 25 mM NaCl, 20 mM DTT, 20 mM EDTA, 2.5% glycerol and concentrated to at least 7.6 mg/mL was used for crystallography. Crystals of BCATm were grown by hanging drop vapor diffusion at 20 °C with microseeding using MDL Morpheus screen condition B2 supplemented with 10 mM DTT in a protein to microseed solution of drop ratio of 1:1. The Hampton Research seed-bead method was used to generate microseeds. The crystals had a yellow hue suggestive of bound PLP cofactor despite none being added during purification or crystallization. The complex with compound **27** was produced from a cocrystal grown under comparable conditions to the holoenzyme but in the presence of the compound (at 25 mM).

X-ray Crystallography: Crystal Structures of BCATm/PLP Complexed with Inhibitors. Holocrystals were transferred to soaking buffer comprising MDL Morpheus screen condition B2 supplemented with 10 mM or 20 mM DTT and the compound of interest (from a stock solution dissolved in DMSO) at the soaking concentration given in the X-ray summary table (in Supporting Information). Crystals were harvested in a cryoloop and plunge-frozen into liquid nitrogen before loading in a puck for mounting with a sample collector. Data from single crystals were collected at 100 K either at the Diamond Light Source (Harwell) or on an in-house RIGAKU FR-E$^+$ SUPERBRIGHT/Saturn A200 detector/ACTOR robotic system. Data processing was achieve using DENZO, MOSFLM, or XDS (within AUTOPROC) and scaled using either SCALEPACK or SCALA within the CCP4 programming suite.[25] Structures were solved by Fourier synthesis using REFMAC (via CCP4) starting from a previously determined in house structure, model-building was performed using COOT and refined using REFMAC via CCP4. The statistics for the data collection and refined coordinates are given in Supporting Information. The final crystal structures are deposited in the Protein Data Bank under the accession codes 5I5S-Y and 5I60.

■ ASSOCIATED CONTENT

Ⓢ Supporting Information

The Supporting Information is available free of charge on the ACS Publications website at DOI: 10.1021/acs.jmedchem.5b01607.

Molecular formula strings (CSV)

Statistics for data collection and refined coordinates for X-ray crystallography (PDF)

■ AUTHOR INFORMATION

Corresponding Author

*E-mail: jennifer.a.borthwick@gsk.com. Phone: +44 (0)1438 763875.

Author Contributions

The manuscript was written through contributions of all authors. All authors have given approval to the final version of the manuscript.

Notes

◼ ABBREVIATIONS USED

BCAT, branched-chain aminotransferase; BCAA, branched-chain amino acid; CLND, chemiluminescent nitrogen detection; FBDD, fragment based drug discovery; DIPEA, diisopropylethylamine; HATU, 1-[bis(dimethylamino)-methylene]-1H-1,2,3-triazolo[4,5-b]pyridinium 3-oxide hexa-fluorophosphate; HTS, high throughput screening; LE, ligand efficiency; LLE_{AT}, lipophilic ligand efficiency defined by Astex; PK, pharmacokinetic; PLP, pyridoxal phosphate; PMP, pyridox-amine phosphate; PPB, plasma protein binding; SAR, structure−activity relationship; STD-NMR, saturation-transfer difference nuclear magnetic resonance; T_m, thermal shift

◼ REFERENCES

(1) Sweatt, A. J.; Wood, M.; Suryawan, A.; Wallin, R.; Willingham, M. C.; Hutson, S. M. Branched-chain Amino Acid Catabolism: Unique Segregation of Pathway Enzymes in Organ Systems and Peripheral Nerves. *Am. J. Physiol.: Endocrinol. Metab.* **2004**, *286*, E64−E76.

(2) She, P.; Reid, T. M.; Bronson, S. K.; Vary, T. C.; Hajnal, A.; Lynch, C. J.; Hutson, S. M. Disruption of BCATm in Mice Leads to Increased Energy Expenditure Associated with the Activation of a Futile Protein Turnover Cycle. *Cell Metab.* **2007**, *6*, 181−194.

(3) She, P.; Zhou, Y.; Zhang, Z.; Griffin, K.; Gowda, K.; Lynch, C. J. Disruption of BCAA Metabolism in Mice Impairs Exercise Metabolism and Endurance. *J. Appl. Physiol.* **2010**, *108*, 941−949.

(4) Bertrand, S. M.; Ancellin, N.; Beaufils, B.; Bingham, R. P.; Borthwick, J. A.; Boullay, A. B.; Boursier, E.; Carter, P. S.; Chung, C. W.; Churcher, I.; Dodic, N.; Fouchet, M. H.; Fournier, C.; Francis, P. L.; Gummer, L. A.; Herry, K.; Hobbs, A.; Hobbs, C. I.; Homes, P.; Jamieson, C.; Nicodeme, E.; Pickett, S. D.; Reid, I. H.; Simpson, G. L.; Sloan, L. A.; Smith, S. E.; Somers, D. O.; Spitzfaden, C.; Suckling, C. J.; Valko, K.; Washio, Y.; Young, R. J. The Discovery of in Vivo Active Mitochondrial Branched-Chain Aminotransferase (BCATm) Inhibitors by Hybridizing Fragment and HTS Hits. *J. Med. Chem.* **2015**, *58*, 7140−7163.

(5) Deng, H.; Zhou, J.; Sundersingh, F. S.; Summerfield, J.; Somers, D.; Messer, J. A.; Satz, A. L.; Ancellin, N.; Arico-Muendel, C. C.; Bedard, K. L.; Beljean, A.; Belyanskaya, S. L.; Bingham, R.; Smith, S. E.; Boursier, E.; Carter, P.; Centrella, P. A.; Clark, M. A.; Chung, C. W.; Davie, C. P.; Delorey, J. L.; Ding, Y.; Franklin, G. J.; Grady, L. C.; Herry, K.; Hobbs, C.; Kollmann, C. S.; Morgan, B. A.; Kaushansky, L. J.; Zhou, Q. Discovery, SAR, and X-ray Binding Mode Study of BCATm Inhibitors from a Novel DNA-Encoded Library. *ACS Med. Chem. Lett.* **2015**, *6*, 919−924.

(6) Scanlon, M. Inhibitors of BCATm: A Tough Nut To Crack. *J. Med. Chem.* **2015**, *58*, 7138−7139.

(7) Whittaker, M.; Law, R. J.; Ichihara, O.; Hesterkamp, T.; Hallett, D. Fragments: Past, Present and Future. *Drug Discovery Today: Technol.* **2010**, *7*, e163−e171.

(8) Schiebel, J.; Radeva, N.; Köster, H.; Metz, A.; Krotzky, T.; Kuhnert, M.; Diederich, W. E.; Heine, A.; Neumann, L.; Atmanene, C.; Roecklin, D.; Vivat-Hannah, V.; Renaud, J. P.; Meinecke, R.; Schlinck, N.; Sitte, A.; Popp, F.; Zeeb, M.; Klebe, G. One Question, Multiple Answers: Biochemical and Biophysical Screening Methods Retrieve Deviating Fragment Hit Lists. *ChemMedChem* **2015**, *10*, 1511−1521.

(9) Alex, A. A.; Flocco, M. M. Fragment-Based Drug Discovery: What has it Achieved so Far? *Curr. Top. Med. Chem.* **2007**, *7*, 1544−1567.

(10) Chessari, G.; Woodhead, A. J. From Fragment to Clinical Candidate − a Historical Perspective. *Drug Discovery Today* **2009**, *14*, 668−675.

(11) Hajduk, P. J.; Greer, J. A Decade of Fragment-Based Drug Design: Strategic Advances and Lessons Learned. *Nat. Rev. Drug Discovery* **2007**, *6*, 211−219.

(12) Hutson, S. Structure and Function of Branched Chain Aminotransferases. *Prog. Nucleic Acid Res. Mol. Biol.* **2001**, *70*, 175−206.

(13) Hann, M. M.; Leach, A. R.; Harper, G. Molecular Complexity and its Impact on the Probability of Finding Leads for Drug Discovery. *J. Chem. Inf. Model.* **2001**, *41*, 856−864.

(14) Ludwig, C.; Guenther, U. L. Ligand Based NMR Methods for Drug Discovery. *Front. Biosci., Landmark Ed.* **2009**, *14*, 4565−4574.

(15) Gozalbes, R.; Carbajo, R. J.; Pineda-Lucena, A. Contributions of Computational Chemistry and Biophysical Techniques to Fragment-Based Drug Discovery. *Curr. Med. Chem.* **2010**, *17*, 1769−1794.

(16) Hopkins, A. L.; Groom, C. R.; Alex, A. Ligand Efficiency: a Useful Metric for Lead Selection. *Drug Discovery Today* **2004**, *9*, 430−431.

(17) Mortenson, P.; Murray, C. Assessing the Lipophilicity of Fragments and Early Hits. *J. Comput.-Aided Mol. Des.* **2011**, *25*, 663−667.

(18) Fischer, M.; Hubbard, R. E. Fragment-Based Ligand Discovery. *Mol. Interventions* **2009**, *9*, 22−30.

(19) Ishikawa, M.; Hashimoto, Y. Improvement in Aqueous Solubility in Small Molecule Drug Discovery Programs by Disruption of Molecular Planarity and Symmetry. *J. Med. Chem.* **2011**, *54*, 1539−1554.

(20) Murray, C. W.; Rees, D. C. The Rise of Fragment-Based Drug Discovery. *Nat. Chem.* **2009**, *1*, 187−192.

(21) Azizian, J.; Mohammadi, A. A.; Karimi, A. R.; Mohammadizadeh, M. R. A Stereoselective Three-Component Reaction: $KAl(SO_4)_2.12H_2O$, an Efficient and Reusable Catalyst for the One-Pot Synthesis of cis-Isoquinolonic Acids. *J. Org. Chem.* **2005**, *70*, 350−352.

(22) Willett, P.; Barnard, J. M.; Downs, G. M. Chemical Similarity Searching. *J. Chem. Inf. Model.* **1998**, *38*, 983−996.

(23) Tversky, A. Features of Similarity. *Psychol. Rev.* **1977**, *84*, 327−352.

(24) Harper, G.; Bravi, G. S.; Pickett, S. D.; Hussain, J.; Green, D. V. S. The Reduced Graph Descriptor in Virtual Screening and Data-Driven Clustering of High-Throughput Screening Data. *J. Chem. Inf. Model.* **2004**, *44*, 2145−2156.

(25) Bailey, S. The CCP4 Suite: Programs for Protein Crystallography. *Acta Crystallogr., Sect. D: Biol. Crystallogr.* **1994**, *50*, 760−763.